EMERGING INFECTIOUS DISEASES®

CDC
CENTERS FOR DISEASE CONTROL AND PREVENTION

Zoonotic Infections

December 2020

Artist Unknown. Cat treatise (Tamrā maeo), 1800–1870. Paper folding book, 12 folios, 2 lines per side, black ink, Thai script. 14.2 in x 4.7 in / 27.31 cm x 28.57 cm. British Library, London, UK. Public Domain.

EMERGING INFECTIOUS DISEASES®

Emerging Infectious Diseases is published monthly by the Centers for Disease Control and Prevention, 1600 Clifton Rd NE, Mailstop H16-2, Atlanta, GA 30329-4027, USA. Telephone 404-639-1960; email, eideditor@cdc.gov

EMERGING INFECTIOUS DISEASES®

Zoonotic Infections

December 2020

On the Cover

Artist Unknown. *Tamrā maeo—Cat treatise*, 1800–1870. Paper folding book, 12 folios, 2 images per side, ink, Thai script. 14.2 in × 4.7 in/27.31 cm × 28.57 cm. British Library (Or 16797), London, UK. Public domain.

About the Cover p. 3108

Synopses

Research

Medscape EDUCATION ACTIVITY

Medscape EDUCATION ACTIVITY

Dispatches

EMERGING INFECTIOUS DISEASES®
December 2020

Research Letters

EMERGING INFECTIOUS DISEASES®
December 2020

Comment Letters

About the Cover

Reviewer Appreciation

Etymologia

Online Report

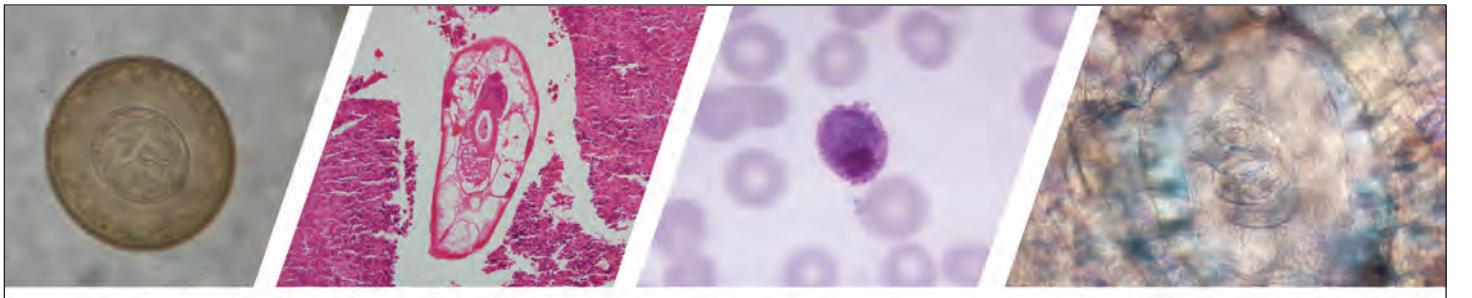

DPDx

Diagnostic Assistance and Training in Laboratory Identification of Parasites

A free service of CDC available to laboratorians, pathologists, and other health professionals in the United States and abroad

- Diagnosis from photographs of worms, histological sections, fecal, blood, and other specimen types
- Expert diagnostic review
- Formal diagnostic laboratory report
- Submission of samples via secure file share

Visit the DPDx website for information on laboratory diagnosis, geographic distribution, clinical features, parasite life cycles, and training via Monthly Case Studies of parasitic diseases.

www.cdc.gov/dpdx
dpdx@cdc.gov

U.S. Department of Health and Human Services
Centers for Disease Control and Prevention

CS272346-DE

Outbreak of Anthrax Associated with Handling and Eating Meat from a Cow, Uganda, 2018

Esther Kisaakye, Alex Riolexus Ario, Kenneth Bainomugisha, Caitlin M. Cossaboom, David Lowe, Lilian Bulage, Daniel Kadobera, Musa Sekamatte, Bernard Lubwama, Dan Tumusiime, Patrick Tusiime, Robert Downing, Joshua Buule, Julius Lutwama, Johanna S. Salzer, Eduard Matkovic, Jana Ritter, Joy Gary, Bao-Ping Zhu

On April 20, 2018, the Kween District Health Office in Kween District, Uganda reported 7 suspected cases of human anthrax. A team from the Uganda Ministry of Health and partners investigated and identified 49 cases, 3 confirmed and 46 suspected; no deaths were reported. Multiple exposures from handling the carcass of a cow that had died suddenly were significantly associated with cutaneous anthrax, whereas eating meat from that cow was associated with gastrointestinal anthrax. Eating undercooked meat was significantly associated with gastrointestinal anthrax, but boiling the meat for >60 minutes was protective. We recommended providing postexposure antimicrobial prophylaxis for all exposed persons, vaccinating healthy livestock in the area, educating farmers to safely dispose of animal carcasses, and avoiding handling or eating meat from livestock that died of unknown causes.

Anthrax is an acute zoonotic bacterial infection caused by *Bacillus anthracis*, a gram-positive, spore-forming bacteria that is thought to survive for as long as decades in the carcasses and burial sites of infected animals (*1*). Anthrax is transmitted to humans through handling or eating meat from infected animal carcasses, contact with their products (e.g., hair, wool, hides, bones), or by breathing in spores (*1*,*2*).

Author affiliations: Uganda Public Health Fellowship Program, Kampala, Uganda (E. Kisaakye, A. Riolexus Ario, K. Bainomugisha, L. Bulage, D. Kadobera); Ministry of Health, Kampala (A. Riolexus Ario, M. Sekamatte, B. Lubwama, P. Tusiime); US Centers for Disease Control and Prevention, Atlanta, Georgia, USA (C.M. Cossaboom, D. Lowe, J.S. Salzer, E. Matkovic, J. Ritter, J. Gary, B. Zhu); Ministry of Agriculture, Entebbe, Uganda (D. Tumusiime); Uganda Virus Research Institute, Entebbe, Uganda (R. Downing, J. Buule, J. Lutwama); US Centers for Disease Control and Prevention, Kampala (B.-P. Zhu)

DOI: https://doi.org/10.3201/eid2612.191373

Human anthrax infection is classified into 4 forms, depending on the route of exposure, each with a different incubation period: cutaneous (1–12 days), inhalational (1–60 days), gastrointestinal (1–6 days), and injectional (1–10 days) (*3*). Cutaneous anthrax is the most frequently reported form of human anthrax infection, accounting for up to 95% of cases (*4*). Both cutaneous and gastrointestinal anthrax outbreaks have been associated with handling or butchering infected animals and consuming their meat (*5*). It is estimated that each year 2,000–20,000 human anthrax cases occur worldwide (*6*). Most reported anthrax outbreaks occur in endemic areas in sub-Saharan Africa and Asia (*1*).

On April 20, 2018, the Kween District of Uganda reported to the Ministry of Health 7 suspected cases of cutaneous anthrax from 2 neighboring villages, Kaplobotwo and Rikwo. We investigated to verify the existence of an anthrax outbreak, determine its scope, identify possible exposures, and recommend evidence-based control and prevention measures.

Methods

Study Area

Kween District is located in eastern Uganda (Figure 1). It is one of the so-called "cattle-keeping corridor" districts, where cattle-rearing is a major agriculture activity.

Case Definition

For this study, we defined a suspected cutaneous anthrax case as onset of skin vesicle or eschar, ≥2 cutaneous signs and symptoms (e.g., itching, redness, swelling), or any cutaneous sign or symptom plus regional lymphadenopathy, that occurred in a resident of Kaplobotwo and Rikwo during April 11–25,

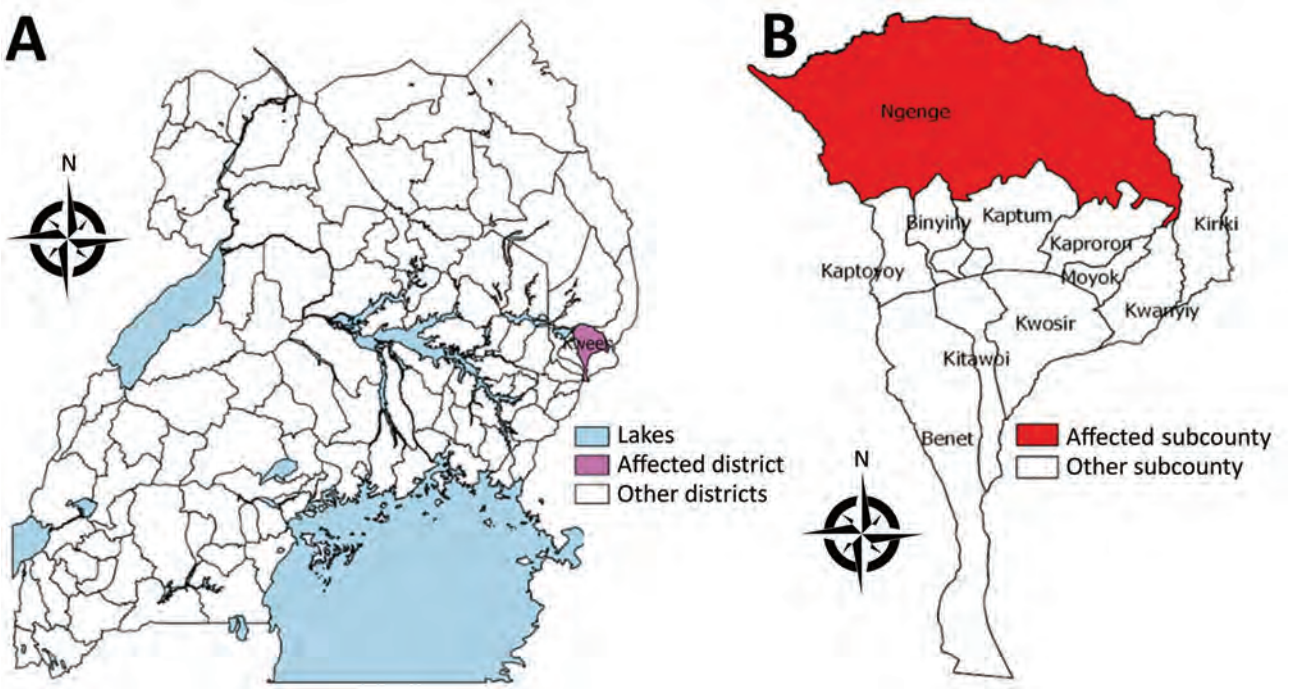

Figure 1. Area where anthrax outbreak occurred in April 2018, Kween District, Uganda. A) Location of Kween District in Uganda; B) Kween District, showing outbreak area.

2018. A suspected gastrointestinal anthrax case was defined as the acute onset of ≥2 signs or symptoms: abdominal pain, vomiting, diarrhea, or sore throat. A confirmed case was a suspected case followed up with a clinical specimen (blood or swab from skin lesion or vesicle) that tested positive for *B. anthracis* by real-time PCR (rPCR).

Case Identification

To identify anthrax cases and possible fatalities, we reviewed medical records from the 3 health facilities nearest the affected communities, Ngenge Health Center III and 2 private clinics. We also conducted a house-to-house search for cases in all 57 households of the 2 affected villages with the help of village leaders and members of the village health team. We developed a list of patients with details about age, sex, residence, date of onset of any signs or symptoms, treatment provided, specimens collected, results of laboratory tests conducted, and date of discharge if the patient was hospitalized.

Descriptive Epidemiology and Hypothesis Generation

We determined the epidemiology of the outbreak by date of symptom onset, location, and demographic characteristics of patients. To identify potential exposures leading to illness, we interviewed 12 suspected anthrax case-patients using convenience sampling in Kaplobotwo. We also conducted key informant interviews with village leaders. From interviews we learned of the sudden death of a cow owned by a resident of Kaplobotwo; the cow was subsequently butchered and eaten by some villagers.

Retrospective Cohort Study

We conducted a retrospective cohort study in the more-affected village, Kaplobotwo, where 96% of the cases occurred, focusing on exposures, which we identified using the methods described. Using a standardized questionnaire developed by the team, we interviewed villagers present in the area at the time of the outbreak. We evaluated the association between exposure to the dead cow and illness onset separately by form of anthrax illness—cutaneous, gastrointestinal, or both. We computed the attack rate (AR) and risk ratio (RR) for each activity that resulted in exposure (e.g., butchering the cow, eating the meat) to assess the association between each individual exposure and subsequent illness. Using modified Poisson regression, we also evaluated the total number of cutaneous exposures for each person interviewed relative to the risk of cutaneous anthrax to assess the dose-response relationship (*7*).

Laboratory Investigations

We collected 6 skin lesion swabs from patients with cutaneous-form anthrax and 8 blood specimens

from patients with gastroenteritis-form anthrax and shipped the samples to the Uganda Virus Research Institute (UVRI; Entebbe, Uganda) for testing. The skin lesion swabs and blood specimens were tested at UVRI using rPCR following standard protocol (*8*).

In addition, upon revisiting the village 1 month later, we tested a specimen collected from the dried hide of the dead cow using the Active Anthrax Detect test (AAD; InBios, https://inbios.com). AAD rapid test, a novel lateral-flow rapid diagnostic test that detects the capsular polypeptide of *B. anthracis*, was developed as a point-of-care test for presumptive human inhalation of anthrax spores and is available as an investigational use only– or research use only–product (*9*, *10*). We suspended the sample in 600 μL of sterile phosphate buffered saline, vortexed for 10 s, and, after pipetting the solution multiple times, applied 10 μL to the AAD cassette.

We shipped a specimen from the same dried hide to the US Centers for Disease Control and Prevention (CDC; Atlanta, GA, USA) for confirmatory testing. DNA extraction on the specimen was performed using a QIAGEN Blood Mini Kit (QIAGEN, https://www.qiagen.com), and the resulting DNA was tested using real-time reverse transcription PCR for *B. anthracis* from the Laboratory Reference Network (https://emergency.cdc.gov/lrn) (*11*). A formalin-fixed sample from the dried hide was routinely processed, embedded in paraffin, and stained with hematoxylin and eosin, Lillie-Twort gram stain, and Warthin-Starry silver stain. Immunohistochemistry assays using mouse monoclonal antibodies targeting the *B. anthracis* cell wall and capsule were performed by using an immunoalkaline phosphatase polymer system as previously described (*10*,*12*).

Trace-Forward Investigations and Environmental Assessment

We conducted in-depth interviews of the district health officer, the village leader, and the owner of the dead cow, as well as a convenience sample of 15 villagers who participated in the processing of the dead cow. The interviews were conducted to investigate the circumstances surrounding the death of the cow, identify people who participated in the butchering, and determine where the meat was distributed and how many people had received the meat. We also walked through the entire village to evaluate evidence of any other dead or sick livestock in the area.

Ethics Considerations

The Office of the Director General of Health Services, Ministry of Health of Uganda, gave the directive and approval to investigate this outbreak. The Office of the Associate Director for Science, Center for Global Health, US CDC, determined that this activity was in response to a public health emergency and not human subjects research. We obtained verbal informed consent from respondents ≥18 years of age or from their parents or guardians if respondents were <18 years of age. We stored all completed questionnaires in a secure location and stored the electronic data in a password-protected laptop to avoid disclosure of respondents' personal information. Data were not shared outside of the investigation team and when being shared within the team, all personal identifying information was deleted in advance.

Results

Descriptive Epidemiology and Hypothesis Generation

We identified 49 cases of human anthrax, 46 suspected and 3 confirmed by rPCR testing. No human deaths were reported. The mean age of the 49 patients was 30 (range 1–84) years. Of the 49 cases, 13 (27%) had cutaneous anthrax only, 16 (33%) had gastrointestinal anthrax only, and 20 (41%) had both cutaneous and gastrointestinal anthrax. Among the 20 patients with both cutaneous and gastrointestinal anthrax, 3 had photophobia, and 2 of those 3 also had neck pain or stiffness, suggesting possible meningeal involvement (*13*) (Table 1).

Key informant interviews indicated that a cow had died suddenly on April 11, 2018, at the residence of a Kaplobotwo resident. Subsequently, the dead cow was skinned and butchered. Most of the adults in Kaplobotwo participated in the butchering and handling of the meat, and many villagers took the meat home to eat. Some of the meat was also sold to neighboring Rikwo. According to local leaders, Kaplobotwo had a total of 234 residents and Rikwo a total of 120 residents. When we analyzed the geographic locations of the cases, 47 (96%) occurred in Kaplobotwo (AR 20%, 47/234) and 2 (4.1%) occurred in Rikwo (AR 1.7%, 2/120). In Kaplobotwo, all cases were within a 600-meter radius of the site where the dead cow was skinned and butchered.

The epidemic curve showed that, after the death and processing of the cow, cases began to appear on April 13, and the number of cases rose, peaking on April 15, suggesting a point-source outbreak. After that, the onset of cases declined, the last being on April 25 (Figure 2, panel A). When the epidemic curve was stratified by anthrax forms (Figure 2, panels B–D), the intervals from exposure to the peak of the epidemic curve was 3 days for cutaneous and 2 days for

Table 1. Clinical manifestations of anthrax by form in patients during an outbreak, Kween District, Uganda, April 2018

Signs and symptoms	No. (%) patients			
	All cases, N = 49	Cutaneous-only, n = 13	Gastrointestinal-only, n = 16	Both, n = 20
Cutaneous				
Skin itching (pruritis)	35 (65)	12 (92)	0	20 (100)
Skin reddening (erythema)	25 (51)	12 (92)	0	13 (65)
Skin swelling (edema)	26 (53)	11 (85)	0	15 (75)
Skin vesicles	17 (35)	8 (62)	0	9 (45)
Skin eschar	9 (18)	3 (23)	0	6 (30)
Regional lymphadenopathy	15 (31)	4 (31)	0	11 (55)
Gastrointestinal				
Abdominal pain	37 (76)	2 (15)	16 (100)	19 (95)
Diarrhea	28 (57)	0	12 (75)	16 (80)
Bloody diarrhea	9 (18)	0	6 (38)	3 (15)
Sore throat	13 (27)	0	6 (38)	7 (35)
Vomiting	10 (20)	0	3 (19)	7 (35)
Swollen neck lymph nodes	2 (4.1)	0	1 (6.3)	1 (5.0)
Systemic				
Fever	25 (51)	2 (15)	8 (50)	15 (75)
Lethargy	24 (49)	1 (7.7)	9 (56)	14 (70)
Anorexia	13 (27)	0	6 (38)	7 (35)
Difficulty breathing	5 (10)	0	1 (6.3)	4 (20)
Cough	5 (10)	0	1 (6.3)	4 (20)
Headache	3 (6.1)	0	0	3 (15)
Other				
Photophobia	3 (6.1)	0	0	3 (15)
Neck pain or stiffness	2 (4.1)	0	0	2 (10)

gastrointestinal. The interval from the initial exposure (April 11–12, 2018) to the end of the epidemic curve was 12–13 days for onset of cutaneous anthrax and 8–9 days for onset of gastrointestinal anthrax. Of the 12 suspected case-patients who participated in the hypothesis-generation interview, 100% carried and ate the meat of the dead cow and were involved in the cutting or butchering, 50% participated in the cleaning of the waste site after the carcass was processed, and 33% participated in skinning the dead cow before butchering.

Retrospective Cohort Study Findings

In our retrospective cohort study in Kaplobotwo, we interviewed 141 persons who resided in the village during April 2018 and therefore could have been exposed to anthrax. Among these 141 villagers, anthrax developed in 47 (AR 33%); cutaneous anthrax developed in 33 (AR 23%), and gastrointestinal anthrax developed in 34 (AR 24%). By anthrax form, the ARs were 9.2% for cutaneous-only, 9.9% for gastrointestinal-only, and 14% for combined cutaneous and gastrointestinal anthrax.

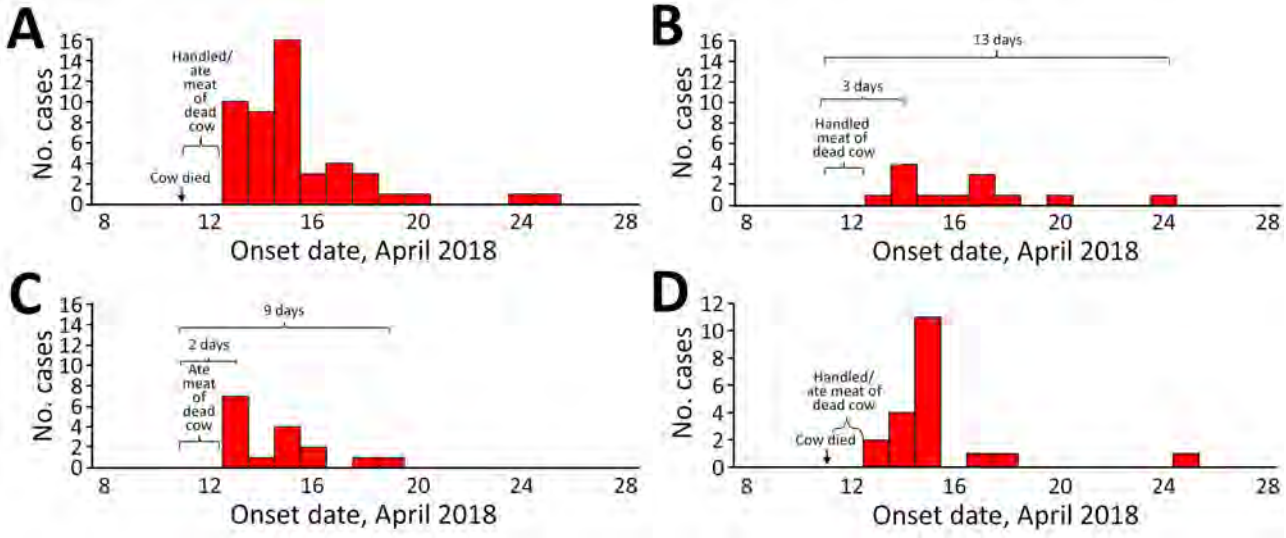

Figure 2. Distribution by date of onset of cases in anthrax outbreak that occurred in April 2018, Kween District, Uganda. A) All anthrax cases; B) cutaneous-only cases; C) gastrointestinal-only cases; D) cases of both cutaneous and gastrointestinal anthrax.

Male residents had a lower AR than female residents for cutaneous-only anthrax (6.5% vs. 13%); however, this difference was not significant (p = 0.175 by Fisher exact test). Conversely, male residents had higher ARs than female residents for both the gastrointestinal-only form (16% vs. 3.1%; p = 0.012 by Fisher exact test) and the combined cutaneous and gastrointestinal form (19% vs. 7.8%; p = 0.039 by Fisher exact test). The cutaneous-only form affected adults more than children, whereas the gastrointestinal-only form affected young children (≤5 years) and older adults (≥30 years) more than older children (5–17 years) and young adults (18–29 years). The mixed cutaneous and gastrointestinal form affected all age groups approximately equally (Table 2).

In the retrospective cohort study, certain activities were significantly associated with developing cutaneous anthrax: carrying the dead cow from the place of death to the place of butchering (RR 4.3, 95% CI 2.4–7.8), participating in the skinning of the cow (RR 4.2, 95% CI 2.6–6.7), participating in cutting and butchering of the dead cow (RR 4.9, 95% CI 3.2–7.9), participating in the removal of the organs (RR 3.5, 95% CI 2.1–6.0), carrying the skin of the dead cow from the butchering site to homes (RR 4.5, 95% CI 2.9–6.9), carrying the cut meat from the place of butchering to homes (RR 4.3, 95% CI 2.4–7.8), and cleaning the waste site after the butchering (RR 4.2, 95% CI 2.6–6.7). The number of cutaneous exposures for each person ranged from 0 to 7. Of the 141 persons who participated in the cohort study, 99 (70%) had no exposures at all, 6 (4.3%) reported only 1 exposure, 22 (16%) reported 2 exposures, 4 (2.8%) reported 3 exposures, 2 (1.4%) reported 4 exposures, 1 (0.71%) reported 5 exposures, 2 (1.4%) reported 6 exposures, and 5 (3.6%) reported having all 7 exposures. For each additional cutaneous exposure, the risk for cutaneous anthrax increased by 30% (RR 1.4, 95% CI 1.3–1.5).

Eating meat from the dead cow was significantly associated with gastrointestinal anthrax (RR ¥, 95% CI 4.3 ¥ by Fisher exact test; p = 0.00). Of the 95 persons who ate the cow meat, eating meat that was boiled for ≤30 minutes was significantly associated with gastrointestinal anthrax (RR 2.5, 95% CI 1.5–4.1); we found that boiling meat for >60 minutes was protective compared with the shorter cooking time (RR 0.34, 95% CI 0.18–0.67) (Table 3).

Table 2. Anthrax attack rates by age and sex for each form, Kaplobotwo, Kween District, Uganda, April 2018*

Anthrax form	Total cohort	No. cases	AR, %
All anthrax	141	47	33
Sex			
M	77	32	42
F	64	15	23
Age range, y			
0–5	30	12	40
6–17	27	6	22
18–29	27	7	26
30–59	40	16	40
≥60	17	6	35
Cutaneous-only	141	13	9.2
Sex			
M	77	5	6.5
F	64	8	13
Age range, y			
0–5	30	1	3.3
6–17	27	1	3.7
18–29	27	3	11
30–59	40	6	15
≥60	17	2	12
Gastrointestinal-only	141	14	9.9
Sex			
M	77	12	16
F	64	2	3.1
Age range, y			
0–5	30	5	17
6–17	27	1	3.7
18–29	27	1	3.7
30–59	40	5	13
≥60	17	2	12
Cutaneous and gastrointestinal	141	20	14
Sex			
M	77	15	19
F	64	5	7.8
Age range, y			
0–5	30	6	20
6–17	27	4	15
18–29	27	3	11
30–59	40	5	13
≥60	17	2	12

*AR, attack rate.

Laboratory Investigation Findings

Of the 6 skin lesion swabs collected, 3 tested positive for *B. anthracis* DNA by rPCR at UVRI. All 8 blood samples were negative for *B. anthracis* by rPCR at UVRI. It should be noted that, at the time of specimen collection, all patients had already started and some had completed antimicrobial treatment. A sample from the dried hide of the cow, taken 1 month after the initial visit to the village, tested positive by AAD in the field and was confirmed to be positive for *B. anthracis* by both rPCR and immunohistochemistry at CDC.

Trace-Forward and Environmental Investigation

According to the village leader, after the cow died on April 11, 2018, a total of 10 residents of Kaplobotwo participated in butchering, skinning, and carrying meat from the cow, and most of the villagers ate meat from the dead cow. Environmental investigations found that the village was near the Panupe Game Reserve. Piles of animal bones were found in the livestock grazing fields, indicating past animal

deaths. Interviews with community leaders revealed that these were remains from animals that had died suddenly and were abandoned in the grazing fields.

Some of the meat from the dead cow was reportedly sold to 2 neighboring villages, Rikwo and Tukumo. Due to resource limitations, we were unable to conduct house-to-house searches for cases in these 2 villages; instead, we contacted the village leaders for case finding. In Rikwo, a family of 2 bought the meat from a meat broker, and gastrointestinal symptoms developed in both family members after they ate the meat. The owner of a bar in the same village also bought the meat, boiled it overnight, poured out the broth from the boiling pot the next morning, fried the boiled meat, and sold it to 28 patrons the next day. None of the patrons reported any gastrointestinal symptoms. In Tukumo, the meat was sold to a bar, a restaurant, and an unknown number of individual families. The village leader was aware of 23 persons who bought and ate the meat; however, he did not know of anyone who had reported gastrointestinal or cutaneous anthrax symptoms.

Discussion

On the basis of epidemiologic, laboratory, and environmental assessments, we determined that this was a point-source cutaneous and gastrointestinal human anthrax outbreak associated with handling and eating meat from a cow that had died from confirmed anthrax infection. Results from this investigation were consistent with those in other anthrax outbreak investigations in which anthrax patients were infected through contact with diseased livestock or contaminated animal products (*14*–*17*).

In our study, although the cause of the cow's death was unknown at the time of death, subsequent laboratory testing confirmed anthrax in the dried hide of the cow. In this area, when a cow is butchered, it is customary to share meat with all households in the village. In this case, this custom exposed the entire village to anthrax. Butchering anthrax-infected animals and disposing of carcasses and waste in environments where ruminants live and graze, combined with limited vaccination of livestock against anthrax, enables further environmental contamination with *B. anthracis* spores and propagation of anthrax outbreaks in animals and zoonotic transmission to humans (*18*). Findings from this investigation are consistent with findings from a previous study in Kuwirirana ward, Gokwe North, Zimbabwe, in which anthrax also resulted from contact with and consumption of anthrax-infected carcasses (*19*).

Among people, anthrax infection is typically an occupational disease, most common among farmers and workers with occupational activities that involve handling animals and animal products, such as the herders, butchers, and others. Infections may also occur among persons who consume infected meat (*4*,*20*,*21*). In this outbreak, cutaneous-only anthrax affected adults more than children, probably because adults were more likely to have been engaged in handling and processing the dead cow.

Spores of *B. anthracis* are refractory to inactivation by boiling and, in this outbreak, eating undercooked meat was significantly associated with developing gastrointestinal anthrax. Conversely, boiling meat for >60 minutes appeared to be protective among persons who ate it, possibly because that length of time could have allowed the heat to rise to a temperature sufficient to inactivate a portion of the spores. Whether or not this actually occurred is unclear. Findings in this study are consistent with those found in a study in Bangladesh in which high rates of cutaneous anthrax but few gastrointestinal anthrax cases occurred in a community that had cooked the meat longer (*22*).

In addition, the risk for gastrointestinal anthrax remained high even when the meat was well cooked (AR 31%) or boiled for >60 minutes (AR 22%). According to World Health Organization guidelines, "any animal that is sick, behaves strangely or has died suddenly should not be used for food or for making any product, as it may have succumbed to an

Table 3. Retrospective cohort study on anthrax risk factors by form during outbreak, Kaplobotwo, Kween District, April 2018

Form	Cases		Attack rate, %		RR (95% CI)
	Exposed	Nonexposed	Exposed	Nonexposed	
Cutaneous anthrax					
Carried dead cow	37	104	54	13	4.3 (2.4–7.8)*
Participated in skinning	10	131	80	19	4.2 (2.6–6.7)*
Participated in cutting/butchering	10	131	90	18	4.9 (3.2–7.5)*
Participated in removing organs	10	131	70	20	3.5 (2.1–6.0)*
Carried the skin of the dead cow	8	133	88	20	4.5 (2.9–6.9)*
Carried cut meat	37	104	54	13	4.3 (2.4–7.8)*
Cleaned the waste	10	131	80	19	4.2 (2.6–6.7)*
For every additional exposure*					1.4 (1.3–1.5)*
Gastrointestinal anthrax					
Ate meat from dead cow, total	95	46	35	0	∞ (4.3–∞)*

infectious disease" (*23*). Following these guidelines can safeguard both animal products and persons involved in handling them.

This study had some limitations. In this outbreak, *B. anthracis* was confirmed by rPCR in 3 of the 6 skin-lesion swab specimens, as well as from the dried hide of the cow. However, the 8 blood specimens from patients with gastroenteritis were negative for *B. anthracis* by both rPCR and culture. These negative findings might be explained by the fact that all patients were already under antimicrobial treatment at the time of specimen collection. Whereas clinical and epidemiologic characteristics strongly suggested gastrointestinal anthrax, we were unable to provide definitive proof without laboratory confirmation. Clinical signs and symptoms of both cutaneous and gastrointestinal anthrax are nonspecific; therefore, some of the identified cases found might actually have been noncases. In addition, the dried hide of the implicated cow tested positive by AAD rapid test. There is great utility for a rapid diagnostic test for presumptive diagnosis of anthrax under field conditions, but care must be taken when interpreting the results of this test. Recent work has identified that the specificity of this assay decreases with carcass age (>24 hours after death), so parallel confirmatory testing is critical when interpreting results from this test (*24*). Also, trace-forward investigation indicated that some meat from the implicated cow might have been sold to neighboring villages, but no house-to-house search was conducted in those villages, possibly resulting in undercounting of cases.

This investigation highlights an outbreak of human cutaneous and gastrointestinal anthrax among persons handling and eating meat from a cow that died of presumed anthrax. As a result of our findings, we made several recommendations to the communities: routinely vaccinate livestock; continue education and mobilization for anthrax; administer antimicrobials to all persons identified with anthrax and prophylaxis to exposed community members; use rapid diagnostic tests at the district level to quickly provide presumptive evidence of anthrax in animal carcasses; and safely bury carcasses under supervision. For burial, carcasses should be disinfected at the site of death with 12.5% formalin solution and buried in a pit ≥6 feet deep with the bottom of the pit ≥3 feet above the water table. We also recommended building capacity and the awareness of healthcare workers to obtain samples from patients before beginning drug administration.

The investigation team worked with the district to conduct community health education on these recommendations and about the dangers of eating meat from animals found dead. We also provided antimicrobial treatment (ciprofloxacin and doxycycline) to all identified patients, offered postexposure antimicrobial prophylaxis to carcass-disposal team members and exposed community members, replenished antimicrobials at Ngenge Health Center III, and provided personal protective equipment and training in its use to the carcass disposal teams. Finally, we advocated for prompt reporting of suspected anthrax cases to the district health office, district veterinary office, and the national One Health coordinator.

Acknowledgments

We are grateful to the Kween District Rapid Response Team for their contribution to the outbreak investigation and response. We thank the staff at the Public Health Emergency Operation Centre and National Task Force in Epidemic Preparedness and Response, Ministry of Health, for coordinating the outbreak response, and staff of Makerere University School of Public Health for their technical support. We also thank all who managed the specimen transport system for ensuring the smooth operations of the system, and staff of CDC's National Center for Emerging and Zoonotic Infectious Diseases, Office of the Deputy Director for Infectious Diseases, Bacterial Special Pathogens Branch (specifically Antonio R. Vieira, William A. Bower, Cari B. Kolton, Chung K. Marston, Robyn A. Stoddard, and Alex R. Hoffmaster) for providing technical assistance and support with the laboratory investigations. Finally, we acknowledge Syamal Raychaudhuri at InBios for providing the AAD lateral flow cassettes.

About the Author

Esther Kisaakye is a field epidemiology training program fellow in the 2018 cohort of the Uganda Public Health Fellowship program. She is currently hosted at the Uganda Ministry of Health to monitor, investigate, and control disease outbreaks in the country, and to conduct disease and mortality surveillance activities.

References

1. Turnbull PCB. Introduction: anthrax history, disease and ecology. In: Koehler TM, editor. Anthrax. Current topics in microbiology and immunology, vol 271. Berlin: Springer; 2002. p. 1–19.
2. Dragon DC, Rennie RP. The ecology of anthrax spores: tough but not invincible. Can Vet J. 1995;36:295–301.
3. Chin J, editor. Control of communicable diseases manual. 17th ed. Washington: American Public Health Association; 2000.
4. Hicks CW, Sweeney DA, Cui X, Li Y, Eichacker PQ. An overview of anthrax infection including the recently

identified form of disease in injection drug users. Intensive Care Med. 2012;38:1092–104. https://doi.org/10.1007/s00134-012-2541-0
5. Inglesby TV, O'Toole T, Henderson DA, Bartlett JG, Ascher MS, Eitzen E, et al.; Working Group on Civilian Biodefense. Anthrax as a biological weapon, 2002: updated recommendations for management. JAMA. 2002;287:2236–52. https://doi.org/10.1001/jama.287.17.2236
6. Martin GJ, Friedlander AM. Bacillus anthracis (anthrax). In: Mandell GL, Bennett JE, Dolin R, editors. Mandell, Douglas, and Bennett's principles and practice of infectious diseases. 7th ed. Philadelphia: Elsevier; 2010. p. 2715–25.
7. Yelland LN, Salter AB, Ryan P. Performance of the modified Poisson regression approach for estimating relative risks from clustered prospective data. Am J Epidemiol. 2011;174:984–92. https://doi.org/10.1093/aje/kwr183
8. Oggioni MR, Meacci F, Carattoli A, Ciervo A, Orru G, Cassone A, et al. Protocol for real-time PCR identification of anthrax spores from nasal swabs after broth enrichment. J Clin Microbiol. 2002;40:3956–63. https://doi.org/10.1128/JCM.40.11.3956-3963.2002
9. Gates-Hollingsworth MA, Perry MR, Chen H, Needham J, Houghton RL, Raychaudhuri S, et al. Immunoassay for capsular antigen of *Bacillus anthracis* enables rapid diagnosis in a rabbit model of inhalational anthrax. PLoS One. 2015;10:e0126304. https://doi.org/10.1371/journal.pone.0126304
10. Guarner J, Jernigan JA, Shieh W-J, Tatti K, Flannagan LM, Stephens DS, et al.; Inhalational Anthrax Pathology Working Group. Pathology and pathogenesis of bioterrorism-related inhalational anthrax. Am J Pathol. 2003;163:701–9. https://doi.org/10.1016/S0002-9440(10)63697-8
11. Hoffmaster AR, Meyer RF, Bowen MD, Marston CK, Weyant RS, Thurman K, et al. Evaluation and validation of a real-time polymerase chain reaction assay for rapid identification of *Bacillus anthracis.* [Erratum in: Emerg Infect Dis. 2003;9:511.] Emerg Infect Dis. 2002;8:1178–82. https://doi.org/10.3201/eid0810.020393
12. Bollweg BC, Silva-Flannery L, Spivey P, Hale GL. Optimization of commercially available Zika virus antibodies for use in a laboratory-developed immunohistochemical assay. J Pathol Clin Res. 2017;4:19–25. https://doi.org/10.1002/cjp2.84
13. Levy LM, Baker N, Meyer MP, Crosland P, Hampton J. Anthrax meningitis in Zimbabwe. Cent Afr J Med. 1981;27:101–4.
14. Mwakapeje ER, Høgset S, Softic A, Mghamba J, Nonga HE, Mdegela RH, et al. Risk factors for human cutaneous anthrax outbreaks in the hotspot districts of Northern Tanzania: an unmatched case-control study. R Soc Open Sci. 2018;5:180479. https://doi.org/10.1098/rsos.180479
15. Yu D, He J, Zhang E, Wang P, Liu D, Hou Y, et al. Investigation and source-tracing of an anthrax outbreak in Gansu Province, China. PLoS One. 2018;13:e0203267. https://doi.org/10.1371/journal.pone.0203267
16. Mwenye KS, Siziya S, Peterson D. Factors associated with human anthrax outbreak in the Chikupo and Ngandu villages of Murewa district in Mashonaland East Province, Zimbabwe. Cent Afr J Med. 1996;42:312–5.
17. Islam MS, Hossain MJ, Mikolon A, Parveen S, Khan MSU, Haider N, et al. Risk practices for animal and human anthrax in Bangladesh: an exploratory study. Infect Ecol Epidemiol. 2013;3:21356. https://doi.org/10.3402/iee.v3i0.21356
18. Rume FI. Epidemiology of anthrax in domestic animals of Bangladesh [PhD thesis]. Dhaka, Bangladesh: University of Dhaka; 2018.
19. Gombe NT, Nkomo BMM, Chadambuka A, Shambira G, Tshimanga M. Risk factors for contracting anthrax in Kuwirirana ward, Gokwe North, Zimbabwe. Afr Health Sci. 2010;10:159–64.
20. Jong EC, Stevens DL, editors. Netteris infectious disease, 1st ed. Philadelphia: Elsevier-Saunders, 2011.
21. Smyth HF, Cheney VS. Anthrax as an occupational disease. Am J Public Health Nations Health. 1930;20:155–60. https://doi.org/10.2105/AJPH.20.2.155
22. Chakraborty A, Khan SU, Hasnat MA, Parveen S, Islam MS, Mikolon A, et al. Anthrax outbreaks in Bangladesh, 2009-2010. Am J Trop Med Hyg. 2012;86:703–10. https://doi.org/10.4269/ajtmh.2012.11-0234
23. World Health Organization. Anthrax: questions and answers. 2019 [cited 2019 July 19]. http://www.euro.who.int/en/health-topics/disease-prevention/food-safety/data-and-statistics/anthrax-questions-and-answers
24. Kolton CB, Marston CK, Stoddard RA, Cossaboom C, Salzer JS, Kozel TR, et al. Detection of *Bacillus anthracis* in animal tissues using InBios active anthrax detect rapid test lateral flow immunoassay. Lett Appl Microbiol. 2019;68:480–4. https://doi.org/10.1111/lam.13134

Address for correspondence: Esther Kisaakye, Uganda Public Health Fellowship Program, Ministry of Health, 4th Floor, Lourdel Towers, Plot 1, Lourdel Rd, Nakasero, P.O. Box 7072, Kampala, Uganda; email: estherkisaakye@musph.ac.ug

Mycoplasma bovis Infections in Free-Ranging Pronghorn, Wyoming, USA

Jennifer L. Malmberg, Donal O'Toole, Terry Creekmore, Erika Peckham, Hally Killion, Madison Vance, Rebecca Ashley, Marguerite Johnson, Christopher Anderson, Marce Vasquez, Douglas Sandidge, Jim Mildenberger, Noah Hull, Dan Bradway, Todd Cornish, Karen B. Register, Kerry S. Sondgeroth

Mycoplasma bovis is 1 of several bacterial pathogens associated with pneumonia in cattle. Its role in pneumonia of free-ranging ungulates has not been established. Over a 3-month period in early 2019, ≈60 free-ranging pronghorn with signs of respiratory disease died in northeast Wyoming, USA. A consistent finding in submitted carcasses was severe fibrinosuppurative pleuropneumonia and detection of *M. bovis* by PCR and immunohistochemical analysis. Multilocus sequence typing of isolates from 4 animals revealed that all have a deletion in 1 of the target genes, *adh-1*. A retrospective survey by PCR and immunohistochemical analysis of paraffin-embedded lung from 20 pronghorn that died with and without pneumonia during 2007–2018 yielded negative results. These findings indicate that a distinct strain of *M. bovis* was associated with fatal pneumonia in this group of pronghorn.

The bacterium *Mycoplasma bovis* is an economically important pathogen of cattle that contributes to the multifactorial bovine respiratory disease complex. In addition to causing respiratory disease, this bacterium can cause polyarthritis, mastitis, otitis media, and a chronic pneumonia–polyarthritis syndrome, impacting beef and dairy cattle worldwide (*1*). Despite increased recognition of its role in economic loss in the cattle industry, *M. bovis* remains a clinical challenge because of a common carrier state in clinically healthy animals, variable disease expression, intermittent shedding, and the lack of rapid accurate diagnostic assays (*1*,*2*).

Clinical disease is not considered necessary to maintain *M. bovis* in populations, and *M. bovis* is commonly detected in asymptomatic adult feedlot cattle (*2*). Although the upper respiratory tract mucosa is a primary site for *M. bovis* colonization, presence of the bacterium in the lung is variable in occurrence and clinical manifestation. In 1 study, *M. bovis* was detected in 46% of cattle with normal lungs, 82% of cattle with acute fibrinous pneumonia, and 98% of cattle with chronic pneumonia (*3*). Manifestation of *M. bovis*–associated respiratory disease is particularly common in the wake of stress (e.g., from transportation, comingling, feedlot entry, and harsh temperatures or conditions).

In the early 2000s, *M. bovis* caused several high-mortality (case-fatality rate 45%) epizootics in bison (*Bison bison*) in North America (*4*). These events raised concern about emergent virulent strains, and research began to characterize isolates from different host species (*5*). An important difference between outbreaks of mycoplasmosis in bison and cattle is that, in the former, few or no co-infecting bacterial or viral pathogens are consistently detected (*4*,*6*–*8*). Although *M. bovis* virulence factors are poorly defined, evasion of immune response is implicated in maintaining chronic infection (*9*). One study found that that up to 79% of bison herds in western Canada have ≥1 *M. bovis*–seropositive animal and that 8 of 11 herds with no history of *M. bovis* disease had seropositive animals (*10*). These findings suggest that host response to *M. bovis* varies; some exposed bison become subclinical carriers and might also

Author affiliations: Wyoming State Veterinary Laboratory, Laramie, Wyoming, USA (J.L. Malmberg, D. O'Toole, H. Killion, M. Vance, R. Ashley, M. Vasquez, T. Cornish, K.S. Sondgeroth); University of Wyoming Department of Veterinary Sciences, Laramie (J.L. Malmberg, D. O'Toole, M. Johnson, C. Anderson, D. Sandidge, T. Cornish, K.S. Sondgeroth); Wyoming Game and Fish Department, Laramie (T. Creekmore); Wyoming Game and Fish Department, Gillette, Wyoming, USA (E. Peckham); Wyoming Public Health Laboratories, Cheyenne, Wyoming, USA (J. Mildenberger, N. Hull); Washington Animal Disease Diagnostic Laboratory, Pullman, Washington, USA (D. Bradway); US Department of Agriculture National Animal Disease Center, Ames, Iowa, USA (K.B. Register)

DOI: https://doi.org/10.3201/eid2612.191375

indicate a strain variation in *M. bovis* that influences the severity of disease.

Despite its recent recognition in bison, documented cases of *M. bovis* in free-ranging ruminants are rare. *M. bovis* was reported in farmed white-tailed deer (*Odocoileus virginianus*) (*11*) and observed in free-ranging mule deer (*Odocoileus hemionus*) (P. Wolff, Wildlife Disease Association, pers. comm., August 2019). Pronghorn (*Antilocapra americana*) are the only extant member of the family *Antilocapridae* and are native to expansive ranges in the western United States, southern Canada, and northern Mexico (*12*). Approximately 0.5–1.0 million pronghorn exist in North America (*12*). Herds are commonly sympatric with range cattle and ranched bison. In this article, we document *M. bovis* as the cause of a high-mortality outbreak of respiratory disease in a new free-ranging host, using a widely employed multilocus sequence typing (MLST) scheme to characterize associated lesions and the allelic profile of *M. bovis*.

Materials and Methods

Diagnostic Workup

Carcasses, tissue samples, or both were obtained from the site of the outbreak comprising a ≈20-km^2 area northeast of Gillette, Wyoming, USA (Figure 1). The samples were submitted on behalf of the Wyoming Game and Fish Department (WGFD) for a diagnostic workup. For 2 of the 9 cases, an entire carcass was submitted and a detailed postmortem examination was performed by a board-certified pathologist, including histopathologic examination of tissues. For 7 of the 9 cases, limited tissue sampling was performed during field autopsy by WGFD. In all 9 cases, fresh or fresh frozen lung tissue was received, and *M. bovis* was detected by PCR. Bacteriology (aerobic and anaerobic culture) was performed on fresh or fresh frozen lung from 5 of 9 cases; 4 cases had advanced tissue autolysis and were not cultured. No consistent bacterial co-infections were detected across multiple cases (Table 1). Because *Mannheimia* spp. and *Histophilus* spp. were detected by culture in 1 case, we performed PCR for both agents on all 9 cases, yielding negative results. Molecular virology was performed on fresh or fresh frozen lung from all 9 cases; PCR assays included bovine herpesvirus 1, parainfluenza virus 3, bovine viral diarrhea virus, bovine respiratory syncytial virus, epizootic hemorrhagic disease virus, blue tongue virus, and a cervid adenovirus originally identified in mule deer and occasionally detected in pronghorn (*13*). No viruses were detected in any case. PCR assays were performed according to validated diagnostic protocols at the Wyoming State Veterinary Laboratory (WSVL). Histopathologic and immunohistochemical (IHC) analysis were performed on a total of 5 cases. In all cases, *M. bovis* was detected by IHC analysis. IHC analysis for *Histophilus somni* was also performed on these 5 cases; *H. somni* was not detected.

Histopathology

Tissues collected at autopsy for histopathologic analysis (Appendix, https://wwwnc.cdc.gov/EID/article/26/12/19-1375-App1.pdf) were fixed in 10% buffered formalin and processed conventionally before embedding in paraffin wax. Sections cut at 5 μm were stained with hematoxylin and eosin. IHC analysis of *M. bovis* and *H. somni* was performed on lung tissue derived from the same blocks as used in the hematoxylin and eosin assays (Appendix).

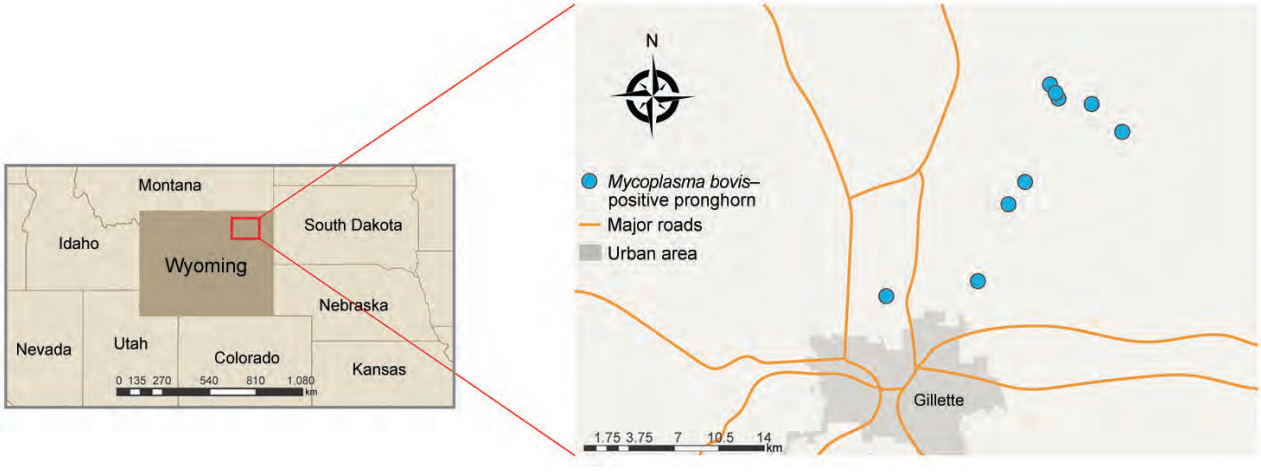

Figure 1. Locations of deaths in free-ranging pronghorn attributable to *Mycoplasma bovis* infection, Wyoming, USA, February–April 2019. Infections were geographically confined to northeast of state (demarcated in inset map).

Table 1. Summary of pronghorn cases associated with pneumonia outbreak, Wyoming, USA, 2019*

Case no.	Age category and sex	Sample type	Histopathologic results	*Mycoplasma bovis* IHC result	*M. bovis* PCR test result	Aerobic culture	*M. bovis* culture
1	Adult male	Lung, kidney, liver, spleen, bone marrow	Exudative pneumonia	Detected	Detected	*Trueperella pyogenes*	Positive
2	Adult female	Lung	Pleuropneumonia with caseous abscesses	Detected	Detected	No growth	Positive
3	Adult female	Whole carcass	Bronchointerstitial pneumonia, fibrinonecrotic and suppurative with fibrinous pleuritis	Detected	Detected	Mixed bacteria	Positive
4	Adult female	Lung, kidney, liver, spleen	Pleuropneumonia with caseonecrotic abscesses	Detected	Detected	Mixed bacteria	Positive
9	Yearling male	Whole carcass	Bronchointerstitial pneumonia, fibrionone crotic and suppurative with fibrinous pleuritis, caseonecrotic abscesses, lymphocytic cuffing	Detected	Detected	*Mannheimia spp., Histophilus spp.*	Positive
5	Adult female	Lung	NE	NA	Detected	NA	Positive
6	Adult female	Lung, kidney, liver, spleen	NE	NA	Detected	NA	Positive
7	Adult female	Lung	NE	NA	Detected	NA	Positive
8	Adult female	Lung	NE	NA	Detected	NA	Positive

*IHC, immunohistochemical; NA, not applicable; NE, not examined.

Mycoplasma Culture

Approximately 20 mg of lung tissue was placed in a mycoplasma enrichment broth (Hardy Diagnostics' Mycoplasma Broth; Hardy Diagnostics, https://hardydiagnostics.com) and incubated with a loose lid at 37°C in 10% CO_2 for 72 h. Subsequently, 100 µL of broth was inoculated onto a commercial *Mycoplasma* spp. medium (Hardy Diagnostics' Mycoplasma Agar with Cefoperazone) and spread evenly over the entire plate with a sterile swab. Plates were incubated at 37°C in 10% CO_2 for 72–240 h, depending on appearance of colony growth. Colonies from each isolate were analyzed by matrix-assisted laser desorption/ionization-time of flight mass spectrometry (Bruker's Biotyper, https://www.bruker.com) according to the manufacturer's instructions for identification. Additional colonies were used for whole-genome sequencing.

Sequencing

16S

After DNA extraction from fresh lung tissue, a portion of the 16S ribosomal RNA gene was amplified by PCR using universal *Mycoplasma* primers (*13*) at the Washington Animal Disease Diagnostic Laboratory. PCR amplicons were directly sequenced, and a GenBank BLAST search was performed (https://blast.ncbi.nlm.nih.gov) on consensus sequence from 2 forward and 2 reverse high-quality reads. This initial confirmation was performed on the first sample only, and isolates from subsequent samples were confirmed by whole-genome sequencing.

Whole-Genome Sequencing

Short-read sequencing technology was used on extractions of pure *M. bovis* isolates. Postsequencing statistics were evaluated by using FastQC (*14*) (Appendix).

Polymerase chain reaction

Diagnostic *M. bovis* PCR

DNA was extracted from fresh lung tissue and PCR was performed targeting the *M. bovis* 16S ribosomal RNA gene (Appendix). Confirmation of diagnosis from case 1 (Table 1) by PCR targeting of the *uvrC* gene was performed at the Washington Animal Disease Diagnostic Laboratory (*15*).

Survey of Formalin-Fixed Paraffin-Embedded Archival Lung Tissue

DNA was extracted from formalin-fixed, paraffin embedded lung tissue curls cut at a thickness of 20 µm. In brief, 1–2 curls per sample were dewaxed by using xylene and ethanol according to the DNeasy Blood and Tissue kit's recommended protocol (QIAGEN, https://www.qiagen.com). The tissue extraction proceeded overnight at 56°C, according to manufacturer

instructions. Cases selected for PCR were based on the availability of lung tissue from pronghorn in archived wax blocks, which are retained for 15 years because of limited storage space. A total of 20 cases (13 in pronghorn with previously diagnosed pneumonia) were identified; all cases originated from Wyoming (Table 2). After DNA extraction, PCR was performed as described previously for the diagnostic *M. bovis* PCR assay.

Diagnostic *M. ovipneumoniae* PCR

A 2 × 2 cm section of fresh lung tissue was placed into 2 mL modified tryptic soy broth and homogenized for 120 seconds. The homogenous solution was transferred to a snap cap tube and incubated at 37°C with 10% CO_2 for 48 h. After centrifugation of 1 mL, the pellet was resuspended and used in a PCR reaction as previously described (*16*).

adh-1 PCR

DNA was extracted from the *Mycoplasma* broth of each sample stored at −80°C by using the QIAGEN DNeasy Blood and Tissue Kit fluid protocol. In brief, 200 µL was extracted following manufacturer instructions. Forward and reverse primers targeting the *adh-1* gene (0.5 µmol/L of each) were used in a 50 µL reaction containing 22.5 µL GoTaq green master mix (Promega, https://www.promega.com), 1.5 µL of 50 nM $MgCl_2$, and nuclease-free water (*5*).

MLST Analysis

Paired fastq reads of ≈250 bp were analyzed as follows: trimming of indexes, primers, low quality (phred <20), and short reads (<50 bp) using Cutadapt (*17*); mapping of trimmed reads to the genome of *M. bovis* international reference strain PG45 (GenBank accession no. NC_014760) using Bowtie2 (*18*); conversion of .sam files to .bam files using Samtools (*19*); and viewing of sorted .bam files in Geneious Prime 2019.1.3 (https://www.geneious.com). Consensus sequences were generated from mapped reads by using the highest quality parameter in Geneious Prime as a threshold. "N" was assigned to sites with coverage <3 to represent missing data. Consensus sequences were trimmed to loci employed in the MLST scheme described by Register et al. (*5*) and concatenated in frame. Concatenated sequences were compared for 4 *M. bovis* isolates recovered from the lung samples of 4 different pronghorn across the following MLST genes: alcohol dehydrogenase (*adh-1*), glutamate tRNA ligase (*gltX*), glycerol-3-phosphate dehydrogenase (*gpsA*), DNA gyrase subunit B (*gyrB*), phosphate acetyltransferase-2 (*pta-2*), thymidine kinase (*tdk*), and transketolase (*tkt*) (*5*). Isolates derived in our study were compared with those from the University of Oxford *Mycoplasma bovis* MLST website (https://pubmlst.org/mbovis) (*20*). An aligned fasta file was obtained for all publicly available isolates missing the *adh-1* gene (i.e., nontypeable isolates). The representative sequence from the 4 identical pronghorn isolates was aligned to the fasta file comprising all nontypeable isolates by using Muscle (*21*), and model selection was performed in MEGA X (*22*). Sequence alignments were subjected to maximum-likelihood phylogenetic analyses under the Hasegawa–Kishono–Yano substitution model using PhyML (*23*) with 10,000 bootstrap replicates for support.

Table 2. Pronghorn with and without pneumonia, Wyoming, USA, 2007–2019

Case no.	Year	Pneumonia	Other diagnosis	Geographic area
1	2007	Yes	None	Southeast
2	2014	Yes	None	Southeast
3	2014	Yes	*Trueperella pyogenes*	South central
4	2015	Yes	*Corynebacterium spp.*	South central
5	2015	Yes	*T. pyogenes*	Central
6	2016	Yes	*T. pyogenes*	West central
7	2016	Yes	None	Northeast
8	2016	Yes	*Protostrongylus spp.* lungworms, *Dermacentor spp.* ticks, *Haemonchus contortus* abomasal worms	Southeast
9	2016	Yes	*Dermatophilus congolensis*	Southeast
10	2017	Yes	*T. pyogenes*	Central
11	2017	Yes	*Dictyocaulus spp.*	Southeast
12	2018	Yes	Epizootic hemorrhagic disease virus	East central
13	2018	Yes	*T. pyogenes*	Central
14	2018	No	Blackleg from *Clostridium chauvoei*	Southeast
15	2018	No	None	West central
16	2018	No	Bluetongue virus	Southeast
17	2018	No	Peritonitis	Southeast
18	2018	No	None	Southeast
19	2019	No	Foot defect	West central
20	2019	No	Trauma from hail	Southeast

Results

Disease Outbreak

At least 60 pronghorn died during February–April 2019 within a total area of ≈13 km^2. WGFD received initial reports of ≈30 carcasses in early February 2019. An additional 20 pronghorn deaths were identified within 8 km of the site of initial reports within 1 month, and the affected area expanded as wintering herds began to disperse with warmer weather. In March, a herd of ≈10 pronghorn moved to the same area and began dying within 2 weeks. Landowners reported that affected pronghorn appeared lethargic. Such animals were typically dead within 24 hours. Because of logistics of finding fresh carcasses in remote areas on private land during 2 major winter storms, only a fraction of the dead pronghorn could be sampled. Two carcasses were obtained for autopsy, and tissues were obtained from an additional 3 cases for histopathologic examination and PCR. Samples were collected from 4 additional animals for PCR only. The extent of the die-off could not be estimated until improved weather conditions allowed WGFD biologists to conduct ground and aerial surveys. Bison, cattle, or other free-ranging ungulates (i.e., deer, elk, and moose) deaths associated with pneumonia were not reported in the area during this outbreak. The closest captive bison herd was located ≈64 km south of the outbreak site. Although pronghorn deaths occur in winter because of starvation, predation, and vehicular collision, 60 deaths in a small area is unusual.

Diagnosis and Characterization of Lesions

Gross lesions were characterized by severe, regionally extensive to diffuse, bilateral fibrinous pleuropneumonia affecting an estimated 50%–100% of lung parenchyma (Figure 2). Histopathologic examination revealed fibrinosuppurative pneumonia with caseonecrotic foci centered on bronchi and bronchioles. Caseonecrotic foci were characterized by central granular eosinophilic material and necrotic leukocytes surrounded by degenerate and intact neutrophils. Some foci were partly mineralized (Figure 3). Lesions were interpreted as acute to subacute, because features of chronic infection, such as extensive fibrosis, were absent (*24*). In all 5 cases for which histopathologic examination was performed, pulmonary lesions were strongly immunoreactive for *M. bovis* antigen, with characteristically strong staining at the margins of necrotic foci as described in affected cattle and bison (*3*) (Figure 4). The pronghorn in case 9 (Table 1) had pulmonary abscesses up to 1 cm diameter characterized by coagulative necrosis surrounded by a thin band of fibrosis. Features characteristic of mannheimiosis, histophilosis, or both, such as neutrophils with oat cell morphology, were absent. The pronghorn in case 9 also had fibrinosuppurative synovitis and conjunctivitis. *M. bovis* antigen was detected in the conjunctiva by IHC analysis. In addition, acute centrilobular hepatic necrosis was identified in case 9. We attributed this finding to hypoxia secondary to severe pneumonia.

Lung samples from the 9 pronghorn cases were positive for *M. bovis* by culture and PCR (Table 1). 16S sequencing revealed that the isolate from case 1 most closely matched that of *M. bovis* (100% sequence identity [553/553 bp]; GenBank no. KX462388). The next closest match was 99% identity (549/553 bp) to *M. agalactiae* (GenBank no. AF332750). *M. ovipneumoniae* PCR was performed on samples of lung; all results were negative (data not shown).

Aside from the consistent detection of *M. bovis*, aerobic culture results were inconsistent. The pronghorn in case 1 contained *Trueperella pyogenes*, the pronghorn in case 9 contained both *Mannheimia* spp. and *Histophilus* spp., and the pronghorn in cases 3 and 4 had a mixture of bacterial species not typically associated with pneumonia interpreted as incidental (Table 1). The pronghorn in cases 2 and 9 had a mild lungworm infection, including nematode larvae and eggs histologically consistent with *Dictyocaulus* spp. parasitic infection.

Retrospective Study

We performed a retrospective survey for *M. bovis* on 20 archived WSVL cases of pronghorn deaths with and without pneumonia (Table 2); embedded lesioned lung from the animals in 2 of the 9 positive cases among the 2019 pronghorn deaths were used as

Figure 2. Free-ranging pronghorn infected with *Mycoplasma bovis* with severe fibrinous pleuropneumonia, Wyoming, USA, February–April 2019. Open thoracic cavity with ribs reflected reveals abundant fibrin on the visceral pleura (arrowhead) and consolidated lungs (asterisk).

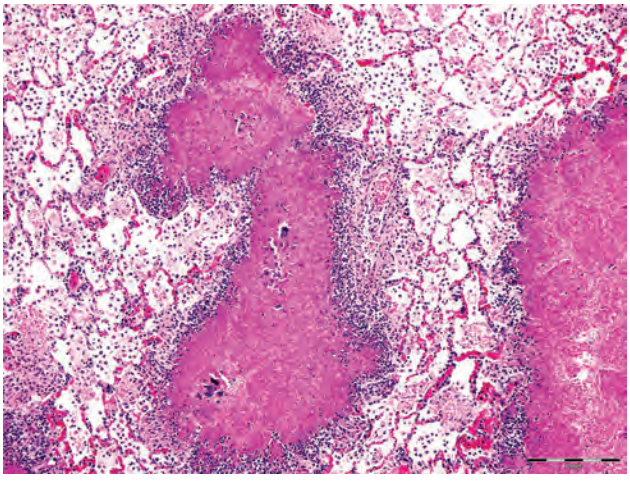

Figure 3. Histologic lung lesions in free-ranging pronghorn, characterized by caseonecrotic foci centered on residual bronchioles, Wyoming, USA, February–April 2019. Alveolar fibrin exudation and suppurative to mixed inflammation throughout. Scale bar indicates 1 mm.

positive controls. All archived pronghorn lung tissues were negative for *M. bovis* by PCR and IHC analysis, and none had lesions suggestive of mycoplasmosis.

MLST and Phylogenetics

Genome sequencing of the 4 *M. bovis* isolates recovered from the pronghorn carcasses was performed at the Wyoming Public Health Laboratory. All isolates from pronghorn had 100% sequence identity at loci used for MLST (*5*). All assemblies contained an apparent deletion of 1 of the 7 MLST target genes, *adh-1* (*5*). Sequences for the 6 remaining loci are available through GenBank (accession nos. MT782331–6). To confirm the *adh-1* deletion, DNA from *M. bovis* pronghorn isolates was amplified by PCR using the *adh-1* primers specified for MLST as described previously (*5*). DNA extracted from a cattle isolate of *M. bovis* was strongly positive, whereas DNA from the pronghorn isolates produced no visible band upon gel electrophoresis.

Deletion of *adh-1* has been identified in *M. bovis* isolates derived from cattle (*25*; https://pubmlst.org/mbovis; K.B. Register, unpub. data). Phylogenetic analysis of these MLST-nontypeable isolates based on DNA sequences of the other 6 MLST targets revealed that the pronghorn isolates we evaluated are divergent from all others typed to date but are most similar to a group of isolates obtained from cattle in the United States since 2011 (Figure 5).

Discussion

M. bovis is uncommon in free-ranging ungulates. Accounts are limited to cases in farmed white-tailed deer (*11*), and free-ranging mule deer (*26*; P. Wolff, Wildlife Disease Association, pers. comm., August 2019). Lesions in lung were compatible with the lesions attributable to *M. bovis* in cattle and bison (*2*,*6*). The distribution of *M. bovis* antigen in IHC preparations of caseonecrotic foci is typical of fatal mycoplasmosis in cattle (*2*,*3*).

To determine whether *M. bovis* had been previously overlooked in Wyoming pronghorn, we queried the WSVL diagnostic database. We identified 20 cases from different geographic regions of Wyoming that occurred during 2007–2019. This group included 13 cases in pronghorn with previously diagnosed pneumonia and 7 without (Table 2). Although the *M. bovis* PCR assay used at WSVL has not been validated for formalin-fixed, wax-embedded tissue, positive dewaxed lung samples from pronghorn in the 2019 cases were used as a control. On the basis of these 20 samples, no *M. bovis* infections in pronghorn before 2019 was evident.

Draft genome sequences were obtained for isolates of *M. bovis* from 4 pronghorn in the 2019 group. Compared with MLST data available on >700 isolates, only 9 complete genome assemblies from other host species, such as goat, bison, or cattle, were available. Thus, we determined sequence type by extracting regions of 7 genes used in MLST typing (*5*). The 4 isolates were identical across these loci and contained a deletion encompassing the *adh-1* gene. This deletion was confirmed by using *adh-1* specific primers as described previously (*5*). These isolates were compared with others with a deletion at the *adh-1* locus (i.e., nontypeable isolates). Although the *adh-1* gene deletion has been identified in *M. bovis* from bison and mule deer (K.B.

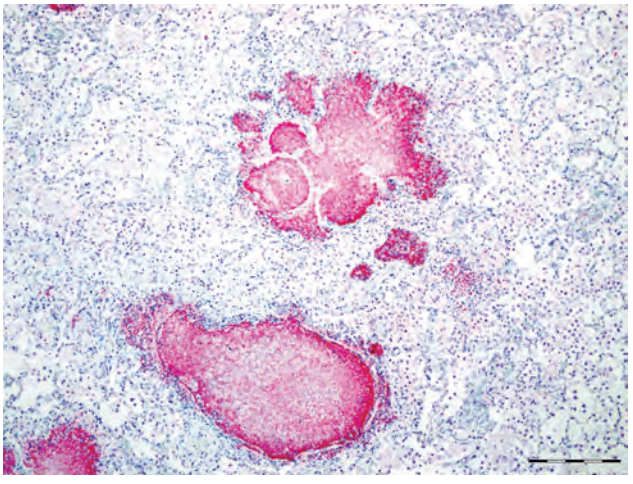

Figure 4. Caseonecrotic lung lesions in free-ranging pronghorn found to be strongly immunopositive for *Mycoplasma bovis* antigen by immunohistochemical analysis, Wyoming, USA, February–April 2019. Positive staining indicated by fast red coloring has strong intensity and specificity for lesions centered on bronchioles. Scale bar indicates 1 mm.

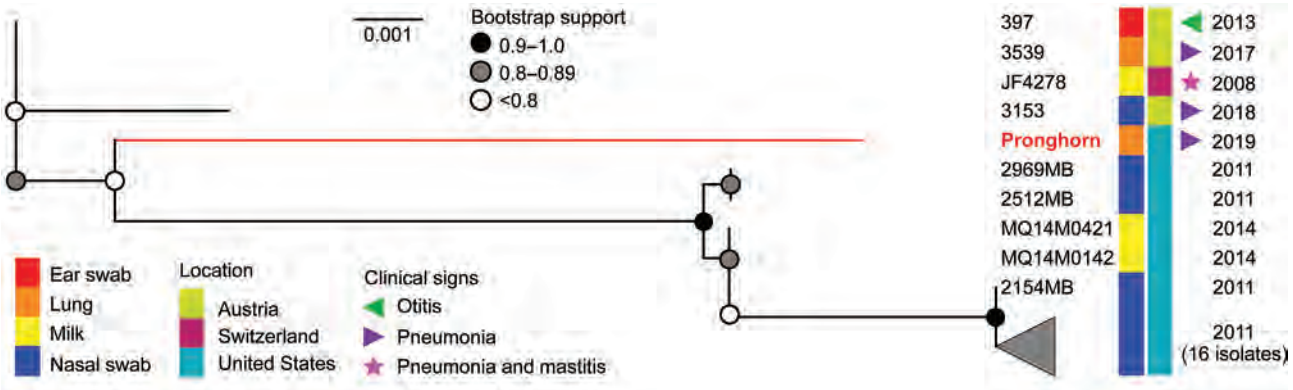

Figure 5. Phylogeny of *Mycoplasma bovis* isolates from free-ranging pronghorn (red branch), Wyoming, USA, February–April 2019. Pronghorn were found to be divergent from all bovine isolates with a deletion of *adh-1* gene but are most similar to those recovered from cattle in the United States. This unrooted maximum-likelihood tree (10,000 bootstrap replicates) comprises all available nontypeable isolates and is based on 6 of 7 sequence typing loci. The health status of cattle sampled during 2011–2014 is unknown, and the absence of reported clinical signs does not necessarily equate to absence of disease. Scale bar indicates substitutions per site.

Register, unpub. data), only sequences from bovine isolates are currently available in the *Mycoplasma bovis* pubMLST database (https://pubmlst.org/mbovis). The isolates from pronghorn are divergent from other published isolates but are most similar to those from US cattle compared with bovine isolates from Austria or Switzerland (Figure 5).

Although the *adh-1* deletion has not yet been thoroughly characterized, the earliest identification of this variant is from 2008. The deletion might be relatively recent and might be associated with expansion of *M. bovis* host range or emergence in new species. Additional research is needed to investigate the possible association between the *adh-1* gene deletion and the recent appearance of *M. bovis* in pronghorn. It will be of interest to investigate the entire genome for other whole-gene deletions or insertions and to correlate whether genomic changes are associated with certain hosts, levels of virulence, or both.

Surveillance of pronghorn samples submitted to WSVL has not identified *M. bovis* in other areas of the state at this time. No additional cases have been diagnosed in northeast Wyoming since April 2019. As part of a surveillance effort, we have recently performed *M. bovis* PCR on lung tissue DNA of any ungulate submitted to WSVL. We have found no evidence of chronically infected pronghorn or other wildlife reservoirs of this bacterium. The host species of origin in this outbreak is unknown. Given the frequency of *M. bovis* in asymptomatic cattle and bison and its rarity of detection in free-ranging ungulates, transmission to pronghorn from a livestock reservoir seems likely.

Our findings strongly implicate *M. bovis* as a primary pathogen in pronghorn, resulting in fatal pneumonia in absence of other respiratory pathogens with changes comparable to those in bison with fatal mycoplasmosis. *M. bovis* as a primary pathogen in bison is in contrast to *M. bovis* in adult cattle, where the bacterium tends to occur most commonly as 1 component of chronic, polymicrobial respiratory disease (*24*,*27*). The pronghorn *M. bovis* infection is more analogous to mycoplasmosis in bison, where it is known to be a primary cause of pneumonia, arthritis, pharyngitis, and reproductive disorders (*6*–*8*).

Our findings document *M. bovis* infection in pronghorn and highlight the possible health implications for other wildlife populations and the potential risk for transmission at the wildlife–livestock interface. Furthermore, we document *M. bovis* genetic variation in association with virulent disease in pronghorn, supporting hypotheses that *M. bovis* might be expanding in host range and in disease expression. We therefore recommend that *M. bovis* be considered as a differential diagnosis for pneumonia in wildlife, particularly in outbreak scenarios. Traditionally, pronghorn are not considered a major source of disease threats to either cattle or bison and are therefore widely tolerated on commercial operations. Additional studies are needed to establish transmission potential and direction, which will elucidate the importance of *M. bovis* at the wildlife–livestock interface.

About the Author

Dr. Malmberg is a veterinary pathologist at the Wyoming State Veterinary Laboratory and an assistant professor at the University of Wyoming in Laramie. Her research interests include transmission of naturally occurring diseases at wildlife–livestock and urban–rural interfaces.

References

1. Pfützner H, Sachse K. *Mycoplasma bovis* as an agent of mastitis, pneumonia, arthritis and genital disorders in cattle. Rev Sci Tech. 1996;15:1477–94. https://doi.org/10.20506/rst.15.4.987
2. Jeff L. Caswell, Archambault M. *Mycoplasma bovis* pneumonia in cattle. Anim Health Res Rev. 2008;8:161–86.
3. Gagea MI, Bateman KG, Shanahan RA, van Dreumel T, McEwen BJ, Carman S, et al. Naturally occurring *Mycoplasma bovis*–associated pneumonia and polyarthritis in feedlot beef calves. J Vet Diagn Invest. 2006;18:29–40. https://doi.org/10.1177/104063870601800105
4. Kyathanahalli S, Janardhan MH. Neil Dyer, Richard D. Oberst, Brad M. DeBey. *Mycoplasma bovis* outbreak in a herd of North American bison (*Bison bison*). J Vet Diagn Invest. 2010; 22:797–801. https://doi.org/10.1177/104063871002200528
5. Karen B. Register, Luke Thole, Ricardo F. Rosenbush, Minion FC. Multilocus sequence typing of *Mycoplasma bovis* reveals host-specific genotypes in cattle versus bison. Vet Micro. 2015;175:92–8. https://doi.org/10.1016/j.vetmic.2014.11.002
6. Dyer N, Hansen-Lardy L, Krogh D, Schaan L, Schamber E. An outbreak of chronic pneumonia and polyarthritis syndrome caused by *Mycoplasma bovis* in feedlot bison (*Bison bison*). J Vet Diagn Invest. 2008;20:369–71. https://doi.org/10.1177/104063870802000321
7. Dyer N, Register KB, Miskimins D, Newell T. Necrotic pharyngitis associated with *Mycoplasma bovis* infections in American bison (*Bison bison*). J Vet Diagn Invest. 2013;25: 301–3. https://doi.org/10.1177/1040638713478815
8. Register KB, Woodbury MR, Davies JL, Trujillo JD, Perez-Casal J, Burrage PH, et al. Systemic mycoplasmosis with dystocia and abortion in a North American bison (*Bison bison*) herd. J Vet Diagn Invest. 2013;25:541–5. https://doi.org/10.1177/1040638713495029
9. Boothby JT, Jasper DE, Zinkl JG, Thomas CB, Dellinger JD. Prevalence of mycoplasmas and immune responses to *Mycoplasma bovis* in feedlot calves. Am J Vet Res. 1983;44:831–8.
10. Bras AL, Suleman M, Woodbury M, Register K, Barkema HW, Perez-Casal J, et al. A serologic survey of *Mycoplasma* spp. in farmed bison (*Bison bison*) herds in western Canada. J Vet Diagn Invest. 2017;29:513–21. https://doi.org/10.1177/1040638717710057
11. Dyer NW, Krogh DF, Schaan LP. Pulmonary mycoplasmosis in farmed white-tailed deer (*Odocoileus virginianus*). J Wildl Dis. 2004;40:366–70. https://doi.org/10.7589/0090-3558-40.2.366
12. International Union for Conservation of Nature. IUCN red list of threatened species 2016: e.T1677A115056938. IUCN SSC Antelope Specialist Group 2016 *Antilocapra americana* [cited 2020 Jul 19]. http://dx.doi.org/10.2305/IUCN.UK.2016-3.RLTS.T1677A50181848.en
13. Kong F, James G, Gordon S, Zelynski A, Gilbert GL. Species-specific PCR for identification of common contaminant mollicutes in cell culture. Appl Environ Microbiol. 2001;67:3195–200. https://doi.org/10.1128/AEM.67.7.3195-3200.2001
14. Andrews S. FastQC: a quality control tool for high throughput sequence data. 2010 [cited 2019 Aug 20]. http://www.bioinformatics.babraham.ac.uk/projects/fastqc
15. Naikare H, Bruno D, Mahapatra D, Reinisch A, Raleigh R, Sprowls R. Development and evaluation of a novel Taqman real-time PCR assay for rapid detection of *Mycoplasma bovis*: comparison of assay performance with a conventional PCR assay and another Taqman real-time PCR assay. Vet Sci. 2015;2:32–42. https://doi.org/10.3390/vetsci2010032
16. Ziegler JC, Lahmers KK, Barrington GM, Parish SM, Kilzer K, Baker K, et al. Safety and immunogenicity of a *Mycoplasma ovipneumoniae* bacterin for domestic sheep (*Ovis aries*). PLoS One. 2014;9:e95698. https://doi.org/10.1371/journal.pone.0095698
17. Martin M. Cutadapt removes adapter sequences from high-throughput sequencing reads. EMBnet J. 2011;17:10–2. https://doi.org/10.14806/ej.17.1.200
18. Langmead B, Salzberg SL. Fast gapped-read alignment with Bowtie 2. Nat Methods. 2012;9:357–9. https://doi.org/10.1038/nmeth.1923
19. Li H, Handsaker B, Wysoker A, Fennell T, Ruan J, Homer N, et al.; 1000 Genome Project Data Processing Subgroup. The sequence alignment/map format and SAMtools. Bioinformatics. 2009;25:2078–9. https://doi.org/10.1093/bioinformatics/btp352
20. Keith A. Jolley, James E. Bray, Maiden MCJ. Open-access bacterial population genomics: BIGSdb software, the PubMLST.org website and their applications. Wellcome Open Res. 2018;3:124.
21. Edgar RC. MUSCLE: multiple sequence alignment with high accuracy and high throughput. Nucleic Acids Res. 2004;32:1792–7. https://doi.org/10.1093/nar/gkh340
22. Kumar S, Stecher G, Li M, Knyaz C, Tamura K. MEGA X: Molecular Evolutionary Genetics Analysis across computing platforms. Mol Biol Evol. 2018;35:1547–9. https://doi.org/10.1093/molbev/msy096
23. Guindon S, Dufayard J-F, Lefort V, Anisimova M, Hordijk W, Gascuel O. New algorithms and methods to estimate maximum-likelihood phylogenies: assessing the performance of PhyML 3.0. Syst Biol. 2010;59:307–21. https://doi.org/10.1093/sysbio/syq010
24. Maunsell FP, Woolums AR, Francoz D, Rosenbusch RF, Step DL, Wilson DJ, et al. *Mycoplasma bovis* infections in cattle. J Vet Intern Med. 2011;25:772–83. https://doi.org/10.1111/j.1939-1676.2011.0750.x
25. Josi C, Bürki S, Stojiljkovic A, Wellnitz O, Stoffel MH, Pilo P. Bovine epithelial in vitro infection models for *Mycoplasma bovis*. Front Cell Infect Microbiol. 2018;8:329. https://doi.org/10.3389/fcimb.2018.00329
26. Register KB, Jelinski MD, Waldner M, Boatwright WD, Anderson TK, Hunter DL, et al. Comparison of multilocus sequence types found among North American isolates of *Mycoplasma bovis* from cattle, bison, and deer, 2007-2017. J Vet Diagn Invest. 2019;31:899–904. https://doi.org/10.1177/1040638719874848
27. Maunsell FP, Donovan GA. *Mycoplasma bovis* infections in young calves. Vet Clin North Am Food Anim Pract. 2009;25:139–77, vii. https://doi.org/10.1016/j.cvfa.2008.10.011

Address for correspondence: Kerry Sondgeroth, Wyoming State Veterinary Laboratory, 1174 Snowy Range Rd, Laramie, WY 82070, USA; email ksondger@uwyo.edu

Control and Prevention of Anthrax, Texas, USA, 2019

Tom Sidwa, Johanna S. Salzer, Rita Traxler, Erin Swaney, Marcus L. Sims, Pam Bradshaw, Briana J. O'Sullivan, Kathy Parker, Kenneth A. Waldrup, William A. Bower, Kate Hendricks

The zoonotic disease anthrax is endemic to most continents. It is a disease of herbivores that incidentally infects humans through contact with animals that are ill or have died from anthrax or through contact with *Bacillus anthracis*–contaminated byproducts. In the United States, human risk is primarily associated with handling carcasses of hoofstock that have died of anthrax; the primary risk for herbivores is ingestion of *B. anthracis* spores, which can persist in suitable alkaline soils in a corridor from Texas through Montana. The last known naturally occurring human case of cutaneous anthrax associated with livestock exposure in the United States was reported from South Dakota in 2002. Texas experienced an increase of animal cases in 2019 and consequently higher than usual human risk. We describe the animal outbreak that occurred in southwest Texas beginning in June 2019 and an associated human case. Primary prevention in humans is achieved through control of animal anthrax.

The zoonotic disease anthrax, caused by the bacterium *Bacillus anthracis*, has been known to humankind for thousands of years and is endemic to most continents (*1*–*3*). It is a naturally occurring disease of herbivores that incidentally infects humans through contact with animals that are ill or have died from anthrax or through contact with *B. anthracis*–contaminated byproducts such as meat, hides, hair, and wool (*4*). Transmission routes include cutaneous, ingestion, inhalation, and injection; cutaneous accounts for most (95%) cases worldwide (*2*,*4*). In the United States, human risk is primarily associated with handling carcasses of hoofstock that have died of anthrax; the primary risk for herbivores is ingestion of *B. anthracis* spores that can persist in suitable alkaline soils in a corridor from Texas through Colorado, the Dakotas, and Montana (*5*–*7*).

The 2 state agencies responsible for anthrax surveillance in Texas are the Texas Department of State Health Services (DSHS) and the Texas Animal Health Commission (TAHC). Samples that are culture-positive for *B. anthracis* at veterinary reference laboratories are reported to DSHS and TAHC. Veterinarians treating animals with illnesses compatible with anthrax must also report to DSHS and TAHC. Suspected cases of human anthrax are immediately reportable to DSHS. Samples or isolates from human cases are forwarded for identification to local public health reference laboratories. In Texas, animal anthrax cases are most commonly reported from the triangular area bounded by the towns of Uvalde, Ozona, and Eagle Pass (Figure 1), which includes portions of Crockett, Val Verde, Sutton, Edwards, Kinney, Uvalde, Zavala, and Maverick Counties in southwestern Texas.

During 2000–2018, a total of 63 animal anthrax cases were confirmed by culture of *B. anthracis* in a reference laboratory (annual mean 3.3, range 0–20 cases/year) (T. Sidwa, unpub. data). Because only 1 animal per affected premise usually is reported in a given year, the number of cases is a substantial underrepresention of the total number of affected animals and properties. The last naturally occurring human case of cutaneous anthrax associated with livestock exposure in Texas was reported in 2001 (*8*,*9*).

Texas Outbreak 2019

Animal Cases

Texas Veterinary Medical Diagnostic Laboratory confirmed the first anthrax case of 2019 in an exotic antelope carcass from Uvalde County on June 19. Overall in 2019, the laboratory reported 25 culture-positive animals, including cattle, horses, white-tailed deer,

Author affiliations: Texas Department of State Health Services, Austin, Texas, USA (T. Sidwa, E. Swaney, B.J. O'Sullivan, K. Parker); Centers for Disease Control and Prevention, Atlanta, Georgia, USA (J.S. Salzer, R. Traxler, W.A. Bower, K. Hendricks); Shannon Health System, Ozona, Texas, USA (M.L. Sims); Shannon Medical Center, San Angelo, Texas, USA (P. Bradshaw); Texas Department of State Health Services, El Paso, Texas, USA (K.A. Waldrup)

DOI: https://doi.org/10.3201/eid2612.200470

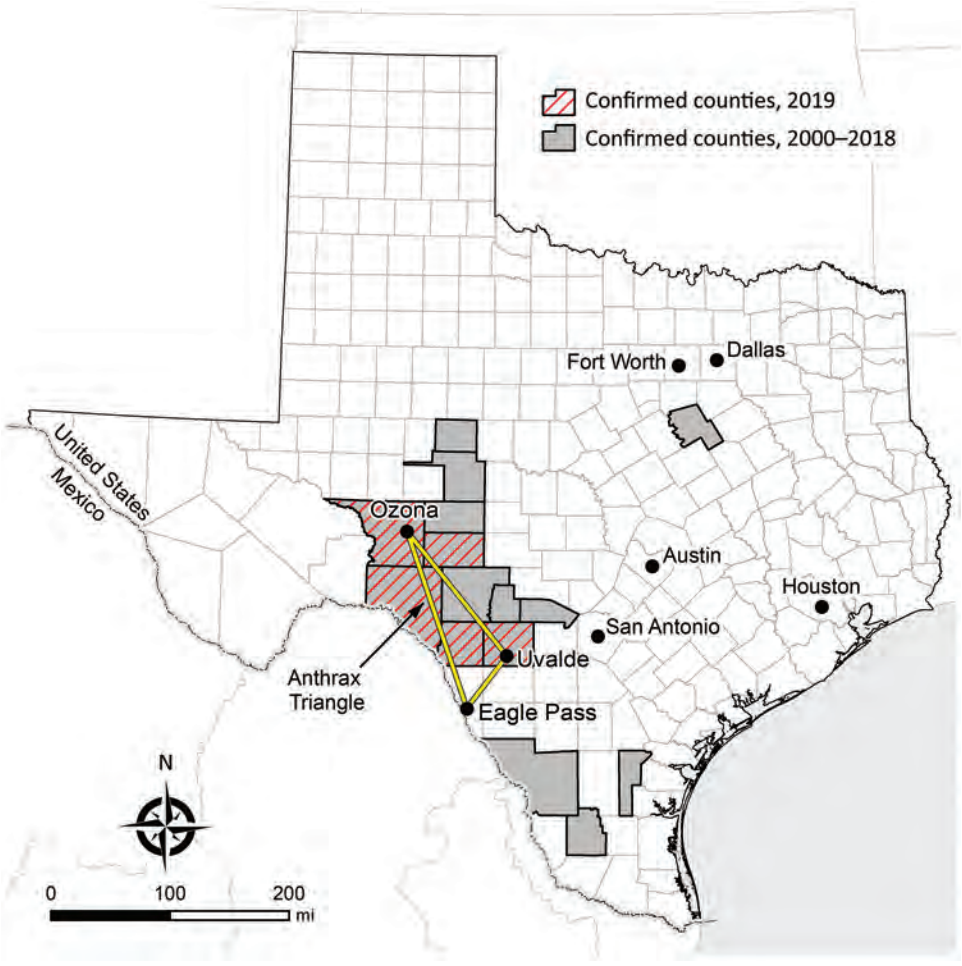

Figure 1. Counties with confirmed animal anthrax cases, Texas, USA, 2000–2019. The location of the "Anthrax Triangle" is indicated.

antelope, and a goat, from Crockett, Kinney, Sutton, Uvalde, and Val Verde counties. The last confirmed animal case was reported on August 21. Unconfirmed numbers reported to DSHS staff suggest that >1,000 animal losses might be attributed to the 2019 outbreak (K. Waldrup, unpub. data).

Implementing control measures (i.e., vaccination and proper carcass disposal) was challenging; thin topsoil over bedrock, vast and inaccessible terrain, and burn bans triggered by hot, dry weather conditions made it difficult for livestock owners and landowners to identify and bury or burn dead animals. Livestock owners can sometimes cover dead animals with tarps if burial or burning is not an option. However, because properties in this area of Texas can be thousands of acres and not particularly navigable, reaching dead animals to cover and protect them from scavengers (that might further distribute *B. anthracis*–contaminated remains) is often not feasible.

Another obstacle to controlling the outbreak was the inability to address the contribution of wildlife to the initiation and perpetuation of disease spread (e.g., lack of a licensed vaccine and impracticality of using physical or chemical restraint to administer vaccine "off label" to wildlife species). In addition, reports of vaccine-associated adverse events among goats and horses (*2*,*10*) made some owners reluctant to vaccinate these species. Among confirmed animal anthrax cases in species for which vaccination is indicated (cattle, goats, horses, sheep, and swine) (*11*), a third are reported to have been vaccinated before illness. Of those, the median number of days from most recent vaccination to specimen collection was 8 days (range 3–82 days) (T. Sidwa, unpub. data). The frequency and effect of antibiotic use subsequent or simultaneous to vaccination was unknown.

Human Case Report

On July 23, 2019, a non-Hispanic White man in his 70s from the anthrax-affected area who had a history of cardiovascular disease and hypertension visited his physician for evaluation of 2 lesions near his right knee. Four days earlier, a small red spot had emerged and gradually enlarged and became painful. He

reported no fever and used no over-the-counter medications. When asked about animal exposures because of where he lived, he reported that he and his daughter had moved 2 fly-covered deer carcasses from beneath his porch before lesion onset. He was wearing shorts and a shirt while moving the carcasses, and his affected leg was scraped by the velvet-covered antlers. He also reported being bitten by a fly. The deer carcasses were not tested for anthrax, and the patient disposed of them.

On examination at his physician's office, the patient's vital signs were as follows: blood pressure 177/87 mm Hg; heart rate 76 beats/min; and temperature 98.3°F. Below and lateral to his right knee was an indurated, raised, erythematous 5-cm lesion with small ulcerations that oozed serosanguinous fluid and was surrounded by a blanched halo. Just proximal to his right knee was a nonindurated erythematous macule (Figure 2). No popliteal or inguinal adenopathy was present. After 2 swab specimens were obtained from the larger lesion, the patient was given a cephalosporin intramuscularly, and a prescription for ciprofloxacin was called in to his pharmacy of choice more than an hour's drive from his home. Because it was too late to send the specimens anywhere for testing on that day, the swabs were mailed directly to the Texas Department of State Health Services Laboratory on Wednesday after a phone consultation with the state health department.

The patient began his ciprofloxacin the next evening (July 24). On July 26, after having taken 4 doses of his antibiotics, he was feeling worse and sought additional care at the emergency department of hospital A, more than an hour's drive from his residence. Concurrently, the state laboratory notified his primary-care physician that a preliminary laboratory report for the specimen was PCR-positive for *B. anthracis*; this result was confirmed by culture the following week (August 1) (Figures 3, 4). His physician relayed the information first to the patient and then to hospital staff. Upon arrival to the hospital, the patient reported pain, difficulty walking, and nausea. He reported intermittent spontaneous drainage of a dark, jelly-like material from the larger wound. He reported no fever, chills, chest pain, shortness of breath, pain at rest, numbness, or tingling. He did not use tobacco products.

At hospital A, he reported that his exposure had been ≈3 weeks earlier. At examination, his vital signs were blood pressure 132/71 mm Hg; heart rate 91 beats/min; and respirations 24 breaths/min. He was afebrile. He had a nondraining, nonerythematous eschar 7.2 cm × 5 cm on the lateral aspect of the right calf and a painless, nondraining, nonerythematous 3.3 cm × 2 cm eschar on the lateral aspect of the right knee (Figure 5). His leukocyte count was 12,000 (10^3 cells/μL); hemoglobin, 15.5 g/dL; hematocrit, 46.9% g/dL; platelets, 83,000 (10^3 cells/mL); blood urea nitrogen, 35 mg/dL; and creatinine, 2.6 mg/dL. His antibiotic was switched to intravenous doxycycline (100 mg every 12 hours). He was discharged on hospital day 13.

Control and Prevention Measures

Control Measures for Animal Outbreaks

Because naturally occurring human anthrax cases in endemic countries are almost always related to exposure to infected animals or their byproducts, control of animal anthrax essentially eliminates human risk. The primary control measure for animal anthrax is annual preventive vaccination; however, once an outbreak occurs, other control measures include ring vaccination, proper carcass disposal to avoid further environmental contamination, and quarantine (i.e., limit animal movement from the affected and nearby properties, animal contact with

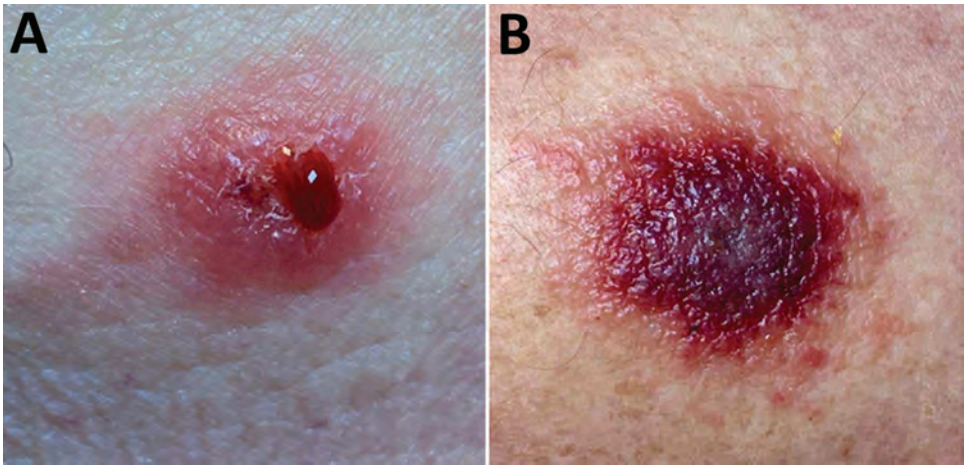

Figure 2. Lesions on right leg of anthrax patient as seen on outpatient visit, Texas, USA, 2019.

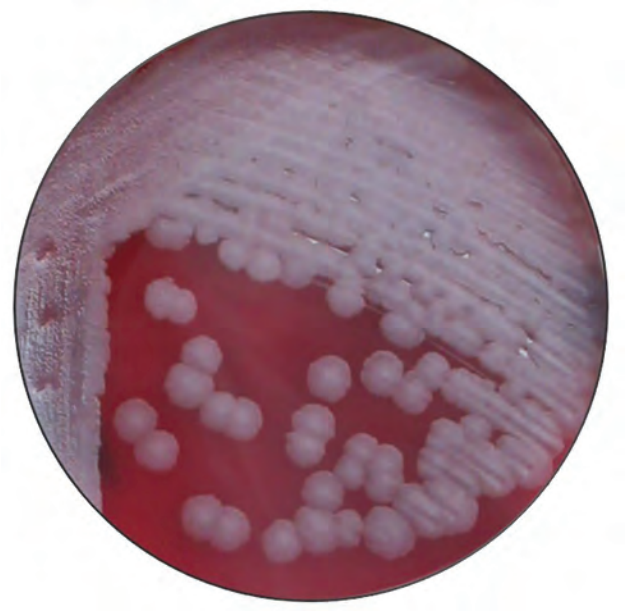

Figure 3. *Bacillus anthracis* 24-hour growth on sheep blood agar from a swab of a cutaneous anthrax lesion from a patient in Texas, USA, 2019. Typical ground glass colony morphology and lack of hemolysis are shown.

anthrax-contaminated sites, and contact between affected and nonaffected herds) (*9*). On the basis of anecdotal reports and 1 small study, tabanid flies (e.g., deer and horse flies) might play a role in transmission; whether fly control is achievable or would be effective remains an open question (*2*,*12*,*13*).

The attenuated Sterne-strain of *B. anthracis* is used globally for vaccination among domestic livestock (*14*). Because the vaccine is live-attenuated, concurrent antibiotic administration can substantially diminish efficacy. If an animal is given antibiotics either 10 days before or after vaccination, revaccination is recommended (*9*,*15*). Whether concurrent administration of antibiotics played a role in diminished vaccine efficacy in the Texas outbreak is unclear.

Proper and safe carcass disposal is critical for controlling anthrax outbreaks in enzootic areas because inappropriate carcass disposal seeds the soil with spores and increases the risk for future epizootics. Global recommendations (*9*) and codified Texas regulations (*16*) for carcass disposal are similar: the carcass should be burned in place, using a pyre or other method that leaves only ash and allows the destruction of the contaminated soil as well (i.e., "burnt until it is thoroughly consumed") (*9*,*16*). When a carcass cannot be burned, global recommendations are to bury it deeply (*9*). The historic practice of adding lime should be avoided (*17*). High soil calcium levels, either from the addition of lime or as occur naturally in southwest Texas, are conducive to *B. anthracis* spore survival (*6*,*7*) and increase the likelihood of future outbreaks. The least desirable disposal method is leaving the carcass in place, because scavenging can further disseminate the spores and increase future exposure risks for susceptible animals. Alternative carcass disposal methods are needed in areas where the standard recommendations to burn or bury carcasses are impractical. This need is particularly pronounced where there is an abundance of susceptible wildlife species that are not vaccinated or where there is poor vaccination coverage of domestic hoofstock.

Prevention of Human Cases in Endemic Areas

Human and animal health authorities should remind at-risk populations of the following prevention measures when animal cases are first identified. During animal outbreaks of anthrax, persons who handle and dispose of infected animals are at highest risk for exposure. However, exposure can be minimized through use of personal protective equipment, which should include gloves that can be disinfected or disposed of, long sleeves and pants, and footwear suitable to the terrain that can be disinfected (*9*). Even in the absence of a recognized anthrax outbreak, veterinarians and ranchers in endemic areas should always keep anthrax in mind as they interact with members of susceptible species that are ill. To do otherwise can result in inadvertent exposure to anthrax.

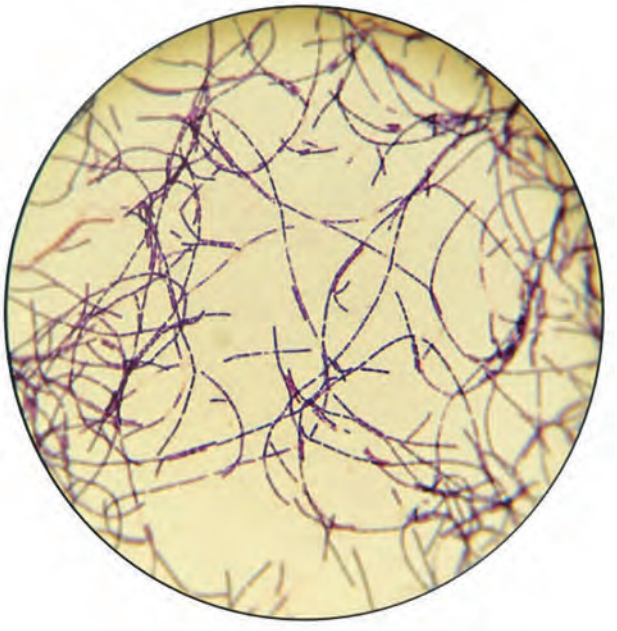

Figure 4. Gram stain from culture of a lesion of an anthrax patient, Texas, USA, 2019.

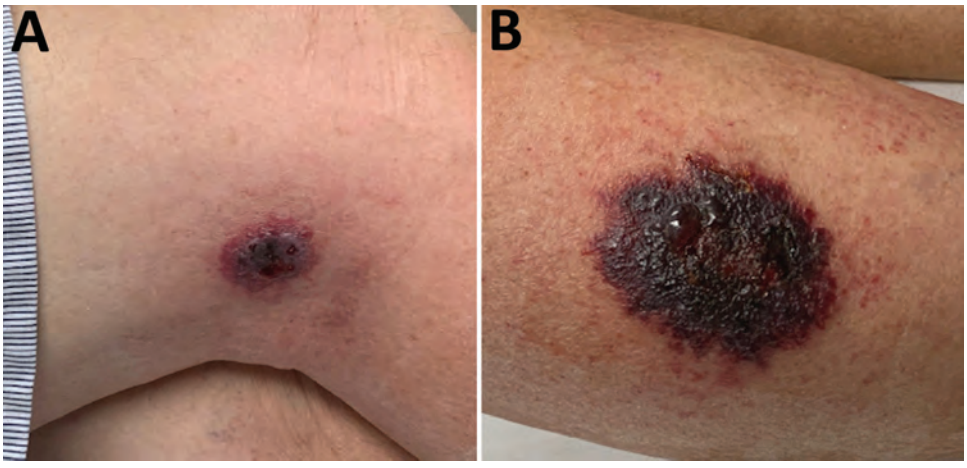

Figure 5. Eschars on right leg of anthrax patient as seen at hospital admission, Texas, USA, 2019.

Antibiotic postexposure prophylaxis (PEP) is another important component of prevention. In the former Soviet Union, before 1965, 58/339 (17%) of patients who did not receive antibiotic prophylaxis after cutaneous exposures had onset of anthrax; in contrast, only 5/287 (2%) who received prophylaxis had onset of anthrax (*18*).

If skin or mucus membrane contact occurs during carcass disposal, persons should seek medical attention and receive antibiotic PEP for 7 days (Table 1) and have their symptoms monitored for 14 days. Although aerosol exposure is unlikely in cases of natural cutaneous exposures, if potential aerosol exposure also occurred, antibiotic PEP should be administered for up to 60 days and anthrax vaccine may be considered.

Persons who live and work in anthrax-endemic areas and who anticipate interacting with animals that are dying or have died of anthrax might wish to consider preexposure prophylaxis with anthrax vaccine adsorbed (AVA). For preexposure prophylaxis of persons at high risk for *B. anthracis* exposure, AVA is administered intramuscularly as a priming series at 0, 1, and 6 months, with booster doses at 12 and 18 months and annually thereafter (*19*). Health departments in endemic areas that have existing vaccination programs can acquire AVA from the manufacturer.

Table 1. Oral antimicrobial drugs for postexposure prophylaxis and treatment of localized cutaneous anthrax*

Postexposure prophylaxis alone or after oral or intravenous therapy	Monotherapy for localized cutaneous anthrax
Antimicrobial drugs before susceptibility testing	For all strains, regardless of penicillin susceptibility or if susceptibility is unknown
Ciprofloxacin 500 mg every 12 h OR **Doxycycline 100 mg every 12 h** OR Levofloxacin 750 mg every 24 h OR Moxifloxacin 400 mg every 24 h OR Clindamycin† 600 mg every 8 h OR For penicillin-susceptible strains Amoxicillin 1 g every 8 h OR Penicillin VK 500 mg every 6 h	**Ciprofloxacin 500 mg every 12 h** OR **Doxycycline 100 mg every 12 h** OR Levofloxacin 750 mg every 24 h OR Moxifloxacin 400 mg every 24 h OR Clindamycin† 600 mg every 8 h OR For penicillin-susceptible strains Amoxicillin 1 g every 8 h OR Penicillin VK 500 mg every 6 h
Because patients who have had aerosol exposures might still have residual spores in their lungs even after treatment, oral postexposure prophylaxis is recommended as follows: for noncases (i.e., no treatment) without AVA, 60 d; with AVA for healthy adults 18–65 y, 14 d after the 3rd dose of AVA; with AVA for children <18 y, adults >65 y, pregnant women, and adults with underlying conditions, 60 d. For cases (i.e., following treatment) after finishing oral or intravenous treatment, patients exposed to aerosolized spores should finish out a 60-d course of antimicrobials (i.e., 60 d minus the duration of treatment)	Duration of therapy for naturally acquired cases, 7 d

*Bold type indicates preferred agent. Nonbolded type indicates alternative selections, which are listed in order of preference for therapy for patients who cannot tolerate first-line therapy or if first-line therapy is unavailable.
†Based on in vitro susceptibility data, rather than studies of clinical efficacy.

Healthcare Infection Control Issues for Cutaneous Anthrax

A person with cutaneous or other type of anthrax (e.g., injection, ingestion, or inhalation) cannot transmit disease through aerosol or droplet. However, spores that could remain on a person's skin, hair, or clothing after an exposure before they bathe or shower and change clothes might possibly transfer to someone else's skin and cause cutaneous anthrax (*20*–*22*). Although incubation periods of ≤1 day are reported, patients usually wait a few days to seek care, making it likely that they would already have bathed and changed clothes before seeking care. It is therefore unlikely that healthcare personnel would be secondarily exposed to spores.

Although cutaneous anthrax lesions can be contagious before the institution of effective antibiotic therapy, they become sterile in <1 day once therapy has begun (*23*). Lesions should be covered until the patient has had 24 hours of effective antibiotics. Contact precautions should be used for the first day; after that, standard precautions are sufficient.

Disposable items that have been in direct contact with the anthrax lesion, any tissue removed during debridement, and potentially infectious wound care materials (*24*,*25*) should be disposed of in a biohazard bag according to guidelines for disposal of any potentially infectious material. No additional disinfection is needed beyond what is regularly scheduled for the facility. Nondisposable surfaces in direct contact with the anthrax lesion or wound drainage can be disinfected with a 0.5% hypochlorite solution, a commercial product such as SporGon (Decon Labs, https://deconlabs.com), or other sporicidal agents such as an Environmental Protection Agency–registered antimicrobial product effective against *B. anthracis* spores (*26*–*28*); products effective against *Clostridium difficile* spores might also be appropriate (*29*,*30*).

Diagnosis

Although an eschar is the cardinal sign of cutaneous anthrax, in its early stages, anthrax can manifest as a group of small vesicles that might be pruritic. The lesion might be surrounded by erythema and swelling but is usually painless. Lymphadenopathy can occur, and constitutional symptoms including fever and headache are also possible. Localized cutaneous anthrax can disseminate to become a systemic disease. Although a substantial portion (10%–40%) of patients with cutaneous anthrax would die if left untreated (*4*), most can recover with treatment (*31*). Meningitis is also a possible, and typically fatal, complication (*32*).

In the United States, cutaneous anthrax is decidedly rare: other causes of eschars and eschar-like lesions include poxvirus infections (e.g., cowpox, vaccinia, orf), rickettsial infections (e.g., scrub typhus and *Rickettsia parkeri* rickettsiosis), ulceroglandular tularemia, staphylococcal or streptococcal infections, and noninfectious causes such as insect or spider bites. Obtaining a good exposure history is key to determining the likelihood of various etiologies among the differential diagnoses and determining the best specimens to collect. Patients seeking care with an eschar or eschar-like lesion should be asked about recent exposure to dead or dying herbivores or biting flies in an anthrax enzootic area; recent animal bites or scratches; and recent contact with lagomorphs, rodents, fleas, ticks, and spiders.

A Gram stain of a swab specimen from the lesion can often quickly identify possible cases and narrow the differential diagnosis (*23*). Specimens for tests such as Gram stain, culture, and PCR to rule anthrax in or out (Table 2) must be collected before the use of antibiotic therapy because they will rapidly become negative after the implementation of therapy (*23*). Specimens can be sent to sentinel laboratories for preliminary assessment. Specimens for which *B. anthracis* is not ruled out by a sentinel laboratory should

Table 2. Diagnostic specimens for cutaneous anthrax (*33*)*

Specimen	Test	Temperature	Laboratory Response Network level
1 swab†	Gram stain‡ and culture	Room temperature	Sentinel laboratory§
1 swab†	PCR	Room temperature	Reference laboratory¶
Single plasma or serum	Lethal factor	Frozen (−70°)	CDC#
Paired serum**	Antiprotective antigen	Frozen (−70°)	CDC
Full thickness punch biopsy of lesion	Immunohistochemistry	Room temperature	CDC

*CDC, Centers for Disease Control and Prevention.
†Dry dacron swabs for swabbing moist lesions (e.g., bullae) or saline-moistened dacron swabs for swabbing beneath dry lesions (i.e., eschars) to be collected before onset of antimicrobial therapy.
‡Direct smear from lesion.
§Sentinel laboratories comprise the first level of the Laboratory Response Network; they include private and commercial laboratories that provide routine diagnostic services, rule-out, and referral steps in the identification process.
¶Reference laboratories, often called Laboratory Response Network member laboratories, are responsible for investigating, confirming, or referring specimens. These laboratories perform testing for multiple agents in high-risk environmental or clinical samples.
#CDC laboratories belong to the top tier of the Laboratory Response Network (national laboratories).
**Acute and convalescent collected 2 weeks apart.

promptly be sent to a Laboratory Response Network (LRN) laboratory for confirmation (*33*). LRN is a network of laboratories established to respond to biologic and chemical threats and other public health emergencies that consists of 3 types of laboratories. Private and commercial laboratories comprise the first tier of the LRN and are described as sentinel laboratories. Laboratories that receive reagents, protocols, and specialized training to perform confirmatory testing for multiple agents in high-risk environmental or clinical samples comprise the second tier of LRN and are referred to as reference laboratories. Specialized characterization of organisms, bioforensics, select agent activity, and handling of highly infectious biologic agents is performed at national laboratories, the third tier of LRN. However, with approval from public health authorities, specimens from lesions that are highly suspicious based on clinical or epidemiologic grounds can be sent directly from clinicians to an LRN laboratory (*34*).

Notification

Clinicians should promptly notify their local or state health department when they suspect anthrax, although the mandated timing varies by jurisdiction. State and territorial health departments should notify the Centers for Disease Control and Prevention (CDC) within 4–24 hours (*24*) of the initial report for patients whose illness meets the probable or confirmed case definition (*35*). Presumptive positive results from an LRN laboratory must be reported within 2 hours to the state and CDC.

Treatment

Cutaneous anthrax lacking systemic manifestations such as fever, tachycardia, tachypnea, hypotension, leukocytosis, or leukopenia can usually be treated with 7 days of an oral antibiotic. Patients with cutaneous anthrax should only continue oral antibiotics for PEP after antibiotic treatment is complete if the patient was also exposed to aerosolized spores; this would rarely be indicated for naturally acquired cutaneous infections because aerosol exposures are unlikely (Table 1).

Systemically ill patients should be evaluated for meningitis; if meningitis can be ruled out, they should be treated with at least 2 intravenous antibiotics (1 that is bactericidal and 1 that inhibits protein synthesis to block toxin production). Antibiotic therapy should continue for ≥2 weeks or until the patient is stable. If meningitis is present, ≥3 antibiotics should be used (≥1 should be bactericidal, ≥1 should inhibit protein synthesis, and all should have good central nervous system penetration). Antibiotic options for treatment and prevention of anthrax are listed in Tables 1 and 3.

Systemically ill patients (whether from cutaneous, ingestion, inhalation, or injection exposures) are candidates for 1 of the Food and Drug Administration–approved anthrax antitoxins. The antitoxins are available through the Strategic National Stockpile pending a consultation with an anthrax subject matter expert at CDC, which can be reached by calling the Emergency Operations Center (770-488-7100).

Surgery might occasionally be indicated for lesions complicated by compartment syndrome. However, surgery usually is not necessary for cutaneous anthrax (*36*).

Public Health Implications and Conclusion

Anthrax is endemic to parts of the United States. Epizootics emerge with varying frequency when climatic conditions favor the uncovering of soilborne *B. anthracis* spores with subsequent consumption by susceptible herbivores. Humans contract cutaneous anthrax through contact with animals that are ill or have died from anthrax or contact with *B. anthracis*–contaminated byproducts; this risk is increased during epizootics. The outbreak we describe was confirmed in June 2019, but its actual start date is unknown; reliable recognition of epizootics might be impeded when they occur in vast, rough, and sparsely populated areas such as those in the anthrax-endemic areas of Texas. These same geographic characteristics create challenges in implementing the recommended disease control interventions, including appropriate carcass disposal and broad use of animal anthrax vaccine in species for which the vaccine is licensed, as well as off-label use in other species. Wild herbivores (e.g., white-tailed deer and exotic hoofstock) contributed to the 2019 Texas outbreak, but effective mitigation (carcass disposal or vaccination) of the risk they posed could not be adequately achieved.

The cutaneous anthrax patient associated with this outbreak was apparently exposed through a scratch on the leg from the antler of an untested deer carcass. The physician he visited in rural Texas included anthrax in the differential diagnosis, obtained and submitted diagnostic samples before treating the patient, and provided the patient with a prescription for oral ciprofloxacin. Anthrax was identified through PCR and confirmed through culture at the state reference laboratory from swab specimens of a leg lesion. The patient was treated as an outpatient with appropriate antibiotics until his condition worsened and required a 13-day hospitalization. The necessity for hospitalization might

have been related to a few-week delay in seeking treatment. Despite the delay, the patient, like most patients with cutaneous anthrax, survived with antibiotic treatment (*4*,*32*).

As soon as anthrax is recognized in an animal population, public health and animal health agencies must collaborate to heighten awareness among medical and animal health communities, as well as among ranchers and other inhabitants of at-risk areas. Timely delivery of information to ranchers on proper carcass disposal and appropriate use of personal protective equipment, as was done through various alerts, might reduce the number of exposures. If exposure is recognized, antibiotic PEP should be considered by medical providers. AVA may be appropriate for persons at high risk for exposure, such as veterinary staff and ranch workers in endemic areas; however, this process involves a long-term commitment to annual booster shots to ensure protection.

Ranchers and veterinarians should receive authoritative information on animal vaccine use to break the cycle of transmission (including emphasis on avoiding administration of antibiotics 10 days before or after vaccine administration). Even in the absence of a recognized anthrax outbreak, veterinarians and ranchers in endemic areas should keep anthrax in mind as they interact with ill members of susceptible species. Doing otherwise might result in inadvertent exposure to anthrax. A survey of ranchers in the outbreak area is planned by TAHC to assess knowledge, attitudes, and practices regarding anthrax, including information on livestock vaccination.

Table 3. Intravenous antimicrobials for treatment of adults with severe anthrax*

Dual therapy for when meningitis has been excluded	Triple therapy for when meningitis might be present
Bactericidal agent	Bactericidal agent (fluoroquinolone)
Antimicrobial drugs before susceptibility testing	
Ciprofloxacin 400 mg every 8 h†	**Ciprofloxacin 400 mg every 8 h†**
OR	OR
Levofloxacin 750 mg every 24 h	Levofloxacin 750 mg every 24 h
OR	OR
Moxifloxacin 400 mg every 24 h	Moxifloxacin 400 mg every 24 h
OR	PLUS
Meropenem 2 g every 8 h	Bactericidal agent (beta-lactam)
OR	For all strains, regardless of penicillin susceptibility or if susceptibility is unknown
Imipenem‡ 1 g every 6 h	**Meropenem 2 g every 8 h**
OR	OR
Doripenem 500 mg every 8 h	Imipenem‡ 1 g every 6 h
OR	OR
Vancomycin 60 mg/kg/day divided every 8 h (maintain serum trough concentrations of 15–20 μg/mL)	Doripenem 500 mg every 8 h
OR	OR
For penicillin-susceptible strains	For penicillin-susceptible strains
Penicillin G 4 million units every 4 h	Penicillin G 4 million units every 4 h
OR	OR
Ampicillin 3 g every 6 h	Ampicillin 3 g every 6 h
PLUS	**PLUS**
Protein synthesis inhibitor	Protein synthesis inhibitor
Clindamycin 900 mg every 8 h	**Linezolid§ 600 mg every 12 h**
OR	OR
Linezolid§ 600 mg every 12 h	Clindamycin 900 mg every 8 h
OR	OR
Doxycycline¶ 200 mg initially, then 100 mg every 12 h	Rifampin# 600 mg every 12 h
OR	OR
Rifampin# 600 mg every 12 h	Chloramphenicol** 1 g every 6–8 h
Duration of therapy for 10–14 d or until clinical criteria for stability are met. Patient exposed to aerosolized spores will require prophylaxis to complete an antimicrobial course of up to 60 d from onset of illness (see postexposure prophylaxis in Table 1)	Duration of therapy for 2–3 weeks or greater, until clinical criteria for stability are met. Patients exposed to aerosolized spores will require prophylaxis to complete an antimicrobial course of up to 60 d from onset of illness (see postexposure prophylaxis in Table 1)

*Bold type indicates preferred agent. Nonbolded type indicates alternative selections, which are listed in order of preference for therapy for patients who cannot tolerate first-line therapy or if first-line therapy is unavailable.
†Severe anthrax includes anthrax meningitis, inhalation, injection, and gastrointestinal anthrax; and cutaneous anthrax with systemic involvement, extensive edema, or lesions of the head or neck.
‡Increased risk for seizures associated with imipenem/cilastatin therapy.
§Linezolid should be used with caution in patients with thrombocytopenia because it might exacerbate it. Linezolid use for >14 d carries additional risk for hematopoietic toxicity.
¶A single 10–14 d course of doxycycline is not routinely associated with tooth-staining.
#**Rifampin is not a protein synthesis inhibitor, it may also be used in combination therapy based on in vitro synergy.
**Should only be used if other options are not available, due to toxicity concerns.

Recent federal anthrax guidance has focused on the treatment of systemic anthrax, including meningitis, rather than on the more common cutaneous form of the disease. Given that half the cases in the 2001 anthrax incident in the United States (*37*) were cutaneous anthrax and most sporadic cases in the United States and worldwide are cutaneous, this article provides an overview of prevention and control measures for animals and a single resource for the prevention, diagnosis, infection control, and treatment of naturally acquired cutaneous anthrax.

Acknowledgments

We thank Amanda Kieffer, Trevor Maness, Amanda Kammen, Kelly Persinger, Laura Robinson, Kelly Broussard, and Bonny Mayes for their assistance with this investigation and contributions to this article. We would also like to thank Thitipong Mongkolrattanothai for assistance with references and Mark Deka for preparing a map of the affected area.

This work is in memory of Robert "Dr. Bob" Dittmar, a friend, colleague, and Texas Parks and Wildlife Department (TPWD) State Wildlife Veterinarian who, along with 2 TPWD colleagues, was killed August 8, 2020, in a helicopter crash while conducting aerial surveys for desert bighorn sheep in TPWD's Black Gap Wildlife Management Area. He is missed.

About the Author

Dr. Sidwa worked for the Texas Department of State Health Services from 1993 to 2020 (retired January 31, 2020), most recently managing the Zoonosis Control Branch and serving as the State Public Health Veterinarian.

References

1. Sternbach G. The history of anthrax. J Emerg Med. 2003;24:463–7. https://doi.org/10.1016/S0736-4679(03)00079-9
2. Fasanella A, Galante D, Garofolo G, Jones MH. Anthrax undervalued zoonosis. Vet Microbiol. 2010;140:318–31. https://doi.org/10.1016/j.vetmic.2009.08.016
3. Shadomy SV, Smith TL. Zoonosis update. Anthrax. J Am Vet Med Assoc. 2008;233:63–72. https://doi.org/10.2460/javma.233.1.63
4. Doganay M, Metan G, Alp E. A review of cutaneous anthrax and its outcome. J Infect Public Health. 2010;3:98–105. https://doi.org/10.1016/j.jiph.2010.07.004
5. Griffin DW, Silvestri EE, Bowling CY, Boe T, Smith DB, Nichols TL. Anthrax and the geochemistry of soils in the contiguous United States. Geosciences (Basel). 2014;2014:114–27. https://doi.org/10.3390/geosciences4030114
6. Blackburn JK, McNyset KM, Curtis A, Hugh-Jones ME. Modeling the geographic distribution of *Bacillus anthracis*, the causative agent of anthrax disease, for the contiguous United States using predictive ecological [corrected] niche modeling. Am J Trop Med Hyg. 2007;77:1103–10. https://doi.org/10.4269/ajtmh.2007.77.1103
7. Yang A, Mullins JC, Van Ert M, Bowen RA, Hadfield TL, Blackburn JK. Predicting the geographic distribution of the *Bacillus anthracis* A1.a/Western North American sub-lineage for the continental United States: new outbreaks, new genotypes, and new climate data. Am J Trop Med Hyg. 2020;102:392–402. https://doi.org/10.4269/ajtmh.19-0191
8. Barnes S, Tull C, Neidert M. Confirmed human cutaneous anthrax in PHR 8. Texas Disease Prevention News. 2001;61:1–4.
9. World Health Organization. Anthrax in humans and animals. 4th ed. 2008 [cited 2020 Jan 31]. https://www.who.int/csr/resources/publications/AnthraxGuidelines2008
10. Wobeser BK. Anthrax vaccine associated deaths in miniature horses. Can Vet J. 2015;56:359–60.
11. World Organization for Animal Health (OIE). Anthrax manual of diagnostic tests and vaccines for terrestrial animals. 8th edition; 2018. p. 307–20.
12. Turell MJ, Knudson GB. Mechanical transmission of *Bacillus anthracis* by stable flies (*Stomoxys calcitrans*) and mosquitoes (*Aedes aegypti* and *Aedes taeniorhynchus*). Infect Immun. 1987;55:1859–61. https://doi.org/10.1128/IAI.55.8.1859-1861.1987
13. Blackburn JK, Van Ert M, Mullins JC, Hadfield TL, Hugh-Jones ME. The necrophagous fly anthrax transmission pathway: empirical and genetic evidence from wildlife epizootics. Vector Borne Zoonotic Dis. 2014;14:576–83. https://doi.org/10.1089/vbz.2013.1538
14. Hugh-Jones M. Overview of Anthrax. Merck veterinary manual 2015 [cited 2020 Aug 12]. https://www.merckvetmanual.com/generalized-conditions/anthrax/overview-of-anthrax
15. Forshaw D, Higgs AR, Moir DC, Ellis TM, Links IJ. Anthrax in cattle in southern Western Australia. Aust Vet J. 1996;74:391–3. https://doi.org/10.1111/j.1751-0813.1996.tb15453.x
16. Texas Legal Code. Anthrax disposal [chapter 31]. §313 adopted to be effective December 18, 1992, 17 TexReg 8286; amended to be effective April 4, 1999, 24 TexReg 2298 1999 [cited 2020 Jan 31]. http://txrules.elaws.us/rule/title4_chapter31_sec.31.3
17. Himsworth CG. The danger of lime use in agricultural anthrax disinfection procedures: the potential role of calcium in the preservation of anthrax spores. Can Vet J. 2008;49:1208–10.
18. Kebedzhiev G. Prophylaxis of anthrax by antibiotics [in Russian]. Antibiotiki. 1970;15:89–93.
19. Bower WA, Schiffer J, Atmar RL, Keitel WA, Friedlander AM, Liu L, et al.; ACIP Anthrax Vaccine Work Group. Use of anthrax vaccine in the United States: recommendations of the Advisory Committee on Immunization Practices, 2019. MMWR Recomm Rep. 2019;68:1–14. https://doi.org/10.15585/mmwr.rr6804a1
20. Herley R. Eight cases of external anthrax. Lancet. 1909;2:1662–5. https://doi.org/10.1016/S0140-6736(01)11260-2
21. Hodgson AE. Anthrax in a 15 months old baby. BMJ. 1929;2:667. https://doi.org/10.1136/bmj.2.3588.667
22. Clarke PS. Chloramphenicol in treatment of cutaneous anthrax. BMJ. 1952;1:86–7. https://doi.org/10.1136/bmj.1.4749.86
23. Amidi S, Dutz W, Kohout E, Ronaghy A. Human anthrax in Iran. Report of 300 cases and review of literature. Tropenmed Parasitol. 1974;25:96–104.

24. Reilly WA, Beeson CR. Antibiotic therapy for cutaneous anthrax: report of five cases. Arch Intern Med (Chic). 1948;82:529. https://doi.org/10.1001/archinte.1948.00220290013002
25. Gaitanis G, Lolis CJ, Tsartsarakis A, Kalogeropoulos C, Leveidiotou-Stefanou S, Bartzokas A, et al. An aggregate of four anthrax cases during the dry summer of 2011 in Epirus, Greece. Dermatology. 2016;232:112–6. https://doi.org/10.1159/000440860
26. Heninger SJ, Anderson CA, Beltz G, Onderdonk AB. Decontamination of *Bacillus anthracis* spores: evaluation of various disinfectants. Appl Biosaf. 2009;14:7–10. https://doi.org/10.1177/153567600901400103
27. Evers DL, Allen KP, Fowler CB, Mason JT, Blacksell SD. Laboratory decontamination of HHS-listed and HHS/USDA overlap select agents and toxins. Appl Biosaf. 2013;18:59–72. https://doi.org/10.1177/153567601301800202
28. Oudejans L, Mickelsen L, McConkey K. Effectiveness of disinfecting and sporicidal wipes against *Bacillus atrophaeus*, a *Bacillus anthracis* surrogate. 2017 [cited 2020 Aug 12]. https://cfpub.epa.gov/si/si_public_record_report.cfm?Lab=NHSRC&dirEntryId=337359
29. US Environmental Protection Agency. List K: EPA's registered antimicrobial products effective against *Clostridium difficile* spores. 2016 [cited 2020 Aug 12]. https://19january2017snapshot.epa.gov/sites/production/files/2016-06/documents/list_k_clostridium.pdf
30. US Environmental Protection Agency. Comparative efficacy of sporicidal technologies for the decontamination of *Bacillus anthracis, B. atrophaeus*, and *Clostridium difficile* spores on building materials. 2015 [cited 2020 Aug 12]. https://cfpub.epa.gov/si/si_public_record_report.cfm?Lab=NHSRC&dirEntryId=303850
31. Davies JC. A major epidemic of anthrax in Zimbabwe. The experience at the Beatrice Road Infectious Diseases Hospital, Harare. Cent Afr J Med. 1985;31:176–80.
32. Lanska DJ. Anthrax meningoencephalitis. Neurology. 2002;59:327–34. https://doi.org/10.1212/WNL.59.3.327
33. American Society for Microbiology. Sentinel level clinical laboratory guidelines for suspected agents of bioterrorism and emerging infectious diseases. *Bacillus anthracis* and *Bacillus cereus* biovar anthracis. 2017 [cited 2020 Aug 12]. https://www.asm.org/ASM/media/Policy-and-Advocacy/LRN/Sentinel%20Files/AnthraxLRN-Aug2017.pdf
34. Centers For Disease Control and Prevention. The Laboratory Response Network: partners in preparedness. 2019 [cited 2020 Aug 12]. https://emergency.cdc.gov/lrn
35. Centers For Disease Control and Prevention. National Notifiable Diseases Surveillance System: anthrax 2018 case definition. 2018 [cited 2020 Aug 12]. https://wwwn.cdc.gov/nndss/conditions/anthrax/case-definition/2018
36. Doganay M. International medicine: major tropical syndromes: systemic infections [section 6]. In: Cohen J, Powderly WG, Opal SM, editors. Infectious diseases. 4th ed: Elsevier; 2017. p. 1123–8.
37. Jernigan DB, Raghunathan PL, Bell BP, Brechner R, Bresnitz EA, Butler JC, et al.; National Anthrax Epidemiologic Investigation Team. Investigation of bioterrorism-related anthrax, United States, 2001: epidemiologic findings. Emerg Infect Dis. 2002;8:1019–28. https://doi.org/10.3201/eid0810.020353

Address for correspondence: Kate Hendricks, Centers for Disease Control and Prevention, 1600 Clifton Rd NE, Mailstop H24-12, Atlanta, GA 30329-4027, USA; email: kah1@cdc.gov

Animal Rabies Surveillance, China, 2004–2018

Ye Feng,[1] Yuyang Wang,[1] Weidi Xu, Zhongzhong Tu, Tingfang Liu, Minghe Huo, Yan Liu, Wenjie Gong, Zheng Zeng, Wen Wang, Yinhong Wei, Changchun Tu

Rabies is a severe zoonotic disease in China, but the circulation and distribution of rabies virus (RABV) within animal reservoirs is not well understood. We report the results of 15 years of surveillance of the first Chinese Rabies Surveillance Plan in animal populations, in which animal brain tissues collected during 2004–2018 were tested for RABV and phylogenetic and spatial–temporal evolutionary analyses performed using obtained RABV sequences. The results have provided the most comprehensive dataset to date on the infected animal species, geographic distribution, transmission sources, and genetic diversity of RABVs in China. In particular, the transboundary transmission of emerging RABV subclades between China and neighboring countries was confirmed. The study highlights the importance of continuous animal rabies surveillance in monitoring the transmission dynamics, and provides updated information for improving current control and prevention strategies at the source.

Rabies is a fatal zoonotic disease of humans and almost all warm-blooded animals, causing severe dysfunction of the central nervous system (*1*). About 99% of human cases occur in developing countries, mainly in Asia and Africa (*2*). Rabies is a major public issue throughout China, resulting in several hundred human deaths every year during 2015–2018 (*3*). More than 95% of human rabies cases are caused by rabid dogs (*4*). In contrast, the numbers of animal rabies cases reported in China are much lower than those of humans; only several provinces, autonomous regions, or municipalities report animal rabies cases to national veterinary authorities, as disseminated by the Veterinary Bulletin, the only official journal to report monthly information on animal infectious diseases in China (*5*). Even so, such scattered studies have still shown an increase in wildlife rabies in red foxes (*Vulpes vulpes*), raccoon dogs (*Nyctereutes procyonoides*), and ferret badgers (*Melogale moschata* in the mainland and *Melogale moschata subaurantiaca* in Taiwan). Rabies in dogs and livestock has also increased and expanded geographically to include Heilongjiang, Inner Mongolia, Xinjiang, Qinghai, Tibet, and Taiwan, provincial regions within which rabies had rarely or never been reported previously (*6*–*11*). These investigations had monitored the emergence of fox- and raccoon dog–specific RABVs in north China that caused the outbreaks in livestock; some wildlife isolates shared a high nucleotide identity with those circulating in neighboring countries (*6*,*7*,*10*). This similarity is a matter for concern because China is surrounded by 14 contiguous countries, all of which are rabies endemic and within which the genetic diversity and phylogenetic characteristics of RABVs have not been well studied.

An understanding of the status of animal rabies is a prerequisite for control and possible elimination of human rabies. Since 2004, China has implemented annual surveillance of animal rabies, with the National Reference Laboratory for Animal Rabies at the Institute of Military Veterinary Medicine, (Changchun, Jilin Province, China) as the project leader (*12*). This surveillance focuses mainly on dogs, cats, livestock, and wild animal reservoirs that have the potential to maintain the circulation and transmission of RABVs in China. As part of this program, using the epidemiologic information collected and nucleoprotein (N) gene sequences of RABV isolates obtained during 2004–2018, we investigated the infected animal species, geographic distribution, animal sources, and

Author affiliations: Academy of Military Medical Sciences, Changchun, China (Y. Feng, Y. Wang, W. Xu, Z. Tu, T. Liu, M. Huo, Y. Liu, W. Gong, C. Tu); Jilin Agricultural University, Changchun (W. Xu, T. Liu); Jilin University College of Veterinary Medicine, Changchun (M. Huo, W. Gong); Center for Animal Disease Control and Prevention of Chongqing, Chongqing, China (Z. Zeng); Animal Health Inspection Institute of Xinjiang Uygur Autonomous Region, Urumqi, China (W. Wang); Center for Animal Disease Control and Prevention of Alxa Youqi, Alxa, China (Y. Wei); Jiangsu Co-Innovation Center for the Prevention and Control of Important Animal Infectious Disease and Zoonoses, Yangzhou University, Yangzhou, China (C. Tu)

DOI: https://doi.org/10.3201/eid2612.200303

[1]These authors contributed equally to this article.

genetic diversity of RABVs in China, as well as their phylogenetic and phylogeographic relationships with those of neighboring countries. Our objective was to provide updated information about the animal rabies situation and its public health impact in China and neighboring countries.

Methods

Sample Collection and Detection of Rabies Virus

Since 2004, the Ministry of Agriculture and Rural Affairs of China has implemented the Rabies Surveillance Plan with a focus on free-roaming and stray dogs and cats, especially those showing abnormal behaviors such as biting humans. The plan also requires the monitoring of suspected rabies outbreaks in livestock and wild animals. During 2004–2018, brain tissues of 185 animals suspected of having rabies (dead dogs, dogs behaving strangely or biting humans, livestock showing rabieslike clinical signs, dead foxes, wolves, and raccoon dogs) were submitted (Appendix Table 1, https://wwwnc.cdc.gov/EID/article/26/12/20-0303-App1.pdf). In addition, 10,118 brain tissues were collected for active surveillance from 3 types of apparently healthy dogs, mostly from rabies-endemic rural areas: free-roaming and ownerless dogs, slaughtered dogs (for meat consumption), and dogs killed during emergencies (culled in rabies outbreak areas to prevent further transmission) (Appendix Table 2). All specimens were collected and submitted to the reference laboratory by the regional Centers of Animal Disease Prevention and Control.

The brain tissues were examined by the direct fluorescent antibody test (FAT) using FITC-conjugated anti-rabies monoclonal antibody (Fujirebio Diagnostics Inc., https://www.fujirebio.com) (*13*). To obtain the complete coding sequence of the N gene, rabies-positive specimens were subjected to RNA extraction using TRIzol Reagent (Invitrogen, https://www.thermofisher.com), followed by reverse transcription PCR with the SuperScript III First-Strand Synthesis System and the Platinum Taq DNA Polymerase High Fidelity kit (Invitrogen) (*6*).

Gene Sequencing and Phylogenetic Analysis

Amplified N gene sequencing was performed commercially by the Sanger method and submitted to GenBank (see Appendix Table 3 for accession numbers). Phylogenetic analysis of the complete N gene was performed on these sequences and on representative sequences retrieved from GenBank, covering samples collected in China and its neighboring countries from the 1940s through 2018 (Appendix Table 3). The MEGA 7 program package was used to construct the phylogenetic trees using the neighbor-joining method with 1,000 bootstrap replicates (*14*). Trees were visualized using Figtree version 1.4.2 (http://tree.bio.ed.ac.uk/software/figtree).

To rank the prevalence of the different RABV phylogroups and to analyze their transmission trends in China, we retrieved the sequences of all RABV strains from China deposited in GenBank. After we removed duplicate sequences and those without clear time information, we phylogenetically classified the remaining sequences, along with those obtained during this study, by the procedure described previously and chronologically sorted them by collection date.

Spatial–Temporal Evolutionary Analysis

To investigate the temporal signal and clock likeness of molecular phylogenies based on the N gene dataset, the linear evolutionary rates of different RABV clades were estimated using the Bayesian Markov chain Monte Carlo in BEAST version 1.8.2 package (*15*,*16*). For these analyses, we selected the general time reversible model as the substitution model and gamma plus invariable sites as the site heterogeneity model based on the calculations of Model Generator (*17*,*18*). An uncorrelated log normal relaxed molecular clock model and the constant size model as a coalescent tree prior were also selected for the analyses, which were run for 100 million steps with sampling at every 10,000 states (*19*). The BEAGLE parallel computation library was used to enhance the speed of the likelihood calculations (*20*). Finally, the resulting log file was checked using TRACER version 1.5 (http://tree.bio.ed.ac.uk/software/tracer) to confirm that all effective sample sizes were >200. The tree file was obtained using TreeAnnotator version 1.8.2 with a burn-in of 10%, and the maximum clade credibility tree was visualized by FigTree version 1.4.2 (*16*). Based on the analyses, estimations were made of the rates of nucleotide substitution and the time to most recent common ancestor (tMRCA) for each RABV clade.

To investigate the phylogeographic spread of RABVs in China and neighboring countries, we used a Bayesian stochastic search variable selection (BSSVS) approach to analyze transmission routes of RABV subclades, in which we applied a Bayes factor to determine the best supported transmission event between 2 geographic locations. Bayes factors were calculated by SpreaD3 software with a value >3 as cutoff (*21*,*22*).

Results

Current Animal Rabies Situation in China

During 2004–2018, animal brain tissues collected from 185 animals with suspected rabies in 17 provinces were submitted to our laboratory; 144 of them (77.8%) were confirmed by FAT as rabies virus positive (Appendix Table 1). Among the positive species, dogs were the main infected animals, accounting for 68.8% of total cases (99/144), followed by cattle (12.5%), sheep (9.7%), camels (4.2%), foxes (2.1%), pigs (1.4%), raccoon dogs (0.7%), and donkeys (0.7%) (Appendix Table 1). Concurrently, 33 (0.33%) of 10,118 brain tissue samples taken during an active surveillance of apparently healthy dogs from 7 provinces across China were found to be FAT-positive. Of the 33 positive specimens, 31 were from free-roaming and ownerless dogs (including stray dogs) and 2 were from dogs killed during an emergency (Appendix Table 2). For livestock rabies, 29 cattle, sheep, and camel cases were reported in Inner Mongolia and Xinjiang during 2013–2018, all of which were caused by fox bites (Appendix Table 1).

Phylogenetic Analysis and Evolution of Animal RABVs in China

A total of 108 complete N genes were amplified from 177 positive brain tissue samples. Of these, we selected 78, representing different years, animal species, outbreaks, and locations, together with 222 reference sequences from China, as well as from neighboring and other countries, to determine their phylogenetic characteristics (Appendix Table 3). Animal RABVs in China were clustered within 4 major clades: Asian, Cosmopolitan, Arctic-related, and Indian Subcontinent, together with different subclades (Figure 1). The Asian clade, the most prevalent one, widely distributed throughout China and Southeast Asia (SEA) countries, shows abundant genetic diversity and is transmitted mainly by dogs. This lineage was further divided into 5 subclades and different lineages. SEA1, 2, 3, and 5 subclades circulate mainly in populous areas within China; however, some lineages and strains in SEA1 and 3 were also found circulating in some countries in Southeast Asia, whereas SEA4 was restricted to the Philippines (Figure 2). Reported only in China, ferret badger RABVs were found to have abundant genetic diversity and were segregated into different lineages within SEA1, 2, and 5 (Figure 1) (*23*). Within the Cosmopolitan clade, which includes some vaccine strains, a steppe-type subclade was fox-transmitted and distributed along north and northwest border areas and neighboring Mongolia, Russia, and Kazakhstan, forming 2 major lineages (Figure 1). Other Cosmopolitan strains were dog-transmitted and mainly distributed in populous inland areas (Figure 2). Arctic-related RABVs in China segregated within the AL2 subclade and formed 2 lineages, one in northeastern China and far eastern Russia, Mongolia, and South Korea with dogs and raccoon dogs as the major hosts, and the other in southwestern China with dogs as the major transmission source (Figures 1,2). The Indian Subcontinent clade had not been identified in China until the first human rabies case caused by this clade was identified in 2017 in the border area of Tibet close to Nepal (*24*). That human case was caused by the bite of a local stray dog and remains the only Indian Subcontinent clade RABV confirmed so far in China.

For the chronological sorting of different subclades, we retrieved all 2,486 RABV sequences from China deposited in GenBank. After removing repeated sequences and those without date information, 1,118 eligible sequences remained, representing 1,118 Chinese strains isolated during 1969–2018 (including those in Figure 1). These sequences included complete genome (n = 45), full length or partial N (n = 819), glycoprotein (G; n = 208), phosphoprotein (P; n = 15), matrix protein (M; n = 25) and RNA-dependent RNA polymerase (L; n = 6) genes. Figure 3 shows the spatial–temporal trends of different RABV subclades in China, in which the 55 Chinese RABV sequences submitted to GenBank between 1969 (the earliest submission) and 2003 (therefore listed chronologically as "before 2004") segregated within 3 SEA and 1 Cosmopolitan subclade. Following initiation of official rabies surveillance in 2004, numbers of sequences submitted to GenBank sharply increased and high numbers of submissions have been maintained thereafter. The resulting data showed clearly that most rabies outbreaks have been caused by strains of the Asian clade (93.3%), with limited involvement of strains of the other 3 clades. Within the Asian clade, the subclade SEA1 predominated in rabies endemics in China (70.1%), followed by SEA2 (16.7%). SEA1 is the most widely distributed of the subclades and continues to spread. The steppe-type subclade first emerged in 2011 and has rapidly become predominant among the livestock RABV strains found along border areas in Inner Mongolia and Xinjiang Province (Figure 2). AL2 was first detected in 2007 and has become a common subclade in recent years (*10*). The Indian Subcontinent clade caused an occasional case in 2017. The result showed that steppe-type, AL2, and Indian Subcontinent strains are emerging RABVs in China. Dog-transmitted Cosmopolitan strains have not been detected during the past decade.

Transmission of Animal Rabies in China and Neighboring Countries

Results of the Bayesian skyline model analysis showed that the mean rate of nucleotide substitution for the tested RABVs was 3.50×10^{-4} substitutions per site per year (95% highest posterior density 2.90–4.11 $\times 10^{-4}$ substitutions per site per year). This finding is consistent with the previous analyses of evolutionary change performed on dog-related RABV N genes (*25*). Differences in evolutionary rates among the clades and subclades were not significant. All representative RABVs in China and neighboring countries shared a tMRCA, predicted to merge 349–563 years ago (Figure 4). Further analysis of transmission routes of RABV subclades by BEAST revealed the transboundary transmissions of rabies in different border regions around China. The significant translocation pathway of SEA1 (Bayes factor 76.9) (Appendix Table 4) from China to Indonesia was identified in accordance with our previous analysis of the G gene (Figure 5) (*26*).

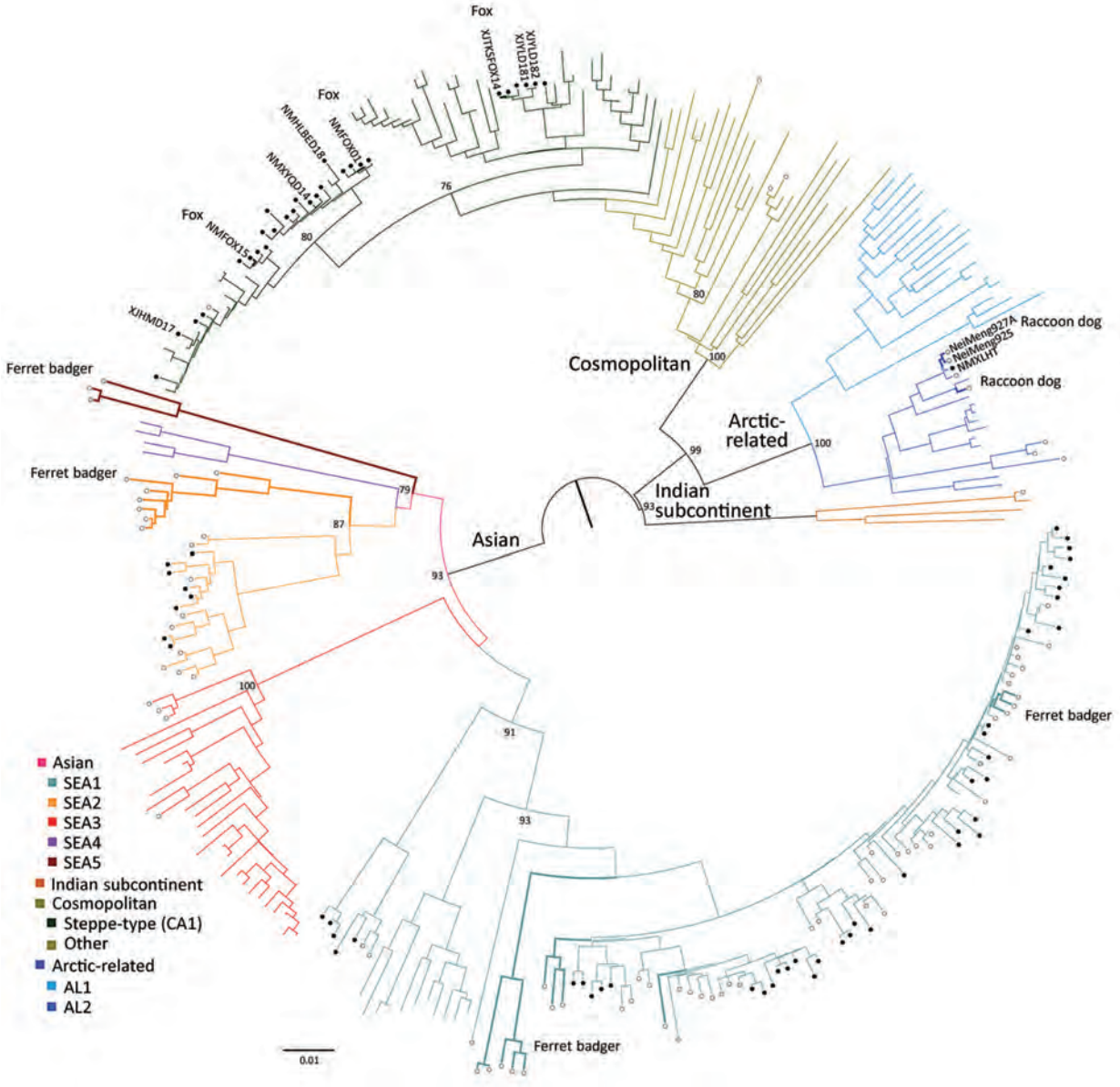

Figure 1. Phylogenetic analysis of 300 full rabies virus nucleoprotein sequences showed that RABVs in China could be classified into 4 major clades and 8 subclades. Bootstrap values = 1,000. Solid circles indicate sequences from this study; open circles indicate representative sequences from China previously published and retrieved from GenBank (Appendix Table 3, https://wwwnc.cdc.gov/EID/article/26/12/20-0303-App1.pdf). Unlabeled sequences are from surrounding countries; a few are vaccine sequences in the subclade of another Cosmopolitan clade. Named branches: dog isolates spilling out from wild animals; bold branches: wild animal isolates as indicated. SEA, Southeast Asia.

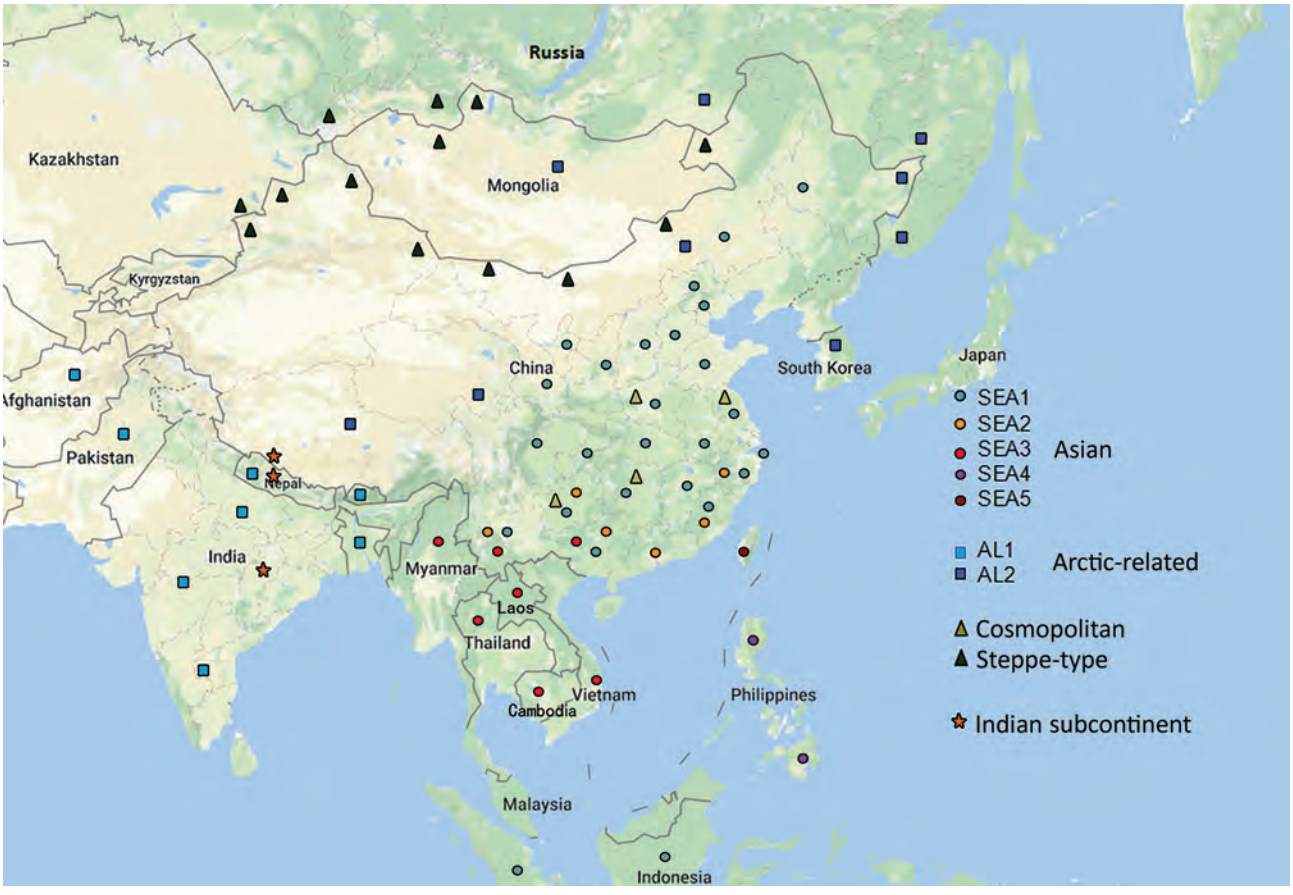

Figure 2. Geographic distribution of rabies virus clades and subclades in China and neighboring countries. The sequence information is from this study and GenBank(Appendix Table 3, https://wwwnc.cdc.gov/EID/article/26/12/20-0303-App3.pdf). . SEA, Southeast Asia.

Moreover, many SEA3 strains in Myanmar, Thailand, Laos, and Vietnam were genetically close to some strains circulating in Yunnan and Guangxi, China, indicating mutual transmission of SEA3 strains between China and bordering SEA countries (Bayes factor 4.3–85.0), as discussed previously (*27*). The same transmission was also found for steppe-type and AL2 subclades in border regions between China and Kazakhstan, Russia, Mongolia, and South Korea (Bayes factor 3.17–229.87). The most noteworthy event was the recent cross-border transmission of an Indian subcontinent strain from Nepal to the border region of Tibet, albeit with a lower Bayes factor (0.9), which caused a human rabies death in 2017 (*24*).

Discussion

There have been studies of the genetic diversity and transmission dynamics of RABVs in China, but the background information was compiled mainly from RABVs collected before 2010 or restricted to several provinces or geographic regions (*26*,*28*–*30*). Information about the molecular epidemiology of RABV within the past 10 years has been lacking, particularly within the context of the recently increasing animal rabies situation in the north, northwest, northeast, and southwest regions of China (*6*,*7*,*31*,*32*). In addition, although all the neighboring countries of China are rabies endemic, phylogenetic relationships and transboundary transmission of RABVs between China and these countries have not been systematically investigated; however, a 2013 study based on N gene sequences of RABV isolates collected before 2010 concluded that national borders effectively halted transboundary rabies transmission from China (*33*). Our study, however, has provided the most comprehensive update of RABV genetic diversity and transmission dynamics in China and has systematically compared these characteristics with those of neighboring countries, using many recent sequences obtained in our continuous surveillance during 2004–2018, along with many representative sequences from GenBank published in the past decade. The results have not only revealed the abundant genetic diversity of RABVs from China with many lineages or strains in most

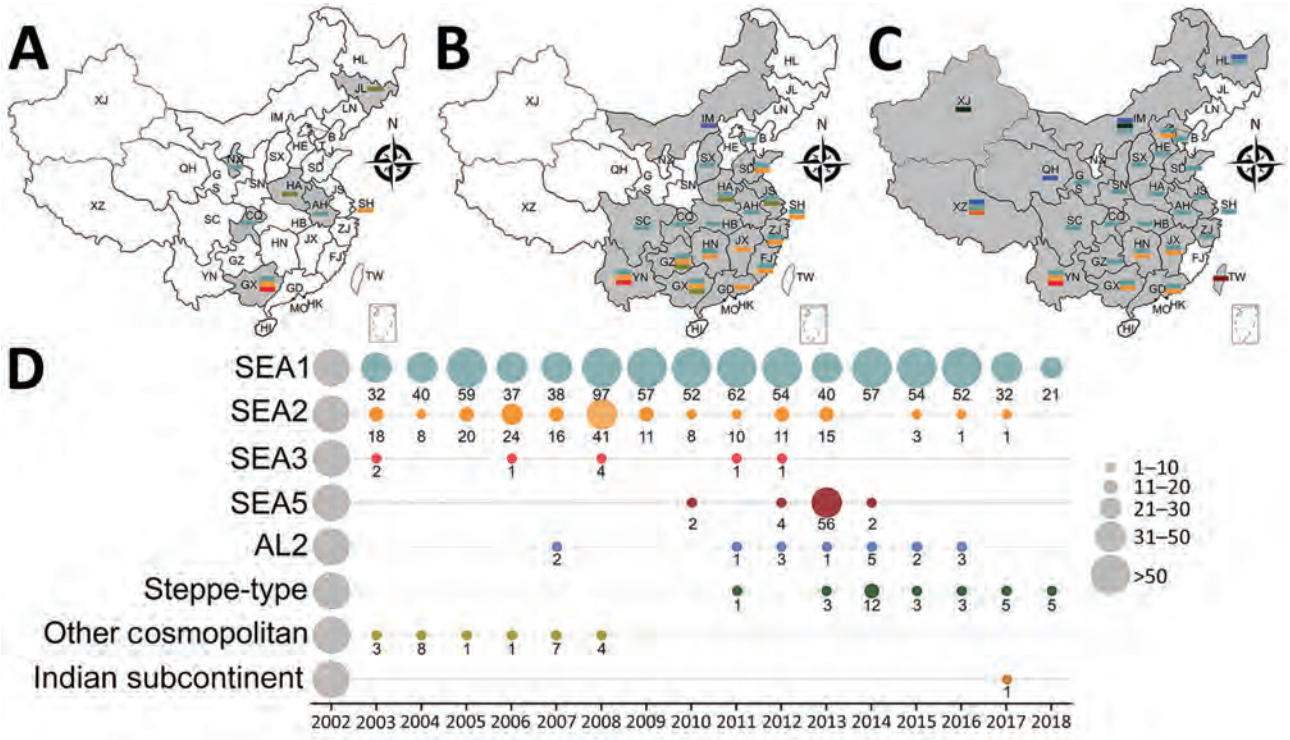

Figure 3. Spatial–temporal dynamics of RABVs in China. Phylogenetic analysis of 1,118 sequences representing 1,118 rabies cases or virus strains, including those obtained in this study using different gene fragments, followed by chronological summation of each subclade. A–C) Distribution of identified subclades during 3 time periods: A) before 2004; B) 2004–2008; C) 2009–2018. D) Quantitative trends of 8 Chinese RABV subclades during 2004–2018. Exact numbers within each subclade are given below the circles. SEA, Southeast Asia.

subclades genetically close to those circulating in neighboring countries (Figure 1) but also delineated the phylogeographic distribution of diverse RABVs in China and neighboring countries (Figure 2). The results have revealed 2 epidemic modes existing in China. The first is the historical dog-mediated rabies epidemic in populous inland provinces mainly in the center, east, and south, in which subclades within the Asian clade, particularly SEA1 followed by SEA 2, play dominant roles. The second consists mainly of outbreaks caused by the emerging subclades AL2, steppe-type, and Indian Subcontinent that have been closely associated over the past decade with cross-border transmission (Figure 5). As determined by analysis of data with a Bayes factor >3 using the BSSVS approach, fox-transmitted steppe-type viruses circulate in north and northwest border areas in Inner Mongolia and Xinjiang Province, with transboundary transmission between China and Mongolia, Russia, and Kazakhstan. Wild foxes have become the main rabies transmitter in these areas (Figure 1; Appendix Table 1). The raccoon dog–transmitted AL2 subclade emerged in the northeast likely through cross-border transmission from Mongolia. The Indian Subcontinent subclade, emerging to cause a human death in Tibet in 2017, is the most recent transboundary transmission event of dog-mediated rabies from a neighboring country (*24*). Our study has also shown transboundary transmission of the SEA3 subclade, mediated by dogs in the border areas between southwest China and SEA countries (Figure 5).

Wild animals remain the major sources of AL2 and steppe-type subclades and usually transmit the viruses causing human and livestock rabies in the steppes of Mongolia (*34*,*35*). Surprisingly, however, the surveillance in our study identified the initial spillover of these 2 subclades into dogs within China. An AL2 strain (NMXLHT) was isolated from an infected dog in 2013 in Inner Mongolia (Appendix Table 1) and grouped together with the first 2 AL2 strains (NeiMeng 927 and 925) isolated from rabid raccoon dogs in 2007 in Inner Mongolia (Figure 1) (*10*). Their collection sites were ≈200 km apart. Two steppe-type isolates (NMXYQD14 and XJHMD17) were also identified from dogs: the first in Inner Mongolia in 2014 and the second in 2017 in Xinjiang (Appendix Table 1). These dogs had exhibited strange behavior and had bitten some humans or other dogs. In 2018,

another 3 dog steppe-type isolates (NMHLBED18, XJYLD181, and XJYLD182) were detected, 1 from a dog suspected of having rabies in Inner Mongolia (Appendix Table 1) and 2 from apparently healthy dogs in Xinjiang Province (Appendix Table 2). All 5 of these dog isolates had a very close phylogenetic relationship with 3 fox isolates (NMFOX01, NMFOX15, and XJTKSFOX14) (Figure 1). A case of fox-mediated human rabies was diagnosed by reverse transcription PCR in Xinjiang Province in 2016, although the causative virus was not sequenced (*9*). These results not only demonstrated the spillover of wildlife RABVs into dogs in the past decade but also indicated that the risk of the spillover is increasing and threatening public health in northern China.

Rabies is still neglected in China, and efforts to increase awareness and strengthen control measures at the animal sources are still insufficient. As a consequence, the number of animal rabies cases officially reported during 2004–2018 (no data are available from before 2004) was only 893 (*5*), a much lower figure than the 25,424 human cases reported in China over

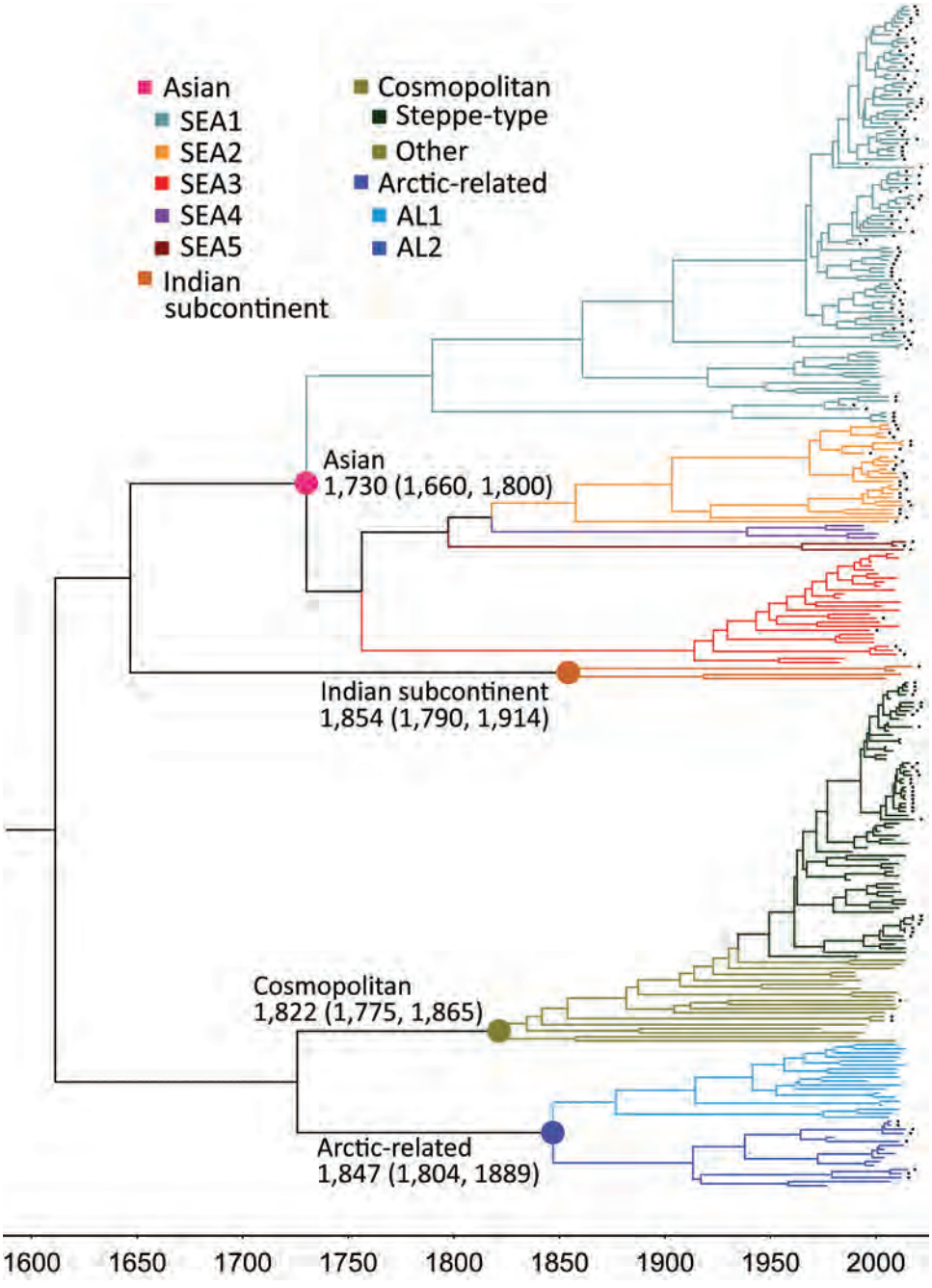

Figure 4. Nucleoprotein gene–based maximum clade credibility tree of rabies viruses. The estimated time to most recent common ancestor of these clades and their 95% highest posterior density values are indicated. The same sequences as in Figure 1 were used, except for those of 5 vaccine strains listed at end of Appendix Table 3 (https://wwwnc.cdc.gov/EID/article/26/12/20-0303-App1.pdf). Black solid squares indicate strains from China. SEA, Southeast Asia.

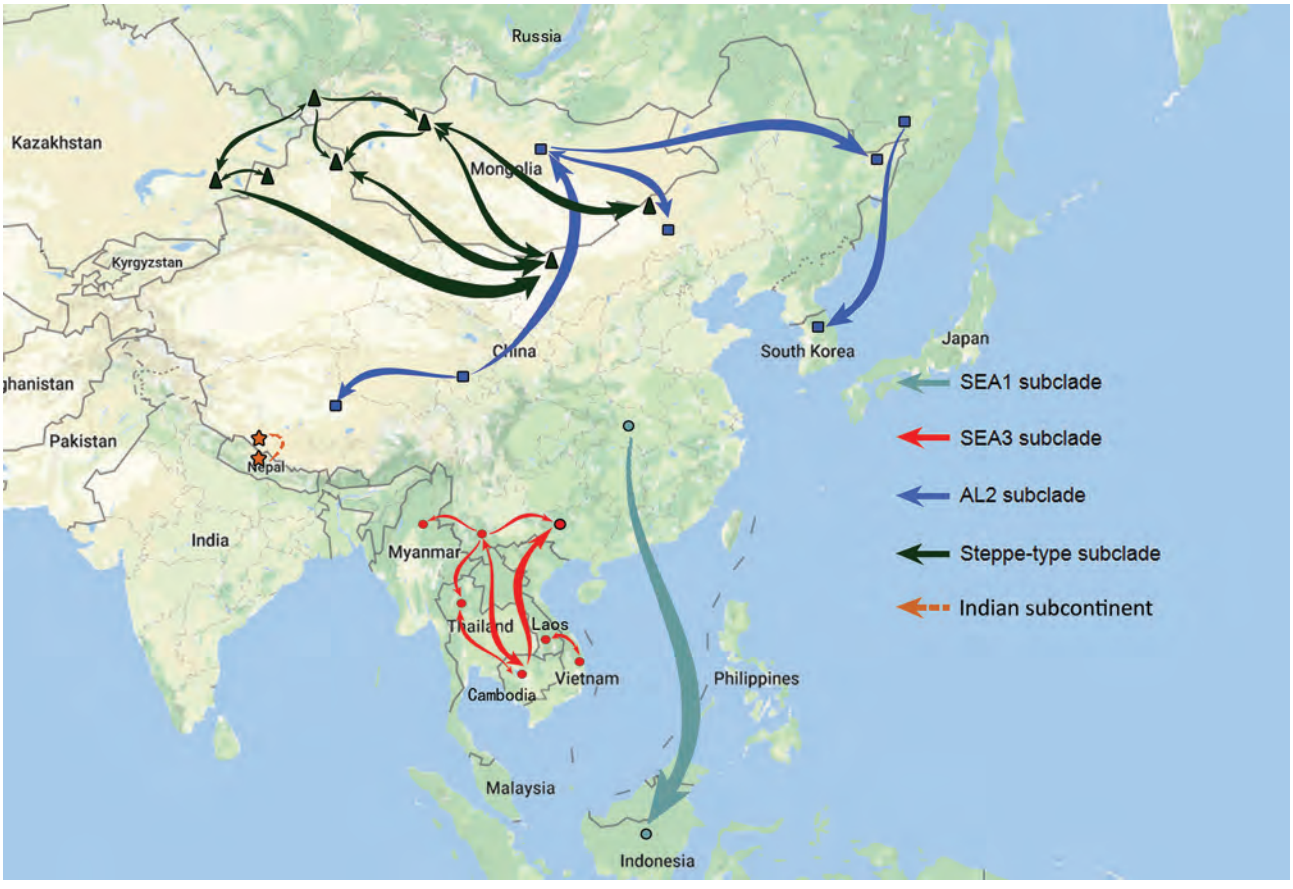

Figure 5. Proposed transboundary transmission of rabies viruses between China and neighboring countries determined by the Bayesian stochastic search variable selection approach. Unbroken lines: transmission events with a Bayes factor >3; broken line: transmission event with a Bayes factor <3. SEA, Southeast Asia.

the same period (3). Of the reported animal rabies cases, only a small proportion was submitted for laboratory diagnosis, and the 185 rabies-suspected animals tested in our study account for most of these. This low figure notwithstanding, 15 years of continuous surveillance have been adequate to reveal the spread of animal rabies (Figure 3) and have highlighted that dog rabies is still widely distributed, accounting for 74.6% (132/177) of total infected animals (Appendix Tables 1, 2). Phylogenetic analyses (Figure 1) have clearly shown that all livestock RABV isolates grouped together with either dog or fox isolates, indicating that dogs and foxes are major transmission sources. These analyses have also shown that some RABV isolates were ferret badger specific, circulating solely in ferret badgers and forming independent lineage (within SEA 2) or even a sublcade (such as SEA 5 in Taiwan). Moreover, the ongoing surveillance has also revealed the spillover of fox- and raccoon dog–transmitted RABVs into dogs, which emphasizes the importance of sequence-based analysis in tracking the sources of animal rabies cases, for which investigation into the retrospective biting history is impossible. In addition, our study has delineated the current status of wildlife rabies in China, emphasizing the roles of the relevant wild reservoir hosts in the current increase of rabies transmission. Altogether, our work has shown that sustained surveillance of animal rabies, combined with sequence-based analysis of collected RABVs, is a robust strategy to track the transmission source.

In conclusion, although animal rabies is largely underreported in China, our continuous surveillance has been able to document the current status and transmission trends of animal rabies within the country, showing that these consist of a combination of historical dog-mediated rabies in populous inland areas and the emergence of wildlife-mediated rabies during the past decade in border areas. We have also completely updated the phylogenetic and phylogeographic characteristics of RABVs in China, with particular attention to the prevalence and transboundary transmission of emerging RABV subclades.

This study was supported by the National Key Research and Development Plan (grant no. 2016YFD0500401) and National Natural Science Foundation of China (grant nos. 31302043, 31972720, and 31902307).

About the Authors

Dr. Feng is an associate professor and epidemiologist at the National Reference Laboratory for Animal Rabies, Changchun, China. Her research interests focus on rabies epidemiology and diagnosis. She is also responsible for the rabies diagnosis training of technicians in China and other countries. Mr. Wang is a master's degree student; his primary research interest is in rabies epidemiology.

References

1. Swanepoel R. Rabies. In: Coetzer JAW, Tustin RC, editors. Infectious disease of livestock: with special reference to southern Africa, 2nd ed. Cape Town (South Africa): Oxford University Press South Africa; 2004. p. 1123–82.
2. Knobel DL, Cleaveland S, Coleman PG, Fèvre EM, Meltzer MI, Miranda ME, et al. Re-evaluating the burden of rabies in Africa and Asia. Bull World Health Organ. 2005;83:360–8.
3. National Health Commission of the People's Republic of China. General situation of national legal infectious diseases [cited 2020 Apr 13]. http://so.kaipuyun.cn/s?token=9762&siteCode=bm24000006&qt=%E6%B3%95%E5%AE%9A%E4%BC%A0%E6%9F%93%E7%97%85&button=
4. Meng S, Sun Y, Wu X, Tang J, Xu G, Lei Y, et al. Evolutionary dynamics of rabies viruses highlights the importance of China rabies transmission in Asia. Virology. 2011;410:403–9. https://doi.org/10.1016/j.virol.2010.12.011
5. Ministry of Agriculture and Rural Affairs of the People's Republic of China. Official veterinary bulletin [cited 2020 Apr 13]. http://www.moa.gov.cn/gk/sygb/
6. Feng Y, Wang W, Guo J, Alatengheli, Li Y, Yang G, et al. Disease outbreaks caused by steppe-type rabies viruses in China. Epidemiol Infect. 2015;143:1287–91. https://doi.org/10.1017/s0950268814001952
7. Liu Y, Zhang S, Zhao J, Zhang F, Li N, Lian H, et al. Fox- and raccoon-dog-associated rabies outbreaks in northern China. Virol Sin. 2014;29:308–10. https://doi.org/10.1007/s12250-014-3484-0
8. Tsai K, Hsu W, Chuang W, Chang J, Tu Y, Tsai H, et al. Emergence of a sylvatic enzootic formosan ferret badger-associated rabies in Taiwan and the geographical separation of two phylogenetic groups of rabies viruses. Vet Microbiol. 2016;182:28–34. https://doi.org/10.1016/j.vetmic.2015.10.030
9. Taxitiemuer A, Tuerdi G, Zhang Y, Wushouer F, Tao X, Talipu J, et al. An investigation of the first case of human rabies caused by a fox in China in May 2016. Biomed Environ Sci. 2017;30:825–8. https://doi.org/10.3967/bes2017.110
10. Shao X, Yan X, Luo G, Zhang H, Chai X, Wang F, et al. Genetic evidence for domestic raccoon dog rabies caused by Arctic-like rabies virus in Inner Mongolia, China. Epidemiol Infect. 2011;139:629–35. https://doi.org/10.1017/s0950268810001263
11. Huang A, Chen W, Huang W, Huang S, Lo Y, Wei S, et al. Public health responses to reemergence of animal rabies, Taiwan, July 16–December 28, 2013. PLoS One. 2015;10:e0132160. https://doi.org/10.1371/journal.pone.0132160
12. Tang X, Luo M, Zhang S, Fooks AR, Hu R, Tu C. Pivotal role of dogs in rabies transmission, China. Emerg Infect Dis. 2005;11:1970–2. https://doi.org/10.3201/eid1112.050271
13. Rupprecht CE, Fooks AR, Abela-Ridder B, editors. Laboratory techniques in rabies, 5th ed. Geneva: World Health Organization; 2018. p. 108–29.
14. Kumar S, Stecher G, Tamura K. MEGA7: Molecular evolutionary genetics analysis version 7.0 for bigger datasets. Mol Biol Evol. 2016;33:1870–4. https://doi.org/10.1093/molbev/msw054
15. Drummond AJ, Nicholls GK, Rodrigo AG, Solomon W. Estimating mutation parameters, population history and genealogy simultaneously from temporally spaced sequence data. Genetics. 2002;161:1307–20.
16. Drummond AJ, Suchard MA, Xie D, Rambaut A. Bayesian phylogenetics with BEAUti and the BEAST 1.7. Mol Biol Evol. 2012;29:1969–73. https://doi.org/10.1093/molbev/mss075
17. Keane TM, Creevey CJ, Pentony MM, Naughton TJ, Mclnerney JO. Assessment of methods for amino acid matrix selection and their use on empirical data shows that ad hoc assumptions for choice of matrix are not justified. BMC Evol Biol. 2006;6:29–0. https://doi.org/10.1186/1471-2148-6-29
18. Nei M, Kumar S, editors. Molecular evolution and phylogenetics. New York: Oxford University Press; 2000.
19. Drummond AJ, Ho SY, Phillips MJ, Rambaut A. Relaxed phylogenetics and dating with confidence. PLoS Biol. 2006;4:e88. https://doi.org/10.1371/journal.pbio.0040088
20. Ayres DL, Darling A, Zwickl DJ, Beerli P, Holder MT, Lewis PO, et al. BEAGLE: an application programming interface and high-performance computing library for statistical phylogenetics. Syst Biol. 2012;61:170–3. https://doi.org/10.1093/sysbio/syr100
21. Lemey P, Rambaut A, Drummond AJ, Suchard MA. Bayesian phylogeography finds its roots. PLoS Comp Biol. 2009;5:e1000520. https://doi.org/10.1371/journal.pcbi.1000520
22. Bielejec F, Baele G, Vrancken B, Suchard MA, Rambaut A, Lemey P. SpreaD3: Interactive visualization of spatiotemporal history and trait evolutionary processes. Mol Biol Evol. 2016;33:2167–9. https://doi.org/10.1093/molbev/msw082
23. Chiou H, Hsieh C, Jeng C, Chan F, Wang H, Pang V. Molecular characterization of cryptically circulating rabies virus from ferret badgers, Taiwan. Emerg Infect Dis. 2014;20:790–8. https://doi.org/10.3201/eid2005.131389
24. Tao X, Li M, Wang Q, Baima C, Hong M, Li W, et al. The reemergence of human rabies and emergence of an Indian subcontinent lineage in Tibet, China. PloS Negl Trop Dis. 2019;13:e0007036. https://doi.org/10.1371/journal.pntd.0007036
25. Troupin C, Dacheux L, Tanguy M, Sabeta C, Blanc H, Bouchier C, et al. Large-scale phylogenomic analysis reveals the complex evolutionary history of rabies virus in multiple carnivore hosts. PLoS Path. 2016;12:e1006041. https://doi.org/10.1371/journal.ppat.1006041
26. Gong W, Jiang Y, Za Y, Zeng Z, Shao M, Fan J, et al. Temporal and spatial dynamics of rabies viruses in China and Southeast Asia. Virus Res. 2010;150:111–8. https://doi.org/10.1016/j.virusres.2010.02.019
27. Zhang Y, Vrancken B, Feng Y, Dellicour S, Yang Q, Yang W, et al. Cross-border spread, lineage displacement and evolutionary rate estimation of rabies virus in Yunnan Province, China. Virol J. 2017;14:102. https://doi.org/10.1186/s12985-017-0769-6

28. Song M, Tang Q, Wang D, Mo Z, Guo S, Li H, et al. Epidemiological investigations of human rabies in China. BMC Infect Dis. 2009;9:210. https://doi.org/10.1186/1471-2334-9-210
29. Wu X, Hu R, Zhang Y, Dong G, Rupprecht CE. Reemerging rabies and lack of systemic surveillance in People's Republic of China. Emerg Infect Dis. 2009;15:1159–64. https://doi.org/10.3201/eid1508.081426
30. Zhang H, Zhang Y, Yang W, Tao X, Li H, Ding J, et al. Molecular epidemiology of reemergent rabies in Yunnan Province, southwestern China. Emerg Infect Dis. 2014;20:1433–42. https://doi.org/10.3201/eid2009.130440
31. Tao X, Guo Z, Li H, Jiao W, Shen X, Zhu W, et al. Rabies cases in the west of China have two distinct origins. PloS Negl Trop Dis. 2015;9:e0004140. https://doi.org/10.1371/journal.pntd.0004140
32. Tian H, Feng Y, Vrancken B, Cazelles B, Tan H, Gill MS, et al. Transmission dynamics of re-emerging rabies in domestic dogs of rural China. PLoS Path. 2018;14:e1007392. https://doi.org/10.1371/journal.ppat.1007392
33. Guo Z, Tao X, Yin C, Han N, Yu J, Li H, et al. National borders effectively halt the spread of rabies: the current rabies epidemic in China is dislocated from cases in neighboring countries. PLoS Negl Trop Dis. 2013;7:e2039. https://doi.org/10.1371/journal.pntd.0002039
34. Botvinkin AD, Otgonbaatar D, Tsoodol S, Kuzmin IV. Rabies in the Mongolian steppes. Dev Biol (Basel). 2008;131:199–205.
35. Boldbaatar B, Inoue S, Tuya N, Dulam P, Batchuluun D, Sugiura N, et al. Molecular epidemiology of rabies virus in Mongolia, 2005–2008. Jpn J Infect Dis. 2010;63:358–63.

Address for correspondence: Changchun Tu, Institute of Military Veterinary Medicine, Academy of Military Medical Sciences, 666 Liuying West Rd, Jingyue Economic Development Zone, Changchun 130122, China; email: changchun_tu@hotmail.com

Small Particle Aerosol Exposure of African Green Monkeys to MERS-CoV as a Model for Highly Pathogenic Coronavirus Infection

Allison Totura,[1] Virginia Livingston, Ondraya Frick, David Dyer, Donald Nichols, Aysegul Nalca

Emerging coronaviruses are a global public health threat because of the potential for person-to-person transmission and high mortality rates. Middle East respiratory syndrome coronavirus (MERS-CoV) emerged in 2012, causing lethal respiratory disease in ≈35% of cases. Primate models of coronavirus disease are needed to support development of therapeutics, but few models exist that recapitulate severe disease. For initial development of a MERS-CoV primate model, 12 African green monkeys were exposed to 10^3, 10^4, or 10^5 PFU target doses of aerosolized MERS-CoV. We observed a dose-dependent increase of respiratory disease signs, although all 12 monkeys survived for the 28-day duration of the study. This study describes dose-dependent effects of MERS-CoV infection of primates and uses a route of infection with potential relevance to MERS-CoV transmission. Aerosol exposure of African green monkeys might provide a platform approach for the development of primate models of novel coronavirus diseases.

Since 2002, three novel coronaviruses have emerged into human populations, causing severe respiratory disease: severe acute respiratory syndrome coronavirus (SARS-CoV) during 2002–2004; Middle East respiratory syndrome coronavirus (MERS-CoV), starting in 2012; and most recently, severe acute respiratory syndrome coronavirus 2 (SARS-CoV-2), starting in 2019 (*1*,*2*). All 3 of these highly pathogenic coronaviruses can cause lethal respiratory disease characterized by acute atypical pneumonia. Subclinical or asymptomatic infection has been reported for both MERS-CoV and SARS-CoV-2, but the actual number of asymptomatic infections and the pathogenesis of mild cases are not well understood (*3*,*4*). Onset of clinical disease from highly pathogenic coronaviruses typically follows an incubation period of 2–14 days, beginning as mild and nonspecific influenza-like illness including fever, fatigue, rhinorrhea, or dry cough. Many patients progress to symptoms of dyspnea and atypical pneumonia, often requiring hospitalization or supportive medical intervention, including ventilation.

Coronaviridae is a family of positive-sense, single-stranded RNA genome enveloped viruses that includes the genera alphacoronavirus, betacoronavirus, gammacoronavirus, and deltacoronavirus. Highly pathogenic coronaviruses, including SARS-CoV, MERS-CoV, and SARS-CoV-2 (all betacoronaviruses), likely emerged from bats, which are a diverse reservoir of alphacoronaviruses and betacoronaviruses (*5*–*8*). Cross-species transmission of MERS-CoV or similar zoonotic precursor viruses from bats to camels established an intermediate reservoir of MERS-CoV in dromedary camels (*9*). MERS-CoV replicates in the upper respiratory tract of camels, but camels demonstrate only mild disease signs, and a high percentage of camels are seropositive for MERS-CoV antibodies (*10*,*11*).

The MERS-CoV enzootic cycle within dromedary camels likely facilitates continued emergence in humans, where animal workers and healthcare workers are at risk for occupational exposure to MERS-CoV transmission (*12*,*13*). Sporadic MERS cases on the Arabian Peninsula continue to seed outbreaks primarily in Saudi Arabia with the potential for exported MERS cases by travelers to other regions. A major outbreak of MERS occurred in 2015 in South Korea, where a single case in a traveler returning from Saudi Arabia resulted in 186 cases and an additional ≈16,000 contacts were traced to prevent viral spread (*13*). Outbreaks of MERS since 2012 have resulted in a total of >2,500 cases of MERS, whereas 8,096 cases were

Author affiliation: US Army Medical Research Institute of Infectious Diseases, Fort Detrick, Maryland, USA

DOI: https://doi.org/10.3201/eid2612.201664

[1]Current affiliation: US Department of Health and Human Services Biomedical Advanced Research and Development Authority, Washington, DC, USA

identified in the SARS epidemic, and >6 million cases of coronavirus disease (COVID-19) have been confirmed globally as of June 1, 2020 (*14*–*16*). Transmission of highly pathogenic coronaviruses is likely complex and thus difficult to characterize. MERS-CoV infection in humans is thought to result from direct and indirect exposure to infected camels, consumption of contaminated camel products, or close contact with infected MERS patients. Respiratory droplets likely facilitate transmission of highly pathogenic coronaviruses, including MERS-CoV (*17*). However, unlike with SARS-CoV and SARS-CoV-2, MERS-CoV person-to-person transmission is somewhat limited and not often observed outside of households or healthcare settings. Within healthcare settings, aerosol-generating procedures are associated with increased risk for transmission of coronaviruses from infected patients to healthcare workers (*18*,*19*).

No proven antiviral therapies or vaccines exist for highly pathogenic coronaviruses. Current treatment regimens for MERS include supportive care and administration of general antiviral drugs. However, most medical countermeasures for MERS lack conclusive anti-coronavirus activity supported by robust in vitro and in vivo models of MERS-CoV infection. Nonhuman primate (NHP) models of SARS-CoV were initially pursued but were never characterized to the extent necessary to support therapeutic evaluation (*20*–*23*). In particular, platform approaches to developing animal models of highly pathogenic coronavirus infection have considerable value in that they could be rapidly applied to novel emerging viruses where medical countermeasures are needed.

Prior development of NHP models of MERS-CoV has been reported in the common marmoset (*Callithrix jacchus*) model and rhesus macaque (*Macaca mulatta*) model. Rhesus macaques experienced only mild, transient respiratory symptoms when infected with 10^6–10^8 PFU of MERS-CoV by either intratracheal route (IT) or multiple route (MR) (IT, intranasal [IN], oral, and ocular routes concurrently) (*24*,*25*). Common marmosets had onset of more severe MERS disease signs in other NHP experiments using similar doses and routes of exposure, but discrepancies have been reported in the marmoset model dependent on route of exposure (*26*–*28*). In rhesus macaque and marmoset models of MERS-CoV infection, endpoints for therapeutic testing are not well defined. A lack of robust primate models that replicate severe MERS disease observed in humans is a major obstacle to evaluation of medical countermeasure against MERS-CoV infection. Therefore, in this study we exposed African green monkeys (AGMs) to aerosolized MERS-CoV to determine whether an AGM model recapitulates severe MERS disease signs to establish a platform that is useful for medical countermeasure development.

Methods

Animals

Animal research was conducted at the United States Army Medical Research Institute of Infectious Diseases (USAMRIID). Twelve wild-caught adult AGMs (*Chlorocebus aethiops*) of Caribbean origin (estimated ages 7–12 years old, weighing 3.9–7.8 kg) were included on this study. Animals were acclimated in Biosafety Level 3 (BSL-3) containment laboratory animal rooms for 7 days before virus exposure and housed individually.

Ethics Statement

These experiments and procedures were reviewed and approved by the USAMRIID Institutional Animal Care and Use Committee. All research was conducted in compliance with the US Department of Agriculture Animal Welfare Act and Public Health Service policy and other federal statutes and regulations relating to animals and experiments involving animals, and adheres to the principles stated in the Guide for the Care and Use of Laboratory Animals, National Research Council, 2011. The facility is fully accredited by the Association for Assessment and Accreditation of Laboratory Animal Care, International. The animals were provided food and water ad libitum and checked at least daily according to the protocol. All efforts were made to minimize painful procedures; the attending veterinarian was consulted regarding painful procedures, and animals were anesthetized before phlebotomy and virus exposure. Animals were humanely euthanized at the end of study under deep anesthesia in accordance with current American Veterinary Medical Association Guidelines on Euthanasia and USAMRIID standard operating procedures.

Virus and Cells

The virus (MERS-CoV EMC/2012, NR-44260) was obtained through the BEI Resources Repository (https://www.niaid.nih.gov/research/bei-resources-repository) at the National Institutes of Health's National Institute of Allergy and Infectious Diseases. Virus was sequence verified with 100% identity to MERS-CoV EMC/2012 (GenBank accession no. JX869059). MERS-CoV was amplified on Vero E6 cells. Supernatants from infected cells were collected and clarified by centrifugation. Plaque assay in Vero (CCL-81) cells was used to titrate the amount of virus in samples, as previously

described (*29*). Neutral red was used to visualize plaques at 2–3 days after inoculation. We used 50% plaque-reduction neutralization titer assays ($PRNT_{50}$) to titrate neutralizing response in AGM serum, as described previously (*30*). Plates were visualized with crystal violet to plaques at 3 days after inoculation.

Aerosol Exposures

Each AGM was anesthetized by intramuscular injection of ketamine (8–12 mg/kg) and challenged by aerosol, as previously described (*31*). In brief, the respiratory function of each of the AGMs was measured by using the Buxco Large Animal Whole Body Plethysmography (Data Sciences International [DSI], https://www.datasci.com) before aerosol challenge. Aerosol procedures were conducted by using a 16-liter, airtight Lexan chamber assembled in a head-only configuration for individual AGM exposures in a class III biologic safety cabinet located inside a BSL-3 suite. The aerosol spray was generated using a Collison Nebulizer (CH Technologies, https://chtechusa.com) to produce a highly respirable aerosol (flow rate 7.5 ± 0.1 L/minute). The system generates a target aerosol of 1–3 μm mass median aerodynamic diameter determined by aerodynamic particle sizer. Samples of the aerosol collected from the exposure chamber using an all-glass impinger during each exposure were assessed using a plaque assay. The exposure dose for each animal was calculated from the minute volume determined with a plexiglass whole body plethysmograph box using Buxco FinePointe software. The total volume of aerosol inhaled was determined by the exposure time required to deliver the estimated inhaled dose (*31*).

Animal Observation and Endpoint Criteria

AGMs were observed at least twice a day after aerosol exposure and scored for clinical signs of disease before (and while under) anesthesia. Any observable disease signs, including dehydration, lymphadenopathy, and respiratory signs, were recorded during physical examinations. Other observations such as biscuit and fruit consumption, condition of stool, and urine output were also documented, if possible. The early endpoint criteria for humane euthanasia were a >4 responsiveness score, or a ≥4°C decrease from baseline body temperature without anesthesia, or agonal breathing (https://wwwnc.cdc.gov/EID/article/26/12/20-1664-App1.pdf).

Telemetry

AGMs were implanted subcutaneously with a radiotelemetry device (DSI) ≥14 days before aerosol exposure. Body temperatures were recorded every 15 minutes using the DataQuest A.R.T. 4.1 system (DSI). Fever was predefined as 2 SDs above individual baseline temperature as determined by autoregressive integrated moving average modeling. Baselines for each animal were calculated by averaging the recorded 15-minute temperature intervals for 3 days before challenge.

Sample Collection

Blood samples and throat swab specimens were collected at indicated days after aerosol exposure to MERS-CoV (Figure 1). Puritan 6-inch 25–800–1PD sterile swabs (https://www.puritanmedproducts.com) were used for collection and were placed in 1-mL virus growth medium and frozen until further processing. Blood samples were collected from the femoral vein of AGMs anesthetized with 3 mg/kg intramuscular ketamine. Samples collected 7 days before exposure served as a reference baseline for each animal. Blood chemistry values were analyzed with VITROS 250 chemistry analyzers

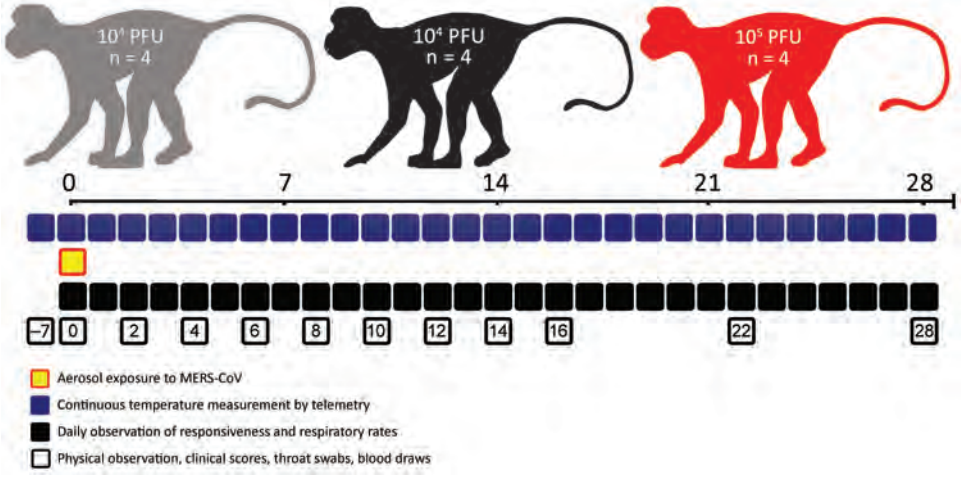

Figure 1. Study schedule for small particle aerosol infection of African green monkeys (AGMs) with MERS-CoV. Three groups of AGMs (4 in each group) were exposed to 3 different target doses of MERS-CoV EMC/2012 strain by small particle aerosol exposure. AGMs were observed at indicated days postinfection (shown by squares) for metrics that would indicate recapitulation of MERS-CoV infection in humans. MERS-CoV, Middle East respiratory syndrome coronavirus.

(Ortho Clinical Diagnostics, https://www.orthoclinical diagnostics.com).

Necropsy and Histology

At the conclusion of this study (day 28 postinfection), each AGM was euthanized with an overdose of pentobarbitol and then submitted for necropsy. The necropsies were performed under BSL-3 biocontainment by a pathologist certified by the American College of Veterinary Pathologists. The samples for histology were fixed by immersion in containers containing 10% neutral-buffered formalin. These containers were held for ≥30 days under BSL-3 biocontainment before being transferred to the USAMRIID histology laboratory. The formalin-fixed tissues were then trimmed, processed, and embedded in paraffin according to standard operating procedures. The paraffin-embedded tissues were cut into sections 5 μ thick, which were placed onto glass microscope slides, stained with hematoxylin and eosin, and coverslipped before histologic evaluation by the study pathologist.

Results

Clinical Disease Signs Observed in AGMs Exposed to Aerosolized MERS-CoV

To enable comparison of aerosol exposure to previously published NHP model development studies, AGMs were exposed to aerosolized MERS-CoV strain EMC/2012, which is the same strain used previously by other research groups (*24*,*26*,*27*). The expected range of doses was 10^3–10^5 PFU. The actual range of the infection was $10^{2.88}$–$10^{4.57}$ PFU (Table 1). All of the AGMs survived the MERS-CoV exposure and subsequent manipulations to the conclusion of the study at 28 days postinfection (Figure 2). Of note, the highest dose group of AGMs exposed to aerosolized MERS-CoV in this study were estimated to have received considerably lower doses than in prior published NHP models using MR (5–7 × 10^6 50% tissue culture infectious dose) or IT only (5 × 10^6 – 5 × 10^7 PFU) routes of infection (*24*–*27*).

Table 1. Inhaled doses of African green monkeys exposed to MERS-CoV*

Animal ID	Sex	Target dose, 10^x PFU	Actual dose, PFU	Actual dose, 10^x PFU
1	F	3	7.60 × 10^2	2.88
2	M	3	1.17 × 10^3	3.07
3	M	3	8.70 × 10^2	2.94
4	F	3	1.11 × 10^3	3.04
5	F	4	6.31 × 10^3	3.80
6	M	4	7.79 × 10^3	3.89
7	M	4	7.25 × 10^3	3.86
8	F	4	4.65 × 10^3	3.67
9	F	5	2.78 × 10^4	4.44
10	M	5	3.75 × 10^4	4.57
11	M	5	2.83 × 10^4	4.45
12	F	5	2.27 × 10^4	4.36

*MERS-CoV, Middle East respiratory syndrome coronavirus.

To determine whether exposure of AGMs to aerosolized MERS-CoV results in observable disease signs that recapitulate MERS disease observed in human cases, physical observations of AGMs were performed, including calculation of respiratory rates (Figure 2, panels A, B) and clinical scores (Figure 2, panels B–D). Clinical scores included observation of disease signs, including responsiveness, lymphadenopathy, dehydration signs, and respiratory signs by physical examination. Clinical disease signs that recapitulated human cases of MERS were observed in all groups but were most pronounced in the group that received the highest dose of MERS-CoV (Figure 1, panels C, D). All groups had increased clinical scores over the course of infection compared with pre-infection clinical scoring. No statistically significant changes in weight of AGMs were observed over the course of the study or between groups (data not shown). The 10^5 PFU group had significantly higher respiratory rates than the 10^3 PFU group, beginning at 3 days postinfection (dpi) and continuing through 10 dpi (Figure 2, panels A and B). Respiratory rates were not significantly different between the 10^4 PFU dose group and 10^3 PFU dose group. Significantly higher clinical scores were observed in the 10^5 PFU group of AGMs than the 10^4 PFU or 10^3 PFU group (Figure 2, panel D). Onset of respiratory disease signs occurred at 6 dpi and persisted in some animals through 16 dpi. All of the AGMs in the 10^5 PFU group displayed observable respiratory disease signs, including chest congestion, rales, or wheezing. Baseline temperatures were measured over a 24-hour period before infection with aerosolized MERS-CoV. Individual AGMs in 10^4 and 10^5 PFU dose group (2 of 4 AGMS in each group) had elevated temperature after exposure to MERS-CoV aerosols during 1–3 dpi but were not febrile (Appendix Figure 1).

Viral Replication and Tissue Damage Resulting from MERS-CoV Infection of AGMs

To determine whether respiratory disease signs observed in AGMs were the result of robust MERS-CoV viral replication, viral loads were titrated from throat swab specimens and serum samples. Virus was detected by plaque assay in throat swab specimens collected 6 dpi from all AGMs after exposure to aerosolized MERS-CoV. Significantly higher viral titers were observed in the throat swab specimens collected from the highest dose group (10^5 PFU) of AGMs than the

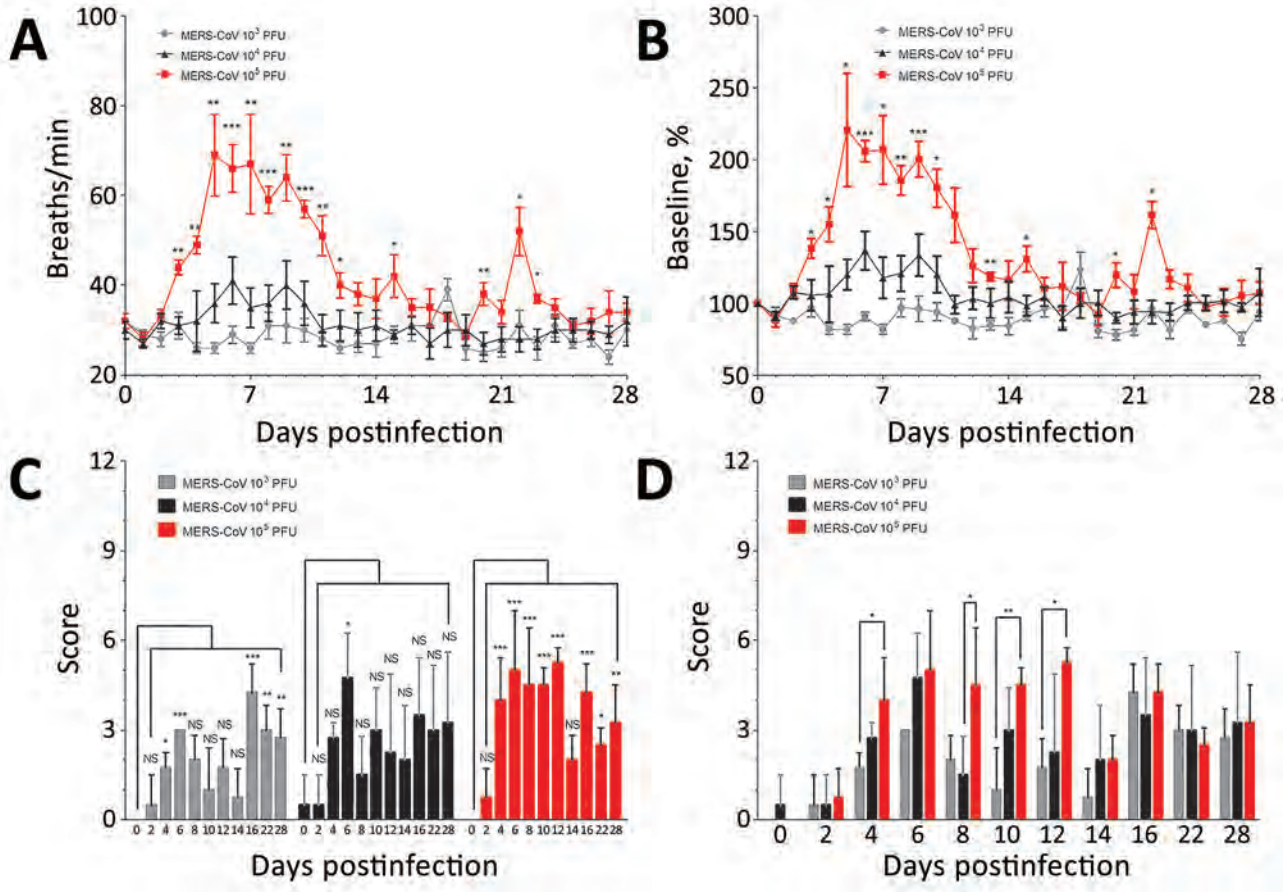

Figure 2. Clinical disease signs in African green monkeys after infection with small particle aerosol MERS-CoV. A, B) Respiratory rates were observed twice daily for all groups and recorded. Statistically significant differences on the graph reflects analysis comparing respiratory rates between the 10^3 and 10^5 PFU dose groups. C, D) Clinical scores incorporated signs of MERS-CoV infection, based in part on observations of responsiveness, respiratory function (other than respiratory rate), lymphadenopathy, and dehydration. Differences between respiratory rate and clinical score groups were determined by using 1-way analysis of variance (Tukey's multiple comparison test; *p<0.05, **p<0.01, ***p<0.001). MERS-CoV, Middle East respiratory syndrome coronavirus.

lower 2 dose groups during 6–12 dpi (Figure 3, panel A). Onset of respiratory symptoms recorded during physical evaluations of AGMs was concurrent with detection of virus in throat swab specimens. Significantly higher viral titers in the serum were observed in the 10^5 PFU group and 10^4 PFU group compared with the 10^3 PFU group in the serum at 6 dpi (Figure 3, panel B). At the conclusion of the study, all of the AGMs had measurable neutralizing antibody titers in the serum, although no statistically significant difference was observed in neutralizing titers between the dose groups (Figure 3, panel C). Elevated blood enzyme chemistry values were observed in AGMs infected with the highest dose of MERS-CoV (Appendix Figure 2). No statistically significant differences were observed in blood urea nitrogen or creatinine levels (Appendix Figure 2, panel A–D). Significantly elevated levels of enzymes indicative of liver damage, aspartate aminotransferase and gamma-glutamyl transferase, were observed in the 10^5 PFU group at 8 dpi and 10 dpi (Appendix Figure 2, panels E–H).

Although the AGMs survived the infection, all of the AGMs exposed to aerosolized MERS-CoV showed mild or minimal lung lesions at 28 dpi (Table 2; Figure 4). At the point in the disease course when lung samples were collected, all of the AGMs were recovering from the infection, although some were still experiencing very mild disease signs correlated by the clinical disease score (Figure 2, panel C). The most common histopathologic observation was multifocal interstitial pneumonia, which was likely attributable to the MERS-CoV aerosol exposure. The location, severity, and type of lung lesion observed appeared to be independent of the dose of aerosolized MERS-CoV. Another common finding was lymphoid hyperplasia in the mediastinal lymph nodes, the tracheobronchial lymph nodes, or both, which can be attributed to antigenic stimulation caused by the viral infection (data

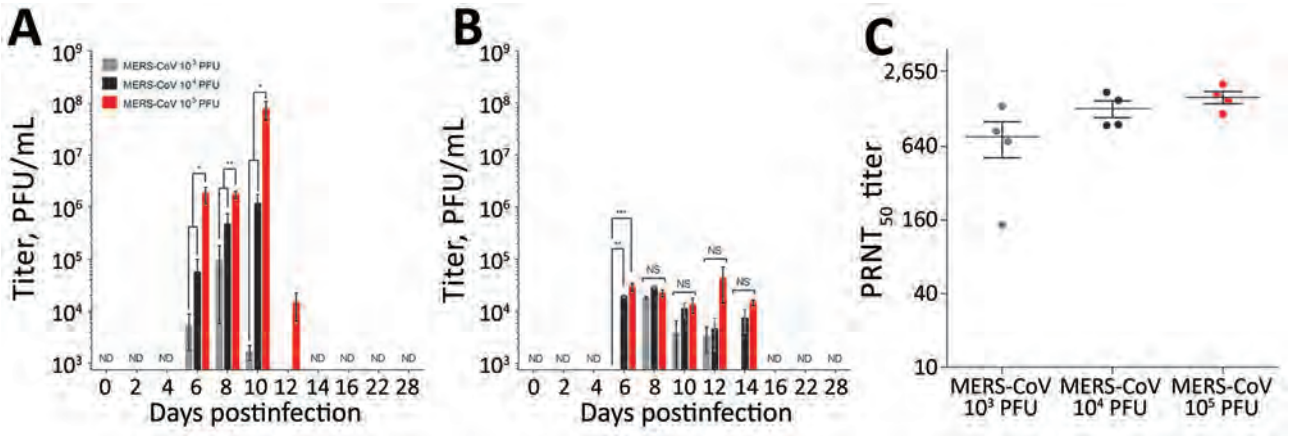

Figure 3. Detection of MERS-CoV viral loads in throat swabs and serum from African green monkeys (AGMs). A, B) Infectious MERS-CoV was titrated on Vero cells from throat swab samples (A) and serum samples (B) collected at indicated days after MERS-CoV aerosol exposure of AGMs. C) $PRNT_{50}$ titers were assessed for AGM serum samples collected at 28 days postinfection. Plaque assays and $PRNT_{50}$ assays were completed for each sample in triplicate. Differences between groups were evaluated by using 1-way analysis of variance (Tukey's multiple comparison test; *p<0.05, **p<0.01, ***p<0.001). MERS-CoV, Middle East respiratory syndrome coronavirus; ND, not detected; NS, not significant; $PRNT_{50}$, 50% reduction plaque reduction neutralization test.

not shown). These observations were not clinically significant and, because these lymph nodes receive lymphatic drainage from the lungs, this finding was not unexpected after an aerosol exposure to a virus. Tissues from other major organs were surveyed for pathologic disease signs, but no other findings were consistent with MERS disease (data not shown).

Discussion

Currently, the world is experiencing a pandemic of a novel coronavirus (SARS-CoV-2). More COVID-19 cases have occurred in the first month since identification than all of the previous SARS-CoV and MERS-CoV epidemics combined. Novel coronaviruses from the *Betacoronavirus* genus have emerged into the human population 3 separate times in <20 years: SARS-CoV (2002), MERS-CoV (2012), and SARS-CoV-2 (2019). In each instance, the novel coronavirus most likely emerged from viruses originally circulating in bats (*5*,*7*,*8*). During the emergence of SARS-CoV and MERS-CoV, spillover into human populations was driven by an intermediate animal reservoir in closer proximity to humans (civets or raccoon dogs for SARS-CoV and dromedary camels for MERS-CoV) (*9*,*31*). Whether SARS-CoV-2 emergence resulted directly through transmission from bats to humans or through another intermediate animal host remains unknown. Human disease from emergent coronaviruses manifested as a respiratory syndrome with the hallmarks of atypical pneumonia, progressing to more severe lung dysfunction accompanied by varying degrees of illness (asymptomatic illness to long-term lung dysfunction) and even death (≈10% mortality rate from SARS, ≈35% from MERS, and yet to be determined from COVID-19) (*32*). Forewarned by the knowledge that coronaviruses circulating in animals

Table 2. Summary of histological findings from African green monkeys exposed to MERS-CoV*

Animal ID	Sex	Target dose, 10^x PFU	Type of lung lesion	Location and severity of lung lesion			
				Left superior	Right superior	Left inferior	Right inferior
1	F	3	Multifocal interstitial pneumonia	Minimal	Minimal	Minimal	Minimal
2	M	3	Multifocal interstitial pneumonia	Minimal	Minimal	NLP	NLP
3	M	3	Multifocal broncho-interstitial pneumonia	Mild	Mild	Minimal	Minimal
4	F	3	Multifocal interstitial pneumonia	Minimal	Minimal	Minimal	Minimal
5	F	4	Multifocal broncho-interstitial pneumonia	Minimal	Minimal	NLP	NLP
6	M	4	Multifocal foreign-body bronchiolitis	NLP	NLP	Mild	Mild
7	M	4	Multifocal broncho-interstitial pneumonia	Minimal	Minimal	NLP	NLP
8	F	4	Multifocal interstitial pneumonia	Minimal	Minimal	Mild	Mild
9	F	5	Multifocal interstitial pneumonia	NLP	NLP	Minimal	Minimal
10	M	5	Multifocal interstitial pneumonia	Mild	Mild	Minimal	Minimal
11	M	5	Multifocal interstitial pneumonia	Minimal	Minimal	Minimal	Minimal
12	F	5	Multifocal interstitial fibrosis	NLP	NLP	Minimal	NLP

*MERS-CoV, Middle East respiratory syndrome coronavirus; NLP, no lesion present.

can cause severe disease in humans, developing platform approaches for the generation of animal models is needed to allow evaluation of medical countermeasures against coronaviruses. The development of well-characterized NHP models of coronavirus infection could provide a complementary approach to small animal models of pathogenesis, transmission, and countermeasure development.

In this study, we initiated development of an AGM model of highly pathogenic coronavirus infection by aerosol as a first step to establishing a platform for medical countermeasure testing against highly pathogenic coronaviruses. A prior study in NHP models of SARS-CoV delivered by combined IN/IT route compared disease signs in multiple NHP species (e.g., rhesus macaques, cynomolgus macaques [*Macaca fascicularis*], and AGMs) (*21*). Although none of the NHPs had onset of severe disease signs from SARS-CoV infection, AGMs had higher titers of virus recovered from nasal swabs and throat lavage than rhesus or cynomolgus macaques, particularly at later times postinfection (4–10 dpi). Building on this observation, we evaluated 3 different target doses of MERS-CoV delivered by aerosol to determine if AGMs have a dose-dependent disease response to MERS-CoV infection. Although we did not observe lethal or severe MERS disease signs, all of the AGMs in the highest dose group had clinical disease signs and elevated respiratory rates.

Previous studies of MERS-CoV in NHPs focused on infection of either rhesus macaques or marmosets. The approaches of different research groups typically used very high titer inoculum delivered by either MR or IT-only routes of infection. Rhesus macaques were observed to have only very mild disease signs (if any) after MERS-CoV infection by either MR or IT route (*24*,*25*). A study of a small particle aerosol exposure of rhesus macaques to MERS-CoV yielded subclinical infection with no disease signs (*33*). Viral replication of MERS-CoV in rhesus macaques is limited and difficult to detect, indicating limitations for the use of this model for evaluation of medical countermeasures to MERS-CoV infection. Marmosets infected with MERS-CoV were observed to have more severe disease signs by MR but not the IT route (*24*–*27*). Marmosets infected by MR had high viral loads in serum and throat swab specimens (*26*), as was observed in this study with AGMs infected by the aerosol route. Although the marmoset model of MERS-CoV infection by MR yields severe respiratory disease, marmosets are a smaller NHP species that might present challenges for researchers evaluating medical countermeasures because of sampling limitations. NHP model development in rhesus and marmoset models used a higher titer inoculum of MERS-CoV than was used in this study of aerosol exposure of AGMs to MERS-CoV and did not compare dose-response. The response of animal models to differing doses of coronavirus infection might play an important role in the evaluation of viral pathogenesis of subclinical disease compared with more severe disease.

Additional refinements to our AGM model of MERS-CoV infection are needed for medical countermeasure testing and evaluation. Although the AGMs had observable disease signs, including elevated respiratory rates and other respiratory disease signs, our model did not recapitulate severe disease or lethality as observed in MERS patients. However, we are encouraged by the dose dependence of the clinical disease signs and response to MERS-CoV infection that we observed, which indicates the potential for increased severity of disease in future iterations of this study using higher titers aerosol exposure. In addition, other NHP studies of MERS-CoV model development used early endpoint euthanasia to explore pathologic outcomes at

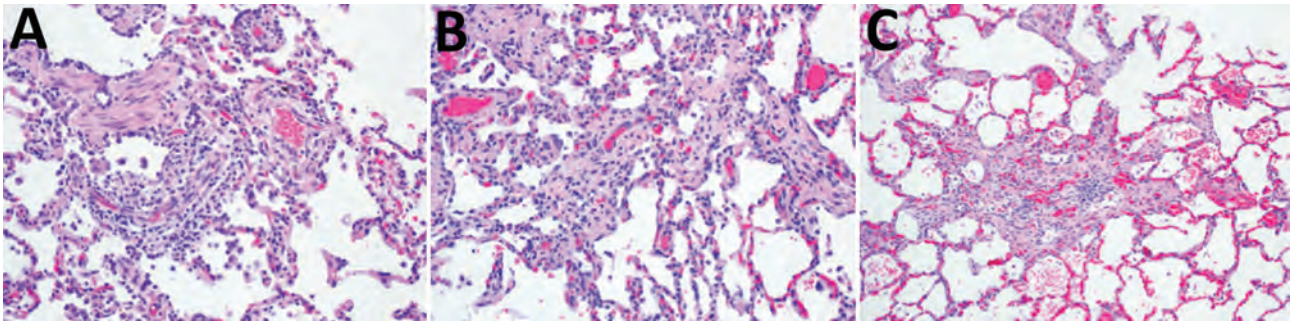

Figure 4. Interstitial pneumonia observed in lung samples from African green monkeys. Hemolysin and eosin–stained lung sample sections were collected from African green monkeys exposed to aerosolized Middle East respiratory syndrome coronavirus at 28 days postinfection. Images shown reflect a sample of lung disease observed in the 10^3 PFU dose group (A) (original magnification × 20), 10^4 PFU dose group (B) (original magnification × 20), and 10^5 PFU dose group (C) (original magnification × 10). Samples were evaluated by a trained pathologist and scored for lesions associated with severe respiratory disease.

acute times during viral infection that we would like to compare in future studies. The presence of pneumonia in all of the AGMs at the end of the study indicates that it is likely that pathologic findings related to MERS disease might be present during the acute phase of infection when respiratory disease signs are observed. In addition, the presence of histologic lesions even after AGMs had mostly recovered from MERS-CoV infection might be of use as a model of long-term lung dysfunction observed in MERS and SARS survivors.

In conclusion, animal models of viral infection must couple methods with desired outcomes; routes and doses of infection must be sufficiently reproducible, but they must also target the viral inoculum to the appropriate tissues to model respiratory disease. Recent efforts to develop an NHP model of SARS-CoV-2 infection for evaluation of vaccines and other medical countermeasures have focused on infection of rhesus macaques or cynomolgus macaques by IN/IT routes or MR with varying respiratory disease signs (*34*–*36*). Animal model development, particularly where it applies to generating a model that is appropriate for medical countermeasure evaluation has been understudied in coronavirus research. We anticipate that the approach we have defined in this study can provide a starting point for additional model development in AGMs or other NHPs using the aerosol route of infection for MERS-CoV, SARS-CoV, SARS-CoV-2, or other novel highly pathogenic coronaviruses.

Acknowledgments

We thank Melek Sunay for careful reading of the manuscript and many helpful scientific discussions and Simon Long for the collection of additional pathology images.

This research was supported, in part, by an appointment to the Postgraduate Research Participation Program at the US Army Medical Research Institute of Infectious Diseases administered by the Oak Ridge Institute for Science and Education through an interagency agreement between the US Department of Energy and the US Army Medical Research and Materiel Command. Opinions, interpretations, conclusions, and recommendations are those of the authors and are not necessarily endorsed by the US Army.

About the Author

Dr. Totura completed this work as a research biologist in the Virology Division of the US Army Medical Research Institute of Infectious Diseases, where her primary research interests were the study of highly pathogenic coronaviruses. She currently works as a biologist at the Biomedical Advanced Research and Development Authority of the US Department of Health and Human Services, where she focuses on the development of animal models for the evaluation of medical countermeasures to infectious diseases.

References

1. Ksiazek TG, Erdman D, Goldsmith CS, Zaki SR, Peret T, Emery S, et al.; SARS Working Group. A novel coronavirus associated with severe acute respiratory syndrome. N Engl J Med. 2003;348:1953–66. https://doi.org/10.1056/NEJMoa030781
2. Zaki AM, van Boheemen S, Bestebroer TM, Osterhaus ADME, Fouchier RAM. Isolation of a novel coronavirus from a man with pneumonia in Saudi Arabia. N Engl J Med. 2012;367:1814–20. https://doi.org/10.1056/NEJMoa1211721
3. Chan JF-W, Yuan S, Kok K-H, To KK-W, Chu H, Yang J, et al. A familial cluster of pneumonia associated with the 2019 novel coronavirus indicating person-to-person transmission: a study of a family cluster. Lancet. 2020;395:514–23. https://doi.org/10.1016/S0140-6736(20)30154-9
4. Omrani AS, Matin MA, Haddad Q, Al-Nakhli D, Memish ZA, Albarrak AM. A family cluster of Middle East respiratory syndrome coronavirus infections related to a likely unrecognized asymptomatic or mild case. Int J Infect Dis. 2013;17:e668–72. https://doi.org/10.1016/j.ijid.2013.07.001
5. Lau SKP, Woo PCY, Li KSM, Huang Y, Tsoi H-W, Wong BHL, et al. Severe acute respiratory syndrome coronavirus-like virus in Chinese horseshoe bats. Proc Natl Acad Sci U S A. 2005;102:14040–5. https://doi.org/10.1073/pnas.0506735102
6. Li W, Shi Z, Yu M, Ren W, Smith C, Epstein JH, et al. Bats are natural reservoirs of SARS-like coronaviruses. Science. 2005;310:676–9. https://doi.org/10.1126/science.1118391
7. Memish ZA, Mishra N, Olival KJ, Fagbo SF, Kapoor V, Epstein JH, et al. Middle East respiratory syndrome coronavirus in bats, Saudi Arabia. Emerg Infect Dis. 2013;19:1819–23. https://doi.org/10.3201/eid1911.131172
8. Zhou P, Yang X-L, Wang X-G, Hu B, Zhang L, Zhang W, et al. A pneumonia outbreak associated with a new coronavirus of probable bat origin. Nature. 2020;579:270–3. https://doi.org/10.1038/s41586-020-2012-7
9. Alagaili AN, Briese T, Mishra N, Kapoor V, Sameroff SC, Burbelo PD, et al. Middle East respiratory syndrome coronavirus infection in dromedary camels in Saudi Arabia. MBio. 2014;5:e00884–14. https://doi.org/10.1128/mBio.01002-14
10. Adney DR, van Doremalen N, Brown VR, Bushmaker T, Scott D, de Wit E, et al. Replication and shedding of MERS-CoV in upper respiratory tract of inoculated dromedary camels. Emerg Infect Dis. 2014;20:1999–2005. https://doi.org/10.3201/eid2012.141280
11. Sikkema RS, Farag EABA, Islam M, Atta M, Reusken CBEM, Al-Hajri MM, et al. Global status of Middle East respiratory syndrome coronavirus in dromedary camels: a systematic review. Epidemiol Infect. 2019;147:e84. https://doi.org/10.1017/S095026881800345X
12. Reusken CBEM, Farag EABA, Haagmans BL, Mohran KA, Godeke GJ V, Raj S, et al. Occupational exposure to dromedaries and risk for MERS-CoV infection, Qatar,

2013–2014. Emerg Infect Dis. 2015;21:1422–5. https://doi.org/10.3201/eid2108.150481
13. Korea Centers for Disease Control and Prevention. Middle East respiratory syndrome coronavirus outbreak in the Republic of Korea, 2015. Osong Public Health Res Perspect. 2015;6:269–78. https://doi.org/10.1016/j.phrp.2015.08.006
14. World Health Organization. MERS situation update, December 2019. 2019 [cited 2020 Feb 12]. http://www.emro.who.int/pandemic-epidemic-diseases/mers-cov/mers-situation-update-december-2019.html
15. World Health Organization. Summary of probable SARS cases with onset of illness from 1 November 2002 to 31 July 2003. 2003 [cited 2020 Feb 12]. http://www.who.int/csr/sars/country/table2004_04_21/en/index.html
16. World Health Organization. Coronavirus disease 2019 (COVID-19) situation report—132. 2020 [cited 2020 Feb 12]. https://www.who.int/docs/default-source/coronaviruse/situation-reports/20200531-covid-19-sitrep-132.pdf
17. Jones RM, Brosseau LM. Aerosol transmission of infectious disease. J Occup Environ Med. 2015;57:501–8. https://doi.org/10.1097/JOM.0000000000000448
18. Tran K, Cimon K, Severn M, Pessoa-Silva CL, Conly J. Aerosol generating procedures and risk of transmission of acute respiratory infections to healthcare workers: a systematic review. PLoS One. 2012;7:e35797. https://doi.org/10.1371/journal.pone.0035797
19. Nam H-S, Yeon M-Y, Park JW, Hong J-Y, Son JW. Healthcare worker infected with Middle East respiratory syndrome during cardiopulmonary resuscitation in Korea, 2015. Epidemiol Health. 2017;39:e2017052. https://doi.org/10.4178/epih.e2017052
20. Haagmans BL, Kuiken T, Martina BE, Fouchier RAM, Rimmelzwaan GF, van Amerongen G, et al. Pegylated interferon-alpha protects type 1 pneumocytes against SARS coronavirus infection in macaques. Nat Med. 2004;10:290–3. https://doi.org/10.1038/nm1001
21. McAuliffe J, Vogel L, Roberts A, Fahle G, Fischer S, Shieh W-J, et al. Replication of SARS coronavirus administered into the respiratory tract of African green, rhesus and cynomolgus monkeys. Virology. 2004;330:8–15. https://doi.org/10.1016/j.virol.2004.09.030
22. Greenough TC, Carville A, Coderre J, Somasundaran M, Sullivan JL, Luzuriaga K, et al. Pneumonitis and multi-organ system disease in common marmosets (*Callithrix jacchus*) infected with the severe acute respiratory syndrome-associated coronavirus. Am J Pathol. 2005;167:455–63. https://doi.org/10.1016/S0002-9440(10)62989-6
23. Smits SL, van den Brand JMA, de Lang A, Leijten LME, van Ijcken WF, van Amerongen G, et al. Distinct severe acute respiratory syndrome coronavirus-induced acute lung injury pathways in two different nonhuman primate species. J Virol. 2011;85:4234–45. https://doi.org/10.1128/JVI.02395-10
24. de Wit E, Rasmussen AL, Falzarano D, Bushmaker T, Feldmann F, Brining DL, et al. Middle East respiratory syndrome coronavirus (MERS-CoV) causes transient lower respiratory tract infection in rhesus macaques. Proc Natl Acad Sci U S A. 2013;110:16598–603. https://doi.org/10.1073/pnas.1310744110
25. Johnson RF, Bagci U, Keith L, Tang X, Mollura DJ, Zeitlin L, et al. 3B11-N, a monoclonal antibody against MERS-CoV, reduces lung pathology in rhesus monkeys following intratracheal inoculation of MERS-CoV Jordan-n3/2012. Virology. 2016;490:49–58. https://doi.org/10.1016/j.virol.2016.01.004
26. Falzarano D, de Wit E, Feldmann F, Rasmussen AL, Okumura A, Peng X, et al. Infection with MERS-CoV causes lethal pneumonia in the common marmoset. PLoS Pathog. 2014; 10:e1004250. https://doi.org/10.1371/journal.ppat.1004250
27. Johnson RF, Via LE, Kumar MR, Cornish JP, Yellayi S, Huzella L, et al. Intratracheal exposure of common marmosets to MERS-CoV Jordan-n3/2012 or MERS-CoV EMC/2012 isolates does not result in lethal disease. Virology. 2015;485:422–30. https://doi.org/10.1016/j.virol.2015.07.013
28. Chan JF-W, Yao Y, Yeung M-L, Deng W, Bao L, Jia L, et al. Treatment with lopinavir/ritonavir or interferon-β1b improves outcome of MERS-CoV infection in a nonhuman primate model of common marmoset. J Infect Dis. 2015;212:1904–13. https://doi.org/10.1093/infdis/jiv392
29. Scobey T, Yount BL, Sims AC, Donaldson EF, Agnihothram SS, Menachery VD, et al. Reverse genetics with a full-length infectious cDNA of the Middle East respiratory syndrome coronavirus. Proc Natl Acad Sci U S A. 2013;110:16157–62. https://doi.org/10.1073/pnas.1311542110
30. Park WB, Perera RAPM, Choe PG, Lau EHY, Choi SJ, Chun JY,et al. Kinetics of serologic responses to MERS coronavirus infection in humans, South Korea. Emerg Infect Dis. 2015;21:2186–9. https://doi.org/10.3201/eid2112.151421
31. Chefer S, Thomasson D, Seidel J, Reba RC, Bohannon JK, Lackemeyer MG, et al. Modeling [^{18}F]-FDG lymphoid tissue kinetics to characterize nonhuman primate immune response to Middle East respiratory syndrome-coronavirus aerosol challenge. EJNMMI Res. 2015;5:65. https://doi.org/10.1186/s13550-015-0143-x
32. Guan Y, Zheng BJ, He YQ, Liu XL, Zhuang ZX, Cheung CL, et al. Isolation and characterization of viruses related to the SARS coronavirus from animals in southern China. Science. 2003;302:276–8. https://doi.org/10.1126/science.1087139
33. Gralinski LE, Baric RS. Molecular pathology of emerging coronavirus infections. J Pathol. 2015;235:185–95. https://doi.org/10.1002/path.4454
34. Munster VJ, Feldmann F, Williamson BN, van Doremalen N, Pérez-Pérez L, Schulz J, et al. Respiratory disease in rhesus macaques inoculated with SARS-CoV-2. Nature. 2020. https://doi.org/10.1038/s41586-020-2324-7
35. Rockx B, Kuiken T, Herfst S, Bestebroer T, Lamers MM, Oude Munnink BB, et al. Comparative pathogenesis of COVID-19, MERS, and SARS in a nonhuman primate model. Science. 2020;368:1012–5. https://doi.org/10.1126/science.abb7314
36. Chandrashekar A, Liu J, Martinot AJ, McMahan K, Mercado NB, Peter L, et al. SARS-CoV-2 infection protects against rechallenge in rhesus macaques. Science. 2020;eabc4776; Epub ahead of print. https://doi.org/10.1126/science.abc4776

Address for correspondence: Aysegul Nalca, US Army Medical Research Institute of Infectious Diseases, 1425 Porter Rd, Fort Detrick, MD 21702, USA; email: aysegul.nalca.civ@mail.mil

Coronavirus Disease Model to Inform Transmission-Reducing Measures and Health System Preparedness, Australia

Robert Moss, James Wood, Damien Brown, Freya M. Shearer, Andrew J. Black, Kathryn Glass, Allen C. Cheng, James M. McCaw, Jodie McVernon

The ability of health systems to cope with coronavirus disease (COVID-19) cases is of major concern. In preparation, we used clinical pathway models to estimate healthcare requirements for COVID-19 patients in the context of broader public health measures in Australia. An age- and risk-stratified transmission model of COVID-19 demonstrated that an unmitigated epidemic would dramatically exceed the capacity of the health system of Australia over a prolonged period. Case isolation and contact quarantine alone are insufficient to constrain healthcare needs within feasible levels of expansion of health sector capacity. Overlaid social restrictions must be applied over the course of the epidemic to ensure systems do not become overwhelmed and essential health sector functions, including care of COVID-19 patients, can be maintained. Attention to the full pathway of clinical care is needed, along with ongoing strengthening of capacity.

As of late September 2020, >30.6 million confirmed cases of coronavirus disease (COVID-19) were reported worldwide, involving all global regions and resulting in >950,000 deaths (*1*). Although most cases are clinically mild or asymptomatic, early reports from China estimated that 20% of all COVID-19 patients progressed to severe disease and required hospitalization, 5%–16% of whom required management in an intensive care unit (ICU) (*2*). Pulmonary disease leading to respiratory failure has been the major cause of death in severe cases (*3*).

The ability of health systems around the world to cope with increasing case numbers is of major concern. All levels of the system will be challenged, from primary care, prehospital and emergency department (ED) services to inpatient units and ultimately ICUs. Stresses on clinical care provision will result in increased illness and death (*4*). Such tragic consequences already have been observed, even in high-income countries that provide the whole population with access to quality medical care. Greater effects can be expected in low- and middle-income countries where access to high-level care is extremely limited. Availability of ICU beds and ventilators has proven critical for the adequate management of severe cases, with overwhelming demand initiating complex ethical discussions about rationing of scarce resources (*5*).

To prepare for this challenge, Australia has drawn on approaches developed over many years to prepare for influenza pandemics (*6*), and rapidly produced a national COVID-19 pandemic plan (*7*). The plan reoriented relevant influenza pandemic response strategies toward this new pathogen, building on emerging understanding of its anticipated transmissibility and severity, which are the determinants of clinical impact (*8*). Early imposition of stringent border measures, high levels of testing, active case-finding, and quarantine of contacts all have bought time to reinforce public health and clinical capacity. However, an influx of cases among travelers returning from countries with rapidly growing epidemics have been associated with community transmission in several states in Australia. By April

Author affiliations: The University of Melbourne, Melbourne, Victoria, Australia (R. Moss, F.M. Shearer, J.M. McCaw, J. McVernon); University of New South Wales, Sydney, New South Wales, Australia (J. Wood); The Peter Doherty Institute for Infection and Immunity at the University of Melbourne and Royal Melbourne Hospital, Melbourne (D. Brown, J.M. McCaw, J. McVernon); University of Adelaide, Adelaide, South Australia, Australia (A.J. Black); Australian National University, Canberra, New South Wales, Australia (K. Glass); Monash University, Melbourne (A.C. Cheng); Murdoch Children's Research Institute, Melbourne (J. McVernon)

DOI: https://doi.org/10.3201/eid2612.202530

Table 1. Parameter assumptions used in a coronavirus disease transmission model, Australia

Parameter	Estimate or assumption	Justification
Fundamental assumptions		
Doubling time	6.4 d	Estimated in from early case growth in Wuhan, China, from Wu et al. (*11*)
Incubation period	5.2 d	Based on Li et al. (*12*) and Lauer et al. (*13*)
Derived assumptions		
R_0	2.53	Based on latent and infectious periods, with doubling time 6.4 d (Appendix, https://wwwnc.cdc.gov/EID/article/26/12/20-2530-App1.pdf)
Latent (noninfectious) period	3.2 d	Assumes 2 d of presymptomatic transmission before completion of incubation period, based on contribution estimates from Ganyani et al. (*14*) and Tindal et al. (*15*)
Infectious period	9.68 d	Estimated, related to doubling time and incubation period (Appendix)

14, 2020, a total of 6,366 cases and 61 deaths had been reported in the country (*9*).

We report on the use of a clinical care pathways model that represents the national capacity of the health system of Australia. This framework initially was developed for influenza pandemic preparedness (*10*) and has been modified to estimate healthcare requirements for COVID-19 patients and inform needed service expansion. The ability of different sectors to meet anticipated demand was assessed by modeling plausible COVID-19 epidemic scenarios, overlaid on available capacity and models of patient flow and care delivery. An unmitigated outbreak is anticipated to completely overwhelm the healthcare system in Australia. Given realistic limits on capacity expansion, these models have made the case for ongoing case-targeted measures, combined with broader social restrictions, to reduce transmission and flatten the curve of the local epidemic to preserve health sector continuity.

Methods

Disease Transmission Model

We developed an age- and risk-stratified transmission model of COVID-19 infection based on a susceptible-exposed-infected-recovered (SEIR) paradigm (Appendix, https://wwwnc.cdc.gov/EID/article/26/12/20-2530-App1.pdf). Transmission parameters were based on information synthesis from multiple sources, with an assumed basic reproduction number (R_0) of 2.53 and a doubling time of 6.4 days (Table 1). Potential for presymptomatic transmission was assumed to be ≤48 hours before symptom onset. Despite an increasing body of evidence regarding requirements of hospitalized patients for critical care, considerable uncertainty remains regarding the full pyramid of mild and moderately symptomatic disease. Therefore, we simulated a range of scenarios by using Latin hypercube sampling from distributions in which the proportion of all infections severe enough to require hospitalization ranged from 4.3%–8.6%. These totals represent the aggregate of strongly age-skewed parameter assumptions (Table 2). For each scenario, corresponding distributions of mild cases being seen by primary care were sampled, ranging from 30%–45% at the lower range of the severe spectrum to 50%–75% for the most extreme cases and increasing linearly between the 2 ranges. Persons not seeking care in the healthcare system were assumed undetected cases without differentiation between those with mild or no symptoms.

Case-Targeted Interventions

We simulated a case-targeted public health intervention. Cases were isolated at the point of diagnosis. We assumed isolation occurred 48 hours after symptom onset, limiting the effective infectious period and reducing infectiousness from the point of identification by 80%, enabling imperfect implementation. Targeted quarantine of close contacts was implemented in the model framework by dynamic assignment of a transient "contact" label. Each time a new infectious case appears in the model, a fixed number of temporary contacts are labeled. Only contacts can progress through the exposed and infectious states, however, most remain

Table 2. COVID-19 model severity parameter assumptions, relative to all denominator infections*

Age group, y	% Hospitalized, range†	% Hospitalized in ICU, range‡
0–9	0.03–0.06	0.01–0.02
10–19	0.03–0.06	0.01–0.02
20–29	0.39–0.78	0.11–0.23
30–39	1.4–2.90	0.43–0.85
40–49	2.55–5.11	0.75–1.50
50–59	4.95–9.90	1.45–2.91
60–69	7.75–15.49	2.27–4.55
70–79	17.88–35.76	5.25–10.50
≥80	32.97–65.94	9.68–19.36
Mean bed-days	8 d	10 d

*COVID-19, coronavirus disease; ICU, intensive care unit.
†Assumed proportional to ICU values and based on calibration to non–Hubei, China, severe case rates (Appendix, https://wwwnc.cdc.gov/EID/article/26/12/20-2530-App1.pdf).
‡Combines use of data from Intensive Care National Audit and Research Centre (*16*) and COVID-19 Task Force of the Department of Infectious Diseases and Computer Service, Italy (*17*), and assumptions used in Ferguson et al. (*18*).
§Based on assumptions used in Ferguson et al. (*18*).

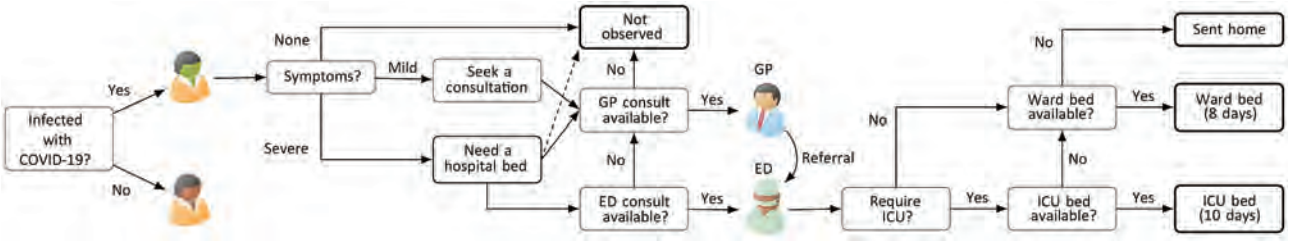

Figure 1. Clinical pathways model for used to assess national health system capacity for managing COVID-19 patients, Australia. The diagram demonstrates clinical pathways for mild and severe illness and assumes minor cases are managed within primary care. Unobserved patients are those who do not seek or are unable to access healthcare services. COVID-19, coronavirus disease; ED, emergency department; GP, general practitioner; ICU, intensive care unit.

uninfected and return to their original noncontact status ≤72 hours. We assumed that 80% of identified contacts adhered to quarantine measures and that the overall infectiousness of truly exposed and infected contacts was halved by quarantine, given delayed and imperfect contact tracing and the risk for transmission to household members.

Clinical Pathways Model

At baseline of our clinical pathways model, we assume that half of available consulting and admission capacity across all healthcare sectors and services is available to COVID-19 patients. Mild cases are seen at primary care until capacity is exceeded. Severe cases access the hospital system through an ED and are triaged to a ward or ICU bed, if available, according to need. Requirements for critical care are assumed to increase steeply with age with the consequence that ≥60% of all infections requiring ICU admission occur in persons ≥70 years of age (Table 2). As ward beds reach capacity, the ability of EDs to adequately assess patients is reduced because of bed block, meaning that not all patients who need care are medically assessed, although some will still be able to access primary care. We assume that secondary infections are not affected by a person's access to clinical care. The model allows for repeat patient visits within and between primary care and hospital services, and progression from ward to intensive care, with length of stay (Figure 1; Table 2). The model structure and assumptions are based on publicly

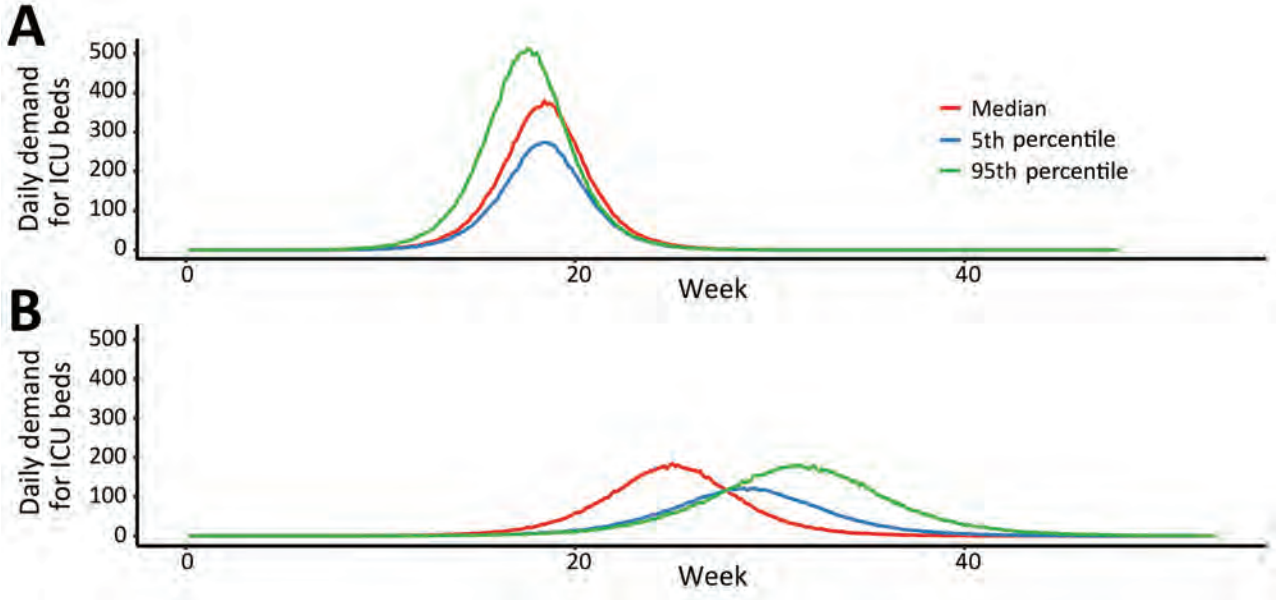

Figure 2. Estimated daily incidence of ICU admission demand per 1 million population during coronavirus disease (COVID-19) epidemic across all age groups, Australia. A) Demand during an unmitigated COVID-19 epidemic. B) COVID-19 epidemic mitigated by case-targeted public health measures. Lines represent single simulations based on median (red), 5th percentile (blue), or 95th percentile (green) final epidemic size. Of note, the more severe epidemic is more delayed by public health interventions due to a higher case proportion seeking medical attention. In a milder event, persons with non–medical seeking cases will continue to transmit in the community. This finding is contingent on the public health response capacity. ICU, intensive care unit.

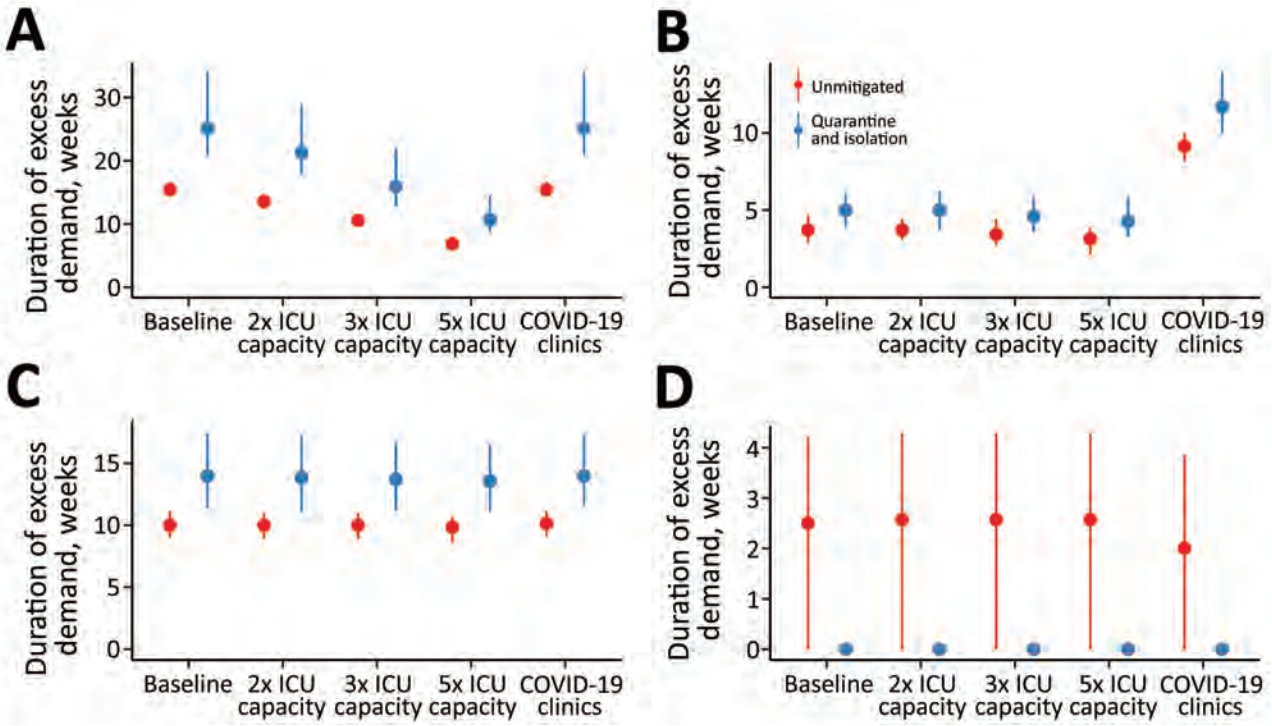

Figure 3. Estimated duration of excess demand for healthcare sector services during COVID-19 epidemic, Australia. The graphs compare exceedance for COVID-19 admissions for A) ICU beds; B) hospital ward beds; C) emergency departments; and D) general practitioner services at baseline, 2×, 3×, and 5× ICU capacity. The COVID-19 clinics scenario reflects an alternative triage pathway and baseline capacity. Red denotes unmitigated scenarios with no public health interventions in place; blue denotes the mitigated scenarios with quarantine and isolation in place. Dots denote the median; lines range from 5th–95th percentiles of simulations. COVID-19, coronavirus disease; ICU, intensive care unit.

available data on the healthcare system of Australia and expert elicitation (Appendix).

Critical Care Capacity Expansion

The baseline assumption in our model was that half of currently available ICU beds would be available to COVID-19 patients. We considered 3 capacity expansion scenarios, assuming routine models of care for patient triage and assessment within the hospital system: total ICU capacity expansion to 150% of baseline, doubling the number of beds available to treat COVID-19 patients (2× ICU capacity); total ICU capacity expansion to 200% of baseline, tripling the number of beds available to treat COVID-19 patients (3× ICU capacity); or total ICU capacity expansion to 300% of baseline, increasing by 5-fold the number of beds available to treat COVID-19 patients (5× ICU capacity).

We also considered a theoretical alternative clinical pathway, COVID-19 clinics, which had constraints on bed numbers but double the capacity to assess severe cases in hospitals. The purpose of including this pathway was to reveal unmet clinical needs arising when bed block constrains ED triage capacity, potentially preventing needed admissions to the ICU.

Social Distancing Interventions

Broad -based social distancing measures overcome ongoing opportunities for transmission arising from imperfect ascertainment of all cases and contacts, and from presymptomatic and asymptomatic persons. In settings where nonpharmaceutical social interventions have been applied, associated case-targeted measures also have been in place, making the effectiveness of each difficult to quantify (*19*). Data from Hong Kong showing a reduction in influenza incidence arising from a combination of distancing measures introduced in response to COVID-19 provides good evidence of generalized transmission reduction (*20*). However, the relative quantitative contributions of different interventions, such as canceling mass gatherings, working remotely, closing schools, and ceasing nonessential services, cannot be differentiated reliably at this time (*18*).

Therefore, we focused on the overall objective of distancing, which is to reduce the reproduction number. We modeled the effect of constraining spread by 25% and 33%, overlaid on existing case-targeted interventions, which is consistent with observed impacts of combined measures less restrictive than

total lockdown (*18*). These reductions in transmission equated to input reproduction numbers of 1.90 at 25% and 1.69 at 33%; the effective reproduction number in each scenario further was reduced by quarantine and isolation measures, which limit spread of established infection.

Results

According to our model, an unmitigated COVID-19 epidemic would dramatically exceed the capacity of the health system of Australia over a prolonged period (Figure 2). Case isolation and contact quarantine applied at the same level of effective coverage throughout the epidemic have the potential to substantially reduce transmission. By flattening the curve, these measures produce a prolonged epidemic with lower peak incidence and fewer overall infections (Figure 2). Epidemic scenarios with higher assumed severity, such as a 95th percentile case, are more effectively delayed by these public health measures than less severe scenarios, such as a 50th percentile case, because a higher proportion of all cases are seen by health services and can be identified for isolation and contact tracing. In a mitigated epidemic, overall use of the health system is increased because more patients are able to access needed care over the extended epidemic duration (Appendix Figure 3, panel A).

Increasing the number of ICU beds available to patients with COVID-19 reduces the time over which ICU capacity is anticipated to be exceeded, potentially by more than half (Figure 3). The duration of exceedance for each capacity scenario is increased by quarantine and isolation because the overall epidemic is longer (Figure 3). During the period of exceedance, a degree of unmet need remains, even for the mitigated scenario (Figure 4). A 5-fold increase in the number of ICU beds available to patients with COVID-19 dramatically reduces the period and peak of excess demand (Figures 3, 4).

These figures do not accurately reflect the true requirement for services, however, because blocks in assessment pathways resulting from ED and ward overload are an upstream constraint on incident ICU admissions. The alternative triage scenario, the COVID-19 clinic, reveals a high level of unmet clinical need for both ward and critical care beds given baseline bed capacity (Figures 3, 4). Case-targeted measures overcame this limitation, to some extent, and

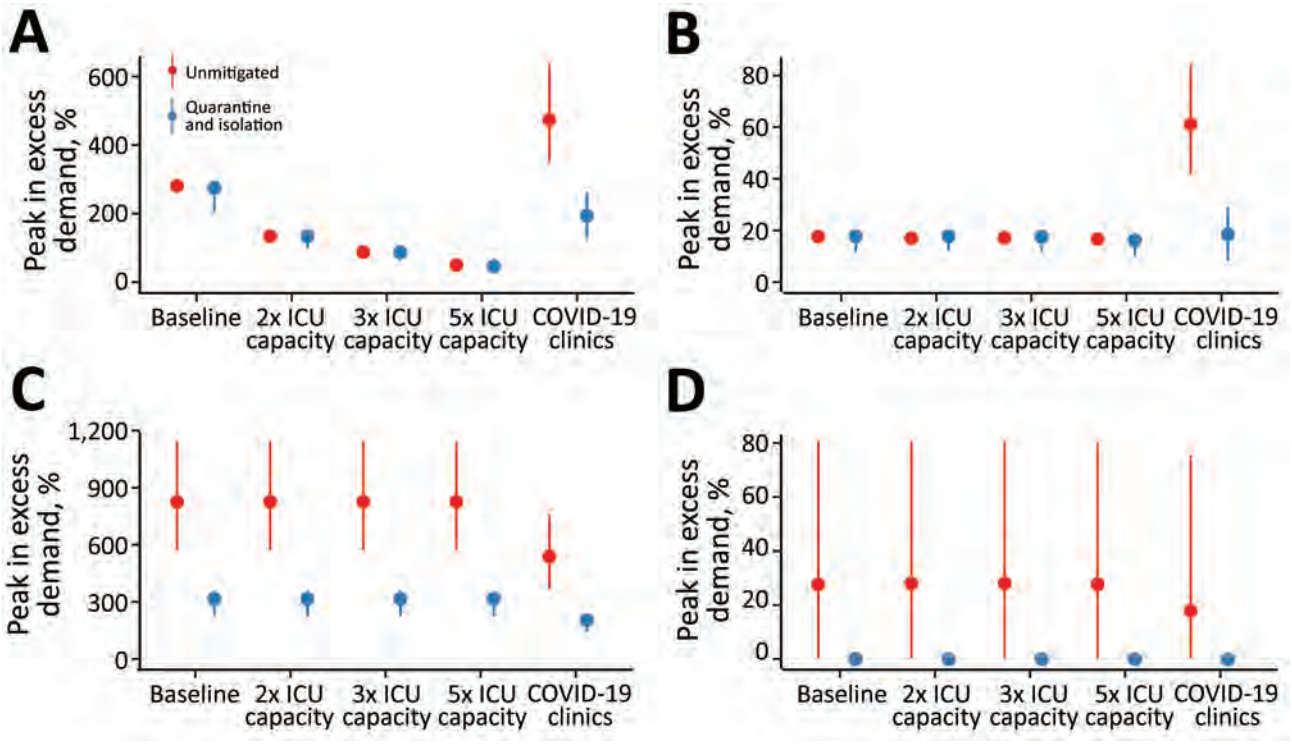

Figure 4. Estimated peak excess demand for healthcare sector services, by percentage, during the COVID-19 epidemic, Australia. The graphs compare exceedance for COVID-19 admissions for A) ICU beds; B) hospital ward beds; C) emergency departments; and D) general practitioner services at baseline, 2×, 3×, and 5× ICU capacity. The COVID-19 clinics scenario reflects an alternative triage pathway and baseline capacity. Red denotes unmitigated scenarios with no public health interventions in place; blue denotes the mitigated scenarios with quarantine and isolation in place. Dots denote the median; lines range from 5th–95th percentiles of simulations. COVID-19, coronavirus disease; ICU, intensive care unit.

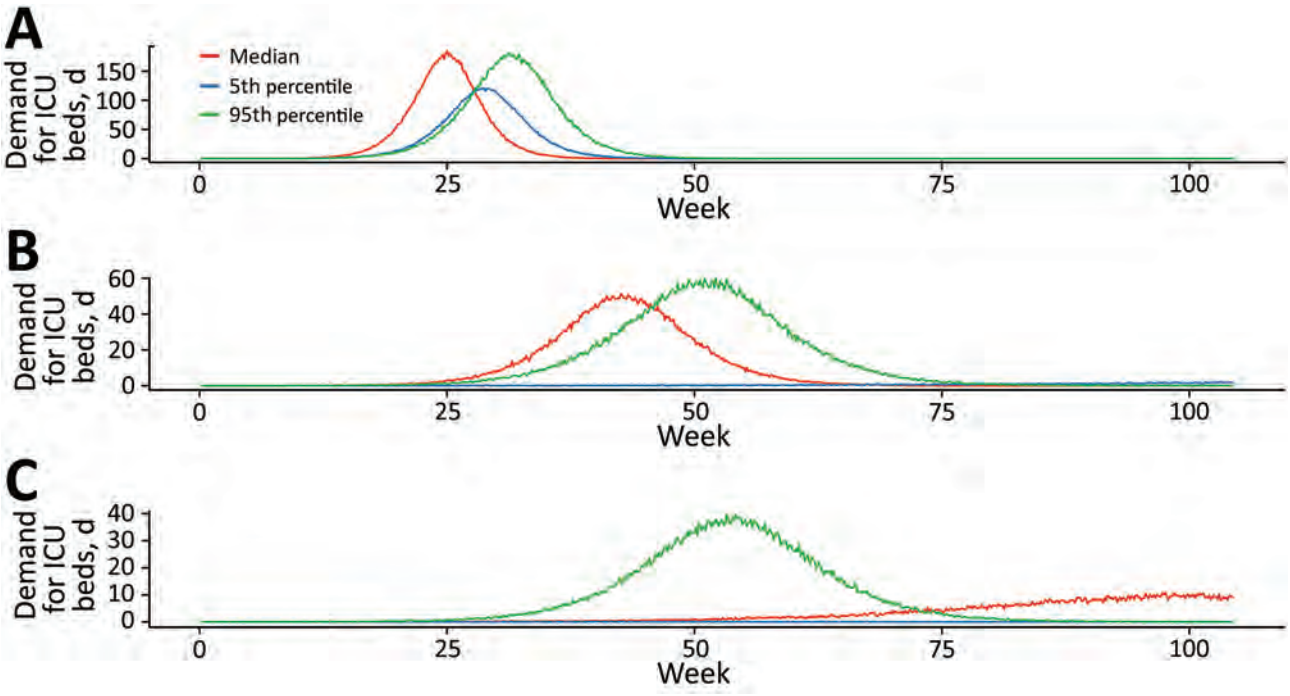

Figure 5. Estimated daily incident ICU admission demand per million population during coronavirus disease (COVID-19) epidemic, Australia. Comparison of mitigation achieved by A) quarantine and isolation alone; B) a further 25% mitigation due to social distancing; and C) a 33% mitigation. Lines represent single simulations based on median (red), 5th percentile (blue), or 95th percentile (green) parameter assumptions. ICU, intensive care unit.

effectively improved overall access to care (Figures 3, 4). Overall, if ICU beds available to COVID-19 patients are doubled, 10%–30% of those who require critical care receive it. The proportion rises to ≥20%–40% if capacity increases by 5-fold (Appendix Figure 3). These figures are quantified as total excess demand per million over the course of the epidemic (Appendix Figure 4).

Our simulated scenarios show that case isolation and contact quarantine alone will be insufficient to keep clinical requirements of COVID-19 cases within plausibly achievable expansion of health system capacity, even if very high and likely unrealistic levels of case finding can be maintained. We therefore explored the effects of additional social distancing measures that reduced input reproduction numbers by 25% and 33% on ICU requirements in relation to the same clinical care capacity constraints (Figure 5). Simulations assume ongoing application of measures of fixed effectiveness, which is also unlikely to be consistently achievable over an extended duration.

The overlay of distancing measures, applied from the initial stages of the epidemic and maintained throughout, suppresses epidemic growth to a level that is within the range of plausible ICU capacity expansion. The duration of ICU exceedance remains long in the 25% case (Figure 6), but this overflow occurs to a far lesser degree than following case-targeted strategies only (Figure 7). As anticipated, a 33% reduction in transmission achieves greater benefits. Of note, pressure on ED consultations and ward beds also is eased substantially in these scenarios, maintaining capacity along the full pathway of care. As a result, the proportion of critical cases that can access care is greatly increased. Transmission reduction of 33% makes treatment for all cases achievable in most simulations if 3- to 5-fold ICU bed capacity can be achieved (Appendix Figure 3, panel B). This improvement is reflected in a large reduction in unmet need (Appendix Figure 4, panel B).

Discussion

This modeling study shows that an unmitigated COVID-19 epidemic would rapidly overwhelm Australia's health sector capacity. Case-targeted measures including isolation of those known to be infected, and quarantine of their close contacts, must remain an ongoing cornerstone of the public health response. These interventions effectively reduce transmission but are unlikely to be maintained throughout the epidemic course at the high coverage modeled here. As public health response capacity is exceeded, greater constraint of disease spread will be essential to ensure that feasible levels of expansion in available health-

care can maintain ongoing system functions, including care of COVID-19 patients. Broader based social and physical distancing measures reduce the number of potential contacts made by each case, minimizing public health workload and supporting sustainable case-targeted disease control efforts.

Our findings are consistent with a recently published model (*21*) that relates the clinical burden of COVID-19 cases to global health sector capacity, characterized at a high level. In unmitigated epidemics, demand rapidly outstrips supply, even in high-income settings, by a factor of 7 (*21*). Because hospital bed capacity is strongly correlated with income, this factor is greatly increased in low- and middle-income countries where underlying health status likely is poorer (*21*). Globally, marked variability in the definition of intensive care is observed, even in high-income countries where the descriptor covers many levels of ventilatory and other support. We concur with our conclusion that social distancing measures to suppress disease are required to save lives. In addition, we acknowledge that the marked social and economic consequences of such measures will limit their ongoing application, particularly in the settings where health systems are least able to cope with disease burden (*21*).

Much attention has been focused on expansion of available ICU beds per se, but our clinical model reveals that critical care admissions are further limited by the ability to adequately assess patients during times of system stress. In line with model recommendations, Australia, along with other countries, has implemented COVID-19 clinics as an initial assessment pathway to reduce impacts on primary care and ED services (*22*). Such facilities have additional benefits of ensuring appropriate testing, aligning local case definitions, and reducing the overall consumption of personal protective equipment by cohorting likely infectious patients. Evidence of bottlenecks as the epidemic progresses indicates that other measures to improve patient flows also should be considered, such as overflow expansion in EDs, encouraging and supporting home-based care, or early discharge to supported isolation facilities.

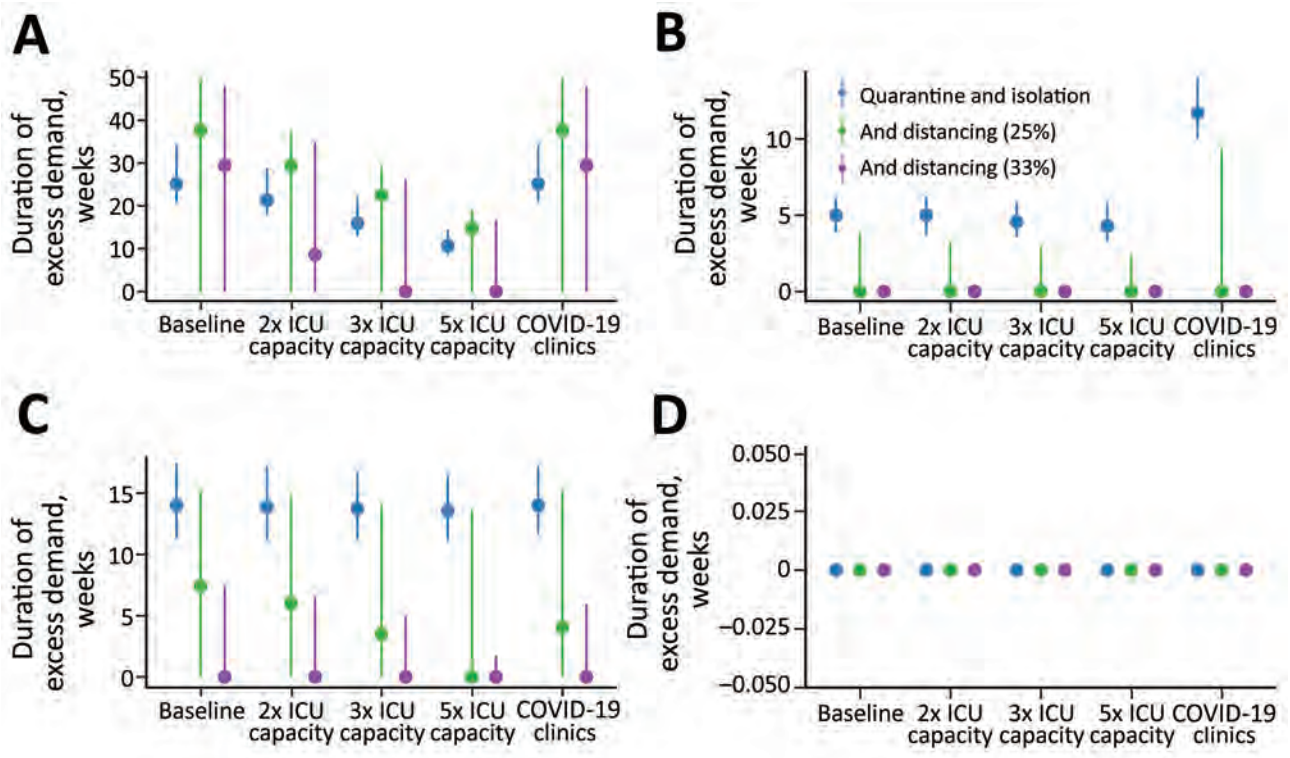

Figure 6. Estimated duration of excess demand for healthcare sector services compared with quarantine and isolation scenarios during the COVID-19 epidemic, Australia. The graphs compare exceedance for COVID-19 admissions for A) ICU beds; B) hospital ward beds; C) emergency departments; and D) general practitioner services at baseline, 2×, 3×, and 5× ICU capacity. Blue lines indicate quarantine and isolation only scenarios; green lines indicate overlaid social distancing measures that reduce transmission by an additional 25%; and purple lines indicate overlaid social distancing measures that reduce transmission by an additional 33%. The COVID-19 clinics scenario reflects an alternative triage pathway, and baseline capacity. Dots denote the median; lines range from 5th–95th percentiles of simulations. COVID-19, coronavirus disease; ICU, intensive care unit.

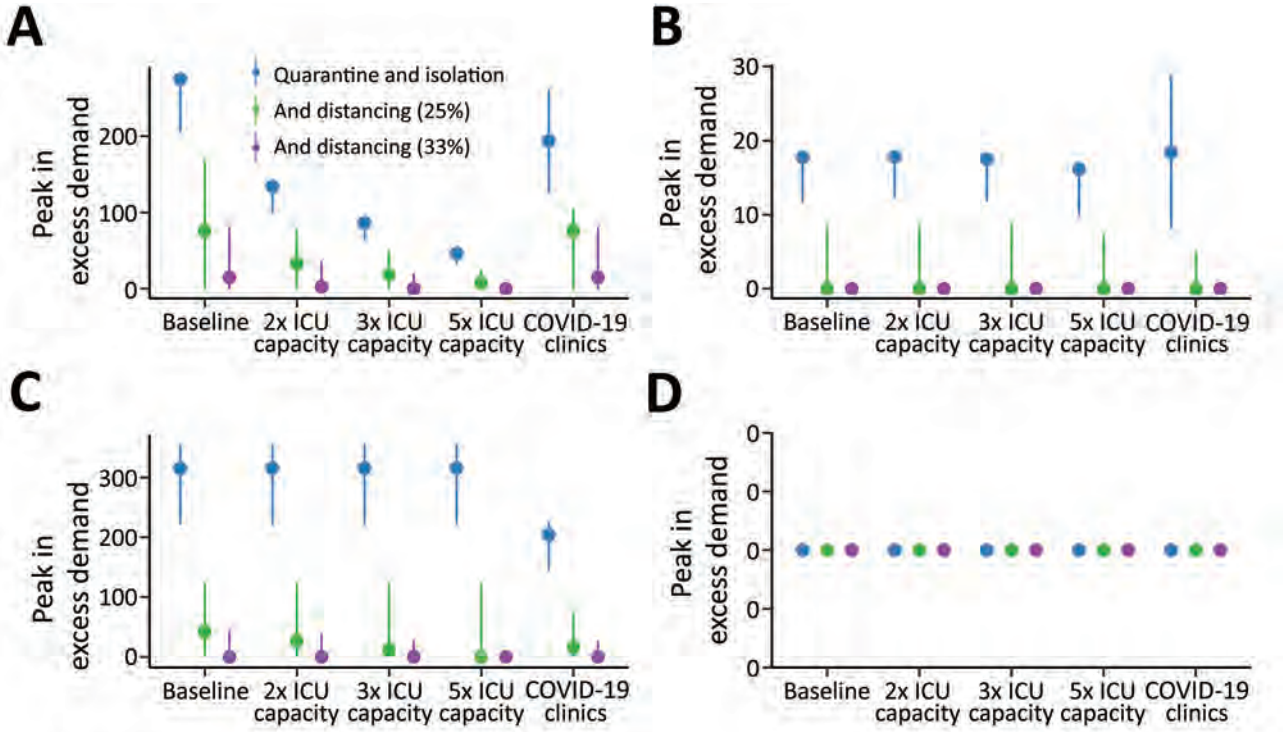

Figure 7. Estimated peak excess demand for healthcare sector services, expressed as percent available capacity, compared with quarantine and isolation scenarios during the COVID-19 epidemic, Australia. The graphs compare exceedance for COVID-19 admissions for A) ICU beds; B) hospital ward beds; C) emergency departments; and D) general practitioner services at baseline, 2×, 3×, and 5× ICU capacity. Blue lines indicate quarantine and isolation only scenarios; green lines indicate overlaid social distancing measures that reduce transmission by an additional 25%; and purple lines indicate overlaid social distancing measures that reduce transmission by an additional 33%. The COVID-19 clinics scenario reflects an alternative triage pathway, and baseline capacity. Dots denote the median; lines range from 5th–95th percentiles of simulations. COVID-19, coronavirus disease; ICU, intensive care unit.

Quantitative findings from our model are limited by ongoing uncertainties about the true disease pyramid for COVID-19 and a lack of nuanced information about determinants of severe disease, which we represented by age as a best proxy. The clinical pathways model assumes that half of available bed capacity is available for patients with the disease but does not anticipate the seasonal surge in influenza admissions that might be overlaid with the epidemic peak, although even in our most recent severe season, 2017, only 6% of hospital beds were occupied by influenza cases (*23*). Available beds will likely be increased by other factors, such as secondary reductions in all respiratory infections and road trauma resulting from social restrictions, and purposive decisions to cancel nonessential surgery. Of note, we did not consider healthcare worker absenteeism due to illness, caregiving responsibilities, or burnout, all of which are anticipated challenges over a very prolonged epidemic accompanied by marked social disruption. We also cannot account for shortages in critical medical supplies because the true extent of these and their likely future impacts on service provision are currently unknown.

Our model indicates that a combination of case-targeted and social measures will need to be applied over an extended period to reduce the rate of epidemic growth. In reality, the stringency of imposed controls, their public acceptability, and compliance, likely will all vary over time. In Australia, compliance with isolation and self-quarantining was largely on the basis of trust in the early response during February–March, but active monitoring and enforcement of these public health measures is now occurring in many jurisdictions. Hong Kong and Singapore initiated electronic monitoring technologies from the outset to track the location of persons and enforce compliance (*24*). Proxy indicators of compliance, such as transport and mobile phone data, have informed understanding of the effect of social and movement restrictions on mobility and behavior in other settings (*19*), and will be further investigated in the context of Australia.

The effectiveness of multiple distancing measures, including lockdown, has been demonstrated in Europe, but the contributions of individual measures cannot yet be reliably differentiated (*18*). The

effect of local measures to curb transmission will be estimated from real time data on epidemic growth in Australia, on the basis of multiple epidemiologic and clinical data streams. Estimates of the local effective reproduction number will enable forecasting of epidemic trajectories (*25*) to be fed into our analysis pathway. Anticipated case numbers will be used to assess the ability to remain within health system capacity represented by the clinical pathways model, given current levels of social intervention. Such evidence will support strengthening and, when appropriate, cautious relaxation of distancing measures. Further work will examine the effects of varying the intensity of measures over time, to inform the necessary conditions that would enable exit strategies from current stringent lockdown conditions to ensure maintenance of social and economic functioning over an extended time.

All these strategies, which combine to flatten the curve, will buy time for further health system strengthening and sourcing of needed supplies. Protecting the health and wellbeing of healthcare workers will be essential to ensure ongoing service provision. ICU capacity will need to be increased several-fold in anticipation of the looming rise in cases.

Multiple challenges must be overcome along the path to delivering safe and effective COVID-19 vaccines, and the timeframe for availability is highly uncertain (*26*). The search for effective therapies continues. Therefore, reducing COVID-19 illness and death relies on broadly applied public health measures to interrupt overall transmission, protect vulnerable groups, and maintain and strengthen the capacity of healthcare systems and workers to manage cases.

This work was directly funded by the Australian Government Department of Health. R.M. is supported by 2 National Health and Medical Research Council (NHMRC) Centres of Research Excellence, the Australian Partnership for Preparedness Research on Infectious Disease Emergencies (APPRISE; grant no. GNT1116530), and Supporting Participatory Evidence use for the Control of Transmissible Diseases in our Region Using Modelling (SPECTRUM; grant no. GNT1170960). J.M. is supported by a NHMRC Principal Research Fellowship (grant no. GNT1117140).

About the Author

Dr. Moss is a senior research fellow at the Melbourne School of Population and Global Health, The University of Melbourne. His research interests include near–real-time forecasting of epidemics and informing recommendations to reduce the burden and impact of infectious diseases.

References

1. World Health Organization. Coronavirus disease (COVID-2019) weekly epidemiological update 21 Sep 2020 [cited 24 Sep 2020]. https://www.who.int/docs/default-source/coronaviruse/situation-reports/20200921-weekly-epi-update-6.pdf
2. Wu Z, McGoogan JM. Characteristics of and important lessons from the coronavirus disease 2019 (COVID-19) outbreak in China: summary of a report of 72,314 cases from the Chinese Center for Disease Control and Prevention. JAMA. 2020;323:1239. https://doi.org/10.1001/jama.2020.2648
3. Chen N, Zhou M, Dong X, Qu J, Gong F, Han Y, et al. Epidemiological and clinical characteristics of 99 cases of 2019 novel coronavirus pneumonia in Wuhan, China: a descriptive study. Lancet. 2020;395:507–13. https://doi.org/10.1016/S0140-6736(20)30211-7
4. Remuzzi A, Remuzzi G. COVID-19 and Italy: what next? Lancet. 2020;395:1225–8. https://doi.org/10.1016/S0140-6736(20)30627-9
5. Emanuel EJ, Persad G, Upshur R, Thome B, Parker M, Glickman A, et al. Fair Allocation of Scarce Medical Resources in the Time of Covid-19. N Engl J Med. 2020;382:2049–55. https://doi.org/10.1056/NEJMsb2005114
6. Australian Government Department of Health. Australian health management plan for pandemic influenza, 2019 [cited 2020 May 24]. https://www1.health.gov.au/internet/main/publishing.nsf/Content/ohp-ahmppi.htm
7. Australian Government Department of Health. Australian health sector emergency response plan for novel coronavirus (COVID-19), 2020 [cited 2020 May 24]. https://www.health.gov.au/resources/publications/australian-health-sector-emergency-response-plan-for-novel-coronavirus-covid-19
8. McCaw JM, Glass K, Mercer GN, McVernon J. Pandemic controllability: a concept to guide a proportionate and flexible operational response to future influenza pandemics. J Public Health (Oxf). 2014;36:5–12. https://doi.org/10.1093/pubmed/fdt058
9. Australian Government Department of Health. Coronavirus (COVID-19) current situation and case numbers [cited 2020 Apr 14]. https://www.health.gov.au/news/health-alerts/novel-coronavirus-2019-ncov-health-alert/coronavirus-covid-19-current-situation-and-case-numbers
10. Moss R, McCaw JM, Cheng AC, Hurt AC, McVernon J. Reducing disease burden in an influenza pandemic by targeted delivery of neuraminidase inhibitors: mathematical models in the Australian context. BMC Infect Dis. 2016;16:552. https://doi.org/10.1186/s12879-016-1866-7
11. Wu JT, Leung K, Leung GM. Nowcasting and forecasting the potential domestic and international spread of the 2019-nCoV outbreak originating in Wuhan, China: a modelling study. Lancet. 2020;395:689–97. https://doi.org/10.1016/S0140-6736(20)30260-9
12. Li Q, Guan X, Wu P, Wang X, Zhou L, Tong Y, et al. Early transmission dynamics in Wuhan, China, of novel coronavirus-infected pneumonia. N Engl J Med. 2020;382:1199–207. https://doi.org/10.1056/NEJMoa2001316
13. Lauer SA, Grantz KH, Bi Q, Jones FK, Zheng Q, Meredith HR, et al. The incubation period of coronavirus disease 2019 (COVID-19) from publicly reported confirmed cases: estimation and application. Ann Intern Med. 2020;172:577–82. https://doi.org/10.7326/M20-0504
14. Ganyani T, Kremer C, Chen D, Torneri A, Faes C, Wallinga J, et al. Estimating the generation interval for COVID-19 based on symptom onset data. Euro Surveill. 2020;25:2000257. https://doi.org/10.2807/1560-7917.ES.2020.25.17.2000257

15. Tindale L, Coombe M, Stockdale J, Garlock E, Lau W, Saraswat M, et al. Transmission interval estimates suggest pre-symptomatic spread of COVID-19. Elife. 2020;9:e57149. https://doi.org/10.7554/eLife.57149
16. Intensive Care National Audit and Research Centre. INRC Case Mix Programme Database, Report on 775 patients critically ill with COVID-19. 2020 Mar 27 [cited 2020 Apr 14]. https://www.icnarc.org/About/Latest-News/2020/03/27/Report-On-775-Patients-Critically-Ill-With-Covid-19
17. COVID-19 Task Force of the Department of Infectious Diseases and Computer Service, Higher Institute of Health, Italy. Epidemiology of COVID-19, 2020 Mar 26 [in Italian] [cited 2020 Apr 14]. https://www.carditalia.com/epidemia-covid-19-aggiornamento-nazionale-iss-26-marzo-2020
18. Ferguson N, Laydon D, Nedjati-Gilani G, Imai N, Ainslie K, Baguelin M, et al.; Imperial College COVID-19 Response Team. Report 9: impact of non-pharmaceutical interventions (NPIs) to reduce COVID-19 mortality and healthcare demand. Imperial College London; 2020 Mar 16. https://doi.org/10.25561/77482
19. Lai S, Ruktanonchai N, Zhou L, Prosper O, Luo W, Floyd J, et al. Effect of non-pharmaceutical interventions for containing the COVID-19 outbreak. Nature. 2020;585:410–3. https://doi.org/10.1038/s41586-020-2293-x
20. Cowling B, Ali S, Ng T, Tsang T, Li J, Fong M, et al. Impact assessment of non-pharmaceutical interventions against COVID-19 and influenza in Hong Kong: an observational study. Lancet Public Health. 2020;5:e279–88. https://doi.org/10.1016/S2468-2667(20)30090-6
21. Walker P, Whittaker C, Watson O, Baguelin M, Ainslie K, Bhatia S, et al.; WHO Collaborating Centre for Infectious Disease Modelling, MRC Centre for Global Infectious Disease Analysis, Abdul Latif Jameel Institute for Disease and Emergency Analytics. The global impact of COVID-19 and strategies for mitigation and suppression. Imperial College London; 2020 Mar 26. https://doi.org/10.25561/77735
22. Zhang J, Zhou L, Yang Y, Peng W, Wang W, Chen X. Therapeutic and triage strategies for 2019 novel coronavirus disease in fever clinics. Lancet Respir Med. 2020;8:e11–2. https://doi.org/10.1016/S2213-2600(20)30071-0
23. Cheng AC, Holmes M, Dwyer DE, Senanayake S, Cooley L, Irving LB, et al. Influenza epidemiology in patients admitted to sentinel Australian hospitals in 2017: the Influenza Complications Alert Network (FluCAN). Commun Dis Intell. 2018;2019:43. https://doi.org/10.33321/cdi.2019.43.39
24. Legido-Quigley H, Asgari N, Teo YY, Leung GM, Oshitani H, Fukuda K, et al. Are high-performing health systems resilient against the COVID-19 epidemic? Lancet. 2020;395:848–50. https://doi.org/10.1016/S0140-6736(20)30551-1
25. Moss R, Fielding JE, Franklin LJ, Stephens N, McVernon J, Dawson P, et al. Epidemic forecasts as a tool for public health: interpretation and (re)calibration. Aust N Z J Public Health. 2018;42:69–76. https://doi.org/10.1111/1753-6405.12750
26. Lurie N, Saville M, Hatchett R, Halton J. Developing Covid-19 vaccines at pandemic speed. N Engl J Med. 2020;382:1969–73. https://doi.org/10.1056/NEJMp2005630

Address for correspondence: Jodie McVernon, Professor and Director of Doherty Epidemiology, Victorian Infectious Diseases Laboratory Epidemiology Unit at The Peter Doherty Institute for Infection and Immunity, The University of Melbourne and Royal Melbourne Hospital, 792 Elizabeth St, Melbourne, VIC 3000, Australia; email: j.mcvernon@unimelb.edu.au

Genomic Epidemiology of Severe Acute Respiratory Syndrome Coronavirus 2, Colombia

Katherine Laiton-Donato, Christian Julián Villabona-Arenas, José A. Usme-Ciro, Carlos Franco-Muñoz, Diego A. Álvarez-Díaz, Liz Stephany Villabona-Arenas, Susy Echeverría-Londoño, Zulma M. Cucunubá, Nicolás D. Franco-Sierra, Astrid C. Flórez, Carolina Ferro, Nadim J. Ajami, Diana Marcela Walteros, Franklin Prieto, Carlos Andrés Durán, Martha Lucia Ospina-Martínez, Marcela Mercado-Reyes

Coronavirus disease (COVID-19) in Colombia was first diagnosed in a traveler arriving from Italy on February 26, 2020. However, limited data are available on the origins and number of introductions of COVID-19 into the country. We sequenced the causative agent of COVID-19, severe acute respiratory syndrome coronavirus 2 (SARS-CoV-2), from 43 clinical samples we collected, along with another 79 genome sequences available from Colombia. We investigated the emergence and importation routes for SARS-CoV-2 into Colombia by using epidemiologic, historical air travel, and phylogenetic observations. Our study provides evidence of multiple introductions, mostly from Europe, and documents ≥12 lineages. Phylogenetic findings validate the lineage diversity, support multiple importation events, and demonstrate the evolutionary relationship of epidemiologically linked transmission chains. Our results reconstruct the early evolutionary history of SARS-CoV-2 in Colombia and highlight the advantages of genome sequencing to complement COVID-19 outbreak investigations.

Coronavirus disease (COVID-19) is a life-threatening respiratory illness caused by severe acute respiratory syndrome coronavirus 2 (SARS-CoV-2), an emerging zoonotic virus first identified in Wuhan, China (*1*). The first confirmed cases of COVID-19 were reported on January 12, 2020, from patients who had respiratory symptoms during December 8, 2019–January 2, 2020 (*2*). Despite early containment and mitigation measures (*3*), the high infectiousness, presymptomatic transmission, and prolonged transmissibility of SARS-CoV-2 (*4*,*5*) combined with other factors, such as globalization, led to the rapid spread of COVID-19 across the world.

Rigorous contact-tracing and physical distancing measures implemented in different countries have been effective in delaying the epidemic during the contention phase (*6*–*9*). However, ensuing lockdowns and travel restrictions to minimize the burden on healthcare systems have led to a decline in wellbeing and an economic downturn and have had profound impacts in low-to-middle income countries (*10*). The contention phase in Colombia started on March 6, 2020, when the Instituto Nacional de Salud (INS; National Institute of Health) confirmed the first case of COVID-19 from a person returning to Colombia from Italy on February 26, 2020 (*11*). On March 23, a total 314 cases had been confirmed, which prompted the closure of all the country borders to contain the outbreak. On March 31, ≥10% of confirmed cases were among persons with no known exposure to a COVID-19 patient (*12*), presumably due to extensive community transmission. Colombia then implemented the mitigation phase, which included physical distancing as the main strategy to limit virus spread. By June 18, a total of 57,046 confirmed cases and 1,864 deaths had been reported in Colombia (*13*).

The unprecedented global health and societal emergency posed by the COVID-19 pandemic urged data sharing and faster-than-ever outbreak research developments that are reflected in the >37,000 complete SARS-CoV-2 genomes made available through

Author affiliations: Instituto Nacional de Salud, Bogotá, Colombia (K. Laiton-Donato, J.A. Usme-Ciro, C. Franco-Muñoz, D.A. Álvarez-Díaz, A.C. Flórez, C. Ferro, D.M. Walteros, F. Prieto, C.A. Durán, M.L. Ospina-Martínez, M. Mercado-Reyes); Centre for the Mathematical Modelling of Infectious Diseases (CMMID) and London School of Hygiene & Tropical Medicine, London, UK (C.J. Villabona-Arenas); Universidad Cooperativa de Colombia, Santa Marta, Colombia (J.A. Usme-Ciro); Universidad Industrial de Santander, Bucaramanga, Colombia (L.S. Villabona-Arenas); Imperial College-London, London, UK (S. Echeverría-Londoño, Z.M. Cucunubá); Instituto de Investigación de Recursos Biológicos Alexander von Humboldt, Colombia (N. Franco-Sierra); Baylor College of Medicine, Houston, Texas, USA (N.J. Ajami)

DOI: https://doi.org/10.3201/eid2612.202969

public databases, mainly GISAID (https://www.gisaid.org). SARS-CoV-2 is an RNA virus with an estimated substitution rate of 0.8–1.1 × 10^{-3} substitutions/site/year (S. Duchene et al., unpub data, https://www.biorxiv.org/content/10.1101/2020.05.04.077735v1; M. Worobey et al., unpub. data, https://www.biorxiv.org/content/10.1101/2020.05.21.109322v1), which means it rapidly evolves as it is transmitted. The availability of SARS-CoV-2 genomes enabled us to detect a rapidly generating variation, demonstrating that genomic epidemiology is a powerful approach for characterizing the outbreak (*14*). Genomic epidemiology relies on phylogenetic analysis and has enabled researchers across the world to detect SARS-CoV-2 emergence in humans, reveal the importation and local transmission chains not detected by travel history and traditional contact-tracing strategies, and trace the geographic spread and prevalence of strains bearing specific mutations of epidemiologic relevance (*15*–*17*; S. Dellicour et al, unpub data, https://www.biorxiv.org/content/10.1101/2020.05.05.078758v4; J.R. Fauver et al., unpub data, https://www.medrxiv.org/content/10.1101/2020.03.25.20043828v1).

Materials and Methods

Sample Collection and Preparation

Colombia is made up of 32 departments, which are groups of municipalities, and a capital district. INS received nasopharyngeal swabs samples from patients with clinical signs and symptoms of SARS-CoV-2 from departments across the country as part of the virological surveillance of COVID-19. INS performed quantitative reverse transcription PCR to diagnose suspected COVID-19 cases by using a method recommended and transferred by the Pan American Health Organization and World Health Organization (*18*). Because of scarce resources, we selected a total of 43 samples for genome sequencing that represented ≥1 of the earliest documented samples in each affected department or samples linked to transmission chains (Appendix 1 Table 1, https://wwwnc.cdc.gov/EID/article/26/12/20-2969-App1.xlsx). We performed viral RNA extraction by using the QIAamp Viral RNA Mini Kit (QIAGEN Inc., https://www.qiagen.com) or the MagNA Pure LC nucleic acid extraction system (Roche Diagnostics GmbH, https://lifescience.roche.com).

Genomic Library Preparation and Sequencing

Library preparation and sequencing were performed following the ARTIC network (https://artic.network) real-time molecular epidemiology for outbreak response protocol and by using both nanopore and next-generation sequencing technologies (*19*). We processed 10 samples by using the MinION sequencer (Oxford Nanopore Technologies, https://nanoporetech.com). We processed the remaining 33 samples by using the Nextera XT DNA library prep kit (Illumina, https://www.illumina.com) and performed sequencing by using the MiSeq Reagent Kit Version 2 and MiSeq sequencer (Illumina).

Genomic Sequence Assembly

We performed base calling on nanopore reads by using Guppy version 3.2.2 (Oxford Nanopore Technologies) and then demultiplexed and trimmed reads by using Porechop version 0.3.2_pre (*20*). We aligned processed reads against a SARS-CoV-2 reference genome (GenBank reference no. NC_045512.2) by using Burrows-Wheeler Aligner's Smith-Waterman Alignment (*21*). We performed base calling for single-nucleotide variants with a depth of ≥200× and then generated polished consensus by using Nanopolish version 0.13.2 (*22*). MiSeq reads were demultiplexed and we used fastp (*23*) to perform quality control using a Q-score threshold of 30. Processed reads were aligned against the SARS-CoV-2 reference genome, we performed bas calling for single nucleotide variants with a depth of ≥100× and generated consensus genomes by using Burrows-Wheeler Aligner's Smith-Waterman Alignment version 0.7.17 (*21*) and BBMap (*24*).

Phylogenetic Analysis of SARS-CoV-2 in Colombia

Sequence data covered the 20 affected departments and the capital district of Colombia. We collected 43 SARS-CoV-2 genome sequences from this study and 79 other sequences from Colombia deposited in GISAID. We combined the 122 sequences from Colombia with 1,461 representative genome sequences from South America–focused subsampling available from NextStrain (https://nextstrain.org) (*25*) as of May 20, 2020 (Appendix 1 Table 2) plus reference MN908947.3 from the GenBank nucleotide database (accesssion no. NC_045512). Across departments, a median of 1.5 sequences (mean 3.9; range 1–45) were available per department. We classified the full genomic dataset into lineages by using Phylogenetic Assignment of Named Global Outbreak LINeages (PANGOLIN) and aligned these with 10 iterative refinements by using MAFFT (*26*–*28*). We removed all alignment positions flagged as problematic for phylogenetic inference, including highly homoplasic positions and 3′ and 5′ ends (*29*). We performed maximum-likelihood phylogenetic reconstruction

on the curated alignment and a Hasegawa-Kishino-Yano plus gamma distribution 4 substitution model by using IQ-TREE (*30*,*31*). We estimated branch support by using an SH-like approximate likelihood ratio test (SH-aLRT) and considered ≥0.75 a high SH-aLRT (*32*). We removed 6 sequences from Colombia from further analysis because they had an inconsistent temporal signal in a clock analysis in TreeTime (*33*). We inferred time-scaled trees and rooted these with least-squares criteria and the evolutionary rate of $\geq 1.1 \times 10^{-3}$ substitutions/site/year estimated by S. Duchene et al. (unpub data, https://www.biorxiv.org/content/10.1101/2020.05.04.077735v1) by using TreeTime (*33*) and least-squares dating (*34*).

We considered geographic locations of sequence data, aggregated by continent except for Colombia, as discrete states, used these data for migration inference, and modeled transitions as a time reversible process by using TreeTime (*33*). We interpreted the number of state transitions into Colombia as a proxy for the minimum number of introductions.

In sensitivity analysis and to measure the effect of the SARS-CoV-2 uneven genomic representativeness across the world, we implemented 2 downsampling strategy datasets in which, based on location, the sequences were randomly resampled 100 times and the phylogenetic and migration inference was replicated. The downsampling strategies were as follows: retaining several sequences per region, when possible, equal to the number of sequences available for Colombia; or retaining 50 sequences per region and the total number of sequences from Colombia, which was the most even sampling per region for the South America–focused subsample.

Potential Routes of SARS-CoV-2 Importation into Colombia

We inferred the relative proportion of expected SARS-CoV-2 importations per country by considering COVID-19 incidence per number of international air passengers arriving in Colombia and the available flight travel. We obtained the number of international flights and number of passengers arriving during January 1–March 9, 2020 from the Special Administrative Unit of Civil Aeronautics of Colombia (Aerocivil, http://www.aerocivil.gov.co). The air travel data consists of direct flights from 14 countries to 7 main cities. We calculated COVID-19 incidence for each of the 14 countries with direct flights to Colombia by using the number of confirmed cases reported by the World Health Organization as of March 17, 2020, the date when travel restrictions started in Colombia (*35*), and the total population for each country for 2019 reported in the United Nations World Population Prospects 2019 database (*36*), as described in D.D.S. Candido, et al. (*37*) (Appendix 2, https://wwwnc.cdc.gov/EID/article/26/12/20-2969-App2.pdf).

Ethics Statement

According to the national law 9/1979, decrees 786/1990 and 2323/2006, the Instituto Nacional de Salud is the reference lab and health authority of the national network of laboratories and in cases of public health emergency or those in which scientific research for public health purposes as required, the Instituto Nacional de Salud may use the biological material for research purposes, without informed consent, which includes the anonymous disclosure of results. The information used for this study comes from secondary sources of data that were previously anonymized and do not represent a risk to the community.

Results

Epidemiologic Investigation of SARS-CoV-2 Introductions, Contact-Tracing, and Community Transmission

In Colombia, preventive isolation and monitoring for passengers arriving from China, Italy, France, and Spain started on March 10, 2020. A national health emergency was declared on March 12, and tougher measures then started to be set in place, including the closing of borders on March 17, the ban of international flights on March 20, and the ban of domestic flights on March 25. Implementations of lockdowns occurred from March 25 onward, including Resolutions 380 and 385 from the Colombian Ministry of Health and Social Protection (*38*,*39*); Decrees 412 and 457 from the Ministry of the Interior (*40*,*41*); and Decree 439 from the Ministry of Transport (*42*). Despite a massive drop in air traffic, >15,500 residents returned to Colombia through humanitarian flights during April–June (*43*). By June 1, >30,000 cases of COVID-19 had been documented in Colombia and 857 cases (2.8%) had been linked to travel abroad (Figure 1, panel A).

Most (816, 95.2%) imported cases were symptomatic. The prominent geographic sources for symptomatic cases were Spain (245 [28.6%] cases), the United States (203 [23.7%] cases), Ecuador (50 [5.8%] cases); Mexico (49 [5.7%] cases), and Brazil (41 [4.8%] cases). The other 41 imported cases were asymptomatic and were detected through contact tracing. Among asymptomatic imported cases, most (16, 39%) were imported from Spain, the United States (13, 31.7%), Brazil (3, 7.3%), and Mexico (2, 4.9%). Overall, most

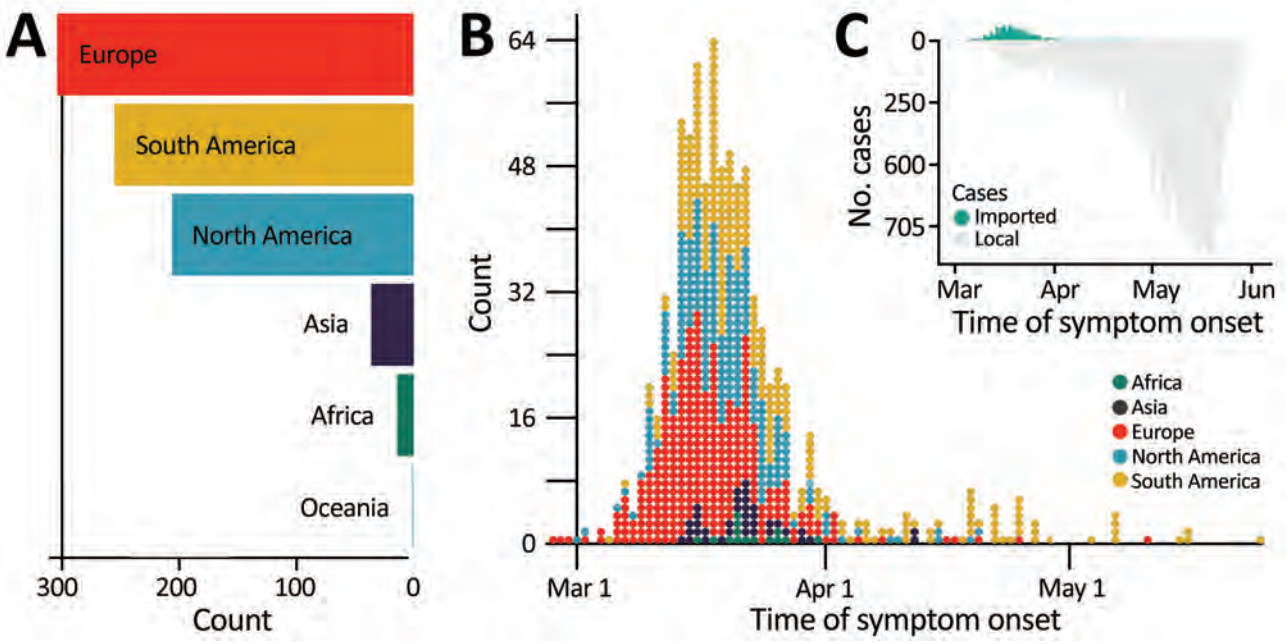

Figure 1. Proportion of imported and local cases early during the COVID-19 pandemic, Colombia. A) Region of origin for the reported imported cases. B) Distribution over time of symptomatic imported and local cases, by region of origin. C) Number of local and imported COVID-19 cases over time. COVID-19, coronavirus disease.

imported cases were from Spain (30.5%), the United States (25.2%), Mexico (6%), Ecuador (5.8%), and Brazil (5.1%). Most symptomatic imported cases were traced back to countries in Europe and the Americas.

The number of symptomatic imported cases steadily increased and peaked on March 14, when local cases were on the rise, but before border closures and the international air travel ban. Our estimate is based on the average incubation time of COVID-19 (*44*) and symptom onset but is 4.8 days earlier than the actual peak on March 18 (Figure 1, panel B). Initial introductions were predominantly linked to Europe; however, both Europe and the Americas were prominent geographic sources of infections during the onset of the epidemic. The introductions after the peak mainly occurred from countries in South America.

SARS-CoV-2 Diversity

To elucidate the dynamics of SARS-CoV-2 spread into Colombia, we combined the 43 whole-genome sequences obtained in our study with sequences from Colombia deposited in GISAID, which provided a set of 122 complete genomes. Sequences from Colombia were classified into 12 sublineages: A.1.2, A.2, A.5, B, B.1, B.1.1, B.1.3, B.1.5, B.1.8, B.1.11, B.2, and B.2.5. The proportion of lineages documented in Colombia seems to reflect founder effects. For example, sublineages B.1, B.1.1, and B.1.5 were found in the early epidemiologically linked transmission chains and consistently were observed most frequently; B.1 was observed in 59 (48.4%) cases, B.1.5 in 31 (25.4%), and B.1.1 in 16 (13.1%) (Figure 2, panel A). From the South America–focused subsampling available from NextStrain, comparable findings were observed for other countries in South America (*45*,*46*), where the most frequently observed lineages were B.1 in 149 (60.8%) cases, B.1.5 in 35 (13.5%) cases, and A.5 in 14 (5.7%) cases.

On average, we identified 1 lineage per department. For instance, the number of documented lineages was highly correlated with the availability of samples (Pearson product-moment correlation coefficient [PPMCC] = 0.72; $p<0.001$) and uncorrelated with the number of local cases (PPMCC = 0.35; $p = 0.049$). We noted 5 different lineages in the departments of Valle del Cauca and Antioquia and 3 different lineages in Cundinamarca; these departments have the most populated capitals and we had more samples from them (Figure 2, panel B). We observed a moderate positive correlation between the number of lineages documented in a department and the number of imported cases (PPMCC = 0.51; $p = 0.002$).

Molecular Evolution of SARS-CoV-2 in Colombia

We identified 133 single-nucleotide variants (NVs) by using the full genome sequences from Colombia and the reference sequence (GenBank accession no. NC_045512.2). Most NVs (131; 98.5%) fell into

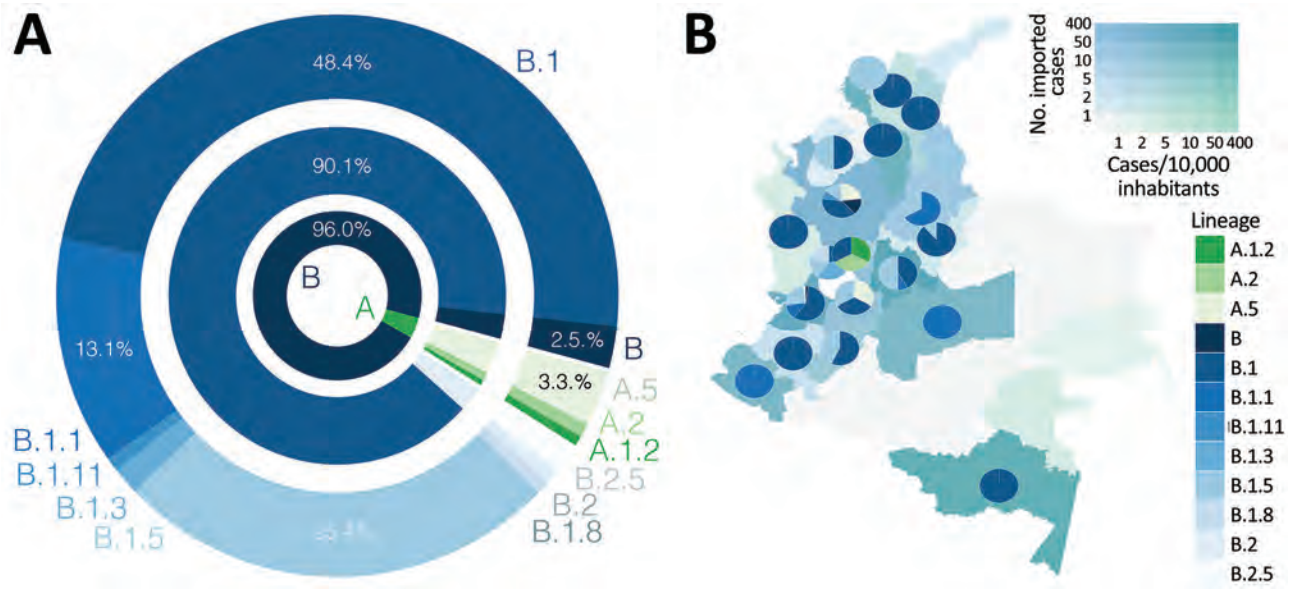

Figure 2. Frequency and distribution of SARS-CoV-2 lineages, Colombia. A) Frequency of A and B lineages and sublineages of SARS-CoV-2 identified. B) Map of distribution of lineages across the country. Departments are colored by the number of imported cases/10,000 inhabitants (inset) and the number of reported introductions. SARS-Co-V-2, severe acute respiratory syndrome coronavirus 2.

the coding region, and 1 NV was identified at each noncoding end. Among NVs in coding sites, 71 (54.2%) led to nonsynonymous substitutions. Most NVs (92/133) were unique to a sequence. Among the shared NVs, 38/41 were associated with a specific lineage (Appendix 1 Tables 3, 4). These observations suggest that the substitutions are not laboratory-specific and most likely the outcome of in situ evolution, shared ancestry, or both (Appendix 2).

In our study, among sequences with complete metadata, 90% (108/120) of sequences from Colombia displayed an amino acid change in region D614G, and the remaining 10% (12 sequences) displayed a change in region D614 (Appendix 1 Table 4). G614 has been associated with higher infectivity (L. Zhang et al., unpub data, https://www.biorxiv.org/content/10.1101/2020.06.12.148726v1) and greater transmissibility with no effects on disease severity outcomes (*46*; E.M. Volz et al., unpub data, https://www.medrxiv.org/content/10.1101/2020.07.31.20166082v2). All G614 sequences also carried mutations that segregate together as described in B. Korber et al. (*47*); we identified the nucleotide substitution C241T at 5′-UTR; the synonymous substitution C3037T at open reading frame 1ab (ORF1ab), the nonstructural protein 3 encoding-gene; and a change in P4715L aa position in ORF1ab, the RNA-dependent RNA polymerase encoding gene. The presence of these and other mutations can be phenotypically and epidemiologically relevant and warrant further monitoring.

Most patients from Colombia for whom genomic sequences were available were symptomatic (n = 90); 59.6% had cough and fever and the others had ≥1 symptom; 10 died, 70% of whom had underlying conditions (Appendix 1 Table 1). However, given the limited number of sequences available, we could not reliably investigate any genomic determinant of clinical outcome.

Evolutionary Relationships between Local and Global SARS-CoV-2 Isolates

The time-stamped phylogeny of 122 isolates from Colombia and 1,462 representative global SARS-CoV-2 isolates showed that the estimated time to the most recent common ancestor for the sampled sequence data is December 7, 2019 (range October 25–December 26, 2019) (Figure 3, panel A). Asia was the inferred ancestral state at the root. Both these observations are in line with the known epidemiology of the pandemic. A root-to-tip regression of genetic distance against sampling time evidenced consistent temporal signal in the sequence data (Figure 3, panel B). The isolates from Colombia were interspersed among the isolates from other countries, suggesting multiple introductions (Figure 3, panels A, C). However, considerable phylogenetic uncertainty appears along the tree and the fine-grained relationships of the isolates from Colombia could not be resolved with confidence (Appendix 2 Figure 1).

Phylogenetic uncertainty and uneven sampling made the quantification of the number of introductions

into the country challenging, let alone dating the time of the introductions. The number of state transitions into Colombia heavily relies on the number and nature of the sequences included from other locations (Figure 4, panel A). By using all sequences in the South America–focused subsampling available from NextStrain, we estimated that an average of 64 (interquartile range [IQR] 62–67) introductions into the country have occurred but this estimate gets lower as we reduce the number of samples (sensitivity analyses) from other locations, down to 22 with the most even downsampled dataset. Independent of the dataset, either the complete or the subsampled datasets, and in line with the epidemiologic information, most geographic source attributions are from Europe (Figure 4, panel B; Appendix 2 Figure 2). This observation also aligns with our estimates using travel data (Figure 4, panel C; Appendix 2 Figure 2).

During January–March 2020, a total of 7 cities in Colombia received 1,593,211 international passengers from 14 countries. Bogotá was the most concentrated city for flights, receiving around 77% of passengers; other cities included Medellín with 11%, Cartagena with 6%, and Cali with 4% of passengers. In total, 35% of international passengers started their journeys in the United States, 17% in Mexico, and 12% in Chile. However, we estimate 87% of all imported COVID-19 cases in Colombia came from Europe, 9.5% from North America, and 3.4% from South America. When stratified by country, the primary source of importation was Spain, which had 71.4% of imported cases; the United States had 8.4%, Germany had 8%, and France had 3.4% (Appendix 2 Figure 2). Our data show most (65.2%) COVID-19 cases were among travelers arriving in Bogotá; 20% were among those arriving in Medellín, and 9% among those arriving in Cali. We estimate that the Spain–Bogotá route carried 42% of the total imported cases.

Since the first COVID-19 case was identified in Colombia on February 26, 2020, contact-tracing efforts had been put in place. We obtained multiple

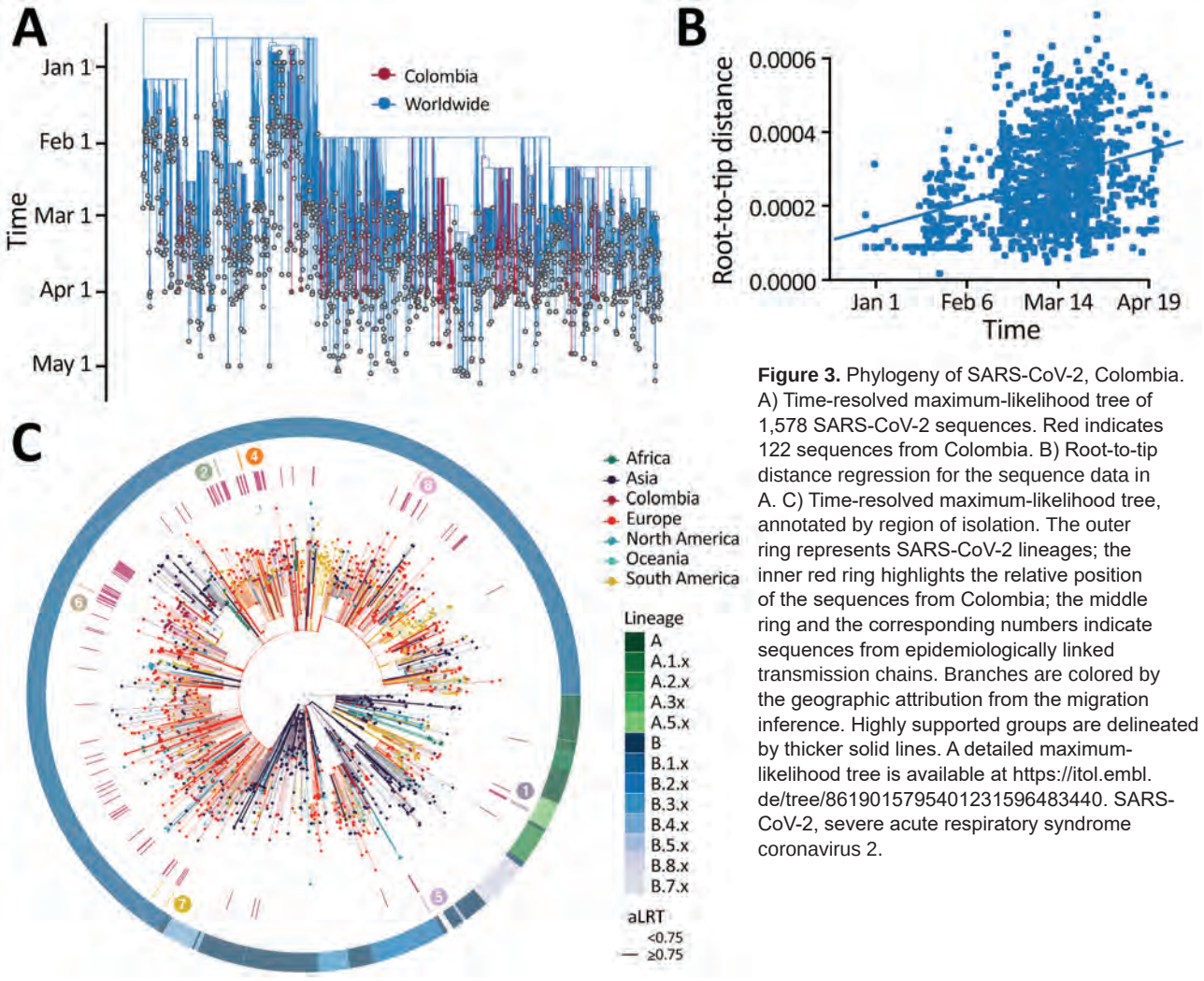

Figure 3. Phylogeny of SARS-CoV-2, Colombia. A) Time-resolved maximum-likelihood tree of 1,578 SARS-CoV-2 sequences. Red indicates 122 sequences from Colombia. B) Root-to-tip distance regression for the sequence data in A. C) Time-resolved maximum-likelihood tree, annotated by region of isolation. The outer ring represents SARS-CoV-2 lineages; the inner red ring highlights the relative position of the sequences from Colombia; the middle ring and the corresponding numbers indicate sequences from epidemiologically linked transmission chains. Branches are colored by the geographic attribution from the migration inference. Highly supported groups are delineated by thicker solid lines. A detailed maximum-likelihood tree is available at https://itol.embl.de/tree/861901579540123159648344O. SARS-CoV-2, severe acute respiratory syndrome coronavirus 2.

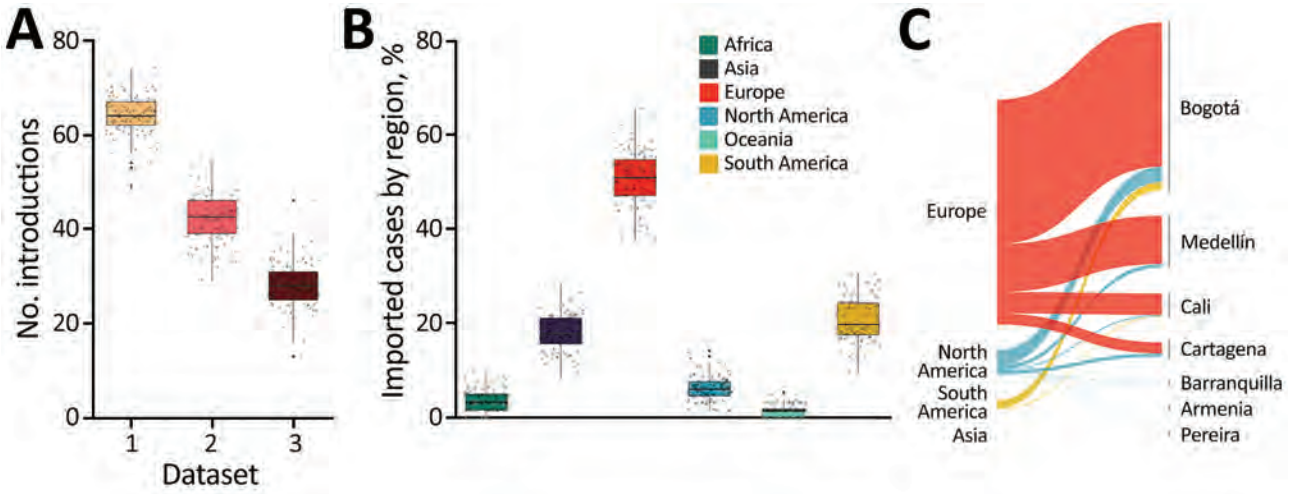

Figure 4. Potential routes of importation for SARS-CoV-2, Colombia. A) The number of transition changes into Colombia following migration inference by using all available sequences per region (dataset 1); retaining several sequences per region, when possible, equal to the number of sequences available for Colombia (dataset 2); and 50 sequences per region and all sequences from Colombia (dataset 3). Box top and bottom lines indicate 25th and 75th percentiles; horizontal lines within boxes indicate means; error bars indicate SDs. B) Geographic source attribution for every transition into Colombia derived from the migration inference using all the available sequences per region. Box top and bottom lines indicate 25th and 75th percentiles; horizontal lines within boxes indicate means; error bars indicate SDs. C) Geographic contribution inferred by using air travel data per country aggregated by region.

sequences from 7 distinct early epidemiologically linked transmission chains (Appendix 1 Table 1) and mapped these data into the phylogeny (Figure 3, panel C). All but 1 set of sequences did not group, but it appeared very close in the tree. These data underscore the potential utility of genomic epidemiology to link persons with incomplete information, such as cases that are disconnected due to intermediate asymptomatic carriers, and complement outbreak transmission investigations.

Our study has some limitations. First, the geographic sources of infection relied on persons self-reporting symptom onset and travel histories, which are subject to inaccuracies. Second, we used air travel data from likely destinations in Colombia, but other locations also might have fueled COVID-19 emergence and dissemination in the country; flight travel data was not available for dates after March 9, 2020. Third, the number of sequences sampled represented a tiny fraction of the documented number of imported cases into Colombia. The sample was selected as a countrywide representation, given limited resources for genome sequencing; thus, the introduced viral diversity also might have been underestimated. Another limitation is the inherent uncertainty stemming from global unsystematic sampling. Therefore, the inferences about the number of introductions and the corresponding geographic sources should be interpreted with caution. We attempted to overcome this by undertaking sensitivity analyses and contrasting the results with the available epidemiologic data and our estimates from travel data. However, more sequence data from Colombia and undersampled countries, together with information of sampling representativeness per country, are needed to account for sampling uncertainty in a more statistically rigorous manner.

Discussion

We describe the complete genome sequences of SARS-CoV-2 from 43 clinical samples, results of an epidemiologic investigation of imported cases, and the phylogenetic findings of 122 genome sequences from Colombia that characterize the epidemic onset of COVID-19 in the country. Our study provides evidence that several independent COVID-19 introductions occurred in Colombia and documents ≥12 SARS-CoV-2 lineages. Most of the notified introductions to countries in Latin America occurred from Europe, an observation that was supported by phylogenetic and air travel data (*48*; C. Salazar et al., unpub data, https://www.biorxiv.org/content/10.1101/2020.05.09.086223v1). Although the sequence data do not represent the actual number of epidemiologically linked transmission chains, our phylogenetic findings validated the linkage for epidemiologically linked transmission chains with available sequence data. Our results further underscore the advantages of genome sequencing to complement COVID-19 outbreak investigations and support the need for a more comprehensive country-wide study of the epidemiology and spread of SARS-CoV-2 in Colombia.

Acknowledgments

The authors thank the National Laboratory Network and Virology Group of INS for routine virologic surveillance of SARS-CoV-2 in Colombia. We also thank all researchers who deposited genomes in GISAID's EpiCoV Database contributing to genomic diversity and phylogenetic relationship of SARS-CoV-2. Finally, we thank Maylin Gonzalez Herrera for her technical assistance.

This work was funded by the Project CEMIN-4-2020 Instituto Nacional de Salud. C.J.V.-A. is supported by an ERC European Research Council Starting Grant (award no. 757688). The funders had no role in study design, data collection and analysis, decision to publish, or preparation of the manuscript.

About the Author

Dr. Laiton-Donato is the head of the Sequencing and Genomics Unit, Dirección de Investigación en Salud Pública, Instituto Nacional de Salud, Colombia. Her research interests include molecular virology of emerging viruses with impact in public health.

References

1. Wu F, Zhao S, Yu B, Chen Y-M, Wang W, Song Z-G, et al. A new coronavirus associated with human respiratory disease in China. Nature. 2020;579:265–9. https://doi.org/10.1038/s41586-020-2008-3
2. World Health Organization. Novel coronavirus—China, 2020 Jan 12 [cited 2020 Jun 16]. https://www.who.int/csr/don/12-january-2020-novel-coronavirus-china
3. Kraemer MUG, Yang C-H, Gutierrez B, Wu C-H, Klein B, Pigott DM, et al.; Open COVID-19 Data Working Group. The effect of human mobility and control measures on the COVID-19 epidemic in China. Science. 2020;368:493–7. https://doi.org/10.1126/science.abb4218
4. He X, Lau EHY, Wu P, Deng X, Wang J, Hao X, et al. Temporal dynamics in viral shedding and transmissibility of COVID-19. Nat Med. 2020;26:672–5. https://doi.org/10.1038/s41591-020-0869-5
5. Li J, Zhang L, Liu B, Song D. Case report: viral shedding for 60 days in a woman with COVID-19. Am J Trop Med Hyg. 2020;102:1210–3. https://doi.org/10.4269/ajtmh.20-0275
6. Jarvis CI, Van Zandvoort K, Gimma A, Prem K, Klepac P, Rubin GJ, et al. CMMID COVID-19 working group. Quantifying the impact of physical distance measures on the transmission of COVID-19 in the UK. BMC Med. 2020;18:124. https://doi.org/10.1186/s12916-020-01597-8
7. Prem K, Liu Y, Russell TW, Kucharski AJ, Eggo RM, Davies N, et al.; Centre for the Mathematical Modelling of Infectious Diseases COVID-19 Working Group. The effect of control strategies to reduce social mixing on outcomes of the COVID-19 epidemic in Wuhan, China: a modelling study. Lancet Public Health. 2020;5:e261–70. https://doi.org/10.1016/S2468-2667(20)30073-6
8. Hellewell J, Abbott S, Gimma A, Bosse NI, Jarvis CI, Russell TW, et al.; Centre for the Mathematical Modelling of Infectious Diseases COVID-19 Working Group. Feasibility of controlling COVID-19 outbreaks by isolation of cases and contacts. Lancet Glob Health. 2020;8:e488–96. https://doi.org/10.1016/S2214-109X(20)30074-7
9. Chinazzi M, Davis JT, Ajelli M, Gioannini C, Litvinova M, Merler S, et al. The effect of travel restrictions on the spread of the 2019 novel coronavirus (COVID-19) outbreak. Science. 2020;368:395–400. https://doi.org/10.1126/science.aba9757
10. Ribeiro F, Leist A. Who is going to pay the price of Covid-19? Reflections about an unequal Brazil. Int J Equity Health. 2020;19:91. https://doi.org/10.1186/s12939-020-01207-2
11. Ministry of Health and Social Protection. Colombia. Minsalud confirms six new cases of coronavirus (COVID-19) in Colombia [in Spanish]. Bogotá, Colombia; Boletín de Prensa no. 057 de 2020. 2020 [cited 2020 May 24]. https://www.minsalud.gov.co/Paginas/Minsalud-confirma-seis-nuevos-casos-de-coronavirus-(COVID-19)-en-Colombia.aspx
12. National Institute of Health. Colombia. COVID-2019 in Colombia daily report 2020 March 31 [in Spanish] [cited 2020 Jun 2]. https://www.ins.gov.co/Noticias/Paginas/Coronavirus.aspx
13. National Institute of Health. Colombia. COVID-2019 in Colombia daily report 2020 Jun 18 [in Spanish] [cited 2020 Jun 2]. https://www.ins.gov.co/Noticias/Paginas/Coronavirus.aspx
14. Grubaugh ND, Ladner JT, Lemey P, Pybus OG, Rambaut A, Holmes EC, et al. Tracking virus outbreaks in the twenty-first century. Nat Microbiol. 2019;4:10–9. https://doi.org/10.1038/s41564-018-0296-2
15. Lu J, du Plessis L, Liu Z, Hill V, Kang M, Lin H, et al. Genomic epidemiology of SARS-CoV-2 in Guangdong Province, China. Cell. 2020;181:997–1003.e9. https://doi.org/10.1016/j.cell.2020.04.023
16. Eden J-S, Rockett R, Carter I, Rahman H, de Ligt J, Hadfield J, et al. An emergent clade of SARS-CoV-2 linked to returned travellers from Iran. Virus Evol. 2020;6:veaa027. https://doi.org/10.1093/ve/veaa027
17. Gudbjartsson DF, Helgason A, Jonsson H, Magnusson OT, Melsted P, Norddahl GL, et al. Spread of SARS-CoV-2 in the Icelandic Population. N Engl J Med. 2020;382:2302–15. https://doi.org/10.1056/NEJMoa2006100
18. Corman VM, Landt O, Kaiser M, Molenkamp R, Meijer A, Chu DK, et al. Detection of 2019 novel coronavirus (2019-nCoV) by real-time RT-PCR. Euro Surveill. 2020;25:2000045. https://doi.org/10.2807/1560-7917.ES.2020.25.3.2000045
19. Quick J. nCoV-2019 sequencing protocol version 1. protocols.io; 2020 Jan 22 [cited 2020 Mar 2]. https://www.protocols.io/view/ncov-2019-sequencing-protocol-bbmuik6w
20. Wick R. Porechop version 0.2.4. 2018 Oct 19 [cited 2020 Jun 18]. https://github.com/rrwick/Porechop
21. Li H, Durbin R. Fast and accurate long-read alignment with Burrows-Wheeler transform. Bioinformatics. 2010;26:589–95. https://doi.org/10.1093/bioinformatics/btp698
22. Simpson J. Nanopolish: signal-level algorithms for MinION data [cited 2020 May 10]. https://github com/jts/nanopolish
23. Chen S, Zhou Y, Chen Y, Gu J. fastp: an ultra-fast all-in-one FASTQ preprocessor. Bioinformatics. 2018;34:i884–90. https://doi.org/10.1093/bioinformatics/bty560
24. Bushnell B. BBMap short read aligner, and other bioinformatic tools [cited 2020 May 10]. https://escholarship.org/uc/item/1h3515gn
25. Hadfield J, Megill C, Bell SM, Huddleston J, Potter B, Callender C, et al. Nextstrain: real-time tracking of pathogen evolution. Bioinformatics. 2018;34:4121–3. https://doi.org/10.1093/bioinformatics/bty407

26. Rambaut A, Holmes EC, Hill V, O'Toole Á, McCrone JT, Ruis C, et al. A dynamic nomenclature proposal for SARS-CoV-2 to assist genomic epidemiology. Nat Microbiol. 2020 Jul 15 [Epub ahead of print]. https://doi.org/10.1038/s41564-020-0770-5
27. O'Toole A, McCrone JT. Pangolin: Phylogenetic Assignment of Named Global Outbreak LINeages [cited 2020 Jun 18]. https://github.com/hCoV-2019/pangolin
28. Katoh K, Misawa K, Kuma K, Miyata T. MAFFT: a novel method for rapid multiple sequence alignment based on fast Fourier transform. Nucleic Acids Res. 2002;30:3059–66. https://doi.org/10.1093/nar/gkf436
29. De Maio N, Walker C, Borges R, Weilguny L, Slodkowicz G, Goldman N. Issues with SARS-CoV-2 sequencing data. 2020 Jul 29 [cited 2020 Jun 16]. https://virological.org/t/issues-with-sars-cov-2-sequencing-data/473
30. Hasegawa M, Kishino H, Yano T. Dating of the human-ape splitting by a molecular clock of mitochondrial DNA. J Mol Evol. 1985;22:160–74. https://doi.org/10.1007/BF02101694
31. Minh BQ, Schmidt HA, Chernomor O, Schrempf D, Woodhams MD, von Haeseler A, et al. IQ-TREE 2: new models and efficient methods for phylogenetic inference in the genomic era. Mol Biol Evol. 2020;37:1530–4. https://doi.org/10.1093/molbev/msaa015
32. Guindon S, Dufayard J-F, Lefort V, Anisimova M, Hordijk W, Gascuel O. New algorithms and methods to estimate maximum-likelihood phylogenies: assessing the performance of PhyML 3.0. Syst Biol. 2010;59:307–21. https://doi.org/10.1093/sysbio/syq010
33. Sagulenko P, Puller V, Neher RA. TreeTime: maximum-likelihood phylodynamic analysis. Virus Evol. 2018;4:vex042. https://doi.org/10.1093/ve/vex042
34. To T-H, Jung M, Lycett S, Gascuel O. Fast dating using least-squares criteria and algorithms. Syst Biol. 2016;65:82–97. https://doi.org/10.1093/sysbio/syv068
35. World Health Organization. Novel coronavirus (2019-nCoV) situation report—57. 2020 March 17 [cited 2020 May 10]. https://www.who.int/emergencies/diseases/novel-coronavirus-2019/situation-reports
36. United Nations Population Division. World population prospects 2019 [cited 2020 Jun 19]. https://population.un.org/wpp/Download/Metadata/Documentation
37. Candido DDS, Watts A, Abade L, Kraemer MUG, Pybus OG, Croda J, et al. Routes for COVID-19 importation in Brazil. J Travel Med. 2020;27:taaa042. https://doi.org/10.1093/jtm/taaa042
38. Ministry of Health and Social Protection, Colombia. Resolution number 0000380 [in Spanish]. 2020 Mar 10 [cited 2020 June 2] https://www.minsalud.gov.co/Normatividad_Nuevo/Resoluci%C3%B3n%20No.%20380%20de%202020.pdf
39. Ministry of Health and Social Protection, Colombia. Resolution number 0000385 [in Spanish]. 2020 Mar 12 [cited 2020 June 2] https://www.minsalud.gov.co/sites/rid/Lists/BibliotecaDigital/RIDE/DE/DIJ/resolucion-385-de-2020.pdf
40. Ministry of the Interior, Colombia. Decree 412 [in Spanish]. 2020 Mar 16 [cited 2020 June 2]. https://dapre.presidencia.gov.co/normativa/normativa/DECRETO%20412%20DEL%2016%20DE%20MARZO%20DE%202020.pdf
41. Ministry of the Interior, Colombia. Decree 457 [in Spanish]. 2020 Mar 22 [cited 2020 June 2] https://dapre.presidencia.gov.co/normativa/normativa/DECRETO%20457%20DEL%2022%20DE%20MARZO%20DE%202020.pdf
42. Ministry of Transport, Colombia. Decree 439 [in Spanish]. 2020 Mar 20 [cited 2020 May 10] https://dapre.presidencia.gov.co/normativa/normativa/DECRETO%20439%20DEL%2020%20DE%20MARZO%20DE%202020.pdf
43. Chancellery of Colombia. Communication on humanitarian flights from 2 to 12 July; 2020 June 17 [cited 2020 Jun 19]. https://www.cancilleria.gov.co/newsroom/publiques/comunicado-vuelos-caracter-humanitario-2-12-julio
44. Sun K, Chen J, Viboud C. Early epidemiological analysis of the coronavirus disease 2019 outbreak based on crowdsourced data: a population-level observational study. Lancet Digit Health. 2020;2:e201–8. https://doi.org/10.1016/s2589-7500(20)30026-1
45. Castillo AE, Parra B, Tapia P, Acevedo A, Lagos J, Andrade W, et al. Phylogenetic analysis of the first four SARS-CoV-2 cases in Chile. J Med Virol. 2020;92:1562–6. https://doi.org/10.1002/jmv.25797
46. Candido DS, Claro IM, de Jesus JG, Souza WM, Moreira FRR, Dellicour S, et al.; Brazil-UK Centre for Arbovirus Discovery, Diagnosis, Genomics and Epidemiology (CADDE) Genomic Network. Evolution and epidemic spread of SARS-CoV-2 in Brazil. Science. 2020;369:1255–60. https://doi.org/10.1126/science.abd2161
47. Korber B, Fischer WM, Gnanakaran S, Yoon H, Theiler J, Abfalterer W, et al.; Sheffield COVID-19 Genomics Group. Tracking changes in SARS-CoV-2 spike: evidence that D614G increases infectivity of the COVID-19 virus. Cell. 2020;182:812–827.e19. https://doi.org/10.1016/j.cell.2020.06.043
48. da Silva Candido D, Watts A, Abade L, Kraemer MUG, Pybus OG, Croda J, et al. Routes for COVID-19 importation in Brazil. J Travel Med. 2020;27:taaa042. https://doi.org/10.1093/jtm/taaa042

Address for correspondence: Katherine Laiton-Donato; Instituto Nacional de Salud, Sequencing and Genomics Unit, Avenida calle 26 No 51-20, Bogotá DC 110221, Colombia; email: kdlaitond@unal.edu.co, klaiton@ins.gov.co

SARS-CoV-2 Seroprevalence among Healthcare, First Response, and Public Safety Personnel, Detroit Metropolitan Area, Michigan, USA, May–June 2020

Lara J. Akinbami, Nga Vuong, Lyle R. Petersen, Samira Sami, Anita Patel, Susan L. Lukacs, Lisa Mackey, Lisa A. Grohskopf, Amy Shehu, Jenny Atas

To estimate seroprevalence of severe acute respiratory syndrome 2 (SARS-CoV-2) among healthcare, first response, and public safety personnel, antibody testing was conducted in emergency medical service agencies and 27 hospitals in the Detroit, Michigan, USA, metropolitan area during May–June 2020. Of 16,403 participants, 6.9% had SARS-CoV-2 antibodies. In adjusted analyses, seropositivity was associated with exposure to SARS-CoV-2–positive household members (adjusted odds ratio [aOR] 6.18, 95% CI 4.81–7.93) and working within 15 km of Detroit (aOR 5.60, 95% CI 3.98–7.89). Nurse assistants (aOR 1.88, 95% CI 1.24–2.83) and nurses (aOR 1.52, 95% CI 1.18–1.95) had higher likelihood of seropositivity than physicians. Working in a hospital emergency department increased the likelihood of seropositivity (aOR 1.16, 95% CI 1.002–1.35). Consistently using N95 respirators (aOR 0.83, 95% CI 0.72–0.95) and surgical facemasks (aOR 0.86, 95% CI 0.75–0.98) decreased the likelihood of seropositivity.

Healthcare, first response (e.g., firefighters, paramedics, emergency medical technicians), and public safety (e.g., law enforcement officers) personnel have served on the front lines of the coronavirus disease (COVID-19) pandemic response in several capacities. Many of these occupations require intensive interaction with persons with suspected or confirmed severe acute respiratory syndrome coronavirus 2 (SARS-CoV-2) infection. Both reverse transcription PCR (RT-PCR) testing for SARS-CoV-2 and assessing COVID-19 symptoms could be used to determine infection status, but not all infected persons develop symptoms or are tested within the necessary time window. Measuring antibodies to SARS-CoV-2 is necessary to inform our understanding of viral transmission dynamics in high-risk situations (*1*).

The Centers for Disease Control and Prevention (CDC) collaborated with the Michigan Department of Health and Human Services (MDHHS) Region 2 South and North Healthcare Coalitions to invite personnel working onsite in hospital, first response, and public safety settings to be tested for SARS-CoV-2 antibodies and to complete a web-based survey about workplace, occupation, use of personal protective equipment (PPE), and selected exposures. The primary study objective was to estimate the prevalence of SARS-CoV-2 antibodies among this population. A second objective was to describe associations between seroprevalence and participant and workplace characteristics.

Methods

The MDHHS Region 2 South Healthcare Coalition area is the most populous region in Michigan and comprises Monroe, Washtenaw, and Wayne (including the city of Detroit) Counties. MDDHS Region 2 North Healthcare Coalition includes Macomb, Oakland, and St. Clair Counties. The Healthcare Coalitions coordinated with 27 hospitals and 7 MDHHS Medical Control Authorities (MCAs), which supervise and

Author affiliations: Centers for Disease Control and Prevention, Hyattsville, Maryland, USA (L.J. Akinbami, S.L. Lukacs); US Public Health Service, Rockville, Maryland, USA (L.J. Akinbami, S.L. Lukacs, L.A. Grohskopf); Centers for Disease Control and Prevention, Fort Collins, Colorado, USA (N. Vuong, L.R. Petersen, L. Mackey); Centers for Disease Control and Prevention, Atlanta, Georgia, USA (S. Sami, A. Patel, L.A. Grohskopf); Epidemic Intelligence Service, Atlanta (S. Sami); Region 2 South Healthcare Coalition, Detroit, Michigan, USA (A. Shehu, J. Atas)

DOI: https://doi.org/10.3201/eid2612.203764

coordinate an emergency medical services (EMS) system for a geographic region, to invite employees to participate. The protocol was reviewed by CDC human subjects research officials, who determined the activity to be public health surveillance and exempt from full institutional review board review (*2*).

Study Participants

Eligible participants for the serology survey included adults ≥18 years of age who worked onsite in a first response, hospital, or public safety setting and consented to phlebotomy and serum sample storage for confirmation of test results if needed. Persons were not eligible to participate if, in the 2 weeks before taking the survey, they reported having new symptoms of cough, shortness of breath, or change in sense of taste or smell, or had tested positive for SARS-CoV-2 by RT-PCR test using a nasal, throat, or saliva sample.

Web-Based Survey

Participating agencies shared information about the secure web-based survey (Appendix Table 1, https://wwwnc.cdc.gov/EID/article/26/12/20-3764-App1.pdf) with employees using email and onsite marketing. There was no face-to-face recruitment. Participation was voluntary and individual results were not shared with employers. CDC did not have access to personal identifiers. The survey was drafted by the investigators, reviewed by CDC subject matter experts, and was designed to require <10 minutes to complete on a personal device. Upon survey completion, participants received information about blood collection sites at their workplace or a nearby MCA location.

Specimen Collection and Testing

Blood samples were collected for SARS-CoV-2 antibody testing during May 18–June 13, 2020. Antibody testing was performed using the Ortho Clinical Diagnostics VITROS Immunodiagnostic Products Anti-SARS-CoV-2 IgG Test (https://www.orthoclinicaldiagnostics.com; specificity 100%, sensitivity 90%) (*3*). Results were reported to participants within 72 hours as negative (signal-to-cutoff ratio <1.0), positive (signal-to-cutoff ratio ≥1.0), or test not performed because of lipemia or insufficient volume.

Statistical Analysis

Of 16,403 participants, 6 (0.04%) had samples that were unable to be tested and were excluded (n = 16,397). Percent SARS-CoV-2 antibody positivity and 95% CIs were calculated. Statistical testing was conducted using Cochran-Armitage trend tests for variables with ordinal categories (2-sided tests with $\alpha = 0.05$). Non-Hispanic Native Hawaiian and other Pacific Islander (n = 31, 0.2%), Non-Hispanic American Indian/Alaska Native (n = 53, 0.3%), and other race (n = 320, 2.0%) participants were categorized as other race. The 398 (2.4%) participants who declined to report race were categorized separately and included in all analyses.

Participants could choose multiple work locations; 17.5% chose >1 location. Each work location category was represented as a separate dichotomous variable (i.e., dummy variable) to enable modeling of non–mutually exclusive categories. Participants were provided with occupation categories and a free text option. The National Institute for Occupational Safety and Health (NIOSH) assisted with coding free-text responses using the NIOSH Industry and Occupation Computerized Coding System (*4*). No categories created from free-text options reached high sample size (n<100) and were coded as "other" except for technicians (e.g., dialysis, telemetry, surgery), which were combined into a "clinical technician" category (n = 365).

Exposure to persons with confirmed COVID-19 (co-worker, household member, patient, and other person) was defined as contact within 6 feet for >10 minutes, but the question did not mention PPE use, which was assessed in separate questions. PPE use was dichotomized for each piece of equipment into "use all the time" (the recommended, or optimal, frequency when PPE is required) versus all other choices. Similarly, exposure to persons with confirmed COVID-19 was dichotomized into "yes" versus all other choices.

Differences between categories were assessed by nonoverlapping 95% CIs for percent positivity. Two participants were excluded from adjusted analyses (1 participant with missing housing information and 1 participant from a nonstudy hospital; n = 16,395). To account for clustering of participants by facility/agency, generalized estimating equations were used to model the likelihood of seropositivity. Covariates were chosen a priori to represent risk of exposure and infection. Model diagnostics performed with regression analysis did not show evidence of collinearity for work location (highest values for variance inflation factor = 1.4, and condition index = 4.1), which was represented by non–mutually exclusive dummy variables entered simultaneously into the multivariable model. No interaction terms were explored. SAS 9.4 software (https://www.sas.com) was used for all analyses. ArcGIS (ESRI, https://www.esri.com) was used to map seroprevalence by agency location.

Results

Of 16,397 participants, 6.9% (95% CI 6.5%–7.3%) were positive for SARS-CoV-2 IgG, indicating previous infection. In contrast, 2.7% (95% CI 2.5%–3.0%) reported having previously tested positive by RT-PCR using a nasal, throat, or saliva sample. Participant age ranged from 19 to 82 years (mean 42.1, SD 12.2). Seroprevalence was lower among those ≥65 years of age (3.2% of the sample; seroprevalence 3.5%, 95% CI 2.1%–5.4%) compared with all younger age groups (Table 1). Women, 68.6% of participants, had a similar seroprevalence to men. Non-Hispanic Black participants made up 7.3% of the sample and had the highest seroprevalence (16.3%, 95% CI 14.2%–18.5%) compared with other race/ethnic groups, including Non-Hispanic White participants (6.0%, 95% CI 5.6%–6.4%), who made up 78.4% of the sample. Seroprevalence among participants by facility ranged from 0.5% to 17.9% and was inversely related to distance of the facility from the Detroit geographic center. Seroprevalence was highest (11.0%, 95% CI 10.3%–11.7%) among participants at facilities within 15 km of Detroit's center and lowest (1.8%, 95% CI 1.4%–2.2%) at locations 30–55 km away (Figure 1). Higher seroprevalence with closer proximity to Detroit was observed among most participants, regardless of occupation and healthcare setting (Appendix Figure 1). Among participants who reported close contact (within 6 feet) with a person with confirmed COVID-19 for ≥10 minutes, seroprevalence was highest among those with exposure to a household member (34.3%, 95% CI 30.2%–38.6%). Participants living in multiunit housing had higher seroprevalence compared with those living in single-family housing (8.4%, 95% CI 7.2%–9.8% vs. 6.7%, 95% CI 6.3%–7.1%).

By work location, seroprevalence was highest among participants who worked in hospital wards (8.8%, 95% CI 8.0%–9.7%) and lowest among those working in police departments (3.9%, 95% CI 2.5%–5.8%) (Table 2). Within hospitals, lower seroprevalence was found among persons working in intensive care units (ICUs; 6.1%) and operating rooms or surgical units (4.5%) compared with participants working in wards (8.8%) and emergency departments (EDs; 8.1%). By occupation, the highest

Table 1. Seropositivity for SARS-CoV-2 among healthcare, first response, and public safety personnel, by demographic characteristics, Detroit metropolitan area, Michigan, USA, May–June 2020*

Characteristics	No. (%)	% Seropositive (95% CI)
Total	16,397 (100.0)	6.9 (6.5–7.3)
Age group, y†		
18–24	686 (4.2)	7.9 (6.0–10.2)
25–34	4,885 (29.8)	6.9 (6.2–7.6)
35–44	3,977 (24.3)	7.0 (6.2–7.9)
45–59	5,222 (31.9)	6.9 (6.2–7.6)
60–64	1,106 (6.8)	7.5 (6.0–9.2)
≥65	521 (3.2)	3.5 (2.1–5.4)
Sex		
M	5,146 (31.4)	6.7 (6.0–10.2)
F	11,251 (68.6)	7.0 (6.5–7.5)
Race/ethnicity		
Non-Hispanic White	12,858 (78.4)	6.0 (5.6–6.4)
Non-Hispanic Black	1,200 (7.3)	16.3 (14.2–18.5)
Non-Hispanic Asian	1,097 (6.7)	7.3 (5.8–9.0)
Hispanic	440 (2.7)	6.8 (4.7–9.6)
Other‡	404 (2.5)	7.2 (4.9–10.2)
Declined to answer	398 (2.4)	7.0 (4.7–10.0)
Distance of work agency/facility from Detroit centroid		
<15 km	7,194 (43.9)	11.0 (10.3–11.7)
15–30 km	4,677 (28.5)	5.5 (4.9–6.2)
31–55 km	4,526 (27.6)	1.8 (1.4–2.2)
Exposure to persons testing positive for COVID-19§		
Co-worker	6,799 (41.5)	10.0 (9.3–10.8)
Household member	519 (3.2)	34.3 (30.2–38.6)
Patient	10,389 (63.4)	7.8 (7.3–8.3)
Other person	2,709 (16.5)	11.5 (10.3–12.7)
Housing		
Multi-unit	1,762 (10.8)	8.4 (7.2–9.8)
Single family	14,634 (89.3)	6.7 (6.3–7.11)

*COVID-19, coronavirus disease; SARS-CoV-2, severe acute respiratory syndrome coronavirus 2.
†Test for trend in seropositivity statistically significant at $\alpha = 0.05$.
‡Other race/ethnicity includes non-Hispanic Native Hawaiian and other Pacific Islander, non-Hispanic American Indian and Alaska Native, and participants who indicated other race.
§Categories are not mutually exclusive.

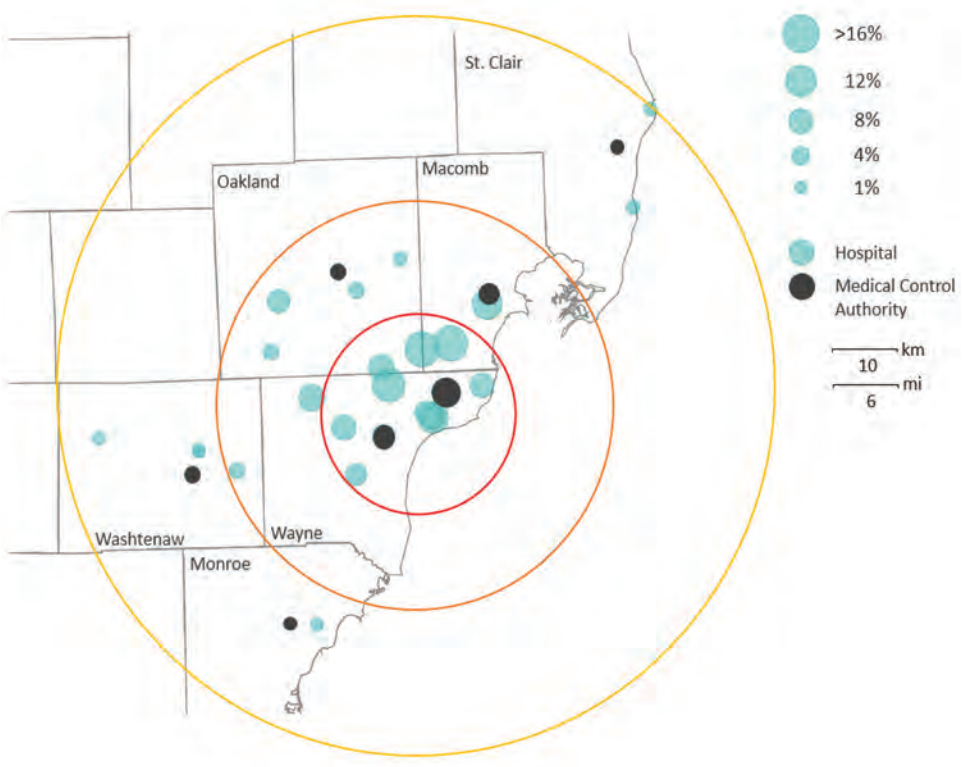

Figure 1. Seropositivity for SARS-CoV-2 among healthcare, first response, and public safety personnel, by hospital and Medical Control Authority agency location, Detroit metropolitan area, Michigan, USA, May–June 2020. Centroid: Detroit city center. Mean SARS-CoV-2 seroprevalence within 15 km was 11.0% (red), 15–30 km, 5.5% (orange), and 31–55 km, 1.8% (yellow). Base map source: ESRI ArcGIS map for Province of Ontario and Oakland County, Michigan (https://www.esri.com). SARS-CoV-2, severe acute respiratory syndrome coronavirus 2.

seroprevalence was found among nurse assistants (12.8%) and physical therapists (10.6%) and the lowest among laboratory technicians (3.4%) and police officers (4.0%). Seroprevalence also varied by hospital-based work locations and occupation (Figure 2). Among participants working on hospital wards, the lower bound of the 95% CI for seropositivity was higher than overall seroprevalence (6.9%) for nurse assistants (13.6%, 95% CI 10.2%–17.5%), administration/clerks (11.9%, 95% CI 7.0%–18.5%), respiratory therapists (10.8%, 95% CI 7.1%–15.6%), and nurses (9.8%, 95% CI 8.5%–11.2%). Nurse assistants who worked in an "other hospital location" (15.9%, 95% CI 8.2%–26.7%) and nurses who worked in EDs (9.9%, 95% CI 8.3%–11.7%) had similarly elevated seroprevalence.

Other occupational risk factors are included in the Appendix. Participants reported the average number of times per shift since March 1, 2020, in which they had participated in aerosol-generating procedures (Appendix Figure 2) and were given a list of examples for reference (Appendix Table 1). Seroprevalence generally increased with increasing procedure frequency ($p = 0.04$ by test for trend), with the highest percent positivity among those who participated in such procedures >25 times per shift on average (9.1%, 95% CI 7.4%–11.0%). Participants also reported how frequently they used each component of PPE, using a Likert scale. Overall, there was no pattern seen in percent antibody positivity with frequency of use with any PPE component (Appendix Table 2). Among those reporting ideal frequency of use ("all the time") for a specific PPE component, seroprevalence was similar to the overall seroprevalence (Table 2).

Multivariable adjustment using generalized estimating equations was performed (Figure 3; Appendix Table 3). Factors most strongly associated with likelihood of seropositivity were exposure to a household member with confirmed COVID-19 (adjusted odds ratio [aOR] 6.18, 95% CI 4.81–7.93) and working within 15 km of the Detroit center (aOR 5.60, 95% CI 3.98–7.89 compared with 30–55 km). Compared with physicians, occupations more likely to be seropositive included nurse assistant (aOR 1.88, 95% CI 1.24–2.83) and nurse (aOR 1.52, 95% CI 1.18–1.95). Working in a hospital ED was the sole location with increased adjusted odds of seropositivity (aOR 1.16, 95% CI 1.00–1.35). Consistently wearing an N95 respirator (aOR 0.83, 95% CI 0.72–0.95) or surgical facemask (vs. using them less than "all the time") lowered the likelihood of being seropositive (aOR 0.86, 95% CI 0.75–0.98).

Discussion

Healthcare, first response, and public safety personnel in 27 hospitals and 7 MCA areas were surveyed

in the Detroit metropolitan area. Among these facilities, seroprevalence of SARS-CoV-2 IgG ranged from 0.5% to 17.9%, indicating wide variation in seroprevalence. A major role for community acquisition of SARS-CoV-2 infection is suggested by the strong association between seropositivity and working closer to the Detroit center and exposure to a household member with confirmed COVID-19. Workers remain vulnerable at home, where social distancing and PPE use may be difficult and likelihood of exposure during presymptomatic or asymptomatic periods is high. Similar patterns have been found in other studies of healthcare worker infections, in which community or household exposure to persons who tested positive for SARS-CoV-2 was the primary predictor of seroconversion (*5*,*6*). The geographic distribution of seroprevalence among first responders in this study was related to population-based cumulative case reporting in Michigan through April 30, 2020: higher percentage positivity for RT-PCR testing was reported for counties near the Detroit center (Oakland, Macomb, and Wayne [0.48%–1.04%]) versus lower levels for the outlying counties (Washtenaw, St. Clair, and Monroe [0.22%–0.32%]) (*7*).

Although 6.9% of participants were seropositive, only 2.7% reported a history of a positive RT-PCR test. This finding of higher seroprevalence compared with confirmed active infection is similar to other serology surveys of the general population (*8*–*10*). A study by Havers et al. estimated 6–24 times as many infections as the number of reported cases detected by RT-PCR (*8*). Our study revealed ≈2.5 times more infections than cases based on self-reported RT-PCR results. The 2.7% positivity for RT-PCR may be higher in the healthcare and first responder population compared with the general public (which ranged from 0.22% to 1.04% in the

Table 2. Seropositivity for SARS-CoV-2 among healthcare, first response, and public safety personnel, by work location, occupation, and PPE use, Detroit metropolitan area, Michigan, USA, May–June 2020*

Characteristic	No. (%)	% Seropositive (95% CI)
Work location		
Hospital emergency department	3,614 (22.0)	8.1 (7.2–9.0)
Hospital ward	4,766 (29.1)	8.8 (8.0–9.7)
Hospital intensive care unit	3,973 (24.2)	6.1 (5.3–6.9)
Hospital operating room/surgical	2,661 (16.2)	4.5 (3.7–5.3)
Other hospital location	3,260 (19.9)	6.1 (5.3–7.0)
Emergency medical services	550 (3.4)	5.3 (3.6–7.5)
Fire services	1,008 (6.2)	5.0 (3.7–6.5)
Police department	615 (3.8)	(2.5–5.8)
Occupation		
Administration/clerk	964 (5.9)	8.0 (6.4–9.9)
Clinical technician†	365 (2.2)	5.5 (3.4–8.3)
EMT/medical first responder/paramedic‡	1,158 (7.1)	5.2 (4.0–6.6)
Firefighter§	330 (2.0)	6.7 (4.2–9.9)
Imaging technician	719 (4.4)	4.2 (2.8–5.9)
Laboratory technician	293 (1.8)	3.4 (1.7– 6.2)
Midlevel clinician	566 (3.5)	4.6 (3.0–6.7)
Nurse	6,426 (39.2)	7.7 (7.1–8.4)
Nurse assistant	641 (3.9)	12.8 (10.3–15.6)
Other¶	688 (4.2)	6.8 (5.1–9.0)
Other health#	200 (4.6)	7.5 (4.3–12.1)
Pharmacist	321 (2.0)	4.4 (2.4–7.2)
Physical therapist	235 (1.4)	10.6 (7.0–15.3)
Physician	2,297 (14.0)	6.1 (5.1–7.1)
Police/corrections officer	785 (4.8)	4.0 (2.7–5.6)
Respiratory therapist	409 (2.5)	8.3 (5.8–11.4)
PPE		
Gown use all the time	9,316 (56.8)	6.9 (6.4–7.5)
Glove use all the time	11,887 (72.5)	7.0 (6.5–7.5)
N95 respirator use all the time	7,316 (44.6)	6.9 (6.3–7.5)
PAPR use all the time	695 (4.2)	7.6 (5.8–9.9)
Goggles/face shield all the time	6,581 (40.1)	6.5 (5.9–7.1)
Surgical facemask all the time	9,452 (57.6)	6.6 (6.1–7.1)

*Work location categories are not mutually exclusive: 17.2% of participants reported ≥1 workplace. EMT, emergency medical technician; PAPR, powered air purifying respirator; PPE, personal protective equipment; SARS-CoV-2, severe acute respiratory syndrome coronavirus 2.
†Includes dialysis, telemetry, cardiovascular, extracorporeal membrane oxygenation (ECMO), respiratory, emergency/critical care, anesthesia, endoscopy, orthopedic, surgical, neurodiagnostic, urology, audiology, and radiation technicians.
‡Includes firefighter/medical first responder.
§Includes fire inspector and fire marshal.
¶Includes dietary staff, environmental staff, social worker/chaplain, maintenance staff, supervisor.
#Includes dentist, medical examiner, orderly, phlebotomist, therapy aide, trainee.

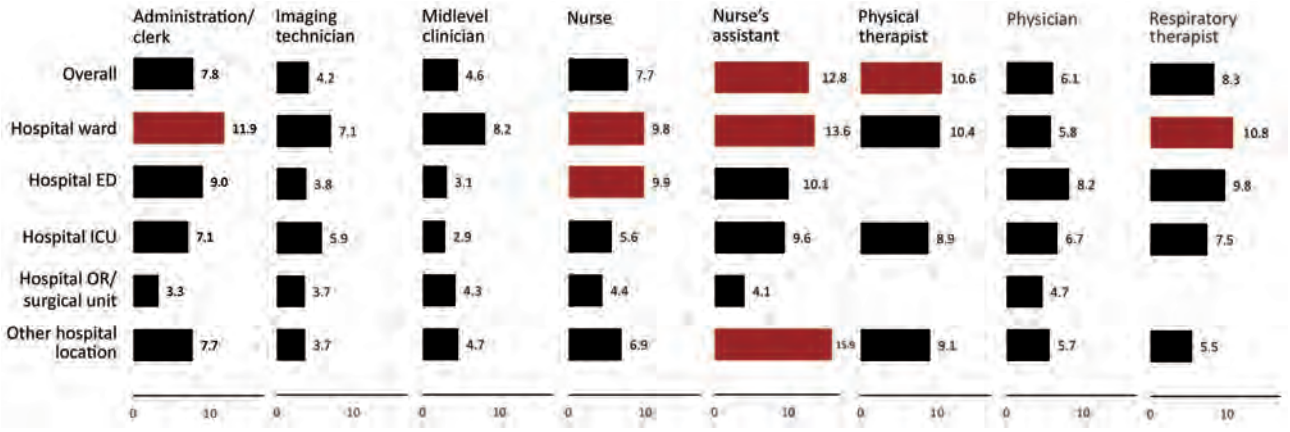

Figure 2. Seropositivity for SARS-CoV-2 among healthcare personnel by selected occupation and hospital work location, Detroit metropolitan area, Michigan, USA, May–June 2020. Red bars: lower 95% CI for percent positive is >6.9% (overall percent positive). Other hospital locations are all other locations not specifically listed in the chart (e.g., radiology, laboratory). Estimates not shown for categories with sample size <25 participants. ED, emergency department; ICU, intensive care unit; OR, operating room; SARS-CoV-2, severe acute respiratory syndrome coronavirus 2.

6 Michigan counties) as a result of targeted and repeated testing of personnel in hospitals and emergency medical services settings (*11*). Even so, surveillance of these occupational groups in Detroit based on self-reported RT-PCR testing results would have identified a minority of infections.

Healthcare workers are known to be at occupational risk for SARS-CoV-2 exposure (*12*). Participants in occupations that may involve frequent and prolonged patient contact, such as nurse assistants and nurses (*13*,*14*), were more likely to be seropositive than physicians. Multivariable analysis revealed a weak association between lower seropositivity and consistent use of N95 respirators and surgical facemasks. Lower seroprevalence was observed among participants who reported high use of PPE despite shortages and reuse/extension protocols that could be hypothesized to lower the observed effectiveness of PPE. These and other confounding factors may obscure the role PPE plays in preventing infection, and it may be necessary to account for multiple factors in studies assessing the effect of PPE. The lower likelihood of seroprevalence associated with working in the controlled environments of a hospital ICU or surgical ward may reflect the impact of additional mitigation measures, including clear identification of infected persons and environmental and engineering controls (*15*). This pattern of lower seropositivity among staff in higher-risk versus lower-risk hospital settings has been described previously (*16*). However, even within healthcare work settings, some workers such as nurse assistants had a higher risk of infection than those in other roles. This finding highlights the concern that certain occupations may require additional focus on assessing and controlling factors related to transmission.

Together, these analyses of community and workplace factors show the contribution of community acquired infection to seropositivity among Detroit area healthcare workers. For 3 hospital settings (hospital ward, ED, and ICU) that could be compared across healthcare occupations, seropositivity rose with closer proximity of the facility to the Detroit center. This pattern suggests that regardless of occupation or work location, community acquisition was a common underlying factor of infection risk. There are 2 related implications. First, the observed impact of PPE may be reduced given the background impact of community acquisition of SARS-CoV-2 infection. Second, reducing community spread through population-based measures may directly protect healthcare workers on 2 fronts: reduced occupational exposure as a result of fewer infected patients in the less controlled workplace settings such as the ED, and reduced exposure in their homes and communities.

After adjusting for other factors, we found that women were less likely than men to be seropositive. This pattern was seen only in adjusted analysis; women's lower risk may have been obscured by their disproportionate representation in the occupations at higher risk of infection. Women represented 69% of the sample but made up 86% of those in nursing and nurse assistance.

Participants ≥65 years of age were less likely to be infected than younger workers. This pattern may be the result of measures to protect older workers

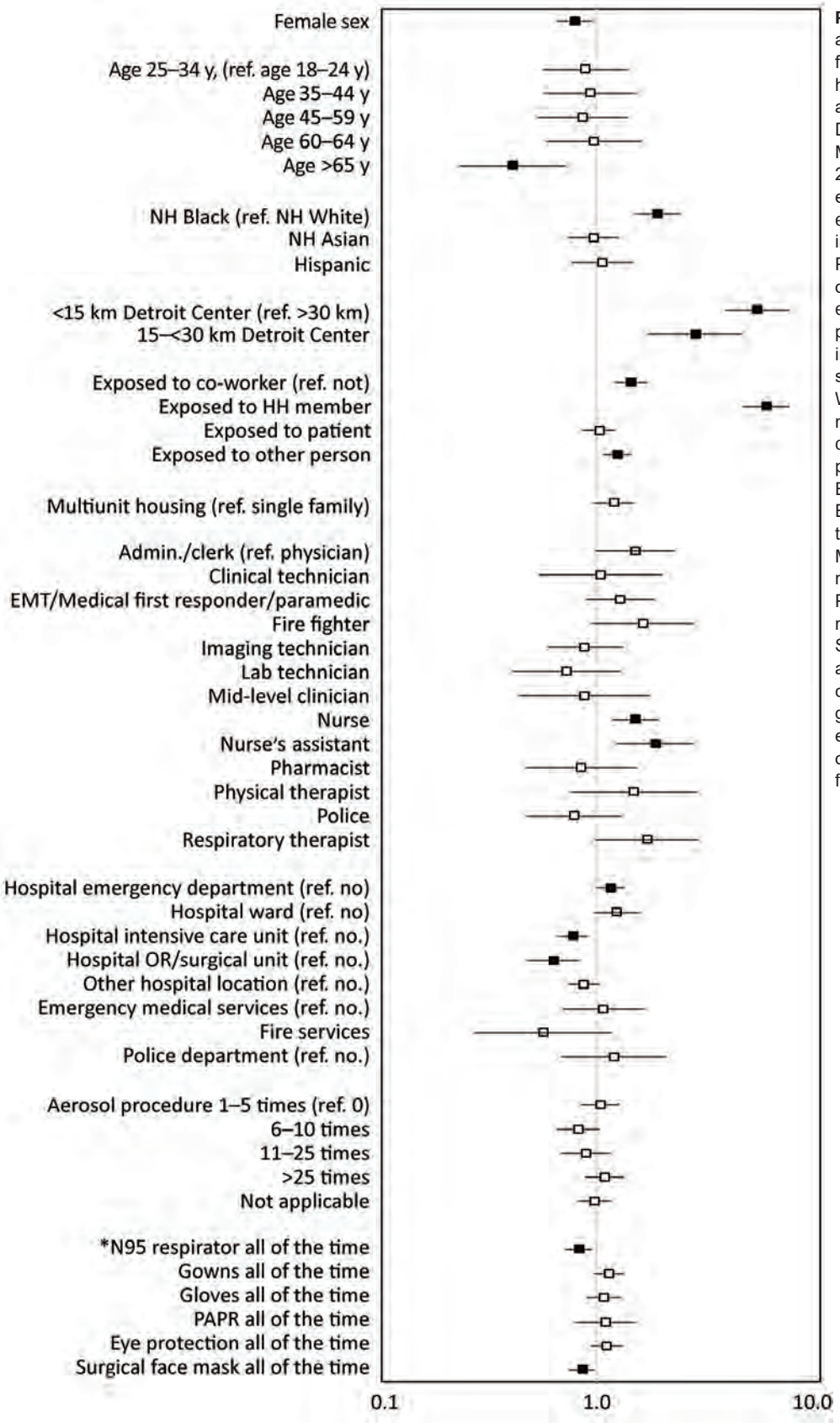

Figure 3. Adjusted odds ratios and 95% CIs for seropositivity for SARS-CoV-2 among healthcare, first response, and public safety personnel, Detroit metropolitan area, Michigan, USA, May–June 2020. Adjusted model was estimated using generalized estimating equations including all variables shown. Participants with other occupations, of other race/ethnicity, or who declined to provide their race/ethnicity are included in the models, but not shown as separate categories. Workplace variables are not mutually exclusive. Reference categories are noted in parentheses for each section. ED, emergency department; EMT, emergency medical technician; HH, household; Med 1st resp, medical first responder; NH, non-Hispanic; PAPR, powered air-purifying respirator; ref., reference; SARS-CoV-2, severe acute respiratory syndrome coronavirus 2. *Reference groups for personal protective equipment variables are all other responses with less frequency than "all the time."

from high-risk situations or from greater precautions taken among this group. A population study that also observed lower seroconversion among older persons found that older persons were less likely to live with a household contact (*17*). Seroconversion may also diminish with age in general (*17*), although other studies showed no pattern by age or higher seroprevalence among older persons (*18*,*19*). Participants of non-Hispanic Black race/ethnicity remained more likely to be seropositive than non-Hispanic white participants, even after adjustment. Community-level surveillance of COVID-19 infection and SARS-CoV-2 infection has demonstrated overrepresentation of minority groups in population-adjusted analyses (*20*,*21*). One hypothesis for the higher risk of infection among Black and Hispanic persons is employment in jobs without possibility of working remotely (*22*). Unfortunately, the survey did not collect information about occupation and workplace of household members. We speculate that the higher risk of exposure/infection among non-Hispanic Black versus non-Hispanic White participants in our study likely reflects uncontrolled confounding by factors for which data were not available.

Some limitations must be considered. The survey was a convenience sample with unknown representativeness: 80% of the 20,650 employees anticipated by MCA and hospital contacts to be eligible participated but agency participation varied, with highest participation among hospital personnel. The cross-sectional design precluded determining the source of exposure. In addition, comprehensive exposure data (e.g., travel, commuting, social exposures) were not collected. Because of the limited questionnaire length, PPE questions did not probe donning and doffing training, participant familiarity with PPE use, or reuse or extension protocols that may have affected effectiveness (*11*). No additional questions were asked about other workplace infection control practices. Another potential source of bias is the healthy worker effect, in which persons with prolonged COVID-19 infection or sequelae would not have been onsite to participate. Seroprevalence may be underestimated, given that the sensitivity of the antibody test was less than 100%. It is also possible that participants who were infected did not seroconvert (*23*; F. Gallais et al., unpub. data, https://www.medrxiv.org/content/10.1101/2020.06.21.2013244 9v1), but it is unknown whether lack of seroconversion may have occurred systematically between occupations (e.g., those exposed more intensely or with more severe illness may be more likely to develop antibodies) (*24*). Although more recent infections may have not been detected, it is unlikely that this varied systematically across groups. Strengths included coverage of a large number of personnel at hospitals and first response/public safety facilities and pairing antibody testing with questionnaire data to enable focus on a high-risk population.

Key implications for the risk of SARS-CoV-2 infection among healthcare, first response, and public safety personnel include the impact of community acquisition, increased odds of exposure associated with specific healthcare occupations, and the protection provided by PPE. Effects of interventions that could be further studied and implemented include providing alternative housing to healthcare workers during times or in areas of high community prevalence and ensuring that workers in high-risk occupations are given adequate PPE, specifically N95 respirators and surgical facemasks, as well as infection control training.

Acknowledgments

The authors thank members of the Quest Diagnostics team: Jeff Chapman, Jeff Crawford, Steve Dudek, Sofija Ivancevic, Brian Jaffa, Kathryn Logan, Christine McKenna, Rebecca Parsons, Sahana Ramprasad, Susan Smart, and Dianna Tate. The authors thank members of the NIOSH Occupational Data Collection and Coding Support and Consultation Teams for their assistance with occupation and workplace classification: Pam Schumacher, Jennifer Cornell, Jeff Purdin, Matthew Groenewold, Sara Luckhaupt, Stacey Marovich, Matt Hirst, Liz Smith, Surprese Watts, Rebecca Purdin, Marie De Perio, Sherry Burrer, Laura Reynolds, and George (Reed) Grimes. The authors also thank members of the CDC Data Collation and Integration for Public Health Event Responses (DCIPHER) team for their assistance in providing secure data transfer and storage: Stephen Sorokin, Nathan Golightly, Sachin Agnihotri, and Serena Burdyshaw. Finally, the authors are grateful to Brian Lein for assistance with survey planning and initial implementation.

Data and specimen collection activities and specimen testing were funded by a US Health and Human Services contract (no. 75P00120C00036).

About the Author

Dr. Akinbami is a pediatrician and epidemiologist in the Division of Health and Nutrition Examination Surveys, National Centers for Health Statistics, CDC, Hyattsville, Maryland, USA. She and her colleagues have undertaken this research while deployed to support the federal COVID-19 response.

References

1. Clapham H, Hay J, Routledge I, Takahashi S, Choisy M, Cummings D, et al. Seroepidemiologic study designs for determining SARS-COV-2 transmission and immunity. Emerg Infect Dis. 2020;26:1978–86. https://doi.org/10.3201/eid2609.201840
2. US Department of Health and Human Services. Title 45 Code of Federal Regulations 46, Protection of human subjects [cited May 1, 2020]. https://www.ecfr.gov/cgi-bin/text-idx?m=08&d=16&y=2020&cd=20200813&submit=GO&SID=83cd09e1c0f5c6937cd9d7513160fc3f&node=pt45.1.46&pd=20180719
3. US Food and Drug Administration. EUA authorized serology test performance; 2020 [cited 2020 Jul 30]. https://www.fda.gov/medical-devices/emergency-situations-medical-devices/eua-authorized-serology-test-performance
4. National Institute for Occupational Safety and Health. NIOSH industry and occupation computerized coding system (NIOCCS) [cited 2020 Jun 25]. https://www.fda.gov/medical-devices/emergency-situations-medical-devices/eua-authorized-serology-test-performance
5. Steensels D, Oris E, Coninx L, Nuyens D, Delforge ML, Vermeersch P, et al. Hospital-wide SARS-CoV-2 antibody screening in 3056 staff in a tertiary center in Belgium. JAMA. 2020;324:195–7. https://doi.org/10.1001/jama.2020.11160
6. Wee LE, Sim XYJ, Conceicao EP, Aung MK, Goh JQ, Yeo DWT, et al. Containment of COVID-19 cases among healthcare workers: the role of surveillance, early detection, and outbreak management. Infect Control Hosp Epidemiol. 2020 May 11 [Epub ahead of print]. https://doi.org/10.1017/ice.2020.219
7. State of Michigan. Coronavirus: Michigan data. 2020 [cited 2020 Jul 23]. https://www.michigan.gov/coronavirus/0,9753,7-406-98163_98173—,00.html
8. Havers FP, Reed C, Lim T, Montgomery JM, Klena JD, Hall AJ, et al. Seroprevalence of antibodies to SARS-CoV-2 in 10 sites in the United States, March 23–May 12, 2020. JAMA Intern Med. 2020 Jul 21 [Epub ahead of print]. https://doi.org/10.1001/jamainternmed.2020.4130
9. Sood N, Simon P, Ebner P, Eichner D, Reynolds J, Bendavid E, et al. Seroprevalence of SARS-CoV-2-specific antibodies among adults in Los Angeles County, California, on April 10–11, 2020. JAMA. 2020;323:2425–7. https://doi.org/10.1001/jama.2020.8279
10. Rosenberg ES, Tesoriero JM, Rosenthal EM, Chung R, Barranco MA, Styer LM, et al. Cumulative incidence and diagnosis of SARS-CoV-2 infection in New York. Ann Epidemiol. 2020;48:23–29.e4. https://doi.org/10.1016/j.annepidem.2020.06.004
11. Nguyen LH, Drew DA, Joshi AD, Guo CG, Ma W, Mehta RS, et al. Risk of COVID-19 among frontline healthcare workers and the general community: a prospective cohort study. Lancet Public Health. 2020 Jul 30 [Epub ahead of print]. https://doi.org/10.1016/S2468-2667(20)30164-X
12. Wei XS, Wang XR, Zhang JC, Yang WB, Ma WL, Yang BH, et al. A cluster of health care workers with COVID-19 pneumonia caused by SARS-CoV-2. J Microbiol Immunol Infect. 2020 Apr 27 [Epub ahead of print]. https://doi.org/10.1016/j.jmii.2020.04.013
13. Weigl M, Müller A, Zupanc A, Angerer P. Participant observation of time allocation, direct patient contact and simultaneous activities in hospital physicians. BMC Health Serv Res. 2009;9:110. https://doi.org/10.1186/1472-6963-9-110
14. Barker AK, Codella J, Ewers T, Dundon A, Alagoz O, Safdar N. Changes to physician and nurse time burdens when caring for patients under contact precautions. Am J Infect Control. 2017;45:542–3. http://dx.doi.org/10.1016/j.ajic.2017.01.026
15. Mani NS, Budak JZ, Lan KF, Bryson-Cahn C, Zelikoff A, Barker GEC, et al. Prevalence of COVID-19 infection and outcomes among symptomatic healthcare workers in Seattle, Washington. Clin Infect Dis. 2020 Jun 16 [Epub ahead of print]. https://doi.org/10.1093/cid/ciaa761
16. Korth J, Wilde B, Dolff S, Anastasiou OE, Krawczyk A, Jahn M, et al. SARS-CoV-2-specific antibody detection in healthcare workers in Germany with direct contact to COVID-19 patients. J Clin Virol. 2020;128:104437. https://doi.org/10.1016/j.jcv.2020.104437
17. Stringhini S, Wisniak A, Piumatti G, Azman AS, Lauer SA, Baysson H, et al. Seroprevalence of anti-SARS-CoV-2 IgG antibodies in Geneva, Switzerland (SEROCoV-POP): a population-based study. Lancet. 2020;396:313–9. https://doi.org/10.1016/S0140-6736(20)31304-0
18. To KK, Tsang OT, Leung WS, Tam AR, Wu TC, Lung DC, et al. Temporal profiles of viral load in posterior oropharyngeal saliva samples and serum antibody responses during infection by SARS-CoV-2: an observational cohort study. Lancet Infect Dis. 2020;20:565–74. https://doi.org/10.1016/S1473-3099(20)30196-1
19. Xu X, Sun J, Nie S, Li H, Kong Y, Liang M, et al. Seroprevalence of immunoglobulin M and G antibodies against SARS-CoV-2 in China. Nat Med. 2020;26:1193–5. https://doi.org/10.1038/s41591-020-0949-6
20. Feehan AK, Fort D, Garcia-Diaz J, Price-Haywood E, Velasco C, Sapp E, et al. Seroprevalence of SARS-CoV-2 and infection fatality ratio, Orleans and Jefferson Parishes, Louisiana, USA, May 2020. Emerg Infect Dis. 2020;26. https://doi.org/10.3201/eid2611.203029
21. Moore JT, Ricaldi JN, Rose CE, Fuld J, Parise M, Kang GJ, et al.; COVID-19 State, Tribal, Local, and Territorial Response Team. Disparities in incidence of COVID-19 among underrepresented racial/ethnic groups in counties identified as hotspots during June 5–18, 2020—22 states, February–June 2020. MMWR Morb Mortal Wkly Rep. 2020;69:1122–6. https://doi.org/10.15585/mmwr.mm6933e1
22. Selden TM, Berdahl TA. COVID-19 and racial/ethnic disparities in health risk, employment, and household composition. Health Aff (Millwood). 2020 Jul 14 [Epub ahead of print]. https://doi.org/10.1377/hlthaff.2020.00897
23. Brandstetter S, Roth S, Harner S, Buntrock-Döpke H, Toncheva AA, Borchers N, et al. Symptoms and immunoglobulin development in hospital staff exposed to a SARS-CoV-2 outbreak. Pediatr Allergy Immunol. 2020 May 15 [Epub ahead of print]. https://doi.org/10.1111/pai.13278
24. Wang X, Guo X, Xin Q, Pan Y, Hu Y, Li J, et al. Neutralizing antibody responses to severe acute respiratory syndrome coronavirus 2 in coronavirus disease 2019 inpatients and convalescent patients. Clin Infect Dis. 2020 Jun 4 [Epub ahead of print]. https://doi.org/10.1093/cid/ciaa721

Address for correspondence: Lara J. Akinbami, Centers for Disease Control and Prevention, 3311 Toledo Rd, Mailstop P08, Hyattsville, MD 20782, USA; email: lea8@cdc.gov

Flight-Associated Transmission of Severe Acute Respiratory Syndrome Coronavirus 2 Corroborated by Whole-Genome Sequencing

Hollie Speake, Anastasia Phillips, Tracie Chong, Chisha Sikazwe, Avram Levy, Jurissa Lang, Benjamin Scalley, David J. Speers, David W. Smith, Paul Effler, Suzanne P. McEvoy

To investigate potential transmission of severe acute respiratory syndrome coronavirus 2 (SARS-CoV-2) during a domestic flight within Australia, we performed epidemiologic analyses with whole-genome sequencing. Eleven passengers with PCR-confirmed SARS-CoV-2 infection and symptom onset within 48 hours of the flight were considered infectious during travel; 9 had recently disembarked from a cruise ship with a retrospectively identified SARS-CoV-2 outbreak. The virus strain of those on the cruise and the flight was linked (A2-RP) and had not been previously identified in Australia. For 11 passengers, none of whom had traveled on the cruise ship, PCR-confirmed SARS-CoV-2 illness developed between 48 hours and 14 days after the flight. Eight cases were considered flight associated with the distinct SARS-CoV-2 A2-RP strain; the remaining 3 cases (1 with A2-RP) were possibly flight associated. All 11 passengers had been in the same cabin with symptomatic persons who had culture-positive A2-RP virus strain. This investigation provides evidence of flight-associated SARS-CoV-2 transmission.

On March 21, 2020, the Western Australia Department of Health was notified that 6 passengers aboard a flight from Sydney, New South Wales, to Perth, Western Australia, Australia, on March 19 had tested positive for severe acute respiratory syndrome coronavirus 2 (SARS-CoV-2) by PCR. All 6 passengers had disembarked from cruise ships that had recently docked in Sydney. In the subsequent 2 weeks, several other cases of SARS-CoV-2 infection were identified among passengers on that flight.

Although the role of cruise ships in SARS-CoV-2 transmission is well documented (*1*), information regarding potential flight-associated transmission of SARS-CoV-2 (*2*,*3*) is limited. We investigated SARS-CoV-2 transmission associated with a 5-hour domestic flight by analyzing epidemiologic and whole-genome sequencing (WGS) data. Ethics approval was not required for this investigation, conducted as part of the public health response to the SARS-CoV-2 outbreak under the Western Australia Public Health Act 2016.

Methods

Public Health Response to Coronavirus Disease in Australia

In Australia, coronavirus disease (COVID-19) is an urgently notifiable disease (*4*); laboratory-confirmed cases and close contacts are investigated and managed according to national guidelines produced by the Communicable Disease Network of Australia (*4*). Details for flights with SARS-CoV-2 infectious persons on board are published at https://www.healthywa.wa.gov.au/coronavirus. Airlines are responsible for the management of crew and are notified of potential in-flight exposure by the National Incident Room (https://www.health.gov.au/initiatives-and-programs/national-incident-room).

Initial Public Health Investigation of the Flight

On the afternoon of March 19, 2020, a domestic flight within Australia departed Sydney and landed 5 hours later in Perth. The aircraft, an Airbus A330-200, had 28 business and 213 economy class passengers on

Author affiliations: University of Notre Dame, Fremantle, Western Australia, Australia (H. Speake); Metropolitan Communicable Disease Control, Perth, Western Australia, Australia (A. Phillips, T. Chong, B. Scalley, S.P. McEvoy); University of Western Australia, Perth (C. Sikazwe, A. Levy, D.J. Speers, P. Effler); PathWest Laboratory Medicine Western Australia, Nedlands, Western Australia, Australia (C. Sikazwe, A. Levy, D.J. Speers, D.W. Smith, J. Lang); Public Health Emergency Operations Centre, Perth (P. Effler)

DOI: https://doi.org/10.3201/eid2612.203910

board. Passengers were persons transiting to Perth through the Sydney International Airport after arriving from overseas and domestic travelers, some of whom had disembarked from 1 of 3 cruise ships that had recently docked in Sydney Harbour (Ovation of the Seas on March 18; Ruby Princess and Sun Princess on March 19).

After the initial 6 persons with COVID-19 were identified among passengers on the flight, all close contacts were informed of their potential exposure to SARS-CoV-2 and directed to quarantine themselves for 14 days. During this investigation, PCR testing for SARS-CoV-2 was limited to persons experiencing symptoms. By April 1, SARS-CoV-2 infection was confirmed for >20 passengers on the flight, and attempts were made to notify all remaining passengers of their potential exposure. The number of infections linked to the flight and the timing of symptom onset among persons with a later diagnosis suggested that flight-associated transmission may have occurred.

Laboratory Methods

For patients with suspected SARS-CoV-2 infection, a throat swab and bilateral nasopharyngeal or deep nasal specimens were collected on flocked nasopharyngeal swabs. The swabs were placed in viral, universal, or Liquid Amies (https://www.copanusa.com) transport medium, then transported and stored at 4°–8°C. Testing was conducted at PathWest Laboratory Medicine WA by use of either the Roche cobas SARS-CoV-2 test (Roche Diagnostics, https://www.roche.com) or combined in-house assays directed at envelope and spike protein gene targets (Table 1) (*5*). The in-house assays were approved for diagnostic use by the National Association of Testing Authorities according to the provisions of the National Pathology Accreditation Advisory Council (*6*).

When a sample was available for genomic testing, it underwent tiled amplicon PCR at PathWest to generate 14 overlapping amplicons representing the whole genome (Appendix Table, https://wwwnc.cdc.gov/EID/article/26/12/20-3910-App1.pdf), which were then sequenced on an Illumina MiSeq sequencer (Illumina, https://www.illumina.com). If multiple samples were available from 1 patient, we used samples with the highest viral loads (i.e., lowest cycle threshold values). Processed reads were mapped to the SARS-CoV-2 reference genome (GenBank accession no. MN908947). Primer-clipped alignment files were imported into Geneious Prime version 2020.1.1 (https://www.geneious.com) for coverage analysis before consensus calling, and consensus sequences were generated by using iVar version 1.2.2 (https://github.com/andersen-lab/ivar).

Genome sequences of SARS-CoV-2 from Western Australia were assigned to lineages (*7*) by using the Phylogenetic Assignment of Named Global Outbreak LINeages (PANGOLIN) tool (https://github.com/cov-lineages/pangolin). On July 17, 2020, we retrieved SARS-CoV-2 complete genomes with corresponding metadata from the GISAID database (https://www.gisaid.org/epiflu-applications/nextthcov-19-app). The final dataset contained 540 GISAID whole-genome sequences that were aligned with the sequences from Western Australia generated in this study by using MAFFT version 7.467 (https://mafft.cbrc.jp/alignment/software). Phylogenetic trees were visualized in iTOL (Interactive Tree Of Life, https://itol.embl.de) and MEGA version 7.014 (*8*). At the time of sequencing, the virologists and scientists overseeing and performing the WGS were blinded as to the epidemiologic details (Appendix).

Virus culture was attempted for primary samples sent directly to the reference laboratory but not for samples received after primary testing at another laboratory. Clinical specimens were inoculated in triplicate wells with Vero-E6 cells at 80% confluency, incubated at 37°C in 5% CO_2, and inspected for cytopathic effect daily for up to 10 days. Identity was confirmed by in-house PCRs as described for previous sequences.

Determining Likely Source of Infection

The likely source of infection for each passenger with PCR-confirmed SARS-CoV-2 infection was determined by using the results of WGS and epidemiologic investigations that assessed the potential for other sources of exposure during the incubation period. For

Table 1. Primers and probe sequences used for in-house diagnostic assays used to test persons with suspected SARS-CoV-2 infection after flight from Sydney to Perth, Australia, March 19, 2020

Oligonucleotide	Sequence, 5′→3′	Concentration, μM
BetaCoV_Wuhan_F22595 (forward)	TGAAGTTTTTAACGCCACCAGAT	0.7
BetaCoV_Wuhan_R22662 (reverse)	CACAGTTGCTGATTCTCTTCCTGTT	0.9
BetaCoV_Wuhan_P22619-HEX (hydrolysis probe)	(HEX)C[+A][+A]GCAT[+A][+A]A[+C]AGATGCA(BHQ1)	0.3
MS2-105F (forward)	GTCGACAATGGCGGAACTG	0.2
MS2-170R (reverse)	TTCAGCGACCCCGTTAGC	0.5
MS2-127-VIC (hydrolysis probe)	(VIC)ACGTGACTGTCGCCCCAAGCAACTT(QSY)	0.2

this investigation, we considered primary cases to be passengers with SARS-CoV-2 infection identified by PCR in Western Australia who probably acquired their infection before boarding the flight.

We defined primary cases as passengers with SARS-CoV-2 who had been on a cruise ship with a known outbreak in the 14 days before illness onset and whose specimen yielded a virus genomic sequence closely matching that of the ship's outbreak strain; any passenger whose illness began before or within 48 hours after the flight's departure (i.e., infectious during the flight); or both. We defined secondary cases as passengers with PCR-confirmed SARS-CoV-2 infection who had not been on a cruise ship with a known SARS-CoV-2 outbreak within 14 days of illness onset and in whom symptoms developed >48 hours after and within 14 days of the flight. We further characterized secondary cases as being flight associated if they were in international passengers who arrived in Sydney on March 19 or domestic Australia travelers who had not been on a cruise ship in the 14 days before illness and whose specimens yielded a WGS lineage not known to be in circulation at their place of origin but that closely matched the lineage of a primary case on the flight. Secondary cases among persons who had recently been on a cruise ship with no known onboard SARS-CoV-2 transmission or domestic passengers who had not been on a cruise ship but for whom WGS information was unavailable were categorized as possibly flight associated (Table 2).

Statistical Analyses

We tested the hypothesis that the risk for flight-associated infections was independent of seat assignment, as might occur if secondary infections were acquired while awaiting the flight in Sydney or after disembarking in Perth. We compared the proportion of secondary cases observed between aircraft cabins and between seating types (i.e., window vs. nonwindow seats) by calculating risk ratios with corrected Mantel-Haenszel χ^2 tests and using EpiInfo Statcalc version 7.2.0.1 (https://www.cdc.gov/epiinfo).

Results

A total of 64 passengers on the flight had or later experienced an illness compatible with COVID-19 and were tested by PCR; 29 were SARS-CoV-2 positive (Figure 1) and 35 were negative. Among PCR-confirmed cases, symptom onset occurred during March 15–April 1, 2020 (Figure 2); median age was 59 (range 4–81) years, 14 were female, and 15 were male. Moreover, 13 had been passengers on the Ruby Princess, 4 on the Ovation of the Seas, and 2 on the Sun Princess. Five others were international travelers transiting through Sydney, and 5 were domestic travelers within Australia who had not been on a cruise ship.

Sufficient viral RNA was available to generate an adequate sequence for 25 of the 29 samples positive by PCR; 100% coverage was obtained for 21 and partial coverage (81%–99%) for 4 samples. The phylogenetic tree for the 21 complete genomes (Figure 3; Appendix Figure, panel A) showed that they belonged to either the A.2 (n = 17) or B.1 (n = 4) sublineages of SARS-CoV-2. All of the complete A.2 sequences belonged to a distinct genomic cluster separated by ≤2 single-nucleotide polymorphisms (Appendix Figure, panel B), which we designated as A2-Ruby Princess (A2-RP). The A2-RP strain had not been identified on the GISAID international database before this outbreak (*9*). The 4 B.1 viruses comprised 3 B.1.31 and 1 phylogenetically more distant B.1 strain. Of the 4 partial sequences, 3 clustered with the A2-RP strains and the other was designated B.1.1 and was phylogenetically close to the B.1.31 sequences (Figure 3). We attempted to culture 17 PCR-positive specimens, 9 of which grew SARS-CoV-2.

Primary Cases

Of the 29 cases of PCR-confirmed SARS-CoV-2 linked to the flight, 18 were classified as primary

Table 2. Criteria for flight-associated and possibly flight-associated secondary cases of SARS-CoV-2 infection in persons aboard a flight from Sydney to Perth, Australia, March 19, 2020

Secondary case classification	Epidemiologic criteria	Virus WGS criteria
Flight associated	International passenger who arrived at Sydney International Airport on March 19, 2020, and transited to the flight OR domestic passenger in Australia not associated with a cruise ship before illness	Specimen yielded lineage not circulating in place of origin AND Lineage closely matched that of passengers with primary cases on flight
Possibly flight associated	Passenger on cruise ship with no known SARS-CoV-2 transmission identified Domestic passenger in Australia not associated with a cruise ship before illness	Specimen from passenger or traveling companion yielded lineage related to that of passengers with primary cases on flight WGS data not available

*WGS, whole-genome sequencing.

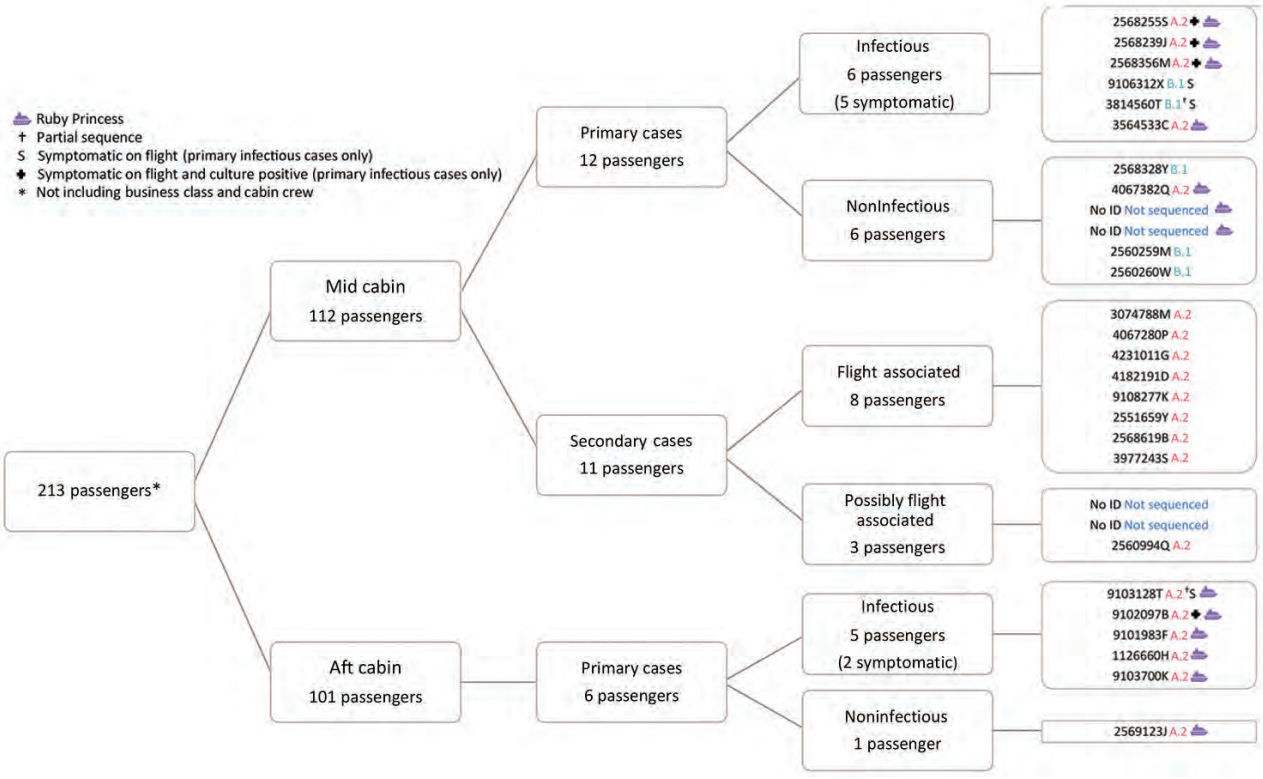

Figure 1. Distribution of SARS-CoV-2 infection cases among passengers on a flight from Sydney to Perth, Australia, on March 19, 2020. Far right column shows passenger identification numbers and SARS-CoV-2 lineage determined by whole-genome sequencing (A.2, B.1, not determined).

cases. Former Ruby Princess passengers accounted for 13 of the primary cases, and all viruses with WGS available were A2-RP strain. Nine Ruby Princess passengers were classified as infectious during the flight based on illness onset; 4 specimens collected on the day after the flight (March 20) were culture positive. Of the remaining 5 primary cases, 4 were in passengers from the Ovation of the Seas (1 classified as infectious during the flight); SARS-CoV-2 virus was B.1.31 for 3 passengers, and for the other passenger a partial B.1.1 sequence clustered near the B.1.31 viruses. Virus of the fifth B.1 lineage was obtained from a traveler returning from the United States who was also infectious during the flight (Figure 3; Appendix Figure 1, panel B).

Secondary Cases

We identified 11 secondary cases with symptom onset during March 22–April 1; among these, 8 cases were classified as flight associated. These 8 persons did not know each other. Four had commenced their journeys from different US cities and had taken an overnight flight from Los Angeles, California, USA, which landed at Sydney Airport on the morning of March 19. All had viruses of the A2-RP strain (3 by full and 1 by partial sequence; Figure 2), which was not circulating in the United States at the time of the flight. As of July 28, 2020, the GISAID database contained 5 sequences from 2 US sites that matched the A2-RP strain; relevant public health authorities confirmed that these sequences were obtained from passengers returning to the United States after disembarking from the Ruby Princess in Australia with specimen collection dates on or after March 22.

The remaining 4 flight-associated cases flew from various locations in New South Wales. Two resided in Sydney, 1 took a short flight from regional New South Wales, and 1 traveled by car several hours to Sydney Airport on March 19. None were previously identified contacts of a person with COVID-19 or had any known interactions with cruise ship passengers before the flight. All had virus with the A2-RP strain. There was no evidence of A2-RP strain circulation in Sydney before disembarkation of passengers from the Ruby Princess on March 19 (*9*,*10*). The median duration from day of flight to illness onset for the 8 persons with flight-associated infections was 4 (range 3–6) days.

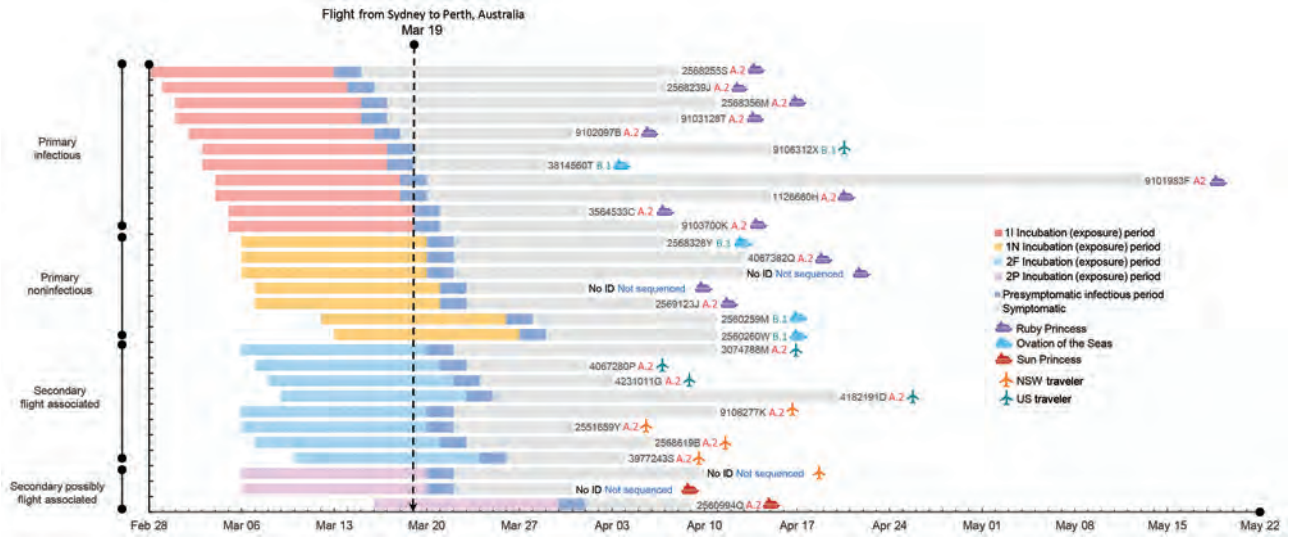

Figure 2. Theoretical maximum incubation (exposure), infectious period, and symptomatic period until time of resolution of illness in passengers on flight from Sydney to Perth, Australia, on March 19, 2020, with primary and secondary SARS-CoV-2 cases, by place of journey origin. Passenger identification numbers and SARS-CoV-2 lineage determined by whole-genome sequencing (A.2, B.1, not determined) indicated to right of bars. NSW, New South Wales, Australia; 1I, primary case, infectious; 1N, primary case, noninfectious; 2F, secondary case, flight associated; 2P, secondary case, possibly flight associated.

Three secondary cases were classified as possibly flight associated. Two traveling companions disembarked from the Sun Princess cruise on March 19; there was no outbreak of SARS-CoV-2 on this cruise ship, and neither person had known contact with anyone with COVID-19. Virus was the A2-RP strain for 1 of these persons, but no specimen was available for WGS for the other. One case in a domestic passenger who spent the incubation period in regional Sydney Airport was classified as possibly rather than flight associated because no specimen was available for WGS.

Overall, the risk of acquiring SARS-CoV-2 in New South Wales or Western Australia from an unknown community source during this time was low. On the day of the flight, New South Wales (population 7.5 million) reported a cumulative total of 307 COVID-19 infections, of which only 26 (3.5 cases/1,000,000 population) were locally acquired from an unknown source (*11*); in Western Australia (population 2.6 million), 52 cumulative cases had been identified, of which only 2 were locally acquired from an unknown source (0.8 cases/1,000,000 population) (*12*).

Spatial Distribution during Flight

Eleven primary cases (6 passengers in mid cabin and 5 in aft cabin) were classified as having been infectious during the flight; 5 were symptomatic. The mid cabin had 3 symptomatic passengers from the Ruby Princess seated together in the same row in the middle section; all had A2-RP (full sequence) viruses and positive virus culture results (Figure 4). In the mid cabin were 1 infectious traveler from the United States, 1 from Ovation of the Seas (both with B.1 lineage virus and culture-negative results), and 1 additional Ruby Princess passenger who was presymptomatic but infectious. The remaining 5 infectious primary cases (all Ruby Princess passengers) were seated in the aft cabin; 2 were symptomatic during the flight. All secondary cases occurred in persons seated in the economy class mid cabin.

Among secondary cases, 8 passengers were seated within 2 rows of infectious Ruby Princess passengers and 3 were more distant (2 possibly flight-associated cases were seated 3 rows away and 1 flight-associated case was seated 6 rows away). Seven (64%) secondary cases were among persons who had window seats (Figure 4).

Risk for Infection by Cabin and Seat Position

The risk for SARS-CoV-2 secondary infections among passengers seated in the mid cabin (11 cases/112 passengers) was significantly greater than for those seated in the aft cabin (0 cases/101 passengers; risk ratio undefined; corrected Mantel–Haenszel $\chi^2 = 8.6$; $p<0.005$). The secondary attack rate among mid-cabin passengers in window seats (7 cases/28 passengers) was significantly greater than among those not in window seats (4/83;

risk ratio 5.2; 95% CI 1.6–16.4; corrected Mantel–Haenszel $\chi^2 = 7.0$; $p<0.007$).

Discussion

This combination of comprehensive epidemiologic investigation and WGS analysis builds a strong case for flight-associated transmission of SARS-CoV-2. Convergence of the following 3 factors enabled this investigation: 1) the emergence of a unique SARS-CoV-2 strain (A2-RP) among cruise ship passengers disembarking in Sydney at the time of the flight, 2) identification of the A2-RP virus sequence among travelers arriving from overseas who did not leave the Sydney Airport before transiting to the flight, and 3) the very limited community transmission of SARS-CoV-2 within Australia at the time.

Other published reports describe suspected flight-associated transmission of SARS-CoV-2 (*2*,*3*,*13*,*14*), but these reports lack supportive genomic evidence. Our investigation demonstrates the value of WGS for elucidating transmission of SARS-CoV-2. Without genomic evidence, we would have assumed that the overseas travelers on this flight acquired their infection in the United States rather than within Australia.

We report several other findings. First, 3 of the 11 persons with secondary infections were outside the usual parameters used to identify close contacts of an infectious passenger on an airplane (2 rows in front and behind). On the flight described, passengers with flight-associated infection spanned 9 rows and were on opposite sides of the airplane. Discussion with airline representatives indicated that no air handling maintenance issues were logged for this flight and no illnesses were reported among the crew (Director of Medical Services for the airline, pers. comm., 2020 Sep 8). Although the results of 1 study of SARS-CoV-1 indicated a significantly increased risk for infection among passengers seated within 2 or 3 rows in front of an index case (*15*), secondary cases have also been reported for passengers seated farther away (*16*). A report funded by the US Federal Aviation Administration concluded that human movement might explain the transmission of SARS-CoV-1 "to passengers seated as far as seven rows from the infected passenger during the SARS outbreak in 2003" (*17*). The spatial distribution of secondary cases on this flight suggests that the current public health practice for contact tracing of passengers exposed to SARS-CoV-2 while aboard aircraft may benefit from additional study (*18*,*19*).

Second, most of the secondary infections were in persons seated at the window, 2 of whom denied ever leaving their seat during the flight. This finding was unanticipated given the widely held view that persons in window seats are at lower risk for exposure to an infectious pathogen during flight, a belief supported by data simulating transmission of droplet-mediated respiratory illnesses during flights of similar duration on single-aisle airplanes in the

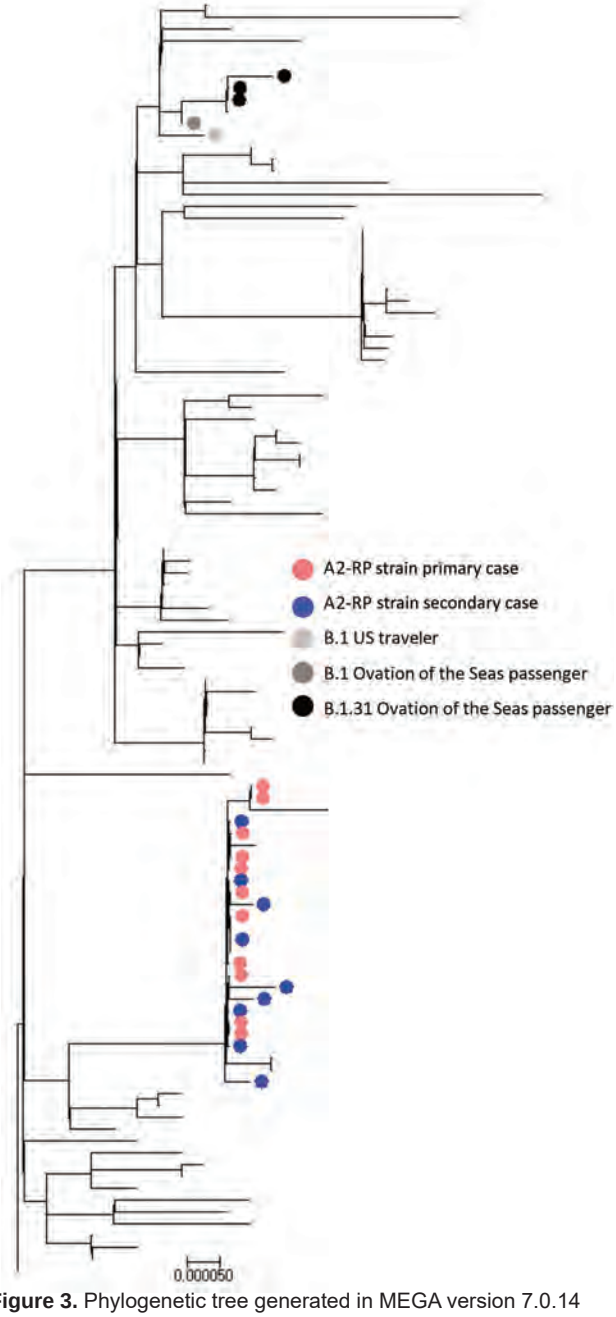

Figure 3. Phylogenetic tree generated in MEGA version 7.0.14 (*8*) for all SARS-CoV-2 whole-genome sequences with ≥80% genome coverage. Colors indicate samples from 458 persons with cases linked to cluster on flight from Sydney to Perth, Australia, on March 19, 2020. Scale bar indicates nucleotide substitutions per site.

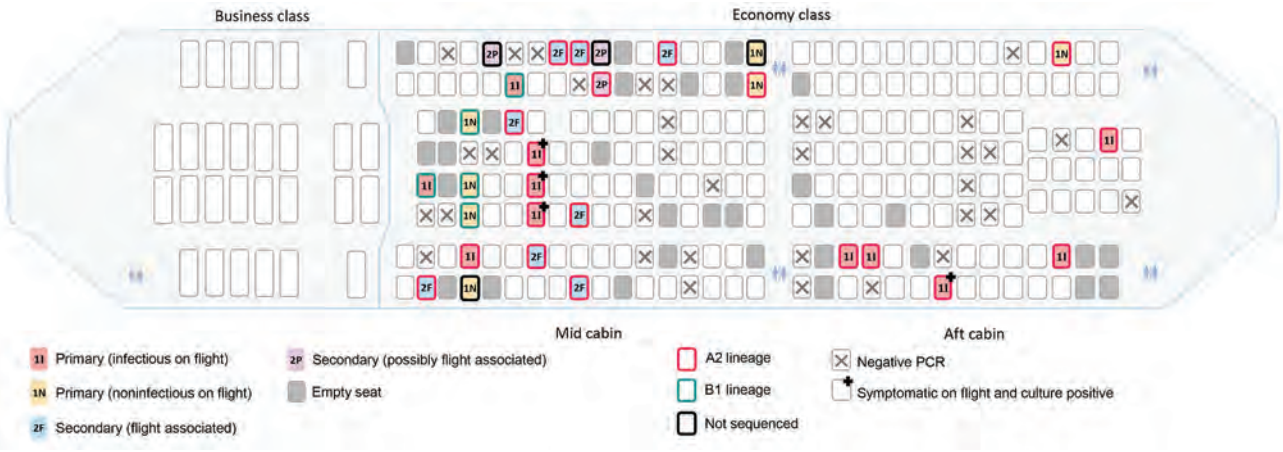

Figure 4. Spatial distribution of primary (infectious and noninfectious) and secondary (flight-associated and possibly flight-associated) cases of SARS-CoV-2 aboard flight from Sydney to Perth, Australia, on March 19, 2020. Passengers are identified by place of origin and SARS-CoV-2 lineage as determined by whole-genome sequencing. 1I, primary case, infectious; 1N, primary case, noninfectious; 2F, secondary case, flight associated; 2P, secondary case, possibly flight associated.

United States (*20*). Other studies, however, have emphasized the difficulty of measuring and understanding the complex airflow inside an aircraft cabin, even under steady-state conditions (*17*). In addition, movement of passengers and crew can also affect airflow patterns on board; further study of the dynamics of airflow on aircraft under real-world conditions is warranted.

Third, the risk for secondary SARS-CoV-2 infections from an infectious passenger during flight does not seem to be uniform. On this flight, there were 2 potentially infectious persons with a B lineage virus, but no B lineage secondary infections were identified. Furthermore, several persons with potentially infectious primary cases with A2-RP virus strain were in the mid and aft cabins (4 mid cabin and 5 aft cabin), and yet no secondary cases were identified in the aft cabin. This disparity raises the possibility that there was ≥1 SARS-CoV-2 superspreader in the mid cabin during the flight (*21*). Although no reports of unwell passengers were logged with the airline for this flight (Director of Medical Services for the airline, pers. comm., 2020 Sep 8), 5 of the 8 passengers with flight-associated secondary cases reported having noted coughing passengers. Anecdotal information obtained via interviews indicates that mask use was rare among the passengers overall, including those who had respiratory symptoms. Of note, 2 passengers with secondary cases reportedly wore masks during the flight but not for the entire flight. Although semiquantitative data on comparative viral loads based on cycle threshold values was available, we could not use these data to further investigate the role of upper respiratory tract viral load for determining transmission risk because samples were collected after the flight. Therefore, viral loads of passengers during the flight are unknown. Of note, 4 persons who were infectious on the flight had culture-positive specimens collected the next day (March 20; Figure 4).

Reports of suspected in-flight transmission of SARS-CoV-2 are relatively few, which probably reflects the challenges of establishing in-flight transmission; the fact that flight-associated transmission may be rare; and the fact that as the pandemic progressed, many airlines adopted measures to decrease risk (e.g., reduced food and beverage services, removal of in-flight entertainment, provision of masks and sanitizing wipes, limitation of movement around the cabin, and enhanced cleaning of the airplane) (*22*). The Australian Health Protection Principal Committee has endorsed a Domestic Passenger Journey Protocol to provide clear guidance regarding risk-minimization principles and processes in domestic airports and on airplanes for domestic passengers (*23*,*24*). This guidance also entails "reminding people not to travel if unwell" (*23*,*24*). As awareness of the threat posed by COVID-19 on cruise ships has grown, it is unlikely that the circumstances that led to exposures on this flight will be repeated.

This study has several limitations. First, we cannot exclude the possibility that the 3 passengers with possibly flight-associated infection might have been exposed before or after their journey; however, the very low levels of community transmission in Australia at the time, combined with the known proximity of these travelers to infectious persons on the airplane,

suggest that this possibility is unlikely. Conversely, we cannot rule out the possibility that the 7 passengers with primary cases who had disembarked from a cruise ship with known SARS-CoV-2 illnesses on board but in whom symptoms developed >48 hours after the flight acquired their infection aboard the airplane; however, given the balance of probabilities, it is more likely that they acquired their infections on the ship. Second, lack of detailed information for all passenger movements within the airport, at the boarding gate, and aboard the aircraft also limits our ability to determine with specificity where flight-associated exposures occurred. However, the spatial clustering of all secondary cases within the mid cabin suggests that transmission most likely occurred aboard the airplane. If persons had been exposed principally at the airport, one might expect the 11 secondary cases to have been distributed beyond the mid cabin. On this flight, all passengers were invited to board at the same time, rather than by rows. Third, categorizing cases as primary or secondary was predicated on the passenger's self-reported date of symptom onset, which may have been subject to recall errors. Fourth, case ascertainment bias is possible because although all passengers were informed of their potential exposure, passengers who had disembarked from a cruise ship that subsequently had a widely publicized outbreak or the close contacts of a primary case who were actively monitored for 14 days may have been more likely to seek testing if they became ill. Last, we cannot be certain that we captured all SARS-CoV-2 infections among persons who traveled on this flight because PCR testing was limited to passengers who reported symptoms and testing is not 100% sensitive (*25*). Given that flight-associated transmission of SARS-CoV-2 from asymptomatic persons has been reported, it is possible that some persons with secondary infections were exposed to passengers other than the infectious cases we identified on the flight (*14*); thus, our findings on the spatial distribution of primary and secondary cases should be interpreted with caution. Attempts to identify additional primary and secondary cases by using SARS-CoV-2 serologic testing are ongoing.

In conclusion, this study documents transmission of SARS-CoV-2 associated with a medium-duration domestic flight within Australia. It also demonstrates the value of WGS for determining SARS-CoV-2 transmission.

Acknowledgments

We thank the Molecular Diagnostics staff of PathWest QE2 Medical Centre and Fiona Stanley Hospital for accessing specimens for sequencing, and we thank the public health nurses in the North Metropolitan Health Service who undertook the initial contact tracing.

About the Author

Dr Speake is a dual trainee in General Practice and Public Health Medicine and is affiliated with the University of Notre Dame in Fremantle. She worked as a Public Health Registrar in the public health response to the SARS-CoV-2 outbreak in Perth.

References

1. Nakazawa E, Ino H, Akabayashi A. Chronology of COVID-19 cases on the Diamond Princess cruise ship and ethical considerations: a report from Japan. Disaster Med Public Health Prep. 2020 Mar 24:1–8 [Epub ahead of print]. https://doi.org/10.1017/dmp.2020.50
2. Eldin C, Lagier JC, Mailhe M, Gautret P. Probable aircraft transmission of Covid-19 in-flight from the Central African Republic to France. Travel Med Infect Dis. 2020;35:101643. https://doi.org/10.1016/j.tmaid.2020.101643
3. Qian GQ, Yang NB, Ding F, Ma AHY, Wang ZY, Shen YF, et al. Epidemiologic and clinical characteristics of 91 hospitalized patients with COVID-19 in Zhejiang, China: a retrospective, multi-centre case series. QJM. 2020;113:474–81. https://doi.org/10.1093/qjmed/hcaa089
4. Australian Government Department of Health. Coronavirus disease 2019 (COVID-19 [cited 2020 May 26]. https://www1.health.gov.au/internet/main/publishing.nsf/Content/cdna-song-novel-coronavirus.htm
5. Corman VM, Landt O, Kaiser M, Molenkamp R, Meijer A, Chu DK, et al. Detection of 2019 novel coronavirus (2019-nCoV) by real-time RT-PCR. Euro Surveill. 2020;25. https://doi.org/10.2807/1560-7917.ES.2020.25.3.2000045
6. National Pathology Accreditation Advisory Council. Requirements for the development and use of in-house in vitro diagnostic medical devices (IVDs) (fourth edition 2018) [cited 2020 Aug 22]. https://www1.health.gov.au/internet/main/publishing.nsf/Content/8838AD5DB81477D5CA257BF00019166E/$File/20180608%20-%20Final%20-%20Reqs%20for%20in-house%20IVDs.pdf
7. Rambaut A, Holmes EC, Hill V, O'Toole Á, McCrone J, Ruis C, et al. A dynamic nomenclature proposal for SARS-CoV-2 to assist genomic epidemiology. Nat Microbiol. 2020 Apr 19 [Epub ahead of print]. https://doi.org/10.1101/2020.04.17.046086
8. Kumar S, Stecher G, Tamura K. MEGA7: Molecular Evolutionary Genetics Analysis version 7.0 for bigger datasets. Mol Biol Evol. 2016;33:1870–4. https://doi.org/10.1093/molbev/msw054
9. Global Initiative on Sharing All Influenza Data [cited 2020 Aug 21]. https://www.gisaid.org
10. New South Wales Government. Special Commission of Inquiry into the Ruby Princess [cited 2020 Aug 28]. https://www.dpc.nsw.gov.au/assets/dpc-nsw-gov-au/publications/The-Special-Commission-of-Inquiry-into-the-Ruby-Princess-Listing-1628/Report-of-the-Special-Commission-of-Inquiry-into-the-Ruby-Princess.pdf
11. New South Wales Government Health. COVID-19 (coronavirus) statistics [cited 2020 May 05]. https://www.health.nsw.gov.au/news/Pages/20200319_00.aspx
12. Western Australian Government Department of Health. COVID-19 update—19 March 2020 [cited 2020 Aug 22].

https://ww2.health.wa.gov.au/Media-releases/2020/COVID19-update–19-March-2020
13. Hoehl S, Karaca O, Kohmer N, Westhaus S, Graf J, Goetsch U, et al. Assessment of SARS-CoV-2 transmission on an international flight and among a tourist group. JAMA Netw Open. 2020;3:e2018044. https://doi.org/10.1001/jamanetworkopen.2020.18044
14. Bae SH, Shin H, Koo H-Y, Lee SW, Yang JM, Yon DK. Asymptomatic transmission of SARS-CoV-2 on evacuation flight. Emerg Infect Dis. 2020 Aug 21 [Epub ahead of print]. https://doi.org/10.3201/eid2611.203353
15. Olsen SJ, Chang HL, Cheung TYY, Tang AF, Fisk TL, Ooi SP, et al. Transmission of the severe acute respiratory syndrome on aircraft. N Engl J Med. 2003;349:2416–22. https://doi.org/10.1056/NEJMoa031349
16. Lei H, Li Y, Xiao S, Lin CH, Norris SL, Wei D, et al. Routes of transmission of influenza A H1N1, SARS CoV, and norovirus in air cabin: comparative analyses. Indoor Air. 2018;28:394–403. https://doi.org/10.1111/ina.12445
17. Airliner Cabin Environment Research. Infectious disease transmission in airliner cabins [cited 2020 Sep 17]. https://www.faa.gov/data_research/research/med_humanfacs/cer/media/InfectiousDiseaseTransmission.pdf
18. Mangili A, Gendreau MA. Transmission of infectious diseases during commercial air travel. Lancet. 2005;365:989–96. https://doi.org/10.1016/S0140-6736(05)71089-8
19. World Health Organization. Contact tracing in the context of COVID-19 [cited 2020 May 14]. https://www.who.int/publications/i/item/contact-tracing-in-the-context-of-covid-19
20. Hertzberg VS, Weiss H, Elon L, Si W, Norris SL; FlyHealthy Research Team. Behaviors, movements, and transmission of droplet-mediated respiratory diseases during transcontinental airline flights. Proc Natl Acad Sci U S A. 2018;115:3623–7. https://doi.org/10.1073/pnas.1711611115
21. Xu X-K, Liu XF, Wu Y, Ali ST, Du Z, Bosetti P, et al. Reconstruction of transmission pairs for novel coronavirus disease 2019 (COVID-19) in mainland China: estimation of super-spreading events, serial interval, and hazard of infection. Clin Infect Dis. 2020;ciaa790. https://doi.org/10.1093/cid/ciaa790
22. qantas.com. Fly Well [cited 2020 Jul 14]. https://www.qantas.com/au/en/travel-info/travel-updates/coronavirus/health-while-flying.html
23. Department of Infrastructure. Domestic passenger journey protocol [cited 2020 Aug 21]. https://www.infrastructure.gov.au/aviation/files/covid-safe-flying-domestic-passenger-journey-protocol.pdf
24. Department of Infrastructure. COVID-safe domestic flying—domestic passenger journey protocol [cited 2020 Aug 21]. https://www.infrastructure.gov.au/aviation/domestic-passenger-journey-protocol.aspx
25. Woloshin S, Patel N, Kesselheim AS. False negative tests for SARS-CoV-2 infection—challenges and implications. N Engl J Med. 2020;383:e38. https://doi.org/10.1056/NEJMp2015897

Address for correspondence: Suzanne McEvoy, Metropolitan Communicable Disease Control, PO Box 332, Northbridge, WA 6865, Australia; email: suzanne.mcevoy@health.wa.gov.au

Risk for Hepatitis E Virus Transmission by Solvent/Detergent–Treated Plasma

Pierre Gallian, Sébastien Lhomme, Pascal Morel, Sylvie Gross, Carole Mantovani, Lisette Hauser, Xavier Tinard, Elodie Pouchol, Rachid Djoudi, Azzedine Assal, Florence Abravanel, Jacques Izopet, Pierre Tiberghien

Hepatitis E has emerged as a major transfusion-transmitted infectious risk. Two recipients of plasma from 2 lots (A and B) of pooled solvent/detergent–treated plasma were found to be infected by hepatitis E virus (HEV) that was determined to have been transmitted by the solvent/detergent–treated plasma. HEV RNA viral loads were 433 IU in lot A and 55 IU in lot B. Retrospective studies found that 100% (13/13) of evaluable lot A recipients versus 18% (3/17) of evaluable lot B recipients had been infected by HEV (p<0.001), albeit not necessarily at time of transfusion. Among evaluable recipients, 86% with a transfused HEV RNA load ≥50,000 IU were infected, most likely by the HEV-containing solvent/detergent–treated plasma, versus only 7% with a transfused HEV RNA load <50,000 IU (p<0.001). Overall, solvent/detergent–treated plasma might harbor HEV. Such an occurrence might result in a dose-dependent risk for transfusion-transmitted hepatitis E.

Hepatitis E virus (HEV) is a small, nonenveloped RNA virus belonging to the family *Hepeviridae*, genus *Orthohepevirus*. HEV genotypes 3 and 4 cause zoonotic infections described in countries in Europe and transmitted mostly by the fecal–oral route in contaminated food or the environment (*1*). Hepatitis E transmission by blood products has been reported, including plasma treated by pathogen-reduction methods (*2*,*3*).

Several studies have indicated that not all HEV-infected blood products cause infection in recipients, suggesting that blood products with a low residual plasma volume and provided by donors with low HEV viral loads might not be infectious (*4*,*5*). The lowest infectious dose resulting in proven or probable HEV transfusion-transmitted infection was 7,056 IU in a platelet concentrate (*6*), 31,600 IU in an erythrocyte concentrate (*4*), and 36,000 IU in a fresh frozen plasma (*7*).

In France, IgG seroprevalence studies indicate that HEV infection is widespread (*8*); high rates in the southern part of the country indicate that this region might be considered a hyperendemic area. Prevalence of HEV RNA in blood donors in France has been estimated to be 1 positive sample/750 donors–1 positive sample/2,218 donors (*9*,*10*). A total of 23 cases of transfusion-transmitted hepatitis with high imputability were reported during 2006–2016, including recipients of solvent/detergent–treated plasma (*3*).

Transfusion-transmitted hepatitis E involving solvent/detergent–treated plasma resulted in the identification of HEV-contaminated solvent/detergent–treated plasma lots, each providing plasma units for ≤350 recipients. We report results and lessons learned from the hemovigilance investigations after identification during 2012 of 2 HEV RNA–positive solvent/detergent–treated plasma lots.

Materials and Methods

Production of Solvent/Detergent–Treated Plasma

Until 2014, the French Transfusion Public Service (Etablissement Français du Sang) produced solvent/detergent–treated plasma that was manufactured

Author affiliations: Aix-Marseille Université, Marseille, France (P. Gallian); Institut National de la Santé et de la Recherche Médicale, Marseille (P. Gallian); Etablissement Français du Sang, La Plaine, Saint-Denis, France (P. Gallian, P. Morel, S. Gross, E. Pouchol, R. Djoudi, P. Tiberghien); Institut National de la Santé et de la Recherche Médicale, Toulouse, France (S. Lhomme, F. Abravanel, J. Izopet); Hôpital Purpan, Toulouse (S. Lhomme, F. Abravanel, J. Izopet); Etablissement Français du Sang Nouvelle Aquitaine, Bordeaux, France (C. Mantovani, A. Assal); Etablissement Français du Sang Ile-de-France, Ivry sur Seine, France (L. Hauser); Etablissement Français du Sang Grand Est, Nancy, France (X. Tinard); Université de Franche-Comté, Besançon, France (P. Tiberghien)

DOI: https://doi.org/10.3201/eid2612.191482

from 100 apheresis plasma donations pooled in a volume of 70 L before being divided into a maximum of 350 individual units of 200 mL. Donations were qualified according to the French regulations. Interruption of solvent/detergent–treated plasma production by the Etablissement Français du Sang resulted from classification of this blood product as a pharmaceutical product according to European Union rules.

HEV Molecular and Serologic Investigations

Samples from solvent/detergent–treated plasma and blood donations were tested for HEV RNA, and viral loads were estimated by using a reverse transcription PCR as described (*11*). Subsequently, genotypes and subtypes were characterized by sequencing and molecular comparison of strains in the open reading frame (ORF) 2/ORF3 genomic region (*12*) and in a fragment of ORF1 covering the polymerase gene (*2*). HEV IgG concentration in solvent/detergent–treated plasma lots and detection of HEV IgG detection in contributed plasma donations were measured by using an HEV IgG Enzyme Immunoassay Kit (Wantai Biologic Pharmacy Enterprise, http://www.ystwt.cn) as described (*13*).

Hemovigilance Inquiries

All contributed plasma donations to a solvent/detergent–treated plasma batch found positive for HEV were tested to identify the involved plasma donor(s). Furthermore, an inquiry was conducted for all recipients transfused with plasma units from an HEV-contaminated solvent/detergent–treated plasma lot. Information collected for each recipient included initial manifestations and outcome, number of solvent/detergent–treated plasma units transfused, and, if available, results of molecular and serologic testing for HEV markers in archived pretransfusion samples and posttransfusion control samples.

Results

Transfusion-Transmitted Hepatitis E Index Case-Patients

Index case-patient 1 was a 50–59 year-old man who had a thrombotic microangiopathy treated by plasma exchange and was found to be infected by HEV in December 2011. Hepatitis E was associated with increased liver cytolysis (increased levels of aspartate aminotransferase and alanine aminotransferase) and resolved spontaneously. This patient had received 150 blood products: 70 solvent/detergent–treated plasma units, 78 Intercept (amotosalen + UVA)–treated plasma units (http://cerus.com), and 2 erythrocyte concentrates. Results for HEV RNA in blood were negative 2 days before transfusion of 2 solvent/detergent–treated plasma units (from lot A) and positive 45 days later. At that time, case-patient 1 was positive for HEV IgG HEV IgM. Investigations on archived samples showed that solvent/detergent–treated plasma was positive for HEV RNA (433 IU).

Further investigations showed that 1 plasma donor who contributed blood to lot A was positive for HEV RNA (HEV-3f, 117,000 IU). All other donors to lot A were negative for HEV RNA. The concentration of HEV IgG in lot A was 0.35 IU/mL

Index case-patient 2 was a 50–59 year old man who was a liver transplant recipient (because of alcoholic cirrhosis) and found to be infected by HEV in October 2012, 3 months after transplantation. Chronic hepatitis E infection developed in the patient. This infection was successfully treated with ribavirin. This patient had received 61 blood products: 30 plasma units, among which 14 were from solvent/detergent–treated plasma (lot B), plus 25 erythrocyte concentrates and 6 platelet concentrates. In the context of liver cytolysis, a blood sample was positive for HEV RNA, IgG, and IgM. The patient was seronegative for HEV IgG and HEV IgM just before transfusion of the involved plasma. Further investigations showed that solvent/detergent–treated plasma from lot B was positive for HEV RNA, albeit with a low viral level (HEV-3f, 55 IU).

Further investigations showed that 1 blood donor (52-year-old man) who contributed to lot B was positive for HEV RNA (HEV-3f, 2,448 IU). All other donors to lot B were negative for HEV RNA. The concentration of HEV IgG in lot B was 1.13 IU/mL.

In both instances, molecular comparison of HEV-3f viral strains from the 2 patients and solvent/detergent–treated plasma lots indicated a 100% nucleic acid sequence homology in ORF1 and 2, thus establishing high imputability. Clinical manifestations and outcomes of both case-patients (recipients) have been documented elsewhere (*3*). Remaining, nontransfused solvent/detergent–treated plasma from both lots at time of notification were immediately quarantined and subsequently discarded.

Hemovigilance Inquiry

A total of 557 solvent/detergent–treated plasma units of lot A (n = 270) or lot B (n = 287) had been transfused into 143 recipients (lot A 61, lot B 82). When recipients were transfused with several solvent/detergent–treated plasmas, all of them were from the same solvent/detergent–treated plasma lot (lot A or lot B). Medical staff in charge of all involved patients

were notified. Among the 143 solvent/detergent–treated plasma recipients, 33.6% (n = 48; lot A 23, lot B 25) had died before investigations of causes related to their primary disease. A total of 21% were evaluable for viral markers (RNA and Ig type), including the 2 index cases (n = 30; lot A 13, lot B 17); results for the remaining 45.4% (n = 65; lot A 25, lot B 40) were not available. No clinical symptoms or biologic abnormalities suggestive of acute or chronic hepatitis E were reported, except for both index case-patients and 1 patient (r3) who were found to be infected by HEV before and after transfusion.

Investigation of Evaluable Recipients

We provide results of hemovigilance follow-up for the 30 recipients (including the 2 index case-patients) for whom results were available (Figure). Intervals between the solvent/detergent–treated plasma transfusion and recipient assessment varied highly and ranged from 2 to 44 months after transfusion; there were no significant differences between lot A and lot B recipients. In addition to the 2 index case-patients, only 1 additional recipient was positive for HEV RNA 37 months after transfusion (lot A recipient). This recipient was a heart transplant recipient for whom an earlier blood sample obtained 1 month before transfusion of 5 solvent/detergent–treated plasma samples from lot A already harbored HEV RNA.

Among the remaining 27 case-patients, 1 recipient was HEV IgG negative and HEV IgM positive (assessed 14 months after transfusion), 5 were IgG positive and IgM positive (4–16 months after transfusion), 7 were IgG positive and IgM negative (2–44 months after transfusion), and 14 were IgG negative and IgM negative (4–31 months after transfusion). In addition to both index case-patients and the other HEV RNA–positive recipient mentioned, pretransfusion results were available for only 5 additional recipients at various times (range 1–21 months) before transfusion. Two were HEV IgG positive and IgM negative before and after transfusion, 1 was IgG negative and IgM negative before transfusion and IgG positive and IgM negative after transfusion, and the remaining 2 were IgG negative and IgM negative before and after transfusion. Both index case-patients (r1 and r2) received similar cumulative HEV viral loads (173,000 IU and 154,000 IU, respectively) (Figure). However, there was a major difference in the number of transfused solvent/detergent–treated plasma units: 2 (r1, lot A) and 14 (r2, lot B). Recipient 3 (r3, lot A) had received a higher viral load (433,000 IU) (Figure).

The frequency of HEV infection differed between recipients of solvent/detergent–treated plasma lots A and B. Although all (13/13, 100%) evaluable recipients of lot A solvent/detergent–treated plasma had been in contact with HEV (posttransfusion positive for HEV RNA or HEV IgG or IgM for all recipients), this finding was not observed for recipients of lot B, for which only 3 evaluable recipients had HEV antibody markers of infection (3/17, 18%) ($p<0.001$ by χ^2 test). After exclusion of recipients who had proof of previous HEV infection (previously positive for HEV Ig or HEV RNA), the trend remained the same (10/10, 100% for lot A vs. 3/17, 18% for lot B). All other recipients who were HEV IgG positive and IgM negative (most of them in lot A) were tested ≥2 months after transfusion, thus potentially too late to detect IgM positivity after putative transfusion-transmitted hepatitis E.

To further evaluate the effect of solvent/detergent–treated plasma HEV RNA viral load on the risk for HEV infection in recipients, we clustered recipient data from both solvent/detergent–treated plasma lots and considered a 50,000 IU viral load threshold for infection, as suggested (*4*). We considered recipients positive for HEV RNA (n = 2 index case-patients) or positive for HEV IgG and HEV IgM (n = 5) (Figure) as most likely infected by a solvent/detergent–treated plasma transfusion and those negative for HEV RNA,

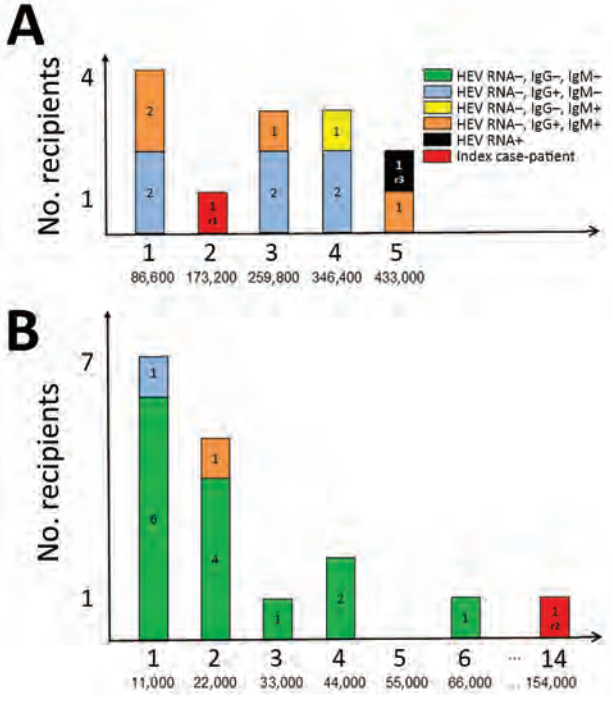

Figure. Transfused, HEV-infected solvent/detergent–treated plasma and recipient HEV status. A) Lot A; B) lot B. Top values along each x-axis indicate the number of solvent/detergent–treated plasma units transfused per recipient; bottom values indicate HEV viral load (IU/recipient). HEV, hepatitis E virus.

HEV IgM, and IgG (n = 14) (Figure) as not infected by HEV. Other case-patients were considered not evaluable because non–transfusion-associated HEV infection had been demonstrated or could not be formally excluded. With such a threshold, a significant difference was observed between likely infected and noninfected recipients: 6/7 (86%) with a viral load ≥50,000 IU of HEV RNA were likely infected but only 1/14 (7%) with a viral load <50,000 IU were likely infected (odds ratio 12.0, 95% CI 1.77–81.3; p<0.001 by Fisher exact test).

Discussion

We report results of investigations undertaken after identification of 2 solvent/detergent–treated plasma lots that contained HEV RNA. Such identification of solvent/detergent–treated plasma lots harboring HEV during December 2012 resulted in immediate introduction of HEV RNA screening of solvent/detergent–treated plasma lots, as well as plasma donors, and destruction of all remaining solvent/detergent–treated plasma units from lots that were positive for HEV RNA.

A portion of plasma units from these lots had been used before HEV RNA detection during December 2012. Efforts to test all involved recipients were only partially successful; 68% of evaluable patients remaining untested. Such a poor response rate, despite nationwide implementation of hemovigilance, highlights the difficulty of performing retrospective studies. Difficulties included lack of response by the medical staff in charge of the recipients despite several solicitations, unwillingness of recipients to undergo further biologic assessment, absence of recipient information, and no further investigations by the medical staff. For this last difficulty, medical staff often did not wish to take the risk for alarming the patient about a potential additional pathology that, if present, would not modify the course of their primary pathology. Furthermore, posttransfusion HEV testing, when undertaken, was most often performed in the absence of pretransfusion testing. Such posttransfusion HEV testing was performed several weeks to months after transfusion (i.e., after resolution of a putative HEV viremia and associated hepatitis E), thus preventing an accurate diagnosis of solvent/detergent–treated plasma transfusion-transmitted infections.

The optimal strategy for assessment of transfusion-transmitted HEV infection requires testing of molecular and serologic HEV markers at several time points before and after transfusion. Partial data (i.e., positive serologic results after transfusion only) and extended delay between informative samples are the main challenges in adequately documenting potential transfusion-transmitted HEV infection. This low frequency of evaluable recipients might have introduced a representative bias that was difficult to resolve precisely. However, one can expect that overall exposure to HEV was similar among nonevaluable recipients. Furthermore, recipients might have been exposed to a variety of infectious sources other than implicated plasma. However, because recipients who were given either lot were exposed similarly to other exposure risks, such occurrences should not greatly affect our findings and their interpretation.

Approximately 25% of the persons residing in France show seroreactivity against HEV (*8*). Accordingly, a recent study reported that HEV infection in transplant recipients resulted most often from sources of contamination other than transfusion (*14*). An additional difficulty is highlighted by the case-patient who was a heart transplant recipient (r3, lot A) and found to be infected by HEV after solvent/detergent–treated plasma transfusion but was also positive for HEV RNA 1 month before the transfusion, thus excluding, in principle, transfusion-transmitted hepatitis E. Investigations of recipients of lot B solvent/detergent–treated plasma showed that 14/17 recipients remained negative for HEV RNA, HEV IgG, and HEV IgM despite transfusion-mediated transmission of 11,000 IU–66,000 IU of HEV RNA (Figure, panel B). This finding could be explained by the low HEV viral level (55 IU) in each unit of lot B solvent/detergent–treated plasma, which might be too low to be infectious, or the presence of HEV IgG (1.13 IU/mL), which potentially provides complete or partial protection against HEV infection. However, the protective role of HEV IgG is controversial because a layer of lipid might encapsulate the virus and shield it from access to specific IgG, which would neutralize epitopes on the viral capsid (*15*,*16*). Conversely, none of the evaluable lot A recipients had a negative HEV IgG serologic status. Lot A plasma units contained a higher HEV RNA load and lower concentration of HEV IgG than lot B plasma units (433 IU vs. 55 IU of HEV RNA and 0.35 IU/mL vs. 1.13 IU/mL of HEV IgG).

These findings strongly suggest that at least a fraction of lot A plasma recipients, in addition to the index case-patient, had transfusion-transmitted hepatitis E that went clinically undetected. The threshold of 50,000 IU of HEV RNA in transfused plasma with regard to posttransfusion immunity against HEV (6/7 who had ≥50,000 IU vs. 1/14 who had <50,000 IU; p<0.001) further suggests that a large fraction of the seropositive recipients was

infected at time of transfusion and that the infectious risk is proportionate to the transfused viral load. Alternatively, difference in frequency of seropositivity between recipients of solvent/detergent–treated plasma lot A versus lot B could be caused by differential geographic nontransfusion HEV infection (*8*). However, widespread issuing of the lot A and lot B solvent/detergent–treated plasma throughout France, in addition to the magnitude of the difference in HEV seroprevalence between recipients of both lots, make this hypothesis unlikely. A threshold of 50,000 IU of HEV RNA for plasma-mediated hepatitis E approaches the 3–4 log IU threshold reported elsewhere for plasma (*4*,*7*).

The lowest reported HEV RNA dose associated with transfusion-transmitted hepatitis E by fresh frozen plasma is 36,000 IU of HEV RNA (*7*). We observed 3 lot B solvent/detergent–treated plasma transfusion recipients who received serial transfusions with cumulative viral loads >36,000 IU of HEV RNA and who nevertheless did not seroconvert after transfusion. This finding might be partly related to a protective effect of the concurrent presence of HEV IgG in solvent/detergent–treated plasma. Overall, the minimal HEV RNA viral load in blood products needed to cause transfusion-transmitted hepatitis E might ultimately be difficult to determine. Risk for transfusion-transmitted hepatitis E might also depend on a combination of additional factors, such as concentration of HEV antibodies in the blood product, recipient immune competence, more specifically immune status with regard to HEV, and viral genotypes and subtypes.

In conclusion, solvent/detergent–treated plasma transfusion technology does not prevent transfusion-transmitted hepatitis E, as can be expected with nonenveloped viruses, such as HEV, hepatitis A virus, and parvovirus B19 (*17*). Plasma donation pooling, most often undertaken when producing solvent/detergent–treated plasma for transfusion, increases the risk for transfusion-transmitted hepatitis E, despite the viral level reduction associated with pooling and the putative protective effect of the low concentration of HEV IgG provided by donors who have resolved their infection. Such transfusion-transmitted hepatitis E might not be diagnosed. HEV testing of solvent/detergent–treated plasma transfusion in regions to which HEV is endemic is now mandatory according to the European pharmacopoeia (*18*). Overall, our observations highlight infectious risks associated with blood donation pooling when an infectious agent goes undetected and is resistant to an applied pathogen reduction technology.

Acknowledgments

We thank the medical staff for helping to conduct hemovigilance inquiries, and Lucile Malard for providing helpful assistance concerning statistical analysis data.

P.G., P.M., S.G., C.M., L.H., X.T., E.P., R.D., A.A., and P.T. are employed by the French Transfusion Public Service (Etablissement Français du Sang).

About the Author

Dr. Gallian is a physician at the Etablissement Français du Sang, Marseille, France. His primary research interest is prevention of transfusion-transmitted, blood-borne pathogens.

References

1. Kamar N, Izopet J, Pavio N, Aggarwal R, Labrique A, Wedemeyer H, et al. Hepatitis E virus infection. Nat Rev Dis Primers. 2017;3:17086. https://doi.org/10.1038/nrdp.2017.86
2. Hauser L, Roque-Afonso AM, Beylouné A, Simonet M, Deau Fischer B, Burin des Roziers N, et al. Hepatitis E transmission by transfusion of Intercept blood system-treated plasma. Blood. 2014;123:796–7. https://doi.org/10.1182/blood-2013-09-524348
3. Gallian P, Pouchol E, Djoudi R, Lhomme S, Mouna L, Gross S, et al. Transfusion-transmitted hepatitis E infection in France. Transfus Med Rev. 2019;33:146–53. https://doi.org/10.1016/j.tmrv.2019.06.001
4. Dreier J, Knabbe C, Vollmer T. Transfusion-transmitted hepatitis E: NAT screening of blood donations and infectious dose. Front Med (Lausanne). 2018;5:5. https://doi.org/10.3389/fmed.2018.00005
5. Hewitt PE, Ijaz S, Brailsford SR, Brett R, Dicks S, Haywood B, et al. Hepatitis E virus in blood components: a prevalence and transmission study in southeast England. Lancet. 2014;384:1766–73. https://doi.org/10.1016/S0140-6736(14)61034-5
6. Huzly D, Umhau M, Bettinger D, Cathomen T, Emmerich F, Hasselblatt P, et al. Transfusion-transmitted hepatitis E in Germany, 2013. Euro Surveill. 2014;19:20812. https://doi.org/10.2807/1560-7917.ES2014.19.21.20812
7. Satake M, Matsubayashi K, Hoshi Y, Taira R, Furui Y, Kokudo N, et al. Unique clinical courses of transfusion-transmitted hepatitis E in patients with immunosuppression. Transfusion. 2017;57:280–8. https://doi.org/10.1111/trf.13994
8. Mansuy JM, Gallian P, Dimeglio C, Saune K, Arnaud C, Pelletier B, et al. A nationwide survey of hepatitis E viral infection in French blood donors. Hepatology. 2016;63:1145–54. https://doi.org/10.1002/hep.28436
9. Gallian P, Lhomme S, Piquet Y, Sauné K, Abravanel F, Assal A, et al. Hepatitis E virus infections in blood donors, France. Emerg Infect Dis. 2014;20:1914–7. https://doi.org/10.3201/eid2011.140516
10. Gallian P, Couchouron A, Dupont I, Fabra C, Piquet Y, Djoudi R, et al. Comparison of hepatitis E virus nucleic acid test screening platforms and RNA prevalence in French blood donors. Transfusion. 2017;57:223–4. https://doi.org/10.1111/trf.13889
11. Abravanel F, Sandres-Saune K, Lhomme S, Dubois M, Mansuy JM, Izopet J. Genotype 3 diversity and quantification

of hepatitis E virus RNA. J Clin Microbiol. 2012;50:897–902. https://doi.org/10.1128/JCM.05942-11
12. Legrand-Abravanel F, Mansuy JM, Dubois M, Kamar N, Peron JM, Rostaing L, et al. Hepatitis E virus genotype 3 diversity, France. Emerg Infect Dis. 2009;15:110–4. https://doi.org/10.3201/eid1501.080296
13. Abravanel F, Lhomme S, Chapuy-Regaud S, Mansuy JM, Muscari F, Sallusto F, et al. Hepatitis E virus reinfections in solid-organ-transplant recipients can evolve into chronic infections. J Infect Dis. 2014;209:1900–6. https://doi.org/10.1093/infdis/jiu032
14. Lhomme S, Bardiaux L, Abravanel F, Gallian P, Kamar N, Izopet J. Hepatitis E virus infection in solid organ transplant recipients, France. Emerg Infect Dis. 2017;23:353–6. https://doi.org/10.3201/eid2302.161094
15. Feng Z, Hirai-Yuki A, McKnight KL, Lemon SM. Naked viruses that aren't always naked: quasi-enveloped agents of acute hepatitis. Annu Rev Virol. 2014;1:539–60. https://doi.org/10.1146/annurev-virology-031413-085359
16. Chapuy-Regaud S, Dubois M, Plisson-Chastang C, Bonnefois T, Lhomme S, Bertrand-Michel J, et al. Characterization of the lipid envelope of exosome encapsulated HEV particles protected from the immune response. Biochimie. 2017;141:70–9. https://doi.org/10.1016/j.biochi.2017.05.003
17. Solheim BG, Rollag H, Svennevig JL, Arafa O, Fosse E, Bergerud U. Viral safety of solvent/detergent-treated plasma. Transfusion. 2000;40:84–90. https://doi.org/10.1046/j.1537-2995.2000.40010084.x
18. The European Directorate for the Quality of Medicines and HealthCare (EDQM). European Pharmacopoeia, 8th ed. Strasbourg (France): Council of Europe; 2016.

Address for correspondence: Pierre Gallian, Etablissement Français du Sang Provence Alpes, Côte d'Azur et Corse, 149 Blvd Baille, 13392 Marseille CEDEX 5, France; email: pierre.gallian@efs.sante.fr

Equine-Like H3 Avian Influenza Viruses in Wild Birds, Chile

Nicolas Bravo-Vasquez,[1] Jiangwei Yao,[1] Pedro Jimenez-Bluhm,[1] Victoria Meliopoulos, Pamela Freiden, Bridgett Sharp, Leonardo Estrada, Amy Davis, Sean Cherry, Brandi Livingston, Angela Danner, Stacey Schultz-Cherry, Christopher Hamilton-West

Since their discovery in the United States in 1963, outbreaks of infection with equine influenza virus (H3N8) have been associated with serious respiratory disease in horses worldwide. Genomic analysis suggests that equine H3 viruses are of an avian lineage, likely originating in wild birds. Equine-like internal genes have been identified in avian influenza viruses isolated from wild birds in the Southern Cone of South America. However, an equine-like H3 hemagglutinin has not been identified. We isolated 6 distinct H3 viruses from wild birds in Chile that have hemagglutinin, nucleoprotein, nonstructural protein 1, and polymerase acidic genes with high nucleotide homology to the 1963 H3N8 equine influenza virus lineage. Despite the nucleotide similarity, viruses from Chile were antigenically more closely related to avian viruses and transmitted effectively in chickens, suggesting adaptation to the avian host. These studies provide the initial demonstration that equine-like H3 hemagglutinin continues to circulate in a wild bird reservoir.

Aquatic birds are the reservoir of influenza A viruses and responsible for the evolution and long-distance spread of the virus (*1*–*3*). Occasionally, spillover into domestic poultry or domesticated mammals can result in human infections (*2*,*4*,*5*) and sustained transmission within a new mammalian host, as shown by equine influenza virus (H3N8) (EIV) (*3*).

The H3N8 EIVs were reported in the southern United States in 1963 during an outbreak in horses imported from Argentina (*6*,*7*). This emergence resulted in a pandemic that led to international cocirculation of H7N7 and H3N8 EIVs during the 1960s and 1970s, causing heterosubtypic reassortment that might have contributed to the extinction of H7N7 EIV (*8*). Today, H3N8 EIVs represent a single genetic lineage capable of inducing serious respiratory disease in susceptible horses.

The origin of the H3N8 lineage is unknown; however, phylogenetic studies and uracil content analysis suggest that these viruses originated in wild birds (*9*). The H3N8 EIV-like polymerase acidic (PA), nucleoprotein (NP), and nonstructural (NS) genes have been identified in avian influenza viruses (AIV) isolated from South American wild birds since the mid-2000s; the most recent isolation was in Argentina during 2016 (*10*–*12*). Time to most recent common ancestor (tMRCA) analysis suggests that these genes likely originated in AIVs during the 1950s (*9*,*12*). However, an EIV-like H3 hemagglutinin (HA) has yet to be identified in AIVs from wild birds.

We performed active surveillance of wild birds in Chile and isolated 6 distinct AIVs with HA, NP, NS, and PA genes having high nucleotide homology with the 1963 H3 EIV. The AIVs were isolated from resident waterfowl belonging to the families *Anatidae* and *Rallidae*, suggesting that circulation of these viruses might be restricted to nonmigratory species found only in the Southern Cone of South America. Although viruses from Chile had nucleotide similarity with H3 EIVs, they were antigenically like avian influenza viruses and could be transmitted into chickens, suggesting adaptations to the avian host. These studies provided the initial evidence that an H3 EIV-like HA continues to circulate in wild birds.

Materials and Methods

Sample Collection, Screening, and Sequencing

Fresh feces from birds were collected from the environment during 2013–2017 at different wetlands

Author affiliations: University of Texas Health Science Center, Houston, Texas, USA (N. Bravo-Vasquez); Centers for Disease Control and Prevention, Atlanta, Georgia, USA (J. Yao); University of Chile, Santiago, Chile (P. Jimenez-Bluhm, C. Hamilton-West); St. Jude Children's Research Hospital, Memphis, Tennessee, USA (V. Meliopoulos, P. Freiden, B. Sharp, L. Estrada, A. Davis, S. Cherry, B. Livingston, A. Danner, S. Schultz-Cherry)

DOI: https://doi.org/10.3201/eid2612.202063

[1]These authors contributed equally to this article.

across the central region of Chile. These samples were collected by using sterile flocked swabs (Copan Italia S.P.A., https://www.copangroup.com) and stored in 1-mL universal transport media tubes (Copan Italia S.P.A). They were then transported at 4°C to the Faculty of Veterinary Science of the University of Chile (Santiago, Chile) and stored at -80°C until analysis.

RNA extraction and quantitative reverse transcription PCR were performed at St. Jude Children's Research Hospital (Memphis, TN, USA) as described (*13*). In brief, RNA was extracted from 50 μL of swab specimen by using the Mag Max-96 IA/ND Viral RNA Isolation Kit (Life Technologies, https://www.thermofisher.com) on a Kingfisher Flex Magnetic Particle Processor (ThermoFisher Scientific, https://www.thermofisher.com). Quantitative reverse transcription PCR was performed on a CFX96 Real-Time PCR System with the 4x TaqMan Fast Virus Master Mix (ThermoFisher Scientific) and primers and probes specific for the influenza A matrix gene (*14*). Samples with a cycle threshold value ≤38 where considered having positive results. Viral isolation was attempted on 9-day old specific pathogen–free (SPF) embryonated chicken eggs as described (*15*).

To identify the host species, genetic barcoding was performed by using primers that amplified the cytochrome oxidase I gene as described (*16*). Sequencing was performed by using either Sanger sequencing and universal oligonucleotide primer sets as described (*17*) or by deep sequencing on an Illumina MiSeq System (https://www.illumina.com) as described (*18*). Sequences were assembled by using CLC Genomic Workbench Version 9 (http://webapp.cabgrid.res.in/biocomp/CLCBio/clc-bio.html). The H3 sequences from Chile used in this study have been deposited into GenBank (accession nos. KX101146, KY644162, MH675632, MH499154, MK163999, and MK164010).

Genetic and Phylogenetic Analysis

Phylogenetic analysis included sequences from avian and equine hosts downloaded from the National Center for Biotechnology Information (Bethesda, MD, USA) Influenza Virus Database. BLAST analysis (https://blast.ncbi.nlm.nih.gov/Blast.cgi) was performed to ensure that sequences from Chile not have higher homology to influenza A virus in other hosts. Representative sequences were selected by clustering similar sequences using CD-HIT-EST (*19*).

Maximum-likelihood trees were constructed by using the DECIPHER and PHANGORN packages in R (*20*,*21*). Sequences were aligned by using DECIPHER with the AlignTranslation function. The modelTest function was used to evaluate which nucleotide substitution with and without gamma-distributed rate variation among sites (γ) and invariant sites (I) is the best fit model. The generalized time reversible (GTR) + γ 4 + I model was best fitting by using Bayesian information criteria. The phylogenetic tree was constructed according to a standard protocol using phangorn (*21*). The starting neighbor-joining tree was constructed by using the distance matrix, and maximum-likelihood trees were generated from the starting tree by using the GTR + γ 4 + I model with stochastic branch rearrangement. The bootstrap method was used to determine the confidence of the tree topology with 1,000 replicate trees. The maximum-likelihood tree was saved with the bootstrap percentage in the Newick format (https://evolution.genetics.washington.edu) and visualized by using the ggtree package (*22*). Alternatively, the maximum-likelihood tree was constructed by using RaxML with a GTR + γ distribution with 1,000 bootstraps (*23*). The tree was visualized in FigTree version 1.4.4 (http://tree.bio.ed.ac.uk).

Clocklikeness of the resulting trees was investigated by using TempEst to determine if the molecular-clock assumption holds for the gene segment (*24*). The NS1 gene segment had no temporal signal and was not further analyzed. The H3, PA, and NP gene segments had positive, linear time vs. root-to-tip distance trend and a moderate scatter with correlation coefficients from 0.55 to 0.7. These gene segments were further analyzed to estimate the age of the most recent common ancestor.

We estimated tMRCAs by using tip date sampling and Bayesian Markov chain Monte Carlo analysis with the BEAST 1.10 package (*25*). Dates were estimated by using coalescent constant size prior with 3 partitions for the 3 codons using the maximum-likelihood estimation tree as the starting tree. Simulations were run using either the GTR or Hasegawa-Kishino-Yano substitution model and either the strict clock or the uncorrelated relaxed clock model to determine the robustness of the date estimates (*26*). The substitution and clock model had minor effects on the divergence date estimates. The maximum clade credibility trees (MCC) generated by the treeannotator package included with BEAST is reported. Figures were visualized and annotated by using the ggtree package (*22*).

Viruses and Cells

We propagated A/California/04/2009(H1N1) and H3Nx viruses A/equine/Miami/1/1963 (H3N8), A/equine/Uruguay/1/1963(H3N8), A/equine/New York/2016(H3N8),A/equine/NewYork/2016(H3N8),

A/red-gartered coot/Chile/C16030/2016(H3N4), A/red-fronted coot/Chile/5/2013(H3N6), A/yellow-billed pintail/Chile/C2014/2015(H3N8), A/mallard/Oregon/449221–105/2006(H3N6), A/duck/Minnesota/34/1976(H3N8), A/mallard/Wisconsin/22/1974 (H3N5), A/blue-winged teal/Wisconsin/279/1975(H3N8), A/green winged teal/Alaska/292/2011 (H3N8), A/northern pintail/Alaska/496/2012(H3N8), and A/northern pintail/Alaska/870/2014(H3N8) in 10-day-old embryonated chicken eggs as described (*27*). MDCK and A549 cells were cultured in modified Eagle medium (Corning 10-010-CV; https://www.corning.com) containing 200 mmol/L GlutaMAX (GIBCO 15290–026; https://www.thermofisher.com/us/en/home/brands/gibco.html) and 10% fetal bovine serum (Atlanta Biologicals, https://www.rndsystems.com). All viruses used were natural isolates.

Hemagglutination Inhibition Assay

We tested 2 equine H3 viruses [A/equine/Uruguay/1/1963(H3N8) and A/equine/Chile/EQCL003/2018(H3N8)]; 3 wild bird viruses from Chile [A/red-gartered coot/Chile/C16030/2016(H3N4), A/red-fronted coot/Chile/5/2013(H3N6), and A/yellow-billed pintail/Chile/2015(H3N6)]; and 7 wild bird origin North American viruses [A/mallard/Oregon/449221–105/2006(H3N6), A/duck/Minnesota/34/1976(H3N8), A/mallard/Wisconsin/22/1974(H3N5), A/blue-winged teal/Wisconsin/279/1975(H3N8), A/green winged teal/Alaska/292/2011(H3N8), A/northern pintail/Alaska/496/201(H3N8), and A/northern pintail/Alaska/870/2014(H3N8)] in a hemagglutination inhibition (HI) assay against a panel of 3 ferret-generated antiserum [A/equine/Miami/1/1963(H3N8), A/equine/New York/2016(H3N8), and A/yellow-billed pintail/Chile/C2014/2015(H3N8)] according to World Health Organization guidelines (*28*). In brief, 25 μL of serum was treated overnight with receptor-destroying enzyme (Denka Seiken, Co., Ltd., https://denka-seiken.com) and serially diluted 2-fold in 25 μL of phosphate-buffered saline in duplicate in a 96 well v-bottom plate. Each homologous virus was adjusted to 4 hemagglutination units, and 25 μL were added to the serum dilutions and incubated for 30 min at 4°C. Finally, 50 μL of 0.5% chicken erythrocytes were added to each of the wells, and the plate was incubated at 4°C for 30 min, after which results of the assay were read.

In Vitro Infections

A549 and MDCK cells were infected at a multiplicity of infection of 0.01 for 1 hour at 37°C. Cells were washed 3 times to remove unbound virus, and infected cells were cultured in appropriate medium containing 0.075% bovine serum albumin and 1 μg/mL l-1-tosylamido-2-phenylethyl chloromethyl ketone–treated trypsin. Aliquots of culture supernatants were collected at 6, 16, 24, 48, and 72 hours postinfection (hpi) and immediately stored at -80°C for the determination of virus titers by 50% median tissue culture infectious dose assay in MDCK cells as described (*29*).

Chicken Transmission Study

The chicken experiment was performed as described (*30*). In brief, 6-week-old SPF leghorn chickens (3/group) were separated into 4 experimental groups: (A/Equine/NY/2/2016 H3N8, A/red-fronted coot/Chile/5/2013 H3N6, A/red-gartered coot/Chile/C16030/2016 H3N4, and A/red-fronted coot/Chile/5/2013 H3N6) and inoculated with 10^6 50% egg infective dose/0.5 mL virus by intraocular, intranasal, and intratracheal routes. These chickens were placed in direct contact with virus-naive chickens (n = 9/group) 24 hours later. All chickens were observed daily for clinical signs of illness, such as body weight loss, labored breathing (including upper respiratory signs, such as coughing and sneezing), and diarrhea. To assess virus shedding, cloacal and tracheal swab specimens were collected at 3, 5, 7, 9, and 12 dpi. Swab specimens were stored in viral transport medium at -80°C until virus titration. Viral titers were established by using the method of Reed and Munch by performing 50% median tissue culture infectious dose assay analysis of the swab specimen inoculum with 50 μL of allantoic fluid and 50 μL of 0.5% chicken erythrocytes (*29*). All birds were euthanized at day 21 pi, and 1 mL blood was collected of each bird to check for seroconversion by HI. Chicken serum samples were tested with their corresponding homologous virus, according to their assigned group.

Statistical Analysis and Ethics

Mean infectious titers were analyzed by 2-way analysis of variance using GraphPad Prism version 8 (https://www.graphpad.com). Area under the curve analysis for measuring cumulative shedding was performed by using GraphPad Prism version 8. All animal experiments, procedures, and sampling activities were approved by the St. Jude Children's Research Hospital Institutional Animal Care and Use Committee.

Results

HA Gene Phylogenetic Nucleotide Analysis

During 2013–2017, a total of 37,171 wild bird fresh fecal samples were collected from various wetlands across Chile. H3 subtypes accounted for 5.8% (n = 8)

of the total HA diversity. Six of the H3 viruses, A/cinnamon teal/Chile/C19368/2016 (H3N8), A/red-fronted coot/Chile/5/2013 (H3N6), A/yellow-billed pintail/Chile/C2014/2015 (H3N8), A/red-gartered coot/Chile/C16030/2016 (H3N4), A/yellow-billed pintail/Chile/C30974/2017 (H3N8), and A/yellow-billed pintail/Chile/C34473/2017 (H3N8), were isolated from different regions of Chile (Figure 1), had highest nucleotide homology with the HA gene of the 1963 H3N8 EIV lineage, and had lower homology to the H3 of AIVs found in other regions (Figure 2; Appendix Figure 1, https://wwwnc.cdc.gov/EID/article/26/12/20-2063-F1.pdf). Maximum-likelihood trees demonstrated that the H3 HA sequences form 4 distinct clusters, with 3 clusters for wild bird origin viruses and 1 cluster for 1963 H3 EIV. The 6 IAVs for Chile form a sister clade relationship with the 1963 H3 EIV and are more phylogenetically related to the 1963 H3N8 EIV than to other avian H3 HAs (Figure 3; Appendix Figure 1).

Bayesian molecular clock analysis was used to estimate the tMRCA between the H3 AIVs from Chile and 1963 H3 EIV, and between avian H3 sequences not from Chile and EIV H3 (Table 1, Figure 4, panel A). The tMRCA of the 1963 EIV H3 is 1954 (95% credible interval 1948–1959). The tMRCA of the H3 HA not from Chile and the 1963 EIV H3 HA is 1916 (95% credible interval 1883–1941). In contrast, the tMRCA of avian H3 HAs not from Chile and the H3/1963 H3N8 EIV from Chile is 1845 (95% credible interval 1795–1882). We provide a complete HA divergence time tree (Appendix Figure 2).

Internal Gene Phylogenetic Nucleotide Analysis

The nucleotide similarity with the EIV H3 HA prompted us to conduct a detailed phylogenetic analysis. Like HA, the H3 viruses from Chile had NS1 (Appendix Figure 3), NP (Appendix Figure 4), and PA (Appendix Figure 5) genes that were phylogenetically more like EIVs than avian viruses at the nucleotide level. Most of the NS1, NP, and PA gene segments obtained from IAVs from South America formed a sister clade relationship with 1963 H3N8 EIV (Appendix Figures 3–5). There was 1 NP sequence collected

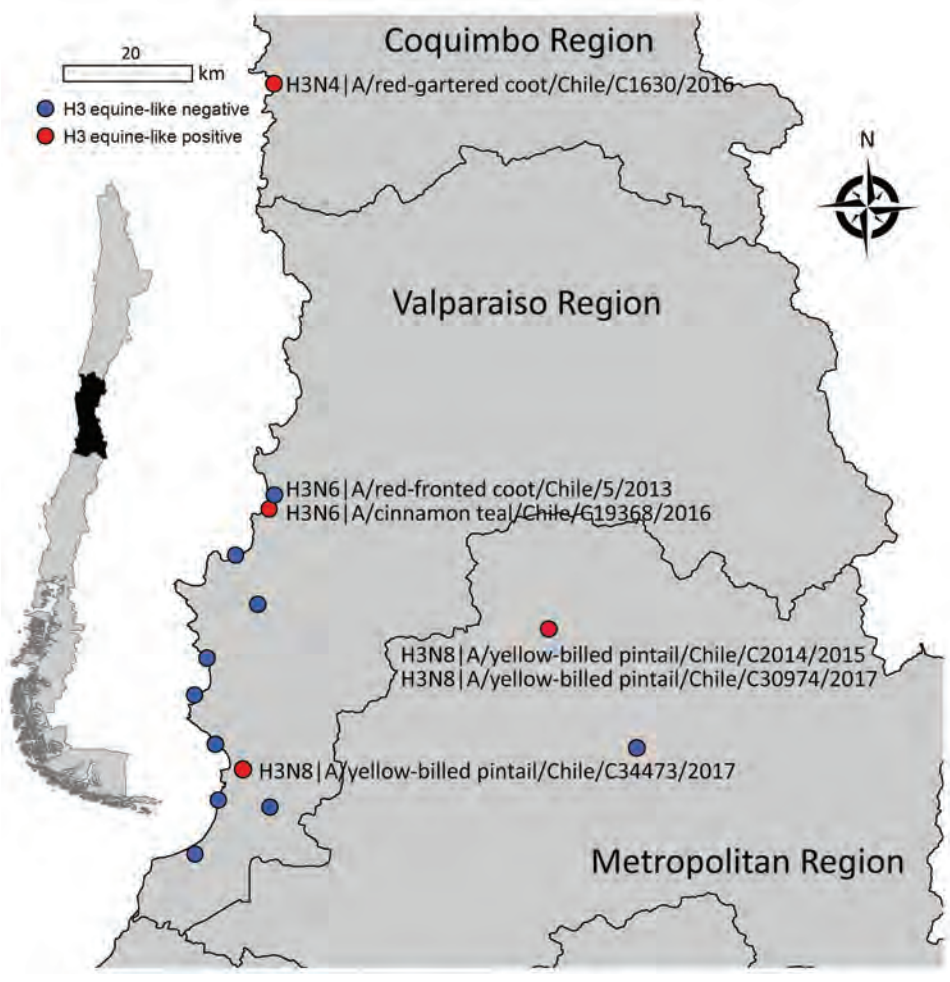

Figure 1. Central region of Chile showing where different equine-like H3Nx influenza viruses were obtained (red dots). Blue dots indicate other avian influenza virus surveillance sites. Isolate names and subtypes are indicated. Inset map indicates location of study area within Chile.

Figure 2. Maximum-likelihood phylogenetic tree showing the relationship between equine influenza (H3N8) viruses (blue), equine-like avian influenza viruses (AIVs) from Chile (red), and AIVs from other locations (green) for the H3 gene fragment. Scale bars indicate average nucleotide substitutions per site. A complete tree, taxon identification, and bootstrap support are shown in Appendix Figure 1 (https://wwwnc.cdc.gov/EID/article/25/12/20-2063-App1.pdf).

from Canada (A/blue-winged teal/ALB/651/1978 (H6N2), GenBank accession no. ABB18989) that was more like these sequences from South America than other AIVs, suggesting that these gene fragments have spread into North America through bird migration, but did not establish a major reservoir to be consistently identified during surveillance. The NA, matrix, polymerase basic 1, and polymerase basic 2

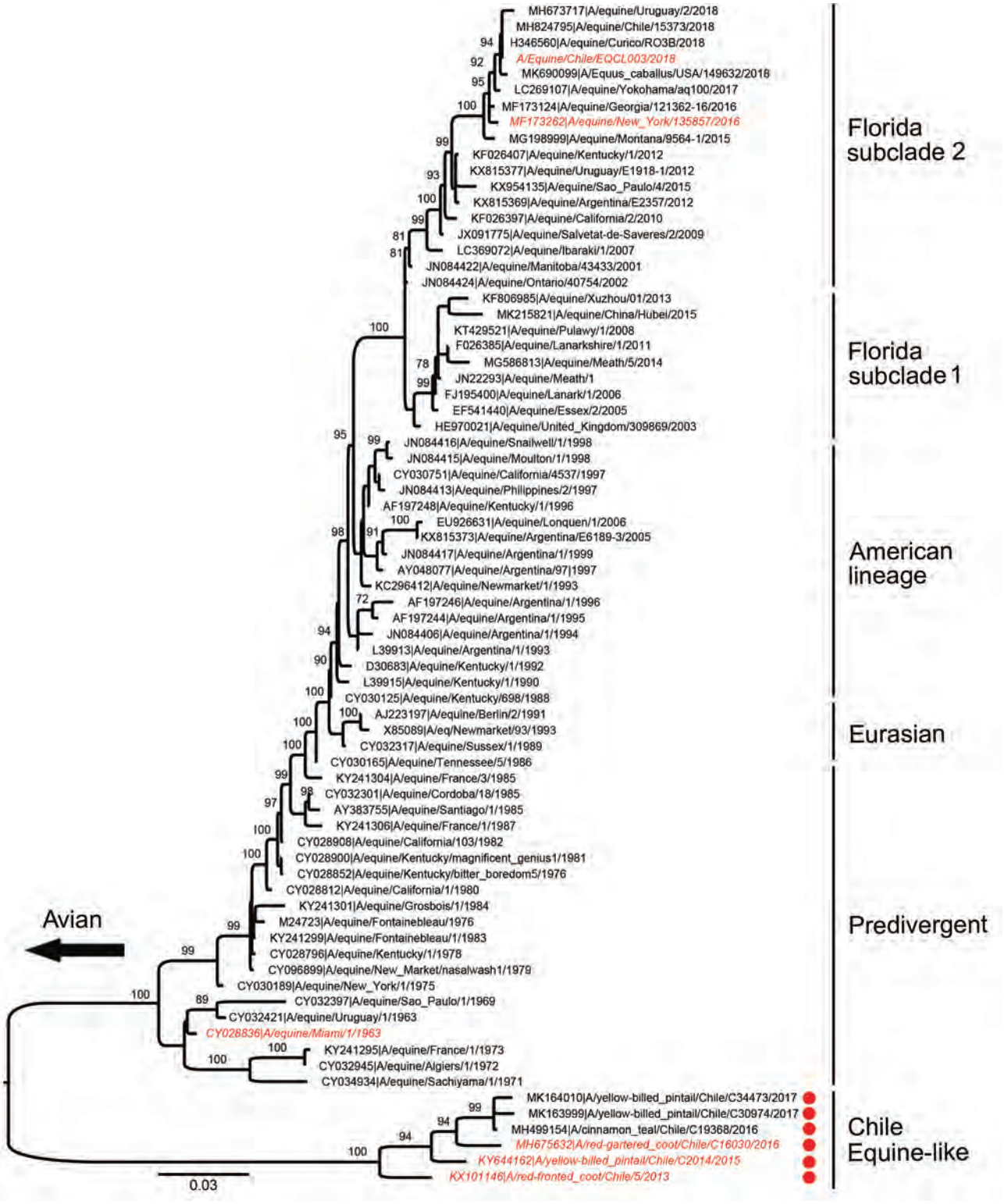

Figure 3. Maximum-likelihood phylogenetic analysis of the hemagglutinin gene of equine-like influenza (H3N8) viruses from Chile sequenced for this study (red dots) and reference sequences. Bootstrap values ≥70 are indicated. Viruses used in antigenic studies are indicated in red and italics. Major equine-like avian influenza virus clades are shown. Scale bars indicate average nucleotide substitutions per site.

Table 1. Divergence dates per gene segment for equine-like H3 avian influenza viruses in wild birds, Chile*

Gene segment	Equine-like, no. positive/no. tested†	GTR relaxed	GTR strict	HKY relaxed	HKY strict
HA	6/8	1916 (1883–1941)	1918 (1909–1927)	1917 (1886–1939)	1918 (1909–1927)
PA	19/26	1948 (1938–1956)	1946 (1941–1950)	1948 (1935–1957)	1946 (1941–1950)
NP	24/29	1947 (1936–1955)	1945 (1940–1950)	1947 (1936–1955)	1945 (1939–1949)
NS1	11/27	NA	NA	NA	NA

*Estimated divergence dates between these sequences from Chile and the 1963 H3N8 equine influenza sequences were estimated by using BEAST version 1.10 (https://beast.community/2018-06-10_BEAST_v1.10.0_released.html) with GTR or HKY substitution models and strict or uncorrelated relaxed clocks. Estimated dates are reported with 95% credible interval dates in parentheses. Because NS1 sequences did not exhibit molecular clock–like behavior, the divergence date could not be estimated. GTR, generalized time reversible; HA, hemagglutinin; HKY, Hasegawa-Kishino-Yano; NA, not available; NP, nucleoprotein; NS1, nonstructural protein 1; PA, polymerase acidic.
†Number of sequences from Chile for the gene segments that have high homology to the 1963 H3N8 equine influenza virus.

gene segments showed greater similarities to typically avian origin gene segments (Appendix Figures 6, 7) and were not further analyzed.

Bayesian molecular clock analysis was performed for the NP and PA gene segments to estimate the age of tMRCA between the 1963 H3 EIV and sequences from Chile (Table 1; Figure 4, panels B, C). The tMRCA of the NP gene segment between most of the sequences from Chile and the 1963 H3N8 EIV is 1947 (95% credible interval 1936–1955) (Appendix Figure 8). The tMRCA for the PA gene is 1948 (95% credible interval 1938–1956) (Appendix Figure 9).

The NS1 segment had insufficient temporal signal for molecular clock analysis. Overall, our phylogenetic analysis suggests that many of the gene segments collected from wild birds in South America were distinct from those collected from wild birds in North America; the H3, PA, NP, and NS1 genes were more closely related to the 1963 H3N8 EIV, supporting the hypothesis that the 1963 H3N8 EIV originated from wild birds in South America. Our results are consistent with those of Rimondi et al., who reported that viruses from birds from Argentina also carry PA and NP sequences with homology to the EIV (*12*). These sequences are closely related to the highlighted sequences from Chile. Rimondi et al. also estimated the tMRCA for PA to be 1943, and the tMRCA for NP to be 1951, which were similar to our estimates.

Antigenicity and Biologic Properties

The H3 HA from Chile and the 1963 EIV H3 HA also show amino acid similarity, having 91.5% amino acid identity to A/equine/Uruguay/1/1963. Thus, antigenicity was assessed by using the HI assay with ferret antisera against equine viruses or viruses from Chile available for these studies. The H3 viruses from Chile were not inhibited by ferret-generated antisera against A/equine/Miami/1963 or A/equine/New York/2016 viruses (Table 2). The equine viruses also failed to cross-react with ferret antisera generated against A/yellow-billed pintail/Chile/C2014/2015 virus (Table 2). Antisera against the avian virus from Chile or equine virus did not inhibit H3 IAVs representing the 3 genetic wild bird clusters identified (Appendix Figure 1). These studies highlight that the H3 viruses from Chile are antigenically unique from equine and other wild bird origin H3 IAVs.

To compare biologic properties, we assessed virus growth in mammalian cells and infections in vivo. The viruses from Chile and 1963 EIV H3 viruses replicated to similar titers and kinetics in MDCK cells (except at 48 hpi) when the eq/Miami/63 virus replicated to significantly higher titers compared with the other H3 viruses ($p<0.05$) (Figure 5, panel A). There was no major difference between eq/Miami/63 virus and the control A/California/2009 H1N1 virus. Replication kinetics and titers were significantly different in human A549 cells in which eq/Miami/63 virus again replicated to significantly higher titers at 24 hpi and 48 hpi ($p<0.05$) (Figure 5, panel B). The IAVs from Chile had lower overall titers and slower kinetics compared with those of eq/Miami/63 virus. This finding is highlighted by area under the curve analysis (Figure 5, panel C). In contrast to the results with eq/Miami/63 virus, the IAVs from Chile had higher viral titers from 24 hpi to 72 hpi than eq/Uruguay/63 virus, which is genetically similar to eq/Miami/63 virus ($p<0.05$) (Figure 5, panel A). A/red-footed Coot/Chile/5/2013 virus also replicated to higher titers than the eq/Uruguay/63 virus in A549 cells ($p<0.05$) (Figure 5, panel B). The reasons for the differential replication kinetics between the genetically similar equine viruses is unknown but was consistent. Attempts to replicate the viruses in EQKC3 and NBL6 equine cell lines were not successful.

In vivo, the equine-like H3 viruses readily infected and transmitted in experimentally infected chicken. In brief, 4 groups of 6 week of age SPF chickens were inoculated with 10^6 50% egg infective dose/0.5 mL virus (n = 3 per group) and then placed in direct contact with virus-naive chickens (n = 9 per group) 24 hours later. Oropharyngeal and cloacal viral shedding was monitored for 12 days postinfection

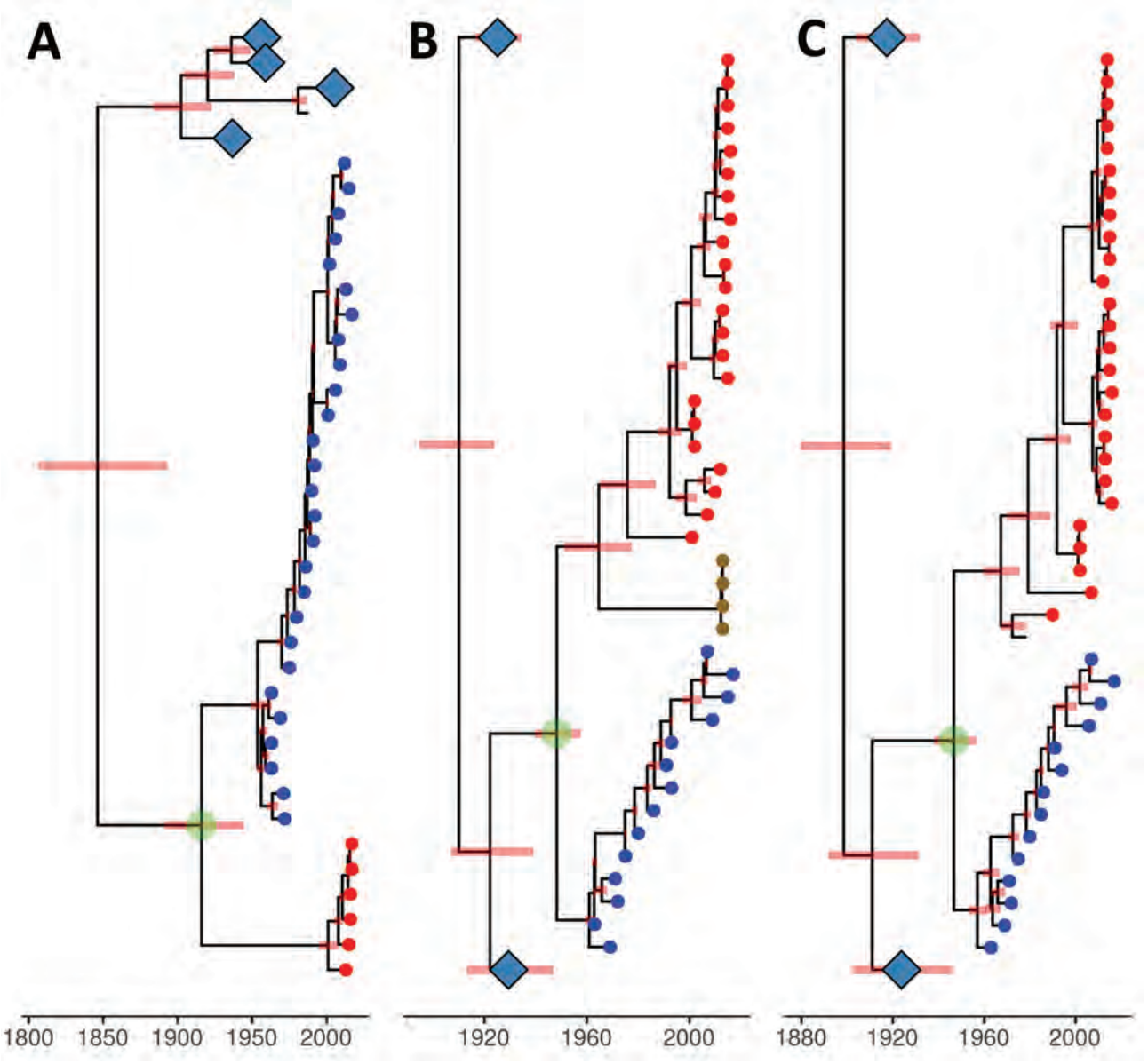

Figure 4. Genetic relationship and divergence date between avian influenza viruses (AIVs) from Chile/South America, the 1963 H3N8 equine-like influenza virus (EIV), and AIVs from other locations. A) Maximum clade credibility tree for the H3 gene segment. B) Maximum clade credibility tree for the polymerase acidic gene segment. AIV samples for penguins from Antarctica are represented by gold circular nodes. C) Maximum clade credibility tree for the nucleoprotein gene segment. Viruses were dated by using Bayesian Markov chain Monte Carlo analysis. Position of tips represent sampled virus for the years they were sampled. H3N8 EIV sequences are represented by blue circular nodes, AIVs from Chile/South America are represented by red circular nodes, and avian sequences from other locations are unlabeled. Internal nodes are reconstructed common ancestors, and pink bars represent 95% credible intervals on their date. Large clades of avian sequences from other locations are collapsed on their common ancestors and represented by light blue diamonds. The common ancestor between most AIVs from South America and the 1963 H3N8 EIV is highlighted by a green circle. Time scale bar indicates years.

(dpi), and seroconversion was measured at 21 dpi. At 3 dpi, each group infected with H3 virus from Chile had at >1 donor bird showing oropharyngeal virus shedding. The group inoculated with A/red-footed Coot/Chile/5/2013(H3N6) (RF Coot) virus also showed shedding by the cloacal route at this time point. After 5 dpi, donors were shedding virus by mixed oropharyngeal and cloacal routes. After 7 dpi, only shedding by the cloacal route was detected in the group inoculated with A/red-gartered coot/Chile/C16030/2016 virus (RG Coot H3N4) (Table 3). Although initially all 3 groups showed similar

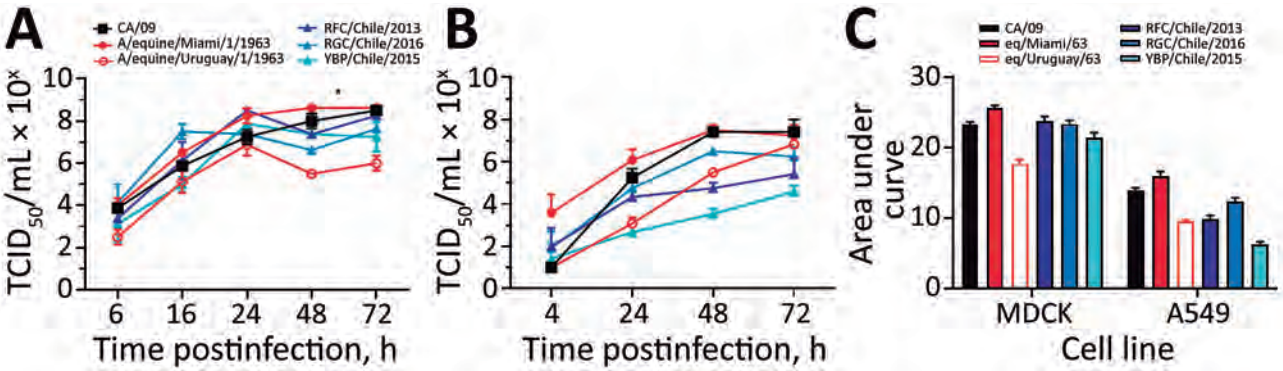

Figure 5. Replicative capacity of H3Nx influenza viruses in vitro. A, B) To evaluate the replication of H3N8 viruses in vitro, MDCK cells (A) and human lung A549 cells (B) were infected at a multiplicity of infection of 0.01, and cell culture supernatants were collected at 6, 16, 24, 48, and 72 hours postinfection. Viral titers were determined by $TCID_{50}$ analysis in triplicate. Values are mean titers of 3 replicates, and error bars indicate SEMs. Differences were considered significant at $p<0.05$ (*). C) Cumulative shedding for each cell line and each viral strain shown. $TCID_{50}$, 50% median tissue culture infectious dose.

infection and transmission (3/3 infected donors and 3–5 infected direct contacts), the direct contact group infected with A/red-fronted coot/Chile/5/2013 virus (RF Coot H3N6) was the only group showing persistent cloacal shedding of virus in 1 of the direct contacts until the end of the experiment at 12 dpi. Equally, RG Coot H3N4 showed cloacal shedding of virus in 1 of the donors until 12 dpi.

Seroconversion, as measured by HI titers at 21 dpi, was similar across all experimental groups and titers ranged from 1:20 to 1:80. In contrast, the eq/Miami/63 or the equine/NY/2016 viruses did not infect or were transmitted in chickens. However, 1 eq/NY/2016 donor chicken did have HI titers (1:60) at 21 dpi, suggesting infection. Overall, these studies demonstrate that there are H3 IAVs circulating in wild birds in Chile that are antigenically unique from H3 EIV and other wild bird AIVs and are capable of infecting and transmitting in poultry.

Discussion

In these studies, we isolated several H3 influenza viruses from wild birds in Chile that contain HA, NP, PA, and NS segments that are genetically similar to the 1963 EIVs, suggesting that the direct descendants of the virus that originated the EIV pandemic continue to circulate in wild birds in Chile. Previous AIV surveillance studies in South America have identified internal genes that were putatively related to the ancestral virus that originated the 1963 equine pandemic (*9*,*13*,*31*); however, we have identified an EIV-like HA in wild birds. Although phylogenetic nucleotide sequence analysis places the H3 viruses from Chile in a monophyletic group together with equine viruses, amino acid composition of the HA and antigenic properties show that viruses from Chile are antigenically unique and can infect and transmit in poultry. However, to better interpret the antigenic data, future studies could benefit from the

Table 2. Hemagglutination inhibition assay used for analysis of equine-like H3 avian influenza viruses in wild birds, Chile*

Virus	Subtype	Ferret antiserum titers		
		eq/Miami/1963	eq/NY/2016	YBP/Chile/2015
A/equine/Miami/1/1963	H3N8	**1:640**	<1:10	<1:10
A/equine/NY/2016	H3N8	1:1,280	**1:640**	<1:10
A/yellow-billed pintail/Chile/2015	H3N6	<1:10	<1:10	**1:160**
Test viruses				
A/equine/Uruguay/1/1963	H3N8	1:320	<1:10	<1:10
A/equine/Chile/EQCL003/2018	H3N8	1:640	1:320	NT
A/red-fronted coot/Chile/5/2013	H3N6	<1:10	<1:10	1:160
A/red-gartered coot/Chile/C16030/2016	H3N4	<1:10	<1:10	1:80
A/mallard/Oregon/449221–105/2006	H3N6	<1:10	<1:10	<1:10
A/duck/Minnesota/34/1976	H3N8	<1:10	<1:10	<1:10
A/mallard/Wisconsin/22/1974	H3N5	<1:10	<1:10	<1:10
A/blue winged teal/Wisconsin/279/1975	H3N8	<1:10	<1:10	<1:10
A/green winged teal/Alaska/292/2011	H3N8	<1:10	<1:10	<1:10
A/northern pintail/Alaska/496/2012	H3N8	<1:10	<1:10	<1:10
A/northern pintail/Alaska/870/2014	H3N8	<1:10	<1:10	<1:10

*Bold indicates homologous serum inhibition values. eq/Miami/1963, A/equine/Miami/1/1963; eq/NY/2016, A/equine/NY/2016; YBP/Chile/2015, A/yellow-billed pintail/Chile/2015; NT, not tested.

Table 3. Infection and transmission in chickens of equine-like H3 avian influenza viruses in wild birds, Chile*

Bird, virus subtype	Type of infection	3 dpi		5 dpi		7 dpi		9 dpi		12 dpi		HI titer, 21 dpi
		OP	CL	OP	CL	OP	CL	OP	CL	OP	CL	
PBS, n = 6	C	0/6	0/6	0/6	0/6	0/6	0/6	0/6	0/6	0/6	0/6	0/6
eq/Miami/1963, H3N8	I	0/3	0/3	0/3	0/3	0/3	0/3	0/3	0/3	0/3	0/3	0/3
	DC	0/9	0/9	0/9	0/9	0/9	0/9	0/9	0/9	0/9	0/9	0/9
eq/NY/2016, H3N8	I	0/3	0/3	0/3	0/3	0/3	0/3	0/3	0/3	0/3	0/3	1/3 (160)
	DC	0/9	0/9	0/9	0/9	0/9	0/9	0/9	0/9	0/9	0/9	0/9
Red-fronted coot, H3N6	I	3/3 (2.75–5.5)	1/3 (8.25)	2/3 (2.25–4.25)	0/3	0/3	0/3	0/3	0/3	0/3	0/3	2/3 (20–80)
	DC	4/9 (3.25–4.5)	0/9	5/9 (2.75–5.75)	1/9 (7.75)	3/9 (2.5–5.5)	1/9 (8.5)	2/9 (2.25–4.75)	1/9 (2.75)	0/9	1/9 (2)	2/9 (20)
Yellow-billed pintail, H3N8	I	3/3 (2.5–5.5)	0/3	1/3 (3.25)	0/3	0/3	0/3	0/3	0/3	0/3	0/3	2/3 (40–80)
	DC	3/9 (3.5–5.5)	1/9 (5.5)	3/9 (2.75–5.5)	1/9 (6.5)	1/9 (5)	1/9 (5.25)	0/9	1/9 (2.75)	0/9	0/9	1/9 (40)
Red-gartered coot, H3N4	I	3/3 (2.25)	0/3	1/3 (2.25)	1/3 (5.5)	0/3	1/3 (5.5)	0/3	1/3 (3.75)	0/3	1/3 (3.25)	2/3 (20–40)
	DC	5/9 (2.25–4)	1/9 (2.25)	4/9 (3–5.5)	0/9	2/9 (3.75–4)	0/9	0/9	0/9	0/9	0/9	4/9 (20–40)

*Values are no. birds infected/total number in group. Values in parentheses are ranges of viral titers (log 50% median tissue culture infectious dose) per timepoint and group. C, control; CL, cloacal; DC, direct contact; dpi, days postinfection; H, hemagglutinin; HI, hemagglutinin inhibition; I, inoculates; N, neuraminidase; OP, oropharyngeal; PBS, phosphate-buffered saline.

use of antigenic cartography to learn about the antigenic evolution of this subtype (*32*).

Although H3 is the most common subtype found in wild birds from North America (*33*), typical avian origin H3 subtypes are seldom recovered in South America. To date, only 4 isolates in Peru and 2 in Chile, all resembling contemporary North American AIVs, have been described (*31*,*34*). This finding could be related to the lack of surveillance throughout Latin America or low-level circulation of H3 viruses in wild birds (*35*). In contrast, we found that the H13 and H16 subtypes comprised up to 54% of the overall subtype diversity of AIVs from Chile deposited in GenBank during the same surveillance period (2013–2017), which could be caused by a biased surveillance effort in the order Charadriiformes. However, if we only consider isolates obtained from waterfowl in South America, the abundance of the H3 subtype (8.5%) is below the relative abundance of more common AIV subtypes, such as H1 (10.6%), H4 (10.6%), H5 (17%), and H7 (14.9%), which illustrates rarity of H3 subtype virus in wild birds in South America.

Global trade of thoroughbred horses from South America carrying the original 1963 H3N8 EIV, and not migratory birds, was responsible for the spread of these avian-origin gene segments (*36*). In comparison, although independent avian-to-equine transmission of lineage H3N8 AIV from Asia to horses was described in eastern Asia in the late 1980s, the epizootic event that followed was self-limited and died out after a few years (*37*). Subsequent active surveillance of wild birds in Mongolia has shown that AIVs carrying several gene segments closely related to H3N8 EIV from Asia are still circulating in wild birds, similar to our findings in Chile (*38*). This finding suggests that avian-to-equine transmission of H3 influenza A viruses is not an uncommon event, but that posterior sustained transmission is more limited. The conditions and key genetic signatures that facilitated the species-jump and rapid adaptation from waterfowl to horses in South America and eastern Asia remain unknown. This limitation reflects our inability to estimate whether the EIV-like HA reassorted together with the PA/NP/NS1 or in a separate event on the basis of our data. However, it is not uncommon to find wild waterfowl next to free-ranging horses in South America, which enables repeated transmission events that might lead to emergence of a new virus strain with pandemic potential in horses.

In summary, our data provide evidence that gene segments, including HA, that are the closest ancestor of the 1963 H3N8 EIV continue to circulate in wild bird reservoirs. We recommend increased surveillance to better clarify the role of this subtype in the context of genetic diversity of IAVs in South America, its epidemiology and ecology, and the risk that this new subtype represents to avian and mammalian hosts.

Acknowledgments

We thank Richard Webby and Scott Krauss for providing viruses and Pablo Galdames, Victor Marambio, and Gabriela Boldt for outstanding field work.

This study was supported by the National Institutes of Health Centers of Excellence in Influenza Virus Research and Surveillance contract HHSN272201400006C to S.S.-C. and from American Lebanese Syrian Associated Charities to S.S.-C.

About the Author

Dr. Bravo-Vasquez is a veterinarian and postdoctoral research scientist in the Department of Neurology, McGovern Medical School, University of Texas Health Science Center at Houston, Houston, TX. His research interests include epidemiology and pathology of infectious and neurodegenerative diseases.

References

1. Webster RG, Bean WJ, Gorman OT, Chambers TM, Kawaoka Y. Evolution and ecology of influenza A viruses. Microbiol Rev. 1992;56:152–79. https://doi.org/10.1128/MMBR.56.1.152-179.1992
2. Webster RG, Govorkova EA. Continuing challenges in influenza. Ann N Y Acad Sci. 2014;1323:115–39. https://doi.org/10.1111/nyas.12462
3. Parrish CR, Murcia PR, Holmes EC. Influenza virus reservoirs and intermediate hosts: dogs, horses, and new possibilities for influenza virus exposure of humans. J Virol. 2015;89:2990–4. https://doi.org/10.1128/JVI.03146-14
4. Joseph U, Su YC, Vijaykrishna D, Smith GJ. The ecology and adaptive evolution of influenza A interspecies transmission. Influenza Other Respir Viruses. 2017;11:74–84. https://doi.org/10.1111/irv.12412
5. Kahn RE, Ma W, Richt JA. Swine and influenza: a challenge to one health research. Curr Top Microbiol Immunol. 2014;385:205–18. https://doi.org/10.1007/82_2014_392
6. Scholtens RG, Steele JH, Dowdle WR, Yarbrough WB, Robinson RQ. Epizootic of equine influenza, 1963. Public Health Rep. 1964;79:393–402. https://doi.org/10.2307/4592142
7. Waddell GH, Teigland MB, Sigel MM. A new influenza virus associated with equine respiratory disease. J Am Vet Med Assoc. 1963;143:587–90.
8. Murcia PR, Wood JL, Holmes EC. Genome-scale evolution and phylodynamics of equine H3N8 influenza A virus. J Virol. 2011;85:5312–22. https://doi.org/10.1128/JVI.02619-10
9. Worobey M, Han GZ, Rambaut A. A synchronized global sweep of the internal genes of modern avian influenza virus. Nature. 2014;508:254–7. https://doi.org/10.1038/nature13016
10. Pereda AJ, Uhart M, Perez AA, Zaccagnini ME, La Sala L, Decarre J, et al. Avian influenza virus isolated in wild waterfowl in Argentina: evidence of a potentially unique phylogenetic lineage in South America. Virology. 2008;378:363–70. https://doi.org/10.1016/j.virol.2008.06.010
11. Spackman E, McCracken KG, Winker K, Swayne DE. An avian influenza virus from waterfowl in South America contains genes from North American avian and equine lineages. Avian Dis. 2007;51(Suppl):273–4. https://doi.org/10.1637/7529-032106R.1
12. Rimondi A, Gonzalez-Reiche AS, Olivera VS, Decarre J, Castresana GJ, Romano M, et al. Evidence of a fixed internal gene constellation in influenza A viruses isolated from wild birds in Argentina (2006–2016). Emerg Microbes Infect. 2018;7:194. https://doi.org/10.1038/s41426-018-0190-2
13. Karlsson EA, Ciuoderis K, Freiden PJ, Seufzer B, Jones JC, Johnson J, et al. Prevalence and characterization of influenza viruses in diverse species in Los Llanos, Colombia. Emerg Microbes Infect. 2013;2:e20. https://doi.org/10.1038/emi.2013.20
14. Hoffmann E, Stech J, Guan Y, Webster RG, Perez DR. Universal primer set for the full-length amplification of all influenza A viruses. Arch Virol. 2001;146:2275–89. https://doi.org/10.1007/s007050170002
15. Moresco KA, Stallknecht DE, Swayne DE. Evaluation and attempted optimization of avian embryos and cell culture methods for efficient isolation and propagation of low pathogenicity avian influenza viruses. Avian Dis. 2010;54(Suppl):622–6. https://doi.org/10.1637/8837-040309-Reg.1
16. Cheung PP, Leung YH, Chow C-K, Ng C-F, Tsang C-L, Wu Y-O, et al. Identifying the species-origin of faecal droppings used for avian influenza virus surveillance in wild-birds. J Clin Virol. 2009;46:90–3. https://doi.org/10.1016/j.jcv.2009.06.016
17. Jiménez-Bluhm P, Karlsson EA, Ciuoderis KA, Cortez V, Marvin SA, Hamilton-West C, et al. Avian H11 influenza virus isolated from domestic poultry in a Colombian live animal market. Emerg Microbes Infect. 2016;5:e121. https://doi.org/10.1038/emi.2016.121
18. Kaplan BS, Russier M, Jeevan T, Marathe B, Govorkova EA, Russell CJ, et al. Novel highly pathogenic avian A (H5N2) and A (H5N8) influenza viruses of clade 2.3. 4.4 from North America have limited capacity for replication and transmission in mammals. MSphere. 2016;1:e00003-16. https://doi.org/10.1128/mSphere.00003-16
19. Li W, Godzik A. Cd-hit: a fast program for clustering and comparing large sets of protein or nucleotide sequences. Bioinformatics. 2006;22:1658–9. https://doi.org/10.1093/bioinformatics/btl158
20. Wright ES. DECIPHER: harnessing local sequence context to improve protein multiple sequence alignment. BMC Bioinformatics. 2015;16:322. https://doi.org/10.1186/s12859-015-0749-z
21. Schliep KP. phangorn: phylogenetic analysis in R. Bioinformatics. 2011;27:592–3. https://doi.org/10.1093/bioinformatics/btq706
22. Yu G, Smith DK, Zhu H, Guan Y, Lam TTY. ggtree: an R package for visualization and annotation of phylogenetic trees with their covariates and other associated data. Methods Ecol Evol. 2017;8:28–36. https://doi.org/10.1111/2041-210X.12628
23. Stamatakis A. RAxML version 8: a tool for phylogenetic analysis and post-analysis of large phylogenies. Bioinformatics. 2014;30:1312–3. https://doi.org/10.1093/bioinformatics/btu033
24. Rambaut A, Lam TT, Max Carvalho L, Pybus OG. Exploring the temporal structure of heterochronous sequences using TempEst (formerly Path-O-Gen). Virus Evol. 2016;2:vew007. https://doi.org/10.1093/ve/vew007
25. Drummond AJ, Rambaut A. BEAST: Bayesian evolutionary analysis by sampling trees. BMC Evol Biol. 2007;7:214. https://doi.org/10.1186/1471-2148-7-214
26. Hasegawa M, Kishino H, Yano T. Dating of the human-ape splitting by a molecular clock of mitochondrial DNA. J Mol Evol. 1985;22:160–74. https://doi.org/10.1007/BF02101694
27. Cline TD, Karlsson EA, Seufzer BJ, Schultz-Cherry S. The hemagglutinin protein of highly pathogenic H5N1 influenza viruses overcomes an early block in the replication cycle to promote productive replication in macrophages. J Virol. 2013;87:1411–9. https://doi.org/10.1128/JVI.02682-12

28. World Health Organization. Manual for the laboratory diagnosis and virological surveillance of influenza. Geneva: The Organization; 2011.
29. Reed LJ, Muench H. A simple method of estimating fifty per cent endpoints. Am J Epidemiol. 1938;27:493–7. https://doi.org/10.1093/oxfordjournals.aje.a118408
30. Jimenez-Bluhm P, Bravo-Vasquez N, Torchetti MK, Killian ML, Livingston B, Herrera J, et al. Low pathogenic avian influenza (H7N6) virus causing an outbreak in commercial turkey farms in Chile. Emerg Microbes Infect. 2019;8:479–85. https://doi.org/10.1080/22221751.2019.1595162
31. Jiménez-Bluhm P, Karlsson EA, Freiden P, Sharp B, Di Pillo F, Osorio JE, et al. Wild birds in Chile harbor diverse avian influenza A viruses. Emerg Microbes Infect. 2018;7:44. https://doi.org/10.1038/s41426-018-0046-9
32. Smith DJ, Lapedes AS, de Jong JC, Bestebroer TM, Rimmelzwaan GF, Osterhaus AD, et al. Mapping the antigenic and genetic evolution of influenza virus. Science. 2004;305:371–6. https://doi.org/10.1126/science.1097211
33. Bahl J, Krauss S, Kühnert D, Fourment M, Raven G, Pryor SP, et al. Influenza a virus migration and persistence in North American wild birds. PLoS Pathog. 2013;9:e1003570. https://doi.org/10.1371/journal.ppat.1003570
34. Nelson MI, Pollett S, Ghersi B, Silva M, Simons MP, Icochea E, et al. The genetic diversity of influenza A viruses in wild birds in Peru. PLoS One. 2016;11:e0146059. https://doi.org/10.1371/journal.pone.0146059
35. Neumann G, Kawaoka Y. Predicting the next influenza pandemics. J Infect Dis. 2019;219(Suppl 1):S14–20. https://doi.org/10.1093/infdis/jiz040
36. Scholtens RG, Steele JH, Dowdle WR, Yarbrough WB, Robinson RQ. US epizootic of equine influenza, 1963. Public Health Rep. 1964;79:393–402. https://doi.org/10.2307/4592142
37. Guo Y, Wang M, Kawaoka Y, Gorman O, Ito T, Saito T, et al. Characterization of a new avian-like influenza A virus from horses in China. Virology. 1992;188:245–55. https://doi.org/10.1016/0042-6822(92)90754-D
38. Zhu H, Damdinjav B, Gonzalez G, Patrono LV, Ramirez-Mendoza H, Amat JAR, et al. Absence of adaptive evolution is the main barrier against influenza emergence in horses in Asia despite frequent virus interspecies transmission from wild birds. PLoS Pathog. 2019;15:e1007531. https://doi.org/10.1371/journal.ppat.1007531

Address for correspondence: Pedro Jimenez-Bluhm or Christopher Hamilton-West, Department of Preventive Veterinary Medicine, Universidad de Chile, Av. Santa Rosa 11735, Santiago, Chile; emails: pedrojimenezb@uchile.cl or christopher.hamilton@veterinaria.uchile.cl

Game Animal Density, Climate, and Tick-Borne Encephalitis in Finland, 2007–2017

Timothée Dub, Jukka Ollgren, Sari Huusko, Ruut Uusitalo, Mika Siljander, Olli Vapalahti, Jussi Sane

Tick-borne encephalitis (TBE) is an endemic infection of public health importance in Finland. We investigated the effect of ecologic factors on 2007–2017 TBE trends. We obtained domestic TBE case data from the National Infectious Diseases Register, weather data from the US National Oceanic and Atmospheric Administration, and data from the Natural Resources Institute in Finland on mammals killed by hunters yearly in game management areas. We performed a mixed-effects time-series analysis with time lags on weather and animal parameters, adding a random effect to game management areas. During 2007–2017, a total of 395/460 (86%) domestic TBE cases were reported with known place of exposure and date of sampling. Overall, we found that TBE incidence increased yearly by 15%. After adjusting for the density of other animals and minimum temperatures, TBE incidence was positively associated with white-tailed deer density. Variation in host animal density should be considered when assessing TBE risks and designing interventions.

Tick-borne encephalitis (TBE) is an endemic vectorborne infectious disease of public health importance in Finland. It is caused by tick-borne encephalitis virus (TBEV), a member of the *Flavivirus* genus of the *Flaviviridae* family. TBEV has 5 subtypes: European and Siberian subtypes, whose presence in Finland has been established (*1*,*2*); recently described Himalayan subtype; Far Eastern subtype (*3*); and Baikalian subtype (*4*). TBEV is most often transmitted through the bite of *Ixodes ricinus* or *I. persulcatus* ticks, 2 species found in Finland that can carry both the European and Siberian TBEV subtypes (*5*–*7*). TBEV may also be transmitted through the consumption of unpasteurized dairy products from infected livestock (*8*,*9*).

Most TBEV infections are asymptomatic (*10*). For clinical infections, the infectious course will differ depending on the TBEV subtype. The European subtype is typically responsible for a biphasic course of the disease: a short incubation period leads to a viremic phase associated with influenza-like symptoms, followed by an asymptomatic interval before onset of acute viral meningoencephalitis. Residual sequelae are reported in up to 50% of patients with European subtype TBE; the case fatality rate (CFR) is <2% (*10*,*11*). The Siberian subtype is associated with direct neurologic signs including focal encephalitis or meningitis in most symptomatic cases and complete recovery occurring in 80% patients; CFR approaches 2% (*10*). Effective TBE vaccines based on purified, formalin-inactivated TBEV are available, but several doses and boosters are required to acquire and maintain immunity.

In Europe, several thousand TBE cases are reported yearly, with the highest incidences in the Baltic countries (*12*,*13*). In Finland, TBE cases are reported from relatively restricted areas, mostly around the archipelago and the coast (*14*). During 1995–2013, the average annual number of cases was 25, ranging from 5 to 43 cases per year (*14*), but the incidence has increased over the past 5 years with the development of new TBE foci (*15*).

Several seasonal or environmental factors, such as temperature (*16*,*17*) and humidity (*18*), along with the number of animal hosts for ticks feeding (*19*), have been shown to affect tick life cycles and activity, which in turn have been associated with transmission of tick-borne infections, such as Lyme disease (*18*,*20*,*21*) and TBE (*21*–*24*). Our aim was to assess the effects of environmental factors, game animal density, and temperatures on TBE emergence and distribution in Finland and to use these findings to inform risk assessment and prevention strategies.

Author affiliations: European Programme for Intervention Epidemiology Training, European Centre for Disease Prevention and Control, Stockholm, Sweden (T. Dub); Finnish institute for Health and Welfare, Helsinki, Finland (T. Dub, J. Ollgren, S. Huusko, J. Sane); University of Helsinki, Helsinki (R. Uusitalo, M. Siljander, O. Vapalahti); Helsinki University Hospital, Helsinki (O. Vapalahti)

DOI: https://doi.org/10.3201/eid2612.191282

Methods

Epidemiologic Data

In Finland, TBE is reportable to the National Infectious Diseases Register (NIDR), maintained by the Finnish Institute for Health and Welfare (Terveyden ja hyvinvoinnin laitos [THL]). An acute laboratory-confirmed TBE case is defined as one in which a patient without a disease-specific medical history (e.g., no previous TBEV exposure) has coherent central nervous system symptomatology, such as meningitis, meningoencephalitis, or encephalomyelitis, and TBEV-specific IgM and IgG detected in either cerebrospinal fluid or serum. Two clinical laboratories in Finland perform TBE diagnostics and report results electronically to the NIDR. Each notification includes the specimen date and the patient's unique national identity code, date of birth, sex, and place of residence.

Since 2007, the Finnish Institute for Health and Welfare has enhanced TBE surveillance in place; because of these additional data, we were able to examine medical records and interview patients to determine the most likely places of exposure (*25*). From these sources, we extracted data on the number of TBE cases for 2007–2017. To account for a median TBE incubation period of ≈7–14 (range 4–28) days (*10*), suspected date of exposure was calculated as 2 weeks before date of symptom onset or 3 weeks before date of sampling if date of onset was unknown.

Weather and Game Animal Density Data

We retrieved temperature data from daily weather reports from multiple meteorologic stations in Finland using the United States National Oceanographic and Atmospheric Administration (NOAA) Climate Data Online open-access platform (https://www.ncdc.noaa.gov/cdo-web) (*26*). Including geographic coordinates for each station, we used QGIS 2.14.20-Essen version software (QGIS, https://qgis.org/en/site) to assign each station to its respective game management area and used Stata version 15 statistical software (StataCorp, https://www.stata.com) to calculate weather data for each game management area (n = 16). We used the difference between reported minimum and maximum daily temperatures to determine temperature variation, then calculated monthly mean values for minimum, maximum, average, and variation for each weather station. We used these data to calculate mean temperature values for the game management areas.

We used mean daily temperature values from each game management area to calculate 2 other weather parameters that affect tick populations. We used the proportion of days in a month with a mean temperature >5°C because ticks are commonly encountered in the northern regions of Europe at that temperature level (*27,28*). We used monthly mean temperature surplus (mean temperature in degrees Celsius above 9°C (or 0, if ≤9°C) because it has been observed that *Ixodes ricinus* larval activity and development occurs at that temperature (*29*).

For the spatial unit in our study, we used game management areas as defined by the Natural Resources Institute Finland. We obtained data for 2006–2017 on the number of animals killed by hunters in game management areas for moose (*Alces alces*), fallow deer (*Dama dama*), roe deer (*Capreolus capreolus*), white-tailed deer (*Odocoileus virginianus*), European hare (*Lepus europaeus*), mountain hare (*Lepus timidus*), and red fox (*Vulpes vulpes*) from the statistical services portal of the Natural Resources Institute Finland (Luonnonvarakeskus [Luke]) (*30*). We used these data on the numbers of animals killed by hunters as a proxy for actual animal density because they have been shown to be strongly correlated (*31,32*). To improve readability of our results, we divided the number of animals killed by hunters per game management areas by 100 (e.g., 5,500 animals = 5.5) and used this number in our models. We used a 1-year lag to estimate the level of TBE incidence based its demonstrated correlation with calculated animal density (*22*).

Statistical Analysis

We calculated the monthly number of cases and temperature values for each game management area, then modeled annual TBE incidence in 2007–2017 at a national level and by game management area using negative binomial regressions, a type of generalized linear model used to model overdispersed count data. As our core model for this time-series analysis, we fit a mixed-effects negative binomial regression model with the monthly numbers of TBE cases reported from each game management area as an outcome and year-month unit (2010m1, 2010m2, etc.), adjusted for a 12-month periodicity as explanatory variables, with a random effect on game management areas to account for regional variability.

For calculations, all temperature variables were used with a 1-month lag period, assuming that ticks would not become fully active again from the beginning of periods with optimal life cycle temperature ranges. By adding the variables to the core model one at a time, we determined the model that showed the best Akaike information criterion/Bayesian information criterion combination. The climatic predictor that offered the best fit was considered the most informative predictor, and we then used it as an adjustment

variable when modeling the effect of the number of animals killed on TBE incidence for each game management area. We then conducted single-variable analyses of all animal density parameters per 100 units, with a 1-year lag.

Finally, we used stepwise backward selection to develop a final multiple-variable analysis model to determine the effect of animal density on TBE incidence in a multilevel mixed-effects negative binomial regression with a random effect on game management areas. We assessed the distribution of Pearson and Deviance residuals and looked for autocorrelation of residuals. Statistical significance was considered at a 5% level. We used Stata to perform modelling; results were displayed with incidence ratios (IR) to 2 decimal places with 95% CIs and, when relevant, negative binomial regression coefficients before exponentiation to 3 decimal places with 95% CIs.

Results

Epidemiology of TBE Cases

During 2007–2017, a total of 488 cases were reported to NIDR, including 28 (6%) with reported exposure in a foreign country (Estonia, 18; Sweden, 5; Russia, 2; other, 3) and 65 cases (13%) without known place of exposure or date of sampling. We included in the analysis the remaining 395 (81%) cases of domestic TBE reported to NIDR. Median yearly number of cases was 28 (interquartile range [IQR] 20–50). Over the study period, the median number of cases was 7 per management area, ranging from 0 in several central game management areas to 120 cases in southern Finland (Varsinais-Suomi) (Figure 1). Overall, nationwide domestic TBE incidence significantly increased by 15% (IR 1.15; 95% CI 1.10–1.20) yearly, with regional variation (Table 1).

Association of TBE Incidence with Game Animal Density and Weather-Based Parameters

We used data from 174 different weather stations in total; the number of stations assigned to each game management area ranged from 3 in the Åland Islands to 47 in the Lappi (Lapland) game management area (Appendix Table 1, https://wwwnc.cdc.gov/EID/article/26/12/19-1282-App1.pdf). The median number of daily reports available per station per month was 30 (IQR 30–31). The number of animals killed by hunters by area was available on a yearly level for all game management areas except for the Åland Islands because the Natural Resources Institute Finland did not collect data for this management area.

Our core mixed-effects negative binomial regression showed a 1% monthly increase (IR 1.01 [1.01–1.01]; coefficient 0.011 [0.008–0.149]) and a significant 12-month periodicity ($p<0.001$). None of the temperature variables showed a significant association with monthly TBE incidence (Table 2). The lowest Akaike information criterion/Bayesian information criterion combination was seen for monthly average minimum temperature; therefore, we adjusted our modeling of hunting data for this weather parameter.

Because data on mammals killed by hunters were not available for the Åland Islands game management area, our analysis was restricted to 15 of the 16 game management areas (Appendix Table 2). Our single hunting data variable analysis, using a mixed-effects negative binomial regression, adjusted for year-month time unit, average minimum temperature, periodicity, and a random effect on game management areas, showed no significant results (Appendix Table 3). The numbers of moose, roe deer, and fallow deer were negatively associated with TBE incidence trends; numbers of fox, white-tailed deer, European hare, and mountain hare were positively associated with TBE incidence trends, although not significantly.

Using a stepwise approach for our analysis of the effect of several animal densities adjusted for average monthly minimum temperature, we obtained a model containing the numbers of moose, roe deer, white-tailed deer, mountain hare, and fox killed by hunters (Appendix Table 4). We found that TBE incidence was positively associated with the number of white-tailed deer killed by hunters (IR 1.04 [1.01–1.07]; coefficient 0.037 [0.009–0.064]), but it was significantly negatively associated with the number of roe deer (IR = 0.94 [0.88–1.00]; coefficient -0.067 [–0.131 to -0.003]). Other animal densities yielded no significant results (Table 3); Pearson and deviance residuals were normally distributed around 0, and residuals only showed autocorrelation in 2 game management areas out of 14 included in the model.

Figure 2 presents the actual monthly number of TBE cases and the model's prediction for the 4 game management areas included the model that contributed the most to TBE incidence: Varsinais-Suomi, Kaakkois-Suomi, Uusimaa, and Lappi. These results show that our model failed to predict some incidence peaks; however, the yearly average difference between the actual number of cases and the model's prediction was 0.04, ranging from -0.05 in Etela Hame to 0.19 in Uusimaa.

Discussion

During 2007–2017, TBE incidence in Finland increased yearly by 15%. Our analysis did not find a statistically

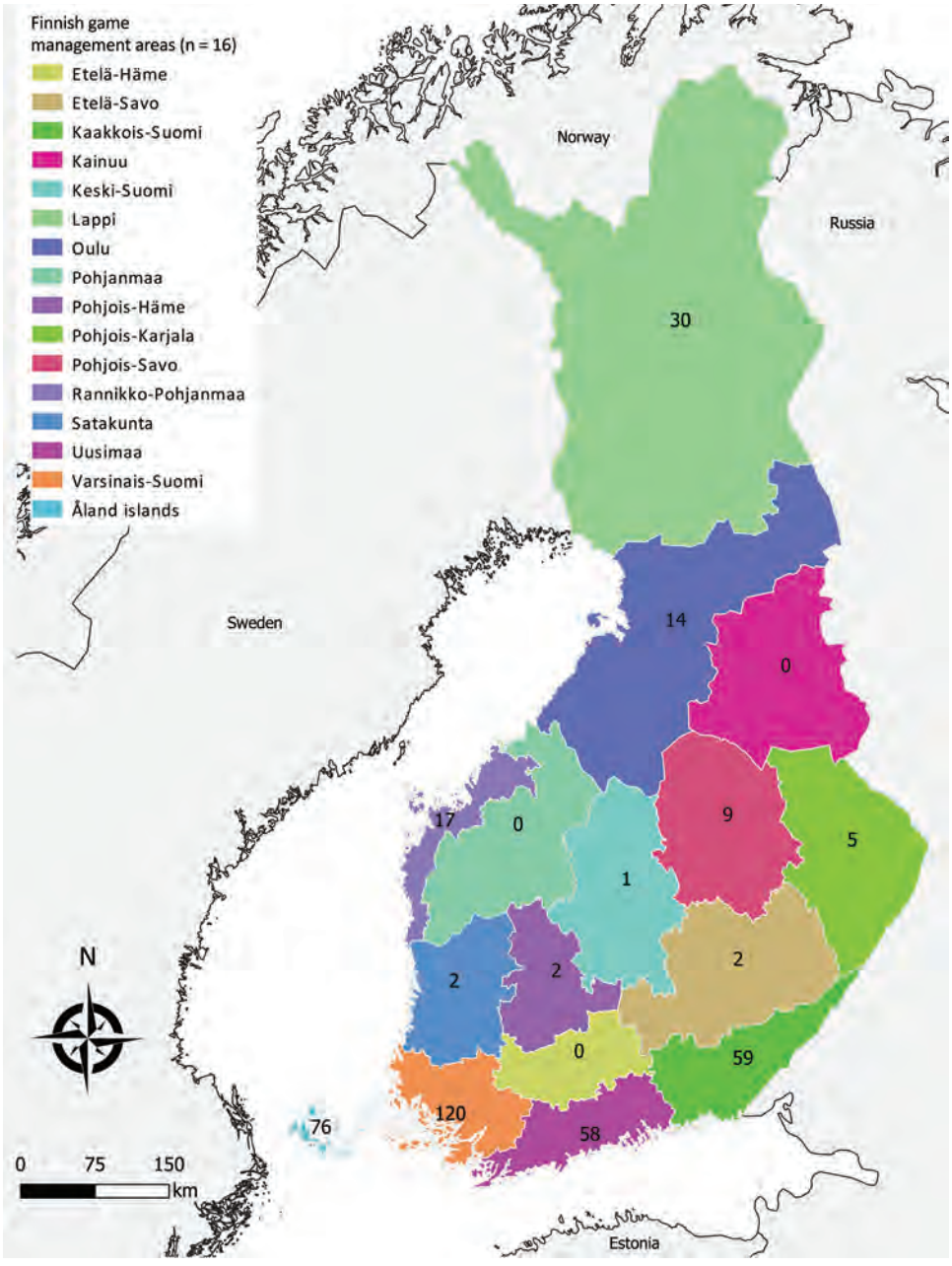

Figure 1. Total number of tick-borne encephalitis cases reported by game management area, Finland 2007–2017.

significant association between temperature and TBE incidence. Multivariable analysis of the effect of several animal densities showed that TBE incidence was positively associated with the number of white-tailed deer, but an increase in the number of roe deer killed by hunters led to a decrease in TBE incidence. Our study provides further evidence on the importance of wildlife in the epidemiology of TBE. Blood meals are necessary for 3 different stages of tick development; large mammals such as deer can both serve as transmission hosts and provide blood meals to ticks, and their numbers can therefore have a strong influence on TBE rates (*22*).

The results of our analysis of weather data were not consistent with those in many other studies on the effect of changes in temperature on TBE incidence (*22*,*33*,*34*). Regarding animal data, our results were partly in line with a 2017 study conducted in Sweden in which single-variable analysis with a 1-year lag showed that the number of fallow deer and moose killed by hunters were negatively associated with TBE incidence, but contrary to our findings, the number of roe deer had a positive effect on TBE increase (*22*). Roe deer abundance is a parameter that has previously been associated with TBE incidence in other

Table 1. Yearly tick-borne encephalitis incidence increase nationwide and by game management area, Finland 2007–2017

Game management area	Median annual no. cases (IQR)†	Annual no. cases, range	IR (95% CI)	p value	Yearly trend, %
Åland islands	7 (2–11)	1–14	0.97 (0.85–1.10)	0.60	–3%
Etelä-Häme	None reported	0–0			
Etelä-Savo	0 (0–0)	0–1	1.17 (0.73–1.87)	0.51	+17%
Kaakkois-Suomi	5 (2–6)	1–15	1.28 (1.04–1.32)	<0.01	+28%
Kainuu	None reported	0–0			
Keski-Suomi	0 (0–0)	0–1	1.46 (0.61–3.52)	0.40	+46%
Lappi	2 (1–3)	0–9	1.23 (1.08–1.40)	<0.01	+23%
Oulu	0 (0–3)	0–4	1.50 (1.18–1.92)	0.001	+50%
Pohjanmaa	None reported	0–0			
Pohjois-Häme	0 (0–0)	0–2	1.34 (0.31–5.80)	0.70	+34%
Pohjois-Karjala	0 (0–1)	0–1	1.21 (0.89–1.65)	0.22	+21%
Pohjois-Savo	0 (0–2)	0–3	1.21 (0.96–1.53)	0.11	+21%
Rannikko-Pohjanmaa	1 (0–2)	0–6	0.80 (0.65–1.00)	0.05	–20%
Satakunta	0 (0–0)	0–1	3.00 (0.60–14.87)	0.18	+200%
Uusimaa	4 (1–9)	0–16	1.39 (1.25–1.54)	0.001	+39%
Varsinais-Suomi	7 (4–17)	3–28	1.23 (1.15–1.31)	0.001	+23%
Finland	28 (20–50)	17–73	1.15 (1.10–1.20)	0.001	+15%

*IQR, interquartile range; IR, incidence ratio.
†None reported indicates that 0 cases were reported in that management area over the entire study period.

TBE endemic areas. In northern Italy, it was shown that roe deer density was higher in areas where more TBE cases were detected (*23*); however, in Slovenia, when both red deer and roe deer density were studied, only red deer density showed a significant positive association with TBE incidence (*24*). Similarly, in the Czech Republic, in a multivariable model adjusted for forest and agriculture area, only the number of wild boars killed by hunters had a significant positive association with TBE incidence, whereas roe deer density was negatively, but nonsignificantly, associated with TBE incidence (*35*). However, the results of these studies cannot all be properly compared with the findings from our work due to different methodologies, fauna, the presence in Finland of 2 tick species (*Ixodes ricinus* and *I. persulcatus*) capable of transmitting TBEV, and differing temperature and environmental characteristics. For example, a study similar to ours was recently conducted in Sweden, a neighboring country with similar climate and fauna, but the species of deer studied differed (*22*).

White-tailed deer are nonnative in Finland, introduced by the mid-20th century; the species' numbers have grown from fewer than 10 to several hundred thousand (*36*,*37*). A geospatial modeling study using similar data recently showed that in Finland, the density of this animal was correlated with concurrent incidence rates of TBE (*38*), which is in line with our findings. These known ticks (*I. ricinus* and *I. persulcatus*) (*39*) and the TBE host (*40*) were also introduced in the Czech Republic (*41*), another TBE-endemic country; however, to our knowledge, their effect on incidence trends there has not been studied.

As in any ecologic study, our results have to be interpreted with caution and should not be generalized to an individual level; some unmeasured characteristics might also differ between game management areas (*42*). In addition, we identified several limitations to our work. First, because we had to use average values for large geographic areas (median area size 19,185 km^2 [IQR 15,826–21,589 km^2]), the effect of temperatures on TBE incidence might have been diluted, which would explain why in our analysis, an increase in temperature was not linked to an incidence increase. This effect would also apply for animal density, which may vary within a game management area. Second, we were not able to use precipitation levels, a parameter with a known influence on tick lifecycle and activity, because data were not collected in a systematic manner throughout Finland.

Table 2. Single-variable modeling of weather parameters' influence on tick-borne encephalitis incidence, Finland, 2007–2017

Weather parameters†	Coefficient (95% CI of coefficient)	IR (95% CI)	p value	AIC	BIC
Monthly average minimum temperature	–0.069 (–0.145 to 0.08)	0.93 (0.87–1.01)	0.08	1,263.0	1,302.6
Monthly average mean temperature	–0.070 (–0.149 to 0.008)	0.93 (0.86–1.01)	0.08	1,263.1	1,302.6
Monthly average maximum temperature	–0.056 (–0.126 to 0.013)	0.95 (0.88–1.01)	0.11	1,263.6	1,303.1
Monthly average of daily temperature variation	0.000 (–0.103 to 0.104)	1.00 (0.90–1.11)	0.99	1,266.1	1,305.6
Proportion of days in a month with a mean temperature >5°C	–0.718 (–1.702 to 0.265)	0.49 (0.18–1.30)	0.15	1,264.1	1,303.6
Monthly average of mean temperature surplus‡	–0.057 (–0.135 to 0.021)	0.94 (0.87–1.02)	0.15	1,264.0	1,303.6

*AIC, Akaike information criterion; BIC, Bayesian information criterion; IR, incidence ratio.
†Adjusted for trend over time and 12 mo periodicity.
‡Temperature surplus: mean temperature minus 9°C if ≥9°C, otherwise 0.

Third, because animal density per game management areas was not available, we used data on animals killed by hunters. Even though these data have been used by several researchers in similar studies on TBE (*22*) and Lyme disease, another tick-borne zoonotic disease (*20*), we cannot assume that it perfectly reflects animal density variations. The reported number of animals killed by hunters can also be affected by changes in hunting habits and wildlife population control regulations. Finally, the effect of density of other potential hosts of ticks and TBEV, such as smaller animals (e.g., rodents), could not be investigated because of lack of available data in Finland. The absence of data on precipitation levels and small rodent

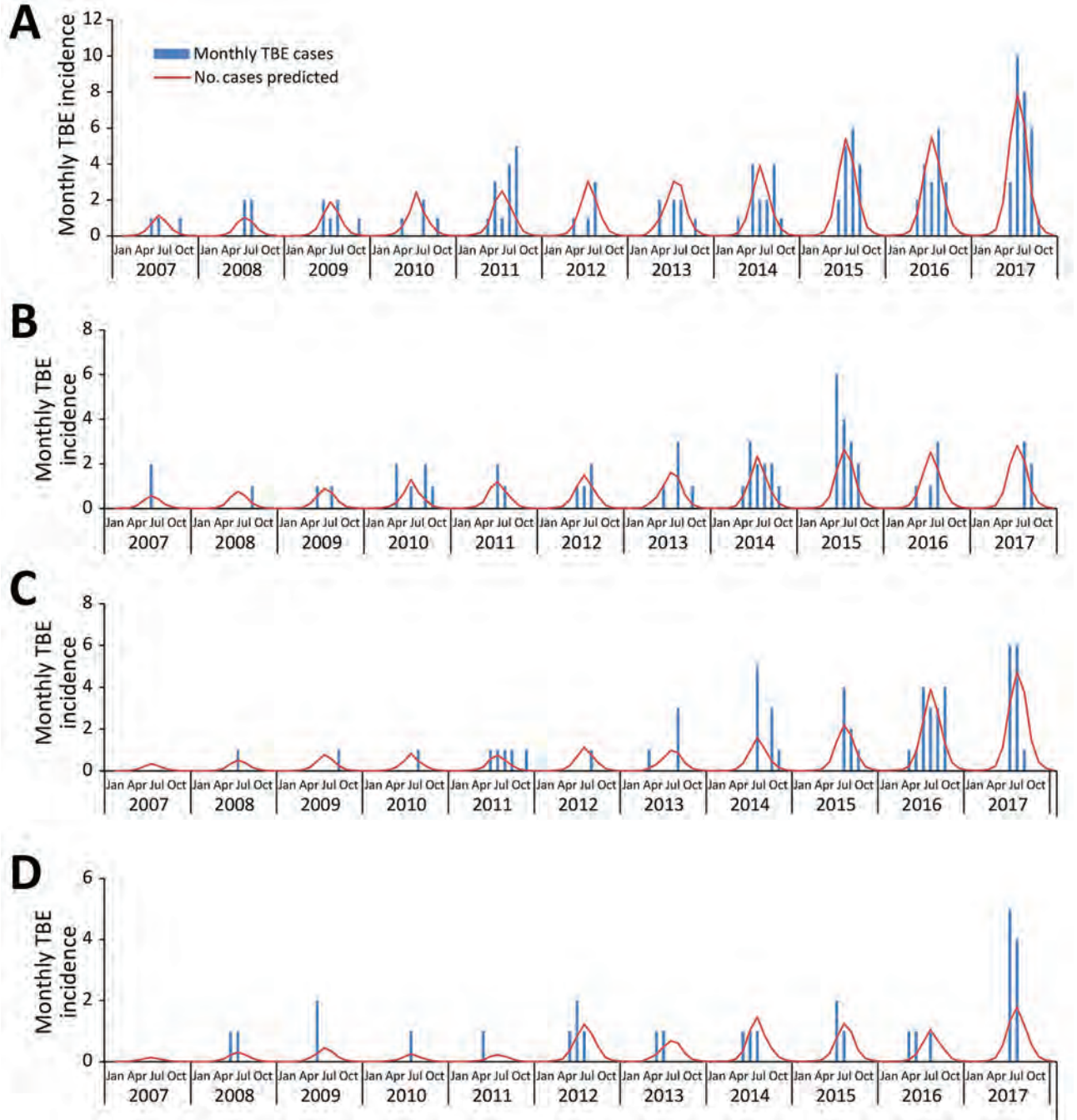

Figure 2. Actual and predicted number of TBE cases in 4 game management areas, Finland, 2007–2017. A) Varsinais-Suomi; B) Kaakkois-Suomi; C) Uusimaa; and D) Lappi. Number of tick-borne encephalitis cases is predicted by a mixed effects multivariable negative binomial model including number of moose, roe deer, white-tailed deer, mountain hare, and red fox killed by hunters adjusted for a 12-month periodicity, minimum temperature, and month, with a random effect on game management areas. TBE, tick-borne encephalitis

Table 3. Ecologic parameters associated with tick-borne encephalitis incidence, Finland, 2007–2017*

Species	Coefficient (95% CI of coefficient)	IR (95% CI)	p value	AIC	BIC
Moose (*Alces alces*)	–0.011 (–0.025 to 0.002)	0.99 (0.98–1.00)	0.11	1034.1	1101.1
Roe deer (*Capreolus capreolus)*	–0.067 (–0.131 to –0.003)	0.94 (0.88–1.00)	0.04		
White-tailed deer (*Odocoileus virginianus)*	0.037 (0.009–0.064)	1.04 (1.01–1.07)	0.01		
Mountain hare (*Lepus timidus)*	0.004 (–0.000 to 0.008)	1.00 (1.00–1.01)	0.08		
Red fox (*Vulpes vulpes*)	0.007 (–0.001 to 0.015)	1.01 (1.00–1.02)	0.09		

*Based on the yearly number of moose, roe deer, white-tailed deer, mountain hare, and red fox killed by hunters, adjusted for average minimum temperature with a 1-month lag, trend over time, and 12-month periodicity. AIC, Akaike information criterion of the multivariable time series model; BIC, Bayesian information criterion of the multivariable times series model; IR, incidence ratio.

density might partially explain why our model failed to properly predict several sudden increases, such as in Varsinais-Suomi in 2017, Kaakkois-Suomi in 2015, or over the final years of the study period in the Uusimaa and Lappi game management areas (Figure 2).

The effect of environmental factors, including climate change and host animal density variations, on vectorborne diseases is a growing concern in Finland. Therefore, over the coming years, the Finnish Institute for Health and Welfare will participate in a national consortium to quantify factors driving vectorborne diseases. The project will use modern analysis tools, empirical field studies, and predictive spatiotemporal modeling to provide information for intervention strategies integrating data on human disease incidence, dynamics of host communities, and vectors and environmental variables, including climate (*43*). We hope this project will lead to better knowledge about the extent and effects of climate change and milder temperatures and the influence of certain animal hosts on TBE incidence because it is growing in the European region (*12*,*13*). The findings of our study, especially that white-tailed deer density is associated with the incidence rates of TBE, show that variations in host animal density should be taken into account when assessing regional TBE risk, forecasting future trends, and designing interventions. Experimental studies on reducing or restricting the movement of deer populations (with fences) should assess whether such interventions can be effective to control tick populations and decrease TBE incidence.

About the Author

Dr. Timothée Dub is a European Programme for Intervention Epidemiology Training (EPIET) fellow based at the Finnish Institute for Health and Welfare in Helsinki, Finland. He has been involved in various projects on vectorborne disease epidemiology.

References

1. Jääskeläinen AE, Tikkakoski T, Uzcátegui NY, Alekseev AN, Vaheri A, Vapalahti O. Siberian subtype tickborne encephalitis virus, Finland. Emerg Infect Dis. 2006;12:1568–71. https://doi.org/10.3201/eid1210.060320
2. Jääskeläinen AE, Sironen T, Murueva GB, Subbotina N, Alekseev AN, Castrén J, et al. Tick-borne encephalitis virus in ticks in Finland, Russian Karelia and Buryatia. J Gen Virol. 2010;91:2706–12. https://doi.org/10.1099/vir.0.023663-0
3. Dai X, Shang G, Lu S, Yang J, Xu J. A new subtype of eastern tick-borne encephalitis virus discovered in Qinghai-Tibet Plateau, China. Emerg Microbes Infect. 2018;7:1–9. https://doi.org/10.1038/s41426-018-0081-6
4. Kovalev SY, Mukhacheva TA. Reconsidering the classification of tick-borne encephalitis virus within the Siberian subtype gives new insights into its evolutionary history. Infect Genet Evol. 2017;55:159–65. https://doi.org/10.1016/j.meegid.2017.09.014
5. Laaksonen M, Sajanti E, Sormunen JJ, Penttinen R, Hänninen J, Ruohomäki K, et al. Crowdsourcing-based nationwide tick collection reveals the distribution of *Ixodes ricinus* and *I. persulcatus* and associated pathogens in Finland. Emerg Microbes Infect. 2017;6:e31. https://doi.org/10.1038/emi.2017.17
6. Jääskeläinen A, Tonteri E, Pieninkeroinen I, Sironen T, Voutilainen L, Kuusi M, et al. Siberian subtype tick-borne encephalitis virus in *Ixodes ricinus* in a newly emerged focus, Finland. Ticks Tick Borne Dis. 2016;7:216–23. https://doi.org/10.1016/j.ttbdis.2015.10.013
7. Jääskeläinen AE, Tonteri E, Sironen T, Pakarinen L, Vaheri A, Vapalahti O. European subtype tick-borne encephalitis virus in *Ixodes persulcatus* ticks. Emerg Infect Dis. 2011;17:323–5. https://doi.org/10.3201/eid1702.101487
8. Offerdahl DK, Clancy NG, Bloom ME. Stability of a tick-borne flavivirus in milk. Front Bioeng Biotechnol. 2016;4:40. https://doi.org/10.3389/fbioe.2016.00040
9. Labuda M, Elecková E, Licková M, Sabó A. Tick-borne encephalitis virus foci in Slovakia. Int J Med Microbiol. 2002;291(Suppl 33):43–7. https://doi.org/10.1016/S1438-4221(02)80008-X
10. Růžek D, Dobler G, Donoso Mantke O. Tick-borne encephalitis: pathogenesis and clinical implications. Travel Med Infect Dis. 2010;8:223–32. https://doi.org/10.1016/j.tmaid.2010.06.004
11. Kaiser R. The clinical and epidemiological profile of tick-borne encephalitis in southern Germany 1994–98: a prospective study of 656 patients. Brain. 1999;122:2067–78. https://doi.org/10.1093/brain/122.11.2067
12. European Centre for Disease Prevention and Control. Tick-borne encephalitis. Annual epidemiological report for 2016. Stockholm: The Centre; 2018.
13. Beauté J, Spiteri G, Warns-Petit E, Zeller H. Tick-borne encephalitis in Europe, 2012 to 2016. Euro Surveill. 2018;23:pii=1800201. https://doi.org/10.2807/1560-7917.ES.2018.23.45.1800201
14. Tonteri E, Kurkela S, Timonen S, Manni T, Vuorinen T, Kuusi M, et al. Surveillance of endemic foci of tick-borne encephalitis in Finland 1995–2013: evidence of emergence of new foci. Euro Surveill 2015;20:pii=30020. https://doi.org/10.2807/1560-7917.ES.2015.20.37.30020

15. Smura T, Tonteri E, Jääskeläinen A, von Troil G, Kuivanen S, Huitu O, et al. Recent establishment of tick-borne encephalitis foci with distinct viral lineages in the Helsinki area, Finland. Emerg Microbes Infect. 2019;8:675–83. https://doi.org/10.1080/22221751.2019.1612279
16. Hancock PA, Brackley R, Palmer SCF. Modelling the effect of temperature variation on the seasonal dynamics of *Ixodes ricinus* tick populations. Int J Parasitol. 2011;41:513–22. https://doi.org/10.1016/j.ijpara.2010.12.012
17. Randolph SE, Green RM, Peacey MF, Rogers DJ. Seasonal synchrony: the key to tick-borne encephalitis foci identified by satellite data. Parasitology. 2000;121:15–23. https://doi.org/10.1017/S0031182099006083
18. Brownstein JS, Holford TR, Fish D. A climate-based model predicts the spatial distribution of the Lyme disease vector Ixodes scapularis in the United States. Environ Health Perspect. 2003;111:1152–7. https://doi.org/10.1289/ehp.6052
19. Estrada-Peña A, de la Fuente J. The ecology of ticks and epidemiology of tick-borne viral diseases. Antiviral Res. 2014;108:104–28. https://doi.org/10.1016/j.antiviral.2014.05.016
20. Ostfeld RS, Canham CD, Oggenfuss K, Winchcombe RJ, Keesing F. Climate, deer, rodents, and acorns as determinants of variation in Lyme-disease risk. PLoS Biol. 2006;4:e145. https://doi.org/10.1371/journal.pbio.0040145
21. Tkadlec E, Václavík T, Široký P. Rodent host abundance and climate variability as predictors of tickborne disease risk 1 year in advance. Emerg Infect Dis. 2019;25:1738–41. https://doi.org/10.3201/eid2509.190684
22. Jaenson TGT, Petersson EH, Jaenson DGE, Kindberg J, Pettersson JH-O, Hjertqvist M, et al. The importance of wildlife in the ecology and epidemiology of the TBE virus in Sweden: incidence of human TBE correlates with abundance of deer and hares. Parasit Vectors. 2018;11:477. https://doi.org/10.1186/s13071-018-3057-4
23. Rizzoli A, Hauffe HC, Tagliapietra V, Neteler M, Rosà R. Forest structure and roe deer abundance predict tick-borne encephalitis risk in Italy. PLoS One. 2009;4:e4336. https://doi.org/10.1371/journal.pone.0004336
24. Knap N, Avšič-Županc T. Correlation of TBE incidence with red deer and roe deer abundance in Slovenia. PLoS One. 2013;8:e66380. https://doi.org/10.1371/journal.pone.0066380
25. Finnish Institute for Health and Welfare. Finnish National Infectious Diseases Register [cited 2017 Dec 22]. https://thl.fi/en/web/infectious-diseases-and-vaccinations/surveillance-and-registers/finnish-national-infectious-diseases-register
26. National Oceanic and Atmospheric Administration. National Centers for Environmental Information. Climate data online. National Climatic Data Center [cited 2019 Apr 26]. https://www.ncdc.noaa.gov/cdo-web
27. Jaenson TGT, Eisen L, Comstedt P, Mejlon HA, Lindgren E, Bergström S, et al. Risk indicators for the tick *Ixodes ricinus* and *Borrelia burgdorferi* sensu lato in Sweden. Med Vet Entomol. 2009;23:226–37. https://doi.org/10.1111/j.1365-2915.2009.00813.x
28. Jaenson TGT, Lindgren E. The range of *Ixodes ricinus* and the risk of contracting Lyme borreliosis will increase northwards when the vegetation period becomes longer. Ticks Tick Borne Dis. 2011;2:44–9. https://doi.org/10.1016/j.ttbdis.2010.10.006
29. Daniel M, Malý M, Danielová V, Kříž B, Nuttall P. Abiotic predictors and annual seasonal dynamics of *Ixodes ricinus*, the major disease vector of Central Europe. Parasit Vectors. 2015;8:478. https://doi.org/10.1186/s13071-015-1092-y
30. National Resources Institute Finland (Luke). Luke's statistical services [cited 2019 Apr 26]. https://stat.luke.fi/en/uusi-etusivu
31. Andrén H, Liberg O. Final report: the lynx project [in Swedish]. Riddarhyttan: Grimsö Research Station, Department of Ecology, Swedish University of Agricultural Sciences; 2008. p. 44.
32. Cattadori IM, Haydon DT, Thirgood SJ, Hudson PJ. Are indirect measures of abundance a useful index of population density? The case of red grouse harvesting.Oikos. 2003;100:439–46. https://doi.org/10.1034/j.1600-0706.2003.12072.x
33. Tokarevich N, Tronin A, Gnativ B, Revich B, Blinova O, Evengard B. Impact of air temperature variation on the ixodid ticks habitat and tick-borne encephalitis incidence in the Russian Arctic: the case of the Komi Republic. Int J Circumpolar Health. 2017;76:1298882. https://doi.org/10.1080/22423982.2017.1298882
34. Czupryna P, Moniuszko A, Pancewicz S, Zajkowska O, Garkowski A, Grygorczuk S, et al. Influence of climatic, demographic and socioeconomic factors on tick-borne encephalitis incidence in 6 counties of Podlaskie region in 1994–2014. Przegl Epidemiol. 2016;70:21–5, 111–4.
35. Kriz B, Daniel M, Benes C, Maly M. The role of game (wild boar and roe deer) in the spread of tick-borne encephalitis in the Czech Republic. Vector Borne Zoonotic Dis. 2014;14:801–7. https://doi.org/10.1089/vbz.2013.1569
36. Yle Uutiset. White-tailed deer in Finland: from 5 to 100,000 in 80 years. 2018 [cited 2019 May 6]. https://yle.fi/uutiset/osasto/news/white-tailed_deer_in_finland_from_5_to_100000_in_80_years/10294577
37. Kekkonen J, Wikström M, Ala-Ajos I, Lappalainen V, Brommer JE. Growth and age structure in an introduced and hunted cervid population: white-tailed deer in Finland. Ann Zool Fenn. 2016;53:69–80. https://doi.org/10.5735/086.053.0206
38. Uusitalo R, Siljander M, Dub T, Sane J, Sormunen JJ, Pellikka P, et al. Modelling habitat suitability for occurrence of human tick-borne encephalitis (TBE) cases in Finland. Ticks Tick Borne Dis. 2020;11:101457. https://doi.org/10.1016/j.ttbdis.2020.101457
39. Huang C-I, Kay SC, Davis S, Tufts DM, Gaffett K, Tefft B, et al. High burdens of Ixodes scapularis larval ticks on white-tailed deer may limit Lyme disease risk in a low biodiversity setting. Ticks Tick Borne Dis. 2019;10:258–68. https://doi.org/10.1016/j.ttbdis.2018.10.013
40. Tonteri E, Jokelainen P, Matala J, Pusenius J, Vapalahti O. Serological evidence of tick-borne encephalitis virus infection in moose and deer in Finland: sentinels for virus circulation. Parasit Vectors. 2016;9:54. https://doi.org/10.1186/s13071-016-1335-6
41. Suchomel J. Non-native mammal species in the Czech Republic. Zooreport. 2015 [cited 2019 May 6]. https://www.zoobrno.cz/img/UK%20ZOO%20profi%20PROSINEC%202015%20K02.pdf
42. Morgenstern H. Ecologic studies in epidemiology: concepts, principles, and methods. Annu Rev Public Health. 1995;16:61–81. https://doi.org/10.1146/annurev.pu.16.050195.000425
43. University of Helsinki. VECLIMIT: vector-borne diseases and climate change in Finland: mapping, modelling, mitigation. 2020 [cited 2020 Jun 28]. https://www.helsinki.fi/en/projects/veclimit

Address for correspondence: Timothée Dub, Department of Health Security, Finnish Institute for Health and Welfare, Mannerheimintie 166 Helsinki 00271, Helsinki, Finland; email: timothee.dub@thl.fi

Trends in Population Dynamics of *Escherichia coli* Sequence Type 131, Calgary, Alberta, Canada, 2006–2016[1]

Gisele Peirano,[2] Tarah Lynch,[2] Yasufumi Matsumara,[2] Diego Nobrega, Thomas J. Finn, Rebekah DeVinney, Johann D.D. Pitout

Global expansion of antimicrobial drug–resistant *Escherichia coli* sequence type (ST) 131 is unrivaled among human bacteria. Understanding trends among ST131 clades will help with designing prevention strategies. We screened *E. coli* from blood samples (n = 1,784) obtained in Calgary, Alberta, Canada, during 2006, 2012, and 2016 by PCR for ST131 and positive samples (n = 344) underwent whole-genome sequencing. The incidence rate per 100,000 residents increased from 4.91 during 2006 to 12.35 during 2012 and 10.12 during 2016. ST131 belonged to clades A (10%), B (9%), and C (81%). Clades C1-nonM27 and B were common during 2006, and C2 containing $bla_{\text{CTX-M-15}}$, C1-M27 containing $bla_{\text{CTX-M-27}}$, and A were responsible for the increase of ST131 during 2012 and 2016. C2 was the most antimicrobial drug–resistant subclade and increased exponentially over time. Eradicating ST131, more specifically the C2 subclade, will lead to considerable public health benefits for persons in Calgary.

Escherichia coli sequence type (ST) 131 is the quintessential example of a successful, global, antimicrobial-resistant, high-risk clone among human bacteria (*1*,*2*). Currently, ST131 is the most common global extraintestinal pathogenic *E. coli* (ExPEC) clone; up to 30% of all ExPEC, 60%–90% of fluoroquinolone-resistant ExPEC, and 40%–80% of ExPEC with extended-spectrum β-lactamases [ESBLs] belong to ST131 (*3*,*4*). Population genetics indicate that ST131 consists of different clades (*5*): clade A contains serotype O16:H5 and *fimH*41, clade B contains mostly serotype O25b:H4 and *fimH*22, and clade C contains serotype O25b:H4 and *fimH*30. Clade C is divided into 2 subclades: C1/H30R (associated with fluoroquinolone resistance) and C2/H30Rx (associated with fluoroquinolone resistance and $bla_{\text{CTX-M-15}}$). A novel ST131 C1 subclade, known as C1-M27 with $bla_{\text{CTX-M-27}}$, was reported in Japan (*6*).

ST131 is the most dominant and most antimicrobial-resistant among *E. coli* causing bloodstream infections in Calgary, Alberta, Canada, infecting mostly the elderly in long-term care centers (*7*). Previous molecular epidemiology studies from the same region showed that ST131 was relatively rare among ESBL-producing and fluoroquinolone-resistant *E. coli* during the early 2000s but showed a major increase toward the end of the 2000s (*8*,*9*). However, limited information is available regarding the changes in population dynamics of ST131 clades over extended periods, especially among nonbiased *E. coli* isolates in large, well-defined, geographic regions.

To address this issue, we conducted a retrospective cohort study that characterized ST131 clades responsible for bloodstream infections in Calgary over an 11-year period (2006–2016). Investigating trends of ST131 clades over long periods by using a population-based surveillance approach will aid in clarifying the evolution of this clone and help with designing superior prevention strategies (*3*,*10*).

Author affiliations: University of Calgary Cummings School of Medicine, Calgary, Alberta, Canada (G. Peirano, T. Lynch, T.J. Finn, R. De Vinney, J.D.D. Pitout); Alberta Precision Laboratories, Calgary (G. Peirano, T. Lynch, J.D.D. Pitout); Kyoto University Graduate School of Medicine, Kyoto, Japan (Y. Matsumara); University of Calgary, Calgary (D. Nobrega); University of Pretoria, Pretoria, South Africa (J.D.D. Pitout)

DOI: https://doi.org/10.3201/eid2612.201221

[1]Accepted as an oral presentation for the 30th European Congress of Clinical Microbiology and Infectious Diseases, Paris, France, April 18–21, 2020.

[2]These authors contributed equally to this article.

Materials and Methods

Study Population

We conducted a retrospective cohort study in Calgary by using all *E. coli* human clinical isolates from blood cultures processed by a centralized laboratory system (Alberta Precision Laboratories) during 2006, 2012, and 2016. All blood culture samples from adults and children in inpatient and outpatient settings were included.

Clinical Data

Clinical information corresponding to source patients at the time of the *E. coli* bloodstream infection was obtained by using Sunrise Clinical Manager (Allscripts Healthcare Solutions, Inc., https://www.allscripts.com). A case-patient with an *E. coli* bloodstream infection was defined as a patient with systemic inflammatory response and documented growth of an *E. coli* isolate in a blood culture. Incident case-patients were defined as Calgary residents with a first isolation of *E. coli* from blood. Repeat *E. coli* from blood were excluded. Bloodstream infections were defined as community acquired, hospital acquired, or healthcare associated (*11*).

Bacterial Isolates, Identification, and Susceptibility Testing

All *E. coli* isolates from blood were routinely stored at Alberta Precision Laboratories and available for this study. Unique isolates recovered during January 1–December 31, 2006, 2012, and 2016 were obtained from the frozen depository.

Identification was conducted by using matrix-assisted laser desorption/ionization time-of-flight mass spectrometry (Vitek; bioMérieux, https://www.biomerieux.com), and susceptibility testing was conducted the VITEK 2 Instrument (bioMérieux). Susceptibilities were determined for amoxicillin/clavulanic acid, piperacillin/tazobactam, ceftriaxone, meropenem, ertapenem, amikacin, gentamicin, tobramycin, ciprofloxacin, and trimethoprim/sulfamethoxazole. Throughout this study, results were interpreted by using the Clinical Laboratory Standards Institute criteria for broth dilution (*12*). Antimicrobial resistance and virulence scores were determined as described (*13*).

Molecular Characterization

All *E. coli* isolates (n = 1,786) were initially screened with a PCR specific for ST131 (*14*). Positive isolates (n = 344) underwent whole-genome sequencing, by using procedures previously (*15*,*16*). The Nextera XT DNA Sample Preparation Kit (Illumina, https://www.illumina.com) was used to prepare libraries for sequencing. Samples were multiplexed and sequenced on an Illumina NextSeq500 for 300 cycles (151-bp paired-end). Draft genomes were obtained by using SPAdes version 3.10.1 (*17*). To define the presence of genes and mutations, BLAST (*18*) in combination with following databases or typing schemes were accessed: National Center for Biotechnology Information Bacterial Antimicrobial Resistance Reference Gene Database (https://www.ncbi.nlm.nih.gov/bioproject/PRJNA313047), ResFinder (*19*), PlasmidFinder (*20*), MLST (*21*) virulence finder (*22*), and virulence factor database (*23*). ST131 clades were identified by using an in silico PCR and primers described elsewhere (*14*).

Statistical Analysis

The Fisher exact test was used to perform pairwise comparisons of factors between clades, *t*-test was used for age comparisons, and p values obtained within individual categories were adjusted for multiple comparisons by using the false discovery rate (*24*). Population data were extracted from census reports from Statistics Canada (https://www.statcan.gc.ca) and used to estimate incidence rates (IRs) on the basis of a Poisson distribution. The Mann-Whitney test was used to compare antimicrobial resistance and virulence scores between clades. The effect of eliminating subclade C2 on nonsusceptibility and IRs was assessed by using Fisher exact and Poisson tests, for which population characteristics were compared with the presence and absence of subclade C2 isolates. The p values were adjusted for multiple comparisons accordingly. All analyses were conducted in R version 3.6.1 (*25*). Statistical significance was set at the 5% level.

Sequence Data Accession Numbers and Ethics

Sequencing data was deposited in the National Center for Biotechnology Information database (submission no. SUB7225977). This study was approved by the University of Calgary Conjoint Health Research Ethics Board (REB16-2457).

Results

E. coli Isolates

E. coli was the most common bacterium obtained from blood in the Calgary region during 2006 (482 [28.9%] of 1,669 isolates), 2012 (691 [29.7%] of 2,084 isolates), and 2016 (685 [31.1%] of 2,201 isolates). A total of 1,786 unique *E. coli* were screened for ST131: 481 from 2006, 621 from 2012, and 684 from 2016. Overall, 344 (19.2%) of 1,786 *E. coli* isolates were PCR positive

for ST131; the prevalence of ST131 increased from 53 (11%) of 481 during 2006 to 150 (24.2%) of 621 during 2012 and 141 (20.6%) of 684 during 2016 (p<0.001 for both comparisons).

Most ST131 isolates belonged to clade C in the following subclades (Table 1, https://wwwnc.cdc.gov/EID/article/26/12/20-1221-T1.htm): C0 (n = 5, 2%), C1-nonM27 (n = 121, 35%), C1-M27 (n = 13, 4%), and C2 (n = 139, 40%). The remainder of ST131 isolates belonged to clades A (n = 34 [10%)] and B (n = 32 [9%]).

Incidence Rates and Population Dynamics of ST131 Clades

The IR per 100,000 residents with ST131 bloodstream infections in Calgary increased from 4.91 during 2006 to 12.35 during 2012 and 10.12 during 2016 (p<0.001 for both comparisons). Overall, the population structure of ST131 was dominated by the C clade. However, the IRs per 100,000 residents and proportions among the different subclades showed a major change over time (Table 2; Figure). The C0 subclade represented 9.4% of the ST131 population during 2006, with an estimated IR of 0.46 cases per 100,000 residents. However, the C0 subclade was not detected during 2012 and 2016 (p = 0.001 for both comparisons).

The C1-nonM27 subclade dominated the population structure of ST131 during 2006 (comprising of 46% of the total population, with an IR of 2.22/100,000 residents). Despite an increased IR during 2012 and 2016 (when compared with that for 2006), the frequency of C1-nonM27 isolates decreased to 37.3% in 2012 and 29% in 2016 (2006 vs. 2016; p = 0.04) (Figure). The C1-M27 subclade increased from 1.9% during 2006 to 5.7% during 2016. There was an association between C1-M27, the presence of $bla_{\text{CTX-M-27}}$, and year of isolation (5 C1-M27 isolates from 2006 and 2012 were negative for $bla_{\text{CTX-M-27}}$, and 7/8 isolates obtained during 2016 were positive for $bla_{\text{CTX-M-27}}$) (p = 0.004) (Figure).

The prevalence of C2 subclade increased substantially from 17% of the total ST131 population during 2006 to 42% during 2012 and 47% during 2016 (p<0.001 for both comparisons) (Figure). The IR per 100,000 residents of the C2 clade increased from 0.83 during 2006 to 5.19 during 2012 and 4.81 during 2016 (p<0.001 for both comparisons) (Table 2). The increase in subclade C2 correlated with the presence of CTX-M-15 (4 [44%] of 9 of C2 isolates from 2006 were positive for $bla_{\text{CTX-M-15}}$ compared with 89 [68%] of 130 isolates obtained during 2012 and 2016) (Figure).

Clade A was absent among ST131 during 2006 and then increased to 12% of the ST131 population during 2012 and 11.3% of the ST131 population during 2016 (p<0.01 for both comparisons) (Figure). The IR of clade A increased from 0 to 1.48/100,001 residents during 2012 and to 1.15/100,000 residents during 2016 (p<0.001 for both comparisons) (Table 2). B was the second most common clade during 2006 (26.4% of the total ST131 population), but decreased to 6% of the ST131 population during 2012 and to 6.4% of the ST131 population during 2016 (p<0.001 for both comparisons) (Figure). The IR of clade B decreased from 1.30/100,000 residents to 0.74/100,000 residents during 2012 and to 0.65/100,000 residents during 2016 (Table 2).

Clinical Characteristics

E. coli ST131 bloodstream infections were evenly distributed between male patients (n = 171, 49.7%) and female patients (n = 173, 50.3%) (Table 1). Just under half (48%) of *E. coli* ST131 bloodstream infections were healthcare-associated, followed by community-acquired (34%) and hospital-acquired (18%) (Table 1). Clades A and B were associated with community-acquired infections, and patients infected with clade C were more likely to be healthcare associated. Patients infected with clade A tended to be younger (Table 1). More than half (n = 186, 54%) of patients had upper urinary tract infections, followed by bloodstream infections with an unknown source (n = 69, 20%), pneumonia (n = 35, 10%), acute biliary tract infections (n = 31, 9%), and intraabdominal infections (n = 23, 7%) (Table 1).

Serotypes, *fim*H Types, and Antimicrobial Susceptibilities

Clade A contained O16:H5, *fim*H41, and *fim*H89. Clade B contained O25:H4, O2:H4, *fim*H22, *fim*H27,

Table 2. Incidence rates/100,000 residents for *Escherichia coli* sequence type 131 clades, Calgary, Alberta, Canada, 2006, 2012, and 2016*

Clade	IR (95% CI)		
	2006	2012	2016
A	0.00[a] (0.00–0.34)	1.48[b] (0.88–2.34)	1.15[b] (0.66–1.87)
B	1.30 (0.71–2.18)	0.74 (0.34–1.41	0.65 (0.30–1.23)
C0	0.46[a] (0.15–1.08)	0.00[b] (0.00–0.30)	0.00[b] (0.00–0.26)
C1-nonM27	2.22[a] (1.55–3.60)	4.61[b] (3.48–5.99)	2.94[a] (2.11–3.99)
C1-M27	0.09[a] (0.00–0.56)	0.33 (0.09–0.84)	0.57[b] (0.25–1.13)
C2	0.83[a] (0.41–1.72)	5.19[b] (3.98–6.63)	4.81[b] (3.73–6.11)
Total	4.91[a] (3.68–6.42)	12.35[b](10.45–14.49)	10.12[b] (8.52–11.94)

*Rates followed by different superscript letters indicate significant differences between years at the 5% level. IR; incidence rate.

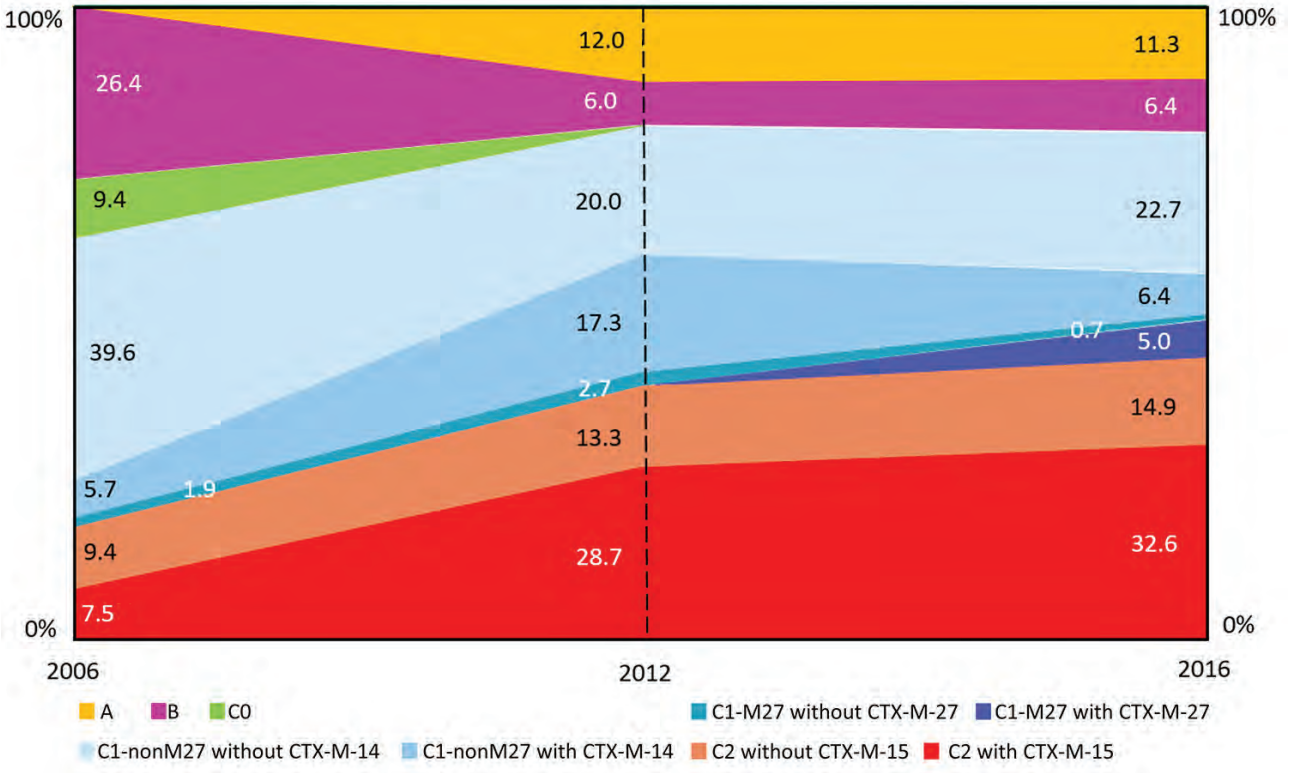

Figure. Proportions of *Escherichia coli* sequence type 131 clades, Calgary, Alberta, Canada, 2006–2016.

*fim*H324, and *fim*H30. Clade C contained O25:H4 and *fim*H30 (Table 1).

Overall, high (>25%), intermediate, or resistant (not susceptible) rates were observed for ceftriaxone, ciprofloxacin, trimethoprim/sulfamethoxazole, gentamicin, and tobramycin. Low rates (<5%) were observed for amikacin, ertapenem, and meropenem. C2 was the most antimicrobial-resistant subclade, followed by C1-nonM27 and C1-M27 (Table 1). Clades B and C0 were the most susceptible clades, and clade A showed high nonsusceptible rates for trimethoprim/sulfamethoxazole, gentamicin, and tobramycin (Table 1).

Removal of Subclade C2

Eliminating subclade C2 would have decreased the incidence rate of ST131 bloodstream infections from 12.35/100,000 residents to 7.16/100,000 residents during 2012 and from 10.12/100,001 residents to 5.31/100,000 residents during 2016 ($p<0.001$ both comparisons). In addition, eliminating subclade C2 would have resulted in a significant reduction of not susceptible rates for amoxicillin/clavulanic acid, ciprofloxacin, ceftriaxone, and tobramycin for ST131 causing bloodstream infections in Calgary (2006, 2012, and 2016) ($p<0.05$ for all comparisons).

Quinolone Resistance–Determining Regions and Antimicrobial Resistance Determinants

The combination of mutations in gyrase A genes (*gyrA* S83L and *gyrA* D87N) and DNA topoisomerase IV genes (*parC* S80I, *parC* E84V, and *parE* I529L) in the quinolone resistance-determining regions were present in all C1 and C2 isolates (Table 3). Nearly all (97%) ST131 isolates contained the *parE* I529L mutation. Most (85%) clade A isolates had the *gyrA* S83L mutation; for 5 isolates, this mutation was combined with *gyrA* D87N and *parC* S80I, and 1 isolate had the *gyrA* S83L, *gyrA* D87N, *parC* S80I, and *parC* E84V combination. Mutations in *gyrA* and *parC* were rare in clade B; 2/32 isolates had the *gyrA* S83L and *parC* S80I mutation combination (Table 3). One subclade C0 isolate had only the *gyrA* S83L mutation, and another C0 isolate had the *gyrA* S83L, *gyrA* D87N, *parC* S80I, and *parC* E84V combination.

CTX-M β-lactamases were detected among 148 (43%) isolates; most were CTX-M-15, followed by CTX-M-14, CTX-M-27, CTX-M-55, and CTX-M-198 (Table 3). CTX-M types were associated with different subclades (e.g., $bla_{\text{CTX-M-14}}$ with C1-nonM27, $bla_{\text{CTX-M-15}}$ with C2, $bla_{\text{CTX-M-27}}$ with C1-M27, and $bla_{\text{CTX-M-55}}$ with A). TEM-1 was common in most clades, with the exception of C2 and C1-M27. Three ST131 isolates were positive for $bla_{\text{CMY-2}}$, and 1 C2 isolate was positive for $bla_{\text{NDM-5}}$.

Certain aminoglycoside-modifying enzymes were common among ST131: *aac(3)-IId, aac(6')-Ib-cr*, *aadA5, aph(3'')-Ib*, and *aph (6)-Id* (Table 3). Some associations between presences of aminoglycoside-modifying enzymes with certain subclades were noted: *aac (3)-IId* were present mainly in clades A, B, and C1-nonM27; *aac(6')-Ib-cr* in subclade C2; *aadA2* in clade B, and *aadA5* in clades A, C0, and C1. The combination of *aph(3'')-Ib* and *aph (6)-Id* was more common in clades A and C1-nonM27 (Table 3). With regard to the presence of other antimicrobial resistance determinants, *qnr* was rare, and *dfrA17*, *sul1*, *sul2*, and *tetA* were common among most of ST131 clades (Table 3).

Plasmids and Replicon Types

Overall, IncF plasmid types (e.g., combinations of FIA, FIB, FIC, and FII) were common among all ST131 clades. Col-like plasmids and other plasmid families (IncI1, IncN, IncX1, IncX4, and IncY) were widely distributed across all clades but less common than IncF types (Table 1).

Table 3. Factors associated with *Escherichia coli* sequence type 131 clades, Calgary, Alberta, Canada, 2006, 2012, and 2016*

Factor	Clade						
	A, n = 34	B, n = 32	C0, n = 5	C1-non-M27, n = 121	C1-M27, n = 13	C2, n = 139	All, n = 344
QRDR mutation							
gyrA S83L	29 (85)[a,b]	2 (6)[c]	2 (40)[b,c]	121 (100)[d]	13 (100)[a,d]	139 (100)[d]	306 (89)
gyrA D87N	5 (15)[a]	0[a]	1 (20)[a]	121 (100)[b]	13 (100)[b]	139 (100)[b]	279 (8)
parC S80I	5 (15)[a]	2 (6)[a]	1 (20)[a]	121 (100)[b]	13 (100)[b]	139 (100)[b]	281 (82)
parC E84V	1 (3)[a]	0[a]	1 (20)[a]	121 (100)[b]	13 (100)[b]	139 (100)[b]	275 (80)
parE I529L	30 (88)[a]	27 (84)[a]	5 (100)	121 (100)[b]	13 (100)	139 (100)[b]	335 (97)
β-lactamase							
CTX-M-15	2 (6)[a]	1 (3)[a]	0[a]	1 (1)[a]	0[a]	93 (67)[b]	97 (28)
CTX-M-14	0[a]	0[a]	0	38 (31)[b]	0	1 (1)[a]	39 (11)
CTX-M-27	1 (3)[a]	0[a]	0	0[a]	7 (54)[b]	0[a]	8 (2)
CTX-M-55	2 (6)	0	0	0	0	0	2 (0.6)
CTX-M-198	0	0	0	1 (1)	0	0	1 (0.3)
NDM-5	0	0	0	0	0	1 (1)	1 (0.3)
OXA-1	0[a]	0[a]	0[a]	1 (1)[a]	0[a]	84 (6)[b]	85 (25)
OXA-9	0	0	0	0	0	1 (1)	1 (0.3)
SHV-12	0	0	0	0	0	2 (1)	2 (0.6)
TEM-1	29 (85)[a,b]	20 (63)[a]	4 (80)[a,b]	103 (85)[b]	1 (8)[c]	26 (19)[c]	183 (53)
TEM other	0	0	0	2 (2)	0	2 (1)	4 (1)
CMY-2	0	2 (6%)	0	1 (1)	0	0	3 (0.9)
Aminoglycoside-modifying enzyme							
Aac(3)-IIa	0[a]	0[a]	0	2 (1)[a]	0[a]	57 (41)[b]	59 (17)
Aac(3))-IId	11 (32)[a,b]	15 (47)[a]	0	63 (52)[a]	0[b,c]	4 (3)[c]	93 (27)
aac(6')-Ib-cr	0[a]	0[a]	0[a]	2 (2)[a]	0[a]	84 (60)[b]	86 (25)
aadA1	0	2 6)	0	0	0	4 (3)	6 (2)
aadA16	0	0	0	1 (1)	0	1 (1)	2 (0.6)
aadA2	0[a]	14 (44)[b]	0	0[a]	0[a]	2 (1)[a]	16 ()
aadA5	23 (68)[a]	1 (3)[b]	3 (60)[a,c]	70 (58)[a]	7 (54)[a,c]	57 (41)[c]	161 (47)
ant(2'')-Ia	0	0	0	0	0	5 (4)	5 (1)
aph(3')-Ia	1 (3)	2	0	1 (11)	0	0	4 (1)
aph(3'')-Ib	20 (59)[a]	3 (9)[b]	0	69 (57)[a]	5 (38)	26 (19)[b]	123 (36)
aph(3')-IIa	0	1 (3)	0	1 (1)	0	0	2 (0.6)
Aph(6)-Ic	0	1 (3)	0	1 (1)	0	0	2 (0.6)
Aph(6)-Id	20 (59)[a]	3 (9)[b]	0	68 (56)[a]	5 (38)	25 (18)[b]	121 (35)
Other							
qnrB	0	0	0	0	0	2 (1)	2 (0.6)
ARR-3	0	0	0	1 (1)	0	1 (1)	2 (0.6)
dfrA1	0	1 (3)	0	0	0	0	1 (0.3)
dfrA12	0[a]	13 (41)[b]	0	0[a]	0[a]	2 (1)[a]	15 (4)
dfrA14	1 (3)	0	0	0	0	8	12 (3)
dfrA17	22 (65)[a]	1 (3)[b]	3 (60)[a]	70 (58)[a]	7 (54)[a]	59 (42)[a]	162 (47)
dfrA27	0	0	0	1 (1)	0	1 (1)	2 (0.6)
dfrA5	0	1 (3)	0	0	0	0	1 (0.3)
sul1	22 (65)	15 (47)	3 (60)	69 (57)	6 (46)	63 (45)	178 (52)
sul2	20 (59)[a]	3 (9)[b]	0	70 (58)[a]	5 (38)	28 (20)[b]	126 (37)
sul3	0	1 (3)	0	0	0	0	1 (0.3)
tetA	19 (56)[a]	5 (16)[b]	0	61 (50)[a]	6 (4)	77 (55)[a]	168 (49)
tetB	2 (6)	3 (9)	0	2 (2)	0	3 (2)	10 (3)

*Values are no. (%). Rates followed by different superscript letters indicate significant differences between clades at the 5% level (adjusted for multiple comparisons).

Using IncF plasmid replicons (FII_1, FIA_2, FIB_20, FII_2, and FIA_1) and a plasmid classification system published recently (*26*), we found that group 1 plasmids (combination of FII_1, FIA_2, and FIB_20) were in clades A, B, C1-nonM27, and C1-M27, and group 2 plasmids (combination of FII_2 and FIA_1) were in clades C0 and C2 (Table 1). Group 1 plasmids were common among C1 clades, and group 2 plasmids were common among C2 isolates.

Virulence-Associated Factors

The presence of 37 putative virulence factors were assessed for different clades (Table 4). The following factors were present among most isolates: *papAIX*, *iha*, *fimH*, *sat*, *fyuA*, *usp*, *iss*, and *malX*. Some virulence factors were associated with certain clades: *pap*BCFJK, *iha*, *hlyA*, and *cnf1* with subclade C2; *afaABCD*, *draABCDP vat*, and *traT* with clade A; *afaABCD*, *draABCDP*, *kpsMII*, and *ibeABC* with clade B; and *kpsMT*III with subclades C0 and C1. No major differences in virulence scores were observed for the different clades.

Discussion

The abrupt global expansion of ST131 during the 2000s is unrivaled among human bacteria and is a real-world model for the evolution of antimicrobial-resistant high-risk clones (*10*). This study describes the clinical features, incidence rates, genomic characteristics, and changes in population structure of ST131 clades causing bloodstream infections in a large centralized region of Canada over an 11-year period (2006–2016). The incidence rates and prevalence of ST131 increased over the time period, mostly caused by an influx of subclades C2 with $bla_{\text{CTX-M-15}}$ and C1-M27 with $bla_{\text{CTX-M-27}}$. Such results reinforce the possible role of CTX-M enzymes in the evolutionary success of ST131 (*10*). The presence of $bla_{\text{CTX-M-14}}$ among C1-nonM27 isolates did not provide a beneficial advantage to this subclade. This finding is probably caused by clonal interference among 2 clones that have acquired different beneficial mutations competing in the same environment (*27*).

The population structure of ST131 in the Calgary region was dominated by clade C, which is similar to results from a previous large global study (*28*). The C clade originated from clade B during the mid to late 1980s by acquisition of several prophages, genomic islands, the *fimH30* allele, and mutations within *gyrA* and *parC* that likely transpired in North America (*29*,*30*). The C clade in this study was mostly responsible for healthcare-associated urinary tract infections. C2 was the most common and most antimicrobial-resistant subclade in this collection and was associated with group 2 plasmids, $bla_{\text{CTX-M-15}}$ and *aac(6′)-Ib-cr*, as well as the virulence factors *iha*, *hlyA*, and *cnf1*. This subclade became prominent during 2012 and 2016 and showed the highest IRs among all subclades during this period. The increase of C2 correlated with the presence of CTX-M-15. Elimination of the C2 subclade through vaccination or phage-therapy programs (*31*), will lead to major decreases in incidence and antimicrobial-resistant rates among ST131 causing bloodstream infections in Calgary.

The C1-nonM27 subclade was the most common subclade during 2006 and associated with group 1 plasmids, $bla_{\text{CTX-M-14}}$, and *aac (3)-IId*. Overall, the C1-M27 subclade was rare (especially during 2006 and 2012) but increased substantially during 2016, which correlated with the presence of $bla_{\text{CTX-M-27}}$. The C1-M27 subclade has previously been responsible for increases in ESBL-producing *E. coli* from Japan and was also present among ST131 obtained from Thailand, Australia, Canada, and the United States (*6*). The ST131 C1-M27 subclade is currently emerging in Germany (*32*) and France (*33*) and is responsible for 27% of 144 clinical ST131 obtained from different sites in Europe (*34*).

Clade A is likely the ancestral lineage of ST131 and probably originated in Southeast Asia during the mid to late 1880s (*30*). Clade A isolates are generally sensitive to antimicrobial drugs and appear to occupy distinct ecologic niches, such as waste water (*35*). Results from this study show that clade A isolates have high not susceptible rates for trimethoprim/sulfamethoxazole, gentamicin, and tobramycin and were associated with community-associated and healthcare-associated urinary tract infections in younger patients. The virulence factors *afaABCD*, *draABCDP*, *vat*, and *traT* were common in clade A. Also, clade A was absent among ST131 from 2006 but became the third most common clade during 2012 and 2016, replacing clades B and C0 during these periods.

Clade B emerged from clade A in the early 1900s and most likely occurred in North America (*10*,*30*). Members of clade B are antimicrobial susceptible, and several intermediate subclades have been identified (*29*). Our study showed that clade B isolates were the second most common clade during 2006 but decreased substantially during 2016. This clade was the most antimicrobial sensitive ST131 clade in Calgary and was associated with community-acquired urinary tract infections and virulence factors *afaABCD*, *draABCDP*, *kpsMII*, and *ibeABC*.

Previous data have shown that *gyrA S83L* mutations occurred first among fluoroquinolone-resistant

Table 4. Virulence factors associated with *Escherichia coli* sequence type 131 clades, Calgary, Alberta, Canada, 2006, 2012, and 2016*

Factor	Clade						
	A, n = 34	B, n = 32	C0, n = 5	C1-nonM27, n = 121	C1-M27, n = 13	C2, n = 139	All, n = 344
Adhesion gene							
papA	34 (100)	28 (88)	5 (100)	121 (100)	13 (100)	139 (100)	340 (99)
papB	1 (3)[a]	11 (34)	0	35 (29)[a]	1 (8)	90 (65)[b]	138 (40)
papC	1 (3)[a]	13 (41)	0	31 (26)[a]	2 (16)	89 (64)[b]	141 (41)
papD	1 (3)[a]	13 (41)	0	36 (30)[a]	1 (8)	89 (64)[b]	140 (41)
papE	1 (3)	11 (34)	0	0	0	9 (6)	21 (6)
papF	2 (6)[a]	12 (38)	0	34 (28)[a]	1 (8)	90 (65)[b]	139 (40)
papG	1 (3)	14 (44)	0	34 (28)	1 (8)	91 (6)	141 (41)
papH	1 (3)	9 (28)	0	33 (27)	0	41 (29)	84 (24)
papI	32 (94)	24 (75)[a]	5 (100)	116 (96)	12 (92)	137 (99)[b]	326 (95)
papJ	1 (3)[a]	11 (34)	0	34 (28)[a]	1 (8)	90 (65)[b]	137 (40)
papK	1 (3)[a]	11 (34)	0	34 (28)[a]	1 (8)	90 (65)[b]	137 (40)
papX	32 (94)	21 (66)[a]	5 (100)	100 (83)	10 (77)	134 (96)[b]	302 (88)
Iha	33 (97)	16 (50)[a]	5 (100)	111 (92)	13 (100)	137 (99)[b]	314 (91)
fimH	34 (100)	32 (100)	5 (100)	121 (100)	13 (100)	139 (100)	344 (100)
Tsh	0	2 (6)	0	0	0	0	2 (0.6)
Hra	1 (1)	0	1 (25)	1 (1)	0	8 (6)	11 (3)
afaABCD	18 (53)[a]	18 (56)[a]	1 (25)	4 (3)[b]	0	28 (20)[b]	69 (20)
draABCDP	18 (53)[a]	18 (56)[a]	1 (25)	4 (3)[b]	0	28 (20)[b]	69 (20)
Toxin gene							
hlyA	1 (1)	11 (34)	0	27 (22)	0	50 (36)	89 (26)
Sat	30 (88)	21 (66)[a]	5 (100)	112 (93)	13 (100)	136 (98)[b]	317 (92)
Vat	34 (100)[a]	7 (22)[b]	0	1 (1)[b]	0[b]	0[b]	42 (1)
astA	1 (3)	1 (3)	0	0	0	6 (4)	8 (2)
cnf1	1 (3)	9 (28)	0	29 (24)	0	52 (37)	91 (26)
Siderophore gene							
iroN	0	9 (28)	0	1 (1)	0	9 (6)	19 (6)
fyuA	34 (100)	32 (100)	5 (100)	121 (100)	13 (100)	139 (100)	344 (100)
ireA	0	0	0	0	0	11 (8)	11 (3)
iutA	29 (85)	27 (84)	5 (100)	112 (93)	12 (92)	137 (99)	322 (94)
Capsular antigen gene							
kpsM II	0	14 (44)	0	0	0	2 (1)	16 (5)
kpsMT III	0[a]	13 (41)	5 (100)	71 (59)[a,b]	13 (100)[b]	37 (26)[c]	139 (40)
Miscellaneous gene							
Usp	33 (97)	32 (100)	5 (100)	121 (100)	12 (92)	137 (99)	340 (99)
traT	28 (82)[a]	13 (41)[b]	0	20 (17)[b]	0[b]	28 (20)[b]	89 (26)
ompT	0	4 (13)	0	2 (2)	0	1 (1)	7 (2)
Iss	9 (26)[a]	31 (97)	5 (100)	118 (98)[b]	13 (100)	139 (100)[b]	315 (92)
malX	34 (100)	32 (100)	5 (100)	118 (98)	13 (100)	138 (99)	340 (99)
cdtB	0	2 (6)	0	0	0	0	2 (0.6)
cvaC	0	4 (13)	0	0	9 (69%)	10 (7%)	14 (6)
ibeABC	0	14 (44)[a]	0	0	0	0[b]	14 (6)
Virulence score, median (range)†	11 (7–15)	10 (6–14)	11 (9–16)	10 (6–15)	10 (9–14)	11 (7–15)	

*Values are no. (%) unless indicated otherwise. Rates followed by different superscript letters indicate significant differences between clades at the 5% level (adjusted for multiple comparisons). *afa,* afimbrial adhesin; *astA*, enteroaggregative *E. coli* toxin; *cdtB,* cytolethal distending toxin B; *cnf1*, cytotoxic necrotizing factor; *cvaC*, factor facilitating colonization; *dra*, Dr binding adhesins; *fimH*, type-1 fimbriae; *fyuA*, yersiniabactin (siderophore) receptor; *hlyA*, α-hemolysin; *hra*, heat-resistant agglutinin; *ibeABC,* invasion of brain endothelium; *iha*, iron-regulated adhesin; *ireA*, iron-regulated element (catecholate siderophore); *iroN*, salmochelin (siderophore) receptor; *iss*, increased serum survival; *iutA*, aerobactin (siderophore) receptor; *kpsM* II, group II capsule variants synthesis; *kpsM* III, group III capsule variants synthesis; *malX*, pathogenicity island marker; *ompT*, outer membrane protein T; *papA*, P fimbriae; *papBCDEFGHIJKX*, genes of P fimbriae operon; *sat*, secreted autotransporter toxin; *traT*, complement inhibition protein; *tsh*, temperature-sensitive hemagglutinin; *usp*, uropathogenic-specific protein; *vat*, vacuolating autotransporter toxin.
†The virulence gene score was the number of virulence operons detected.

E. coli and is a major initial step for establishing relative fitness among antimicrobial-resistant isolates (*36*). Our study showed that *gyrA* mutations were rare among clade B isolates, but *parE* I529L mutations were common. This finding suggests that *parE* I529L mutations are the first to occur among fluoroquinolone-resistant ST131. The order in which these mutations arise might play a major role in establishing fitness in ST131 (*37*).

Our study had some limitations. Only patients in Calgary who had positive blood cultures for *E. coli* were included, which excluded those with *E. coli* bloodstream infections from whom no blood samples were submitted for culture. Therefore, incidence rates should be considered as conservative estimates of ST131 bloodstream infections in Calgary, especially for patients infected with clades A and B, who tended to be younger (i.e., clade A infections) and from the

community (i.e., clade B infections). Such patients were less likely to have had blood cultures taken than patients who are older or who had previous contact with the healthcare system.

The novel approach for our study used population-based surveillance to describe the incidence rates, specific characteristics, and trends among ST131 clades over an 11-year period in a well-defined human population. We showed major differences in IRs, frequencies, resistance patterns, antimicrobial resistance determinants, grouped plasmid types, virulence factors, and trends over time for different clades. We provided insights into the evolution of ST131 clades in a large well-defined region of Canada. The population structure of ST131 in large geographic healthcare regions is dynamic and has continuous interplay between different subclades.

A previous study showed that eliminating ST131 would substantially decrease the overall IR and antimicrobial-resistant burden within *E. coli* causing bloodstream infections in the Calgary region (*7*). This study identified ST131 subclade C2 as the predominant and most antimicrobial-resistant subclade in Calgary, which is increasing exponentially over time. Eradicating ST131, more specifically the C2 subclade, will lead to considerable public health benefits for persons in Calgary.

This study was supported by research grant #10016015 from the Joint Programming Initiative on Antimicrobial Resistance/Canadian Institute Health Research Program.

About the Author

Dr. Peirano is a research associate at Alberta Precision Laboratories and the University of Calgary, Calgary, Alberta, Canada. Her research interests include the molecular epidemiology of antimicrobial drug–resistant organisms.

References

1. Mathers AJ, Peirano G, Pitout JD. The role of epidemic resistance plasmids and international high-risk clones in the spread of multidrug-resistant *Enterobacteriaceae*. Clin Microbiol Rev. 2015;28:565–91. https://doi.org/10.1128/CMR.00116-14
2. Peirano G, Pitout JD. Molecular epidemiology of *Escherichia coli* producing CTX-M beta-lactamases: the worldwide emergence of clone ST131 O25:H4. Int J Antimicrob Agents. 2010;35:316–21. https://doi.org/10.1016/j.ijantimicag.2009.11.003
3. Manges AR, Geum HM, Guo A, Edens TJ, Fibke CD, Pitout J. Global extraintestinal pathogenic *Escherichia coli* (ExPEC) lineages. Clin Microbiol Rev. 2019;32:e00135-18. https://doi.org/10.1128/CMR.00135-18
4. Peirano G, Pitout JDD. Extended-spectrum β-lactamase–producing *Enterobacteriaceae*: update on molecular epidemiology and treatment options. Drugs. 2019;79:1529–41. https://doi.org/10.1007/s40265-019-01180-3
5. Pitout JD, DeVinney R. *Escherichia coli* ST131: a multidrug-resistant clone primed for global domination. F1000 Res. 2017;6:6. https://doi.org/10.12688/f1000research.10609.1
6. Matsumura Y, Pitout JD, Gomi R, Matsuda T, Noguchi T, Yamamoto M, et al. Global *Escherichia coli* sequence type 131 clade with $bla_{CTX-M-27}$ gene. Emerg Infect Dis. 2016;22:1900–7. https://doi.org/10.3201/eid2211.160519
7. Holland MS, Nobrega D, Peirano G, Naugler C, Church DL, Pitout JDD. Molecular epidemiology of *Escherichia coli* causing bloodstream infections in a centralized Canadian region: a population-based surveillance study. Clin Microbiol Infect. 2020;S1198-743X(20)30101-4. https://doi.org/10.1016/j.cmi.2020.02.019
8. Peirano G, Pitout JD. Fluoroquinolone-resistant *Escherichia coli* sequence type 131 isolates causing bloodstream infections in a Canadian region with a centralized laboratory system: rapid emergence of the H30-Rx sublineage. Antimicrob Agents Chemother. 2014;58:2699–703. https://doi.org/10.1128/AAC.00119-14
9. Peirano G, van der Bij AK, Gregson DB, Pitout JD. Molecular epidemiology over an 11-year period (2000 to 2010) of extended-spectrum β-lactamase-producing *Escherichia coli* causing bacteremia in a centralized Canadian region. J Clin Microbiol. 2012;50:294–9. https://doi.org/10.1128/JCM.06025-11
10. Pitout JDD, Finn TJ. The evolutionary puzzle of *Escherichia coli* ST131. Infect Genet Evol. 2020;81:104265. https://doi.org/10.1016/j.meegid.2020.104265
11. Friedman ND, Kaye KS, Stout JE, McGarry SA, Trivette SL, Briggs JP, et al. Health care–associated bloodstream infections in adults: a reason to change the accepted definition of community-acquired infections. Ann Intern Med. 2002;137:791–7. https://doi.org/10.7326/0003-4819-137-10-200211190-00007
12. Clinical and Laboratory Standards Institute. Perfomance standards for antimicrobial susceptibility testing. 25th information supplement. CLSI document M100–S25. Wayne (PA): The Institute; 2015.
13. Johnson JR, Porter S, Thuras P, Castanheira M. The pandemic *H*30 subclone of sequence type 131 (ST131) as the leading cause of multidrug-resistant *Escherichia coli* infections in the United States (2011–2012). Open Forum Infect Dis. 2017;4:ofx089. https://doi.org/10.1093/ofid/ofx089
14. Matsumura Y, Pitout JD, Peirano G, DeVinney R, Noguchi T, Yamamoto M, et al. RapidiIdentification of different *Escherichia coli* sequence type 131 clades. Antimicrob Agents Chemother. 2017;61:e00179-17. https://doi.org/10.1128/AAC.00179-17
15. Lowe M, Kock MM, Coetzee J, Hoosien E, Peirano G, Strydom KA, et al. *Klebsiella pneumoniae* ST307 with $bla_{OXA-181}$, South Africa, 2014–2016. Emerg Infect Dis. 2019;25:739–47. https://doi.org/10.3201/eid2504.181482
16. Peirano G, Matsumura Y, Adams MD, Bradford P, Motyl M, Chen L, et al. Genomic epidemiology of global carbapenemase-producing *Enterobacter* spp., 2008–2014. Emerg Infect Dis. 2018;24:1010–9. https://doi.org/10.3201/eid2406.171648
17. Nurk S, Bankevich A, Antipov D, Gurevich AA, Korobeynikov A, Lapidus A, et al. Assembling single-cell genomes and mini-metagenomes from chimeric MDA products. J Comput Biol. 2013;20:714–37. https://doi.org/10.1089/cmb.2013.0084
18. Camacho C, Coulouris G, Avagyan V, Ma N, Papadopoulos J, Bealer K, et al. BLAST+: architecture and applications.

BMC Bioinformatics. 2009;10:421. https://doi.org/10.1186/1471-2105-10-421
19. Zankari E, Hasman H, Cosentino S, Vestergaard M, Rasmussen S, Lund O, et al. Identification of acquired antimicrobial resistance genes. J Antimicrob Chemother. 2012;67:2640–4. https://doi.org/10.1093/jac/dks261
20. Carattoli A, Zankari E, García-Fernández A, Voldby Larsen M, Lund O, Villa L, et al. In silico detection and typing of plasmids using PlasmidFinder and plasmid multilocus sequence typing. Antimicrob Agents Chemother. 2014;58:3895–903. https://doi.org/10.1128/AAC.02412-14
21. Zhou Z, Alikhan NF, Mohamed K, Fan Y, Achtman M; Agama Study Group. The EnteroBase user's guide, with case studies on *Salmonella* transmissions, *Yersinia pestis* phylogeny, and *Escherichia* core genomic diversity. Genome Res. 2020;30:138–52. https://doi.org/10.1101/gr.251678.119
22. Joensen KG, Scheutz F, Lund O, Hasman H, Kaas RS, Nielsen EM, et al. Real-time whole-genome sequencing for routine typing, surveillance, and outbreak detection of verotoxigenic *Escherichia coli*. J Clin Microbiol. 2014;52:1501–10. https://doi.org/10.1128/JCM.03617-13
23. Liu B, Zheng D, Jin Q, Chen L, Yang J. VFDB 2019: a comparative pathogenomic platform with an interactive web interface. Nucleic Acids Res. 2019;47(D1):D687–92. https://doi.org/10.1093/nar/gky1080
24. Benjamini Y, Hochberg Y. Controlling the false discovery rate: a practical and powerful approach to multiple testing. J R Stat Soc B. 1995;57:289–300. https://doi.org/10.1111/j.2517-6161.1995.tb02031.x
25. R Core Team. R: a language and environment for statistical computing. Vienna: R Foundation for Statistical Computing; 2017.
26. Kondratyeva K, Salmon-Divon M, Navon-Venezia S. Meta-analysis of pandemic *Escherichia coli* ST131 plasmidome proves restricted plasmid–clade associations. Sci Rep. 2020;10:36. https://doi.org/10.1038/s41598-019-56763-7
27. Hughes JM, Lohman BK, Deckert GE, Nichols EP, Settles M, Abdo Z, et al. The role of clonal interference in the evolutionary dynamics of plasmid–host adaptation. MBio. 2012;3:e00077–12. https://doi.org/10.1128/mBio.00077-12
28. Decano AG, Downing T. An *Escherichia coli* ST131 pangenome atlas reveals population structure and evolution across 4,071 isolates. Sci Rep. 2019;9:17394. https://doi.org/10.1038/s41598-019-54004-5
29. Ben Zakour NL, Alsheikh-Hussain AS, Ashcroft MM, Khanh Nhu NT, Roberts LW, Stanton-Cook M, et al. Sequential acquisition of virulence and fluoroquinolone resistance has shaped the evolution of *Escherichia coli ST131*. mBio. 2016;7:e00347–16.
30. Stoesser N, Sheppard AE, Pankhurst L, De Maio N, Moore CE, Sebra R, et al.; Modernizing Medical Microbiology Informatics Group (MMMIG). Evolutionary history of the global emergence of the *Escherichia coli* epidemic clone ST131. MBio. 2016;7:e02162. https://doi.org/10.1128/mBio.02162-15
31. Galtier M, De Sordi L, Maura D, Arachchi H, Volant S, Dillies MA, et al. Bacteriophages to reduce gut carriage of antibiotic resistant uropathogens with low impact on microbiota composition. Environ Microbiol. 2016;18:2237–45. https://doi.org/10.1111/1462-2920.13284
32. Ghosh H, Doijad S, Falgenhauer L, Fritzenwanker M, Imirzalioglu C, Chakraborty T. bla$_{CTX-M-27}$-encoding *Escherichia coli* sequence type 131 lineage C1-M27 clone in clinical isolates, Germany. Emerg Infect Dis. 2017;23:1754–6. https://doi.org/10.3201/eid2310.170938
33. Birgy A, Bidet P, Levy C, Sobral E, Cohen R, Bonacorsi S. CTX-M-27-producing *Escherichia coli* of sequence type 131 and clade C1-M27, France. Emerg Infect Dis. 2017;23:885. https://doi.org/10.3201/eid2305.161865
34. Merino I, Hernández-García M, Turrientes MC, Pérez-Viso B, López-Fresneña N, Diaz-Agero C, et al.; R-GNOSIS Study Group. Emergence of ESBL-producing *Escherichia coli* ST131-C1-M27 clade colonizing patients in Europe. J Antimicrob Chemother. 2018;73:2973–80. https://doi.org/10.1093/jac/dky296
35. Finn TJ, Scriver L, Lam L, Duong M, Peirano G, Lynch T, et al. A comprehensive account of *Escherichia coli* sequence type 131 in wastewater reveals an abundance of fluoroquinolone-resistant clade A strains. Appl Environ Microbiol. 2020;86:e01913-19. https://doi.org/10.1128/AEM.01913-19
36. Huseby DL, Pietsch F, Brandis G, Garoff L, Tegehall A, Hughes D. Mutation supply and relative fitness shape the genotypes of ciprofloxacin-resistant *Escherichia coli.* Mol Biol Evol. 2017;34:1029–39. https://doi.org/10.1093/molbev/msx052
37. Johnson JR, Johnston B, Kuskowski MA, Sokurenko EV, Tchesnokova V. Intensity and mechanisms of fluoroquinolone resistance within the H30 and H30Rx subclones of *Escherichia coli* sequence type 131 compared with other fluoroquinolone-resistant *E. coli.* Antimicrob Agents Chemother. 2015;59:4471–80. https://doi.org/10.1128/AAC.00673-15

Address for correspondence: Johann D.D. Pitout, Department of Pathology and Laboratory Medicine, University of Calgary, #9 3535 Research Rd NW, Calgary T2L 2K8, Alberta, Canada; email: jpitout@ucalgary.ca

Outbreak of Haff Disease along the Yangtze River, Anhui Province, China, 2016

Huilai Ma,[1] Jiabing Wu,[1] Wei Qin,[1] Chao Lin, Dan Li, Bing Zha, Qi Chen, Yan Ma, Tichao Zhou, Shicong Li, Lei Gong, Wanwan Ma, Dafang Ge, Zhouxiang Cheng, Jian Chen, Qun Li

We investigated a large outbreak of Haff disease that occurred along the Yangtze River in Anhui Province, China, in 2016. Of the 672 cases identified during the outbreak, 83.3% (560/672) occurred in Wuhu and Ma'anshan. Patients experienced myalgia (100%) and muscle weakness (54.7%). The mean value of myoglobin was 330 ± 121.2 ng/mL and of serum creatine kinase 5,439.2 ± 4,765.1 U/L. Eating crayfish was the only common exposure among all cases; 96.8% (240/248) of implicated crayfish were caught on the shores of the Yangtze River or its connected ditches. Mean incubation period was 6.2 ± 3.8 hours. This case–control study demonstrated that eating the liver of crayfish and eating a large quantity of crayfish were associated with an increased risk for Haff disease. The seasonal increases in crayfish population along the Yangtze River might explain the seasonal outbreaks of Haff disease.

Haff disease is an unexplained rhabdomyolysis that occurs within 24 hours after consumption of certain types of freshwater or saltwater fish (*1*,*2*). It was first reported in 1924 in the vicinity of Königsberg along the Baltic coast near Frisches Haff (*1*–*3*). Over the next 9 years, an estimated 1,000 persons were affected by similar outbreaks, occurring seasonally in the summer and autumn in this area (*3*). Although subsequent outbreaks were identified in several other countries, such as Sweden (*4*), the former Soviet Union (*5*), Brazil (*6*,*7*), Japan (*8*), and China (*9*,*10*), the etiology has not yet been determined. An unidentified heat-stable toxin similar to cyanotoxins or palytoxin, but primarily myotoxic and not neurotoxic, is thought to be the cause of Haff disease (*1*); however, evidence supporting this hypothesis has been scant.

In July 2016, the number of rhabdomyolysis cases reported to the National Foodborne Disease Surveillance System (NFDSS) in China dramatically increased in Anhui Province compared with previous years. Most of the cases were reported in Wuhu and Ma'anshan, cities in Anhui Province in eastern China. Epidemiologic features were compatible with Haff disease (*3*,*6*). Preliminary investigation implicated crayfish as the vector. On August 5, the number of cases surpassed 200, prompting an emergency investigation by the Chinese Field Epidemiology Training Program, together with the Anhui Province Center for Disease Control and Prevention (CDC). The objectives of the investigation were to describe the epidemiologic and clinical characteristics, trace back the implicated vectors, identify possible risk factors, and recommend control measures.

Methods

Case Definition and Finding

We defined a case of rhabdomyolysis as any person with elevation in creatine kinase (CK) value plus clinical manifestations of myalgia or limb weakness (*10*,*11*). We defined a Haff disease case as illness in any person with acute onset of rhabdomyolysis after ingestion of freshwater fish or seafood within 24 hours in Anhui Province during June–August 2016. We searched for physician-diagnosed rhabdomyolysis cases from the NFDSS, an internet-based, passive surveillance system for foodborne

Author affiliations: Chinese Center for Disease Control and Prevention, Beijing, China (H. Ma, W. Qin, C. Lin, D. Li, Q. Chen, Y. Ma, T. Zhou, S. Li, Q. Li); Anhui Center for Disease Control and Prevention, Hefei, China (J. Wu, L. Gong, W. Ma); Lu'an Center for Disease Control and Prevention, Lu'an (W. Qin); Wuhu Center for Disease Control and Prevention, Wuhu, China (C. Lin, Z. Cheng); Ma'anshan Center for Disease Control and Prevention, Ma'anshan (B. Zha, D. Ge, J. Chen)

DOI: https://doi.org/10.3201/eid2612.191186

[1]These authors contributed equally to this article.

diseases searchable by food source in China. We also reviewed the outpatient and inpatient medical records in hospitals in Wuhu and Ma'anshan during the outbreak period to search for potential rhabdomyolysis cases.

Local Anhui Province CDC staff or Chinese Field Epidemiology Training Program trainees interviewed all rhabdomyolysis case-patients, either in-person or by telephone, using a structured questionnaire. Information collected included age, sex, date of onset, disease duration, clinical symptoms, potential risk factors (e.g., food, drugs, alcohol consumption, intense exercise, allergy history, underlying chronic illness), and the quantity of crayfish consumed. The researchers also obtained laboratory test findings from hospital medical records. They applied the Haff disease case definition to rhabdomyolysis cases to identify Haff disease cases and collected blood and urine specimens from Haff disease case-patients for further analysis.

In total, 673 rhabdomyolysis cases were identified in Anhui Province during June–August 2016. Of these, 99.9% (672/673) were compatible with the definition of Haff disease. All but 1 patient consumed cooked crayfish before symptom onset. The patient who did not eat cooked crayfish was a steelworker who had been working in the factory before onset, suggesting his illness might have been caused by heatstroke.

Case–Control Study

Although nearly all Haff disease case-patients ate cooked crayfish, we did not know what percent of persons who did not become ill also ate meals containing crayfish, given that crayfish were widely available during June–August 2016. Therefore, we conducted a matched case–control study to assess the association between eating crayfish and Haff disease. Cases in this study were persons who met the definition for Haff disease, had shared a meal with someone else before symptom onset, and consented to participate in the study. We identified $\geq$1 control per case; controls were selected among persons who shared the suspected meal of exposure with the case-patient before symptom onset. Controls had no clinical symptoms compatible with rhabdomyolysis and consented to participate in the study. Persons with other illnesses (e.g., fever, cold, injury, etc.) were disqualified as controls. In total, 67 cases and 108 controls were enrolled in the case–control study. Trained investigators conducted telephone-based interviews August 7–15, 2016, using a standardized questionnaire.

Traceback of Food and Environmental Investigation

For all Haff disease cases, we conducted a traceback investigation for the source of the implicated food by interviewing case-patients, restaurant owners, fishermen, and crayfish sellers. We conducted an environmental investigation of potential contamination along the distribution chain or unusual events during the outbreak period. We investigated the restaurants where case-patients had a meal before onset to find out where the crayfish came from and how they were cooked. We also visited crayfish farms, settings where crayfish were caught, and factories along the Yangtze River to identify whether the implicated crayfish or the environment in which the crayfish were raised had been contaminated.

Data Analysis

We performed statistical analysis using SPSS Statistics 20 (IBM, https://www.ibm.com). We compared cases and controls by χ^2 test. Significant risk factors ($p<0.05$) in the χ^2 tests were included in a multivariate Cox proportional hazard model to determine the odds ratio (OR) and 95% CI for the potential risk factors associated with Haff disease. All of the p values were 2-sided, and $p<0.05$ was considered significant.

Results

Confirmation of the Outbreak

In total, we verified 672 Haff disease cases in Anhui Province during June–August 2016. All cases occurred in 7 cities along the Yangtze River in Anhui Province; 83.3% (560/672) of the cases occurred in Wuhu (334 cases) and Ma'anshan (226 cases). We focused our investigation on the cases that occurred in Wuhu and Ma'anshan. Of the 560 case-patients in Wuhu and Ma'anshan, 495 (88.4%) completed the questionnaires; all 495 had consumed crayfish within 24 hours before symptom onset. The epidemic curve suggested a continuing common-source outbreak (Figure).

Descriptive Epidemiology

The outbreak started at the end of June, peaked in mid-July to early August, and lasted through August 17. Of the 495 case-patients, 197 (39.8%) were hospitalized; mean length of hospital stay was 7.3 ± 3.2 days. No deaths were reported. The mean age of the case-patients was 38.7 ± 13.5 years; 323/495 (65.3%) patients were female. Although cases were widely distributed in the 2 cities, 87.7% (434/495) were in residents from urban areas close to the

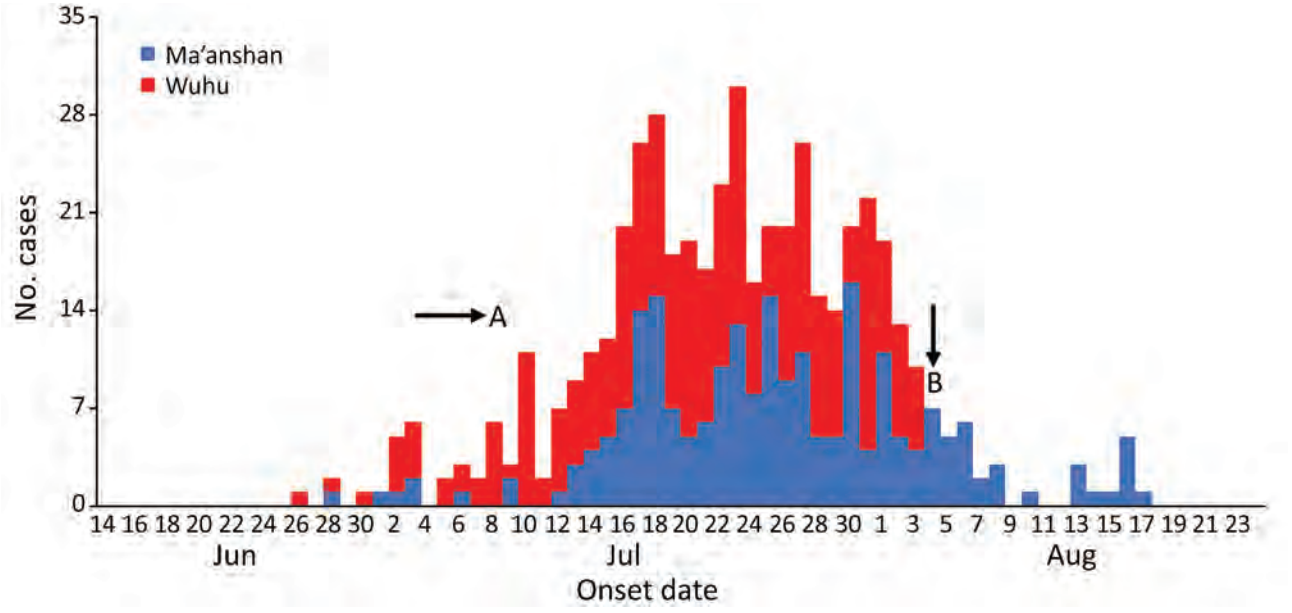

Figure. Outbreak of Haff disease in 2 cities along the Yangtze River, Anhui Province, China, 2016. A indicates period of heavy rainfall in Anhui Province; B indicates time at which local government warned residents not to eat crayfish.

Yangtze River. Each case-patient consumed a mean of 11.6 ± 6.1 crayfish pieces. The mean incubation period was 6.2 ± 3.8 hours.

Clinical Characteristics

All 495 case-patients experienced myalgia that was local or diffuse, involving the back, waist, whole body, neck, limbs, and chest (Table 1). A total of 271/495 (54.7%) experienced muscle weakness. Additional symptoms included brown urine, dyspnea, vomiting, abdominal pain, dizziness, and headache. Symptoms of nerve paralysis and fever were rare. Acute renal failure was not observed.

Table 1. Clinical characteristics during Haff disease outbreak in Anhui Province, China, 2016

Symptoms	No. cases (%), N = 495
Myalgia	495 (100.0)
Back	241 (48.7)
Waist	194 (39.2)
Whole-body	186 (37.6)
Neck	186 (37.6)
Lower limbs	111 (22.4)
Upper limbs	89 (18.0)
Chest	59 (11.9)
Muscle weakness	271 (54.7)
Brown urine	99 (20.0)
Dyspnea	60 (12.1)
Headache	49 (9.9)
Abdominal pain	46 (9.3)
Diarrhea	32 (6.5)
Vomiting	29 (5.9)
Dizziness	25 (5.1)
Nausea	21 (4.2)
Nerve paralysis	11 (2.2)
Fever	1 (0.2)

Laboratory Characteristics

We reviewed the laboratory test findings of blood and urine for some cases. The mean value of myoglobin was 330.0 ± 121.2 ng/mL, and mean CK level was 5,439.2 ± 4,765.1 U/L. In >80% of the cases, the levels of muscle-type CK and aspartate aminotransferase were abnormally elevated. In addition, 50.0% of case-patients were positive for urinary occult blood and proteinuria (Table 2).

Case–Control Study

In the case–control study, 100% of the 67 cases and 93.3% (101/108) of controls ate crayfish during their shared meal (OR = ∞, 95% CI 0.92–∞). We observed a significant dose-response relationship between the number of pieces of crayfish eaten and Haff disease (χ^2 = 29.225; p<0.001) (Table 3). Further analysis showed that eating crayfish liver was associated with increased disease risk (OR = 4.0, 95% CI 1.2–12.7).

Traceback and Environmental Investigation

Wuhu and Ma'anshan are located in the middle to lower reaches of the Yangtze River. Crayfish is a popular dish for residents of these 2 cities. Before the Haff disease outbreak, Anhui Province experienced heavy rainfall, which caused the largest flood disaster in decades. Consequently, rain or floodwater was retained in irrigation ditches and detention ponds for an extended time, and the amount of crayfish caught on the shores of the Yangtze River

Table 2. Laboratory test values from cases during Haff disease outbreak in Anhui, China, 2016*

Variables	Reference range	Median (range)	Mean ± SD	No. cases	% Abnormal cases
Serologic test					
Myoglobin, ng/mL	<25	344.3 (25.0–500.0)	330.0 ± 121.2	97	100
CK, U/L	30–135	4,192.0 (165.0–17,470.0)	5,439.2 ± 4,765.1	191	100
CK-MM, U/L	0–25	79.0 (10.0–980.0)	161.2 ± 185.9	104	82.7
AST, U/L	14–36	73.0 (14.0–1,346.0)	164.6 ± 207.0	103	84.5
ALT, U/L	9–52	52.0 (20.0–515.0)	85.9 ± 88.2	101	49.5
LDH, U/L	313–618	684.0 (333.0–8,170.0)	1,161.0 ± 1,334.9	99	53.5
Cre, μmol/L	62–106	63.6 (34.6–108.3)	66.4 ± 14.5	102	44.1
Urea, mmol/L	2.5–6.1	5.7 (2.3–256.1)	8.1 ± 24.84	102	32.4
Cl^+, mmol/L	98–107	104.70 (98.20–109.80)	104.46 ± 2.42	97	12.4
Ka^+, mmol/L	3.6–5.0	3.95 (3.14–5.17)	3.97 ± 0.34	97	10.3
Ca^{2+}, mmol/L	2.10–2.55	2.30 (2.07–2.65)	2.29 ± 0.13	47	8.5
Na^+, mmol/L	137–145	139.20 (133.80–144.50)	139.25 ± 1.9	97	8.2
Urinalysis					
Proteinuria	−	No. positive results: 9		50.0	18
Urinary occult blood	−	No. positive results: 10		50.0	20

*ALT, alanine aminotransferase; AST, aspartate aminotransferase; CK, creatine kinase; CK-MM, muscle-type creatine kinase; LDH, lactate dehydrogenase; Cre, serum creatinine; Ka^+, serum potassium, Na^+, serum sodium; Cl^+, Serum chloride; Ca^{2+}, serum calcium.

or its connected ditches was 5–10 times more during the outbreak period. However, no industrial or chemical contamination along the Yangtze River was reported.

The only common risk factor for all cases was eating crayfish, which were cooked thoroughly. We conducted a traceback investigation of the source for the implicated crayfish in Ma'anshan and Wuhu by interviewing persons in markets, restaurants, fisheries, and settings where crayfish were caught, as well as fishermen; we were able to trace 50.1% (248/495) of the implicated crayfish to their sources. Of these, 96.8% (240/248) were wild crayfish caught on the shores of the Yangtze River or its connected ditches. When we consulted with crayfish biologists, we found that the species of crayfish implicated during this outbreak was *Procambarus clarkii*.

Public Health Measures

Local governments issued a warning about the dangers of eating crayfish. In addition, public health departments instituted continuous surveillance and investigation of the outbreak.

Discussion

The epidemiologic and traceback investigations of a large outbreak of Haff disease in Anhui Province, China, indicated that all case-patients consumed crayfish within 24 hours before symptom onset; the implicated crayfish were caught on the shores of the Yangtze River or its connected ditches. The case–control study revealed that eating the liver of crayfish was associated with an increased risk for disease; the risk increased as the quantity of crayfish eaten increased.

Table 3. Analysis of probable risk factors associated with Haff disease in case–control study, Anhui, China, 2016*

Variables	Cases, N = 67	Controls, N = 108	p value	Multivariable OR (95% CI)
Sex			0.033	
M	19 (28.4)	48 (44.4)		Referent
F	48 (71.6)	60 (55.6)		1.6 (0.9–2.7)
Mean age, y (SD)	37.3 (11.3)	39.4 (18.9)	0.227	NA
Consumption of crayfish (SD)			0.084	NA
No	0	7 (6.5)		
Yes	67 (100)	101 (93.5)		
No. crayfish consumed			<0.001	
1−9	27 (40.3)	84 (77.8)		Reference
10−19	26 (38.8)	12 (11.1)		2.4 (1.4–4.2)
≥20	14 (20.9)	5 (4.6)		2.6 (1.3–5.1)
Ate liver of crayfish			<0.001	
No	3 (4.5)	32 (29.6)		Reference
Yes	64 (95.5)	76 (70.4)		4.0 (1.2–12.7)
Alcohol consumption			0.015	
No	51 (76.1)	97 (89.8)		Reference
Yes	16 (23.9)	11 (10.2)		1.6 (0.9–2.8)
Fish consumption†			0.648	—
No	64 (95.5)	100 (92.6)		
Yes	3 (4.5)	8 (7.4)		

*Values are no. (%) except as indicated. NA, not applicable; OR, odds ratio. SD, standard deviation.
†Corrected χ^2 value and p value for univariate analysis.

In China, the earliest reported outbreak of Haff disease was in Beijing in 2000 and involved 6 cases (*12*). An epidemiologic study revealed that all patients ate crayfish before onset, suggesting a link between crayfish and Haff disease (*12*). Although the literature shows that eating several species of fish, such as buffalo fish (*3*), salmon (*13*), freshwater pompano (*7*), marine boxfish (*8*), and pomfrets (*9*), could trigger Haff disease, almost all Haff disease cases in China were associated with eating crayfish (*2*). In recent years, Haff disease outbreaks have been reported in other cities in China (*14*–*19*). These outbreaks prompted the China CDC to conduct a thorough investigation of Haff disease. Crayfish have become a popular seafood for residents in central and eastern China, especially in June–September. Previous studies have reported that Haff disease shows a seasonal pattern, and outbreaks usually occur in the summer and fall months (*1*,*3*,*10*). Although a large Haff disease outbreak caused by eating freshwater pomfret occurred in October 2009 in southern China (*9*), most crayfish-related outbreaks (*10*,*20*,*21*), clusters (*18*,*22*), and sporadic cases (*16*) occurred predominantly in the summer. Seasonal crayfish harvest and consumption in June–September likely increases the opportunities for exposure, which may partially explain the seasonal pattern of Haff disease in China (*10*).

The most commonly reported clinical features in this outbreak were myalgia and muscle weakness, as well as abnormal levels of myoglobin and CK. Increased serum myoglobin concentration is the basis for early diagnosis of rhabdomyolysis (*23*); however, myoglobin concentrations tend to normalize within 6–8 hours following exposure. Thus, the window of opportunity for diagnosis is short (*24*). Of note, elevated myoglobin concentrations were observed in all case-patients who were tested in this study; this may be due to prompt medical care and timely laboratory testing in the hospital.

Rhabdomyolysis is a common life-threatening syndrome characterized by the injury of skeletal muscle resulting in the leakage of intracellular contents into the circulatory system (*25*). Patients with rhabdomyolysis usually experience myalgia, muscle weakness, raised serum CK, and brown urine (*24*). The etiologic spectrum of rhabdomyolysis is extensive, including crush injuries, ischemia, strenuous exercise, extreme body temperatures, drugs, toxins, infections, hereditary causes, and inflammatory or autoimmune muscle disease (*23*,*25*). A substantial number of patients may have no cause identified. We found that nerve paralysis and fever were rare symptoms, all crayfish were cooked thoroughly, and no industrial or chemical contamination was identified; therefore, this outbreak was unlikely to have been caused by infectious or chemical etiologies. Diaz et al. reported that an unidentified, heat-stable, algal toxin with primarily myotoxic rather than neurotoxic properties in seafood has been proposed as a cause of Haff disease (*1*); whether this toxin also exists in crayfish remains unknown.

Although many Haff disease cases have occurred in cities located in the middle to lower reaches of the Yangtze River, the association between Haff disease and crayfish caught from Yangtze River has not been elucidated in the published literature (*10*,*18*,*20*,*26*). In recent years, 3 other large Haff disease outbreaks have been reported in Nanjing and Tongling, 2 other cities located in the middle to lower reaches of the Yangtze River (*10*,*19*–*21*). The fact that these outbreaks all occurred in the middle to lower reaches of the Yangtze River suggests that crayfish could be their common etiology.

Studies using a mouse model have found that the hazardous substance from crayfish could cause rhabdomyolysis (*27*,*28*). This hazardous substance is specific to certain batches of crayfish. A dose-response relationship has also been observed. These findings in laboratory animals were consistent with the results of human epidemiologic investigation (*21*,*28*) and with our case–control study findings.

Our study had several limitations. First, because we lacked data on how many persons ate crayfish in the 2 study cities, we could not calculate the attack rates. Second, not all crayfish were traced back to their sources. Third, we were unable to conduct animal experiments to prove causation.

In conclusion, during this outbreak, the risk for Haff disease was associated with eating crayfish along the Yangtze River. The etiology of Haff disease remains elusive due to lack of knowledge of the underlying disease mechanism of rhabdomyolysis. Our findings might help researchers isolate the toxin that causes this disease.

Acknowledgments

We acknowledge the contributions of all participants of the outbreak investigation, especially public health workers from Wuhu and Ma'anshan.

About the Author

Dr. Ma is an epidemiologist and the director of the Chinese Field Epidemiology Training Program, China Center for Disease Control and Prevention. Her research interests include emergency outbreak investigation, epidemiologic, and surveillance projects.

References

1. Diaz JH. Global incidence of rhabdomyolysis after cooked seafood consumption (Haff disease). Clin Toxicol (Phila). 2015;53:421–6. https://doi.org/10.3109/15563650.2015.1016165
2. Chan TY. The emergence and epidemiology of Haff disease in China. Toxins (Basel). 2016;8:359. https://doi.org/10.3390/toxins8120359
3. Buchholz U, Mouzin E, Dickey R, Moolenaar R, Sass N, Mascola L. Haff disease: from the Baltic Sea to the U.S. shore. Emerg Infect Dis. 2000;6:192–5. https://doi.org/10.3201/eid0602.000215
4. Berlin R. Haff disease in Sweden. Acta Med Scand. 1948; 129:560–72.
5. Sidorova LD, Ierusalimskaia LA, Valentik MF, Razenko TN, Bredikhin AV. Kidney lesions in dietary and toxic paroxysmal myoglobinuria (Iuksovsk-Sartlansk disease) [in Russian]. Ter Arkh. 1985;57:120–3.
6. Bandeira AC, Campos GS, Ribeiro GS, Cardoso CW, Bastos CJ, Pessoa TL, et al. Clinical and laboratory evidence of Haff disease—case series from an outbreak in Salvador, Brazil, December 2016 to April 2017. Euro Surveill. 2017;22:30552. https://doi.org/10.2807/1560-7917.ES.2017.22.24.30552
7. Santos MC, Albuquerque BC, Pinto RC, Aguiar GP, Lescano AG, Santos JH, et al. Outbreak of Haff disease in the Brazilian Amazon. Rev Panam Salud Publica. 2009;26:469–70. https://doi.org/10.1590/S1020-49892009001100012
8. Taniyama S, Sagara T, Nishio S, Kuroki R, Asakawa M, Noguchi T, et al. Survey of food poisoning incidents in Japan due to ingestion of marine boxfish and their toxicity [in Japanese]. Shokuhin Eiseigaku Zasshi. 2009;50:270–7. https://doi.org/10.3358/shokueishi.50.270
9. Huang X, Li Y, Huang Q, Liang J, Liang C, Chen B, et al. A past Haff disease outbreak associated with eating freshwater pomfret in South China. BMC Public Health. 2013;13:447. https://doi.org/10.1186/1471-2458-13-447
10. Chen Y, Yuan B, Xie G, Zhen S, Zhou Y, Shao B, et al. Outbreak of Haff disease caused by consumption of crayfish (*Procambarus clarkii*), Nanjing, Jiangsu Province, China. Food Control. 2016;59:690–4. https://doi.org/10.1016/j.foodcont.2015.06.031
11. Bagley WH, Yang H, Shah KH. Rhabdomyolysis. Intern Emerg Med. 2007;2:210–8. https://doi.org/10.1007/s11739-007-0060-8
12. Yuan Y, Chen QT. Clinical analysis of six cases with Haff disease after eating crayfish [in Chinese]. Zhonghua Yi Xue Za Zhi. 2001;81:1530–1.
13. Langley RL, Bobbitt WH III. Haff disease after eating salmon. South Med J. 2007;100:1147–50. https://doi.org/10.1097/SMJ.0b013e3181583673
14. Sun S. Investigation on a case of rhabdomyolysis caused by crayfish [in Chinese]. Zhi Ye Yu Jian Kang. 2011;27:788.
15. Zhu L. Investigation of two crayfish cases related to rhabdomyolysis syndromes [in Chinese]. Yu Fang Yi Xue Lun Tan. 2015;21:700–3.
16. Feng G, Luo Q, Zhuang P, Guo E, Yao Y, Gao Z. Haff disease complicated by multiple organ failure after crayfish consumption: a case study. Rev Bras Ter Intensiva. 2014;26:407–9.
17. Gan L, Li Q, Gong NK. Two cases of rhabdomyolysis diagnosis caused by eating crayfish [in Chinese]. Journal of Jinzhou Medical University. 2015;36:111–2.
18. Zhang B, Yang G, Yu X, Mao H, Xing C, Liu J. Haff disease after eating crayfish in east China. Intern Med. 2012;51:487–9. https://doi.org/10.2169/internalmedicine.51.6786
19. Liu JJ, Yong H, Shenwei Q, Yixin H. Epidemiological investigation of crayfish related rhabdomyolysis in Tongling, 2016–2017 [in Chinese]. China Trop Med. 2018;18:899–903.
20. Ma S, Xu C, Liu S, Hu Z, Liu W, Zhang J, et al. [Epidemiology characteristics of crawfish related rhabdomyolysis in Nanjing, 2016: a multicenter retrospective investigation [in Chinese]. Zhonghua Wei Zhong Bing Ji Jiu Yi Xue. 2017;29:805–9.
21. Guo B, Xie G, Li X, Jiang Y, Jin D, Zhou Y, et al. Outbreak of Haff disease caused by consumption of crayfish (*Procambarus clarkii*) in Nanjing, China. Clin Toxicol (Phila). 2019;57:331–7. https://doi.org/10.1080/15563650.2018.1529318
22. Yang WX, Fan KL, Leung LP. A cluster of patients with rhabdomyolysis after eating crayfish. CJEM. 2018; 20(S2):S48–S50.
23. Warren JD, Blumbergs PC, Thompson PD. Rhabdomyolysis: a review. Muscle Nerve. 2002;25:332–47. https://doi.org/10.1002/mus.10053
24. Cervellin G, Comelli I, Lippi G. Rhabdomyolysis: historical background, clinical, diagnostic and therapeutic features. Clin Chem Lab Med. 2010;48:749–56. https://doi.org/10.1515/CCLM.2010.151
25. Khan FY. Rhabdomyolysis: a review of the literature. Neth J Med. 2009;67:272–83.
26. He F, Ni J, Huang JA, Liu Y, Wu C, Wang J. Clinical features of Haff disease and myositis after the consumption of boiled brackish water crayfish: a retrospective study of 96 cases at a single centre. Intern Emerg Med. 2018;13:1265–71. https://doi.org/10.1007/s11739-018-1870-6
27. Chen XF, Lin JW, Pan TM, Cao MJ, Shi CL, Cai QF, et al. Investigation of the hazardous substance causing crayfish-induced rhabdomyolysis via a mouse model, a hemolysis assay, and a cytotoxicity assay. Fish Sci. 2015;81:551–8. https://doi.org/10.1007/s12562-015-0856-9
28. Huang Q, Zhao M, Wang FY, Tan JB, Chen BF, Li XQ, et al. Population epidemiological investigation of crayfish-related rhabdomyolysis syndrome and triggering experiments in mice [in Chinese]. Zhongguo Shipin Weisheng Zazhi. 2017;29:269–76.

Address for correspondence: Qun Li, Public Health Emergency Center, Chinese Center for Disease Control and Prevention, Beijing, China; email: liqun@chinacdc.cn

Clinical and Multimodal Imaging Findings and Risk Factors for Ocular Involvement in a Presumed Waterborne Toxoplasmosis Outbreak, Brazil[1]

Camilo Brandão-de-Resende, Helena Hollanda Santos, Angel Alessio Rojas Lagos, Camila Munayert Lara, Jacqueline Souza Dutra Arruda, Ana Paula Maia Peixoto Marino, Lis Ribeiro do Valle Antonelli, Ricardo Tostes Gazzinelli, Ricardo Wagner de Almeida Vitor, Daniel Vitor Vasconcelos-Santos

Medscape EDUCATION ACTIVITY

In support of improving patient care, this activity has been planned and implemented by Medscape, LLC and Emerging Infectious Diseases. Medscape, LLC is jointly accredited by the Accreditation Council for Continuing Medical Education (ACCME), the Accreditation Council for Pharmacy Education (ACPE), and the American Nurses Credentialing Center (ANCC), to provide continuing education for the healthcare team.

Medscape, LLC designates this Journal-based CME activity for a maximum of 1.00 ***AMA PRA Category 1 Credit(s)™***. Physicians should claim only the credit commensurate with the extent of their participation in the activity.

Successful completion of this CME activity, which includes participation in the evaluation component, enables the participant to earn up to 1.0 MOC points in the American Board of Internal Medicine's (ABIM) Maintenance of Certification (MOC) program. Participants will earn MOC points equivalent to the amount of CME credits claimed for the activity. It is the CME activity provider's responsibility to submit participant completion information to ACCME for the purpose of granting ABIM MOC credit.

All other clinicians completing this activity will be issued a certificate of participation. To participate in this journal CME activity: (1) review the learning objectives and author disclosures; (2) study the education content; (3) take the post-test with a 75% minimum passing score and complete the evaluation at http://www.medscape.org/journal/eid; and (4) view/print certificate. For CME questions, see page 3121.

Release date: November 19, 2020; Expiration date: November 19, 2021

Learning Objectives

Upon completion of this activity, participants will be able to:

- Describe clinical and multimodal imaging findings at presentation and prevalence of and risk factors for ocular involvement in toxoplasmosis reported during an outbreak in 2015 in Gouveia, Brazil
- Determine recurrences and complications of toxoplasmosis reported during an outbreak in 2015 in Gouveia, Brazil
- Identify clinical implications of findings, course, and risk factors for ocular involvement in toxoplasmosis reported during an outbreak in 2015 in Gouveia, Brazil.

CME Editor

Amy J. Guinn, BA, MA, Copyeditor, Emerging Infectious Diseases. *Disclosure: Amy J. Guinn, BA, MA, has disclosed no relevant financial relationships.*

CME Author

Laurie Barclay, MD, freelance writer and reviewer, Medscape, LLC. *Disclosure: Laurie Barclay, MD, has disclosed no relevant financial relationships.*

Authors

Disclosure: ***Camilo Brandão-de-Resende, BEng, MD, PhD,*** *and* ***Daniel Vitor Vasconcelos-Santos, MD, PhD,*** *have disclosed the following relevant financial relationships: co-founder/partner of Alsculapius Medicina Inteligente Ltda.* ***Helena Hollanda Santos, MD, MSc; Angel Alessio Rojas Lagos, PhD; Camila Munayert Lara, MD; Jacqueline Souza Dutra Arruda, MD; Ana Paula Maia Peixoto Marino, PhD; Lis Ribeiro do Valle Antonelli, PhD; Ricardo Tostes Gazzinelli, PhD;*** *and* ***Ricardo Wagner de Almeida Vitor, PhD,*** *have disclosed no relevant financial relationships.*

Author affiliations: Universidade Federal de Minas Gerais, Belo Horizonte, Brazil (C. Brandão-de-Resende, H.H. Santos, A.A.R. Lagos, C.M. Lara, J.S.D. Arruda, R.W.A, Vitor, D.V. Vasconcelos-Santos);Centro de Pesquisas René Rachou, Fundação Oswaldo Cruz, Belo Horizonte (A.P.M.P. Marino, L.R.V. Antonelli, R.T. Gazzinelli).

DOI: https://doi.org/10.3201/eid2612.200227

[1]Presented in part at the 2015 American Uveitis Society Fall meeting, November 15, 2014, Las Vegas, Nevada, USA

In 2015, an outbreak of presumed waterborne toxoplasmosis occurred in Gouveia, Brazil. We conducted a 3-year prospective study on a cohort of 52 patients from this outbreak, collected clinical and multimodal imaging findings, and determined risk factors for ocular involvement. At baseline examination, 12 (23%) patients had retinochoroiditis; 4 patients had bilateral and 2 had macular lesions. Multimodal imaging revealed 2 distinct retinochoroiditis patterns: necrotizing focal retinochoroiditis and punctate retinochoroiditis. Older age, worse visual acuity, self-reported recent reduction of visual acuity, and presence of floaters were associated with retinochoroiditis. Among patients, persons ≥40 years of age had 5 times the risk for ocular involvement. Five patients had recurrences during follow-up, a rate of 22% per person-year. Recurrences were associated with binocular involvement. Two patients had late ocular involvement that occurred ≥34 months after initial diagnosis. Patients with acquired toxoplasmosis should have long-term ophthalmic follow-up, regardless of initial ocular involvement.

Toxoplasmosis is caused by *Toxoplasma gondii*, an obligate intracellular apicomplexan parasite that infects up to one third of the human population (*1*–*4*). Humans are mainly infected by ingesting tissue cysts in undercooked or raw meat or oocysts excreted in cat feces that contaminate water or food (*1*–*4*). Ocular disease is the major clinical repercussion in immunocompetent patients; toxoplasmosis is the leading cause of infectious posterior uveitis worldwide and can potentially lead to severe ocular complications (*1*,*3*,*5*,*6*). Although congenital toxoplasmosis more frequently leads to retinochoroiditis, postnatally acquired infection now is acknowledged as being associated with a large proportion of cases (*2*,*3*,*6*,*7*). Association between ocular toxoplasmosis and older age is not completely understood (*8*), but previous studies found increased prevalence of ocular involvement in persons >30 years of age (*9*,*10*).

Toxoplasmosis outbreaks are good opportunities to clarify clinical aspects of this complex disease because patients are infected at known times, by similar routes, and presumably by parasites of the same genotype (*11*–*19*). In 2015, an outbreak of presumed waterborne toxoplasmosis was reported in Gouveia, a small city of ≈10,000 inhabitants in the center of the state of Minas Gerais in southeastern Brazil (*20*). Municipal, state, and federal health authorities investigated several cases of fever, malaise, weight loss, and lymphadenopathy. Recent toxoplasmic infection was eventually confirmed in 52 cases. All patients had the disease after drinking water from a single, presumably contaminated, source (*20*).

We performed complete ophthalmic examination and multimodal fundus imaging evaluation on all 52 patients. The objective of this study was to describe clinical and multimodal imaging findings and determine the prevalence of ocular involvement, incidence of recurrences and complications, and to analyze risk factors for ocular involvement in this cohort.

Methods

We used a prospective cohort approach to address our main goal. The study was approved by institutional review boards of René Rachou Research Center, Oswaldo Cruz Foundation (CAAE no. 37614314.7.3001.5091), and Federal University of Minas Gerais (CAAE no. 37614314.7.3001.5149). All patients provided written informed consent.

We defined a case as illness in a person in the city of Gouveia with a history of fever, headache, lymphadenopathy, asthenia, or myalgia during February 12–May 18, 2015. From 5,276 local health charts, a task force comprised of municipal, state, and federal health authorities identified 201 persons suspected of meeting case definition criteria. Before confirmation of toxoplasmosis, differential diagnosis was made with consultation of an infectious disease specialist and serologic tests for dengue fever, visceral leishmaniasis, and leptospirosis.

We contacted the 201 persons with suspected toxoplasmosis. We were able to reach 151 (75.1%) persons whom we subsequently interviewed and tested for toxoplasmosis. We defined confirmed cases of acute toxoplasmosis as persons having *T. gondii* IgM and low avidity IgG on enzyme-linked fluorescence assay by using Vidas Toxo IgM, IgGII, and IgG avidity assays (bioMérieux, https://www.biomerieux.com).

Among the 151 suspected cases interviewed and tested, 52 (34.4%) had serologic evidence of *T. gondii* IgM and low avidity IgG, indicating acute toxoplasmosis. We performed a complete ophthalmic examination on each of the 52 case-patients, including assessment of best-corrected visual acuity (VA), applanation tonometry, slit-lamp examination (SLE; biomicroscopy), and indirect ophthalmoscopy. All case-patients also underwent multimodal imaging evaluation, including fundus photography, reflectances, fundus autofluorescence, and spectral-domain optical coherence tomography (SD-OCT). For patients with confirmed ocular involvement, we also performed fluorescein angiography. We determined prevalence and incidence of ocular changes and clinical characteristics on the basis of clinical and multimodal imaging findings. All patients with ocular involvement received standard therapy for 35–45

days, which consisted of sulfadiazine (1 g 4×/d), pyrimethamine (25–50 mg/d), folinic acid (7.5 mg/d), and prednisone (40–60 mg/d). One patient was allergic to sulfa and was switched from sulfadiazine to clindamycin 300 mg 4×/d. Complete blood counts were monitored at baseline and every 2 weeks during treatment.

For 3 years, we conducted follow-up examinations on case-patients at 5–8-month intervals and conducted the same ophthalmic examination protocol periodically. We reexamined case-patients with active primary or recurrent retinochoroiditis 3–6 weeks after therapy, or more often, if needed. We defined severe ocular involvement as binocular or macular involvement, or extensive necrotizing retinochoroiditis of >3 disk diameter (DD).

We prospectively collected and stored in an electronic database clinical and ophthalmological data, including symptoms, best-corrected VA, applanation tonometry, SLE, indirect ophthalmoscopy, and multimodal imaging. We assessed best-corrected VA by using an early treatment of diabetic retinopathy study chart and reported results in logarithm of the minimum angle of resolution (logMAR) scale. Previous studies suggested increased prevalence of ocular involvement among patients ≥30 years of age and among patients ≥50 years of age (*9*,*10*). We also analyzed age ≥40 years at time of infection as a potential risk factor for occurrence and severity of ocular involvement.

We defined the time of primary infection for each case-patient as the time of ocular or systemic symptom onset. To calculate time intervals among persons with new active retinochoroidal lesions during follow-up, we assumed eye disease occurred when patients first noted ocular symptoms. For case-patients without ocular symptoms, we assumed eye disease occurred when consistent retinochoroidal lesions were identified. Among case-patients who displayed new retinochoroidal scars during follow-up exams, we assumed eye disease occurred when ocular symptoms first were perceived; if the case-patient did not notice any ocular symptoms, we assumed eye disease occurred in the time between the prior ocular examination and identification of the scar. We also noted the first instance of retinochoroidal recurrences in either eye.

We performed statistical analyses by using R version 3.5.2 (*21*) by nonparametric methods and considered $p<0.05$ statistically significant. We used Mann-Whitney-Wilcoxon test to compare continuous variables, including age, length of follow-up, and VA at baseline. We used the mid-p exact test to compare proportions between subgroups, such as age ≥40 years, sex, and presence of underlying conditions and symptoms. We reported continuous variables as median (interquartile range [IQR]) and proportions as no. (%). We estimated the 95% CI of relative risks by using a maximum-likelihood estimator and described the follow-up by using the rate of recurrence per person-year (*22*), rate of recurrence per person-month, and Kaplan-Meier survival plot (*23*). We estimated survival probability and cumulative risk for ocular involvement and ocular recurrence by using the Kaplan-Meier method and compared results by using a log-rank test (*24*,*25*).

Results

Baseline Examination

All 52 patients with serologic evidence of acute toxoplasmosis underwent a baseline examination in the first 4 months after onset of systemic symptoms; 40 (77%) patients had a baseline exam within the first month (Table 1). Median age at infection was 34 years (IQR 27–40 years); 8 (15.4%) patients were female and 44 (84.6%) were male. The most common systemic signs or symptoms were fever (52/52; 100%), headache (33/52; 63%), myalgia (30/52; 58%), and lymphadenopathy (8/52; 15%). Ocular symptoms were reported by 17 (32.6%) patients, among whom 9 (52.9%) reported recent VA decrease, 8 reported eye pain (47%), and 3 (17.6%) reported floaters.

At baseline, 12 (23%) patients had retinochoroiditis (Figure 1), 4 (33%) of whom had bilateral involvement and 2 (17%) of whom had macular involvement. Necrotizing lesions or scars were found in 10 (58%) patients; subtle punctate active lesions were found in 4 (33%) patients. Among 4 (33%) patients, we observed multiple necrotizing lesions or multifocal punctate active lesions in different retinal quadrants (Table 2). SLE revealed all 12 patients with toxoplasmic retinochoroiditis had inflammatory cells in the anterior vitreous; however, only 3 (25%) had inflammatory cells in the anterior chamber with standardization of uveitis nomenclature (SUN) grade ranging from 0.5+ to 3+. Intraocular pressure was within normal limits in all but 1 patient with granulomatous keratic precipitates and SUN of 3+ in the anterior chamber. Two (17%) patients with retinochoroiditis did not report any eye symptoms (Table 3).

We observed other fundus changes among patients with confirmed acute toxoplasmosis but without ocular involvement. One patient had unspecific focal retinal pigment epithelium (RPE) hyperplasia in 1 eye; a patient with nyctalopia had

Table 1. Characteristics and ocular signs and symptoms among patients with confirmed acute toxoplasmosis infection at baseline examination, Brazil*

Characteristics	Total, n = 52	No ocular involvement, n = 40	Ocular involvement, n = 12	p value
Age at infection, y, median (IQR)†	34 (27–40)	32 (22–38)	43 (40–47)	<0.01
≥40 years of age†	14 (27)	6 (15)	9 (75)	<0.01
Sex				
M	44 (84.6)	33 (82.5)	11 (91.7)	0.50
F	8 (15.4)	7 (17.5)	1 (8.3)	0.50
Follow-up length, mo, median (IQR)	36 (19–36)	36 (12–36)	35 (24–37)	0.32
Underlying conditions				
Arterial hypertension	7 (13.5)	4 (10.0)	3 (25.0)	0.23
Diabetes mellitus	1 (1.9)	0	1 (8.3)	0.23
General signs and symptoms				
Fever	49 (94.2)	38 (95.0)	11 (91.7)	0.68
Headache	33 (63.5)	25 (62.5)	8 (66.7)	0.81
Myalgia	30 (57.7)	22 (55.0)	8 (66.7)	0.50
Lymphadenopathy	8 (15.4)	7 (17.5)	1 (8.3)	0.50
Ocular signs and symptoms				
VA at baseline, logMAR, median (IQR)†‡	0.0 (0.0–0.0)	0.0 (0.0–0.0)	0.1 (0.0–0.6)	0.01
Eye pain	8 (15.4)	5 (12.5)	3 (25.0)	0.33
Self-reported recent reduction of VA†	10 (19.2)	1 (2.5)	9 (75.0)	<0.01
Floaters†	3 (5.7)	0	3 (25.0)	0.01

*Values are no. (%), except as indicated. Mann-Whitney-Wilcoxon test was used to compare continuous and the mid-p exact tests for proportions between subgroups. IQR, interquartile range; logMAR, logarithm of the Minimum Angle of Resolution scale; VA, visual acuity.
†Statistical significant at α = 5%.
‡For visual acuity baseline, binocular involvement was considered the worst VA.

bilateral optic disc pallor, vascular attenuation and RPE changes consistent with retinitis pigmentosa; another patient with severe systemic arterial hypertension had bilateral nerve-fiber layer infarcts. One patient with ocular toxoplasmosis in 1 eye had findings consistent with Leber miliary aneurysms in the contralateral eye.

Among the 12 patients with ocular disease at baseline, 9 (75%) had severe ocular involvement, defined by binocular, macular, or extensive (>3 DD) necrotizing retinochoroiditis. Among 9 patients with severe ocular involvement, the median age was 43 years (IQR 40–47 years); among 3 patients without severe ocular involvement the median age was 31 years (IQR 29–38 years), but the difference was not statistically significant (p = 0.14).

Age, self-reported recent reduction of VA, presence of floaters, and greater reduction in VA were associated with ocular involvement at baseline (Table 1). Among patients with ocular involvement, the median age at infection was 43 years (IQR 40–47 years) vs. 31 years (IQR 22–38 years) for patients without ocular involvement (p = 0.02); 9 (75%) patients with ocular involvement were ≥40 years of age at infection compared with 6 (15%) patients without ocular involvement (relative risk [RR] = 5.0, 95% CI 2.2–11.2; p<0.01). Among these same subgroups, median logMAR VA at examination was 0.1 (IQR 0.0–0.6) for patients with ocular involvement compared with 0.0 (0.0–0.0) for patients without ocular involvement (p = 0.01).

Multimodal imaging revealed 2 distinct patterns of active retinochoroiditis: the typical pattern of focal necrotizing retinochoroiditis and punctate retinochoroiditis. Necrotizing retinochoroiditis subsequently left a variably pigmented scar and was more extensive in some cases, simulating a viral retinitis (Figure 2). Punctate retinochoroiditis displayed a much more subtle pattern, which was not seen as

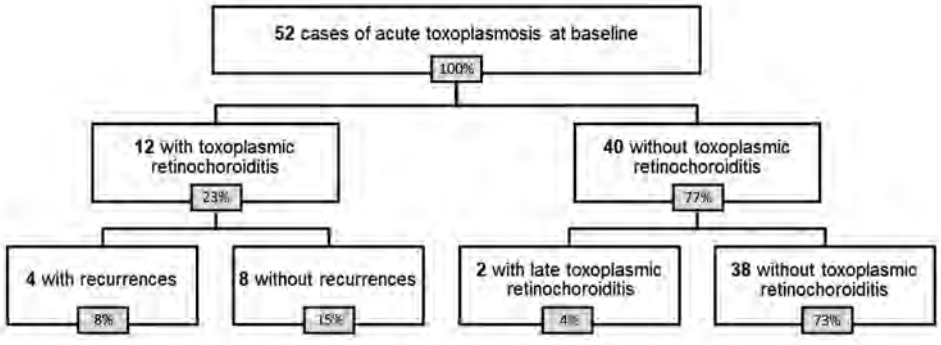

Figure 1. Flowchart of patients in study of ocular involvement associated with a presumed waterborne toxoplasmosis outbreak, Brazil.

Table 2. Characterization of patterns of retinochoroiditis seen in multimodal imaging among patients with toxoplasmosis treated with antiparasitic drugs and oral corticosteroids, Brazil*

Type of lesion, fundus imaging modality	Patterns of retinochoroiditis	
	Active phase, before treatment	Cicatricial phase, after treatment
Focal necrotizing retinochoroiditis		
Fundus photo or examination	Dense focal retinal whitening with indistinct borders, associated with overlying vitreous haze	Initially hypopigmented retinochoroidal scar, but frequently evolving with variable degree of pigmentation and subretinal fibrosis or preretinal gliosis
SD-OCT	Focal full-thickness hyper-reflectivity and disorganization of retinal layers indicating necrotizing retinitis; surrounding retinal thickening, signaling edema; numerous overlying hyper-reflective dots at the vitreous indicating vitreal inflammatory cell exudate; and underlying fusiform choroidal thickening, with loss of stromal/luminal pattern indicating reactive choroiditis	Disorganization of retinal architecture; hyper-reflectivity at the level of the scar, but without perilesional retinal thickening; resolution of choroidal thickening; marked decrease in the number of overlying vitreal hyper-reflective dots; and frequent tent-like focal detachment of the less thickened overlying posterior hyaloid
FAF reflectances	Subtle hypo- or hyper-autofluorescence changes at the level of the active lesion; near infrared reflectance can indicate active focus but not as remarkably as red-free reflectance	Increased autofluorescence signal in the first weeks, then hypo-autofluorescence at the level of the scar after several months; scars less clearly delineated by near-infrared than red-free reflectance, but both reveal retinal wrinkling in the presence of epiretinal membrane
FFA	Early hypofluorescence, with progressive hyperfluorescence and late leakage at the retinochoroiditis lesion; reactive changes, including hyperfluorescence, of optic disc indicating edema; staining of venular walls, signaling periphlebitis	Variable window defects and blockage at the level of the scar; staining in the presence of subretinal fibrosis and epiretinal gliosis
Punctate retinochoroiditis		
Fundus photo or examination	Multiple subtle, indistinct, or confluent gray-whitish punctate retinal infiltrates with minimal vitreous haze	Very subtle changes in retinal reflex, sometimes with minor hypopigmentation, but frequently with no apparent abnormality
SD-OCT	Multifocal hyper-reflectivity at the inner retinal layers, demonstrating retinitis, occasionally extending to deeper layers, with surrounding retinal thickening (edema); numerous overlying hyper-reflective dots indicating vitreal inflammatory cell exudate, along with thickening and shallow detachment of the posterior hyaloid; mild choroidal thickening without apparent major change in reflectivity	Frequent normalization of the retinal architecture, sometimes with mild disruption of outer retinal layers or retinal pigment epithelium; normalization of choroidal thickening; marked decrease in the number of overlying vitreal hyper-reflective dots and frequent tent-like focal detachment of the less-thickened overlying posterior hyaloid
FAF reflectances	Subtle hypo- or hyper-autofluorescence changes at the level of the punctate active lesions; near-infrared reflectance can show changes at the area of active foci but not as remarkably as red-free reflectance	Autofluorescence and reflectance changes are minimal or absent
FFA	Progressive but mild hyperfluorescence or late leakage at the site of punctate lesions; reactive changes, including hyperfluorescence of optic disc, demonstrating edema; staining of venular walls indicating periphlebitis	Normal or showing minimal punctate window defects

*FAF, fundus autofluorescence; FFA, fundus fluorescein angiography; SD-OCT, spectral-domain optical coherence tomography.

easily on fundus examination, but was nicely delineated by SD-OCT (Figure 3). All 12 patients with toxoplasmic retinochoroiditis promptly responded to antiparasitic treatment; 11 received standard therapy with sulfadiazine, pyrimethamine, and folinic acid, supplemented with oral prednisone; 1 had clindamycin instead of sulfadiazine because of sulfa allergy. All 12 patients had resolution of intraocular inflammation within 5–6 weeks. However, the pattern of retinochoroiditis resolution differed between patients with focal necrotizing retinochoroiditis and those with punctate retinochoroiditis (Table 2).

Follow-up Examinations

Among all 52 patients in the cohort, the median length of follow-up after infection was 36 months (IQR 19–36 months); most (47; 90%) patients were followed for >6 months. Among the 12 patients with ocular involvement at baseline examination, 5 (42%) had recurrent retinochoroiditis during

follow-up examinations (Figure 1). The median time for first recurrence was 11 months after starting standard therapy for the first episode of ocular involvement, and the 5 patients had recurrences at 2, 9, 11, 12, and 22 months (Table 3). All 5 reported adequate treatment adhesion.

Rate of recurrence of retinochoroiditis among the 12 patients with ocular involvement at baseline was 22% per person-year (1.8% per person-month). All patients with binocular involvement (n = 4) had recurrent lesions during the follow-up period compared with only 13% (1/8) of patients with monocular involvement (RR = 8.0, 95% CI 1.3–50.0; p = 0.01). Rate of recurrence was 8.5% per person-month among patients with binocular involvement and 0.4% per person-month among the patients

Table 3. Ocular characteristics, recurrences, and complications of patients with ocular involvement from toxoplasmosis, Brazil*

Age, y/sex	Baseline eye examination			Follow-up findings	Complications	Last VA, mo; result
	RC	Right	Left			
38/M†	Bilateral	VA 0.0; SLE, AV cells and AC cells (0.5+/4+); FE, multifocal PR and peripheral large FNR	VA 0.0; SLE, AV cells; FE, PR	1 OD recurrence; month 2, satellite active lesion	None	21; 0.0 OU
47/M†	Bilateral	VA 0.2; SLE, AV cells;FE, peripheral large FNR	VA 0.0; SLE, AV cells; FE, multiple peripheral large FNR	1 OD recurrence; month 22, new peripheral scar	Month 22, epiretinal membrane OD	34; 0.0 OU
40/M†	Bilateral	VA 0.0; SLE, AV cells; FE, multifocal PR	VA 0.0; SLE, AV cells; FE, multifocal PR and peripheral large FNR	Multiple recurrences OU; months 11, 21, and 24, active peripheral lesions; month 27, active peripheral lesion OS	Month 21, epiretinal membrane OD; month 27, rhegmatogenous RD OS	36; 0.0 OD, 0.8 OS
48/M†	Bilateral	VA 2.1; SL, EAV cells; FE, macular FNR	VA 0.3; SLE, AV cells; FE, peripheral FNR	2 recurrences OS; new peripheral scar in months 12 and 15	Month 9, epiretinal membrane OD; month 34, epiretinal membrane OS	34; 1.9 OD, 0.4 OS
43/M†	Unilateral	VA 0.0; SLE, normal; FE, Leber miliary aneurysms	VA 0.7; SLE, fine KP, AC cells 2+/4+, and AV cells; FE, peripheral large FNR	–	None	36; 0.1 OS
27/M	Unilateral	VA 0.0; SLE, AV cells; FE, PR	VA 0.0; normal SLE and FE	–	None	23; 0.0 OD
42/M†	Unilateral	VA 0.5; SLE, granulomatous KP, AC cells (3+/4+), AV cells; IOP, 28 mmHg; FE, peripheral large FNR	VA 0.0; normal SLE and FE	1 recurrence OD; month 9, multiple active peripheral lesions OD	Baseline transient IOP elevation OD, 28mmHg	24; 0.0 OD
31/M	Unilateral	VA 0.0; normal SLE and FE	VA 0.0; SLE OS, AV cells; FE, multiple peripheral FNR	–	None	8; 0.0 OS
50/M†	Unilateral	VA 0.5; SLE, AV cells; FE, peripheral large FNR	VA 0.0; normal SLE and FE	–	Month 6, posterior vitreous detachment OD	37; 0.0 OD
47/F†	Unilateral	VA 1.6; SLE, AV cells; FE, macular FNR	VA 0.0; normal SLE and FE	–	None	37; 1.9 OD
40/M†	Unilateral	VA 0.0; SLE, AV cells; FE, peripheral large FNR	VA 0.0; normal SLE and FE	–	None	37; 0.0 OD
45/M	Unilateral	VA 0.0; SLE, AV cells; FE, PR	VA 0.0; normal SLE and FE	–s	None	37; 0.0 OD
15/M‡	NA	VA 0.0; normal SLE and FE	VA 0.0; normal SLE and FE	Late ocular involvement; OD VA 0.1; month 34, new peripheral scar	None	34; 0.1 OD
28/F‡	NA	VA 0.0; normal SLE and FE	VA 0.0; normal SLE and FE	Late ocular involvement; OD VA 0.0; month 37, peripheral FNR	None	39; 0.0 OD

*Age represents age at detection of first ocular lesion or scar. AC cells, grading of anterior chamber cells according to Standardization of Uveitis Nomenclature (SUN) working group (*29*); AV cells, anterior vitreous cells; FE, fundus examination; FNR, focal necrotizing retinochoroiditis, large FNR is >3 disk diameters; IOP, intraocular pressure; KP, keratic precipitates; NA, not applicable; OD, oculus dexter (right eye); OS, oculus sinister (left eye); OU, oculus uterque (both eyes); PR, punctate retinochoroiditis; RC, retinochoroiditis; RD, retinal detachment; SLE, slit-lamp examination; VA, visual acuity (log MAR); –, no recurrence or no new lesion.
†Patients with severe ocular involvement, including binocular, macular, or extensive necrotizing retinochoroiditis (>3 disk diameters).
‡Patients with initial normal ophthalmic examination.

with monocular involvement (log-rank p = 0.01; Figure 4) (*24*,*25*).

Among patients without ocular involvement at baseline, 2/40 (5%) had late ocular involvement. A 15-year-old boy had a new peripheral scar in his right eye (VA 0.1) 34 months after infection, referring a transient VA reduction that started 3 months earlier; the patient recovered spontaneously after a couple of weeks. A 28-year-old woman had a peripheral active lesion in her right eye (VA 0.0) at her 37-month follow-up examination but had no other ocular symptoms (Figure 5).

Overall, 14/52 (27%) patients had ocular involvement at some point during the study. The rate of ocular involvement was 16% per person-year (1.3% per person-month).

Complications and Visual Outcomes

Among the 16 eyes (15%) of 12 patients (23%) with retinochoroiditis at baseline, ocular complications developed in 7 eyes (44%) of 5 patients (42%) during follow-up; 2 patients had complications in both eyes. Four (25%) eyes had epiretinal membranes develop, detected at 9-, 21-, 22-, and 34-month follow-up visits. One (6%) eye had rhegmatogeneous retinal detachment at the 27-month follow-up, which required pars plana vitrectomy. One (6%) eye had transient intraocular pressure elevation at baseline, and 1 (6%) had posterior vitreous detachment detected at the 6-month follow-up visit.

Among patients with retinochoroiditis at baseline, 4 (25%) eyes among 3 (25%) patients had logMAR VA >0.3 at the last follow-up examination. Two eyes had macular involvement at baseline examination and a final VA of 1.9; an epiretinal membrane developed in 1 eye (final VA 0.4), and rhegmatogeneous retinal detachment developed in the other, which underwent pars plana vitrectomy (final VA 0.8).

Discussion

We investigated ocular involvement of 52 patients with serologically confirmed acute toxoplasmosis acquired in a presumed waterborne outbreak. We described clinical and multimodal imaging findings and determined the prevalence of retinochoroiditis,

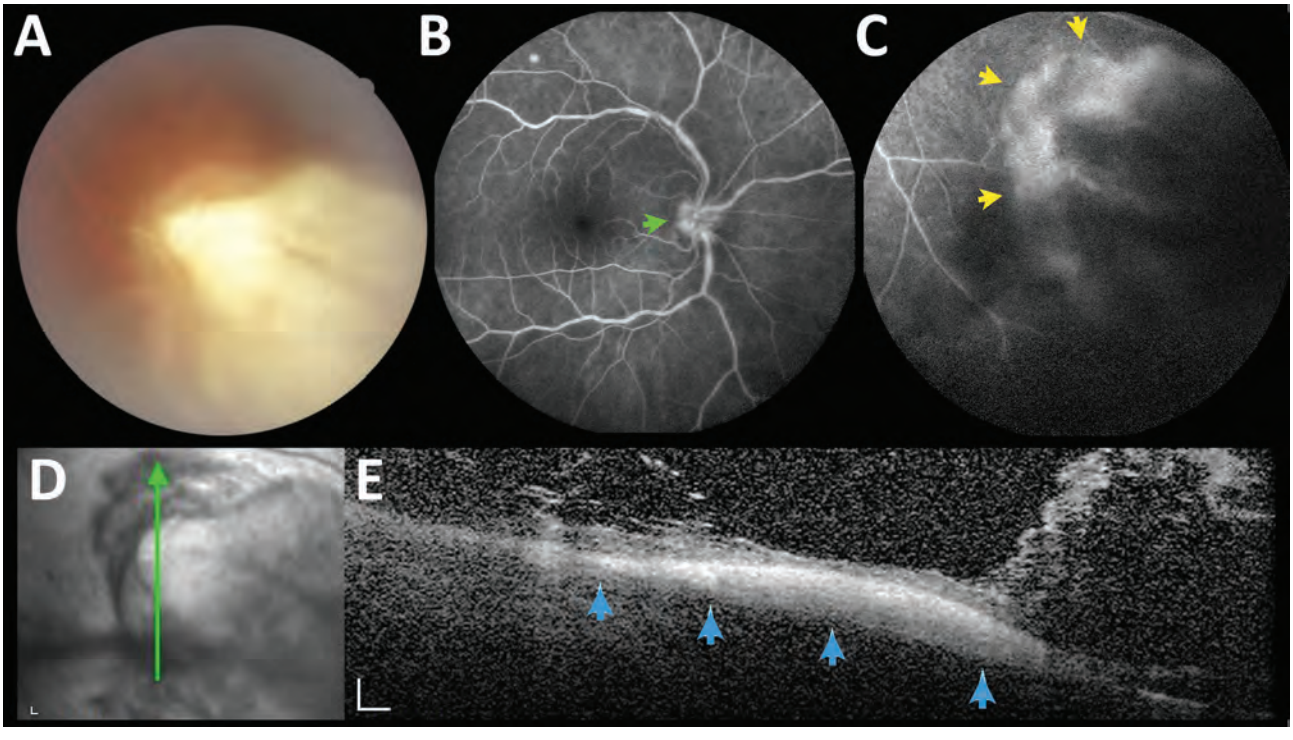

Figure 2. A large necrotizing retinochoroiditis lesion in the right eye, detected in baseline examination (VA 0.5) of a 42-year-old man in a presumed waterborne toxoplasmosis outbreak, Brazil. A) Fundus photograph showing dense focal retinal whitening with indistinct borders, associated with overlying vitreous haze. B) Fundus fluorescein angiography; green arrow indicates hyperfluorescence of optic disc. C) Fundus fluorescein angiography; yellow arrows indicate hyperfluorescence indicating late leakage at the margins of the retinochoroiditis lesion. D) Red-free reflectance showing changes at the level of the active lesion. Green line indicates site of optical coherence tomography scan. E) Spectral-domain optical coherence tomography; blue arrows indicate focal full-thickness hyperreflectivity and disorganization of retinal layers, surrounding retinal thickening, and numerous overlying hyper-reflective dots and bands, indicating exuberant inflammatory vitreous exudation. Scale bars indicate 200 μm. VA, visual acuity.

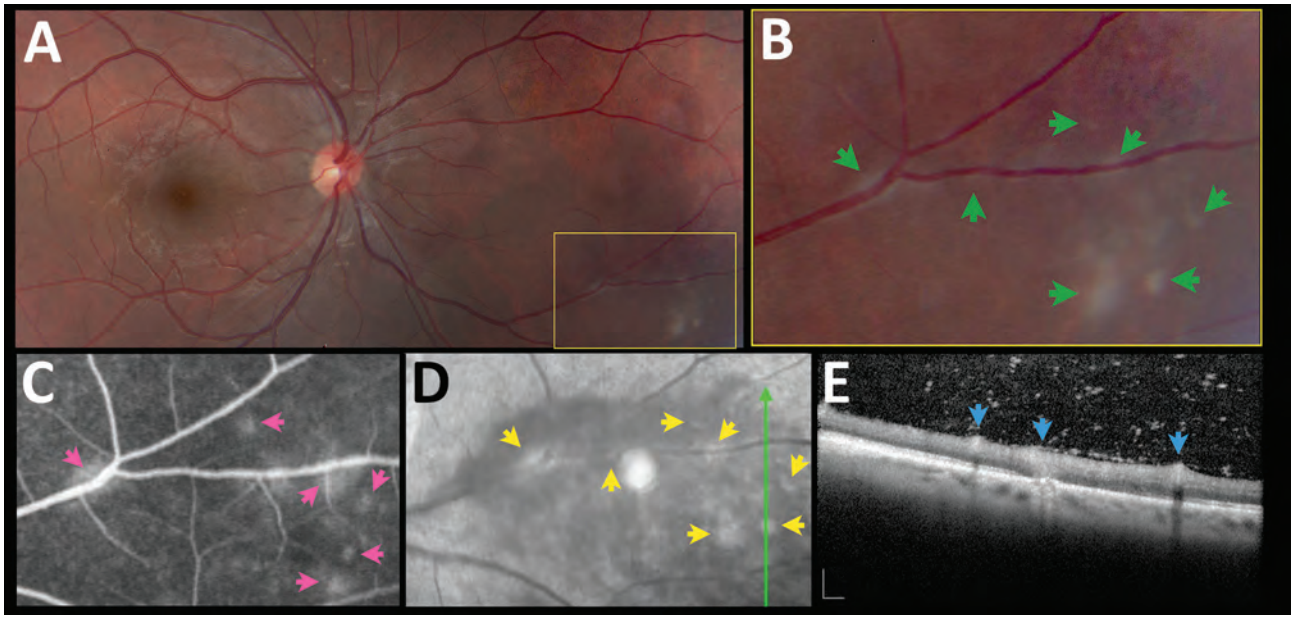

Figure 3. Asymptomatic retinochoroiditis in the right eye, detected in baseline examination (VA 0.0) of a 27-year-old man in a presumed waterborne toxoplasmosis outbreak, Brazil. A) Fundus photograph showing minimal vitreous haze; box indicates enlarged area on B); green arrows indicate multiple subtle and confluent gray-whitish punctate retinal infiltrates. C) Fundus fluorescein angiography. Pink arrows indicate leakage at the site of some of the punctate lesions. D) Fundus fluorescein angiography with red-free reflectance. Green line indicates site of optical coherence tomography scan. Yellow arrows indicate changes in the area of active focuses. E) Spectral-domain optical coherence tomography showing retinal thickening, and numerous overlying hyper-reflective dots. Blue arrows indicate multifocal hyper-reflectivity at the inner retinal layers. Scale bar indicates 200 μm. VA, visual acuity.

the incidence of recurrences and complications, and analyzed risk factors for ocular involvement.

In addition to the standard pattern of necrotizing retinochoroiditis, multimodal imaging revealed a distinct pattern of punctate retinal infiltrates (Figure 3), which might be overlooked if the retina is not examined carefully. This pattern also has been reported in neonates with congenital toxoplasmosis (5) and might represent the result of the primary parasite insult to the retina before a more robust immune response develops.

In this study, 12 (23%) patients displayed toxoplasmic retinochoroiditis at baseline examination; 14 (27%) had ocular involvement at some point during the study (Table 3), a rate of 16% per person-year. Variable rates of ocular involvement have been reported in toxoplasmosis outbreaks. For instance, risk for ocular involvement was 31% during the first 10.5 months after the Santa Isabel do Ivaí outbreak in Paraná, Brazil during 2001–2002 (*15*), and 21% after a mean follow-up of 114 weeks in an outbreak in Victoria, British Columbia, Canada in 1995 (*13*,*14*).

As expected, eye symptoms, particularly self-reported recently decreased VA and floaters, were associated with ocular involvement, suggesting that clinicians should inquire about symptoms routinely during and after an outbreak. Nevertheless, 2/12 (16.6%) patients had retinochoroiditis at baseline in the absence of symptoms, reinforcing the importance of examining the eyes of every patient with confirmed acute *T. gondii* infection.

Older age was frequently associated with a higher risk for ocular involvement at baseline and patients ≥40 years of age at the time of infection had a 5 times greater risk for retinochoroiditis than younger patients. Patients in the subgroup with ocular involvement were much older than patients in the subgroup without ocular involvement, consistent with reports in other studies. In a study from the Netherlands, most patients with serologic evidence of recently acquired ocular toxoplasmosis were older, with a mean age of 50.6 years (*26*). A study from Brazil found age was a major risk factor for ocular involvement, with higher prevalence in patients ≥50 years of age, and ≈50% of patients >60 years of age had ocular involvement (*10*). Another study from Brazil found that persons >30 years of age with recently acquired *T. gondii* infection were more likely to have ocular involvement by the time of study enrollment (*9*).

At baseline examination, 75% (9/12) of patients with toxoplasmic retinochoroiditis in our study had severe ocular involvement, defined by large (>3 DD)

necrotizing, macular, or bilateral retinochoroiditis (Figure 2). The median age of the 9 patients with severe ocular involvement (43 years of age) was higher than the median age of the 3 patients with less severe disease (31 years of age), but the differences were not statistically significant, probably because of the small number of patients in each subgroup. These findings also are in line with the literature (*8*), agreeing with 2 previous studies focusing on ocular toxoplasmosis in patients ≥50 years of age (median 67.5 years) in which 22/34 (64.7%) patients had severe disease, defined as either multiple active lesions, large lesions (>3 DD), or prolonged disease (duration >8 weeks) (*27*,*28*). Another possible explanation for the higher rate and severity of ocular involvement in our cohort is involvement of a virulent atypical *T. gondii* strain. However, this possibility remains elusive because parasite isolation for subsequent genotyping was not successful in the presumably contaminated water source, or in blood samples of patients with serologically confirmed infection (*20*).

Recurrence of retinochoroiditis was associated with bilateral ocular involvement at initial examination (Figure 4). One possible explanation is that patients with bilateral lesions at initial examination might have had a higher parasite load systemically and in the retina, leading to an increased risk for local reactivation. This finding also might have been associated with some degree of subclinical immune dysfunction in these cases.

The most common complication was epiretinal membrane development in 25% of eyes with retinochoroiditis, a finding consistent with a transversal study including 248 patients with acquired toxoplasmosis in India, which also reported development of epiretinal membranes at 25.1% (*12*). At the last follow-up examination 3/12 (25%) patients with retinochoroiditis had logMAR VA >0.3, one of them in both eyes. Complications underlying this visual impairment included unilateral macular involvement at baseline in 2 patients (VA 1.9) and other late complications, including 1 eye with an epiretinal membrane (VA 0.4), and the other with a rhegmatogenous retinal detachment (VA 0.8 after pars plana vitrectomy).

In addition to the 4 patients who developed recurrences of retinochoroiditis at 2, 9, 11, 12, or even at 22 months of follow-up, 2 patients without retinochoroiditis had new primary retinal lesions detected ≥34

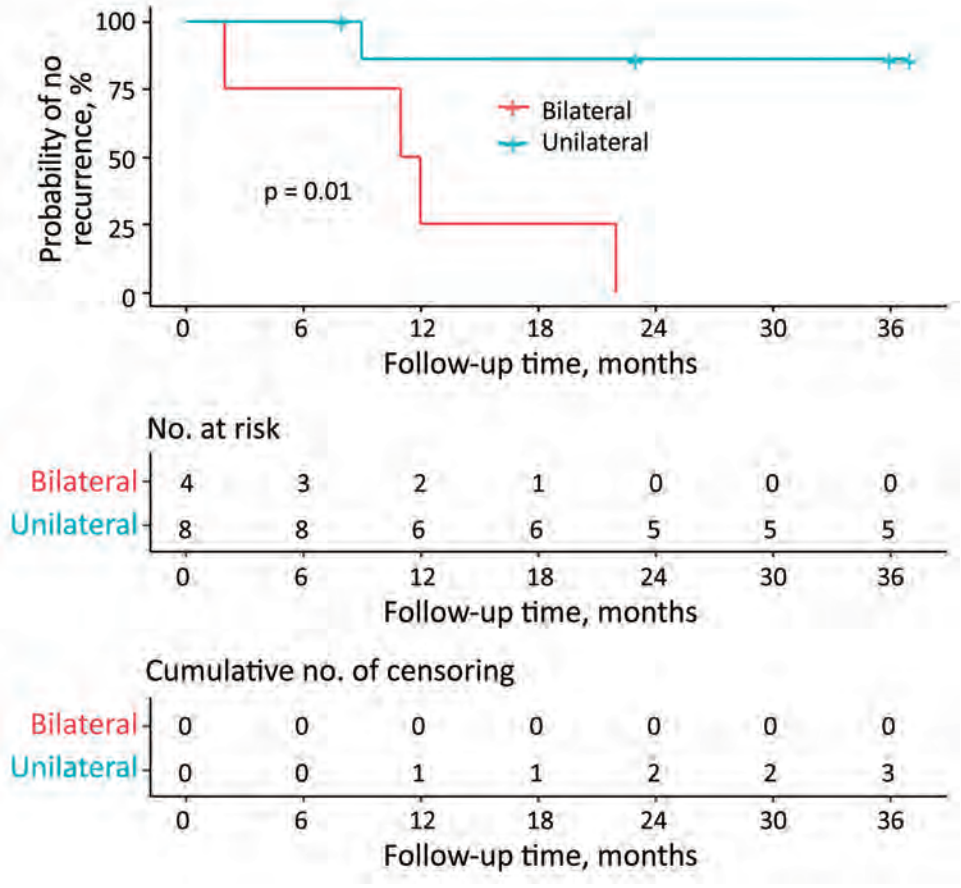

Figure 4. Kaplan-Meier plot showing proportion of patients with toxoplasmic retinochoroiditis at baseline who remain free of recurrence during follow-up. Bilateral retinochoroidal involvement at baseline was statistically significantly associated with recurrences by log-rank test (p = 0.01).

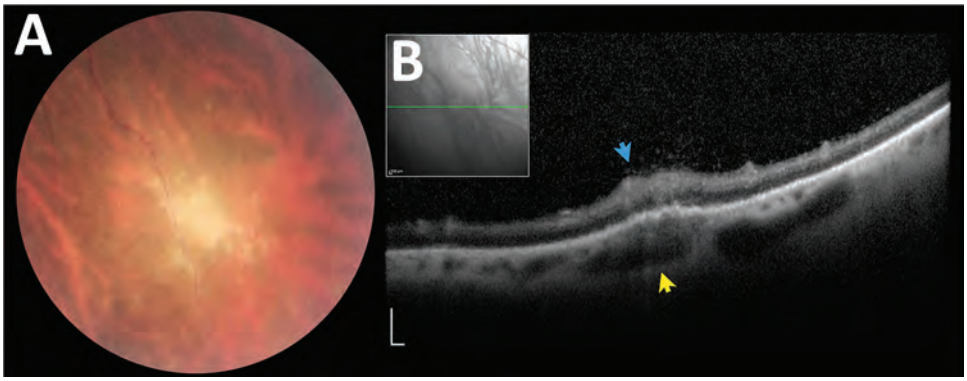

Figure 5. Asymptomatic late retinochoroiditis in right eye detected in follow-up examination at month 37 (visual acuity 0.0) in 28-year-old woman from a presumed waterborne toxoplasmosis outbreak, Brazil. A) Fundus photograph showing focal retinal whitening with indistinct borders. B) Spectral-domain optical coherence tomography showing hyper-reflectivity, disorganization, and thickening OF inner retinal layers (blue arrow), and numerous overlying hyper-reflective dots at the overlying vitreous and fusiform thickening of underlying choroid (yellow arrows). Scale bars indicate 200 μm.

months of follow-up (Figure 5). This finding highlights the need for long-term ophthalmologic follow-up in patients with postnatally acquired toxoplasmosis, regardless of previous ocular involvement.

This study has some limitations. We only considered symptomatic patients as having suspected cases of acute toxoplasmosis, and that might represent only a small portion of infected persons; several asymptomatic persons probably were not included, and this selection bias might justify, at least in part, the high prevalence of ocular changes. However, selecting for symptomatic cases has been the rule in most investigations of outbreaks of toxoplasmosis because serologic survey of all persons in affected areas is difficult. Finally, incidence calculations were based on few events, especially within subgroups of cases with ocular involvement, and some statistical tests were underpowered, such as the comparison of age in relation to severity of ocular involvement.

Despite the limitations, our study provides objective documentation of ocular changes in the context of a toxoplasmosis outbreak. By using multimodal imaging, we were able to characterize more subtle lesions, such as punctate retinochoroiditis among 33% of cases with ocular involvement. By comparison, previous reports of ophthalmic assessment of patients during outbreaks mostly were based on indirect ophthalmoscopy alone. Among 52 patients with confirmed infection, 47 (90%) had ≥6 months of follow-up; the median length for follow-up was 36 months, which enabled us to estimate the incidence of new lesions, recurrences, and complications during a relatively long period. We noted a substantial prevalence of early ocular involvement, with recurrences and new lesions occurring up to 39 months after infection. Thus, patients diagnosed with toxoplasmosis should receive long-term ophthalmic follow-up, regardless of initial ocular involvement. In addition, older patients had higher risk for ocular involvement, possibly reflecting age-related changes in the immune system, which could predispose persons ≥40 years of age to more severe disease.

Acknowledgments

The authors thank the teams from the Brazilian Ministry of Health, especially Juliane Malta; from the State Secretary of Health of Minas Gerais, especially Marcela Lencine Ferraz; and from the Secretary of Health of Gouveia, especially Leticia Miranda, for participation and support.

D.V.V.S. is supported in part by the National Council for Scientific and Technological Development, Brazil (research productivity scholarship no. 313293/2018-0) and received lecture fees from Abbvie.

About the Author

Dr. Brandão-de-Resende is an engineer and ophthalmologist and recently earned his PhD at the Federal University of Minas Gerais, Brazil. His research interests encompass uveitis, glaucoma, and applications of machine learning and artificial intelligence in ophthalmology.

References

1. Montoya JG, Liesenfeld O. Toxoplasmosis. Lancet. 2004; 363:1965–76. https://doi.org/10.1016/S0140-6736(04)16412-X
2. Holland GN. Ocular toxoplasmosis: a global reassessment. Part I: epidemiology and course of disease. Am J Ophthalmol. 2003;136:973–88. https://doi.org/10.1016/j.ajo.2003.09.040
3. Vasconcelos-Santos DV. Ocular manifestations of systemic disease: toxoplasmosis. Curr Opin Ophthalmol. 2012;23:543–50. https://doi.org/10.1097/ICU.0b013e328358bae5
4. Aguirre AA, Longcore T, Barbieri M, Dabritz H, Hill D, Klein PN, et al. The One Health approach to toxoplasmosis: epidemiology, control, and prevention strategies. EcoHealth. 2019;16:378–90. https://doi.org/10.1007/s10393-019-01405-7

5. Holland GN. Ocular toxoplasmosis: a global reassessment. Part II: disease manifestations and management. Am J Ophthalmol. 2004;137:1–17. https://doi.org/10.1016/S0002-9394(03)01319-9
6. Vasconcelos-Santos DV, Machado Azevedo DO, Campos WR, Oréfice F, Queiroz-Andrade GM, Carellos EVM, et al. Congenital toxoplasmosis in southeastern Brazil: results of early ophthalmologic examination of a large cohort of neonates. Ophthalmology. 2009;116:2199–2205.e1. https://doi.org/10.1016/j.ophtha.2009.04.042
7. Arantes TE, Silveira C, Holland GN, Muccioli C, Yu F, Jones JL, et al. Ocular involvement following postnatally acquired *Toxoplasma gondii* infection in southern Brazil: a 28-year experience. Am J Ophthalmol. 2015;159:1002–12.e2. https://doi.org/0.1016/j.ajo.2015.02.015
8. Holland GN. Ocular toxoplasmosis: the influence of patient age. Mem Inst Oswaldo Cruz. 2009;104:351–7. https://doi.org/10.1590/S0074-02762009000200031
9. Dadgostar H, Silveira C, Jones JL, Lee G, Muccioli C, Belfort R Jr., et al. Risk factors for ocular toxoplasmosis among individuals recently infected by *Toxoplasma gondii* in Southern Brazil. In: Abstracts of the Association for Research in Vision and Ophthalmology annual meeting. Invest Ophthalmol Vis Sci. 2008;49:5529.
10. Portela RW, Bethony J, Costa MI, Gazzinelli A, Vitor RW, Hermeto FM, et al. A multihousehold study reveals a positive correlation between age, severity of ocular toxoplasmosis, and levels of glycoinositolphospholipid-specific immunoglobulin A. J Infect Dis. 2004;190:175–83. https://doi.org/10.1086/421505
11. Bahia-Oliveira LM, Jones JL, Azevedo-Silva J, Alves CC, Oréfice F, Addiss DG. Highly endemic, waterborne toxoplasmosis in north Rio de Janeiro state, Brazil. Emerg Infect Dis. 2003;9:55–62. https://doi.org/10.3201/eid0901.020160
12. Balasundaram MB, Andavar R, Palaniswamy M, Venkatapathy N. Outbreak of acquired ocular toxoplasmosis involving 248 patients. Arch Ophthalmol. 2010;128:28–32. https://doi.org/10.1001/archophthalmol.2009.354
13. Bowie WR, King AS, Werker DH, Isaac-Renton JL, Bell A, Eng SB, et al.; The BC Toxoplasma Investigation Team. Outbreak of toxoplasmosis associated with municipal drinking water. Lancet. 1997;350:173–7. https://doi.org/10.1016/S0140-6736(96)11105-3
14. Burnett AJ, Shortt SG, Isaac-Renton J, King A, Werker D, Bowie WR. Multiple cases of acquired toxoplasmosis retinitis presenting in an outbreak. Ophthalmology. 1998;105:1032–7. https://doi.org/10.1016/S0161-6420(98)96004-3
15. Silveira C, Muccioli C, Holland GN, Jones JL, Yu F, de Paulo A, et al. Ocular involvement following an epidemic of *Toxoplasma gondii* infection in Santa Isabel do Ivai, Brazil. Am J Ophthalmol. 2015;159:1013–21e3. https://doi.org/10.1016/j.ajo.2015.02.017
16. Teutsch SM, Juranek DD, Sulzer A, Dubey JP, Sikes RK. Epidemic toxoplasmosis associated with infected cats. N Engl J Med. 1979;300:695–9. https://doi.org/10.1056/NEJM197903293001302
17. Perkins ES. Ocular toxoplasmosis. Br J Ophthalmol. 1973;57:1–17. https://doi.org/10.1136/bjo.57.1.1
18. Benenson MW, Takafuji ET, Lemon SM, Greenup RL, Sulzer AJ. Oocyst-transmitted toxoplasmosis associated with ingestion of contaminated water. N Engl J Med. 1982;307:666–9. https://doi.org/10.1056/NEJM198209093071107
19. Akstein RB, Wilson LA, Teutsch SM. Acquired toxoplasmosis. Ophthalmology. 1982;89:1299–302. https://doi.org/10.1016/S0161-6420(82)34629-1
20. Malta JMAS, Cabral CM, Nóbrega AA, Leite PL, de Souza Alves RM, Almeida SML, et al. Outbreak of toxoplasmosis in the municipality of Gouveia, Minas Gerais [in Portuguese]. J Health Biol Sci. 2019;7:233–41. https://doi.org/10.12662/2317-3076jhbs.v7i3.2375.p233-241.2019
21. R: a language and environment for statistical computing. 2017; Vienna, Austria: R Foundation for Statistical Computing [cited 2020 Feb 2]. https://www.r-project.org
22. Becker S. A comparison of maximum likelihood and Jewell's estimators of the odds ratio and relative risk in single 2 x 2 tables. Stat Med. 1989;8:987–96. https://doi.org/10.1002/sim.4780080809
23. Jabs DA. Improving the reporting of clinical case series. Am J Ophthalmol. 2005;139:900–5. https://doi.org/10.1016/j.ajo.2004.12.009
24. Harrington DP, Fleming TR. A class of rank test procedures for censored survival data. Biometrika. 1982;69:553–66. https://doi.org/10.1093/biomet/69.3.553
25. Mantel N. Evaluation of survival data and two new rank order statistics arising in its consideration. Cancer Chemother Rep. 1966;50:163–70.
26. Bosch-Driessen LE, Berendschot TT, Ongkosuwito JV, Rothova A. Ocular toxoplasmosis: clinical features and prognosis of 154 patients. Ophthalmology. 2002;109:869–78. https://doi.org/10.1016/S0161-6420(02)00990-9
27. Labalette P, Delhaes L, Margaron F, Fortier B, Rouland JF. Ocular toxoplasmosis after the fifth decade. Am J Ophthalmol. 2002;133:506–15. https://doi.org/10.1016/S0002-9394(02)01324-7
28. Johnson MW, Greven GM, Jaffe GJ, Sudhalkar H, Vine AK. Atypical, severe toxoplasmic retinochoroiditis in elderly patients. Ophthalmology. 1997;104:48–57. https://doi.org/10.1016/S0161-6420(97)30362-5
29. Jabs DA, Nussenblatt RB, Rosenbaum JT; Standardization of Uveitis Nomenclature (SUN) Working Group. Standardization of uveitis nomenclature for reporting clinical data. Results of the First International Workshop. Am J Ophthalmol. 2005;140:509–16. https://doi.org/10.1016/j.ajo.2005.03.057

Address for correspondence: Daniel Vitor Vasconcelos-Santos, Av. Alfredo Balena 190, Sala 199, Belo Horizonte, MG 30190-090, Brazil. email: dvitor@ufmg.br

Tuberculosis among Children and Adolescents at HIV Treatment Centers in Sub-Saharan Africa

Anna M. Mandalakas,[1] Alexander W. Kay,[1] Jason M. Bacha, Tara Devezin, Rachel Golin, Katherine R. Simon, Dilsher Dhillon, Sandile Dlamini, Andrew DiNardo, Mogo Matshaba, Jill Sanders, Lineo Thahane, Pauline M. Amuge, Saeed Ahmed, Moorine P. Sekadde, Neway G. Fida, Bhekumusa Lukhele, Nodumo Chidah, David Damba, Joseph Mhango, Moses Chodota, Makhorong Matsoso, Angelina Kayabu, Richard S. Wanless, Gordon E. Schutze

Medscape EDUCATION ACTIVITY

In support of improving patient care, this activity has been planned and implemented by Medscape, LLC and Emerging Infectious Diseases. Medscape, LLC is jointly accredited by the Accreditation Council for Continuing Medical Education (ACCME), the Accreditation Council for Pharmacy Education (ACPE), and the American Nurses Credentialing Center (ANCC), to provide continuing education for the healthcare team.

Medscape, LLC designates this Journal-based CME activity for a maximum of 1.00 ***AMA PRA Category 1 Credit(s)™***. Physicians should claim only the credit commensurate with the extent of their participation in the activity.

Successful completion of this CME activity, which includes participation in the evaluation component, enables the participant to earn up to 1.0 MOC points in the American Board of Internal Medicine's (ABIM) Maintenance of Certification (MOC) program. Participants will earn MOC points equivalent to the amount of CME credits claimed for the activity. It is the CME activity provider's responsibility to submit participant completion information to ACCME for the purpose of granting ABIM MOC credit.

All other clinicians completing this activity will be issued a certificate of participation. To participate in this journal CME activity: (1) review the learning objectives and author disclosures; (2) study the education content; (3) take the post-test with a 75% minimum passing score and complete the evaluation at http://www.medscape.org/journal/eid; and (4) view/print certificate. For CME questions, see page 3121.

Release date: November 20, 2020; Expiration date: November 20, 2021

Learning Objectives

Upon completion of this activity, participants will be able to:

- Describe TB incidence and period prevalence among children and adolescents with HIV (C/ALHIV), according to an analysis of data from 7 integrated pediatric HIV/TB centers in 6 countries in sub-Saharan Africa
- Determine TB outcomes and risk factors among C/ALHIV, according to an analysis of data from 7 integrated pediatric HIV/TB centers in 6 countries in sub-Saharan Africa
- Identify clinical implications of the association between antiretroviral therapy and TB prevalence and risk factors for adverse TB outcomes among C/ALHIV, according to an analysis of data from 7 integrated pediatric HIV/TB centers in 6 countries in sub-Saharan Africa

CME Editor

Deanna Altomara, BA, Copyeditor, Emerging Infectious Diseases. *Disclosure: Deborah Wenger, MBA, has disclosed no relevant financial relationships.*

CME Author

Laurie Barclay, MD, freelance writer and reviewer, Medscape, LLC. *Disclosure: Laurie Barclay, MD, has disclosed no relevant financial relationships.*

Authors

Disclosure: ***Anna M. Mandalakas, MD, PhD; Alexander W. Kay, MD; Jason M. Bacha, MD, MS; Tara Devezin, BA, MID; Rachel Golin, MD, MHS; Katherine R. Simon, MD; Dilsher Dhillon, MS; Sandile Dlamini, BA; Andrew DiNardo, MD; Mogomotsi Matshaba, MB, BCh, BAO; Jill E. Sanders, MD; Lineo Thahane, MD; Pauline M. Amuge, MBChB, MMed; Saeed Ahmed, MD; Moorine P. Sekadde, MMed, MPH; Neway G. Fida, MD; Bhekumusa Lukhele, PhD; Nodumo Chidah, MBA; David Damba, MS; Joseph Mhango, MS; Moses Chodota, BA; Makhorong Matsoso, BSc; Angelina Kayabu, BSc;*** *and* ***Gordon E. Schutze, MD,*** *have disclosed no relevant financial relationships.* ***Richard Sebastian Wanless, MBChB, PhD,*** *has disclosed the following relevant financial relationships: served as an advisor or consultant for Bristol-Myers Squibb Foundation; INNOCIMAB PTE. LTD.*

[1]These authors contributed equally to this article.

HIV-infected children and adolescents are at increased risk for tuberculosis (TB). Antiretroviral therapy (ART) reduces TB risk in HIV-infected adults, but its effectiveness in HIV-infected children and adolescents is unknown. We analyzed data from 7 integrated pediatric HIV/TB centers in 6 countries in sub-Saharan Africa. We used a Bayesian mixed-effect model to assess association between ART and TB prevalence and used adaptive lasso regression to analyze risk factors for adverse TB outcomes. The study period encompassed 57,525 patient-years and 1,160 TB cases (2,017 cases/100,000 patient-years). Every 10% increase in ART uptake resulted in a 2.33% reduction in TB prevalence. Favorable TB outcomes were associated with increased time in care and early ART initiation, whereas severe immunosuppression was associated with death. These findings support integrated HIV/TB services for HIV-infected children and adults and demonstrate the association of ART uptake with decreased TB incidence in high HIV/TB settings.

Tuberculosis (TB) is an underestimated cause of death in children (*1*); it is accurately diagnosed and reported in only 45% of children with the disease (*2*). When accounting for underdetection, the World Health Organization (WHO) estimated that, in 2017, a total of 1.12 million TB cases developed in infants, children, and adolescents ≤14 years of age and 1.60 million cases in adolescents and young adults 15–24 years of age (*2*). WHO also estimated that TB was associated with 205,000 deaths in children, including 32,000 in HIV-infected children and adolescents; these deaths account for 13% of total TB-associated deaths in HIV-infected persons, although only 5% of HIV-infected persons are children (*2*). Children might be at increased risk for TB because they receive antiretroviral therapy (ART) at lower rates than adults. According to the Joint United Nations Programme on HIV/AIDS (*3*), only 53% of eligible children worldwide received ART in 2019.

Before ART was widely available, TB incidence and TB-related deaths were substantially higher among HIV-infected children and adolescents than among peers without HIV (*4*). Multiple studies have demonstrated declines in TB incidence among this group after ART scale-up initiatives (*5*,*6*). A meta-analysis of data from children estimated a pooled hazard ratio of 0.3 (95% CI 0.21–0.39) and declining TB risk for 2 years after ART initiation (*5*,*7*). However, TB remains a major cause of illness and death in children receiving ART (*8*).

Although risk factors for TB and adverse TB outcomes are well-documented among HIV-infected adults (*9*), risk factors among HIV-infected children and adolescents are poorly understood, particularly since the 2016 recommendations for universal ART for all HIV-infected persons (*10*). Some systematic reviews suggest that immunosuppression predicts TB incidence (*7*) among HIV-infected children and adolescents. Studies examining data sourced from a single country typically demonstrate that 1 or 2 risk factors, such as age <2 years, extrapulmonary TB, malnutrition, severe immunosuppression, WHO HIV clinical stage, or TB treatment status (*11*–*14*) can predict death among children with HIV-associated TB. Large or multinational studies of TB risk factors and outcomes among HIV-infected children and adolescents are few (*15*,*16*) and urgently needed.

Limited and conflicting data exist on outcomes among HIV-infected children and adolescents in whom TB developed before versus after ART initiation. In a multinational cohort of children from predominantly resource-limited countries, no association existed between TB outcomes and disease onset relative to ART initiation (*15*). In contrast, other studies have demonstrated lower death rates among children on ART at the time of TB diagnosis (*17*). WHO

Author affiliations: Texas Children's Hospital, Houston, Texas, USA (A.M. Manadalakas, A.W. Kay, J.M. Bacha, T. Devezin, K.R. Simon, D. Dhillon, S. Dlamini, A. DiNardo, M. Matshaba, J. Sanders, L. Thahane, S. Ahmed, N. Chidah, D. Damba, M. Chodota, M. Matsoso, A. Kayabu, R.S. Wanless, G.E. Schutze); Baylor College of Medicine, Houston (A.M. Manadalakas, A.W. Kay, J.M. Bacha, T. Devezin, D. Dhillon, A. DiNardo, B. Lukhele, R.S. Wanless, G.E. Schutze); Baylor College of Medicine Children's Foundation Swaziland, Mbabane, Swaziland (A.W. Kay, S. Dlamini, B. Lukhele); Baylor College of Medicine Children's Foundation Tanzania, Mbeya, Tanzania (J.M. Bacha); US Agency for International Development, Washington, DC, USA (R. Golin); Baylor College of Medicine Children's Foundation Malawi, Lilongwe, Malawi (K.R. Simon, S. Ahmed, J. Mhango); Technical Support to PEPFAR Programs in the Southern Africa Region, Lilongwe (K.R. Simon, S. Ahmed, J. Mhango); Botswana-Baylor Children's Clinical Centre of Excellence, Gaborone, Botswana (M. Matshaba, N. Chidah); Baylor College of Medicine Children's Foundation Lesotho, Maseru, Lesotho (J. Sanders, L. Thahane, M. Matsoso); Baylor College of Medicine Children's Foundation Uganda, Kampala, Uganda (P.M. Amuge, D. Damba); National Tuberculosis and Leprosy Programme, Kampala, Uganda (M.P. Sekkade); US Agency for International Development, Pretoria, South Africa (N.G. Fida); Baylor College of Medicine Children's Foundation Tanzania, Mwanza, Tanzania (M. Chodota, A. Kayabu)

DOI: https://doi.org/10.3201/eid2612.202245

recommends that HIV-infected children and adolescents start ART as soon as possible and within ≤8 weeks of beginning TB treatment (*18*). Recent evidence derived from the same multinational cohort demonstrates that this recommendation was poorly implemented; only 46% of ART-naive children began treatment within ≤8 weeks of starting TB treatment. However, when implemented successfully, this measure was associated with favorable TB treatment outcomes (64% vs. 40%; p = 0.04) (*15*).

Data regarding TB incidence, management, and outcomes among HIV-infected children and adolescents are mostly sourced from single healthcare centers, limiting their generalizability. We analyzed these variables in the largest reported multinational study of TB in HIV-infected children and adolescents in countries in sub-Saharan Africa.

Materials and Methods

Strengthening the Reporting of Observational Studies in Epidemiology Statement

This study was conducted in accordance with the Strengthening the Reporting of Observational Studies in Epidemiology guidelines (*19*). Our primary objectives were to estimate longitudinal TB incidence within the context of increasing ART coverage and identify risk factors for death from TB in HIV-infected children and adolescents in various stages of ART.

Participants

We examined TB outcomes of HIV-infected children and adolescents receiving care at 7 treatment centers (Centers of Excellence; COEs) within the Baylor International Pediatric AIDS Initiative at Texas Children's Hospital network, spanning 6 countries: Botswana, Swaziland, Lesotho, Malawi, Tanzania (locations in Mbeya and Mwanza), and Uganda. To avoid sampling bias, we included data from all children receiving care during from January 2013 through June 2017.

Outcomes of Interest

We used TB case and outcome definitions from WHO (*20*) (Appendix Table 1, https://wwwnc.cdc.gov/EID/article/26/12/20-2245-App1.pdf). We categorized TB outcomes as favorable (cured or treatment completed), unfavorable (death), lost to follow-up (LTFU), or transferred out of the COE.

Data Extraction

We analayzed data from Janaury 2013 through June 2017 from the electronic medical records of HIV-infected children and adolescents ≤19 years of age. The deidentified data from the 7 COEs enables follow-up of individual patients for longitudinal analysis.

The duration of each COE's study period depended on when that COE began collecting TB data using electronic medical records. Data collection began in 2013 at all COEs (except for Malawi, which began data collection in 2016) and continued through June 2017.

Statistical Approach

We calculated the annual TB incidence for all HIV-infected children and adolescents at each COE. We modeled the TB incidence as a function of time, ART uptake, and COE. We included a random intercept for the COE, enabling us to visualize how ART uptake varied by COE and by year. We ran this model under a Bayesian framework using R with the library brms (*21*). We used a similar Bayesian mixed-effect model to determine association between isoniazid preventive therapy (IPT) use and TB incidence (*22*). Data on IPT use were available from 4 COEs: Swaziland, Tanzania-Mbeya, Tanzania-Mwanza, and Uganda. We considered children to be eligible for IPT if they were >12 months of age and had not previously received IPT.

We examined variables in bivariate analysis if >75% of data were available. We excluded some variables, such as specific anthropometrics (e.g., height, mid-upper arm circumference) and *Mycobacterium bovis* BCG vaccination status because of missing data. We considered CD4 values and viral loads if measured ≤60 days before or after the analytic baseline. For bivariate analysis, we used a χ^2 test for categorical independent variables and a Wilcoxon rank-sum test for continuous independent variables. We used multinomial logistic regression to study the univariate association between age and outcome. To relax the assumption of age having a constant effect on outcome, we modeled age using natural cubic splines, using the splines package in R, with 3 knots at equally spaced quantiles. To determine age-related risk for death we calculated the instantaneous rate of change using the method of finite differences.

We used an adaptive lasso logistic regression model to examine the association between TB outcome and 13 independent variables (*23*). Adaptive lasso normalizes coefficients; therefore, no reference level is preselected. Instead, the model minimizes the influence of coefficients unassociated with the outcome; these coefficients set the reference levels for the remaining coefficients. We selected the penalty parameter to minimize deviance using leave-one-out cross-validation; we used the selected penalty to

fit the final model. We included risk factors that we hypothesized, a priori, would affect TB outcomes (Appendix Table 2). We conducted the adaptive lasso procedure using library glmnet in R (*23*) and postselection inference of the selected coefficients using library selective Inference, also in R (*24*). We developed 3 models to examine associations with favorable outcomes (cure or treatment completion) against death. We examined the outcome within all participants, participants on ART at time of TB diagnosis, and participants not on ART at diagnosis. We conducted sensitivity analyses of HIV-infected children and adolescents who were LTFU or died. We developed additional models evaluating outcomes categorized by WHO as favorable (cure or treatment completion) or unfavorable (death, LTFU, or not evaluated/transferred out) (Appendix Tables 3–5).

Ethics Statement

All clinical investigation supporting the data handling, analysis, and reporting of these findings was conducted according to the principles expressed in the Declaration of Helsinki. Approval was obtained from all necessary ethics bodies in each country (i.e., the Baylor College of Medicine Children's Foundation or Trust, the national ethics committee in each country, and the Baylor College of Medicine Institutional Review Board).

Results

TB Incidence

We analyzed data on 1,160 HIV-infected children and adolescents in whom TB was diagnosed during the study period, which encompassed 57,525 patient-years. During the 4-year study period, overall TB incidence was 2,017 cases/100,000 patient-years (range 454 cases/100,000 patient-years in Botswana to 4,385 cases/100,000 patient-years in Tanzania-Mwanza). These incidences were substantially higher than those estimated by WHO for the general populations of the respective countries (Table 1).

The age distribution of the cohort was similar across sites. TB incidence was highest among infants and children <5 years of age but was elevated among school-aged children, a trend that persisted into early and late adolescence (Figure 1). Increasing age was associated with more favorable outcomes. Children ≤7 years of age had a higher risk for death than school-aged children (i.e. 8–10 years of age) and adolescents (i.e., 11–19 years of age) (Figure 2, panels A, B). Of patients receiving TB treatment, 32% had TB infection confirmed by bacteriologic testing, usually GeneXpert (Cepheid, https://www.cepheid.com); this percentage excludes children at the Lesotho COE because it had incomplete data. Confirmation rates ranged from 24% for infants and children ≤2 years of age to 51% for adolescents 10–19 years of age.

Throughout the study, rates of ART administration increased and the prevalence of TB declined at most sites (Figure 3, panels A, B). For every 10% increase in the number of HIV-infected children and adolescents who received ART, the overall prevalence of TB in the clinical network decreased 2.33% (95% credible interval 0.58%–4.4%) (Figure 3, panel C).

We also observed an increase in the number of eligible children starting IPT. Average rates of IPT use across all COEs increased from 8.68% in 2014 to 27.5% in 2017. When we limited our analysis to the 4 COEs with available IPT data, we observed no effect on TB prevalence (0.4% increase, 95% credible interval –0.3% to 1.0%) associated with each 10% increase in the number of HIV-infected children and adolescents receiving IPT.

TB Outcomes and Risk Factor Analysis

Most children and adolescents had favorable outcomes: across all sites, 75% (95% CI 67%–87%) of patients, including those who were LTFU or had transferred out, had favorable outcomes (Table 2). On average, children with favorable TB outcomes had received care at the clinics nearly a year longer than children who died (p<0.01). Ten percent (95%

Table 1. Comparison of country-specific incidence of HIV-associated TB, 2013–2017*

Country	TB incidence no. per 100,000 patient-years (95% CI)	WHO 2017 country estimates, no. per 100,000 persons (95% CI)		TB incidence/WHO 2017 TB country estimate fold difference
		TB	HIV-associated TB	
Botswana	454 (299–608)	300 (232–376)	144 (93–206)	1.5
Eswatini	2,612 (2,205–3,020)	308 (236–389)	213 (138–304)	8.5
Lesotho	3,762 (3,376–4,148)	665 (430–949)	470 (298–680)	5.6
Malawi	1,159 (791–1,528)	131 (70–210)	65 (42–93)	8.8
Tanzania-Mwanza	4,385 (3,747–5,024)	269 (127–464)	84 (54–120)	16.3
Tanzania-Mbeya	3,995 (3,498–4,492)	269 (127–464)	84 (54–120)	14.8
Uganda	656 (546–766)	201 (118–305)	80 (52–114)	3.2

*Incidence reflects the estimated new cases of TB disease among HIV-infected children and adolescents at each HIV treatment center. TB, tuberculosis; WHO, World Health Organization.

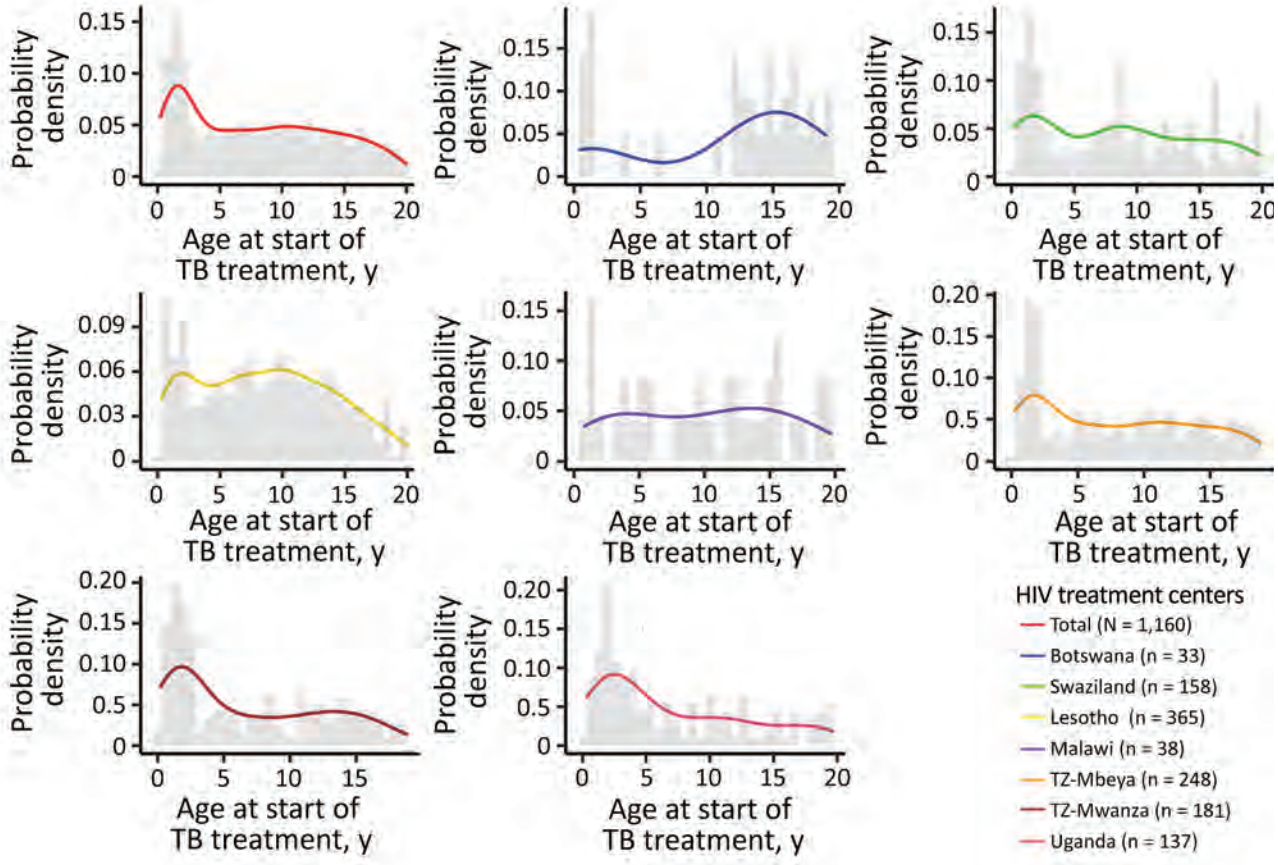

Figure 1. Incidence of tuberculosis (TB) among HIV-infected children and adolescents, 2013–2017. The age at start of TB treatment is plotted as a smoothed line and histogram against the probability of TB diagnosis on the basis of the prevalence of that age within the overall cohort of HIV-infected children and adolescents. The data are presented combined and stratified by HIV treatment center.

CI 5%–15%) of HIV-infected children and adolescents with TB died. If we assumed all HIV-infected children and adolescents who were LTFU died, the death ratio would increase to 13% (95% CI 6%–20%).

We used bivariate analysis to identify factors associated with TB outcome (Table 2). Extrapulmonary disease increased the odds of death (p<0.01). The death ratio for patients who had previously been treated for TB was similar to the death ratio for patients who had not, even if we assumed all patients

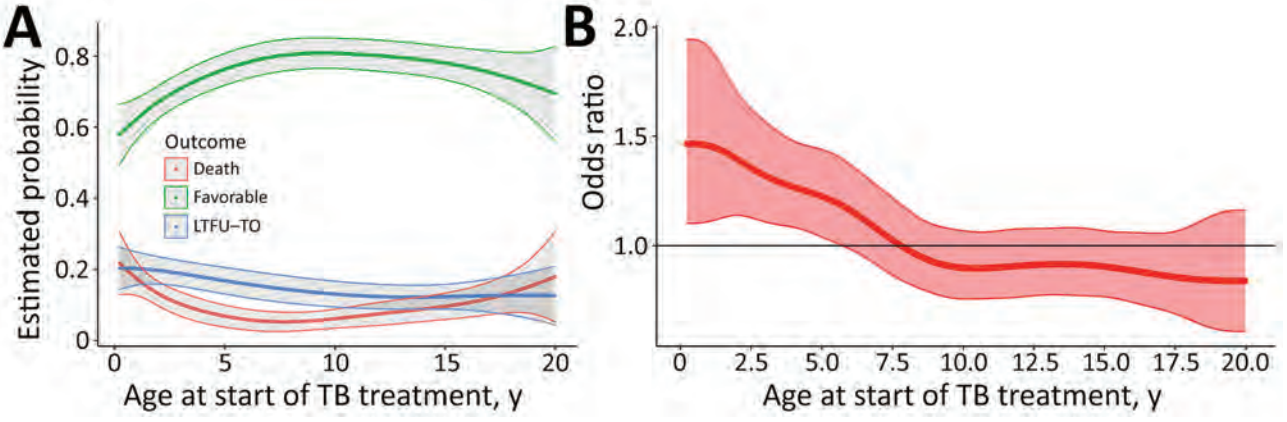

Figure 2. Probabilities of specific outcomes for TB in HIV-infected children and adolescents, 2013–2017. A) Probability (with 95% CIs) of outcomes stratified by age at start of TB treatment. B) Instantaneous odds ratios for death at each age. The odds ratio reflects the change in odds of death according to age at start of TB treatment. LTFU-TO, lost to follow-up or transferred out; TB, tuberculosis.

who were LTFU died. HIV-infected children and adolescents who had engaged in facility-based HIV care for more time were more likely to have favorable outcomes (p<0.01).

HIV-infected children and adolescents who never started ART were less likely than those in all other groups to have a favorable outcome (Figure 4, panel A). HIV-infected children and adolescents who began ART during the 6 months before the start of their TB treatment had the highest death ratio (14%); children who had never been on ART but began it within 8 weeks of TB diagnosis had the lowest death ratio (8%). Immune status was highly predictive of death (Figure 4, panel B). HIV-infected children and adolescents with severe immunosuppression had >5-fold increased odds of death compared with those without immune suppression (16% vs. 3%; p<0.01); we defined severe immunosuppression as a CD4 percentage of <25% in children <5 years of age or CD4 count <200 cells/mm^3 in children ≥5 years of age.

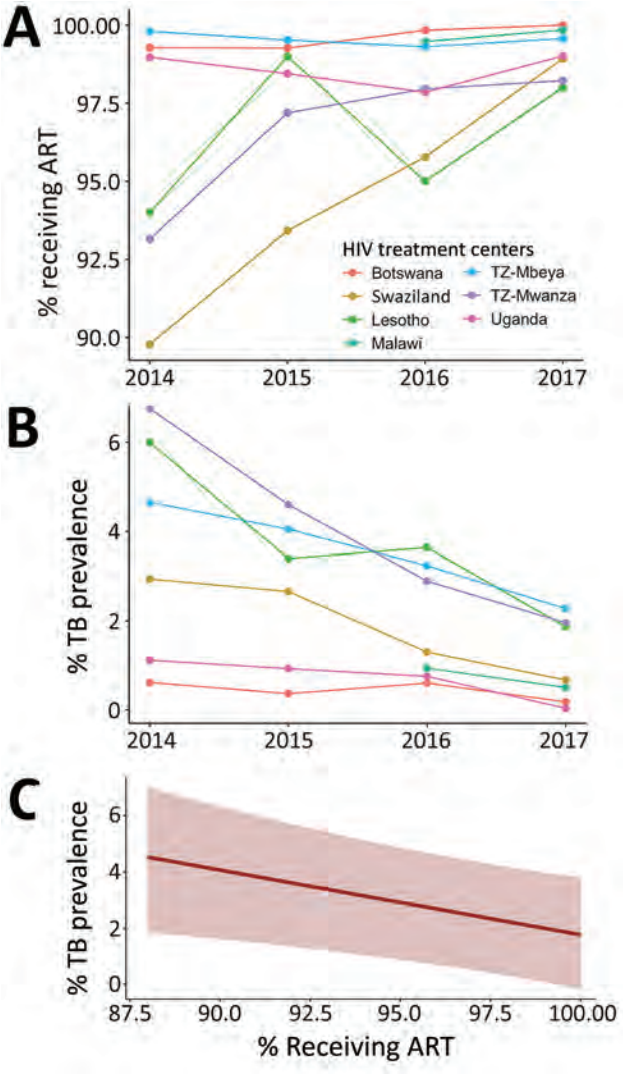

Figure 3. ART use and TB prevalence in HIV-infected children and adolescents, 2013–2017. A) Annual percentage of the cohort at each HIV treatment center receiving ART. B) Annual percentage of the cohort at each treatment center in whom TB was diagnosed. C) Declining TB prevalence with increase in ART uptake, averaged across all treatment centers in the study period. ART, antiretroviral therapy; TB, tuberculosis.

We developed 3 multivariate models to comprehensively examine associations with favorable outcomes against death, considering a patient's history of ART. The model comparing all 1,029 patients considered 11 factors (Table 3). This model demonstrated the influence of immune status at the time of TB diagnosis, showing that HIV-infected children and adolescents without immune suppression (CD4 percentage >30% in children <5 years of age or CD4 count >350 cells/mm^3 in children ≥5 years of age) at TB diagnosis had a 58% lower odds of death (odds ratio [OR] 0.42 [95% CI 0.13–0.94]; p = 0.04) than children with advanced immune suppression. In addition, patients who had never been on ART but received it ≤8 weeks after TB diagnosis had a 59% lower odds of death than those who received ART >8 weeks after TB diagnosis (OR 0.41 [95% CI 0.14–0.60]; p<0.01). The multivariate analysis did not demonstrate an increased odds of death for HIV-infected children and adolescents who started ART in the 6 months before TB diagnosis.

The model comparing the 597 patients who had received ART before TB diagnosis considered 13 factors (Table 4). Children with severe immunosuppression at TB diagnosis had a 4 times higher odds of death than children with advanced immune suppression (OR 4.29 [95% CI 1.23–29.28]; p = 0.03). A patient's odds of death increased with each advance in WHO stage at TB diagnosis (OR 2.18 [95% CI 1.91–5.98]; p<0.01).

The final model of patients who had never received ART, prior to TB diagnosis, comprised 391 patients with favorable outcomes and 41 patients who died; this model was intractable and did not converge. Results evaluating associations with programmatic outcomes were similar to the results described in the previous paragraphs (Appendix Tables 3–5).

Discussion

TB is the leading cause of death in HIV-infected persons (2). This multicountry study of TB in HIV-infected children and adolescents revealed high TB incidences that greatly exceeded estimated population level TB incidences of all individual countries represented by the cohort. Consistent with recent systematic reviews and meta-analyses (7), our evidence demonstrates that although ART significantly reduc-

Table 2. Bivariate analysis of associations with TB treatment outcomes in HIV-infected children and adolescents, 2013–2017*

Variable	Total	Outcome			p value†
		Completed TB treatment or cured	Died	Lost to follow up or transferred out	
Sex					0.98
F	591 (50.95)	438 (51.11)	61 (50.41)	92 (50.55)	
M	569 (49.05)	419 (48.89)	60 (49.59)	90 (49.45)	
HIV treatment center					<0.01
Botswana	33 (2.84)	31 (3.62)	0	2 (1.10)	
Eswatini	365 (32.39)	302 (35.24)	15 (12.40)	48 (26.37)	
Lesotho	38 (4.99)	33 (3.85)	3 (2.48)	2 (1.10)	
Malawi	158 (13.62)	134 (15.64)	15 (12.40)	9 (4.95)	
Tanzania–Mbeya	248 (21.38)	160 (18.67)	41 (33.88)	47 (25.82)	
Tanzania–Mwanza	181 (15.60)	106 (12.37)	18 (14.88)	57 (31.32)	
Uganda	137 (11.81)	91 (10.62)	29 (23.97)	17 (9.34)	
Site of TB					<0.01
Pulmonary TB	997 (88.39)	760 (90.15)	87 (78.38)	150 (86.21)	
Extrapulmonary TB	131 (11.61)	83 (9.85)	24 (21.62)	24 (13.79)	
TB treatment category					0.08
Newly treated TB patient	1,007 (90.56)	764 (91.50)	96 (91.43)	147 (85.47)	
Previously treated TB patient	105 (9.44)	71 (8.50)	9 (8.57)	25 (14.53)	
TB drug resistance testing					<0.01
Not tested	837 (75.61)	612 (73.38)	82 (78.10)	143 (90.51)	
Not detected	258 (23.31)	220 (26.38)	23 (21.70)	15 (9.04)	
Mono-resistance detected	6 (0.54)	2 (0.24)	1 (0.94)	3 (1.81)	
Multidrug-resistance detected	6 (0.54)	0	0	5 (3.01)	
ART regimen at start of TB treatment					0.41
Efavirenz-based	225 (40.61)	177 (42.34)	20 (31.75)	28 (38.36)	
Nevirapine-based	166 (29.96)	130 (31.10)	16 (25.40)	20 (27.40)	
Lopinavir-based	134 (24.19)	91 (21.77)	23 (36.51)	20 (27.40)	
Atazanavir-based	17 (3.07)	12 (2.87)	3 (4.76)	2 (2.74)	
Other	9 (1.62)	6 (1.44)	1 (1.59)	2 (2.74)	
Azidothymidine + lamivudine + abacavir	3 (0.54)	2 (0.48)	0	1 (1.37)	
ART relative to start of TB treatment					<0.01
On ART >6 mos	421 (34.59)	327 (36.01)	42 (34.71)	52 (27.66)	
On ART ≤8 wks after TB treatment	396 (32.54)	315 (34.69)	26 (21.49)	55 (29.26)	
On ART ≤6 mos	276 (22.68)	190 (20.93)	38 (31.40)	48 (25.53)	
Never started ART	97 (7.97)	58 (6.39)	12 (9.92)	27 (14.36)	
On ART >8 wks after TB treatment	27 (2.22)	18 (1.98)	3 (2.48)	6 (3.19)	
Immune status at start of TB treatment					<0.01
Nonadvanced	468 (55.19)	387 (58.46)	15 (22.73)	66 (55.00)	
Severe	252 (29.72)	174 (26.28)	41 (62.12)	37 (30.83)	
Advanced	128 (15.09)	101 (15.26)	10 (15.15)	17 (14.17)	
Mean time receiving care before TB diagnosis, d		635.5	363.3	342	<0.01
Mean time on ART before TB diagnosis, d		697.6	624	508.6	0.12

*Values are no (%) except as indicated. ART, antiretroviral therapy; TB, tuberculosis.
†χ^2 test.

es the prevalence of TB in HIV-infected children and adolescents, the risk for TB remains elevated even among a population with excellent ART coverage. TB-related deaths decreased in adults during 1996–2011, when ART use increased in various countries (*25*). Although we cannot ascribe causality between increasing ART coverage and declining TB prevalence, this association is notable given the very high initial ART coverage in our study. Increasing ART uptake >90% was associated with ongoing declines in TB incidence, suggesting that the Joint United Nations Programme on HIV/AIDS 95-95-95 targets for HIV might also reduce TB incidence. Likewise, HIV-infected children and adolescents with favorable TB outcomes had received care for nearly a year longer, on average, than children who died. These findings highlight the importance of early HIV diagnosis, prompt treatment, and patient retention in HIV-infected children and adolescents.

Of HIV-infected children and adolescents with TB, 32% had a confirmed TB diagnosis; the rate of TB confirmation increased with age. This high rate of disease confirmation is consistent with prior studies, which have found that HIV infection does not significantly reduce the likelihood of disease confirmation in children (*26*–*28*). However, other multinational cohorts have reported lower rates of disease confirmation in HIV-infected children and adolescents, a discrepancy that might reflect the greater testing capacity at the COEs (*15*). Most HIV clinics treating children in sub-Saharan Africa do not have the capacity to collect TB specimens in children (*29*). Confirmatory

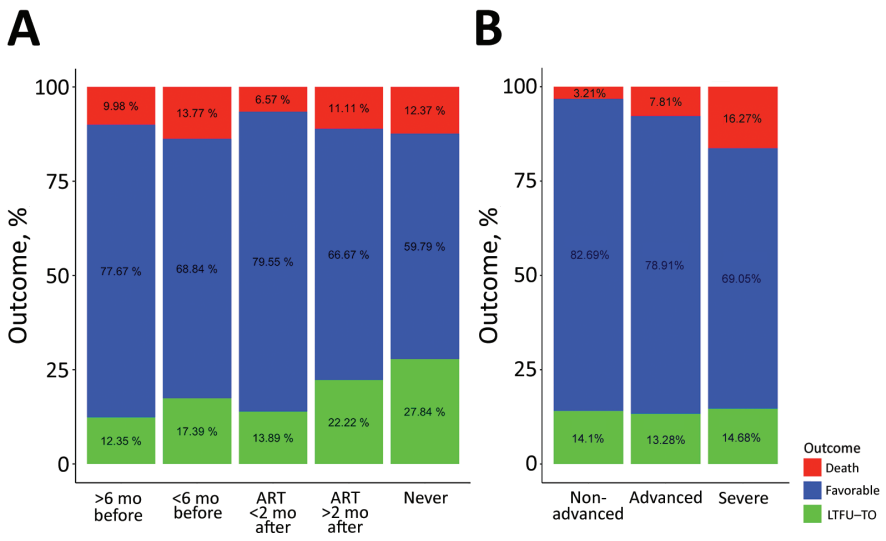

Figure 4. Bivariate analyses of factors relating to TB treatment outcome in HIV-infected children and adolescents, 2013–2017. A) ART treatment category: received ART >6 months or <6 months before TB diagnosis or started on ART <2 months or >2 months after TB diagnosis. B) Immune status. Advanced immunosuppression was define as a CD4 percentage of <25% in children <5 years of age or CD4 count <200 cells/mm3 in children >5 years of age. ART, antiretroviral therapy; TB, tuberculosis.

diagnostic testing remains a challenge more broadly across low and middle-income countries in sub-Saharan Africa; furthermore, current testing strategies are invasive and extremely uncomfortable, necessitating the development of child-friendly diagnostic tools.

Within the cohort, HIV-infected children and adolescents <5 years of age had the greatest risk for TB, a finding consistent with existing literature (*14*). Likewise, children in this age range were more likely to die (*4*). However, TB incidence did not decline significantly among school-age children ≤10 years of age, an age group in HIV-negative cohorts that has a significantly reduced risk for TB (*30*). This analysis, like others (*31*), suggests that HIV reduces the protective effect of age on TB risk.

Overall, 75% of HIV-infected children and adolescents in this cohort had favorable treatment outcomes, whereas 10% died. Existing literature estimates that in sub-Saharan Africa, 16% of HIV-infected children and adolescents who are LTFU die, regardless of TB status (*32*). Because 4% of patients in our study were LTFU, the death rate of our cohort might be closer to 10%–13%. Recent evidence estimates a cumulative all-cause death rate of 3% at 3 months, 5% at 6 months, 6% at 12 months, and 7% at 24 months after ART initiation in HIV-infected children and adolescents in sub-Saharan Africa (*33*).

Approximately 60% of HIV-infected children and adolescents have severe immunosuppression at TB diagnosis (*13*). In contrast, 33% of children in this cohort had advanced or severe immunosuppression at TB diagnosis. Severe immunosuppression was associated with up to a 4-fold higher risk for death than advanced immunosuppression. Similarly, advanced WHO stage (noted before TB diagnosis) was associated with a 2-fold increased risk for death. This finding highlights the need for scale-up of HIV identification and treatment methods, such as family index

Table 3. Predictors of favorable TB outcomes against death in HIV-infected children and adolescents, 2013–2017

Variable	Odds ratio (95% CI)	p value
Country		
Swaziland, Lesotho, Malawi, Tanzania-Mbeya, Tanzania-Mwanza, and Uganda	Referent	
Botswana	0.09 (0.00–22.83)	0.1811
TB drug resistance		
Not tested, multidrug resistance, and not detected	Referent	
Monoresistance	18.11 (0.00–31,381.00)	0.4642
ART category		
On ART >6 mos before TB treatment, on ART <6 mos before TB treatment, and on ART >8 wks after starting TB treatment	Referent	
Never on ART	3.38 (0.21–20.02)	0.2168
On ART ≤8 wks after TB treatment	0.41 (0.14–0.60)	0.0051†
Immune status		
Advanced	Referent	
Not advanced	0.42 (0.13–0.94)	0.0412†
Severe	1.88 (0.70–4.80)	0.1233
Each increasing WHO stage	3.64 (2.50–7.17)	<0.001‡

Table 4. Predictors of favorable TB outcomes against death in HIV-infected children and adolescents on ART at TB diagnosis, 2013–2017

Variable	Odds ratio (95% CI)	p value
Country		
Swaziland, Lesotho, Malawi, Tanzania-Mbeya, Tanzania-Mwanza, and Uganda	Referent	
Botswana	0.22 (0.01–1.90)	0.0858
TB drug resistance		
Not tested, multidrug resistance, not detected	Referent	
Mono INH resistance	23.64 (0.00–28,630.46)	0.3917
Immune status		
Advanced	Referent	
Not advanced	0.59 (0.12–5.17)	0.2767
Severe	4.29 (1.23–29.28)	0.0294*
Each increasing WHO stage	2.18 (1.91–5.98)	0.001*

*Significant result (p<0.05)

testing, provider-initiated testing and counseling, Test and Start models (*10*), and prompt ART initiation. Public health officials must further evaluate the care of children and adolescents with advanced HIV to develop strategies that promote survival (*34*).

The bivariate and multivariate analyses demonstrate a dramatic reduction of death in children who started ART within ≤8 weeks after TB diagnosis. Multivariate analysis shows that starting ART within ≤8 weeks after beginning TB treatment was associated with a 59% reduction in death compared with children on ART before their TB diagnosis or beginning it >8 weeks after starting TB treatment. Furthermore, children who never initiated ART had a >3 times higher risk for death than those who were on ART before their TB diagnosis or began ART >8 weeks after starting TB treatment. We need more data to ascertain whether ART can further reduce HIV-associated TB death in children when initiated within ≤2 weeks after TB treatment. Most HIV-infected children and adolescents with TB have paucibacillary disease, which can inhibit confirmatory TB testing and might reduce children's risk for immune reconstitution syndrome after starting ART. Furthermore, children have lower risk for adverse reactions to TB treatment and ART than adults. Thus, early simultaneous initiation of ART and TB treatment might be a safer treatment strategy in children. Starting ART at the same time as TB treatment might reduce the number of HIV-infected children and adolescents with TB who are LTFU before starting ART. This promising treatment strategy should be evaluated in controlled studies.

Among HIV-infected children and adolescents who were not on ART at TB diagnosis, 85% started ART within ≤8 weeks of beginning TB treatment, confirming that this intervention is attainable in a setting with high HIV/TB prevalence. Children who started ART ≤8 weeks after TB treatment had the lowest odds of death, even lower than those of children on ART at TB diagnosis. We hypothesize that many children who develop TB while on ART are not virologically surpressed and are therefore more likely to die from this disease. The bivariate analysis, but not the multivariate analysis, indicated an increased odds of death among children who began ART ≤6 months before TB diagnosis. This finding suggests that HIV-infected children and adolescents with unmasking TB-immune reconstitution syndrome, an exaggerated inflammatory manifestation of TB during early ART, might have an increased odds of death. Prospective studies evaluating time from TB diagnosis to ART initiation has benefitted the treatment of adults with HIV (*35*). Similar prospective trials are needed to inform treatment of HIV-infected children and adolescents.

This study has some limitations. Because we used data from clinical settings, missing data precluded analysis of some variables. Nevertheless, this evidence is representative of well-managed clinics in countries in sub-Saharan Africa with consistent access to diagnostic technology and ART medications. We identified an association between ART and TB prevalence but cumulative IPT coverage also increased over time across a subset of COEs. We did not observe an association between IPT uptake and TB prevalence. This lack of association might have been caused by sample size limitations, inconsistent IPT availability, or heterogeneity of IPT guidelines; therefore, we cannot draw strong conclusions about the effects of IPT on TB prevalence. Because only a subset of COEs provided data on IPT, we did not include it in the TB outcomes models. We could not compare annual incidence of TB at the clinic level with national trends because of recent changes in WHO's estimation methods (*36*). Last, as with all retrospective analysis, the possibility exists for inaccurate entry of clinical data. We attempted to limit this source of error through manual data checks.

The strong association between immune suppression at TB diagnosis and death highlights the importance of early TB case detection and ART initiation among HIV-infected children and adolescents. Furthermore, we found a strong association between favorable TB outcome and increased length of time in care. These associations emphasize the importance of early HIV case detection and prompt ART initiation. Finally, we found an association between increased ART coverage and decreased TB incidence, as well as ART initiation within ≤8 weeks after starting TB treatment and favorable outcomes. Collectively, these findings support the continued need to promote policies and implement practices that fully integrate optimal HIV and TB treatment in countries with high burdens of these diseases.

Acknowledgments

We thank the local Ministry of Health officials, the Baylor teams, children, adolescents, and families across the Baylor International Pediatric AIDS Initiative at Texas Children's Hospital network who contributed to this analysis.

This work is in memory of Peter Nicholas Kazembe (1955–2020), who made monumental contributions to the health of children and families in Malawi and beyond.

This study was supported by the US President's Emergency Plan for AIDS Relief through the US Agency for International Development (USAID) award no. AID-674-A-16-00003. In addition to USAID funding, Texas Children's Hospital provided funds to support this research and disseminate findings.

The contents in this manuscript are those of the authors and do not necessarily reflect the view of the US Agency for International Development, the U.S. President's Emergency Plan for AIDS Relief, or the United States Government. This manuscript was made possible by the support of the American people through the United States Agency for International Development under the President's Emergency Plan for AIDS Relief. The contents in this article are the sole responsibility of the authors, and do not necessarily reflect the views of USAID, PEPFAR or the United States Government. USAID Award Number AID-674-A-16-00003.

About the Author

Dr. Mandalakas is the director of the Global Tuberculosis Program at Texas Children's Hospital. Her research interests include child TB and TB/HIV.

References

1. Dodd PJ, Yuen CM, Sismanidis C, Seddon JA, Jenkins HE. The global burden of tuberculosis mortality in children: a mathematical modelling study. Lancet Glob Health. 2017;5:e898–906. https://doi.org/10.1016/S2214-109X(17)30289-9
2. World Health Organization. Global tuberculosis report. 2018 [cited 2020 Mar 20]. https://www.who.int/tb/publications/global_report/gtbr2018_main_text_28Feb2019.pdf
3. UNAIDS. Global HIV & AIDS statistics—2020 fact sheet. 2020 [cited 2020 Aug 1]. https://www.unaids.org/en/resources/fact-sheet#:~:text=38.0%20million%20%5B31.6%20million%E2%80%9344.5,AIDS%2Drelated%20illnesses%20in%202019
4. Jenkins HE, Yuen CM, Rodriguez CA, Nathavitharana RR, McLaughlin MM, Donald P, et al. Mortality in children diagnosed with tuberculosis: a systematic review and meta-analysis. Lancet Infect Dis. 2017;17:285–95. https://doi.org/10.1016/S1473-3099(16)30474-1
5. Bakeera-Kitaka S, Conesa-Botella A, Dhabangi A, Maganda A, Kekitiinwa A, Colebunders R, et al. Tuberculosis in human immunodeficiency virus infected Ugandan children starting on antiretroviral therapy. Int J Tuberc Lung Dis. 2011;15:1082–6. https://doi.org/10.5588/ijtld.10.0538
6. Martinson NA, Moultrie H, van Niekerk R, Barry G, Coovadia A, Cotton M, et al. HAART and risk of tuberculosis in HIV-infected South African children: a multi-site retrospective cohort. Int J Tuberc Lung Dis. 2009;13:862–7.
7. Dodd PJ, Prendergast AJ, Beecroft C, Kampmann B, Seddon JA. The impact of HIV and antiretroviral therapy on TB risk in children: a systematic review and meta-analysis. Thorax. 2017;72:559–75. https://doi.org/10.1136/thoraxjnl-2016-209421
8. B-Lajoie MR, Drouin O, Bartlett G, Nguyen Q, Low A, Gavriilidis G, et al. Incidence and prevalence of opportunistic and other infections and the impact of antiretroviral therapy among HIV-infected children in low- and middle-income countries: a systematic review and meta-analysis. Clin Infect Dis. 2016;62:1586–94. https://doi.org/10.1093/cid/ciw139
9. Nguyen DT, Jenkins HE, Graviss EA. Prognostic score to predict mortality during TB treatment in TB/HIV co-infected patients. PLoS One. 2018;13:e0196022. https://doi.org/10.1371/journal.pone.0196022
10. World Health Organization. Consolidated guidelines on the use of antiretroviral drugs for treating and preventing HIV infection: recommendations for a public health approach. 2016 [cited 2020 Sep 22]. https://apps.who.int/iris/bitstream/handle/10665/208825/9789241549684_eng.pdf;jsessionid=C22AB630B33C95684E57DA59D7B9F56D?sequence=1
11. Atalell KA, Birhan Tebeje N, Ekubagewargies DT. Survival and predictors of mortality among children co-infected with tuberculosis and human immunodeficiency virus at University of Gondar Comprehensive Specialized Hospital, Northwest Ethiopia. A retrospective follow-up study. PLoS One. 2018;13:e0197145. https://doi.org/10.1371/journal.pone.0197145
12. Hicks RM, Padayatchi N, Shah NS, Wolf A, Werner L, Sunkari VB, et al. Malnutrition associated with unfavorable outcome and death among South African MDR-TB and HIV co-infected children. Int J Tuberc Lung Dis. 2014;18:1074–83. https://doi.org/10.5588/ijtld.14.0231
13. Buck WC, Olson D, Kabue MM, Ahmed S, Nchama LK, Munthali A, et al. Risk factors for mortality in Malawian children with human immunodeficiency virus and tuberculosis co-infection. Int J Tuberc Lung Dis. 2013;17:1389–95. https://doi.org/10.5588/ijtld.13.0030
14. Wiseman CA, Schaaf HS, Cotton MF, Gie RP, Jennings T, Whitelaw A, et al. Bacteriologically confirmed tuberculosis

in HIV-infected infants: disease spectrum and survival. Int J Tuberc Lung Dis. 2011;15:770–5. https://doi.org/10.5588/ijtld.10.0501
15. Carlucci JG, Blevins Peratikos M, Kipp AM, Lindegren ML, Du QT, Renner L, et al.; International Epidemiology Databases to Evaluate AIDS (IeDEA) Network. Tuberculosis treatment outcomes among HIV/TB-coinfected children in the International Epidemiology Databases to Evaluate AIDS (IeDEA) Network. J Acquir Immune Defic Syndr. 2017; 75:156–63. https://doi.org/10.1097/QAI.0000000000001335
16. Osman M, Lee K, Du Preez K, Dunbar R, Hesseling AC, Seddon JA. Excellent treatment outcomes in children treated for tuberculosis under routine operational conditions in Cape Town, South Africa. Clin Infect Dis. 2017;65:1444–52. https://doi.org/10.1093/cid/cix602
17. Walters E, Cotton MF, Rabie H, Schaaf HS, Walters LO, Marais BJ. Clinical presentation and outcome of tuberculosis in human immunodeficiency virus infected children on anti-retroviral therapy. BMC Pediatr. 2008;8:1. https://doi.org/10.1186/1471-2431-8-1
18. World Health Organization. Consolidated guidelines on the use of antiretroviral drugs for treating and preventing HIV infection: recommendations for a public health approach—second edition. 2016 [cited 2020 Mar 24]. https://www.who.int/hiv/pub/arv/arv-2016
19. von Elm E, Altman DG, Egger M, Pocock SJ, Gøtzsche PC, Vandenbroucke JP; STROBE Initiative. The Strengthening the Reporting of Observational Studies in Epidemiology (STROBE) statement: guidelines for reporting observational studies. Lancet. 2007;370:1453–7. https://doi.org/10.1016/S0140-6736(07)61602-X
20. World Health Organization. Definitions and reporting framework for tuberculosis—2013 revision. 2013 [cited 2020 Mar 24]. https://www.who.int/tb/publications/definitions/en
21. Bürkner PC. brms: an R package for Bayesian multilevel models using Stan. J Stat Softw. 2017;80:1–28. https://doi.org/10.18637/jss.v080.i01
22. Goodrich B, Gabry J, Ali I, Brilleman S. rstanarm: Bayesian applied regression modeling via Stan. R package. Version 2174 [cited 2020 Mar 20]. http://mc-stanorg/2018
23. Friedman J, Hastie T, Tibshirani R. Regularization paths for generalized linear models via coordinate descent. J Stat Softw. 2010;33:1–22. https://doi.org/10.18637/jss.v033.i01
24. Tibshirani R, Tibshirani R, Taylor J, Loftus J, Reid S, Markovic J. Selective inference: tools for post-selection inference. 2019 [cited 2020 Mar 20]. https://cran.r-project.org/web/packages/selectiveInference/selectiveInference.pdf
25. Yan I, Bendavid E, Korenromp EL. Antiretroviral treatment scale-up and tuberculosis mortality in high TB/HIV burden countries: an econometric analysis. PLoS One. 2016;11:e0160481. https://doi.org/10.1371/journal.pone.0160481
26. Connell TG, Zar HJ, Nicol MP. Advances in the diagnosis of pulmonary tuberculosis in HIV-infected and HIV-uninfected children. J Infect Dis. 2011;204(Suppl 4):S1151–8. https://doi.org/10.1093/infdis/jir413
27. Zar HJ, Workman L, Isaacs W, Dheda K, Zemanay W, Nicol MP. Rapid diagnosis of pulmonary tuberculosis in African children in a primary care setting by use of Xpert MTB/RIF on respiratory specimens: a prospective study. Lancet Glob Health. 2013;1:e97–104. https://doi.org/10.1016/S2214-109X(13)70036-6
28. Detjen AK, DiNardo AR, Leyden J, Steingart KR, Menzies D, Schiller I, et al. Xpert MTB/RIF assay for the diagnosis of pulmonary tuberculosis in children: a systematic review and meta-analysis. Lancet Respir Med. 2015;3:451–61. https://doi.org/10.1016/S2213-2600(15)00095-8
29. Reid MJ, Saito S, Fayorsey R, Carter RJ, Abrams EJ. Assessing capacity for diagnosing tuberculosis in children in sub-Saharan African HIV care settings. Int J Tuberc Lung Dis. 2012;16:924–7. https://doi.org/10.5588/ijtld.11.0816
30. Seddon JA, Chiang SS, Esmail H, Coussens AK. The wonder years: what can primary school children teach us about immunity to Mycobacterium tuberculosis? Front Immunol. 2018;9:2946. https://doi.org/10.3389/fimmu.2018.02946
31. Marais BJ, Graham SM, Cotton MF, Beyers N. Diagnostic and management challenges for childhood tuberculosis in the era of HIV. J Infect Dis. 2007;196(Suppl 1):S76–85. https://doi.org/10.1086/518659
32. Braitstein P, Songok J, Vreeman RC, Wools-Kaloustian KK, Koskei P, Walusuna L, et al. "Wamepotea" (they have become lost): outcomes of HIV-positive and HIV-exposed children lost to follow-up from a large HIV treatment program in western Kenya. J Acquir Immune Defic Syndr. 2011;57:e40–6. https://doi.org/10.1097/QAI.0b013e3182167f0d
33. U.S. President's Emergency Plan for AIDS Relief. PEPFAR 2019 country operational plan guidance for all PEPFAR countries. 2019 [cited 2020 Apr 20]. https://www.state.gov/wp-content/uploads/2019/08/PEPFAR-Fiscal-Year-2019-Country-Operational-Plan-Guidance.pdf
34. World Health Organization. Package of care for children and adolescents with advanced HIV disease: stop AIDS. 2020 [cited 2020 Jul 10]. https://www.aidsdatahub.org/sites/default/files/resource/who-package-care-children-and-adolescents-advanced-hiv-disease-2020.pdf
35. Havlir DV, Kendall MA, Ive P, Kumwenda J, Swindells S, Qasba SS, et al.; AIDS Clinical Trials Group Study A5221. Timing of antiretroviral therapy for HIV-1 infection and tuberculosis. N Engl J Med. 2011;365:1482–91. https://doi.org/10.1056/NEJMoa1013607
36. García-Basteiro AL, Brew J, Williams B, Borgdorff M, Cobelens F. What is the true tuberculosis mortality burden? Differences in estimates by the World Health Organization and the Global Burden of Disease study. Int J Epidemiol. 2018;47:1549–60. https://doi.org/10.1093/ije/dyy144

Address for correspondence: Anna M. Mandalakas, Baylor College of Medicine, 1102 Bates St, Ste 630, Houston, TX 77030, USA; email: anna.mandalakas@bcm.edu

Human-Pathogenic Kasokero Virus in Field-Collected Ticks

Amy J. Schuh, Brian R. Amman, Ketan Patel, Tara K. Sealy, Robert Swanepoel, Jonathan S. Towner

Kasokero virus (KASV; genus *Orthonairovirus*) was first isolated in 1977 at Uganda Virus Research Institute from serum collected from *Rousettus aegyptiacus* bats captured at Kasokero Cave, Uganda. During virus characterization studies at the institute, 4 laboratory-associated infections resulted in mild to severe disease. Although orthonairoviruses are typically associated with vertebrate and tick hosts, a tick vector of KASV never has been reported. We tested 786 *Ornithodoros* (*Reticulinasus*) *faini* tick pools (3,930 ticks) for KASV. The ticks were collected from a large *R. aegyptiacus* bat roosting site in western Uganda. We detected KASV RNA in 43 tick pools and recovered 2 infectious isolates, 1 of which was derived from host blood–depleted ticks. Our findings suggest that KASV is maintained in an enzootic transmission cycle involving *O.* (*R.*) *faini* ticks and *R. aegyptiacus* bats and has the potential for incidental virus spillover to humans.

The genus *Orthonairovirus* (family *Nairoviridae*) comprises ≈40 viruses (*1*), including human pathogens such as Crimean-Congo hemorrhagic fever virus. The orthonairoviruses are assigned to 14 species (*1*), most of which have been associated with a single vertebrate subphylum (Vertebrata: bats, birds, rodents, shrews, or ungulates) and tick order (Ixodida: argasids or ixodids) (*2*). The species *Kasokero orthonairovirus* comprises 3 viruses isolated from bats belonging to the suborder Yinpterochiroptera (*3*,*4*) (Pteropodiformes) (*5*) in Africa, namely Yogue virus (YOGV; *Rousettus aegyptiacus*, Senegal), Leopards Hill virus (LPHV; *Hipposideros gigas*, Zambia), and Kasokero virus (KASV; *Rousettus aegyptiacus*, Uganda) (*2*,*6*,*7*).

KASV was first isolated in 1977 by scientists at Uganda Virus Research Institute (UVRI) from 2.7% (2/74) of serum samples collected from *R. aegyptiacus* bats captured at Kasokero Cave in Uganda (*6*). Two months after the KASV bat isolates were introduced to the UVRI laboratory and 3 weeks after the isolates were used in virus characterization assays, a laboratory staff member became ill. Shortly thereafter, 2 additional laboratory staff members became ill. Two of these laboratory staff members had participated in KASV characterization studies that involved virus antigen extraction and serologic testing; the third laboratory staff member had prepared KASV mouse brain suspensions for inoculation and examined virus-infected mice. Sixteen days after symptom onset in the index patient, a UVRI driver who reported no direct contact with the laboratory rooms used to handle the KASV isolates became ill. Manifestations ranged in severity from mild febrile illness to prolonged systemic disease characterized by fever, headache, myalgia, arthralgia, abdominal pain, nausea, diarrhea, chest pain, coughing, and hyperactive reflexes. Intracerebral inoculation of suckling mice with acute phase blood specimens collected from each of the 4 humans yielded a KASV isolate. KASV-specific antibodies were detected in serum from the 4 patients at various times after illness, as well as in 9.5% (10/105) of serum samples collected from other UVRI laboratory staff members and 67.6% (50/74) of the original *R. aegyptiacus* serum. In susceptibility studies, KASV killed suckling and adult mice by intracerebral and intraperitoneal inoculation within 8 days (*6*). In addition, nearly all naive adult mice that nursed KASV-inoculated suckling mice died of KASV infection, indicating horizontal transmission of virus infection.

The home range of *R. aegyptiacus* bats extends throughout sub-Saharan Africa; the bats prefer subterranean environments, such as caves or mines. At multiple locations, *Ornithodoros* (*Reticulinasus*) *faini* ticks (family Argasidae) (*8*) have been observed living within rock crevices and feeding on *R. aegyptiacus* bats (*9*–*13*). Although chiropteran ticks typically exhibit high host-specificity (*9*,*14*), miners, researchers, and other persons entering *R. aegyptiacus* bat roosts have reported being bitten by *O.* (*R.*) *faini* ticks (*13*).

Author affiliations: US Public Health Service Commissioned Corps, Rockville, Maryland, USA (A.J. Schuh); Centers for Disease Control and Prevention, Atlanta, Georgia, USA (A.J. Schuh, B.R. Amman, K. Patel, T.K. Sealy, J.S. Towner); University of Pretoria, Onderstepoort, South Africa (R. Swanepoel)

DOI: https://doi.org/10.3201/eid2612.202411

Because most orthonairoviruses have been associated with a tick host, *O.* (*R.*) *faini* ticks are likely to be involved in the enzootic transmission and maintenance of KASV and have the potential to be vectors for virus spillover into humans. In 1994 and 1995, KASV was isolated by 1 author (R.S.) from *O.* (*R.*) *faini* ticks collected in Lanner Gorge Cave (22.450°S, 31.150°E) in South Africa, where *R. aegyptiacus* bats roosted. The isolations were made by intracerebral inoculation of suckling mice and identified in cross-neutralization tests in mice using homologous and reference mouse antiserum and the prototype KASV UG Z-52969 isolate obtained from Yale Arbovirus Research Unit (New Haven, CT, USA) and methods described by Shope and Sather (*15*). At the time, KASV was considered a possible bunyavirus, and the isolations remained unpublished. No molecular studies were attempted, and the isolations are no longer available for sequencing. Members of the team that entered Lannar Gorge Cave were bitten by ticks, and in 2 team members, a moderately severe, transient febrile illness developed with headache, malaise, and myalgia a few days later; they refused to seek medical attention or to donate blood samples for virologic examination.

In this study, we tested 786 tick pools (3,930 total *O.* [*R.*] *faini* ticks) for KASV. We collected the ticks from a large *R. aegyptiacus* bat roosting site in western Uganda in 2013 and 2017.

Methods

Tick Collection and Processing

After obtaining approval from the Uganda Wildlife Authority, we collected adult and nymph *O.* (*R.*) *faini* ticks with forceps from rock crevices in Python Cave, Queen Elizabeth National Park, Uganda, over 4 days in April 2013 (*12*) and 1 day in September 2017. A chiropteran population consisting solely of ≈40,000 *R. aegyptiacus* bats inhabit the cave (*11*). Ticks collected in 2013 were pooled in groups of 5, placed directly into grinding vials (OPS Diagnostics, https://opsdiagnostics.com) containing 250 μL of a 1:1 ratio of MagMax Lysis Binding Solution Concentrate (Thermo Fisher Scientific, https://www.thermofisher.com) to 100% isopropanol (MagMax Lysis Binding Buffer) and then homogenized using the GenoGrinder 2000 (OPS Diagnostics). After we added 550 μL of MagMax Lysis Binding Buffer, we transferred the tick pool lysates to cryovials and stored them under liquid nitrogen (*12*).

Ticks collected in 2017, also pooled in groups of 5, were placed directly into cryovials containing Dulbecco's Modified Eagle Medium supplemented with 20% heat-inactivated fetal bovine serum (FBS) and antimicrobial drugs and then stored under liquid nitrogen. After thawing the tick pools, we transferred the contents to grinding vials, homogenized them using the GenoGrinder 2000, and then transferred them to a cryovial containing 250 μL of Dulbecco's Modified Eagle Medium supplemented with 2% heat-inactivated FBS and antimicrobial drugs. We transferred a portion of each tick pool homogenate (100-μL) into a 400-μL aliquot of MagMax Lysis Binding Buffer.

RNA Extraction and Quantitative Reverse Transcriptase PCR

We extracted RNA (90 μL) from the 2013 (800 μL) and 2017 (500 μL) tick pool lysates using the MagMax Pathogen RNA/DNA Kit on the MagMax Express-96 Deep Well Magnetic Particle Processor (Thermo Fisher Scientific). KASV has an 18.3-kb single-stranded, negative-sense, trisegmented RNA genome comprising large segment that encodes for the viral RNA-dependent RNA polymerase (RdRp), medium segment that encodes for the glycoprotein precursor (GP), and small segment that encodes for the nucleoprotein (N) (*2*). We analyzed RNA by quantitative reverse transcription PCR (qRT-PCR) using the SuperScript III Platinum One-Step qRT-PCR Kit (Thermo Fisher Scientific) with primers and probes (Appendix Table 1, https://wwwnc.cdc.gov/EID/article/26/12/20-2411-App1.pdf) targeting the KASV N gene, tick mitochondrial 16S ribosomal RNA (rRNA) gene (*16*), and eukaryotic 18S rRNA gene (Thermo Fisher Scientific; 2017 tick pools only). Relative KASV RNA copies/tick pool were interpolated from a standard curve generated from a serial dilution of a known concentration of a synthetic KASV RNA oligo.

KASV Infection Prevalence Calculations

We calculated maximum-likelihood estimates of KASV infection prevalence in individual ticks with exact 95% CIs using an online pooled prevalence calculator (https://epitools.ausvet.com.au). The calculator implemented a frequentist approach and assumed a fixed tick pool size (n = 5) and 100% KASV qRT-PCR sensitivity and specificity (*17*,*18*).

Virus Isolation and Immunofluorescence Assay

We attempted virus isolation on the four 2017 KASV RNA-positive tick pools. After clarifying the tick pool homogenates (650 μL) by centrifugation, we transferred 200 μL supernatant to a vial containing antimicrobials and incubated it at room temperature for 1 h. Monolayers of Vero E6 cells in 12-well plates were inoculated with 210 μL of antimicrobial-treated supernatant and incubated for 1 h at 37°C under 5%

CO_2. After the addition of 1.3 mL maintenance media, cultures were incubated at 37°C under 5% CO_2 and monitored daily for cytopathic effect. After 7 d, we transferred 1 mL culture media to a cryovial and replaced with an equal volume of fresh maintenance media. We transferred a portion of the day 7 media (100 µL) into MagMax Lysis Binding Buffer (400 µL) for RNA extraction and qRT-PCR. After 9–10 d, tissue cultures monolayers that were KASV RNA positive at day 7 were scraped to release virus-infected cells. Part of each cellular medium (1 mL) was suspended in 5 mL of borate saline, and 100 µL was placed into MagMax Lysis Binding Buffer (400 µL) for RNA extraction and qRT-PCR. After the cell suspensions were pelleted by centrifugation, the borate saline was decanted, the cells were resuspended in 500 µL borate saline, and 12-well spot slides were spotted with 25 µL of the cellular suspensions. The slides were fixed in acetone before receiving 2 megarads of γ-irradiation.

Six spots on each slide were incubated with 25 µL of a 1:100 dilution of KASV mouse immune ascitic fluid (World Reference Center for Emerging Viruses and Arboviruses, https://www.utmb.edu/gnl/research/wrceva), and the other 6 spots were incubated with normal mouse ascitic fluid for 30 min at 37°C. After the incubation, the spot slides were rinsed 2 times with phosphate buffered saline (PBS), incubated with 24 µL of a 1:40 dilution of goat anti-mouse fluorescein isothiocyanate (MP Biomedicals, https://www.mpbio.com) for 30 min at 37°C, rinsed with PBS, stained with Eriochrome Black T, rinsed with PBS, and then observed under a fluorescence microscope.

KASV Genome Sequencing

First-strand cDNA was synthesized directly from RNA extracted from 9 of the 2013 KASV RNA-positive tick pools using the qScript XLT cDNA SuperMix Kit (Quantabio, https://www.quantabio.com). KASV amplicons were generated from first-strand cDNA using the Q5 High-Fidelity 2X Master Mix (New England BioLabs, https://www.neb.com) and 6 multiplex pools of KASV-specific tiling primers (Appendix Table 2) that were designed using the Primal Scheme software (http://primal.zibraproject.org) (*19*). We prepared purified KASV amplicons for sequencing using the Accel-NGS 2S DNA Library Kit (Swift Biosciences, https://swiftbiosci.com). Indexed DNA libraries were pooled and then pair-end sequenced using a 500-cycle MiSeq Reagent Kit v2 on the MiSeq System (Illumina, https://www.illumina.com).

After thawing media collected from the two 2017 KASV isolates, we clarified the media by centrifugation and transferred 100 µL supernatant into 400 µL TriPure Isolation Reagent (MilliporeSigma, https://www.emdmillipore.com). We extracted RNA from the KASV isolate lysates using the 5PRIME Phase Lock Gel (Quantabio) system and then purified it using the Monarch Total RNA Miniprep Kit (New England Biolabs). We prepared purified RNA for sequencing using the NEB rRNA Depletion and NEBNext Ultra II RNA Library Kits for Illumina (New England Biolabs). Indexed DNA libraries were pooled and then pair-end sequenced using a 300-cycle MiSeq Reagent Kit v2 on the MiSeq System (Illumina).

Sequence and Phylogenetic Analyses

KASV sequence data were imported into Geneious 11.1.2 (Biomatters, https://www.geneious.com). After removing KASV-specific primers from the sequences (2013 tick pools), we used BBDuk to trim adaptors and low-quality reads from both sequence ends (minimum quality 30). Long sequence reads were retained (>93% of maximum read length) and normalized to a target coverage level of 40 with a minimum depth of 2. Merged reads were mapped to the concatenated genome sequence of the KASV Z-52963 isolate using the Geneious mapper (minimum mapping quality 30), and consensus sequences were then extracted and parsed according to gene.

We used the MUSCLE algorithm (https://www.ebi.ac.uk/Tools/msa/muscle) to generate N, GP, and RdRp nucleotide and deduced amino acid alignments from the new KASV sequences and existing KASV, YOGV, and LPHV sequences. We constructed maximum-likelihood phylogenies using the PhyML 3.0 algorithm (*20*) in conjunction with the best-fit nucleotide substitution model (*21*) on the ATGC Montpellier Bioinformatics Platform (http://www.atgc-montpellier.fr). We visualized phylogenies using TreeGraph 2 (http://treegraph.bioinfweb.info) (*22*). We estimated the global ratio of the rate of nonsynonymous (d_N) nucleotide substitutions to the rate of synonymous (d_S) nucleotide substitutions (d_N:d_S) across the KASV nucleotide alignments using the fixed effects likelihood method with the HyPhy version 1.8.2 software (https://www.hyphy.org).

Results

Description of the *O.* (*R.*) *faini* Tick Collections

We collected 3,125 *O.* (*R.*) *faini* ticks (625 pools of 5 each) from the rock crevices within *R. aegyptiacus* bat roosting sites in Python Cave, Uganda, in 2013 and 975 *O.* (*R.*) *faini* ticks (195 pools of 5 each) from the same location in 2017. We confirmed the *O.* (*R.*) *faini* species designation by comparative genetic analysis

of the 16S rRNA gene of a set of ticks and by morphologic examination (*12*). Screening the *O.* (*R.*) *faini* tick pools for the tick-specific 16S rRNA gene revealed that 4.3% (27/625) of the 2013 pools and 3.6% (7/195) of the 2017 pools were negative, indicating that these samples contained RNA inhibitors and were unsuitable for downstream KASV qRT-PCR analysis.

Detection of KASV RNA in Ticks

We detected KASV RNA in 39/598 of the 2013 *O.* (*R.*) *faini* tick pools and 4/188 of the 2017 *O.* (*R.*) *faini* tick pools, resulting in maximum-likelihood estimates of KASV infection prevalence at the individual tick level of 1.34% (95% CI 0.94%–1.83%) and 0.43% (95% CI 0.12%–1.10%), respectively. Based off a standard curve using synthetic KASV RNA, the mean KASV load of the positive 2013 tick pools was 5.5 (range 0.6–7.0) $\log_{10}$ RNA copies, and the mean KASV load of the positive 2017 tick pools was 7.1 (range 1.5–7.6) $\log_{10}$ RNA copies (Figure 1).

Isolation of Infectious KASV from Ticks

We isolated infectious KASV from 50% (2/4) of the 2017 KASV RNA-positive tick pools. As expected, the 2 KASV isolates were derived from the tick pools with the highest KASV RNA loads (UGA-Tick-20170048: 7.6 $\log_{10}$ RNA copies and UGA-Tick-20170128: 7.0 $\log_{10}$RNA copies) (Figure 1). A qRT-PCR targeting the eukaryotic 18S rRNA gene was used to screen the KASV-isolation positive tick pools for *R. aegyptiacus* blood. We found no trace of *R. aegyptiacus* blood in tick pool UGA-Tick-20170048, indicating that the 5 ticks in this pool had not recently taken a blood meal from an actively KASV-infected *R. aegyptiacus* bat. This finding suggests that KASV in this tick pool resulted from active virus replication in ≥1 tick.

Circulation of Genetically Diverse KASVs

We attempted genomic sequencing on 9 of the 2013 KASV RNA-positive tick pools with KASV loads ≥3.6 $\log_{10}$ RNA copies and on the two 2017 KASV tick isolates. We obtained complete sequence coverage for the N (1,545 nt) for 11 of the KASV-positive tick pools, the GP (4,314 nt) for 4 of the KASV-positive tick pools, and the RdRp (11,919 nt) genes for 4 of the KASV-positive tick pools. Maximum-likelihood phylogenies constructed from N, GP, and RdRp gene sequences from the 2013 and 2017 KASV-positive tick pools, as well as prototype KASV (Z-52963, *R. aegyptiacus*, Uganda, 1977), YOGV (DakAnD 56, *R. aegyptiacus*, Senegal, 1968), and LPHV (11SB17, *H. gigas*, Zambia, 2011) isolate sequences, had similar topologies and virus species groupings (Figure 2). Consistent with

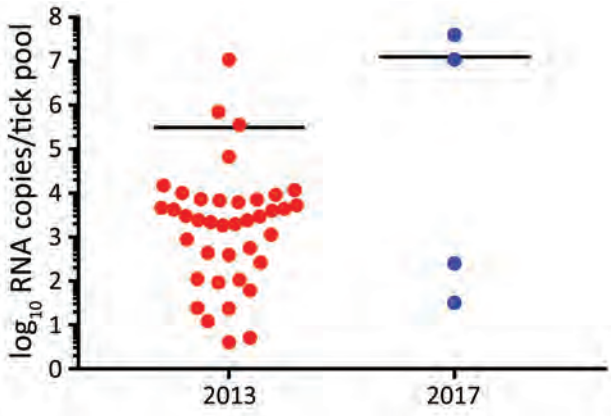

Figure 1. Kasokero virus RNA loads in *Ornithodoros* (*Reticulinasus*) *faini* tick pools from *Rousettus aegyptiacus* bats, western Uganda, 2013 and 2017. Black horizontal bars represent mean viral loads.

previous results (*2*,*23*,*24*), YOGV diverged first followed by LPHV, and finally the KASV lineage. The N phylogeny showed 2 distinct KASV lineages defined by >9.2% interlineage nucleotide divergences, and the RdRp phylogeny showed 2 distinct KASV lineages defined by ≥12.0% interlineage nucleotide divergences; the first lineage included the prototype Z-52963 sequence plus the 2013 tick sequences and the second lineage included the 2017 tick sequences (Appendix Tables 3, 4). Deduced amino acid alignments of the N and RdRp proteins revealed that most KASV lineage-defining nucleotide substitutions were synonymous with interlineage amino acid divergences ranging from 0.6% to 1.0% for the N protein and 2.4% to 2.6% for the RdRp protein. In contrast to the N and RdRp phylogenies, the GP phylogeny shows that the Z-52963 sequence diverged first, followed by the divergence of the 2013 and the 2017 tick sequence groups. Furthermore, the KASV sequences in the GP phylogeny are considerably more similar to one another at the nucleotide level (≤2.2% nt divergence and ≤0.9% aa divergence) and do not form 2 distinct lineages (Appendix Table 5). Consistent with the phylogenetic and KASV gene/protein divergence data, d_N:d_S estimates demonstrated that the N gene was under the strongest purifying selection (0.0110), followed by the RdRp (0.0264) and GP (0.0650) genes.

Discussion

We detected KASV RNA in 43 *O.* (*R.*) *faini* tick pools collected from a large *R. aegyptiacus* bat colony at Python Cave, Uganda, over a 4-year span. The mean KASV RNA load for the 39 positive 2013 tick pools stored in MagMax Lysis Binding Buffer was lower (5.5 [range 0.6–7.0] log10 RNA copies) than the 4 positive 2017 tick

pools stored in sterile media supplemented with FBS and antimicrobial drugs (7.1 [range 1.5–7.6] log10 RNA copies). Although this difference might have resulted from the choice of sample preservation buffer, it could also be attributed to the type of storage vial (internally threaded for 2017 ticks vs. externally threaded for 2013 ticks), number of RNA freeze-thaw cycles (0 for 2017 ticks vs. 1 for 2013 ticks), month of tick collection in relation to the natural history of KASV infection in *O.* (*R.*) *faini* ticks (September for ticks collected in 2017 vs. April for ticks collected in 2013), or sample size effect (39 KASV-positive tick pools in 2013 vs. 4 KASV-positive tick pools in 2017). We could not attempt virus isolation on the 2013 KASV-positive tick pools because they were placed directly in virucidal buffer; however, we isolated infectious KASV from 2 of the 2017 KASV RNA-positive tick pools. Importantly, molecular evidence of *R. aegyptiacus* blood was not detected in 1 of the KASV isolation-positive tick pools. This finding indicates that the presence of infectious KASV in this tick pool resulted from active virus replication in ≥1 tick and not from ingestion of a recent blood meal by a tick feeding on a viremic *R. aegyptiacus* bat. Although we did not assess whether KASV can disseminate to the salivary glands of *O.* (*R.*) *faini* ticks and then be successfully transmitted to *R. aegyptiacus* bats, our data coupled with the results of a previous study demonstrating a 2.7% prevalence of active KASV infection and a 67.6% KASV seroprevalence in *R. aegyptiacus* captured at Kasokero Cave, Uganda (*6*), suggest that this virus is maintained in an enzootic transmission cycle involving *R. aegyptiacus* bats and *O.* (*R.*) *faini* ticks. The isolation of KASV from *O.* (*R.*) *faini* ticks collected from a *R. aegyptiacus* bat roost in Lanner Gorge Cave, South Africa, in 1994–1995 (R. Swanepoel, unpub. data) supports this notion and suggests that KASV has a widespread geographic distribution. Tick transmission of KASV also is consistent with our knowledge

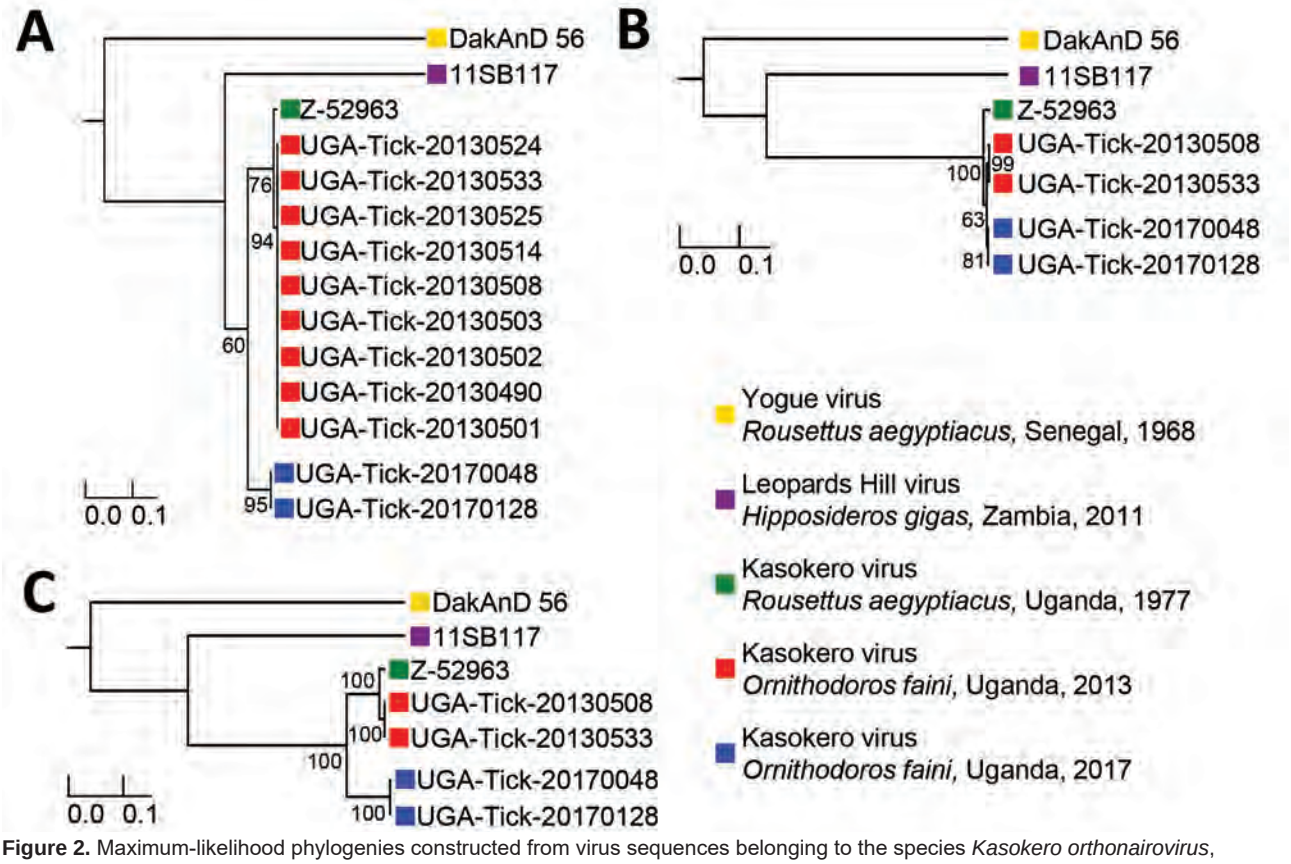

Figure 2. Maximum-likelihood phylogenies constructed from virus sequences belonging to the species *Kasokero orthonairovirus*, including viruses collected from *Ornithodoros* (*Reticulinasus*) *faini* tick pools from *Rousettus aegyptiacus* bats, western Uganda, 2013 and 2017. The midpoint rooted phylogenies were generated from complete nucleoprotein (N) (A), glycoprotein precursor (GP) (B), and RNA-dependent RNA-polymerase (RdRp) (C) gene sequences. The N and RdRp gene phylogenies were generated using the general time-reversible nucleotide substitution model with the addition of invariant sites, and the GP gene phylogeny was generated using the general time-reversible nucleotide substitution model with a gamma distribution of rates across sites. Horizontal branch lengths are proportional to the genetic distance between the sequences. Numbers at the end of the branches represent percent bootstrap values based on 1,000 replicates. Only percent bootstrap values ≥50% are shown. GenBank accession numbers for the new Kasokero virus tick sequences from this study are MT309080–98. Scale bars indicate nucleotide substitutions per site.

of the vector status of the orthonairoviruses (*2*). Of the 14 currently recognized orthonairovirus species (*1*), 13 have now been associated with a tick host.

Genetic analysis of the KASV nucleotide alignment showed that the N and RdRp gene sequences were highly divergent, whereas the GP gene sequences were highly conserved. However, the low d_N:d_S estimates, together with the high level of conservation between the deduced amino acid sequences for the N, GP, and RdRp proteins, suggest that strong purifying selection purged deleterious mutations. This finding is consistent with findings of previous studies demonstrating that arbovirus evolution is constrained to enable alternating infection of disparate vertebrate and arthropod hosts (*25*–*27*).

Additional work is needed to fully understand the roles that *R. aegyptiacus* bats and *O.* (*R.*) *faini* ticks play in maintaining KASV over time (*9*). Collection and separation of *O.* (*R.*) *faini* ticks according to life history stage, as well as experimental tick work, will be important in determining whether these ticks serve as amplification or reservoir hosts for KASV. Detection of infectious KASV in larval, nymphal, and adult stages of *O.* (*R.*) *faini* ticks would suggest that the virus is transtadially transmitted, and ticks serve as virus amplification hosts. Likewise, detection of KASV in nymphs and adults originating from KASV-artificially infected *O.* (*R.*) *faini* larvae would suggest the virus is transtadially transmitted from one generation to the next. Isolation of KASV in *O.* (*R.*) *faini* eggs found in nature or in larvae originating from KASV-artificially infected female ticks would indicate that the virus is transovarially transmitted and that ticks are reservoir hosts for the virus because a vertebrate host is not required for long-term virus survival. Similarly, a longitudinal ecologic investigation of KASV infection in *R. aegyptiacus* bats, as well as experimental KASV infection of captive bats, is critical in defining the relationship this virus has with its vertebrate host. Although KASV has previously been isolated from 2 wild-caught *R. aegyptiacus* bats (*6*), the isolation of actively replicating KASV over several days in experimentally infected *R. aegyptiacus* bats will confirm the ability of this bat species to serve as an amplification host for the virus. The detection of KASV in oral, rectal, or urogenital shedding collected from experimentally infected or wild-caught *R. aegyptiacus* bats will not only provide evidence that these bats are reservoir hosts of the virus but also indicate that they are capable of transmitting the virus to humans that encroach upon their habitat.

Although no human cases of KASV infection have been reported since the initial UVRI-associated cases described in 1977 (*6*), surveillance of populations at risk for KASV infection has never been conducted. Miners, herders, tourists, and researchers often frequent mines and caves occupied by large colonies of *R. aegyptiacus* bats. Entry into *R. aegyptiacus* bat–inhabited environments has been linked to the spillover of several pathogenic agents into the human population, including Marburg virus (*11*,*28*,*29*), Sosuga virus (*30*,*31*), and *Borrelia* spirochetes (*13*). Similarly, humans who enter environments occupied by *R. aegyptiacus* bats and *O.* (*R.*) *faini* ticks are likely to be at risk for KASV infection. Surveillance of these at-risk populations for evidence of active or past infection KASV infection is needed to determine the true burden of KASV infection in humans.

Acknowledgments

We thank Margret Driciru and the Uganda Wildlife Authority rangers at Python Cave in Queen Elizabeth National Park for providing support during the tick collections and Shannon Whitmer for providing Illumina sequencing advice. We are grateful to Kenneth Plante, Scott Weaver, Nikos Vasilakis, Robert Tesh, and Thomas Ksiazek for providing the KASV Z-52963 isolate and KASV mouse immune ascitic fluid from the World Reference Center for Emerging Viruses and Arboviruses.

This work was funded in part through an interagency agreement with the Defense Threat Reduction Agency, HDTRA16-025-33037.

About the Author

Dr. Schuh is a research scientist with the Viral Special Pathogens Branch, Division of High-Consequence Pathogens and Pathology, National Center for Emerging and Zoonotic Infectious Diseases, Centers for Disease Control and Prevention. Her research interests include investigating the enzootic transmission dynamics of tickborne and batborne viruses and identifying ecologic drivers underlying the spillover of zoonotic viruses into the human population.

References

1. Maes P, Adkins S, Alkhovsky SV, Avšič-Županc T, Ballinger MJ, Bente DA, et al. Taxonomy of the order *Bunyavirales*: second update 2018. Arch Virol. 2019;164:927–41. https://doi.org/10.1007/s00705-018-04127-3
2. Walker PJ, Widen SG, Firth C, Blasdell KR, Wood TG, Travassos da Rosa AP, et al. Genomic characterization of Yogue, Kasokero, Issyk-Kul, Keterah, Gossas, and Thiafora viruses: nairoviruses naturally infecting bats, shrews, and ticks. Am J Trop Med Hyg. 2015;93:1041–51. https://doi.org/10.4269/ajtmh.15-0344
3. Springer MS. Phylogenetics: bats united, microbats divided. Curr Biol. 2013;23:R999–1001. https://doi.org/10.1016/j.cub.2013.09.053

4. Lei M, Dong D. Phylogenomic analyses of bat subordinal relationships based on transcriptome data. Sci Rep. 2016;6:27726. https://doi.org/10.1038/srep27726
5. Hutcheon JM, Kirsch JAW. A moveable face: deconstructing the Microchiroptera and a new classification of extant bats. Acta Chiropt. 2006;8:1–10. https://doi.org/10.3161/1733-5329(2006)8[1:AMFDTM]2.0.CO;2
6. Kalunda M, Mukwaya LG, Mukuye A, Lule M, Sekyalo E, Wright J, et al. Kasokero virus: a new human pathogen from bats (*Rousettus aegyptiacus*) in Uganda. Am J Trop Med Hyg. 1986;35:387–92. https://doi.org/10.4269/ajtmh.1986.35.387
7. Ishii A, Ueno K, Orba Y, Sasaki M, Moonga L, Hang'ombe BM, et al. A nairovirus isolated from African bats causes haemorrhagic gastroenteritis and severe hepatic disease in mice. Nat Commun. 2014;5:5651. https://doi.org/10.1038/ncomms6651
8. Mans BJ, Featherston J, Kvas M, Pillay K-A, de Klerk DG, Pienaar R, et al. Argasid and ixodid systematics: implications for soft tick evolution and systematics, with a new argasid species list. Ticks Tick Borne Dis. 2019;10:219–40. https://doi.org/10.1016/j.ttbdis.2018.09.010
9. Hoogstraal H. Argasid and nuttalliellid ticks as parasites and vectors. Adv Parasitol. 1985;24:135–238. https://doi.org/10.1016/S0065-308X(08)60563-1
10. Braack LEO. Arthropod inhabitants of a tropical cave 'island' environment provisioned by bats. Biol Conserv. 1989;48:77–84. https://doi.org/10.1016/0006-3207(89)90027-X
11. Amman BR, Carroll SA, Reed ZD, Sealy TK, Balinandi S, Swanepoel R, et al. Seasonal pulses of Marburg virus circulation in juvenile *Rousettus aegyptiacus* bats coincide with periods of increased risk of human infection. PLoS Pathog. 2012;8:e1002877. https://doi.org/10.1371/journal.ppat.1002877
12. Schuh AJ, Amman BR, Apanaskevich DA, Sealy TK, Nichol ST, Towner JS. No evidence for the involvement of the argasid tick *Ornithodoros faini* in the enzootic maintenance of Marburgvirus within Egyptian rousette bats *Rousettus aegyptiacus*. Parasit Vectors. 2016;9:128. https://doi.org/10.1186/s13071-016-1390-z
13. Qiu Y, Nakao R, Hang'ombe BM, Sato K, Kajihara M, Kanchela S, et al. Human borreliosis caused by a New World relapsing fever *Borrelia*-like organism in the Old World. Clin Infect Dis. 2019;69:107–12. https://doi.org/10.1093/cid/ciy850
14. Sándor AD, Corduneanu A, Péter Á, Mihalca AD, Barti L, Csősz I, et al. Bats and ticks: host selection and seasonality of bat-specialist ticks in eastern Europe. Parasit Vectors. 2019;12:605. https://doi.org/10.1186/s13071-019-3861-5
15. Shope RE, Sather GE. Diagnostic procedures for viral, rickettsial and chlamydial infections. In: Schmidt NJ, Lennette EH, editors. Arboviruses. 5th ed. Washington (DC): American Public Health Association; 1979. p. 767–814.
16. Shone SM, Dillon HJ, Hom SS, Delgado N. A novel real-time PCR assay for the speciation of medically important ticks. Vector Borne Zoonotic Dis. 2006;6:152–60. https://doi.org/10.1089/vbz.2006.6.152
17. Cowling DW, Gardner IA, Johnson WO. Comparison of methods for estimation of individual-level prevalence based on pooled samples. Prev Vet Med. 1999;39:211–25. https://doi.org/10.1016/S0167-5877(98)00131-7
18. Andreassen A, Jore S, Cuber P, Dudman S, Tengs T, Isaksen K, et al. Prevalence of tick borne encephalitis virus in tick nymphs in relation to climatic factors on the southern coast of Norway. Parasit Vectors. 2012;5:177. https://doi.org/10.1186/1756-3305-5-177
19. Quick J, Grubaugh ND, Pullan ST, Claro IM, Smith AD, Gangavarapu K, et al. Multiplex PCR method for MinION and Illumina sequencing of Zika and other virus genomes directly from clinical samples. Nat Protoc. 2017;12:1261–76. https://doi.org/10.1038/nprot.2017.066
20. Guindon S, Dufayard JF, Lefort V, Anisimova M, Hordijk W, Gascuel O. New algorithms and methods to estimate maximum-likelihood phylogenies: assessing the performance of PhyML 3.0. Syst Biol. 2010;59:307–21. https://doi.org/10.1093/sysbio/syq010
21. Lefort V, Longueville JE, Gascuel O. SMS: Smart Model Selection in PhyML. Mol Biol Evol. 2017;34:2422–4. https://doi.org/10.1093/molbev/msx149
22. Stöver BC, Müller KF. TreeGraph 2: combining and visualizing evidence from different phylogenetic analyses. BMC Bioinformatics. 2010;11:7. https://doi.org/10.1186/1471-2105-11-7
23. Walker PJ, Widen SG, Wood TG, Guzman H, Tesh RB, Vasilakis N. A global genomic characterization of nairoviruses identifies nine discrete genogroups with distinctive structural characteristics and host-vector associations. Am J Trop Med Hyg. 2016;94:1107–22. https://doi.org/10.4269/ajtmh.15-0917
24. Aguilar PV, Marciel de Souza W, Silvas JA, Wood T, Widen S, Fumagalli MJ, et al. Genetic characterization of the Patois serogroup (genus *Orthobunyavirus*; family *Peribunyaviridae*) and evidence that Estero Real virus is a member of the genus *Orthonairovirus*. Am J Trop Med Hyg. 2018;99:451–7. https://doi.org/10.4269/ajtmh.18-0201
25. Coffey LL, Vasilakis N, Brault AC, Powers AM, Tripet F, Weaver SC. Arbovirus evolution in vivo is constrained by host alternation. Proc Natl Acad Sci U S A. 2008;105:6970–5. https://doi.org/10.1073/pnas.0712130105
26. Vasilakis N, Deardorff ER, Kenney JL, Rossi SL, Hanley KA, Weaver SC. Mosquitoes put the brake on arbovirus evolution: experimental evolution reveals slower mutation accumulation in mosquito than vertebrate cells. PLoS Pathog. 2009;5:e1000467. https://doi.org/10.1371/journal.ppat.1000467
27. Grubaugh ND, Rückert C, Armstrong PM, Bransfield A, Anderson JF, Ebel GD, et al. Transmission bottlenecks and RNAi collectively influence tick-borne flavivirus evolution. Virus Evol. 2016;2:vew033. https://doi.org/10.1093/ve/vew033
28. Swanepoel R, Smit SB, Rollin PE, Formenty P, Leman PA, Kemp A, et al.; International Scientific and Technical Committee for Marburg Hemorrhagic Fever Control in the Democratic Republic of Congo. Studies of reservoir hosts for Marburg virus. Emerg Infect Dis. 2007;13:1847–51. https://doi.org/10.3201/eid1312.071115
29. Towner JS, Amman BR, Sealy TK, Carroll SA, Comer JA, Kemp A, et al. Isolation of genetically diverse Marburg viruses from Egyptian fruit bats. PLoS Pathog. 2009;5:e1000536. https://doi.org/10.1371/journal.ppat.1000536
30. Amman BR, Albariño CG, Bird BH, Nyakarahuka L, Sealy TK, Balinandi S, et al. A recently discovered pathogenic paramyxovirus, Sosuga virus, is present in *Rousettus aegyptiacus* fruit bats at multiple locations in Uganda. J Wildl Dis. 2015;51:774–9. https://doi.org/10.7589/2015-02-044
31. Albariño CG, Foltzer M, Towner JS, Rowe LA, Campbell S, Jaramillo CM, et al. Novel paramyxovirus associated with severe acute febrile disease, South Sudan and Uganda, 2012. Emerg Infect Dis. 2014;20:211–6. https://doi.org/10.3201/eid2002.131620

Address for correspondence: Jonathan S. Towner, Centers for Disease Control and Prevention, 1600 Clifton Rd NE, Mailstop H18-B, Atlanta, GA 30329-4027, USA; email: jit8@cdc.gov

Characterization and Source Investigation of Multidrug-Resistant *Salmonella* Anatum from a Sustained Outbreak, Taiwan

Ye Feng, Yi-Jung Chang, Shih-Chuan Pan, Lin-Hui Su, Hsin-Chieh Li, Hsin-Ping Yang, Min-Jia Yu, Cheng-Hsun Chiu

An ongoing outbreak of multidrug-resistant *Salmonella enterica* serovar Anatum began in Taiwan in 2015. Pork and poultry were identified as vehicles for transmission. Contaminated meat contributed to the high rate of infections among children. Nearly identical *Salmonella* Anatum strains have been identified in the United Kingdom, the United States, and the Philippines.

Nontyphoidal *Salmonella* (NTS) is a major cause for foodborne diseases worldwide. In Taiwan, the ambient climate and flourishing pig-raising industry makes NTS infections rampant. As in other countries, salmonellosis was primarily caused by *Salmonella enterica* serovars Enteritidis and Typhimurium in Taiwan (*1*), but rare serovars such as *Salmonella* Goldcoast have appeared in recent years (*2*). Recommended antimicrobial treatment options for salmonellosis include fluoroquinolones and extended-spectrum cephalosporins (*1*). However, resistance to these antibiotics has been emerging in many countries, leading to increased disease prevalence, disease severity, and death and the requirement of last-line antimicrobial drugs (e.g., carbapenems) (*3*–*5*).

Author affiliations: Sir Run Run Shaw Hospital, Zhejiang University School of Medicine, Hangzhou, China (Y. Feng); Institute for Translational Medicine, Zhejiang University School of Medicine, Hangzhou (Y. Feng); Key Laboratory of Microbial Technology and Bioinformatics of Zhejiang Province, Hangzhou (Y. Feng); Division of Pediatric Infectious Diseases, Chang Gung Memorial Hospital, Chang Gung University College of Medicine, Taoyuan (Y.-J. Chang, S.-C. Pan, C.-H. Chiu); Molecular Infectious Disease Research Center, Chang Gung Memorial Hospital, Chang Gung University College of Medicine, Taoyuan, Taiwan (Y.-J. Chang, L.-H. Su, H.-C. Li, H.-P. Yang, M.-J. Yu, C.-H. Chiu)

DOI: https://doi.org/10.3201/eid2612.200147

Since 2015, northern Taiwan has seen an increase in *Salmonella* infections, caused by previously rare *Salmonella* Anatum. The infections were also reported in central Taiwan, indicating that this outbreak had already prevailed throughout the entire island (*6*). Co-resistance to ceftriaxone and ciprofloxacin are the main feature of the outbreak clone. Evidence from epidemiologic, laboratory, and supply-chain investigations identified raw pork and poultry as the vehicle for spread of this strain. More important, genomic comparisons against the global public database indicated that this clone has appeared in Europe, Asia, and America. Given the increasing globalization of foodstuffs, these findings prompt an urgent global sharing of whole-genome sequencing (WGS) data to facilitate disease surveillance and early recognition of international foodborne outbreaks (*7*,*8*).

The Study

Chang Gung Memorial Hospital is a main referral hospital for cities in northern Taiwan, including Taipei, New Taipei, and Taoyuan. The population in this region is ≈7 million. In 2012, the hospital's clinical microbiology laboratory launched a program to monitor the NTS serovars causing human infections. All *Salmonella* isolates from patients were collected and serotyped. Before 2015, very few *Salmonella* Anatum isolates were recovered, and most were susceptible to antimicrobial agents. Since then, an increase has been observed, peaking in 2017 (Figure 1, panel A). As of June 2019, a total of 319 nonrepetitive isolates have been identified; of these, 197 (61.8%) isolates were ceftriaxone-resistant (MIC ≥2 μg/mL), 301 (94.4%) were ciprofloxacin-resistant (MIC ≥0.12 μg/mL), and 197 (61.8%) were resistant to both. In addition, 292 (91.5%) isolates were resistant to chloramphenic, and 295 (92.5%) were resistant to trimethoprim/

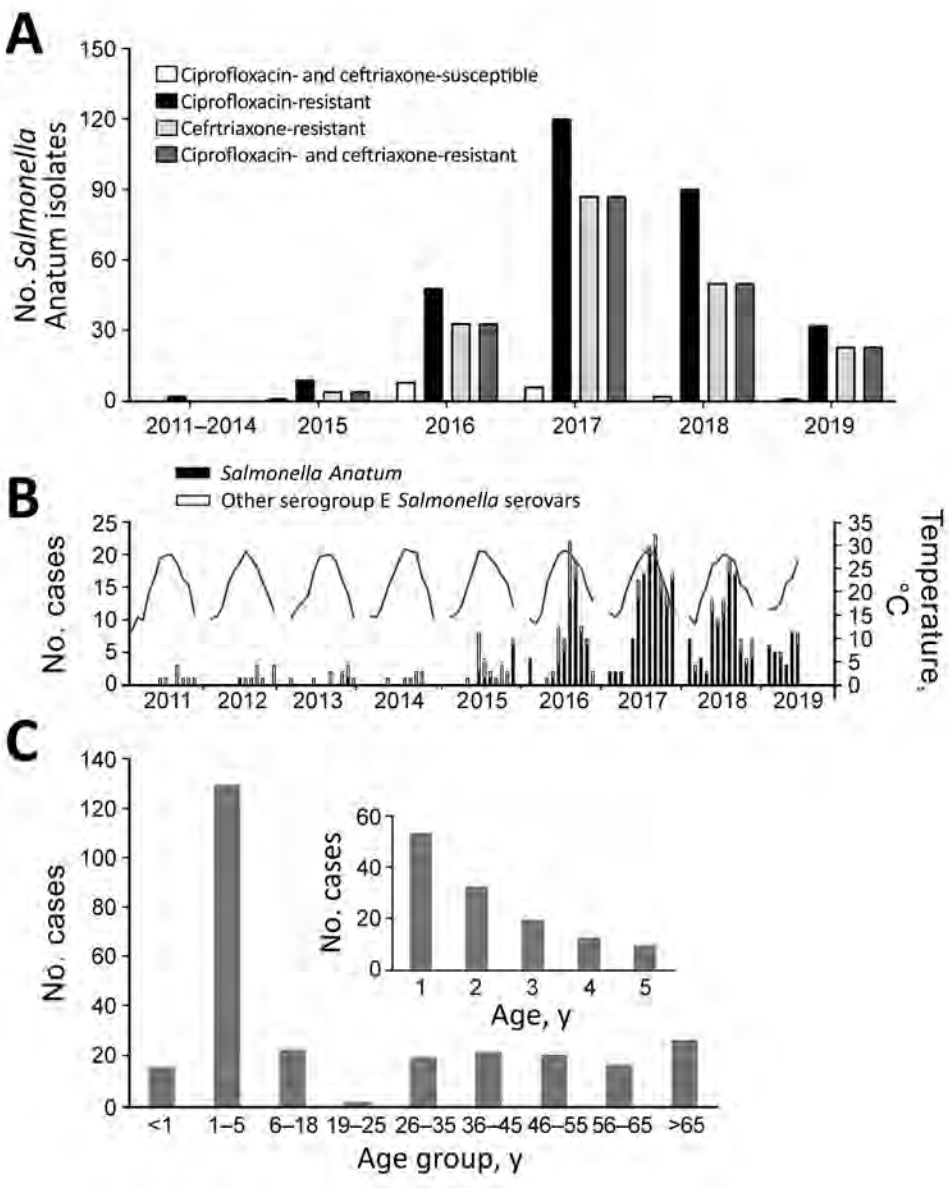

Figure 1. *Salmonella enterica* serotype Anatum infection and antimicrobial resistance, Taiwan. A) Antimicrobial resistance of the *Salmonella* Anatum isolates collected in Chang Gung Memorial Hospital. B) Monthly case number (bar plot) and temperature (line). C) Age distribution of patients diagnosed during 2015–2018.

sulfamethoxazole. A positive correlation was found between higher temperatures and the infections (r = 0.4; p<0.05) (Figure 1, panel B); however, no notable effects on *Salmonella.* Anatum infections have been associated with precipitation or humidity (r<0.3; p>0.05).

Detailed methods are described in the Appendix (https://wwwnc.cdc.gov/EID/article/26/12/20-0147-App1.pdf). We first reviewed the clinical and laboratory characteristics of 278 patients from 2015–2018. Most patients had acute gastroenteritis, whereas a few (14/278, 5%) had invasive diseases, such as bacteremia and sepsis. In terms of age distribution, the highest number of cases were in young children (Figure 1, panel C). Pediatric patients (n = 169) had significantly higher rates than adult patients (n = 109) for hospitalization (79.2% vs. 55.0%; p<0.05), diarrhea (89.9% vs. 68.8%; p<0.05), and fever (89.2% vs. 58.1%; p<0.05).

Multilocus sequence typing indicated that the entire collection of clinical *Salmonella* Anatum isolates belonged to sequence type 64. We randomly selected 54 clinical isolates for WGS (Appendix Table 1). Both core genome multilocus sequence typing and whole-genome single-nucleotide polymorphism analyses, performed by using the BacWGSTdb database (*9*), further divided these isolates into 3 clades (Figure 2, panel A, B). Clades I and II were more closely related to each other; their most recent common ancestor occurred >21 years ago.

Clade III was more distantly connected to these 2 clades. Typing based on PCR assay was performed on the unsequenced isolates. Clade I accounted for 95.6% (305/319) of all isolates, suggesting it was the cause of the outbreak. The isolates resistant to ceftriaxone, ciprofloxacin, or both clustered within clade I, whereas the isolates of clades II and III were more susceptible. Most of the clade I isolates harbored a 90-kb IncA/C plasmid carrying *bla*DHA-1 (encoding a class C β-lactamase) and *qnrB* (conferring resistance to quinolones). A conjugation assay demonstrated that this plasmid conferred ceftriaxone and ciprofloxacin resistance. In addition, 31 (9.7%) clinical isolates carried bla_{CMY-2}, which was located within a >100-kb IncI1 plasmid and also encoded a class C β-lactamase. These 31 isolates carried bla_{DHA-1} simultaneously. In 11 of them, the bla_{DHA-1}–carrying and bla_{CMY-2}–carrying plasmids were fused into 1 large plasmid (Figure 2, panel C).

By comparing these findings against sequences in GenBank, we found nearly identical genomic sequences for isolates in the United Kingdom, the

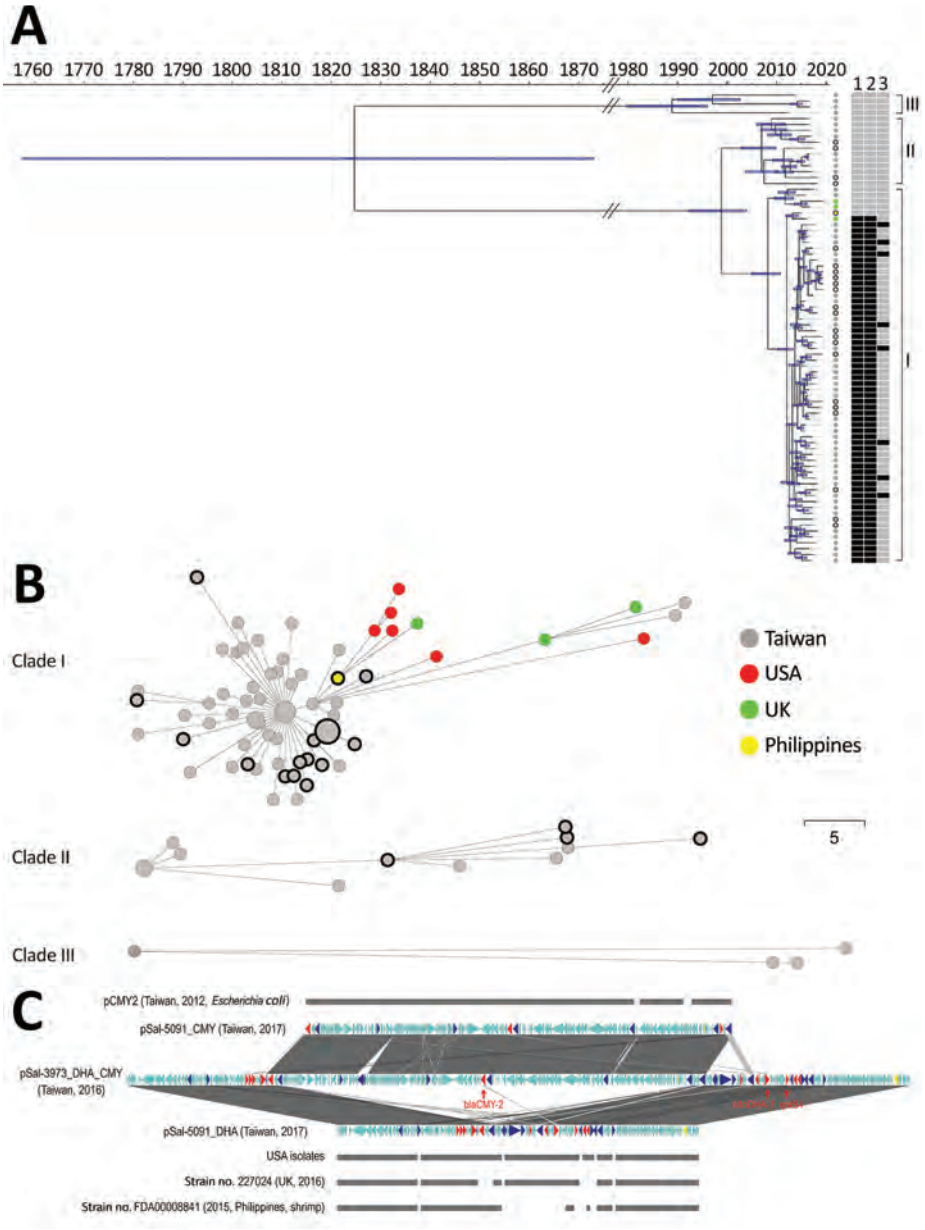

Figure 2. Genomic analysis of the outbreak caused by *Salmonella enterica* serotype Anatum, Taiwan. A) Dated phylogeny for *Salmonella* Anatum clinical isolates and food and environmental isolates. All isolates were divided into 3 clades, shown at right. The nodes' colors represent the geo source; nodes with black rings were from meat or the environment, and the remainder were derived from the patients. The right heatmap represents the presence (in black) or absence (in gray) of key antimicrobial-resistance genes (1, bla_{DHA-1}; 2, *qnrB4*; 3, bla_{CMY-2}). B) Minimal spanning tree based on alleles identified through core genome multilocus sequence typing. Dots with black circles represent food isolates; the others are clinical isolates. The collection date for the 6 US isolates in panel B was missing in GenBank and therefore not included in panel A. Scale bar indicates 5 single nucleotide polymorphisms. C) Gene structure of multidrug-resistant plasmids in *Salmonella* Anatum in Taiwan compared with international isolates. Two types of plasmids were identified in the clade I *Salmonella.* Anatum isolates in Taiwan. One carried bla_{CMY-2}, with its structure being shown by pSal-5091_CMY. A similar plasmid, pCMY2 (GenBank accession no. LC019731.1), is shown. The other carried bla_{DHA-1}; its structure is shown by pSal-5091_DHA. International isolates shown in the figure, whose genomes also were downloaded from GenBank (Appendix Table 1, https://wwwnc.cdc.gov/EID/article/26/12/20-0147-App1.pdf), possess very similar plasmids. In certain isolates, the 2 plasmids can integrate into 1 large plasmid, with its structure shown by pSal-3973_DHA_CMY. Red genes represent antimicrobial-resistance genes; blue genes represent transposase/integrase genes; and yellow genes represent Inc-determinant genes.

United States, and the Philippines. The collection time for these isolates also occurred during 2015–2019, which nearly coincided with the outbreak in Taiwan. These international *Salmonella* Anatum isolates also carried the 90-kb IncA/C plasmid (Figure 2, panel A, C); therefore, they were likely ceftriaxone- and ciprofloxacin-resistant concomitantly. The only distinction of these international isolates was their lack of the bla_{CMY-2}–carrying plasmid. Accordingly, we speculated that the *Salmonella* Anatum clone had arrived in Taiwan through food trade and later acquired the bla_{CMY-2}–carrying plasmid.

To trace the source of *Salmonella* Anatum, we investigated food samples from supermarkets and traditional markets of 8 districts with high density of *Salmonella* patients in New Taipei City and Taoyuan City, Taiwan (Appendix Figure 1). A total of 11 *Salmonella* Anatum isolates were collected from pork, 4 from poultry, and 1 from beef in these regions (Appendix Table 2, Figure 1). WGS showed that they all belonged to clades I and II, providing strong evidence that raw meats were the outbreak vehicle. All 16 isolates harbored the bla_{DHA-1}–carrying IncA/C plasmid. Other *Salmonella* serovars also were detected in this investigation. The overall *Salmonella* isolation rate from retail meats was significantly higher in traditional markets than in the supermarkets ($p<0.001$) (Appendix Table 3). In Taiwan, pork in the supermarkets is usually provided through the cold transportation chain, whereas for traditional markets pork is usually provided through the traditional chain, with notable differences. Temperatures were much lower in the cutting factory and butcher shop in the cold chain than in the traditional chain (Appendix Figure 2). Furthermore, pork was wrapped by plastic tissue and bags in the cold chain, but the traditional chain did not do any wrapping or packaging during transportation.

To clarify the contradictory findings that most infections occurred in young children even though pork is not a major food for infants, we conducted a questionnaire survey among parents of 20 infants (<1 year of age) with NTS infections and 80 parents of infants without (controls) (Appendix). Parents of the infected infants more often touched, rinsed, and cooked meat before feeding other foods to their infants (Appendix Table 4). Moreover, these parents were more willing to purchase meat from traditional markets rather than supermarkets. A possibility is that they bought meat from the traditional markets, then their frequent rinsing flushed the *Salmonella* on the surface of the meats, cutting boards and knives, and sinks, and finally onto fresh vegetables, fruit, and other ready-to-eat foods that were cross-contaminated and reached the infants through parents or other caregivers. This transmission mode is of particular importance in infants and has already been reported for other bacterial pathogens such as *Yersinia enterocolitica* (*10*).

Conclusions

Our study sought to describe an outbreak in Taiwan caused by a multidrug-resistant *Salmonella* Anatum clone. The questionnaire and supply-chain investigations we conducted found that the infection cases were closely associated with improper packaging during transportation and unhygienic food handling in the customers' kitchen. The high similarity of genomic sequence between the Taiwan isolates and international isolates indicates the global dissemination of this clone and highlights the public health value of multicountry sharing of epidemiologic, trace-back, microbiologic, genomic, and food trade data.

This study was financially supported by the National Natural Science Foundation, China (grant no. 31670132); the Chang Gung Memorial Hospital, Taiwan (grant nos. CRRPG3F0084, CMRPG3D1721-3, CMRPG3G1451-3, and CMRPG3E1371-3); and the Ministry of Health and Welfare, Taiwan (grant nos. MOHW106-CDC-C-114-113702, MOHW107-CDC-C-114-123505, and MOHW108-CDC-C-114-133505).

About the Author

Dr. Feng is an associate professor at the Institute for Translational Medicine, Zhejiang University School of Medicine, Hangzhou, China. His research interests are the epidemiology, genomics, and drug-resistance mechanisms of nontyphoidal *Salmonella*.

References

1. Chen HM, Wang Y, Su LH, Chiu CH. Nontyphoid *Salmonella* infection: microbiology, clinical features, and antimicrobial therapy. Pediatr Neonatol. 2013;54:147–52. https://doi.org/10.1016/j.pedneo.2013.01.010
2. Feng Y, Chang YJ, Fang SH, Su LH, Li HC, Yang HP, et al. Emergence and evolution of high-level cephalosporin-resistant *Salmonella* Goldcoast in Northern Taiwan. Open Forum Infect Dis. 2019;6:ofz447. https://doi.org/10.1093/ofid/ofz447
3. Qi X, Li P, Xu X, Yuan Y, Bu S, Lin D. Epidemiological and molecular investigations on *Salmonella* responsible for gastrointestinal infections in the southwest of Shanghai from 1998 to 2017. Front Microbiol. 2019;10:2025. https://doi.org/10.3389/fmicb.2019.02025
4. Jean SS, Lu MC, Shi ZY, Tseng SH, Wu TS, Lu PL, et al. In vitro activity of ceftazidime-avibactam, ceftolozane-tazobactam, and other comparable agents against clinically important Gram-negative bacilli: results from the 2017

Surveillance of Multicenter Antimicrobial Resistance in Taiwan (SMART). Infect Drug Resist. 2018;11:1983–92. https://doi.org/10.2147/IDR.S175679
5. Zhan Z, Xu X, Gu Z, Meng J, Wufuer X, Wang M, et al. Molecular epidemiology and antimicrobial resistance of invasive non-typhoidal *Salmonella* in China, 2007–2016. Infect Drug Resist. 2019;12:2885–97. https://doi.org/10.2147/IDR.S210961
6. Chiou CS, Hong YP, Liao YS, Wang YW, Tu YH, Chen BH, et al. New multidrug-resistant *Salmonella enterica* serovar Anatum clone, Taiwan, 2015–2017. Emerg Infect Dis. 2019;25:144–7. https://doi.org/10.3201/eid2501.181103
7. Ruan Z, Yu Y, Feng Y. The global dissemination of bacterial infections necessitates the study of reverse genomic epidemiology. Brief Bioinform. 2020;21:741–50. https://doi.org/10.1093/bib/bbz010
8. Nadon C, Van Walle I, Gerner-Smidt P, Campos J, Chinen I, Concepcion-Acevedo J, et al.; FWD-NEXT Expert Panel. PulseNet International: vision for the implementation of whole genome sequencing (WGS) for global food-borne disease surveillance. Euro Surveill. 2017;22:30544. https://doi.org/10.2807/1560-7917.ES.2017.22.23.30544
9. Ruan Z, Feng Y. BacWGSTdb, a database for genotyping and source tracking bacterial pathogens. Nucleic Acids Res. 2016;44(D1):D682–7. https://doi.org/10.1093/nar/gkv1004
10. Lee LA, Gerber AR, Lonsway DR, Smith JD, Carter GP, Puhr ND, et al. *Yersinia enterocolitica* O:3 infections in infants and children, associated with the household preparation of chitterlings. N Engl J Med. 1990;322:984–7. https://doi.org/10.1056/NEJM199004053221407

Address for correspondence: Cheng-Hsun Chiu, Department of Pediatrics, Chang Gung Memorial Hospital, No. 5, Fu-Hsin St, Kweishan 333, Taoyuan, Taiwan; email: chchiu@adm.cgmh.org.tw

etymologia

Salmonella [sal''mo-nel'ə]

Daniel F. M. Monte, Fábio P. Sellera

Named in honor of Daniel Elmer Salmon, an American veterinary pathologist, *Salmonella* is a genus of motile, gram-negative bacillus, nonspore-forming, aerobic to facultatively anaerobic bacteria of the family *Enterobacteriaceae*. In 1880, Karl Joseph Eberth was the first to observe *Salmonella* from specimens of patients with typhoid fever (from the Greek *typhōdes* [like smoke; delirious]), which was formerly called *Eberthella typhosa* in his tribute. In 1884, Georg Gaffky successfully isolated this bacillus (later described as *Salmonella* Typhi) from patients with typhoid fever, confirming Eberth's findings. Shortly afterward, Salmon and his assistant Theobald Smith, an American bacteriologist, isolated *Salmonella* Choleraesuis from swine, incorrectly assuming that this germ was the causative agent of hog cholera. Later, Joseph Lignières, a French bacteriologist, proposed the genus name *Salmonella* in recognition of Salmon's efforts.

With a complicated taxonomy, the genus *Salmonella* is currently classified into 2 species (*S. enterica* and *S. bongori*), encompassing 2,659 serotypes based on somatic O and H flagellar antigens as specified in the Kauffmann–White–Le Minor scheme. *S. enterica* is divided into 6 subspecies: e*nterica, salamae, arizonae, diarizonae, houtenae,* and *indica*. Arguably, this zoonotic pathogen remains one of the most pressing global concerns. It causes a spectrum of diseases in several hosts, and there is much to be learned and deciphered about its continuous evolution.

Drug-resistant, nontyphoidal, *Salmonella* sp. bacteria showing numerous flagella. Taken from Antibiotic Resistance Threats in the United States, 2019 (AR Threats Report); Centers for Disease Control and Prevention. Illustration: James Archer/CDC, 2019.

Sources

1. Dorland's Illustrated Medical Dictionary. 32nd ed. Philadelphia: Elsevier Saunders; 2012.
2. Gossner CM, Le Hello S, de Jong B, Rolfhamre P, Faensen D, Weill FX, et al. Around the world in 1,475 *Salmonella* geo-serotypes [Another Dimension]. Emerg Infect Dis. 2016;22:1298–302. https://doi.org/10.3201/eid2207.141678
3. Issenhuth-Jeanjean S, Roggentin P, Mikoleit M, Guibourdenche M, de Pinna E, Nair S, et al. Supplement 2008–2010 (no. 48) to the White-Kauffmann-Le Minor scheme. Res Microbiol. 2014;165:526–30. https://doi.org/10.1016/j.resmic.2014.07.004
4. Salmon DE. The discovery of the germ of swine-plague. Science. 1884;3:155–8. https://doi.org/10.1126/science.ns-3.=53.155
5. Su LH, Chiu CH. *Salmonella*: clinical importance and evolution of nomenclature. Chang Gung Med J. 2007;30:210–9.

Author affiliations: University of São Paulo, São Paulo, Brazil

Address for correspondence: Daniel F. M. Monte, Department of Food and Experimental Nutrition, Faculty of Pharmaceutical Sciences, University of São Paulo, São Paulo-SP 05508-900, Brazil; email: monte_dfm@usp.br

DOI: https://doi.org/10.3201/eid2612.ET2612

Outbreaks of Highly Pathogenic Avian Influenza (H5N6) Virus Subclade 2.3.4.4h in Swans, Xinjiang, Western China, 2020

Yanbing Li, Minghui Li, Yulei Li, Jingman Tian, Xiaoli Bai, Cen Yang, Jianzhong Shi, Ridengcaicike Ai, Weidong Chen, Wentao Zhang, Jie Li, Yufei Kong, Yuntao Guan, Hualan Chen

In January 2020, the subclade 2.3.4.4h of highly pathogenic avian influenza (H5N6) virus infected migratory whooper swans and mute swans in Xinjiang, western China. The virus is lethal to chickens and ducks but has low pathogenicity in mice. Antigenically, this subclade is similar to the H5N1 vaccine seed virus Re-11.

The H5 highly pathogenic avian influenza viruses (HPAIVs) of clade 2.3.4.4 are of great concern because of their global spread and circulation. Ample evidence indicates that clade 2.3.4.4 H5 viruses derived neuraminidase (NA) gene from other low-pathogenicity avian influenza viruses (LPAIVs) co-circulating in migratory birds, and new subtypes of H5N2, H5N5, H5N6, and H5N8 HPAIVs have been detected in wild bird species and poultry globally (*1*,*2*). To date, H5 viruses of clade 2.3.4.4 have evolved into 8 subclades (2.3.4.4a to 2.3.4.4h) according to the World Health Organization's (WHO) nomenclature system (*1*). Among them, H5N6 is the only subtype that has caused human infections. As of August 2019, a total of 24 human cases have been reported to WHO; the mortality rate is 67% (*3*,*4*).

H5N6 virus of subclade 2.3.4.4a was first detected in poultry in Laos in 2013, then spread to Vietnam and China and caused numerous cases in these areas. H5N8 virus of subclade 2.3.4.4b caused disease outbreaks in wild birds and poultry in Korea in 2014, then spread to North America through bird migration and established a new subclade, 2.3.2.4c. When the H5N8 virus of subclade 2.3.4.4b landed in Europe and Africa, it reassorted with the local LPAIV and produced H5N6 with a novel internal gene cassette in 2017 (*5*). Simultaneously, the H5N6 viruses of subclades 2.3.4.4d, 2.3.4.4e, 2.3.4.4f, 2.3.4.4g, and 2.3.4.4h established in poultry and wild birds in Southeast Asia (*1*,*6*–*8*). Among the 8 subclades of 2.3.4.4, only 3 (H5N6 2.3.4.4b, 2.3.4.4e, and 2.3.4.4f) had been previously detected in swans (*1*).

Since 2004, different vaccines have been developed and widely administered among poultry flocks in China and other countries for H5 avian influenza control, and the vaccine seed viruses used in China have been updated regularly to ensure antigenic match between the vaccine strain and the prevalent strains (*9*,*10*). After the H7N9 HPAIVs emerged in China in 2017, an H5/H7 combined inactivated vaccine was developed and used in poultry (*11*,*12*). Currently, the vaccine seed virus Re-11 is being used to control the clade 2.3.4.4 viruses (*10*). In our study, we analyzed the genetic evolution, antigenicity, and pathogenicity of the H5N6 HPAIVs isolated from migratory whooper swans (*Cygnus cygnus*) and mute swans (*C. olor*) in Xinjiang, western China, in January 2020.

The Study

The first sick whooper swan was found on December 29, 2019, in Sala Village, Samuyuzi Township, Yining City, Xinjiang Uyghur Autonomous Region. The bird died on January 1, 2020. By January 17, deaths had been reported in 58 swans in 6 locations (Table 1; Figure 1, panel A). We received 5 batches of clinical

Author affiliations: State Key Laboratory of Veterinary Biotechnology, Harbin Veterinary Research Institute, Chinese Academy of Agricultural Sciences, Harbin, Heilongjiang, China (Yanbing Li, M. Li, Yulei Li, J. Tian, X. Bai, J. Shi, C. Yang, Y. Kong, Y. Guan, H. Chen); Preventive and Control Center for Animal Disease of Xinjiang Uyghur Autonomous Region, Urumqi, Xinjiang Wei Autonomous Region, China (R. Ai, J. Li); Preventive and Control Center for Animal Disease of Xinjiang Crops, Urumqi (W. Zhang, J. Li)

DOI: https://doi.org/10.3201/eid2612.201201

Table 1. Avian influenza (H5N6) outbreaks among migratory whooper swans (*Cygnus cygnus*) and mute swans (*C. olor*), Xinjiang Province, China, January 2020

Time	Location description	Bird information		
			No. swans†	
		Flock size*	Total	Dead
2019 Dec 29 to 2020 Jan 5	Small lake in Yining County, Ili Kazak City	>100	100	10
2020 Jan 1–6	Natural park in Yining County, Ili Kazak City	>2,300	40 (270)	6 (3)
2020 Jan 1–8	Natural park in Bole County, Botorla City	160	55	6
2020 Jan 8–10	Natural park in Hejing County, Bayingola City	1150	150	1
2020 Jan 12–14	Wetland in Manas County, Changji City	2,000	800	13
2020 Jan 17–20	Water reservoir in Maguan Chu County, Shihezi City	1,000	150	19

*Estimated number of total migratory birds at that location.
†Numbers are whooper swans, except numbers in parentheses, which are mute swans.

samples from 13 dead birds (11 whooper swans and 2 mute swans), and 13 H5N6 viruses were isolated. The hemagglutinin (HA) subtypes were identified by a hemagglutinin-inhibition test with a panel of H1–H16 subtype antisera, whereas the NA subtypes were detected by reverse transcription PCR with a panel of N1–N9 subtype-specific primers (*11*).

To trace the origin of the viruses and understand their genetic relationship, we sequenced the genome of the 13 viruses and performed comparative phylogenetic analysis with the representative H5 HPAIVs that were recommended by WHO (*1*). All 13 H5N6 viruses possess high identity with each other (99.5%–100%); 7 of 8 segments are closely related to the H5N6 virus isolated from environmental samples in Guangdong Province in 2017, whereas the other 1, nonstructural protein gene, is closest to A/chicken/Nghe An/01VTC/2018(H5N6) (Appendix Table 1, https://wwwnc.cdc.gov/EID/article/26/12/20-1201-App1.pdf). The HA gene has the typical highly pathogenic amino acid sequence -RRKR- in its cleavage site, and a few mammalian adaptation mutations were detected in the genome (Table 2) (*13*). In the maximum clade credibility tree, the HA genes of the 13 H5N6 viruses are grouped into subclade 2.3.4.4h with the HA genes of the strains recently found in Vietnam, China, and Russia (*1*) (Figure 1, panel B). The neighbor-joining phylogenic trees of the 8 gene segments are shown in Appendix Figure 1.

The hemagglutinin-inhibition test was performed with polyclonal antiserum generated from the SW/XJ/1/2020(H5N6) and the currently used H5N1

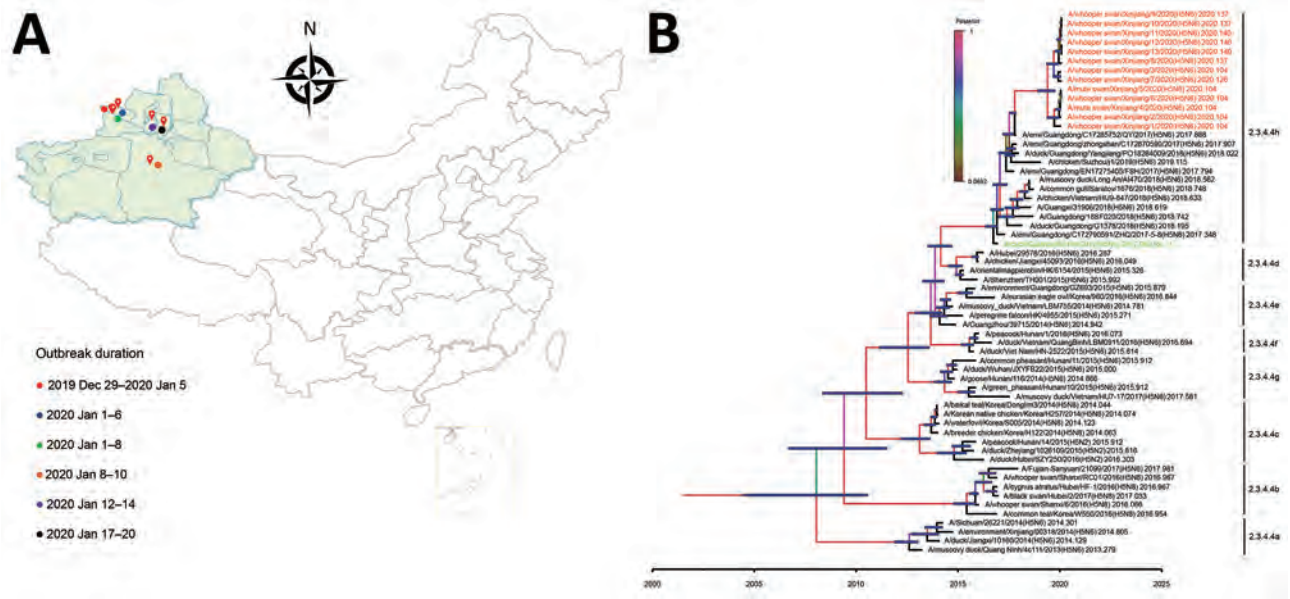

Figure 1. Geography and phylogeny of avian influenza (H5N6) outbreaks among migratory whooper swans (*Cygnus cygnus*) and mute swans (*C. olor*), Xinjiang Province, China, January 2020. A) Disease outbreak sites are marked with red drops, and dates of the outbreaks are indicated. Inset map shows islands in the South China Sea. B) Phylogenetic tree of the hemagglutinin (HA) genes of H5 viruses. The HA gene maximum clade credibility tree of the H5 viruses was constructed by using the BEAST 1.8.4 software package (https://beast-dev.github.io/beast-mcmc). Node bars indicate 95% highest posterior density of the node height. Each branch is colored by posterior probability: the 13 H5N6 viruses reported in this study are shown in red and the HA donor of the H5N1 vaccine Re-11 in green. The time to the most recent common ancestor is labeled at the bottom of the tree, which was estimated by using the Bayesian Markov chain Monte Carlo method in the BEAST 1.8.4 software package.

Table 2. Virulence related molecular markers detected in the WS/XJ/1/2020 (H5N6) virus detected among migratory whooper swans (*Cygnus cygnus*) and mute swans (*C. olor*), Xinjiang Province, China, January 2020

Protein	Amino acid/motif	Phenotypic consequences
Hemagglutinin	Cleavage site motif: -RRKR¯G-	Polybasic cleavage motif sequence required for high pathogenicity of avian influenza viruses in chickens
Neuraminidase	Stalk deletion 58–68	Increased virulence in mice
Polymerase acidic protein	515T	Increased polymerase activity in mammalian cells
Matrix protein 1	30D	Increased virulence in mice
	215A	Increased virulence in mice
Nonstructural protein 1	80–84 deletion	Increased virulence in mice
	42S	Increased virulence in mice
	98F	Increased virulence in mice
	101M	Increased virulence in mice
	222–225 ESEV (PDZ domain)	Increased virulence in mice

inactivated vaccine Re-11, which carries the HA gene from A/duck/Guizhou/S4184/2017(H5N6) virus (*10*). We found that the SW/XJ/1/2020(H5N6) cross-reacted well with Re-11 antisera, and vice versa (Appendix Table 2), yielding a cross-reactivity R value of 0.26.

We conducted an intravenous pathogenicity index test in chickens with the index virus, WS/XJ/1/2020(H5N6), by following the protocol of the World Organisation for Animal Health (OIE) (*14*). Ten 6-week-old specific-pathogen–free chickens were inoculated with 0.2 mL of virus intravenously, and all the birds died within 3 days postinoculation, yielding an intravenous pathogenicity index test value of 2.59.

We tested the virulence and transmission of the WS/XJ/1/2020(H5N6) in ducks as previously described (*2*). Eight 3-week-old specific-pathogen–free ducks were intranasally inoculated with 10^6 50% egg infective dose (EID_{50}) WS/XJ/1/2020(H5N6), and 3 uninfected ducks were put in the same cage 24 hours later for monitoring transmission. Three virus-inoculated ducks were euthanized on day 3 postinoculation, and high titers of virus were detected in the tested organs (Figure 2, panel A). Virus was also detected in the oropharyngeal and cloacal swabs of the surviving virus-inoculated ducks and the contact ducks on days 3 and 5 postinoculation (Figure 2, panel B). All

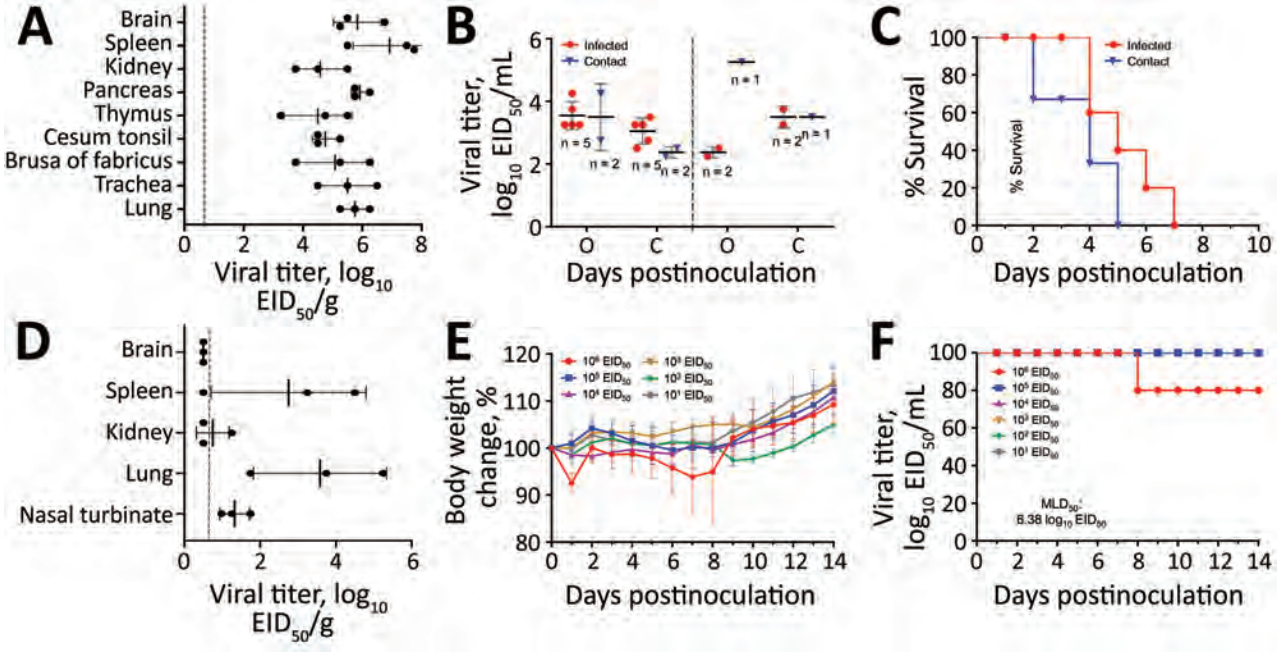

Figure 2. Replication and virulence of the WS/XJ/1/2020(H5N6) isolate in ducks and mice in a laboratory test performed after H5N6 avian influenza (H5N6) outbreaks among migratory whooper swans (*Cygnus cygnus*), Xinjiang Province, China, January 2020. A) Viral titer in organs of ducks that were euthanized on day 3 postinoculation. B) Viral titers in oropharyngeal and cloacal swabs from all surviving ducks were collected on days 3 and 5 postinoculation. C) Lethality of the virus in ducks. D) Viral titer in organs of mice that were euthanized on day 3 postinoculation. E) Bodyweight change of mice after inoculation with different doses of the virus. F) MLD_{50} of the virus. Viral titers in panels A, B, and D are shown as the mean ± SD. The dashed lines indicate the lower limit of detection. EID_{50}, 50% egg infective dose; MLD_{50}, 50% mouse lethal dose.

5 virus-inoculated ducks and 3 contact ducks died within 7 days postinoculation (Figure 2, panel C).

The replication and 50% mouse lethal dose (MLD_{50}) of the WS/XJ/1/2020(H5N6) were evaluated in BALB/c mice as previously reported (2). Three mice were intranasally inoculated with 10^6 EID_{50} of WS/XJ/1/2020(H5N6) in a volume of 50 μL and were euthanized on day 3 postinoculation to assess virus replication in organs, and we found the virus in the brain of 1 mouse, the spleens of 2 mice, and the nasal turbinates and lungs of all 3 mice, but not in the kidneys of any mouse (Figure 2, panel D). To test the MLD_{50}, groups of five 6-week-old mice were intranasally inoculated with 10^1 to 10^6 EID_{50} of WS/XJ/1/2020(H5N6) in a volume of 50 μL and were monitored for bodyweight loss and death for 14 days. Only 1 of 5 mice that received the highest dose of 10^6 EID_{50} died on day 8 postinoculation; all other mice survived the 14-day observation period, yielding an MLD_{50} value of 6.38 $\log_{10}$ EID_{50} (Figure 2, panel E, F).

Conclusions

A total of 58 swans died from H5N6 virus infection in 6 wild bird habitats in Xinjiang in January 2020, and we isolated 13 similar H5N6 HPAIVs from the swan specimens. These viruses bear the HAs of subclade 2.3.4.4h, which were previously detected in other bird species but not in swans.

The WS/XJ/1/2020(H5N6) is highly pathogenic to chickens and ducks, and antigenically close to the H5N1 vaccine seed virus Re-11. Although the virus is low pathogenic in mice, it bears multiple residues that can increase its virulence in mammals, and thus might pose a potential threat to public health.

Wild birds carry and spread the H5 HPAIV, as evidenced by the dissemination of the clade 2.2 viruses from Asia to Europe and Africa in 2005, and the intercontinental distribution of the clade 2.3.4.4b viruses in 2014 (*5*,*15*). The prospect of these H5N6 viruses detected in swans being distributed widely by wild birds is worrisome. Therefore, with the migratory season coming, surveillance and preventive measures should be implemented in poultry raised on the migration routes of wild birds.

Acknowledgments

We thank the researchers who submitted H5N6 HPAIVs sequences to GISAID. The sequence data from this study were deposited in GISAID with the accession numbers EPI1718935–9038.

This study was supported by the National Key R&D Program of China (grant no. 2016YFD0500201), the National Natural Science Foundation of China (grant no. 31521005), the Natural Science Foundation of the Heilongjiang Province of China (grant no. ZD2018007), the Central Public-interest Scientific Institution Basal Research Fund for Chinese Academy of Agricultural Sciences (grant no. 1610302017001), and the China Agriculture Research System (grant no. CARS-41-G12).

About the Author

Dr. Li is a veterinary epidemiologist and virologist at Harbin Veterinary Research Institute, Chinese Academy of Agricultural Sciences, China. Her research focuses on the molecular epidemiology and pathogenicity of avian influenza viruses.

References

1. World Health Organization. Antigenic and genetic characteristics of zoonotic influenza A viruses and development of candidate vaccine viruses for pandemic preparedness. 2020 [cited 2020 Mar 10]. https://www.who.int/influenza/vaccines/virus/202002_zoonotic_vaccinevirusupdate.pdf
2. Cui Y, Li Y, Li M, Zhao L, Wang D, Tian J, et al. Evolution and extensive reassortment of H5 influenza viruses isolated from wild birds in China over the past decade. Emerg Microbes Infect. 2020;9:1793–803. https://doi.org/10.1080/22221751.2020.1797542
3. Yang L, Zhao X, Li X, Bo H, Li D, Liu J, et al. Case report for human infection with a highly pathogenic avian influenza A(H5N6) virus in Beijing, China 2019. Biosafety and Health. 2020;2:49–52. https://doi.org/10.1016/j.bsheal.2020.02.003
4. Yang L, Zhu W, Li X, Bo H, Zhang Y, Zou S, et al. Genesis and dissemination of highly pathogenic H5N6 avian influenza viruses. J Virol. 2017;91:e02199. https://doi.org/10.1128/JVI.02199-16
5. Poen MJ, Venkatesh D, Bestebroer TM, Vuong O, Scheuer RD, Oude Munnink BB, et al. Co-circulation of genetically distinct highly pathogenic avian influenza A clade 2.3.4.4 (H5N6) viruses in wild waterfowl and poultry in Europe and East Asia, 2017–18. Virus Evol. 2019;5:vez004. https://doi.org/10.1093/ve/vez004
6. Yu Z, Gao X, Wang T, Li Y, Li Y, Xu Y, et al. Fatal H5N6 avian influenza virus infection in a domestic cat and wild birds in China. Sci Rep. 2015;5:10704. https://doi.org/10.1038/srep10704
7. Tsunekuni R, Yaguchi Y, Kashima Y, Yamashita K, Takemae N, Mine J, et al. Spatial transmission of H5N6 highly pathogenic avian influenza viruses among wild birds in Ibaraki Prefecture, Japan, 2016–2017. Arch Virol. 2018;163:1195–207. https://doi.org/10.1007/s00705-018-3752-7
8. Hiono T, Okamatsu M, Matsuno K, Haga A, Iwata R, Nguyen LT, et al. Characterization of H5N6 highly pathogenic avian influenza viruses isolated from wild and captive birds in the winter season of 2016–2017 in Northern Japan. Microbiol Immunol. 2017;61:387–97. https://doi.org/10.1111/1348-0421.12506
9. Li C, Bu Z, Chen H. Avian influenza vaccines against H5N1 'bird flu'. Trends Biotechnol. 2014;32:147–56. https://doi.org/10.1016/j.tibtech.2014.01.001
10. Zeng X, Chen X, Ma S, Wu J, Bao H, Pan S, et al. Protective efficacy of an H5/H7 trivalent inactivated vaccine produced from Re-11, Re-12, and H7-Re2 strains against challenge

with different H5 and H7 viruses in chickens. J Integr Agric. 2020;19:2294–300. https://doi.org/10.1016/S2095-3119(20)63301-9
11. Shi J, Deng G, Ma S, Zeng X, Yin X, Li M, et al. Rapid evolution of H7N9 highly pathogenic viruses that emerged in China in 2017. Cell Host Microbe. 2018;24:558–568.e7. https://doi.org/10.1016/j.chom.2018.08.006
12. Zeng X, Tian G, Shi J, Deng G, Li C, Chen H. Vaccination of poultry successfully eliminated human infection with H7N9 virus in China. Sci China Life Sci. 2018;61:1465–73. https://doi.org/10.1007/s11427-018-9420-1
13. Suttie A, Deng YM, Greenhill AR, Dussart P, Horwood PF, Karlsson EA. Inventory of molecular markers affecting biological characteristics of avian influenza A viruses. Virus Genes. 2019;55:739–68. https://doi.org/10.1007/s11262-019-01700-z
14. World Organisation for Animal Health. Avian influenza ((infection with avian influenza viruses). In: Manual of diagnostic tests and vaccines for terrestrial animals. 2019 [cited Mar 10]. https://www.oie.int/fileadmin/Home/eng/Health_standards/tahm/3.03.04_AI.pdf
15. Chen H, Li Y, Li Z, Shi J, Shinya K, Deng G, et al. Properties and dissemination of H5N1 viruses isolated during an influenza outbreak in migratory waterfowl in western China. J Virol. 2006;80:5976–83. https://doi.org/10.1128/JVI.00110-06

Address for correspondence: Hualan Chen, Harbin Veterinary Research Institute, Chinese Academy of Agricultural Sciences, No. 678 Haping Rd, Harbin, Heilongjiang, 150069, China; email: chenhualan@caas.cn

Differential Tropism of SARS-CoV and SARS-CoV-2 in Bat Cells

Susanna K.P. Lau,[1] Antonio C.P. Wong,[1] Hayes K.H. Luk,[1] Kenneth S.M. Li, Joshua Fung, Zirong He, Flora K.K. Cheng, Tony T.Y. Chan, Stella Chu, Kam Leng Aw-Yong, Terrence C.K. Lau, Kitty S.C. Fung, Patrick C.Y. Woo

Severe acute respiratory syndrome coronavirus 2 did not replicate efficiently in 13 bat cell lines, whereas severe acute respiratory syndrome coronavirus replicated efficiently in kidney cells of its ancestral host, the *Rhinolophus sinicus* bat, suggesting different evolutionary origins. Structural modeling showed that RBD/*Rs*ACE2 binding may contribute to the differential cellular tropism.

Coronavirus disease (COVID-19) is a global pandemic, affecting 213 countries with >2.7 million confirmed cases and 190,000 fatalities as of April 25, 2020 (*1*). Its causative agent was identified as severe acute respiratory syndrome coronavirus (SARS-CoV) 2 (SARS-CoV-2), which belongs to the same coronavirus species as SARS-CoV and SARS-related CoVs (SARSr-CoVs) in horseshoe bats (genus *Rhinolophus*) (*2*,*3*). Given the history among some early case-patients of visiting the Huanan seafood market in Wuhan, China, and its genetic close relatedness to SARSr-CoVs in bats and pangolins (*2*,*4*), SARS-CoV-2 was suspected to have emerged from wild animals, particularly bats, similar to SARS-CoV. SARS-CoV was a recombinant virus that originated from Chinese horseshoe bats (*Rhinolophus sinicus*) before it infected palm civets and then humans (*5*).

Studying cellular tropism may provide clues to the host range and possible origin of zoonotic viruses. For example, SARS-CoV could replicate efficiently in kidney cells of its primary origin, *R. sinicus*, but not in other tested bat cells (*6*). To elucidate the possible origin of SARS-CoV-2, we tested susceptibilities of bat cell lines developed from different species commonly found in southern China to infection by SARS-CoV-2 in comparison with SARS-CoV. The selected bat species harbored a diverse set of coronaviruses, including SARSr-CoVs and Middle East respiratory syndrome–related coronaviruses (MERSr-CoVs), which pose potential health threats to humans (*7*). We also performed structural modeling of the virus/host receptor-binding interface.

The Study

SARS-CoV strain HKU-39849 was isolated in Hong Kong during the SARS epidemic as previously described (*8*). SARS-CoV-2 strain HK20 was isolated from a patient with COVID-19 in Hong Kong in early February 2020 (*3*). Thirteen primary or immortalized bat cell lines from 6 different bat species were subjected to infection with SARS-CoV and SARS-CoV-2 at multiplicity of infection of 0.1 as described previously (*6*,*9*,*10*), except with the addition of 2 μg/mL trypsin. The bat species included *Miniopterus pusillus*, *Pipistrellus abramus* (harboring *Pipistrellus*-BatCoV-HKU5), *R. sinicus* (harboring SARSr-BatCoVs, *Rhinolophus*-BatCoV-HKU2, *Rhinolophus sinicus*-BatCoV-HKU32), *Tylonycteris pachypus* (harboring *Tylonycteris*-BatCoV-HKU4), *Rousettus leschenaultii* (harboring many viruses, including *Rousettus*-BatCoV-HKU9 and *Rousettus*-BatCoV-HKU10), and *Myotis ricketii* (harboring *Myotis*-BatCoV-HKU6). Vero cells from African green monkey kidney were used as positive control (Figure 1; Appendix, https://wwwnc.cdc.gov/EID/article/26/12/20-2308-App1.pdf). We determined viral replication efficiency by quantitative reverse transcription PCR (qRT-PCR) on cell culture supernatants (Table 1) (*6*). Cells were considered susceptible to viral infection if qRT-PCR on day 5 postinfection showed $\geq$1 $\log_{10}$ increase in viral titer with statistical significance ($p<0.05$ by Student *t*-test).

Author affiliations: The University of Hong Kong, Hong Kong, China (S.K.P. Lau, A.C.P. Wong, H.K.K. Luk, K.S.M. Li, J. Fung, Z. He, F.K.K. Cheng, T.T.Y. Chan, S. Chu, K.L. Aw-Yong, P.C.Y. Woo); City University of Hong Kong, Hong Kong (T.C.K. Lau); United Christian Hospital, Kwun Tong, Hong Kong (K.S.C. Fung)

DOI: https://doi.org/10.3201/eid2612.202308

[1]These authors contributed equally to this article.

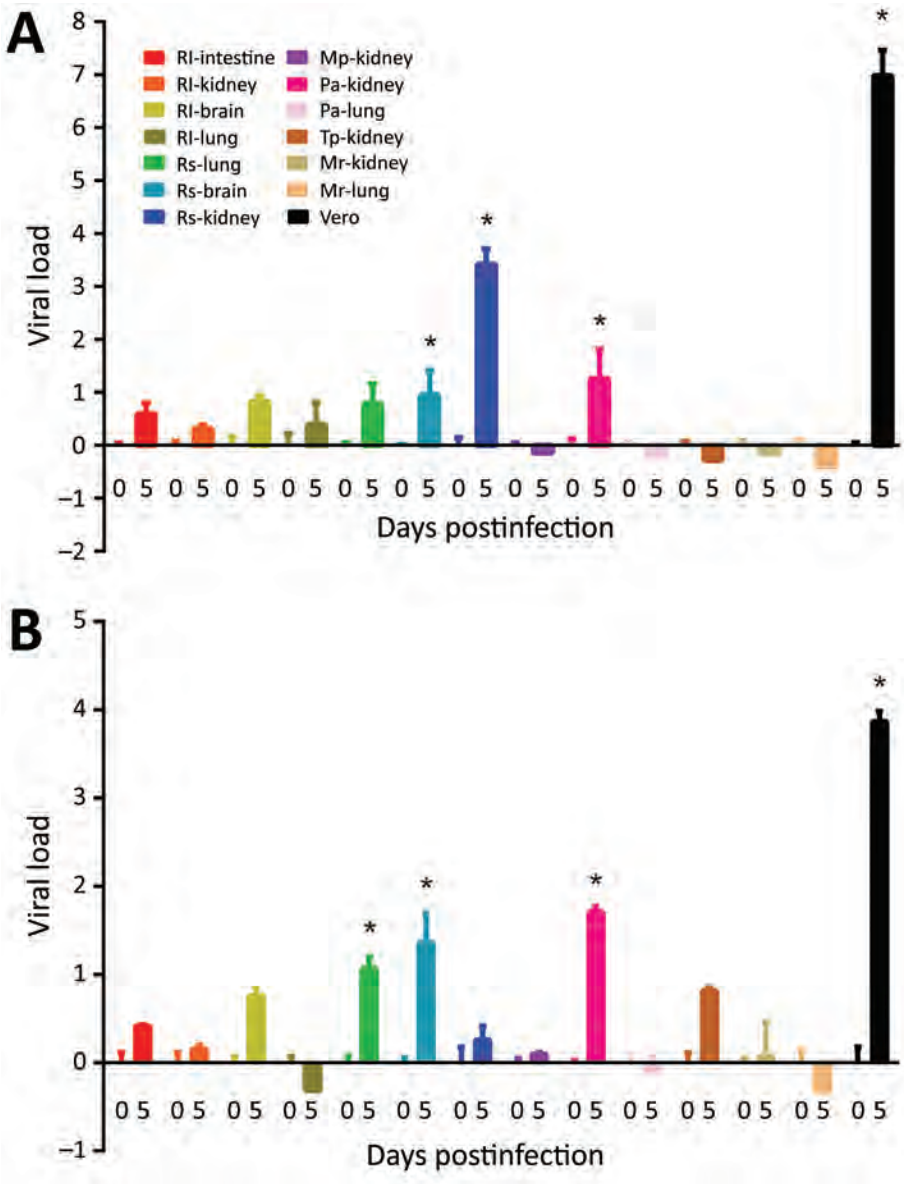

Figure 1. Susceptibilities of 13 bat cell lines to infection by SARS-CoV (A) and SARS-CoV-2 (B) shown from harvest of supernatants and cell lysates at day 0 and 5 postinfection. Viral titers and β-Actin mRNA were determined by real-time quantitative reverse transcription PCR. Viral load is expressed as normalized fold change in $\log_{10}$. Error bars indicate SDs of triplicate samples. Bat cell lines are listed by species and organ. Vero cells served as controls. Asterisk (*) indicates $p<0.05$ and increase in viral load ≥1 $\log_{10}$. Mp, *Miniopterus pusillus*, Mr, *Myotis ricketti;* Pa, *Pipistrellus abramus*, Rl, *Rousettus leschenaultii*, Rs, *Rhinolophus sinicus*, Tp, *Tylonycteris pachypus.* SARS-CoV, severe acute respiratory syndrome coronavirus.

SARS-CoV but not SARS-CoV-2 can replicate efficiently in *R. sinicus* kidney cells; SARS-CoV showed 3.48 $\log_{10}$-fold increase in viral titer. In contrast, only SARS-CoV-2 can replicate in *R. sinicus* lung cells, but at a low viral titer (1.08 $\log_{10}$-fold increase). Moreover, SARS-CoV-2 can replicate more efficiently (1.46 $\log_{10}$-fold increase) in *R. sinicus* brain cells than SARS-CoV (1.09 $\log_{10}$-fold increase), albeit still at low viral titer (Table 2; Figure 1). Both SARS-CoV and SARS-CoV-2 can also replicate in *P. abramus* kidney cells with low viral titers: 1.45 $\log_{10}$-fold increase for SARS-CoV and 1.71 $\log_{10}$-fold increase for SARS-CoV-2. We observed cytopathic effects in SARS-CoV–infected *R. sinicus* kidney cells and SARS-CoV– or SARS-CoV-2–infected *P. abramus* kidney cells with rounding of cells (Appendix Figure 1). We performed immunofluorescence assay on those cell lines with >1 $\log_{10}$-fold increase in viral load (Appendix Figure 2). *M. pusillus* kidney cells; *R. leschenaultii* kidney, brain, intestine, and lung cells; *T. pachypus* kidney cells; and *M. ricketii* kidney and lung cells did not support SARS-CoV or SARS-CoV-2 infection. Furthermore, both SARS-CoV and SARS-CoV-2 replicated less efficiently in Vero cells at 33°C than at 37°C, whereas no difference in viral replication in *R. sinicus* kidney cells was observed between 33°C and 37°C (Appendix Figure 3).

To elucidate whether the receptor-binding interface is a contributing factor for cellular tropism, we modeled the structure of the SARS-CoV-2 receptor binding domain (RBD) with that of human

Table 1. Primers used for reverse transcription quantitative PCR in study of coronavirus in bats*

Target	Primers, 5′ → 3′		
	Forward	Reverse	Probe
SARS-CoV N gene CDC_N3	GGGAGCCTTGAATACACCAAAA	TGTAGCACGATTGCAGCATTG	(FAM) AYCACATTGGCACCCGCAATCCTG (BHQ1)
β-actin	CTCTTCCAGCCCTCCTTCCT (for bat cells) or CTCTTCCAGCCTTCCTTCCT (for human cells)	TTCATCGTGCTGGGAGCC (for bat cells) or TTCATTGTGCTGGGTGCC (for human cells)	(FAM) CATGAAGTGYGACGTBGACATCC G(BHQ1)

*CoV, coronavirus; N, nucleocapsid protein; SARS, severe acute respiratory syndrome.

angiotensin-converting enzyme 2 (hACE2), *R. sinicus* angiotensin-converting enzyme 2 (Rs-ACE2), and *P. abramus* angiotensin-converting enzyme 2 (Pa-ACE2) using homology modeling by SWISS-MODEL (https://swissmodel.expasy.org) as described previously (*11*), based on the crystal structure of SARS-CoV-RBD/hACE2. The sequence identity between SARS-CoV RBD (template) and SARS-CoV-2 RBD (template) was >50% and the interface for all RBD/ACE2 was similar (Figure 2). We identified 11 aa differences between SARS-CoV RBD and SARS-CoV-2 RBD sequences that involved 4 of 5 critical residues for hACE2 binding in SARS-CoV RBD. Y442 was one of the 5 critical residues in SARS-CoV RBD. Because F456 is more hydrophobic than Y442 in SARS-CoV-2 RBD, it may disturb the electrostatic interaction with hACE2/Rs-ACE2. The interface for RBD/Pa-ACE 2 was similar to that of RBD/hACE2 (Figure 2), implying that Pa-ACE2 may also serve as the host receptor for SARS-CoV and SARS-CoV-2.

Conclusions

The ability of SARS-CoV but not SARS-CoV-2 to replicate in *R. sinicus* kidney cells, consistent with previous findings (*12*), may suggest a different evolutionary origin and path of SARS-CoV-2. SARS-CoV was most closely related to SARSr-*Rs*-BatCoVs from Yunnan, China, suggesting *R. sinicus* as its primary origin. It could also use *Rs*-ACE2 as receptor for cell entry (*13*), which may explain the efficient replication of SARS-CoV in *R. sinicus* kidney cells. Although SARS-CoV-2 is closely related to SARSr-CoVs in bats and pangolins, none of the existing animal viruses represents the immediate ancestor of SARS-CoV-2. SARS-CoV-2 was most closely related to SARSr-*Ra*-BatCoV-RaTG13 (96.1% genome identity) in *Rhinolophus affinis* from Pu'er, Yunnan (*2*), except that its RBD region was closest to pangolin-SARSr-CoV-MP789 (86.9% nucleotide identity) in smuggled pangolins from Guangdong, suggesting that SARS-CoV-2 may have evolved through recombination (*3*). The inability of SARS-CoV-2 to efficiently infect and replicate in *R. sinicus* cells may imply that *R. sinicus* bats were unlikely to be its proximal origin. However, bats are the primary origin of SARS-CoV, human coronavirus 229E (HCoV-229E), and probably MERS-CoV; therefore, SARS-CoV-2 most likely originated from bats. One possibility is that SARS-CoV-2 has restricted bat species tropism. Other bat species, such as *R. affinis*, may harbor the ancestor of SARS-CoV-2 and can be tested for cellular susceptibilities in future studies. It is also possible that SARS-CoV-2 can no longer

Table 2. Viral load changes and cytopathic effects of severe acute respiratory syndrome coronavirus and coronavirus 2 in different cell lines on day 5 postinfection*

Cell lines	SARS-CoV			SARS-CoV-2		
	Viral load change, $\log_{10}$	p value	CPE	Viral load change, $\log_{10}$	p value	CPE
Rousettus leschenaultii intestine	0.63	0.0083	–	0.59	0.0039	–
Rousettus leschenaultii kidney	0.33	0.0071	–	0.15	0.0950	–
Rousettus leschenaultii brain	0.84	0.0019	–	0.77	0.0004	–
Rousettus leschenaultii lung	0.39	0.2345	–	–0.31	0.1224	–
Rhinolophus sinicus lung	0.91	0.0226	–	1.08	0.0002	–
Rhinolophus sinicus brain	1.09	0.0251	–	1.46	0.0022	–
Rhinolophus sinicus kidney	3.48	<0.0001	+	0.28	0.1280	–
Miniopterus pusillus kidney	–0.14	0.0372	–	0.10	0.0241	–
Pipistrellus abramus kidney	1.45	0.0176	+	1.71	<0.0001	+
Pipistrellus abramus lung	–0.21	0.2401	–	–0.09	0.4218	–
Tylonycteris pachypus kidney	–0.27	0.0051	–	0.82	0.0003	–
Myotis ricketti kidney	–0.14	0.1683	–	0.07	0.7615	–
Myotis ricketti lung	–0.41	0.0289	–	–0.32	0.0240	–
Vero	7.12	<0.0001	+	3.88	<0.0001	+

*CoV, coronavirus; CPE, cytopathic effects; SARS, severe acute respiratory syndrome.

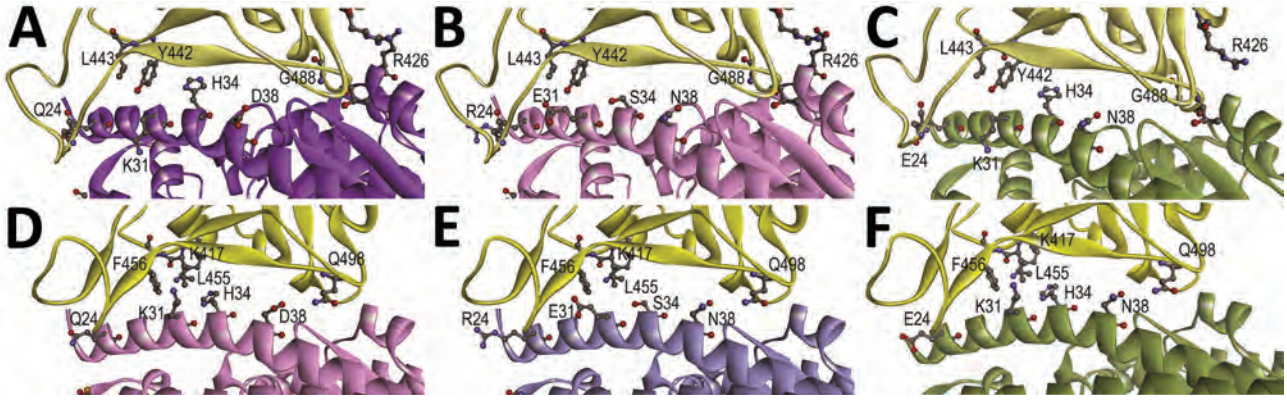

Figure 2. Structural modeling of the human (A, D), *Rhinolophus sinicus* bat (Rs-bat) (B, E), and *Pipistrellus abramus* bat (Pa-bat) (C, F) ACE2 with the receptor-binding domain (RBD) of the spike proteins of SARS-CoV and SARS-CoV-2. The models of RBDs of SARS-CoV and SARS-CoV-2 (yellow) are shown with human (purple), Rs-bat (pink). and Pa-bat (green) ACE2 structures in ribbon diagrams. The interface of different RBDs and human/bat ACE2 are shown and the residues with potential impact on binding affinity are shown in ball-and-stick format. Images were produced using Discovery Studio visualizer (Accelrys, https://www.accelrys.com).

replicate in bat cells because of substantial genetic adaptation, such as through natural evolution in an intermediate host before infecting humans.

The difference in critical residues for receptor binding between SARS-CoV and SARS-CoV-2 may have contributed to their differential infectivities in *R. sinicus* cells, as suggested by results from structural modeling of the receptor-binding interface. Whereas SARS-Cov RBD was most closely related to SARSr-*Rs*-BatCoV-WIV1 from *R. sinicus*, SARS-CoV-2 RBD was most closely related to the RBD region of pangolin-SARSr-CoV-MP789 from pangolins (*14*). Mutagenesis studies are needed to investigate whether changes of these amino acid sites may affect binding affinity to the ACE2 of different hosts and restore the infectivity of SARS-CoV-2 in *R. sinicus* cells.

The restricted cellular tropism of SARS-CoV and SARS-CoV-2 is different from that of MERS-CoV, which showed broad species tropism in bat cells. MERS-CoV could replicate in ≥5 bat cell lines (*M. ricketti* lung, *P. abramus* kidney, *R. sinicus* kidney and lung, and *R. leschenaultii* kidney cells) from 3 bat families (*6*). Although dromedary camels were the immediate source of MERS-CoV, bats were suggested to be the ultimate evolutionary origin (*10*,*15*). Of note, SARS-CoV, SARS-CoV-2, and MERS-CoV could all replicate in *P. abramus* kidneys at low titers. Structural modeling supported that *P. abramus* ACE2 could serve as host receptor for SARS-CoV and SARS-CoV-2. *P. abramus* is known to harbor *Pi*-BatCoV-HKU5 from the subgenus *Merbecovirus* (containing MERS-CoV) but not members of *Sarbecovirus* (containing SARS-CoV and SARS-CoV-2) (*10*,*15*). *P. abramus* is a potential accidental host for spillover of and source for emergence of diverse coronaviruses including SARSr-CoVs.

Acknowledgments

We thank Agriculture, Fisheries and Conservation Department, Government of Hong Kong, for capture of bats for bat cell development and expert opinion.

This study was partly supported by the theme-based research scheme (project no. T11-707/15-R) of the University Grant Committee; Health and Medical Research Fund of the Food and Health Bureau of HKSAR; Consultancy Service for Enhancing Laboratory Surveillance of Emerging Infectious Disease for the HKSAR Department of Health and the University Development Fund of the University of Hong Kong.

About the Author

Dr. Lau is a professor and head of the Department of Microbiology at the University of Hong Kong. Her research focuses on microbial genomics for studying emerging infectious diseases including coronaviruses.

References

1. World Health Organization. Coronavirus disease 2019 (COVID-19) situation report 96. 2020 Apr 25 [cited 2020 Apr 26]. https://www.who.int/docs/default-source/coronaviruse/situation-reports/20200425-sitrep-96-covid-19.pdf?sfvrsn=a33836bb_2
2. Zhou P, Yang XL, Wang XG, Hu B, Zhang L, Zhang W, et al. A pneumonia outbreak associated with a new coronavirus of probable bat origin. Nature. 2020;579:270–3. https://doi.org/10.1038/s41586-020-2012-7
3. Lau SKP, Luk HKH, Wong ACP, Li KSM, Zhu L, He Z, et al. Possible bat origin of severe acute respiratory syndrome coronavirus 2. Emerg Infect Dis. 2020;26:1542–7.
4. Lam TT, Jia N, Zhang YW, Shum MH, Jiang JF, Zhu HC, et al. Identifying SARS-CoV-2-related coronaviruses in Malayan pangolins. Nature. 2020;583:282–5. https://doi.org/10.1038/s41586-020-2169-0

5. Lau SK, Woo PC, Li KS, Huang Y, Tsoi HW, Wong BH, et al. Severe acute respiratory syndrome coronavirus-like virus in Chinese horseshoe bats. Proc Natl Acad Sci U S A. 2005;102:14040–5. https://doi.org/10.1073/pnas.0506735102
6. Lau SKP, Fan RYY, Luk HKH, Zhu L, Fung J, Li KSM, et al. Replication of MERS and SARS coronaviruses in bat cells offers insights to their ancestral origins. Emerg Microbes Infect. 2018;7:1–11. https://doi.org/10.1038/s41426-018-0208-9
7. Wong ACP, Li X, Lau SKP, Woo PCY. Global epidemiology of bat coronaviruses. Viruses. 2019;11:174. https://doi.org/10.3390/v11020174
8. Peiris JS, Lai ST, Poon LL, Guan Y, Yam LY, Lim W, et al.; SARS study group. Coronavirus as a possible cause of severe acute respiratory syndrome. Lancet. 2003;361:1319–25. https://doi.org/10.1016/S0140-6736(03)13077-2
9. Lau SKP, Wong ACP, Zhang L, Luk HKH, Kwok JSL, Ahmed SS, et al. Novel bat alphacoronaviruses in southern China support Chinese horseshoe bats as an important reservoir for potential novel coronaviruses. Viruses. 2019;11:423. PubMed https://doi.org/10.3390/v11050423
10. Woo PC, Wang M, Lau SK, Xu H, Poon RW, Guo R, et al. Comparative analysis of twelve genomes of three novel group 2c and group 2d coronaviruses reveals unique group and subgroup features. J Virol. 2007;81:1574–85. https://doi.org/10.1128/JVI.02182-06
11. Lau SKP, Zhang L, Luk HKH, Xiong L, Peng X, Li KSM, et al. Receptor usage of a novel bat lineage C betacoronavirus reveals evolution of Middle East respiratory syndrome-related coronavirus spike proteins for human dipeptidyl peptidase 4 binding. J Infect Dis. 2018;218:197–207. https://doi.org/10.1093/infdis/jiy018
12. Chu H, Chan JF-W, Yuen TT-T, Shuai H, Yuan S, Wang Y, et al. Comparative tropism, replication kinetics, and cell damage profiling of SARS-CoV-2 and SARS-CoV with implications for clinical manifestations, transmissibility, and laboratory studies of COVID-19: an observational study. Lancet Microbe. 2020;1:e14–23. https://doi.org/10.1016/S2666-5247(20)30004-5
13. Ge XY, Li JL, Yang XL, Chmura AA, Zhu G, Epstein JH, et al. Isolation and characterization of a bat SARS-like coronavirus that uses the ACE2 receptor. Nature. 2013;503:535–8. https://doi.org/10.1038/nature12711
14. Menachery VD, Yount BL Jr, Sims AC, Debbink K, Agnihothram SS, Gralinski LE, et al. SARS-like WIV1-CoV poised for human emergence. Proc Natl Acad Sci U S A. 2016;113:3048–53. https://doi.org/10.1073/pnas.1517719113
15. Lau SK, Li KS, Tsang AK, Lam CS, Ahmed S, Chen H, et al. Genetic characterization of *Betacoronavirus* lineage C viruses in bats reveals marked sequence divergence in the spike protein of *Pipistrellus* bat coronavirus HKU5 in Japanese pipistrelle: implications for the origin of the novel Middle East respiratory syndrome coronavirus. J Virol. 2013;87:8638–50. https://doi.org/10.1128/JVI.01055-13

Address for correspondence: Susanna K.P. Lau or Patrick C.Y. Woo, Department of Microbiology, Li Ka Shing Faculty of Medicine, The University of Hong Kong, Room 26, 19/F, Block T, Queen Mary Hospital, 102 Pokfulam Road, Hong Kong, China; email: skplau@hku.hk or pcywoo@hku.hk

Highly Pathogenic Avian Influenza A(H7N3) Virus in Poultry, United States, 2020

Sungsu Youk,[1] Dong-Hun Lee,[1] Mary L. Killian, Mary J. Pantin-Jackwood, David E. Swayne, Mia K. Torchetti

An outbreak of low-pathogenicity avian influenza A(H7N3) virus of North American wild bird lineage occurred on commercial turkey farms in North Carolina and South Carolina, USA, during March–April 2020. The virus mutated to the highly pathogenic form in 1 house on 1 farm via recombination with host 28S rRNA.

Highly pathogenic avian influenza viruses (HPAIVs) have devastating impacts on the poultry industries. With infections in poultry, H5 and H7 low-pathogenicity avian influenza viruses (LPAIVs) have spontaneously mutated into HPAIVs by different mechanisms, one of which is acquisition of basic amino acids at the hemagglutinin (HA) cleavage site (*1*).

In March 2020, an outbreak of LPAIV H7N3 occurred in turkey farms, affecting 11 premises in North Carolina and 1 in South Carolina, USA. The initial decision to depopulate LPAIV-affected flocks was based on a risk assessment that included the location of affected premises, the poultry density in the area, and the presence of a basic amino acid substitution at the cleavage site among the initial LPAIV detections (PEKPKTR/GLF; substitution sequence is underscored). During the ongoing response for this event, the Clemson Veterinary Diagnostic Center in Columbia, South Carolina, a member of the National Animal Health Laboratory Network, detected an influenza A(H7) outbreak in a second turkey location in South Carolina, with increased death and respiratory signs; oropharyngeal and cloacal swab samples were forwarded to the National Veterinary Services Laboratories in Ames, Iowa, USA. On April 8, the National Veterinary Services Laboratories confirmed 1 of 6 pooled samples as HPAIV H7N3. Subsequent testing from all infected barns on the premises determined that HPAIV was present in only 1 of the 5 barns, but LPAIV was identified in the other 4 barns. All the premises affected by LPAIV and HPAIV H7N3 were located in 3 adjacent counties and 1 across state lines, indicating that geographic proximity was relevant to the outbreaks. Immediate depopulation was performed on the LPAIV- and HPAIV-affected premises, affecting 361,000 birds.

Complete genome sequencing and phylogenetic analyses were conducted to trace the origin and evolution of the H7N3 viruses. A total of 29 H7N3 viruses from 13 premises were sequenced (Appendix Table 1, https://wwwnc.cdc.gov/EID/article/26/12/20-2790-App1.pdf). Complete genome sequences have been deposited in GenBank (accession nos. MT444183–350 and MT444352–415). The intravenous pathogenicity index of selected LPAIV strains was 0 and of selected HPAIV strains, 2.46. Based on the HA cleavage site motif and supported by the intravenous pathogenicity index, 2 H7N3 viruses from 1 house in South Carolina were considered to be HPAIV. For the 2 HPAIVs, 34 (5.7%) and 1,076 (38.8%) reads had no insertion, whereas the rest of the reads were found to have an identical 27 nucleotides insertion from host cellular 28S rRNA in the cleavage site.

The presence of LPAIV and HPAIV in 1 barn at the same time suggests that the mutation was caught early. The 27-nt insertion coding for 9 amino acids at the HA cleavage site (PENPKTDRKSRHRRIR/GLF; insertion sequence is underscored) is identical to that found in a 2017 HPAIV H7N9 from a poultry outbreak that occurred in Tennessee (*2*). The potential role of a palindromic sequence was suggested to be a cause of RNA recombination with host 28S rRNA (*3*), and similar structure is often observed among the

Author affiliations: Southeast Poultry Research Laboratory, US Department of Agriculture Agricultural Research Service, Athens, Georgia, USA (S. Youk, M. Pantin-Jackwood, D. Swayne); University of Connecticut, Storrs, Connecticut, USA (D.-H. Lee); US Department of Agriculture, Ames, Iowa, USA (M. Killian, M. Torchetti)

DOI: https://doi.org/10.3201/eid2612.202790

[1]These authors contributed equally to this article.

H7 subtype (*4*); however, the exact mechanism of recombination for this particular insert remains to be elucidated. Another notable change was a 66-nt deletion in the NA stalk region from 2 premises in North Carolina. The NA stalk deletions are commonly associated with adaptation of wild bird avian influenza viruses to gallinaceous poultry (*5*); for these isolates, all reads had the same 66-nt deletion (e.g., no mixed population was detected). No significant amino acid change indicating adaptation to mammalian hosts was identified by using the Influenza Research Database (Appendix Table 2).

Maximum-likelihood and Bayesian relaxed clock phylogenies of each gene were generated (*6*,*7*). All phylogenies indicate that the North Carolina and South Carolina H7N3 viruses were genetically distinct from recent Mexico H7N3 HPAIV, 2016 Indiana H7N8, and 2017 Tennessee H7N9 poultry outbreak strains (Appendix Figures 1, 2) (*2*,*8*,*9*). All H7N3 viruses from North Carolina and South Carolina clustered together in phylogenies across all 8 gene segments and showed high levels of nucleotide identity (>99.28%). These data support a single source of LPAIV H7N3 being introduced to turkey farms in North Carolina, spreading laterally to other turkey premises, and mutating once to HPAIV during replication in turkeys from a single barn on a turkey premises in South Carolina, with no further reassortment with any other influenza strains. Furthermore, the H7 HA genes of recent US poultry events (2016, 2017, and 2020) originated from the same North American wild bird H7 clade. With several recent incursions, this H7 HA clade represents a repetitive threat to domestic poultry and carries with it the potential to mutate to HPAIV.

To increase phylogenetic resolution, nucleotide sequences from the entire protein coding regions of each virus were concatenated, with 2 modifications: the insertion at the HA cleavage site for the HPAIV was excluded, and the deletion at the NA stalk region for the 2 LPAIVs was removed. The concatenated sequences were then analyzed with Bayesian and median-joining network phylogenetic analysis (*7*,*10*). This analysis highlights that the LPAIV H7N3 diverged early into 3 well-supported genetic clusters (A, B, and C) with high posterior probabilities (posterior probability [PP] >0.99) (Figure 1). Cluster A was detected most frequently from 10 premises in both North Carolina and South Carolina and mutated to HPAIV in a single turkey location in South Carolina (Figure 2). The estimated mean time to most recent common ancestor (tMRCA) of the concatenated whole genome of

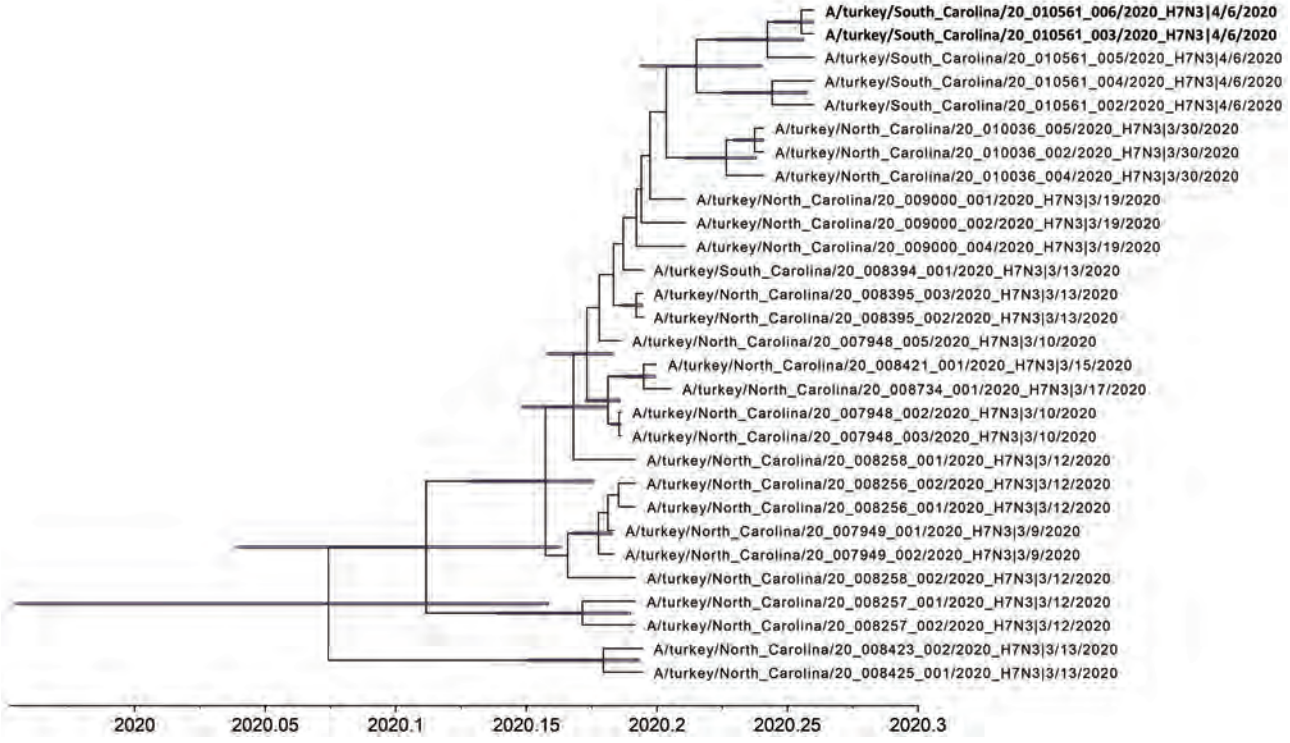

Figure 1. Time-scaled Bayesian maximum clade credibility tree of the concatenated whole genome of highly pathogenic avian influenza A(H7N3) viruses from South Carolina (bold) and North Carolina, USA. Node bars represent 95% Bayesian credible intervals for estimates of common ancestry.

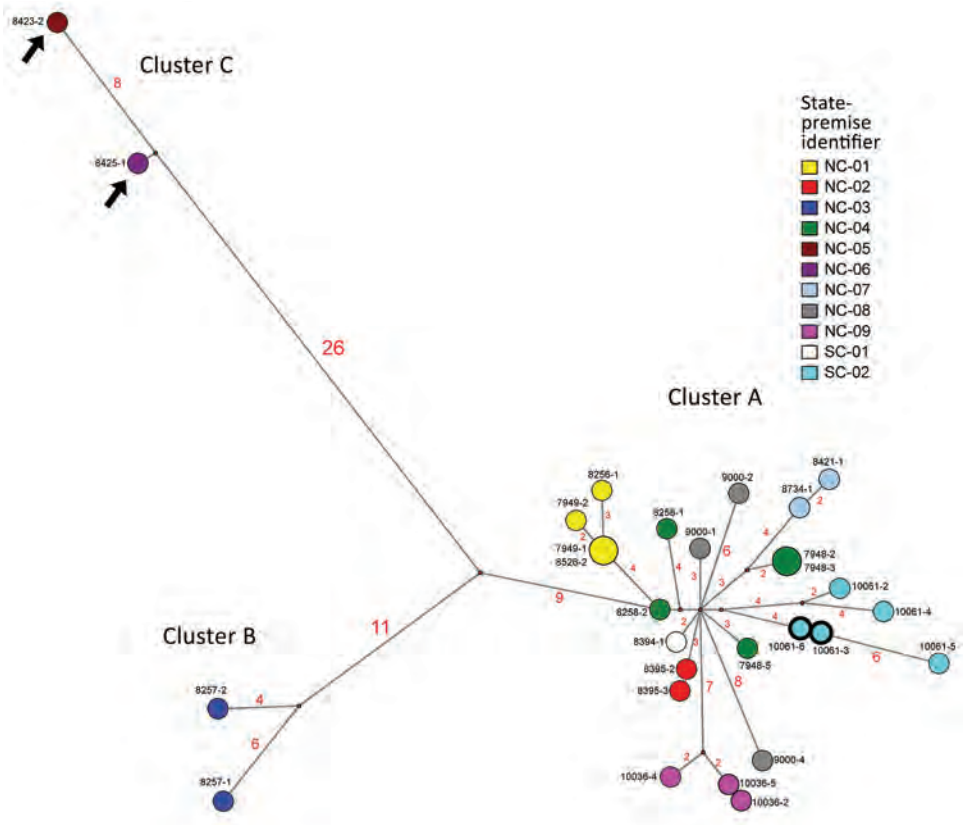

Figure 2. Median-joining phylogenetic network of the concatenated whole genome of highly pathogenic avian influenza (HPAIV) A(H7N3) viruses from South Carolina and North Carolina , USA. This network tree includes all the most parsimonious trees linking the sequences. Each unique sequence is represented by a circle sized relative to its frequency. The number of nucleotide differences between viruses is indicated on the branches. Isolates are colored according to the source premises. The black arrows indicate the H7N3 viruses with the 66-nt deletion at the neuraminidase stalk region (the NA of these 2 viruses was modified to exclude the deletion for this analysis). Both low-pathogenicity (turquoise) and HPAIV (turquoise with bolded black outline) viruses were recovered from the SC-02 premises (the hemagglutinin of the 2 HPAIVs excludes the insertion for this analysis).

H7N3 viruses from North Carolina and South Carolina was January 25, 2020 (95% Bayesian credible interval [BCI] December 14, 2019–February 28, 2020; PP = 1.0). The tMRCA, in addition to the NA stalk deletion indicating adaptation to gallinaceous poultry, potentially extends that estimate before the first detections. The estimated tMRCA of LPAIV and HPAIV from the HPAIV-positive premises was March 19, 2020 (95% BCI March 11, 2020–March 28, 2020; PP = 0.99); however, these estimates are countered by serial weekly negative diagnostic tests obtained from the same flock before onset of clinical signs. Other indicators suggestive of early detection of LPAI and mutation to HPAI include HPAIV being identified in only 1 of the 5 houses, each of the HPAIV isolates demonstrating a mixed LPAIV/HPAIV population by next-generation sequencing; active virus replication (relative cycle threshold values for each of the houses: 37, 20, 18, 23, 29) with a low level of seropositivity (only 1 detectable H7 titer [1:32] of 10 serum samples collected in the HPAIV-affected house).

Although no wild bird–origin precursor had all 8 segments that corresponded to the North Carolina and South Carolina H7N3 viruses, the most probable progenitor gene was identified for each individual segment as LPAIV originating from wild waterfowl migrating along the Mississippi flyway (PP 0.92–1.00). These findings suggest that a precursor virus most likely emerged in wild waterfowl in the Mississippi flyway, with subsequent introduction into poultry via occasional virus spread between migratory flyways (*11*). The genomes of North American LPAIVs appear to reassort at a remarkably high rate with no apparent pattern of gene segment association (*12*).

Wild bird origin H7 LPAIVs have repeatedly spilled over from wild birds into poultry in North and South America, Europe, Asia, Africa, and Australia (*13*); on 28 recorded occasions, they have mutated into HPAIV (*1*). These findings highlight the importance of global surveillance in wild birds and continued vigilance in biosecurity and surveillance in worldwide poultry populations.

Acknowledgments

The authors are grateful for the diagnostic testing laboratories (the Rollins Animal Disease Diagnostic Laboratory and the Clemson Veterinary Diagnostic Center, both members of the National Animal Health Laboratory Network) and state animal health authorities in North Carolina and South Carolina, including the state veterinarians (Douglas Meckes in North Carolina and

Boyd Parr in South Carolina), as well as their respective National Poultry Improvement Program officials (Michael Martin for North Carolina and Julie Helm for South Carolina) for their rapid response and recovery efforts.

This research was supported by the United States Department of Agriculture (USDA), Agricultural Research Service (ARS) project no. 6612-32000-066-00D and by the USDA/ARS Animal and Plant Health Inspection Service (APHIS) Interagency Agreement no. 60-6040-6-005. Its contents are solely the responsibility of the authors and do not necessarily represent the official views of the USDA.

About the Author

Dr. Youk is a postdoctoral researcher at the Southeast Poultry Research Laboratory, Agricultural Research Service, US Department of Agriculture, Athens, Georgia, USA. His research interests focus on molecular epidemiology and pathobiology of avian influenza viruses.

References

1. Lee DH, Criado MF, Swayne DE. Pathobiological origins and evolutionary history of highly pathogenic avian influenza viruses. Cold Spring Harb Perspect Med. 2020 Jan 21 [Epub ahead of print]. https://doi.org/10.1101/cshperspect.a038679
2. Lee DH, Torchetti MK, Killian ML, Berhane Y, Swayne DE. Highly pathogenic avian influenza A(H7N9) virus, Tennessee, USA, March 2017. Emerg Infect Dis. 2017;23:1860–3. https://doi.org/10.3201/eid2311.171013
3. Khatchikian D, Orlich M, Rott R. Increased viral pathogenicity after insertion of a 28S ribosomal RNA sequence into the haemagglutinin gene of an influenza virus. Nature. 1989;340:156–7. https://doi.org/10.1038/340156a0
4. Maurer-Stroh S, Lee RT, Gunalan V, Eisenhaber F. The highly pathogenic H7N3 avian influenza strain from July 2012 in Mexico acquired an extended cleavage site through recombination with host 28S rRNA. Virol J. 2013;10:139. https://doi.org/10.1186/1743-422X-10-139
5. Li J, Zu Dohna H, Cardona CJ, Miller J, Carpenter TE. Emergence and genetic variation of neuraminidase stalk deletions in avian influenza viruses. PLoS One. 2011;6:e14722. https://doi.org/10.1371/journal.pone.0014722
6. Stamatakis A. RAxML version 8: a tool for phylogenetic analysis and post-analysis of large phylogenies. Bioinformatics. 2014;30:1312–3. https://doi.org/10.1093/bioinformatics/btu033
7. Suchard MA, Lemey P, Baele G, Ayres DL, Drummond AJ, Rambaut A. Bayesian phylogenetic and phylodynamic data integration using BEAST 1.10. Virus Evol. 2018;4:vey016. https://doi.org/10.1093/ve/vey016
8. Youk S, Lee DH, Ferreira HL, Afonso CL, Absalon AE, Swayne DE, et al. Rapid evolution of Mexican H7N3 highly pathogenic avian influenza viruses in poultry. PLoS One. 2019;14:e0222457. https://doi.org/10.1371/journal.pone.0222457
9. Lee DH, Torchetti MK, Killian ML, Swayne DE. Deep sequencing of H7N8 avian influenza viruses from surveillance zone supports H7N8 high pathogenicity avian influenza was limited to a single outbreak farm in Indiana during 2016. Virology. 2017;507:216–9. https://doi.org/10.1016/j.virol.2017.04.025
10. Bandelt HJ, Forster P, Röhl A. Median-joining networks for inferring intraspecific phylogenies. Mol Biol Evol. 1999;16:37–48. https://doi.org/10.1093/oxfordjournals.molbev.a026036
11. Fourment M, Darling AE, Holmes EC. The impact of migratory flyways on the spread of avian influenza virus in North America. BMC Evol Biol. 2017;17:118. https://doi.org/10.1186/s12862-017-0965-4
12. Dugan VG, Chen R, Spiro DJ, Sengamalay N, Zaborsky J, Ghedin E, et al. The evolutionary genetics and emergence of avian influenza viruses in wild birds. PLoS Pathog. 2008;4:e1000076. ihttps://doi.org/10.1371/journal.ppat.1000076
13. World Organization for Animal Health. World Animal Health Information Database Interface: disease information [cited 2020 May 5]. https://www.oie.int/wahis_2/public/wahid.php/Diseaseinformation/Immsummary

Address for correspondence: Dong-Hun Lee, University of Connecticut, 61 N Eagleville Rd, Storrs, CT 06269 USA; email: dong-hun.lee@uconn.edu

Sensitive Detection of SARS-CoV-2–Specific Antibodies in Dried Blood Spot Samples

Gabriella L. Morley, Stephen Taylor, Sian Jossi, Marisol Perez-Toledo, Sian E. Faustini, Edith Marcial-Juarez, Adrian M. Shields, Margaret Goodall, Joel D. Allen, Yasunori Watanabe, Maddy L. Newby, Max Crispin, Mark T. Drayson, Adam F. Cunningham, Alex G. Richter,[1] Matthew K. O'Shea[1]

Dried blood spot (DBS) samples can be used for the detection of severe acute respiratory syndrome coronavirus 2 spike antibodies. DBS sampling is comparable to matched serum samples with a relative 98.1% sensitivity and 100% specificity. Thus, DBS sampling offers an alternative for population-wide serologic testing in the coronavirus pandemic.

A confirmed diagnosis of acute coronavirus disease (COVID-19) depends on the detection of RNA from the causative pathogen, severe acute respiratory syndrome coronavirus 2 (SARS-CoV-2). In contrast, although serologic testing is less useful for diagnosing the acute stages of infection, it can aid in diagnosing atypical manifestations of SARS-CoV-2 infection (M. Perez-Toledo et al., unpub. data, https://doi.org/10.1101/2020.06.05.20123117) and in determining prior virus exposure at a population level (*1*), knowledge which could substantially influence public health and social policies (*2*,*3*).

Currently, antibody testing for SARS-CoV-2 uses serum or plasma collected by venipuncture. The use of such sampling in large-scale seroepidemiologic studies is limited by logistic challenges, resources, and costs, as well as the risk for SARS-CoV-2 exposure from direct patient contact. In contrast, dried blood spot (DBS) sampling is simple, inexpensive, and can be self-collected and then sent by postal services to laboratories for processing (*4*). It is a well-established method for detecting antibodies against various infections (*5*,*6*), and antibodies collected by DBS are stable for prolonged periods (*7*). Moreover, DBS sampling provides a solution to widening access to serologic platforms in low- and middle-income countries. Nevertheless, the potential role of DBS sampling in studying SARS-CoV-2 seroprevalence has not been fully explored, and knowledge regarding the recovery of antibody from the DBS is limited. We describe the validation of DBS samples against matched serum in a highly sensitive and specific SARS-CoV-2 ELISA.

The Study

We collected 87 samples from 80 volunteers at the University Hospitals Birmingham NHS Foundation Trust (under approved protocol for blood donations use in clinical assays, UK Research Ethics Committee reference no. 2002/201 and Clinical Immunology Service Reference no. ERN_16-178) during May 18–June 3, 2020. Three matched samples were from SARS-CoV-2 serum antibody–negative volunteers. The remaining samples were from SARS-CoV-2 serum antibody–unknown volunteers; 5 volunteers provided duplicate and 1 volunteer provided triplicate matched samples (Appendix Figure, https://wwwnc.cdc.gov/EID/article/26/12/20-3309-App1.pdf). To refine negative thresholds, we included 17 pre–August 2019 DBS-only samples (UK Research Ethics Committee reference no. 2002/20, Integrated Research Application System reference no. 132132, University Hospitals Birmingham project reference no. RRK4136). Volunteers were healthy at the time of sampling. Thirty-one matched samples (31/87 [35.6%]) were from PCR-positive volunteers, on average, 54 days (SD ± 17 days) from reported symptom onset and 45 days (SD ± 15 days)

Author affiliations: University of Birmingham, Birmingham, UK (G.L. Morley, S. Taylor, S. Jossi, M. Perez-Toledo, S.E. Faustini, E. Marcial-Juarez, A.M. Shields, M. Goodall, M.T. Drayson, A.F. Cunningham, A.G. Richter, M.K. O'Shea); The Saving Lives Charity, Birmingham (S. Taylor); University Hospitals Birmingham NHS Foundation Trust, Birmingham (S. Taylor, A.M. Shields, A.G. Richter, M.K. O'Shea); University of Southampton, Southampton, UK (J.D. Allen, Y. Watanabe, M.L. Newby, M. Crispin); University of Oxford, Oxford, UK (Y. Watanabe)

DOI: https://doi.org/10.3201/eid2612.203309

[1]These senior authors contributed equally to this article.

Table 1. Mean concentrations of SARS-CoV-2 IgG, IgA, and IgM measured in matched DBS eluate and serum samples

Sample type	Mean immunoglobulin concentration, g/L*		
	IgG (range)	IgA (range)	IgM (range)
DBS	1.08 (0.17–2)	0.25 (0.1–0.6)	0.13 (0.1–0.3)
Serum	11.77 (8.18–18.59)	2.55 (1.5–5.2)	0.99 (0.3–1.5)

*DBS, dried blood spot; SARS-CoV-2, severe acute respiratory syndrome coronavirus 2.
†Includes 10 matched DBS and serum and 5 pre–August 2019 DBS.

from PCR testing. All participants were anonymized, and SARS-CoV-2 PCR status was recorded as positive or unknown.

For DBS collection, we collected capillary blood samples onto forensic-grade 226 DBS cards (Ahlstrom Munksjo, https://www.ahlstrom-munksjo.com) by using finger-prick lancets (*4*,*8*). We stored DBS cards at room temperature in individual sample bags with desiccant. Concomitantly, we collected venous blood from volunteers and separated serum by using centrifugation at 9,700 × *g* for 5 min at room temperature. Laboratory analysis was blinded to PCR status, and we reported SARS-CoV-2–specific antibody results as positive, negative, or equivocal.

To elute antibody from DBS cards, we isolated individual preperforated DBS spots by using a sterile pipette tip and placed them into a universal tube at a ratio of 1 spot to 250 μL 0.05% phosphate-buffered saline (PBS)–Tween 20 (PBS-T) (PBS, xoid; Tween-20; Sigma-Aldrich, https://www.sigmaaldrich.com). We briefly vortexed and incubated tubes overnight at room temperature. We then harvested DBS eluate into a microtube and centrifuged it at 10,600 × *g* for 10 min at room temperature. We stored eluate at 4°C for ≤14 days in accordance with standard protocols (*4*). We quantified total IgG, IgA, and IgM concentrations in matched serum and DBS eluate, plus pre–August 2019 DBS samples, with nephelometry by using the automated COBAS 6000 (Roche, https://www.roche.com).

We performed a highly sensitive and specific in-house ELISA (now under peer review) to measure IgG, IgA and IgM against soluble, stabilized, trimeric SARS-CoV-2 spike (S) glycoprotein (*9*,*10*), as previously described (S.E. Faustini et al., unpub. data, https://doi.org/10.1101/2020.06.16.2013302. In brief, we coated Nunc 96-well plates (ThermoFisher, https://www.thermofisher.com) with 50 μL of 2 μg/mL S glycoprotein (M. Perez-Toledo et al.; S.E. Faustini et al.). We blocked plates and diluted samples with 2% BSA 0.1% PBS-T (PBS, Oxoid; Tween-20 and BSA, Sigma-Aldrich) at starting dilutions of 1:3 DBS eluate and 1:15 serum, with 3-fold serial dilutions; or single dilutions of 1:10 DBS eluate and 1:100 serum. We diluted mouse monoclonal anti–human horseradish peroxidase conjugated antibodies (anti–IgG R-10 1:8,000, anti–IgA MG4.156 1:4,000, and anti–IgM AF6 1:2,000; Abingdon Health, https://www.abingdonhealth.com) in 0.1% PBS-T. We developed plates with TMB Core (Bio-Rad, https://www.bio-rad.com) and stopped them after 5 min with 0.2M H_2SO_4 (Sigma-Aldrich). We recorded optical densities at 450 nm (OD_{450}) by using the Dynex Revelation (Dynex Technologies, https://www.dynextechnologies.com). We reported results as SARS-CoV-2 S antibody positive, negative, or equivocal. The cutoff for negativity was less than the highest negative control (DBS 0.399 OD_{450} and serum 0.449 OD_{450}), and for positivity, the mean of the negative controls +3 SD (DBS 0.444 OD_{450} and serum 0.62 OD_{450}); a result between this range was considered equivocal.

We performed statistical analyses by using Prism 8 (GraphPad, https://www.graphpad.com) and

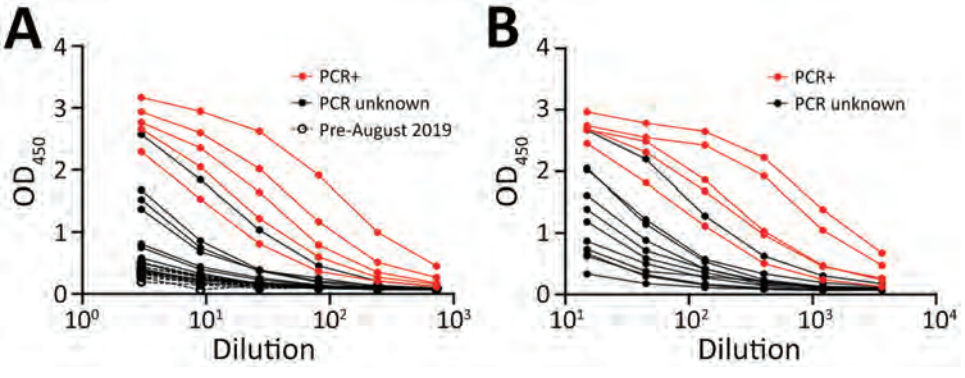

Figure 1. Elution of SARS-CoV-2 anti-spike glycoprotein antibodies from DBS samples, showing 3-fold DBS eluate (A) (initial 1:3 dilution) and serum (B) (initial 1:15 dilution) titrations. Dashed line indicates pre–August 2019 DBS samples (n = 11). Red circles indicate PCR-positive samples (n = 5). Black circles indicate PCR-unknown samples (n = 11), from matched contemporaneous samples. All samples were selected at random for inclusion. DBS, dried blood spot; OD_{450}, optical density at 450 nm; SARS-CoV-2, severe acute respiratory syndrome coronavirus 2.

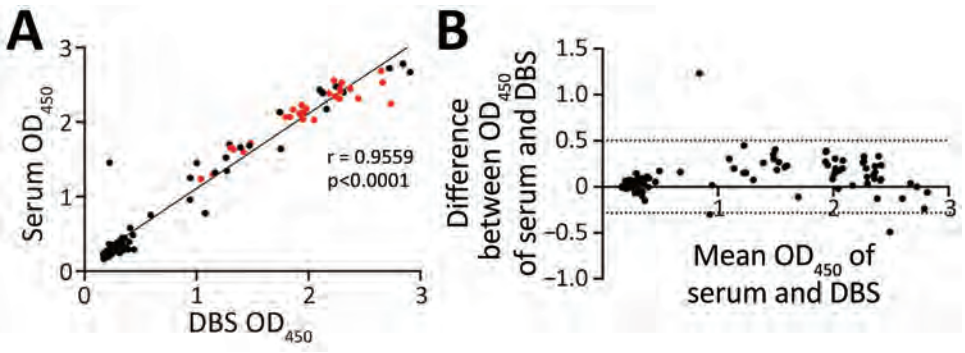

Figure 2. Effectiveness of DBS sampling for SARS-CoV-2 anti-spike glycoprotein detection. A) Correlation between matched DBS eluate (1:10) and serum (1:100) OD_{450} ELISA results (n = 87). Red circles indicate PCR-positive samples (n = 31). Black circles indicate PCR-unknown samples (n = 56). B) Bland-Altman mean-difference comparison of DBS eluate (1:10) and serum (1:100) OD_{450} ELISA results (dashed lines indicate 95% limits of agreement [-0.281 to 0.504]). DBS, dried blood spot; OD_{450}, optical density at 450 nm; SARS-CoV-2, severe acute respiratory syndrome coronavirus 2.

assessed correlations between continuous data by using Spearman's rank test ($p<0.05$ was considered statistically significant). We assessed DBS sample ELISA performance, relative to the serum assay, by calculating the comparative sensitivity, specificity, and positive and negative predictive values, with 95% CIs. We assessed the agreement between DBS and serum ELISA results by determining the Cohen κ coefficient and Bland-Altman mean-difference.

We performed quantification of total immunoglobulin concentrations in serum and DBS eluate. We observed 7- to 11-fold reduction in mean immunoglobulin concentration (IgG, IgA, and IgM) in DBS eluate compared with matched serum (Table 1). Matched serum and DBS titration curves showed the detection of SARS-CoV-2 S glycoprotein antibodies in both serum and DBS eluate with the limits of detection and the optimal detection dilution indicated (1:10 for DBS eluate and 1:100 for serum). PCR-positive matched samples showed higher responses, whereas pre–August 2019 DBS samples were negative across all dilutions (Figure 1).

We measured OD_{450} detected by ELISA for matched DBS eluate (diluted 1:10) and serum (diluted 1:100). We observed a significant correlation between matched serum and DBS samples (r = 0.96 [95% CI 0.93–0.97]; $p<0.0001$) (Figure 2, panel A) and minimal differences in results observed by sample type (Bland-Altman bias 0.11 ± 0.20) (Figure 2, panel B). Discordance occurred between only 1 matched sample (κ = 0.975). Relative to serum samples, DBS samples achieved 98.11% sensitivity and 100% specificity for detecting S glycoprotein antibodies (Table 2); 100% of the PCR-positive samples (n = 31) were also antibody-positive in DBS eluate.

Table 2. DBS eluate SARS-CoV-2 ELISA sensitivity and specificity relative to serum samples*

Sample type		Serum +	Serum –
DBS	+	52	0
	–	1	31
Sensitivity, % (95% CI)		98.11 (89.93–99.95)	
Specificity, % (95% CI)		100 (88.78–100.00)	
PPV, %		100	
NPV, % (95% CI)		96.88 (81.65–99.54)	
Cohen's kappa coefficient (95% CI)		0.975 (0.925–1.00)	

*Includes 87 matched DBS and serum samples tested for the detection of SARS-CoV-2 anti-spike glycoprotein; positive or negative matched samples (n = 84) were included, and equivocal results (n = 3) were excluded from the sensitivity and specificity analysis. DBS, dried blood spot; NPV, negative predictive value; PPV, positive predictive value; SARS-CoV-2, severe acute respiratory syndrome coronavirus 2.

Conclusions

We show that DBS samples can be used for the detection of SARS-CoV-2–specific antibodies with results comparable to serum samples, supporting the findings of recent preliminary studies (*11*,*12*). Although individual laboratories should optimize DBS-derived antibody detection, considering dilution-factor and cutoff thresholds for their relevant downstream assay, these results demonstrate that DBS sampling could complement venipuncture for serologic assessments, such as seroprevalence studies, during the COVID-19 pandemic.

A current limitation of antibody assays is the necessity for venipuncture by skilled phlebotomists; DBS sampling overcomes this limitation and introduces the opportunity for wider population-level testing and improved surveillance in groups at heightened risk for infection. For example, DBS could be delivered using postal services (*4*) to patients with chronic conditions, the immunocompromised, and the elderly, all of which are groups disproportionately affected by COVID-19 (*13*). Furthermore, the DBS method is simple and inexpensive (*4*), which could enhance sampling in low- and middle-income countries, among groups where venipuncture is culturally unacceptable or in a geographically dispersed population.

Acknowledgments

We would like to thank the University of Birmingham Clinical Immunology Service for their invaluable support in sample collection and processing. We also thank Cynthia D'Aguilar and Julie Williams for logistic support in sample collection. We are grateful for the expertise of Margaret Goodall in generating the mouse monoclonal anti–human horseradish peroxidase conjugated antibodies.

This work was supported by the Wellcome Trust and the National Institute for Health Research Birmingham Biomedical Research Centre at the University Hospitals Birmingham NHS Foundation Trust and the University of Birmingham. The views expressed are those of the authors and not necessarily those of the National Institute for Health Research or the Department of Health and Social Care. This project was supported by the Saving Lives Charity (UK Charity Commission no. 1144855) who kindly provided the dried blood spot collection cards. The work, conducted in Max Crispin's laboratory, was funded by the International AIDS Vaccine Initiative, Bill and Melinda Gates Foundation through the Collaboration for AIDS Vaccine Discovery (grants nos. OPP1196345/INV-008813, OPP1084519, and OPP1115782), the Scripps Consortium for HIV Vaccine Development (National Institutes of Health National Institute for Allergy and Infectious Diseases grant no. AI144462), and the University of Southampton Coronavirus Response Fund.

S.T. is the medical director of the Saving Lives Charity. M.T.D. and M.G. report stocks in Abingdon Health (outside the submitted work).

About the Author

Dr. Morley is a clinician specializing in public health, currently undertaking her PhD research, which is focused on humoral immunology, at the University of Birmingham. She worked on SARS-CoV-2 diagnostics and research during the COVID-19 pandemic at the University of Birmingham.

References

1. Wang W, Xu Y, Gao R, Lu R, Han K, Wu G, et al. Detection of SARS-CoV-2 in different types of clinical specimens. JAMA. 2020;323:1843–4. https://doi.org/10.1001/jama.2020.3786
2. Long Q-X, Tang X-J, Shi Q-L, Li Q, Deng H-J, Yuan J, et al. Clinical and immunological assessment of asymptomatic SARS-CoV-2 infections. Nat Med. 2020;26:1200–4. https://doi.org/10.1038/s41591-020-0965-6
3. Shields A, Faustini SE, Perez-Toledo M, Jossi S, Aldera E, Allen JD, et al. SARS-CoV-2 seroprevalence and asymptomatic viral carriage in healthcare workers: a cross-sectional study. Thorax. 2020 Sep 11 [Epub ahead of print]. https://doi.org/10.1136/thoraxjnl-2020-215414
4. Page M, Atabani SF, Wood M, Smit E, Wilson S, Atherton C, et al. Dried blood spot and mini-tube blood sample collection kits for postal HIV testing services: a comparative review of successes in a real-world setting. Sex Transm Infect. 2019;95:43–5. https://doi.org/10.1136/sextrans-2018-053567
5. Vázquez-Morón S, Ryan P, Ardizone-Jiménez B, Martín D, Troya J, Cuevas G, et al. Evaluation of dried blood spot samples for screening of hepatitis C and human immunodeficiency virus in a real-world setting. Sci Rep. 2018;8:1858. https://doi.org/10.1038/s41598-018-20312-5
6. Condorelli F, Scalia G, Stivala A, Gallo R, Marino A, Battaglini CM, et al. Detection of immunoglobulin G to measles virus, rubella virus, and mumps virus in serum samples and in microquantities of whole blood dried on filter paper. J Virol Methods. 1994;49:25–36. https://doi.org/10.1016/0166-0934(94)90052-3
7. Behets F, Kashamuka M, Pappaioanou M, Green TA, Ryder RW, Batter V, et al. Stability of human immunodeficiency virus type 1 antibodies in whole blood dried on filter paper and stored under various tropical conditions in Kinshasa, Zaire. J Clin Microbiol. 1992;30:1179–82. https://doi.org/10.1128/JCM.30.5.1179-1182.1992
8. Grüner N, Stambouli O, Ross RS. Dried blood spots—preparing and processing for use in immunoassays and in molecular techniques. J Vis Exp. 2015;97:52619. https://doi.org/10.3791/52619
9. Wrapp D, Wang N, Corbett KS, Goldsmith JA, Hsieh C-L, Abiona O, et al. Cryo-EM structure of the 2019-nCoV spike in the prefusion conformation. Science. 2020;367:1260–3. https://doi.org/10.1126/science.abb2507
10. Watanabe Y, Allen JD, Wrapp D, McLellan JS, Crispin M. Site-specific glycan analysis of the SARS-CoV-2 spike. Science. 2020;369:330–3. https://doi.org/10.1126/science.abb9983
11. McDade TW, McNally EM, Zelikovich AS, D'Aquila R, Mustanski B, Miller A, et al. High seroprevalence for SARS-CoV-2 among household members of essential workers detected using a dried blood spot assay. PLoS One. 2020;15:e0237833. https://doi.org/10.1371/journal.pone.0237833
12. Thevis M, Knoop A, Schaefer MS, Dufaux B, Schrader Y, Thomas A, et al. Can dried blood spots (DBS) contribute to conducting comprehensive SARS-CoV-2 antibody tests? Drug Test Anal. 2020;12:994–7. https://doi.org/10.1002/dta.2816
13. Jordan RE, Adab P, Cheng KK. Covid-19: risk factors for severe disease and death. BMJ. 2020;368:m1198. https://doi.org/10.1136/bmj.m1198

Address for correspondence: Matthew K. O'Shea. Institute of Immunology and Immunotherapy, College of Medical and Dental Sciences, University of Birmingham, Birmingham B15 2TT, UK; email: m.k.oshea@bham.ac.uk

Antibody Profiles According to Mild or Severe SARS-CoV-2 Infection, Atlanta, Georgia, USA, 2020

William T. Hu, J. Christina Howell, Tugba Ozturk, Karima Benameur, Leda C. Bassit, Richard Ramonell, Kevin S. Cashman, Shama Pirmohammed, John D. Roback, Vincent C. Marconi, Irene Yang, Valerie V. Mac, Daniel Smith, Ignacio Sanz, Whitney Wharton, F. Eun-Hyung Lee, Raymond F. Schinazi

Among patients with coronavirus disease (COVID-19), IgM levels increased early after symptom onset for those with mild and severe disease, but IgG levels increased early only in those with severe disease. A similar pattern was observed in a separate serosurveillance cohort. Mild COVID-19 should be investigated separately from severe COVID-19.

Coronavirus disease (COVID-19) emerged in December 2019 (*1*,*2*), and by June 2020, ≈10 million persons worldwide had acquired the disease. The confirmatory test for severe acute respiratory syndrome virus 2 (SARS-CoV-2) infection remains real-time reverse transcription PCR, but this test poses challenges in terms of sensitivity (*3*), reagent or equipment availability, and specialized personnel training. Serologic assays can be readily performed in most clinical laboratories, with faster turnaround times, but their association with COVID-19 has largely been reported for hospitalized patients with severe disease (*4*; E. Adams et al., unpub. data, https://www.medrxiv.org/content/10.1101/2020.04.15.20066407v1.full.pdf). Whether mild and severe COVID-19 represent 2 interlinked stages on a severity continuum or 2 distinct phenotypes of an infectious process (*5*) remains incompletely understood; detailed cross-sectional characterization of IgM and IgG reactive against SARS-CoV-2 antigens may provide insight into the temporal evolution of antibodies. Detection of cross-reactive antibodies from a pre-2020 cohort can also indicate whether past exposure to other coronaviruses is associated with cross-reactive protection against SARS-CoV-2.

In addition to IgG targeting the receptor-binding domain (RBD) of the spike protein subunit S1 (*6*), we developed and validated an IgM assay targeting the full-length S1 protein. We further developed and validated an IgM assay targeting the small full-length envelope (E) protein, which is highly shared between SARS-CoV and SARS-CoV-2 (*2*), is accessible on the surface, and increases during virus replication (*7*). Using these assays, we characterized the IgM and IgG profiles of participants with COVID-19, pre-2020 control participants, and a community cohort of 116 persons who had recovered from self-limited illness during March and April 2020 in Atlanta, Georgia, USA.

The Study

We recruited 28 participants hospitalized for severe COVID-19 (20 requiring artificial ventilation; samples collected during hospitalization a median of 15.5 days after symptom onset) and 15 participants who had recently recovered from mild COVID-19 (samples collected a median of 15 days after symptom onset; Table 1). Compared with hospitalized participants, participants with mild illness were less likely to be African American (*8*) and more likely to be younger and to have nasal congestion or anosmia.

Compared with control participants, hospitalized participants had higher levels of IgG against S1-RBD ($\log_{10}$ transformed because of nonnormal distribution; Student t [56.7] = 12.183; p<0.0001; Figure 1, panel A), IgM against S1 (Student t [33.29] = 3.713; p<0.001; Figure 1, panel B), and IgM against E (t [129] = 2.279; p = 0.024; Figure 1, panel C). The same was true among participants with mild illness for IgG against S1-RBD (Student t [116] = 4.246; p<0.0001; Figure 1, panel A), IgM against S1 (Student t [116] = 6.764; p<0.0001; Figure 1, panel B), and IgM against E (Student t [116] = 3.398; p = 0.001; Figure 1, panel C). However, an IgG diagnostic

Author affiliation: Emory University, Atlanta, Georgia, USA

DOI: https://doi.org/10.3201/eid2612.203334

Table 1. Demographic and other information for persons with known coronavirus disease, pre-2020 controls, and persons with influenza-like illness but negative for SARS-CoV-2, Atlanta, Georgia, USA, 2020*

Characteristic	Hospitalized, n = 28	Mild disease, n = 15	Pre-2020 control, n = 103	p value
Sex, %				0.273
F	14 (50)	7 (47)	65 (63)	
M	14 (50)	8 (53)	38 (37)	
Median age, y (range)	61.5 (29–85)†	32 (26–81)†	62.5 (24–87)	<0.0001
Race, no. (%)				<0.0001
Asian	3 (11)	0	2 (2)	
African American	18 (64)†	1 (7)†	15 (14)	
Non-Hispanic Caucasian	6 (21)	12 (80)	82 (80)	
Hispanic	1 (4)	1 (7)	0	
Other	0	1 (7)	4 (4)	
Clinical features				
Inpatient/outpatient	28/0	1/14	NA	<0.0001
Respiratory failure requiring intubation, %	20 (71)†	0†	NA	<0.0001
Median days since symptom onset (range)	15.5 (4–42)	15 (9–33)	NA	0.427
Clinical signs/symptoms				
Cough	22 (79)	10 (67)	NA	0.473
Fever/chills	22 (79)	9 (64)	NA	0.287
Shortness of breath	20 (71)	5 (33)	NA	0.024
Myalgia	7 (25)	9 (60)	NA	0.045
Headaches	7 (25)	7 (47)	NA	0.184
Sore throat	5 (18)	6 (40)	NA	0.150
Nasal congestion/rhinorrhea	2 (7)	8 (53)	NA	0.001
Diarrhea	5 (18)	3 (20)	NA	1.000
Anosmia	1 (4)	7 (47)	NA	0.001
Fatigue	3 (11)	3 (20)	NA	0.647
Vomiting	0	1 (7)	NA	0.349
Never symptomatic	0	0	NA	0.012
Laboratory features				
SARS-CoV-2 detected by rRT-PCR	28/28	10/10	NA	<0.0001
Mean anti-S1-RBD IgG (± SD), OD	1.72 (0.72)†	0.71 (0.60)†	0.26 (0.36)	<0.0001
Mean anti-S1 IgM (± SD), OD	1.76 (0.74)	2.12 (0.53)	1.21 (0.48)	<0.0001
Mean anti-E IgM (± SD), OD	1.85 (0.90)	2.16 (0.72)	1.48 (0.71)	0.001

*E, envelope protein; NA, not applicable; OD, optical density, RBD, receptor-binding domain; rRT-PCR, real-time reverse transcription PCR; SARS-CoV-2, severe acute respiratory syndrome coronavirus 2; S1, spike protein subunit S1.
†Different between patients who were hospitalized and who had mild disease at p<0.005.

threshold of 0.82 optical density (OD) (Appendix, https://wwwnc.cdc.gov/EID/article/26/12/20-3334-App1.pdf) from the hospitalized participants identified only 4 (26.7%) of 15 participants with mild disease because of the lower IgG levels early after symptom onset in the group with mild disease. Elevated IgG only weeks after symptom onset among participants with mild COVID-19 is consistent with prior reports (*9*; E. Adams et al., unpub. data, https://www.medrxiv.org/content/10.1101/2020.04.15.20066407v1.full.pdf), and linear regression analysis projected that their IgG would reach the threshold of hospitalized participants an average of 29 days after symptom onset.

Conversely, IgM negatively correlated with time since symptom onset for hospitalized participants but not for those with mild disease. An anti-S1 IgM level of 1.60 OD from hospitalized patients during the first 21 days—before significant IgM decline—and 50-fold randomly selected control participants showed sensitivity of 81.0% and median specificity of 80.4% (range 76%–85.5%). The threshold of 1.60 OD was in range with values derived from pre-adsorption experiments that used S1 antigen (1.75 OD; Appendix) and identified participants with mild disease with sensitivity of 80.0% and median specificity of 80.5% (range 80%–86.7%). Anti-E IgM levels showed similar associations with time from symptom onset and severity but did not increase identification of COVID-19 participants.

Because many persons with mild influenza-like (ILI) symptoms in the metropolitan Atlanta area did not or could not access SARS-CoV-2 testing during early 2020, we also analyzed antibody levels in 116 adults who had recovered from self-limited ILI symptoms (Table 2). Compared with participants with mild COVID-19, this cohort was less likely to have anosmia (11% vs. 47%; p = 0.002) or fatigue (4% vs. 20%; p = 0.048) but was otherwise similar in terms of sex, race, age, and signs/symptoms. Of 31 participants with symptom onset 7–29 days before blood collection, 1 (3%) had elevated IgG, and 11 (12.9%) of 85 with symptom onset 30–60 days before participation had elevated IgG. None of the clinical signs/symptoms

strongly predicted antibody levels. A liberal threshold of anti-S1 IgM ≥1.60 OD identified 18/31 (58%) and 57/85 (67%) participants, and a more stringent threshold of 2.00 OD to reduce false positives identified 7/31(22%) and 41/85 (48%) participants.

Last, we performed plaque-reduction neutralization assays (PRNT; Appendix) for a subgroup of participants with confirmed or probable COVID-19 and pre-2020 control participants (75% with elevated antibody levels; Figure 2, panel A). All 6 hospitalized participants and 5 participants with mild disease (2 weak neutralizing results ≤1:40) demonstrated >90% plaque reduction in Vero cells compared with 2 of 15 control participants who also showed weak neutralization. Using positive PRNT at >1:40 as a specific threshold, we found simultaneously elevated IgM and IgG most predictive of positive PRNT (p = 0.008 compared with IgM alone, p = 0.07 compared with IgG alone; Appendix), although plasma from 1 hospitalized participant with neutralizing plasma had reference IgM and IgG levels. PRNT for community participants

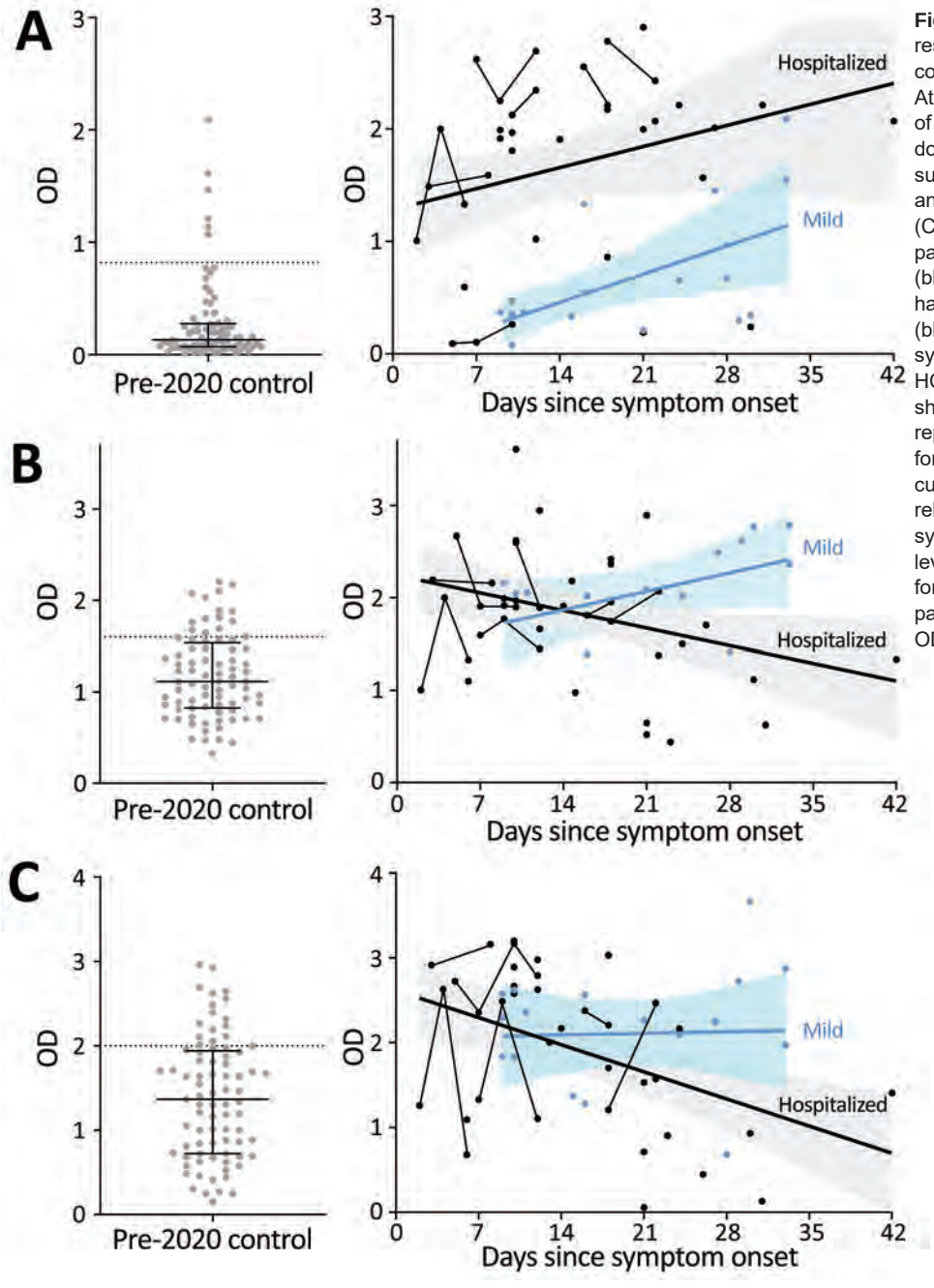

Figure 1. Serologic assay results for study participants with coronavirus disease (COVID-19), Atlanta, Georgia, USA, 2020. Levels of IgG against the receptor-binding domain (RBD) of the spike protein subunit S1 (A), IgM against S1 (B), and IgM against envelope protein (C) were analyzed for hospitalized patients with severe COVID-19 (black circles) and patients who had recovered from mild COVID-19 (blue circles) according to time from symptom onset. Levels in pre-2020 HC participants (gray circles) are shown for comparison; dotted lines represent optimal threshold levels for receiver operating characteristic curve analysis. Best fit lines for relationships between time since symptom onset and antibody levels were calculated separately for hospitalized participants and participants with mild COVID-19. OD, optical density.

Table 2. Demographic and other information for a prospective cohort who recovered from an influenza-like illness, Atlanta, Georgia, USA, 2020

Characteristic	IgG <0.82, IgM <2.00, n = 60	IgG <0.82, IgM ≥2.00, n = 44	IgG ≥0.82, IgM <2.00, n = 8	IgG ≥0.82, IgM ≥2.00, n = 4	p value
Symptom onset, no. (%)					0.029
7–29 d earlier	23 (38)	7 (16)	1 (12)	0	
30–60 d earlier	37 (62)	37 (84)	7 (88)	4 (100)	
Sex, no. (%)					0.042
F	29 (48)	33 (75)	4 (50)	3 (75)	
M	31 (52)	11 (25)	4 (50)	1 (25)	
Median age, y (range)	45.5 (19.4–73.7)	34.9 (25.9–73.3)	43.6 (31.7–62.3)	37.3 (33.5–48.2)	0.113
Non-Hispanic Caucasian	47 (78)	36 (82)	6 (75)	4 (100)	0.715
Healthcare worker	35 (58)	27 (61)	4 (50)	2 (50)	0.918
Potential exposure to coronavirus disease	37 (62)	22 (50)	5 (62)	2 (50)	0.662
Never smoker	51 (85)	38 (86)	7 (88)	2 (50)	0.119
Clinical signs/symptoms					
Cough	38 (63)	37 (84)	2 (25)	4 (100)	0.002
Fever/chills	21 (35)	21 (48)	2 (25)	3 (75)	0.214
Shortness of breath	21 (35)	13 (29)	1 (12)	3 (75)	0.166
Myalgia	34 (57)	21 (48)	4 (50)	4 (100)	0.228
Headaches	38 (63)	21 (48)	3 (37)	3 (75)	0.238
Sore throat	27 (45)	25 (57)	3 (37)	4 (100)	0.117
Nasal congestion/rhinorrhea	37 (62)	30 (68)	3 (37)	0	0.029
Diarrhea	11 (18)	13 (29)	2 (25)	2 (50)	0.352
Anosmia	6 (10)	5 (11)	0	2 (50)	0.067
Fatigue	1 (2)	4 (9)	0	0	0.262
Vomiting	2 (3)	3 (7)	0	0	0.717

with the 10 most elevated IgG levels showed a similar trend (Figure 2, panel B).

Conclusions

IgM reactive toward S1 and E proteins increased early regardless of disease severity, but IgG increased early only in hospitalized participants with severe COVID-19. This pattern was observed in a separate cohort of community participants who had recovered from self-limited ILI. Positive PRNT—a surrogate for antibody-mediated immune protection—may be better associated with elevated IgM and IgG than either antibody alone.

A diagnostic algorithm of IgG from hospitalized participants performed poorly for detection of mild COVID-19. Similarly, other studies found delayed or low-to-medium neutralizing antibody titers in persons who recovered from mild COVID-19 (E. Adams et al., unpub. data, https://www.medrxiv.org/content/10.

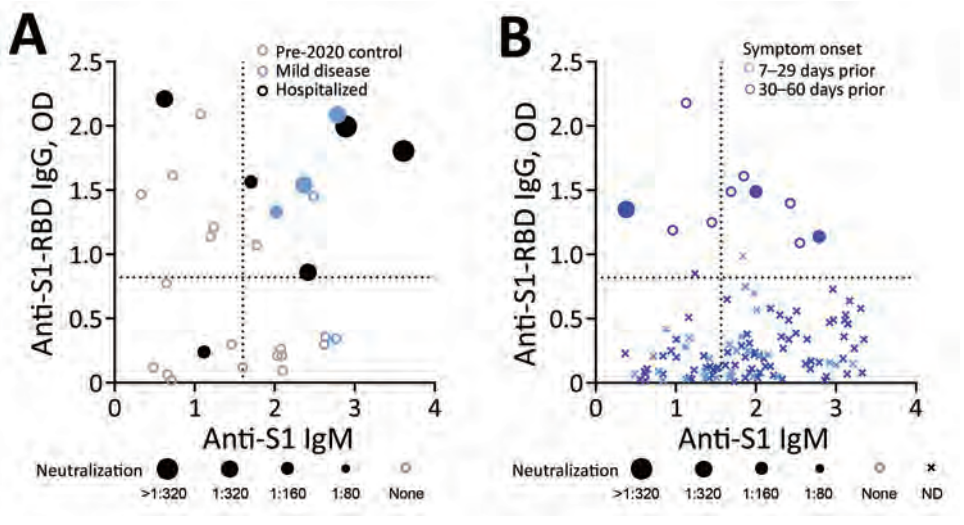

Figure 2. Severe acute respiratory syndrome coronavirus 2 virus neutralization measures according to anti-S1-RBD IgG and anti-S1 IgM levels, Atlanta, Georgia, USA, 2020. Open circles represent negative plaque-reduction neutralization test (PRNT) result, and solid circles represent positive PRNT result (sizes of filled circles are proportional to maximal dilution with positive PRNT result). Dotted lines indicate threshold values. A) Among participants with coronavirus disease (COVID-19) (mild disease and hospitalized), pre-2020 controls with elevated antibody levels, and pre-2020 controls with normal antibody levels, positive PRNT results were most associated with simultaneously elevated IgM and IgG levels (Appendix, https://wwwnc.cdc.gov/EID/article/26/12/20-3334-App1.pdf). B) Analysis of a group of 116 persons who reported recovery from self-limited illness 7–60 days prior showed a similar trend. ND, not done; RBD, receptor-binding domain; S1, spike protein subunit 1.

1101/2020.04.15.20066407v1.full.pdf; F. Wu et al., unpub. data, https://www.medrxiv.org/content/10.1101/2020.03.30.20047365v2). The delayed increase in IgG and neutralizing antibodies in persons with mild COVID-19 also suggests that mild cases do not necessarily represent an intermediate stage between severe and asymptomatic COVID-19. A corollary of slow IgG increases in persons with mild COVID-19 may be longer persistence of IgM, but more definitive characterization of IgM+ memory B cells (*10*) and long-term decay of antibody levels (*11*) is needed.

Our study has limitations. Our small cross-sectional cohort of patients with well-characterized and laboratory-confirmed COVID-19 limits generalization. The overrepresentation of African Americans in the more severely ill cohort may mediate some differences in antibody profiles (*8*), and we did not measure IgA levels or antibodies targeting other SARS-CoV-2 gene products (currently under development and validation). We also did not measure antibody levels in historic SARS or MERS case-patients, and cross-reactive antibody response against homologous regions cannot be ruled out.

We did confirm a complex relationship between antibody levels, disease severity, and time since symptom onset. Examining IgM and IgG against multiple SARS-CoV-2–related antigens may thus better inform natural history and vaccine studies than any one antibody.

This article was preprinted at https://www.medrxiv.org/content/10.1101/2020.05.10.20097535v1

This work was supported by National Institutes of Health grants R01 AG 054046, R01 AG054991, and T32HL116271.

W.T.H. and Emory University have licensed the IgM assay panel for SARS-CoV-2, have a patent on the cerebrospinal fluid–based diagnosis of frontotemporal lobar degeneration with TDP-43 inclusions, and have a patent pending on the cerebrospinal fluid–based prognosis of spinal muscular atrophy. W.T.H. has consulted for ViveBio, LLC; AARP, Inc.; and Biogen, Inc. and has received research support from Fujirebio US. F.E.-H.L. is the founder of MicroB-plex, Inc., and has research grants with Genentech, Inc.

About the Author

Dr. Hu is a physician-scientist at Emory University in Atlanta, GA. His research interests involve reliable fluid biomarkers for human diseases related to inflammation.

References

1. Huang C, Wang Y, Li X, Ren L, Zhao J, Hu Y, et al. Clinical features of patients infected with 2019 novel coronavirus in Wuhan, China. Lancet. 2020;395:497–506. https://doi.org/10.1016/S0140-6736(20)30183-5
2. Wu F, Zhao S, Yu B, Chen YM, Wang W, Song ZG, et al. A new coronavirus associated with human respiratory disease in China. Nature. 2020;579:265–9. https://doi.org/10.1038/s41586-020-2008-3
3. Wang W, Xu Y, Gao R, Lu R, Han K, Wu G, et al. Detection of SARS-CoV-2 in different types of clinical specimens. JAMA. 2020. https://doi.org/10.1001/jama.2020.3786
4. Amanat F, Nguyen THO, Chromikova V, Strohmeier S, Stadlbauer D, Javier A, et al. A serological assay to detect SARS-CoV-2 seroconversion in humans. Nat Med 2020;26:1033–6. https://doi.org/10.1038/s41591-020-0913-5
5. Okba NMA, Müller MA, Li W, Wang C, GeurtsvanKessel CH, Corman VM, et al. Severe acute respiratory syndrome coronavirus 2-specific antibody responses in coronavirus disease patients. Emerg Infect Dis. 2020;26:1478–88. https://doi.org/10.3201/eid2607.200841
6. Wan Y, Shang J, Graham R, Baric RS, Li F. Receptor recognition by the novel coronavirus from Wuhan: an analysis based on decade-long structural studies of SARS coronavirus. J Virol. 2020;94:e00127-20. https://doi.org/10.1128/JVI.00127-20
7. Nieto-Torres JL, Dediego ML, Alvarez E, Jiménez-Guardeño JM, Regla-Nava JA, Llorente M, et al. Subcellular location and topology of severe acute respiratory syndrome coronavirus envelope protein. Virology. 2011;415:69–82. https://doi.org/10.1016/j.virol.2011.03.029
8. Bernard NJ. Double-negative B cells. Nat Rev Rheumatol. 2018;14:684. https://doi.org/10.1038/s41584-018-0113-6
9. Bao M, Zhang Y, Wan M, Dai L, Hu X, Wu X, et al. Anti-SARS-CoV immunity induced by a novel CpG oligodeoxynucleotide. Clin Immunol. 2006;118:180–7. https://doi.org/10.1016/j.clim.2005.09.014
10. Pape KA, Taylor JJ, Maul RW, Gearhart PJ, Jenkins MK. Different B cell populations mediate early and late memory during an endogenous immune response. Science. 2011;331:1203–7. https://doi.org/10.1126/science.1201730
11. Liu X, Wang J, Xu X, Liao G, Chen Y, Hu CH. Patterns of IgG and IgM antibody response in COVID-19 patients. Emerg Microbes Infect. 2020;9:1269–74. https://doi.org/10.1080/22221751.2020.1773324

Address for correspondence: William T. Hu, Neurology, Emory University, 615 Michael St, 505F, Atlanta, GA 30322; email: wthu@emory.edu

Experimental Infection of Cattle with SARS-CoV-2

Lorenz Ulrich, Kerstin Wernike, Donata Hoffmann, Thomas C. Mettenleiter, Martin Beer

We inoculated 6 cattle with severe acute respiratory syndrome coronavirus 2 and kept them together with 3 in-contact, virus-naive cattle. We observed viral replication and specific seroreactivity in 2 inoculated animals, despite high levels of preexisting antibody titers against a bovine betacoronavirus. The in-contact animals did not become infected.

After spilling over from an unknown animal host to humans, a novel betacoronavirus called severe acute respiratory syndrome coronavirus 2 (SARS-CoV-2) emerged in December 2019 (*1*,*2*) and induced a global pandemic. This virus, which causes coronavirus disease, was first identified in humans in Wuhan, China (*3*). The role of livestock and wildlife species at the human-animal interface in disease emergence and dynamics was extensively discussed, focusing on the identification of susceptible species, potential reservoirs, and intermediate hosts. Natural or experimental infections have demonstrated the susceptibility of fruit bats (*Rousettus aegyptiacus*), ferrets, felids, dogs, and minks to the virus; however, pigs, chicken, and ducks are not susceptible (*4*–*6*). Besides ducks, chicken, and pigs, other major livestock species, including >1.5 billion cattle (*Bos taurus*), live with close contact with humans. Non-SARS-CoV-2 betacoronaviruses are widespread in bovines (*7*); seroprevalences reach up to 90% (*8*), but these infections are usually subclinical (*7*). However, whether any ruminant species are susceptible to SARS-CoV-2 infection or whether there is any cross-reactivity of antibodies against bovine coronaviruses (BCoVs) and SARS-CoV-2 is unknown. We examined the susceptibility of cattle to SARS-CoV-2 infection and characterized the course of infection.

The Study

From a group of 9 dairy calves, we intranasally inoculated 6 with 1 x 10^5 50% tissue culture infectious dose of SARS-CoV-2 (strain 2019_nCoV Muc-IMB-1). We reintroduced the other 3 SARS-CoV-2–naive (hereafter in-contact) cattle to the 6 infected animals 24 hours after inoculation. We monitored body temperature and clinical signs daily. We also obtained and processed blood samples and nasal, oral, and rectal swab samples (Appendix, https://wwwnc.cdc.gov/EID/article/26/12/20-3799-App1.pdf). The experimental protocol was assessed and approved by the ethics committee of the State Office of Agriculture, Food Safety, and Fisheries in Mecklenburg–Western Pomerania, Germany (permission no. MV/TSD/7221.3–2-010/18).

Before infection, all animals tested negative for SARS-CoV-2 RNA in nasal, oral, and rectal swab samples and antibodies against SARS-CoV-2 in serum samples. Veterinarians conducted daily physical examinations and noted that none of the animals (inoculated or not) showed signs of clinical SARS-CoV-2 infection (Appendix). Throughout the study, the animals' body temperatures, feed intake, and general condition remained within normal limits (Appendix).

We demonstrated viral replication in 2 of the inoculated animals. One animal (no. 776) tested positive for viral RNA in the nCoV IP4 real-time reverse transcription PCR (RT-PCR) on days 2 (quantification cycle [Cq] value 29.97) and 3 (Cq 33.79) after infection. Another calf (no. 768) tested positive on day 3 (Cq 38.13) (Figure, panel A). We confirmed the results with a second real-time RT-PCR selective for the *E* gene; we measured Cq values of 29.26 (no. 776, day 2 after infection), 32.12 (no. 776, day 3), and 36.18 (no. 768, day 3). We verified the results with real-time RT-PCR using the ID GENE SARS-COV-2 DUPLEX kit (IDvet, https://www.id-vet.com) (Cq values 29.17 [no. 776, day 2 after infection], 30.55 [no. 776, day 3], and 36.07 [no. 768, day 3]). These animals tested positive only in the nasal swab samples.

We tested serum samples with an indirect ELISA specific to the SARS-CoV-2 receptor binding domain (RBD-ELISA). An increase in seroreactivity was observed for animal 776 from day 12 onward, indicating seroconversion (Figure, panel B). On day 20, we took serum samples that confirmed the positive ELISA findings and used an indirect immunofluorescence assay

Author affiliation: Friedrich-Loeffler-Institut, Insel Riems, Germany

DOI: https://doi.org/10.3201/eid2612.203799

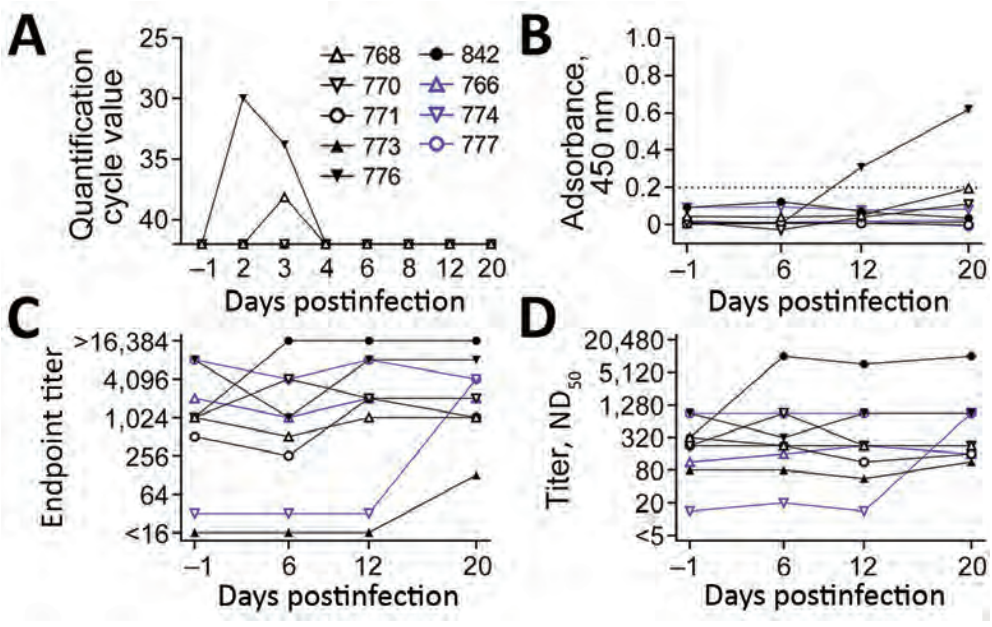

Figure. Characterization of SARS-CoV-2 infection in cattle. Animals directly inoculated shown in black. In-contact animals shown in blue. Individual animals are indicated by the same symbol in every figure panel. A) Viral load in nasal swab samples measured by real-time RT-PCR. Animals 776 and 768 had detectable viral loads on days 2 and 3 (no. 776) or day 3 only (no. 768). B) Results of indirect ELISA specific to the SARS-CoV-2 receptor binding domain. Serum samples taken on days -1 before infection and 6, 12, and 20 days after infection. Values below the dashed line are considered negative for antibodies against SARS-CoV-2. C) Results of indirect immunofluorescence assay for BCoV. D) Results of virus neutralization test for BCoV. Indirect immunofluorescence and virus neutralization test showed that animal 842, which tested positive for BCoV in the nasal swab sample by real-time RT-PCR, had an increase in antibody titer against BCoV. Preinfection antibody titers against BCoV did not affect infection with SARS-CoV-2, as animals 776 and 768, which tested positive for SARS-CoV-2, showed no infection-related reaction of BCoV antibody titers. BCoV, bovine coronavirus; ND_{50}, 50% neutralizing dose, RT-PCR, reverse transcription PCR; SARS-CoV-2, severe acute respiratory syndrome coronavirus 2.

(iIFA) to measure a low antibody titer of 1:4. In addition, a virus neutralization test (VNT) (serum dilution 1:2) showed a visible, although incomplete, inhibition of viral replication. Samples taken on day 20 from animal 768 showed only slightly increased seroreactivity in ELISA, whereas iIFA and VNT results remained negative. These differences might be attributable to varying test sensitivities or a possible restriction of viral replication to the upper respiratory tract. Throughout the study, the other animals tested negative for antibodies against SARS-CoV-2 by ELISA, iIFA, and VNT.

We also tested the BCoV status of each calf. Before SARS-CoV-2 infection, all animals had neutralizing antibodies against BCoV, although the titers differed substantially among individual animals (Figure, panel D). Three animals showed an increase in antibody titers against BCoV by iIFA (no. 842 and 773, which were directly infected with SARS-CoV-2, and no. 774, an in-contact animal) and 2 also by VNT (no. 842 and 774) within the study period (Figure). To show that this increase was caused by a natural BCoV infection and not SARS-CoV-2, we tested nasal swab samples for BCoV using RT-PCR selective for the *RdRp* region (*9*). Animal 842 tested positive by PCR for BCoV RNA 1 day before our experimental SARS-CoV-2 infection and 2 days after infection. We used Sanger sequencing to confirm the BCoV infection, which had increased the titer of antibodies against BCoV in this animal (Figure). Animal 842 presumably infected animal 774 with BCoV. However, we did not observe any cross-reactivity of the bovine coronavirus with the applied SARS-CoV-2 tests, because all animals tested negative by the nCoV IP4 PCR for SARS-CoV-2, the iIFA and VNT specific to SARS-CoV-2, and the RBD-ELISA (Figure) before infection. Moreover, 2 animals (nos. 776 and 768) with high BCoV seroreactivity tested positive for SARS-CoV-2 RNA after inoculation, whereas those with lower BCoV-specific titers could not be infected, further confirming a lack of any cross-reactivity or cross-protection.

Conclusions

Our findings demonstrate that under experimental conditions cattle show low susceptibility to SARS-CoV-2 infection. This finding corresponds with a predicted medium susceptibility of cattle species on the basis of a computational modelling of their angiotensin-I-converting enzyme 2, the cellular receptor for SARS-CoV-2 (*10*).

We inoculated 6 cattle with SARS-CoV-2; of these animals, 2 later tested positive for the virus in PCR of nasal swab samples and show specific seroconversion by RBD-ELISA. Even though the genome loads detected in animal 768 at day 3 were low, there is evidence that this animal was confronted with real viral

replication. RNA residues from inoculation are only detectable shortly after inoculation; here, the day 2 nasal swab tested repeatedly PCR negative. Furthermore, other studies using the same infection dose and vaporization device also found no residual RNA on day 2 (*5*). In addition, the low-level viral replication led to a slight, but detectable, serologic reaction in the applied ELISA (Figure, panel B).

In our study, we did not observe intraspecies transmission to in-contact cattle. Thus, we have no indication that cattle play any role in the human pandemic, and no reports of naturally infected bovines exist. Nevertheless, in regions with large cattle populations and high prevalence of SARS-CoV-2 infection in humans, such as the United States or countries in South America, close contact between livestock and infected animal owners or caretakers could cause anthropo-zoonotic infections of cattle, as has been already described for highly susceptible animal species such as minks, felids, and dogs (*6*,*11*). When assessing the risk for virus circulation within bovine populations, one should consider the age, husbandry practices, and underlying health conditions of the animals. Outbreak investigations might include cattle, particularly if direct contact has occurred between animals and persons infected with SARS-CoV-2. In addition to direct detection by PCR, serologic screenings with sensitive and specific ELISAs should also be taken into consideration. In this context, the wide distribution of BCoV is of special interest, especially because the presence of a preexisting coronavirus did not protect from infection with another betacoronavirus in this study. Double infections of individual animals might lead to recombination events between SARS-CoV-2 and BCoV, a phenomenon already described for other pandemic coronaviruses (*12*). A resulting chimeric virus, comprising characteristics of both viruses, could threaten human and livestock populations and should therefore be monitored.

This article was preprinted at https://www.biorxiv.org/content/10.1101/2020.08.25.254474v1.

Acknowledgments

We thank Doreen Schulz, Bianka Hillmann, Mareen Lange, and Constantin Klein for excellent technical assistance and the animal caretakers for their dedicated work.

The study was supported by intramural funding of the German Federal Ministry of Food and Agriculture provided to the Friedrich-Loeffler-Institut and resources of the VetBioNet consortium (grant agreement no. EU731014), an initiative of the European Commission's Horizon 2020 program.

About the Author

Mr. Ulrich is a veterinarian and doctoral candidate at the Friedrich-Loeffler-Institut, Greifswald-Insel Riems, Germany. His research interests include pathogenesis and prevention of zoonotic viruses.

References

1. World Health Organization. COVID-19 strategy update—14 April 2020. 2020 [cited 2020 May 16]. https://www.who.int/publications/i/item/covid-19-strategy-update---14-april-2020
2. Andersen KG, Rambaut A, Lipkin WI, Holmes EC, Garry RF. The proximal origin of SARS-CoV-2. Nat Med. 2020;26:450–2. https://doi.org/10.1038/s41591-020-0820-9
3. Zhu N, Zhang D, Wang W, Li X, Yang B, Song J, et al.; China Novel Coronavirus Investigating and Research Team. A novel coronavirus from patients with pneumonia in China, 2019. N Engl J Med. 2020;382:727–33. https://doi.org/10.1056/NEJMoa2001017
4. Shi J, Wen Z, Zhong G, Yang H, Wang C, Huang B, et al. Susceptibility of ferrets, cats, dogs, and other domesticated animals to SARS-coronavirus 2. Science. 2020;368:1016–20. https://doi.org/10.1126/science.abb7015
5. Schlottau K, Rissmann M, Graaf A, Schön J, Sehl J, Wylezich C, et al. SARS-CoV-2 in fruit bats, ferrets, pigs, and chickens: an experimental transmission study. Lancet Microbe. 2020 Jul 7 [Epub ahead of print]. https://doi.org/10.2807/1560-7917.ES.2020.25.23.2001005
6. Oreshkova N, Molenaar RJ, Vreman S, Harders F, Oude Munnink BB, Hakze-van der Honing RW, et al. SARS-CoV-2 infection in farmed minks, the Netherlands, April and May 2020. Euro Surveill. 2020;25:25. https://doi.org/10.2807/1560-7917.ES.2020.25.23.2001005
7. Hodnik JJ, Ježek J, Starič J. Coronaviruses in cattle. Trop Anim Health Prod. 2020 Jul 17 [Epub ahead of print]. https://doi.org/10.1007/s11250-020-02354-y
8. Boileau MJ, Kapil S. Bovine coronavirus associated syndromes. Vet Clin North Am Food Anim Pract. 2010;26:123–46. https://doi.org/10.1016/j.cvfa.2009.10.003
9. Dominguez SR, O'Shea TJ, Oko LM, Holmes KV. Detection of group 1 coronaviruses in bats in North America. Emerg Infect Dis. 2007;13:1295–300. https://doi.org/10.3201/eid1309.070491
10. Damas J, Hughes GM, Keough KC, Painter CA, Persky NS, Corbo M, et al. Broad host range of SARS-CoV-2 predicted by comparative and structural analysis of ACE2 in vertebrates. Proc Natl Acad Sci U S A. 2020;117:22311–22. https://doi.org/10.1073/pnas.2010146117
11. Sailleau C, Dumarest M, Vanhomwegen J, Delaplace M, Caro V, Kwasiborski A, et al. First detection and genome sequencing of SARS-CoV-2 in an infected cat in France. Transbound Emerg Dis. 2020 Jun 5 [Epub ahead of print]. https://doi.org/10.1111/tbed.13659
12. Forni D, Cagliani R, Clerici M, Sironi M. Molecular evolution of human coronavirus genomes. Trends Microbiol. 2017;25:35–48. https://doi.org/10.1016/j.tim.2016.09.001

Address for correspondence: Martin Beer, Institute of Diagnostic Virology, Friedrich-Loeffler-Institut, Südufer 10, 17493 Greifswald-Insel Riems, Germany; email: martin.beer@fli.de

Susceptibility of Raccoon Dogs for Experimental SARS-CoV-2 Infection

Conrad M. Freuling,[1] Angele Breithaupt,[1] Thomas Müller, Julia Sehl, Anne Balkema-Buschmann, Melanie Rissmann, Antonia Klein, Claudia Wylezich, Dirk Höper, Kerstin Wernike, Andrea Aebischer, Donata Hoffmann, Virginia Friedrichs, Anca Dorhoi, Martin H. Groschup, Martin Beer, Thomas C. Mettenleiter

Raccoon dogs might have been intermediate hosts for severe acute respiratory syndrome–associated coronavirus in 2002–2004. We demonstrated susceptibility of raccoon dogs to severe acute respiratory syndrome coronavirus 2 infection and transmission to in-contact animals. Infected animals had no signs of illness. Virus replication and tissue lesions occurred in the nasal conchae.

Severe acute respiratory syndrome coronavirus 2 (SARS-CoV-2) emerged in Wuhan, China, at the end of 2019. Researchers have identified close relatives to SARS-CoV-2 in bats (*1*) and pangolins (order Pholidota) (*2*,*3*). Whether the pandemic was initiated by direct transmission from bats or through an intermediate mammalian host is still under debate (*4*). During the 2002–2004 severe acute respiratory syndrome pandemic, researchers documented the causative virus in raccoon dogs (*Nyctereutes procyonoides*) in China, indicating that these animals might have been intermediate hosts for the virus (*5*). Fur producers in China own >14 million captive raccoon dogs, accounting for ≈99% of the global share of raccoon dogs (6) (Appendix Figure 1, panel A, https://wwwnc.cdc.gov/EID/article/26/12/20-3733-App1.pdf). However, whether these animals are susceptible to SARS-CoV-2 is unknown. Using our established study design (*7*), we characterized susceptibility, viral shedding, transmission potential, serologic reactions, and pathologic lesions of raccoon dogs after experimental SARS-CoV-2 infection.

The Study

We intranasally inoculated 9 naive raccoon dogs with 10^5 50% tissue culture infectious dose ($TCID_{50}$) SARS-CoV-2 2019_nCoV Muc-IMB-1. We introduced 3 naive animals 24 hours after inoculation to test for direct transmission (Figure 1). We sorted animals into 4 groups of 3 individual cages separated by meshed wire and placed each naive contact animal between 2 inoculated animals (Appendix Figure 2). We also used 2 naive animals as controls. Although several animals (animal nos. 4, 5, and 10) were slightly lethargic 4 days after inoculation, none of the exposed or contact animals had fever, weight loss, or other signs of clinical infection.

To monitor viral shedding, we collected nasal, oropharyngeal, and rectal swab samples on days 2, 4, 8, 12, 16, 21, and 28. We measured viral RNA by quantitative reverse transcription PCR and the levels of infectious virus by titration on Vero E6 cells (Figure 2). We observed viral shedding in 6 (66.7%) of 9 inoculated animals. Because we did not detect viral shedding in animal nos. 4, 8, and 9 during the 28-day observation period, we concluded that these animals were not successfully infected. The infected animals shed virus in nasal and oropharyngeal swab samples on days 2–4; we found viral RNA in nasal swab samples until day 16 (animal no. 7). The mean viral genome load was 3.2 (range 1.0–6.45) $\log_{10}$ genome copies/mL for nasal swab samples, 2.9 (range 0.54–4.39) $\log_{10}$/mL for oropharyngeal swab samples, and 0.71 (range 0.31–1.38) $\log_{10}$/mL for rectal swab samples. Titrations showed the same trend; viral titers peaked at 4.125 $\log_{10}$ $TCID_{50}$/mL in nasal swabs on day 2. We successfully isolated virus from all except 2 RNA-positive samples that had a cycle threshold of ≤27. However, we could not isolate virus from samples that had a cycle threshold >27 (Appendix Figure 3).

We detected infection in 2 (66.7%) of 3 contact animals (nos. 10 and 11) (Figure 2; Appendix Figure 2). We first detected viral RNA in animal no. 10 on day 8 (i.e., 7 days after contact). Viral shedding, mainly

Author affiliation: Friedrich-Loeffler-Institut, Greifswald-Insel Riems, Germany

DOI: https://doi.org/10.3201/eid2612.203733

[1]These first authors contributed equally to this article.

in nasal secretions, lasted until day 16 (15 days after contact), and we identified viral titers of 1.625 $\log_{10}$ $TCID_{50}$/mL in nasal swab samples on day 8 (7 days after contact). One contact raccoon dog (no. 12) remained negative for SARS-CoV-2 because infection did not develop in either of his inoculated cage neighbors (nos. 8 and 9) (Appendix Figure 2).

On days 4, 8, 12, and 28, we euthanized and conducted autopsies on 2 animals in sequential order. We tested tissues and body fluids for SARS-CoV-2 RNA and replicating virus (Appendix Figure 4). We found viral loads of up to 4.87 $\log_{10}$ genome copies/mL in the nasal mucosa on day 4 but only minute amounts in other organs. We cultivated infectious virus from the nasal conchae of animal nos. 1 (2.86 $\log_{10}$ $TCID_{50}$/mL) and 2 (1.63 $\log_{10}$ $TCID_{50}$/mL). None of the lung samples tested positive for viral RNA.

In the autopsies, we did not find gross lesions definitively caused by SARS-CoV-2 infection. We used hematoxylin and eosin staining on tissues taken at autopsy on days 4, 8, and 12 to identify mild rhinitis affecting the respiratory and olfactory regions in all infected animals (Appendix Figure 5) but not in negative controls. We used immunohistochemical tests to verify the presence of intralesional SARS-CoV-2 antigen in the nasal respiratory and olfactory epithelium on days 4 and 8 (Appendix Figure 5). We did not find the antigen at later time points, possibly because of virus clearance or the limited sensitivity of the immunohistochemical test. We did not detect histopathologic lesions nor viral antigen in animal no. 4, which had not been successfully infected, on day 8. On day 28, 1 infected (no. 7) and 1 contact animal (no. 10) had histologic lesions indicative of SARS-CoV-2 replication in the nasal conchae (Appendix Figure 6). We still detected viral RNA but no antigen. We did not detect further lesions definitively caused by SARS-CoV-2-infection. All other tissues tested negative for SARS-CoV-2 antigen (Appendix).

We took serum samples on days 4, 8, 12, 16, 21, and 28. We tested these samples for antibodies against SARS-CoV-2 using the indirect immunofluorescence assay and virus neutralization test as described (*7*). We detected SARS-CoV-2–specific antibodies in 4 (57.1%) of 7 inoculated animals on day 8 using ELISA (Appendix Figure 7, panel A) and indirect immunofluorescence assay (>1:64) (Table). Titers increased to 1:1,024 on day 28 (animal no. 7). We observed neutralizing antibodies in 2 of the infected animals (nos. 6 and 7) as early as day 8 (animal no. 6, 1:5.04) (Table). The highest titer of neutralizing antibodies was 1:12.7 (found in no. 6 on day 12, and no. 7 on day 28). We characterized SARS-CoV-2–specific immunoglobulins, revealing that IgM, IgG, and IgA developed

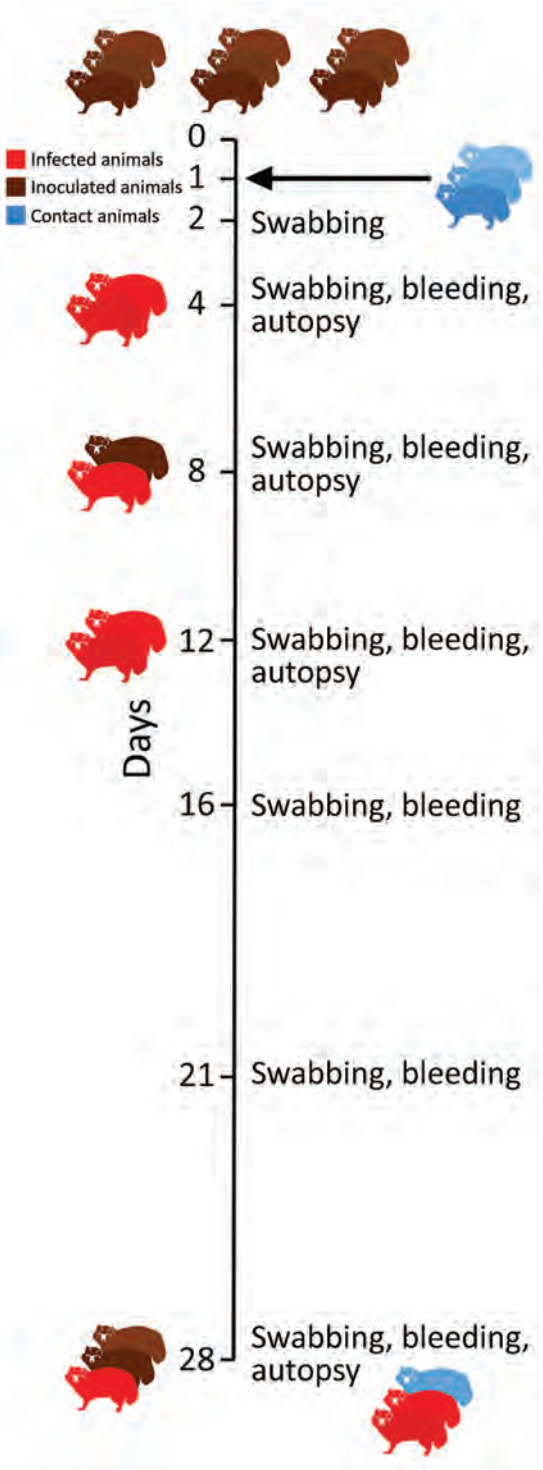

Figure 1. Study design for experimental infection of raccoon dogs with severe acute respiratory syndrome coronavirus 2. Outline of the in vivo experiment with an observation period of 28 days; 9 animals were inoculated intranasally with 10^5 50% tissue culture infectious dose/mL, and 3 naive direct contact animals were introduced 24 hours later. On days 4, 8 and 12, two raccoon dogs were euthanized and autopsied. All remaining animals were euthanized on day 28. Red indicates infected animals.

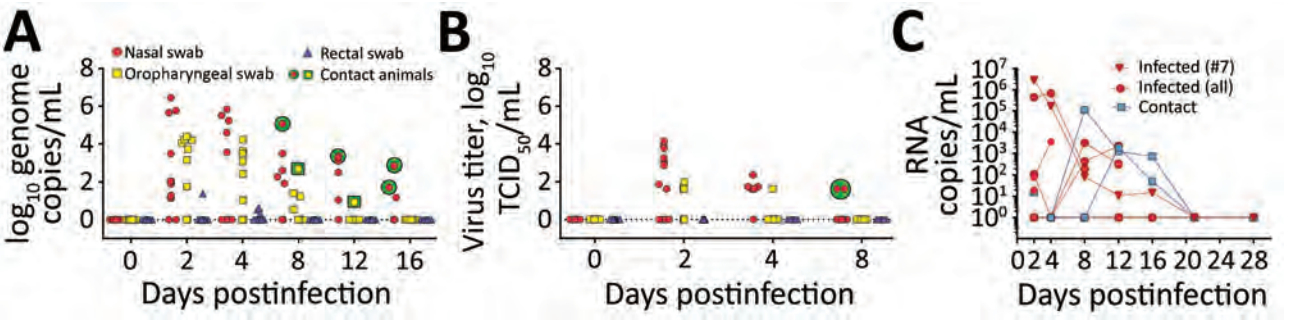

Figure 2. Detection of severe acute respiratory syndrome coronavirus 2 in swab samples from experimentally infected raccoon dogs. A) Viral genome loads in swab samples isolated on Vero E6 cells; B) viral genome loads in virus titers isolated on Vero E6 cells. Two replicates per sample were analyzed. C) Individual viral loads of nasal swab specimens taken from infected and contact animals.

within 8 days after infection; IgM levels peaked on day 8 and IgG on day 12 (Appendix Figure 7, panels B–G). On days 8 and 12, we also detected antibodies specific for the receptor-binding domain of SARS-CoV-2 in saliva samples from animals that developed serum antibodies (Appendix Figure 7, panels H–I). In contrast to SARS-CoV-2 isolates from infected ferrets (*7*), the isolates from nasal swabs of infected raccoon dogs (animal no. 2 on day 2 and no. 10 on day 8) demonstrated 100% sequence identity to the inoculum.

Conclusions

Our experimental study demonstrates that raccoon dogs are susceptible to SARS-CoV-2 infection and can transmit the virus to direct in-contact animals. In our study, raccoon dogs had only subtle clinical signs. We found evidence of viral replication and tissue lesions in only the nasal conchae.

Increasing evidence supports the potential of carnivore species, including farmed fur animals, to become infected by SARS-CoV-2 (*8*–*12*). This transmission could eventually cause zoonotic infections in humans (B.B. Oude Munnink, unpub. data, https://www.biorxiv.org/content/10.1101/2020.09.01.277152v1). Our results indicate that affected farms might be reservoirs for SARS-CoV-2. Thus, efficient and continuous surveillance should target susceptible animals, including raccoon dogs, especially in China, which is a key player in global fur production (*6*). We also need to initiate large-scale epidemiologic field studies with historic samples that might elucidate the role of farmed animals in the current pandemic.

This article was preprinted at https://www.biorxiv.org/content/10.1101/2020.08.19.256800v1.

Acknowledgments

We acknowledge Jeannette Kliemt, Mareen Lange, Silvia Schuparis, Gabriele Czerwinski, Bianka Hillmann, and Patrick Zitzow for their technical assistance. We thank Frank Klipp, Doreen Fiedler, Harald Manthei, René Siewert, Christian Lipinski, Ralf Henkel, and Domenique Lux for their support during animal experiments.

This study was supported by funding from the German Federal Ministry of Food and Agriculture that was provided to the Friedrich-Loeffler-Institut, and partial funding from the

Table. Serologic response of raccoon dogs to experimental SARS-CoV-2 infection, by day after inoculation*

	Day 8		Day 12		Day 16		Day 21		Day 28	
Animal no.	iIFA	VNT	iIFA	VNT	iIFA	VNT	iIFA	VNT	iIFA	VNT
Inoculated										
1										
2										
3	1:128	<1:4								
4	<1:20	<1:2								
5	1:64	<1:2	1:64	<1:2						
6	1:128	1:5.04	1:64	1:12.7						
7	1:128	<1:4	1:64	<1:2	1:64	1:4	1:128	1:10.08	1:1,024	1:12.7
8	<1:20	<1:2	<1:20	<1:2	<1:20	<1:2	<1:20	<1:2	<1:20	<1:2
9	<1:20	<1:2	<1:20	<1:2	<1:20	<1:2	<1:20	<1:2	<1:20	<1:2
In-contact										
10	<1:20	<1:2	<1:20	<1:2	1:64	<1:2	1:128	<1:4	1:512	<1:4
11	<1:20	<1:2	<1:20	<1:2	1:64	<1:2	1:128	1:5.04	1:256	<1:4
12	<1:20	<1:2	<1:20	<1:2	<1:20	<1:2	<1:20	<1:2	<1:20	<1:2

*No serologic response recorded for days 0 and 4. Animal nos. 4, 8, and 9 did not show signs of infection. Each day, 2 raccoon dogs were euthanized and autopsied. iIFA, indirect immunofluorescence assay; SARS-CoV-2, severe acute respiratory syndrome coronavirus 2; VNT, virus neutralization test.

European Union Horizon 2020 project ("Versatile Emerging infectious disease Observatory" grant no. 874735).

About the Author

Dr. Freuling is a research scientist at the Friedrich-Loeffler-Institut. His research interests include viral zoonotic diseases, in particular associated with bats, e.g. rabies.

References

1. Zhou P, Yang X-L, Wang X-G, Hu B, Zhang L, Zhang W, et al. A pneumonia outbreak associated with a new coronavirus of probable bat origin. Nature. 2020;579:270–3. https://doi.org/10.1038/s41586-020-2012-7
2. Zhang T, Wu Q, Zhang Z. Probable pangolin origin of SARS-CoV-2 associated with the COVID-19 outbreak. Curr Biol. 2020;30:1346–1351.e2. https://doi.org/10.1016/j.cub.2020.03.022
3. Xiao K, Zhai J, Feng Y, Zhou N, Zhang X, Zou J-J, et al. Isolation of SARS-CoV-2-related coronavirus from Malayan pangolins. Nature. 2020;583:286–9. https://doi.org/10.1038/s41586-020-2313-x
4. Andersen KG, Rambaut A, Lipkin WI, Holmes EC, Garry RF. The proximal origin of SARS-CoV-2. Nat Med. 2020;26:450–2. https://doi.org/10.1038/s41591-020-0820-9
5. Guan Y, Zheng BJ, He YQ, Liu XL, Zhuang ZX, Cheung CL, et al. Isolation and characterization of viruses related to the SARS coronavirus from animals in southern China. Science. 2003;302:276–8. https://doi.org/10.1126/science.1087139
6. ACTAsia.org. China's fur trade and its position in the global fur industry. 2019 Jul [cited 2019 Jul 7]. https://www.actasia.org/wp-content/uploads/2019/10/China-Fur-Report-7.4-DIGITAL-2.pdf
7. Schlottau K, Rissmann M, Graaf A, Schön J, Sehl J, Wylezich C, et al. SARS-CoV-2 in fruit bats, ferrets, pigs, and chickens: an experimental transmission study. Lancet Microbe. 2020;1:e218-e225. https://10.1016/S2666-5247(20)30089-6.
8. Oreshkova N, Molenaar RJ, Vreman S, Harders F, Oude Munnink BB, Hakze-van der Honing RW, et al. SARS-CoV-2 infection in farmed minks, the Netherlands, April and May 2020. Euro Surveill. 2020;25. https://doi.org/10.2807/1560-7917.ES.2020.25.23.2001005
9. International Society for Infectious Diseases. COVID-19 update (227): Denmark (North Jutland) animal, farmed mink, spread. 2020 Jul 2 [cited 2020 Jul 9]. https://promedmail.org/promed-post/?id=7533033
10. International Society for Infectious Diseases. COVID-19 update (319): Spain (AR) animal, farmed mink, 1st rep. 2020 Jul 17 [cited 2020 Jul 29]. https://promedmail.org/promed-post/?id=20200717.7584560
11. Enserink M. Coronavirus rips through Dutch mink farms, triggering culls. Science. 2020;368:1169. https://doi.org/10.1126/science.368.6496.1169
12. International Society for Infectious Diseases. COVID-19 update (366): animal, USA (UT) mink. 2020 Aug 18 [cited 2020 Sep 8]. https://promedmail.org/promed-post/?id=20200818.7692815

Address for correspondence: Conrad Freuling, Friedrich-Loeffler-Institute Federal Research Institute for Animal Health - Institute of Molecular Virology and Cell Biology, Südufer 10, 17493 Greifswald-Insel Riems, Germany; email: Conrad.Freuling@fli.de

Zoonotic Pathogens in Ticks from Migratory Birds, Italy

Elena Battisti, Katharina Urach, Adnan Hodžić, Leonida Fusani, Peter Hufnagl, Gerit Felsberger, Ezio Ferroglio, Georg Gerhard Duscher

Migratory birds can transport infected ticks across continents. We evaluated pathogens in ticks collected from migratory birds in Italy. We found DNA from *Rickettsia aeschlimannii*, *R. africae*, and *R. raoultii* bacteria, all of which can cause disease in humans. Bird migrations might facilitate the spread of these pathogens into new areas.

Migratory birds can be biological and mechanical carriers of viruses, bacteria, and protozoa. They also can transport infected ectoparasites, such as ticks, across continents, enabling the spread of these vectors and their pathogens into new ecologic niches. Several studies have reported the *Borrelia burgdorferi* sensu lato, spotted fever group (SFG) rickettsiae, and Crimean-Congo hemorrhagic fever virus (CCHFV) in *Ixodes ricinus* and *Hyalomma marginatum* ticks collected from birds that migrate annually from Africa to Europe (*1*,*2*). The role of migratory birds as carriers of vectorborne pathogens in Italy is poorly understood. To assess the risk for introduction of zoonotic microbial agents in Europe by migratory birds, we investigated microorganisms in ticks collected from migratory birds in Italy.

The Study

We conducted fieldwork activities at the Ponza Ringing Station on the island of Ponza (Central Tyrrhenian Sea, Italy; 40°55′N, 12°58′E) during spring (March–May) 2016 and 2017. We captured 744 migratory birds belonging to 20 different species (Table) during regular ringing procedures and checked them for ticks. Fourteen bird species were long-distance migrants that wintered in sub-Saharan Africa, and 6 were partial migrants, such as the blackbird (*Turdus merula*), the dunnock (*Prunella modularis*), the Eurasian blackcap (*Sylvia atricapilla*), the European robin (*Eithacus rubecula*), the song thrush (*Turdus philomenos*), and the subalpine warbler (*Sylvia cantillas*).

We collected 231 engorged ticks and identified them using standard morphologic keys (*3*) and PCR amplification of the internal transcribed spacer (ITS) region when possible (*4*). We used commercial kits for RNA (High Pure Viral Nucleic Isolation Kit; Roche Diagnostics, https://diagnostics.roche.com) and DNA (High Pure PCR Template Preparation Kit; Roche Diagnostics) extraction. We used the RealStar CCHFV RT-PCR Kit 1.0 (Altona Diagnostics, https://www.altona-diagnostics.com) for CCHFV detection; we used conventional PCR with protocols described elsewhere (*5*) to detect DNA from *Babesia* spp., *Anaplasma* spp., *Ehrlichia* spp., SFG rickettsiae, and *Borrelia* spp. We used DNA from *Babesia canis* (dog 825/08, 1:10 diluted), *Anaplasma phagocytophilum* (cattle 2008/13, 1:10 diluted), *Ehrlichia canis* (clone), *Rickettsia raoultii* (clone) and *B. burgdorferi* (clone) as positive controls for each amplification.

Using PCR amplification of the ITS region, we identified 94 ticks at the species level: *H. marginatum* complex (5 larvae, 82 nymphs), *I. frontalis* (3 nymphs), *I. ventalloi* (3 nymphs), and *Amblyomma marmoreum* (1 nymph). Amplification of the ITS region failed in the remaining ticks, identifying only the genus; these ticks were mostly *Hyalomma* spp. (1 larva, 118 nymphs) or *Ixodes* spp. (3 larvae, 14 nymphs, and 1 adult).

Of the analyzed ticks, 50 tested positive for SFG rickettsiae DNA; the overall prevalence was 21.7% (95% CI 16.8%–27.4%). To determine the species, we amplified a fragment of the *ompA* gene in all the SFG rickettsiae–positive ticks (*5*). Positive amplicons were sequenced by LGC Genomics (https://www.lgcgroup.com) and compared with sequences deposited in GenBank. Results revealed *R. aeschlimannii* DNA in 47 (94.0% [95% CI 83.8%–97.9%]) of 50 ticks (Table). We identified 46 sequences identical to an *R. aeschlimanni* strain documented from Egypt (GenBank accession no. HQ335157), Turkey (GenBank accession no. MF379299), and Italy (GenBank accession no. MH532239) and 1 sequence identical to *R. aeschlimanni* strain RH (GenBank

Author affiliations: Università degli Studi di Torino, Turin, Italy (E. Battisti, E. Ferroglio); University of Veterinary Medicine Vienna, Vienna, Austria (K. Urach, A. Hodžić, L. Fusani, G.G. Duscher); University of Vienna, Vienna (K. Urach, L. Fusani); Austrian Agency for Health and Food Safety, Vienna (P. Hufnagl, G. Felsberger, G.G. Duscher)

DOI: https://doi.org/10.3201/eid2612.181686

Table. Sampled bird species, ticks, and *Rickettsia* PCR positivity, Italy, 2016–2017*

Year, bird species	No. birds	Tick species found	No. pathogen-positive ticks/no. tested ticks	*Rickettsia*		
				R. aeschlimanni	*R. africae*	*R. raoultii*
2016						
Barn swallow (*Hirundo rustica*)	18	NA	NA			
Blackbird (*Turdus merula*)	1	*Ixodes ventalloi*	0/1			
Black redstart (*Phoenicuros ochruros*)	29	*I. ventalloi*	0/2			
		Hyalomma sp.	1/3	1	0	0
Eurasian blackcap (*Sylvia atricapilla*)	1	NA	NA			
European robin (*Erithacus rubecula*)	22	*I. frontalis*	0/1			
Garden warbler (*Sylvia borin*)	83	NA	NA			
Icterine warbler (*Hippolais icterina*)	19	*Hyalomma* sp.	1/2	0	1	0
Northern weathear (*Oenanthe oenanthe*)	1	*Hyalomma* sp.	1/1	1	0	0
Pied flycatcher (*Ficedula hypoleuca*)	21	*Hyalomma* sp.	1/5	1	0	0
Redstart (*Phoenicuros phoenicuro*)	14	*Hyalomma* sp.	7/9	7	0	0
Spotted flycatcher (*Muscicapa striata*)	25	NA	NA			
Subalpine warbler (*Sylvia cantillas*)	1	*I. frontalis*	0/1			
Tree pipit (*Anthus trivialis*)	1	*Hyalomma* sp.	1/2	1	0	0
Whinchat (*Saxicola rubetra*)	38	*I. frontalis*	0/1			
		Hyalomma sp.	4/13	4	0	0
Whitethroat (*Sylvia communis*)	92	*Ixodes* sp.	0/1			
		Hyalomma sp.	10/24	9	0	1
Willow warbler (*Phylloscopus trochilus*)	1	NA	NA			
Wood warbler (*Phylloscopus sibilatrix*)	1	*Hyalomma* sp.	0/3			
2017						
Barn swallow (*H. rustica*)	20	*Hyalomma* sp.	0/1			
Black redstart (*P. ochruros*)	3	*H. rufipes*	1/1	0	1	0
Collared flycatcher (*Ficedula albicollis*)	1	*H. rufipes*	1/1	1	0	0
Dunnock (*Prunella modularis*)	1	*Hyalomma* sp.	0/1			
Eurasian blackcap (*S. atricapilla*)	48	NA	NA			
European robin (*E. rubecula*)	39	*H.rufipes*	2/10	2	0	0
Garden warbler (*S. borin*)	30	NA	NA			
Icterine warbler (*H. icterina*)	41	NA	NA			
Northern weathear (*O. oenanthe*)	1	*H. rufipes*	1/1	1		
Pied flycatcher (*F. hypoleuca*)	30	*Hyalomma* sp.	0/1			
Redstart (*P. phoenicuros*)	25	*H. rufipes*	8/12	8	0	0
Song thrush (*Turdus philomenos*)	4	*H. rufipes*	1/1	1	0	0
		Hyalomma sp.	0/3			
Spotted flycatcher (*M. striata*)	24	*H. rufipes*	1/2	1	0	0
Subalpine warbler (*S. cantillas*)	1	*Hyalomma* sp.	0/1			
Tree pipit (*A. trivialis*)	2	*Amblyomma marmoreum*	1/1	1	0	0
		Hyalomma sp.	0/1			
Whinchat (*S. rubetra*)	43	*H. rufipes*	5/7	5	0	0
Whitethroat (*S. communis*)	57	*H. rufipes*	2/5	2	0	0
Willow warbler (*P. trochilus*)	1	*Hyalomma* sp.	0/1			
Wood warbler (*P. sibilatrix*)	5	*H. rufipes*	1/1	1	0	0
		Hyalomma sp.	0/4			

*NA, no ticks collected.

accession no. HM050286) from Senegal; the latter strain differed from the others by 1 nt (T instead of C at nt 425). Two (4.0% [95% CI 1.1%–13.5%]) sequences were identical to *R. africae* (GenBank accession no. HQ335132), and 1 (2.0% [95% CI 0.4%–10.5%]) sequence was identical to *R. raoultii* (GenBank accession no. MF166732). We also screened a subset of positive ticks using primers targeting a fragment of the *gltA* gene (*5*), confirming the results obtained with the *ompA* gene. No ticks tested positive for other microorganisms.

Conclusions

Although ticks of the *H. marginatum* species complex (i.e., *H. marginatum*, *H. rufipes*, *H. turanicum*, and *H. isaaci*) are the most widespread ticks in Africa, they also have been found in some countries in Europe, such as the United Kingdom (*6*). These tick species are also vectors for CCHFV, which occurs mainly in Africa and southeastern Europe and can cause life-threatening disease in humans. *Hyalomma* ticks are vectors and reservoirs of this virus; birds, which are the primary hosts for the immature stages of these ticks, can maintain and spread the virus into new areas through migration (*7*).

R. aeschlimannii and *R. africae*, which are zoonotic bacterial species endemic to Africa, are transmitted by ticks belonging to the genera *Hyalomma* and *Amblyomma*. However, these bacteria have also been detected in ticks from other regions, such as Oceania, the

Caribbean islands, and Europe (*7*–*9*). Autochthonous cases of human rickettsiosis caused by *R. aeschlimannii* have been recently described in Greece (*10*) and Italy (*11*). We detected *R. africae* in *H. rufipes* and *R. raoultii* in *Hyalomma* sp., which are not known vectors for these pathogens. Because we did not test the birds for *Rickettsia* spp. and the ticks were engorged, we cannot exclude the possibility that the ticks acquired these microorganisms by feeding on positive birds. Nevertheless, our results agree with those observed in a study in Italy (*12*) and confirm the circulation of these *Rickettsia* species into areas to which they are not endemic. They also highlight the role of migratory birds in the passive transportation of infected ticks.

Although no ticks tested positive for CCHFV in our study, some studies report this virus in *H. marginatum* complex ticks attached to birds migrating from Africa to Europe (*13*). Migratory birds might have contributed to the establishment of the CCHFV in Spain (*14*). Moreover, climate change could cause prolonged, warmer, and drier summers and autumns. These seasonal changes might lead to the establishment of autochthonous populations of *Hyalomma* ticks in areas previously free of these vectors. Finally, RNA of another relevant human pathogen, the recently discovered Alkhurma hemorrhagic virus (*15*), has been detected in ticks of the *H. marginatum* complex.

In summary, we found zoonotic bacteria in ticks carried by birds across their migratory routes and assessed the risk for pathogen introduction in Italy. However, further studies are needed to clarify the role of these ticks in the epidemiology of zoonotic pathogens.

Acknowledgments

We thank Marco Pombi and 2 anonymous reviewers who provided helpful comments and suggestions to improve this manuscript.

About the Author

Dr. Battisti is a postdoctoral researcher at the Department of Veterinary Science, University of Turin. Her main research focuses on zoonotic s transmitted by vectors.

References

1. Comstedt P, Bergström S, Olsen B, Garpmo U, Marjavaara L, Mejlon H, et al. Migratory passerine birds as reservoirs of Lyme borreliosis in Europe. Emerg Infect Dis. 2006;12:1087–95. https://doi.org/10.3201/eid1207.060127
2. Palomar AM, Portillo A, Mazuelas D, Roncero L, Arizaga J, Crespo A, et al. Molecular analysis of Crimean-Congo hemorrhagic fever virus and *Rickettsia* in *Hyalomma marginatum* ticks removed from patients (Spain) and birds (Spain and Morocco), 2009–2015. Ticks Tick Borne Dis. 2016;7:983–7. https://doi.org/10.1016/j.ttbdis.2016.05.004
3. Palomar AM, Portillo A, Santibáñez P, Mazuelas D, Arizaga J, Crespo A, et al. Crimean-Congo hemorrhagic fever virus in ticks from migratory birds, Morocco. Emerg Infect Dis. 2013;19:260–3. https://doi.org/10.3201/eid1902.121193</jrn>
4. Lv J, Wu S, Zhang Y, Chen Y, Feng C, Yuan X, et al. Assessment of four DNA fragments (COI, 16S rDNA, ITS2, 12S rDNA) for species identification of the Ixodida (Acari: Ixodida). Parasit Vectors. 2014;7:93. https://doi.org/10.1186/1756-3305-7-93
5. Hodžić A, Fuehrer HP, Duscher GG. First molecular evidence of zoonotic bacteria in ticks in Bosnia and Herzegovina. Transbound Emerg Dis. 2017;64:1313–6. https://doi.org/10.1111/tbed.12473
6. Jameson LJ, Morgan PJ, Medlock JM, Watola G, Vaux AGC. Importation of *Hyalomma marginatum*, vector of Crimean-Congo haemorrhagic fever virus, into the United Kingdom by migratory birds. Ticks Tick Borne Dis. 2012;3:95–9. https://doi.org/10.1016/j.ttbdis.2011.12.002
7. Palomar AM, Portillo A, Mazuelas D, Roncero L, Arizaga J, Crespo A, et al. Molecular analysis of Crimean-Congo hemorrhagic fever virus and Rickettsia in *Hyalomma marginatum* ticks removed from patients (Spain) and birds (Spain and Morocco), 2009–2015. Ticks Tick Borne Dis. 2016;7:983–7. https://doi.org/10.1016/j.ttbdis.2016.05.004
8. Kelly PJ. *Rickettsia africae* in the West Indies. Emerg Infect Dis. 2006;12:224–6. https://doi.org/10.3201/eid1202.050903
9. Eldin C, Mediannikov O, Davoust B, Cabre O, Barré N, Raoult D, et al. Emergence of *Rickettsia africae*, Oceania. Emerg Infect Dis. 2011;17:100–2. https://doi.org/10.3201/eid1701.101081
10. Germanakis A, Chochlakis D, Angelakis E, Tselentis Y, Psaroulaki A. *Rickettsia aeschlimannii* infection in a man, Greece. Emerg Infect Dis. 2013;19:1176–7. https://doi.org/10.3201/eid1907.130232
11. Tosoni A, Mirijello A, Ciervo A, Mancini F, Rezza G, Damiano F, et al.; Internal Medicine Sepsis Study Group. Human *Rickettsia aeschlimannii* infection: first case with acute hepatitis and review of the literature. Eur Rev Med Pharmacol Sci. 2016;20:2630–3.
12. Toma L, Mancini F, Di Luca M, Cecere JG, Bianchi R, Khoury C, et al. Detection of microbial agents in ticks collected from migratory birds in central Italy. Vector Borne Zoonotic Dis. 2014;14:199–205. https://doi.org/10.1089/vbz.2013.1458
13. Mancuso E, Toma L, Polci A, d'Alessio SG, Di Luca M, Orsini M, et al. Crimean-Congo hemorrhagic fever virus genome in tick from migratory bird, Italy. Emerg Infect Dis. 2019;25:1418–20. https://doi.org/10.3201/eid2507.181345
14. Negredo A, de la Calle-Prieto F, Palencia-Herrejón E, Mora-Rillo M, Astray-Mochales J, Sánchez-Seco MP, et al.; Crimean Congo Hemorrhagic Fever Madrid Working Group. Autochthonous Crimean–Congo hemorrhagic fever in Spain. N Engl J Med. 2017;377:154–61. https://doi.org/10.1056/NEJMoa1615162
15. Hoffman T, Lindeborg M, Barboutis C, Erciyas-Yavuz K, Evander M, Fransson T, et al. Alkhurma hemorrhagic fever virus RNA in *Hyalomma rufipes* ticks infesting migratory birds, Europe and Asia Minor. Emerg Infect Dis. 2018;24:879–82. https://doi.org/10.3201/eid2405.171369>

Address for correspondence: Georg Gerhard Duscher, Institute of Parasitology, Department of Pathobiology, University of Veterinary Medicine, Veterinaerplatz 1, 1210 Vienna, Austria; email: georg.duscher@vetmeduni.ac.at

Coyotes as Reservoirs for *Onchocerca lupi*, United States, 2015–2018

Chandler C. Roe, Hayley Yaglom, April Howard, Jennifer Urbanz, Guilherme G. Verocai, Lela Andrews, Veronica Harrison, Riley Barnes, Ted Lyons, Jolene R. Bowers, David M. Engelthaler

The *Onchocerca lupi* nematode infects dogs, cats, and humans, but whether it can be spread by coyotes has been unknown. We conducted surveillance for *O. lupi* nematode infection in coyotes in the southwestern United States. We identified multiple coyote populations in Arizona and New Mexico as probable reservoirs for this species.

Onchocerca lupi is a species of zoonotic, filarial nematode that causes onchocerciasis in dogs, cats, and humans. It was first described in 1967 in Georgia, then part of the USSR, in the periocular tissues of a wolf (*Canis lupus lupus*) (*1*) and has been reported in dogs (*C. lupus domesticus*). Since 2013, increased detection of *O. lupi* infections in dogs and humans in the United States and Europe has renewed interest in this parasite, its geographic distribution, and the range of its natural hosts (*2*).

The geographic distribution and prevalence of the *O. lupi* nematode in the United States is unknown. US veterinarians are not required to report *O. lupi* infections in canines, making it difficult to identify the parasite's geographic distribution. The first documented case of *O. lupi* infection in the United States affected a dog in California in 1991 (*3*); since then, *O. lupi* infections have been reported in dogs, cats, and humans in Arizona, California, Colorado, New Mexico, Texas, and Utah (*2*,*4*,*5*,*6*). This parasitic nematode is now endemic in domesticated canines in the southwestern United States (*7*). Reports of *O. lupi* infection in Canada (Alberta and Prince Edward Island) (*7*) associated with dog importation from the southwestern United States and travel of US companion animals suggest an anthropogenic spread of the *O. lupi* nematode. Whether wild canids, including coyotes (*C. latrans*), might be reservoirs for the *O. lupi* nematode is unknown.

Because of the growing number of *O. lupi* infections in canines and humans, public health officials must understand the prevalence and distribution of this parasite in wildlife. Toward that goal, we investigated coyote populations in Arizona, New Mexico, and Nevada as potential primary hosts and natural reservoirs for the *O. lupi* nematode.

The Study

From December 2015 through July 2018, we collected skin tissue samples from coyotes harvested for predation management conducted by the Arizona Game and Fish Department, and from hunters in Arizona, New Mexico, and Nevada. We did not euthanize any coyotes for the specific purpose of this study. Skin tissue from the interocular frontal area of the animal's head was removed and stored in 80% ethanol until we extracted the DNA. We screened 707 DNA sequences for an *O. lupi* cytochrome c oxidase (COI) gene (*8*) using SYBR Green–real-time PCR on a QuantStudio 7 Flex Real Time PCR System (Thermo Fisher Scientific, https://www.thermofisher.com). We used DNA from an adult worm from an infected dog in northern Arizona as a positive control (GenBank accession no. MT878136). We included a no-template control in every real-time PCR reaction plate. We compared the product's melting curve to the positive control using a dissociation curve. We prepared every sample that had a melting curve resembling that of the positive

Author affiliations: Translational Genomics Research Institute, Flagstaff, Arizona, USA (C.C. Roe, H. Yaglom, V. Harrison, R. Barnes, T. Lyons, J.R. Bowers, D.M. Engelthaler); Northern Arizona University, Flagstaff (C.C. Roe, L. Andrews); Arizona Department of Health Services, Phoenix, Arizona, USA (H. Yaglom); Arizona Game and Fish Department, Phoenix (A. Howard); Eye Care for Animals, Scottsdale, Arizona, USA (J. Urbanz); Texas A&M University, College Station, Texas, USA (G.G. Verocai); University of Georgia, Athens, Georgia, USA (G.G. Verocai)

DOI: https://doi.org/10.3201/eid2612.190136

Table. Coyotes tested for *Onchocerca lupi* nematodes, United States, 2015–2018

Location	No. samples	No. (%) positive samples	Coyote sex		Coyote age group	
			M	F	Adult	Youth
Arizona						
Coconino	189	5 (2.7)	97	92	177	12
Apache	106	10 (9.4)	56	50	88	18
Yavapai	86	1 (1.2)	49	37	78	8
Cochise	75	0	44	31	66	9
Mohave*	56	1 (1.8)	29	26	53	3
Navajo*	48	17 (35.4)	31	16	45	3
Graham	48	0	24	24	46	2
Maricopa	42	1 (2.4)	19	23	32	10
La Paz	14	1 (7.1)	5	9	12	2
Pima	6	0	2	4	6	0
Pinal	3	0	1	2	3	0
Yuma	1	0	1	0	1	0
Unknown†	1	0	0	1	1	0
Unknown†	1	0	0	1	1	0
New Mexico						
Catron	7	0	5	2	6	1
McKinley	1	0	0	1	1	0
San Juan	4	0	1	3	4	0
Torrence	4	0	3	1	3	1
Tucamari	3	0	1	2	3	0
Quay	3	0	3	0	3	0
Hildago	2	1 (50.0)	1	1	2	0
Zuni	1	0	1	0	1	0
Nevada						
Elko	4	0	3	1	4	0
Nye	2	0	1	1	2	0

*Mohave and Navajo Counties each had 1 sample for which host sex was not recorded.
†2 samples from Arizona did not have a recorded county.

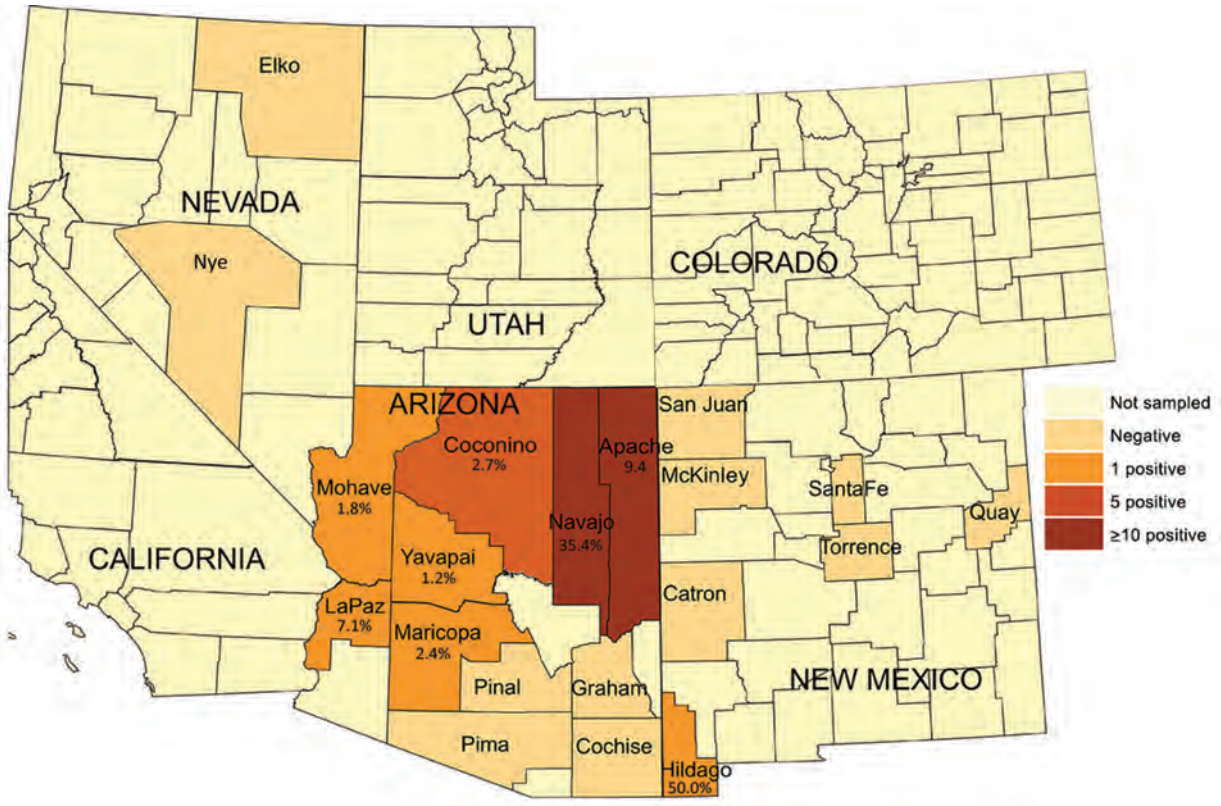

Figure 1. Number of *Onchocerca lupi* nematode–positive coyotes collected, southwestern United States, 2015–2018. Positivity rates are provided for each county with *O. lupi*–positive coyotes.

control for amplicon sequencing using neat DNA and Illumina (https://www.illumina.com) technologies.

Thirty-seven (5.2%) samples from 8 counties in Arizona and New Mexico (Table 1) had sequences that aligned with the reference gene. Of these samples, 36 were from Arizona and 1 was from Hildago County, New Mexico. In Arizona, the highest prevalences of *O. lupi* infection were in Navajo County (17 [35.4%] positive coyotes) and Apache County (10 [9.4%]) (Figure 1). Coconino County had the third

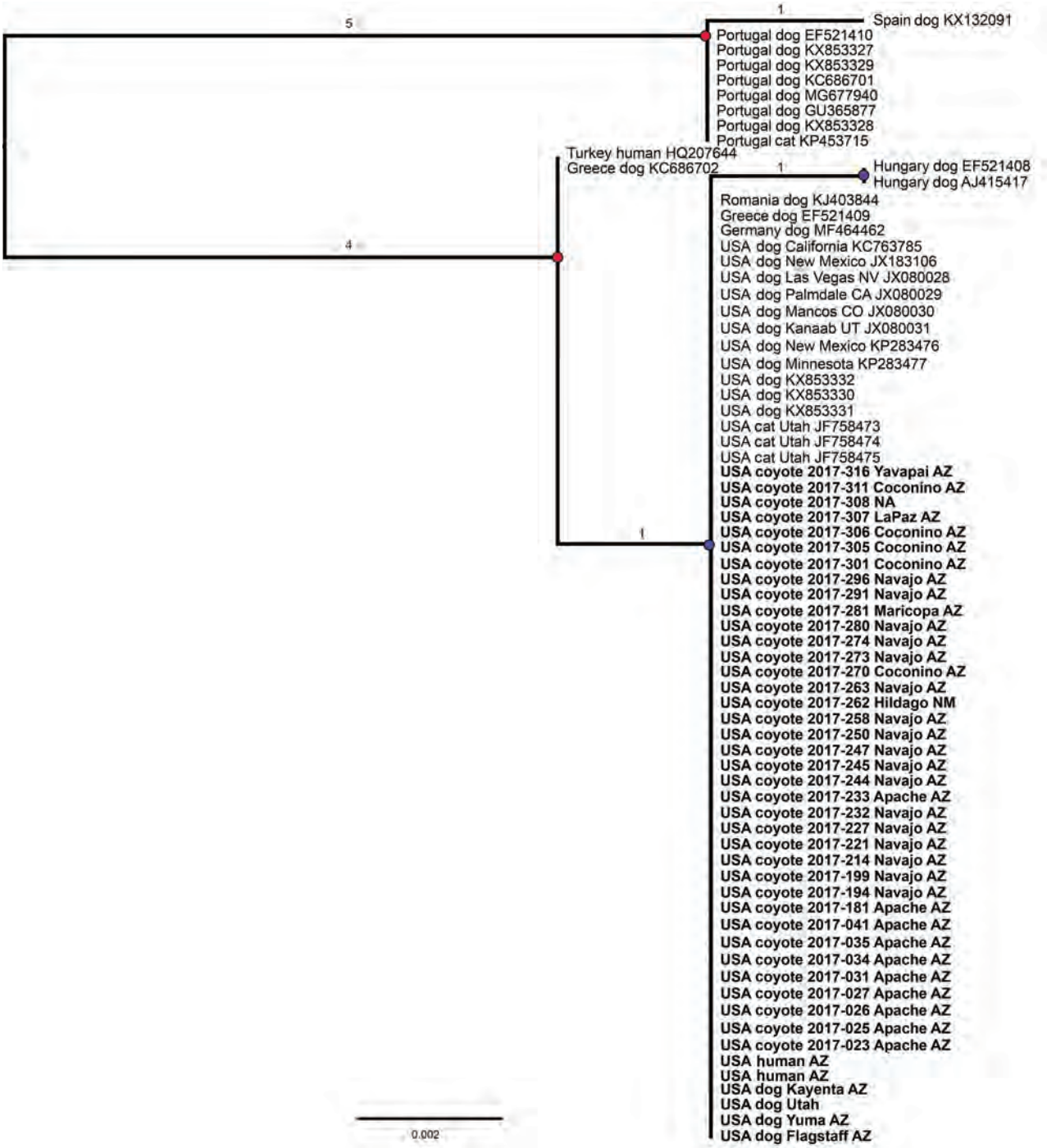

Figure 2. Rooted maximum-likelihood phylogenetic tree based on the cytochrome oxidase c gene sequence from 73 *Onchocerca lupi* nematode samples, including 43 newly obtained samples from 37 coyotes, 4 dogs, and 2 humans, southwestern United States, 2015–2018. This analysis covers 432 bases. Branch lengths indicate the number of single-nucleotide polymorphisms; red dots indicate bootstrap values >99; blue dots indicate bootstrap values <65. Countries of collection, host species, and year of collection are indicated. Newly sequenced specimens are in bold. Scale bar indicates number of nucleotide substitutions per site.

highest number (5) of coyotes that tested positive for the *O. lupi* nematode but a lower positivity rate (2.7%) than other counties. For example, in Hidalgo County we sampled only 2 coyotes, 1 of which tested positive.

We produced a phylogenetic tree of our 43 COI sequences (including 4 that were isolated from infected dogs and 2 from humans [GenBank accession nos. MT878134–9]) in addition to 30 *O. lupi* COI genes on GenBank spanning 432 total bases containing 12 single-nucleotide polymorphisms (SNPs) (Figure 2) using IQTREE version 1.6.9 (*9*) software with 1,000 bootstrap replicates. Examining only this region of the COI gene, we determined the US samples (from dogs, cats, coyotes, and humans) clustered within a single clade with dog samples from Germany, Romania, and Greece. Within this clade, we detected no SNP differences. This clade was separated from a sample from Hungary by 1 SNP and from a single clade containing a human isolate from Turkey and a dog sample from Greece by 1 SNP.

Conclusions

O. lupi infection has been reported mainly in domestic dogs and cats in the southwestern United States (*4*,*2*). However, international transportation (purchasing, adopting, and exporting) of dogs from that area has introduced this parasite into environments to which it is not endemic (*7*,*10*). We hypothesize coyotes are reservoirs for the *O. lupi* nematode and could spread this parasite throughout the southwestern United States.

We consider the probable importance of coyotes as natural reservoirs and dispersal agents. In the United States, the average home territory covered by a resident coyote population (either a pack or lone coyote) is 5–41 km^2, whereas solitary transient coyote territories are up to 155 km^2 (*11*,*12*). The large geographic range and widespread occurrence of not only coyotes, but also the putative black fly vector (Diptera: *Simuliidae*) (*13*), might facilitate the spread and establishment of the *O. lupi* nematode in the southwestern United States. Furthermore, many North American wild canids, such as wolves and foxes, have never been assessed for the *O. lupi* nematode but also should be considered as potential reservoirs. Although the *O. lupi* nematode is only endemic to the southwestern United States, without appropriate surveillance and mitigation strategies it might spread across the United States and into Canada and Mexico. We are not aware of any reports of *O. lupi* nematodes in Mexico; however, we identified a coyote that tested positive for *O. lupi* infection in Hildago County, which borders Mexico. Increasing surveillance in nearby counties upon identification of *O. lupi* nematode–positive coyotes would be prudent. Furthermore, the overlap of rural human residences with coyote and black fly populations probably increases the risk for human exposure.

In summary, canine onchocerciasis is an ongoing emerging infectious threat to wildlife, companion animals, and humans. The expanding range to which the *O. lupi* nematode is endemic, coupled with increased incidence of onchocerciasis in humans and canines in the southwestern United States, reinforces the need to understand, respond to, and potentially mitigate this threat. This understanding will enable the development of surveillance and mitigation strategies, determine the risk of spread to nonendemic regions, and identify human populations at high risk of infection.

Acknowledgments

We thank Yvonne Qvarnstrom for providing 2 *O. lupi* nematode–positive samples from 2 humans in Arizona that were included in this study. We also acknowledge Laura Adams for her contribution.

This study was funded in part by contract 200-2016-92313 with the Centers for Disease Control and Prevention under its Advanced Molecular Detection Initiative.

About the Author

Ms. Roe is a research coordinator at the Pathogen and Microbiome Institute and a doctoral student in the School of Informatics and Computing at Northern Arizona University. Her primary research interests include pathogen genomics of parasites, fungi, and bacteria.

References

1. Rodonaja TE. A new species of nematode, *Onchocerca lupi* n. sp., from *Canis lupus cubanensis*. Soobshchenyia Akad Nuak Gruz Ssr. 1967;45:715–9.
2. Cantey PT, Weeks J, Edwards M, Rao S, Ostovar GA, Dehority W, et al. The emergence of zoonotic *Onchocerca lupi* infection in the United States—a case-series. Clin Infect Dis. 2016;62:778–83. https://doi.org/10.1093/cid/civ983
3. Orihel TC, Ash LR, Holshuh HJ, Santenelli S. Onchocerciasis in a California dog. Am J Trop Med Hyg. 1991;44:513–7. https://doi.org/10.4269/ajtmh.1991.44.513
4. McLean NJ, Newkirk K, Adema CM. Canine ocular onchocerciasis: a retrospective review of the diagnosis, treatment, and outcome of 16 cases in New Mexico (2011–2015). Vet Ophthalmol. 2017;20:349–56. https://doi.org/10.1111/vop.12433
5. Eberhard ML, Ostovar GA, Chundu K, Hobohm D, Feiz-Erfan I, Mathison BA, et al. Zoonotic *Onchocerca lupi* infection in a 22-month-old child in Arizona: first report in the United States and a review of the literature. Am J Trop Med Hyg. 2013;88:601–5. https://doi.org/10.4269/ajtmh.12-0733

6. Labelle AL, Maddox CW, Daniels JB, Lanka S, Eggett TE, Dubielzig RR, et al. Canine ocular onchocercosis in the United States is associated with *Onchocerca lupi*. Vet Parasitol. 2013;193:297–301. https://doi.org/10.1016/j.vetpar.2012.12.002
7. Verocai GG, Conboy G, Lejeune M, Marron F, Hanna P, MacDonald E, et al. *Onchocerca lupi* nematodes in dogs exported from the United States into Canada. Emerg Infect Dis. 2016;22:1477–9. https://doi.org/10.3201/eid2208.151918
8. Hassan HK, Bolcen S, Kubofcik J, Nutman TB, Eberhard ML, Middleton K, et al. Isolation of *Onchocerca lupi* in dogs and black flies, California, USA. Emerg Infect Dis. 2015;21:789–96. https://doi.org/10.3201/eid2105.142011
9. Nguyen L-T, Schmidt HA, von Haeseler A, Minh BQ. IQ-TREE: a fast and effective stochastic algorithm for estimating maximum-likelihood phylogenies. Mol Biol Evol. 2015;32:268–74. https://doi.org/10.1093/molbev/msu300
10. Colella V, Lia RP, Di Paola G, Cortes H, Cardoso L, Otranto D. International dog travelling and risk for zoonotic *Onchocerca lupi*. Transbound Emerg Dis. 2018;65:1107–9. https://doi.org/10.1111/tbed.12842
11. Gehrt SD, Anchor C, White LA. Home range and landscape use of coyotes in a metropolitan landscape: conflict or coexistence? J Mammal. 2009;90:1045–57. https://doi.org/10.1644/08-MAMM-A-277.1
12. Howard VW, Delfrate GG. Home ranges and movements of coyotes in the northern Chihuahuan desert. 1991 [cited 2019 Jan 4]. https://digitalcommons.unl.edu/cgi/viewcontent.cgi?article=1014&context=gpwdcwp
13. Adler PH, Currie DC, Wood M, Idema RM, Zettler LW. The black flies (Simuliidae) of North America. Ithaca (NY): Cornell University Publishing; 2004.

Address for correspondence: Chandler Roe, Northern Arizona University, Pathogen and Microbiome Institute, 1395 S. Knoles Dr, Bldg 56, Ste 210, Flagstaff, AZ 86011, USA; email: chandler.roe@nau.edu

Direct Transmission of Severe Fever with Thrombocytopenia Syndrome Virus from Domestic Cat to Veterinary Personnel

Atsushi Yamanaka, Yumi Kirino, Sho Fujimoto, Naoyasu Ueda, Daisuke Himeji, Miho Miura, Putu E. Sudaryatma, Yukiko Sato, Hidenori Tanaka, Hirohisa Mekata, Tamaki Okabayashi

Two veterinary personnel in Japan were infected with severe fever with thrombocytopenia syndrome virus (SFTSV) while handling a sick cat. Whole-genome sequences of SFTSV isolated from the personnel and the cat were 100% identical. These results identified a nosocomial outbreak of SFTSV infection in an animal hospital without a tick as a vector.

Severe fever with thrombocytopenia syndrome (SFTS) is caused by the species *Dabie bandavirus* (family *Phenuiviridae*, genus *Bandavirus*), generally called severe fever with thrombocytopenia syndrome virus (SFTSV) (*1*,*2*). Cases of SFTS were identified in patients in China during 2009 (*3*) and subsequently in Japan and South Korea (*2*,*4*). Clinical signs include high fever, fatigue, gastrointestinal symptoms, neurologic symptoms, thrombocytopenia, leukocytopenia, and multiorgan failure (*5*). SFTS is potentially fatal, and mortality rates have reached 27% in Japan (*6*). Although the clinical information regarding SFTS in most animals is unclear, cats show fatal symptoms similar to those in humans (*7*). Enzootic SFTSV transmission is primarily tickborne; tick bites can also spread the virus to humans (*8*) and animals (*9*). Human-to-human transmission occurs rarely through contact with infected blood, body fluids, or mucus (*10*) and possibly by aerosols (*11*). In this study, we provide evidence for the direct cat-to-human transmission of the virus, leading to a nosocomial outbreak of SFTSV infection.

Author affiliations: Miyazaki Prefectural Miyazaki Hospital, Miyazaki, Japan (A. Yamanaka, S. Fujimoto, N. Ueda, D. Himeji); University of Miyazaki, Miyazaki (Y. Kirino, P.E. Sudaryatma, Y. Sato, H. Tanaka, H. Mekata, T. Okabayashi); Miyazaki Prefectural Institute for Public Health and Environment, Miyazaki (M. Miura)

DOI: https://doi.org/10.3201/eid2612.191513

The Study

Confirmatory testing of veterinary personnel samples was performed at the Laboratory of Microbiology, Miyazaki Prefecture Institute for the Public Health and Environment, Miyazaki, Japan. Cat sample analysis was performed at the Center for Animal Disease Control, University of Miyazaki. A 1-year-old male domestic cat was hospitalized on August 15, 2018, with jaundice, poor appetite, vomiting, and a rectal temperature of 40.4°C. Hematologic examination showed leukocytopenia (1,080 cells/μL, reference range 4–30 × 10^3 cells/μL), thrombocytopenia (19,000 cells/μL, reference range 9–90 × 10^4 cells/μL), and an increased level of total bilirubin (3.1 mg/dL, reference range 0–0.5 mg/dL) (*12*) (Table). The cat died 3 days after hospitalization.

Serum samples, saliva samples, and anal swab specimens (sampled on the first day of hospitalization) were sent to the Center for Animal Disease Control, University of Miyazaki, for molecular test targeting the small segment RNA of SFTSV by reverse transcription PCR (RT-PCR) and real-time RT-PCR (*3*). The amounts of SFTSV RNA were quantified as RNA copies per milliliter of serum. We detected a viral load of 1.5 × 10^{11} copies/mL (Table).

During hospitalization, the cat came into contact with a veterinarian (44-year-old woman) and a veterinary technician (20-year-old woman). During contact, both veterinary personnel wore protective clothing (gloves and surgical masks), but their eyes remained unprotected; they were not bitten or scratched by the cat. In addition, neither was bitten by ticks.

After the death of the cat, symptoms consistent with SFTS developed in both veterinary personnel (Figure 1). Ten days after the death of the cat, on August 27, the veterinarian (patient 1) was hospitalized with a high fever (body temperature 39.2°C),

Table. Hematologic and diagnostic results from a nosocomial outbreak of infection with severe fever with thrombocytopenia syndrome virus in animal hospital, Japan, 2018*

Characteristic	Cat,† Aug 15	Patient 1						Patient 2	
		Aug 27	Aug 28	Aug 29	Aug 30	Sep 5	Sep 11	Aug 28	Sep 11
RT-PCR	+	–	–	+	+	ND	ND	+	ND
Virus-specific IgG	+	–	–	ND	–	ND	+	–	+
Real-time RT-PCR, copies/mL	1.5×10^{11}	ND	ND	3.9×10^{6}	6.0×10^{6}	ND	ND	5.7×10^{6}	ND
Isolation‡	J1	ND	ND	J1	J1	ND	ND	J1	ND
Leukocytes/μL	1, 080 (4–30 x 10^3)	1,970	1,300	1,060	1,450	2,570	4,070	2,850	4,630
Hemoglobin, g/dL	14.6 (9–18)	13.1	12.6	12.3	13.4	11.6	12.6	13.4	13.1
Platelet count/μL	19,000 (9–90 x 10^4)	81,000	63,000	53,000	59,000	155,000	214,000	254,000	261,000
Total bilirubin, mg/dL	3.1 (0–0.5)	0.36	0.26	ND	0.28	0.44	0.69	0.44	0.42
AST, IU/L	ND	18	17	20	27	51	11	25	24
ALT, IU/L	91 (47.4–97.3)	12	10	12	16	60	25	37	28
LDH, IU/L	ND	134	123	149	157	130	156	213	267
C-reactive protein, mg/dL	ND	0.04	0.04	ND	0.03	0.01	0.002	0.17	0.19

*ALT, alanine aminotransferase; AST, aspartate aminotransferase; J1, J1 genotype; LDH, lactate dehydrogenase; ND, not done; RT-PCR, reverse transcription PCR; –, negative; +, positive.
†Values in parentheses are standard feline hematologic parameters reported by O'Brien et al. (*12*).
‡Virus isolated on Vero cells and genotyping.

fatigue, widespread myalgia, ocular pain, and bicytopenia. No abnormal symptoms were noted on cardiac, pulmonary, or abdominal examination. Hematologic examinations showed leukocytopenia and thrombocytopenia. On postadmission days 2 and 3, the presence of SFTSV RNA was confirmed in the serum samples by RT-PCR and real-time PCR (day 2, 3.9×10^6 virus RNA copies/mL; day 3, 6.0×10^6 virus RNA copies/mL) (Table). By postadmission day 10, the symptoms of SFTS abated, and patient 1 was discharged. Five days after discharge (September 11, 2018), SFTSV-specific IgG were detected in serum samples (*13*) (Table).

Eleven days after the death of the cat, on August 28, the veterinary technician (patient 2) also had fever and general malaise but less severe leukocytopenia. Serum samples collected from patient 2 were positive for SFTSV RNA by RT-PCR, and SFTSV RNA copies were quantified by using real-time RT-PCR (5.7×10^6 virus RNA copies/mL) (Table). However, patient 2 recovered without being hospitalized. Similar to patient 1, IgG against SFTSV was present in serum collected from patient 2 on September 11.

We also isolated the virus. Vero cells were inoculated with SFTSV-positive serum samples taken from the cat, patient 1, and patient 2. The cells were adjusted

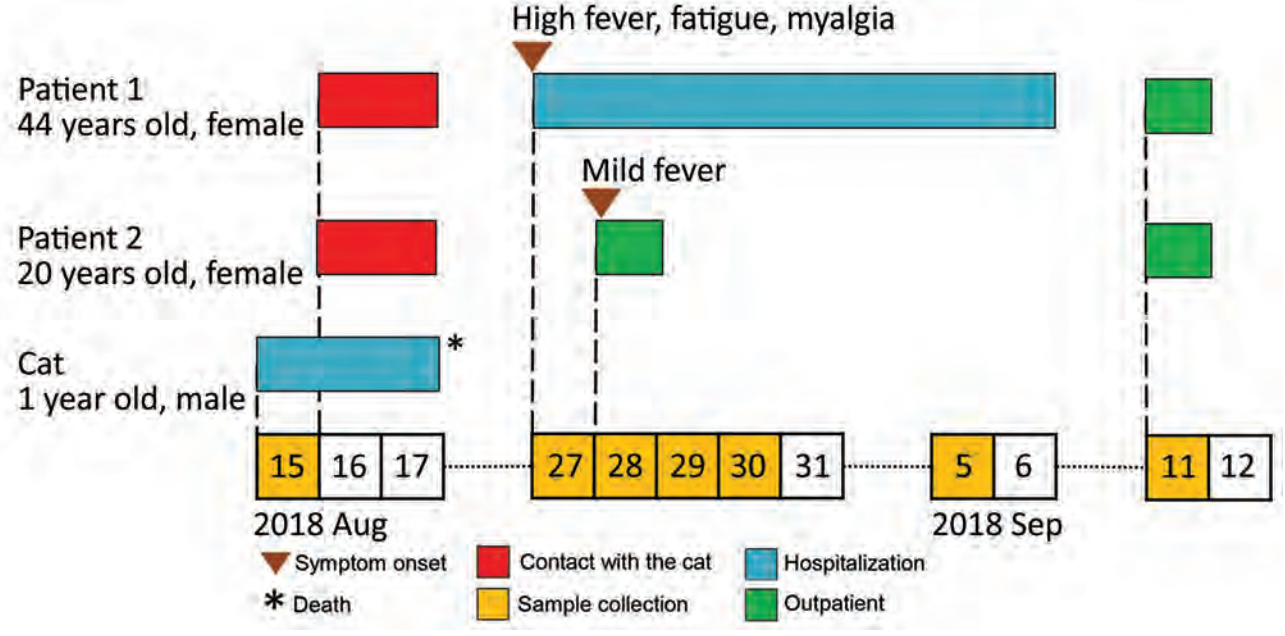

Figure 1. Timeline for transmission of severe fever with thrombocytopenia syndrome virus from cat to veterinary personnel in animal hospital, Japan, 2018. Patient 1, veterinarian; patient 2, veterinary technician.

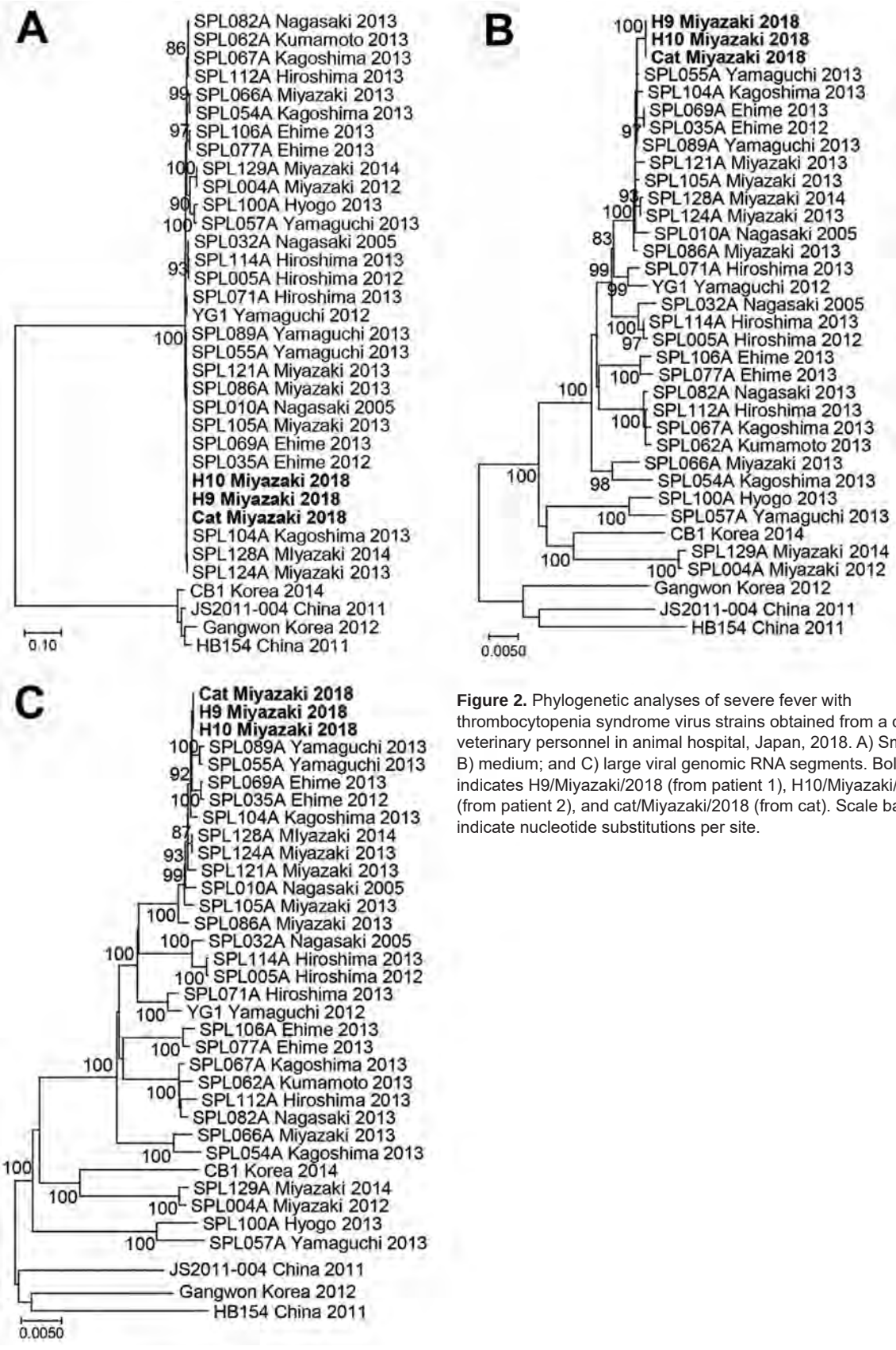

Figure 2. Phylogenetic analyses of severe fever with thrombocytopenia syndrome virus strains obtained from a cat and veterinary personnel in animal hospital, Japan, 2018. A) Small; B) medium; and C) large viral genomic RNA segments. Bold indicates H9/Miyazaki/2018 (from patient 1), H10/Miyazaki/2018 (from patient 2), and cat/Miyazaki/2018 (from cat). Scale bars indicate nucleotide substitutions per site.

to 10^5 cells/mL and seeded onto a 12-well plate (Sumilon, http://www.sumilon.com) overnight as a monolayer (>60% confluence). A total of 200 μL of serum samples was inoculated into the cells. For all 3 serum samples (cat, patient 1, and patient 2), extensive cytopathic effects were observed after 3 days of incubation, and a high copy number of SFTSV RNA was detected in the cell supernatants.

Whole-genome sequencing (MiSeq; Illumina, https://www.illumina.com) of the viruses (named Cat/Miyazaki/2018, H9/Miyazaki/2018, and H10/Miyazaki/2018) was conducted as described (*14*), and sequences were submitted to DDBJ (accession nos. LC462229–37). For each viral RNA segment (small, medium, and large), the viral sequences from the cat and the 2 veterinary personnel showed 100% homology (Figure 2) and were closely related to the reference SFTSV strain YG1 from Japan (YG1/Yamaguchi/2012, accession nos. AB817995, AB817997, and AB817999). Furthermore, the sequence of the small segment was closely related to the SFTSV strains SPL128A Miyazaki 2014 and SPL124A Miyazaki 2013 (Figure 2, panel A), which were obtained from SFTS patients in the same prefecture during 2013–2014. Sequences of the medium and large segments were more distantly related to the SPL128A Miyazaki 2014 and SPL124A Miyazaki 2013 viruses, suggesting that they might have evolved from these strains (Figure 2, panels B, C).

SFTS is an emerging epizootic infectious disease and is transmitted primarily by ticks. However, some cases of SFTS do not involve ticks, and human-to-human transmission by aerosols (*10*) or through contact with infected blood or other body fluids (*6*,*9*) has been reported. Furthermore, a transmission route of SFTSV from a cat to a human has been confirmed with a partial nucleotide sequence of SFTSV in serum samples (*15*). In this report, we demonstrated a direct cat-to-human nosocomial outbreak of SFTSV with the following evidence: SFTSV was isolated from serum samples obtained from a cat and 2 veterinary personnel; the complete nucleotide sequence (segments small, medium, and large) of SFTSV from the cat and the 2 veterinary personnel showed 100% identity; the veterinary personnel were not bitten by ticks, nor were they bitten or scratched by the cat; and SFTS-like symptoms developed in the 2 veterinary personnel ≈10 days after close contact with the cat.

Conclusions

Our results show that SFTSV can be transmitted to humans in the absence of ticks and that wearing limited protective clothing (e.g., face masks and rubber gloves) is insufficient to protect veterinary personnel from infection when handling infected animals. It is likely that cat-to-human transmission occurred by aerosols or contact with infected cat blood or other body fluids. This study draws attention to occupational exposure to potentially fatal zoonotic pathogens and highlights the need for stringent biosafety measures (i.e., personal protective clothing and equipment) to be in place when handling animals with symptoms of SFTS. These measures should include protection against aerosols that can be generated during treatment.

Acknowledgments

We thank the patients for providing permission to report their clinical symptoms and disease course.

This study was supported by the Special Education and Research Expenses, Ministry of Education, Culture, Sports, Science and Technology, Japan.

About the Author

Dr. Yamanaka is a chief physician in the Department of Internal Medicine, Miyazaki Prefectural Miyazaki Hospital, Miyazaki, Japan. His primary research interests are emerging infectious diseases and clinical microbiology.

References

1. International Committee on Taxonomy of Viruses. Virus taxonomy. 2019 release EC 51. Berlin, July 2019; Email ratification 2020 (MSL #35) [cited 2020 Jul 9]. https://talk.ictvonline.org/taxonomy/p/taxonomy-history?taxnode_id=20141803
2. Takahashi T, Maeda K, Suzuki T, Ishido A, Shigeoka T, Tominaga T, et al. The first identification and retrospective study of severe fever with thrombocytopenia syndrome in Japan. J Infect Dis. 2014;209:816–27. https://doi.org/10.1093/infdis/jit603
3. Yu XJ, Liang MF, Zhang SY, Liu Y, Li JD, Sun YL, et al. Fever with thrombocytopenia associated with a novel bunyavirus in China. N Engl J Med. 2011;364:1523–32. https://doi.org/10.1056/NEJMoa1010095
4. Kim KH, Yi J, Kim G, Choi SJ, Jun KI, Kim NH, et al. Severe fever with thrombocytopenia syndrome, South Korea, 2012. Emerg Infect Dis. 2013;19:1892–4. https://doi.org/10.3201/eid1911.130792
5. Kato H, Yamagishi T, Shimada T, Matsui T, Shimojima M, Saijo M, et al.; SFTS epidemiological research group-Japan. Epidemiological and clinical features of severe fever with thrombocytopenia syndrome in Japan, 2013–2014. PLoS One. 2016;11:e0165207. https://doi.org/10.1371/journal.pone.0165207
6. Kobayashi Y, Kato H, Yamagishi T, Shimada T, Matsui T, Yoshikawa T, et al.; SFTS Epidemiological Research Group Japan. Severe fever with thrombocytopenia syndrome, Japan, 2013–2017. Emerg Infect Dis. 2020;26:692–9. https://doi.org/10.3201/eid2604.191011

7. Matsuu A, Momoi Y, Nishiguchi A, Noguchi K, Yabuki M, Hamakubo E, et al. Natural severe fever with thrombocytopenia syndrome virus infection in domestic cats in Japan. Vet Microbiol. 2019;236:108346. https://doi.org/10.1016/j.vetmic.2019.06.019
8. Yun SM, Lee WG, Ryou J, Yang SC, Park SW, Roh JY, et al. Severe fever with thrombocytopenia syndrome virus in ticks collected from humans, South Korea, 2013. Emerg Infect Dis. 2014;20:1358–61. https://doi.org/10.3201/eid2008.131857
9. Oh SS, Chae JB, Kang JG, Kim HC, Chong ST, Shin JH, et al. Detection of severe fever with thrombocytopenia syndrome virus from wild animals and ixodidae ticks in the Republic of Korea. Vector Borne Zoonotic Dis. 2016;16:408–14. https://doi.org/10.1089/vbz.2015.1848
10. Liu Y, Li Q, Hu W, Wu J, Wang Y, Mei L, et al. Person-to-person transmission of severe fever with thrombocytopenia syndrome virus. Vector Borne Zoonotic Dis. 2012;12:156–60. https://doi.org/10.1089/vbz.2011.0758
11. Gong Z, Gu S, Zhang Y, Sun J, Wu X, Ling F, et al. Probable aerosol transmission of severe fever with thrombocytopenia syndrome virus in southeastern China. Clin Microbiol Infect. 2015;21:1115–20. https://doi.org/10.1016/j.cmi.2015.07.024
12. O'Brien M, Murphy MG, Lowe JA. Hematology and clinical chemistry parameters in the cat (*Felis domesticus*). J Nutr. 1998;128(Suppl):2678S–9S. https://doi.org/10.1093/jn/128.12.2678S
13. Fukuma A, Fukushi S, Yoshikawa T, Tani H, Taniguchi S, Kurosu T, et al. Severe fever with thrombocytopenia syndrome virus antigen detection using monoclonal antibodies to the nucleocapsid protein. PLoS Negl Trop Dis. 2016;10:e0004595. https://doi.org/10.1371/journal.pntd.0004595
14. Mekata H, Yamamoto M, Hamabe S, Tanaka H, Omatsu T, Mizutani T, et al. Molecular epidemiological survey and phylogenetic analysis of bovine influenza D virus in Japan. Transbound Emerg Dis. 2018;65:e355–60. https://doi.org/10.1111/tbed.12765
15. Kida K, Matsuoka Y, Shimoda T, Matsuoka H, Yamada H, Saito T, et al. A case of cat-to-human transmission of severe fever with thrombocytopenia syndrome virus. Jpn J Infect Dis. 2019;72:356–8. https://doi.org/10.7883/yoken.JJID.2018.526

Address for correspondence: Tamaki Okabayashi, Center for Animal Disease Control, University of Miyazaki, 1-1 Gakuenkibanadai Nishi, Miyazaki 889-2192, Japan; email: okbys81@cc.miyazaki-u.ac.jp

Endovascular Infection with *Kingella kingae* Complicated by Septic Arthritis in Immunocompromised Adult Patient

Mona Mustafa-Hellou, Neta Sagi, Yishai Ofran, Yuval Geffen, Nesrin Ghanem-Zoubi

We report a case of *Kingella kingae* endovascular infection in an immunocompromised elderly patient in Israel who had culture-negative septic arthritis. This case highlights potential sources of metastatic infection other than infective endocarditis, and emphasizes the need for molecular diagnostic methods in detection of pathogens in culture-negative septic arthritis in immunocompromised patients.

Kingella kingae, a gram-negative coccobacillus, might be part of the normal flora of the upper respiratory tract. It is a well-recognized causative agent of osteoartricular infections in children ≤4 years of age (*1*). In adults, it rarely causes infections; the most well-known is infective endocarditis as part of the HACEK (*Haemophilus* species, *Aggregatibacter* species, *Cardiobacterium* hominis, *Eikenella corrodens*, and *Kingella* species) group.

Predisposing factors for *K. kingae* infection are poor oral hygiene, pharyngitis, and mucosal ulcerations (*2*). Few cases of isolated septic arthritis in immunocompetent and immunocompromised adult patients had been described. We report a rare case of endovascular infection caused by *K. kingae* in an immunocompromised adult patient in Israel who had septic arthritis.

The Study

A 74-year-old woman was admitted to an emergency department because of pain and swelling in her left knee. No fever or chills were reported. She reported no history of a recent invasive procedure, trauma, exposure to animals, or consumption of unpasteurized dairy products. Her medical history indicated that she was a heavy smoker. A high-risk myelodysplastic syndrome had been diagnosed 18 months before her coming to the emergency department. The main manifestations of the myelodysplastic syndrome were anemia, thrombocytopenia, and preserved leukocyte and neutrophils counts. She was given decitabine. She was subsequently given a diagnosis of acute myeloid leukemia and was found to have an isocitrate dehydrogenase 2 gene mutation. Therefore, therapy with enasidenib, an isocitrate dehydrogenase 2 gene blocker, was initiated. She showed a good response for 8 months. Near the time of her admission, the disease progressed, and venetoclax, a B-cell lymphoma 2 inhibitor, was added to her treatment.

At admission, the patient was stable hemodynamically and afebrile. Physical examination showed arthritis in the left knee. A unilateral, nontender, erythematous, maculopapular rash was observed on the sole of the left foot (Figure 1). Peripheral pulses were absent distal to left femoral artery, and there were no signs of ischemia of the lower limb. A murmur was heard over the left femoral artery. No heart murmurs were noted on auscultation. White plaques were observed on her tongue and buccal mucosa.

Laboratory tests showed a leukocyte count of 30,000 cells/μL (reference range 4,500 cells/μL–11,000 cells/μL), a hemoglobin level of 8.1 g/dL (reference range 13.8 g/dL–17.2 g/dL), and a platelet count of 22,000/μL (reference range 150,000 cells/μL–400,000 cells/μL). The C-reactive protein level was high (29 mg/dL; reference value <0.3 mg/dL). Blood cultures were drawn before initiating empiric antimicrobial treatment with cefazolin and ciprofloxacin for suspected septic arthritis. An arthrocentesis of the left knee was performed the day after admission and showed a leukocyte count of 83,000 cells/μL with 93% neutrophils. A negative gram stain result was followed by negative synovial fluid and blood cultures.

A PCR was performed for ≈1 mL of synovial fluid. DNA extraction was performed by using the

Author affilations: Rambam Health Care Campus, Haifa, Israel (M. Mustafa-Hellou, Y. Ofran, Y. Geffen, N. Ghanem-Zoubi); Technion Israel Institute of Technology. Haifa (N. Sagi)

DOI: https://doi.org/10.3201/eid2612.191665

Figure 1. Unilateral, painless, maculopapular, erythematous rash over the sole of the left foot of an immunocompromised patient in Israel with suspected Janeway lesions who had endovascular infection with *Kingella kingae* complicated by septic arthritis. The rash disappeared a few days after initiation of antimicrobial drug treatment.

QIAamp DNA Mini Kit (QIAGEN, https://www.qiagen.com) according to the manufacturer's instructions. Amplification was performed with 2 sets of primers, 1 of ≈500 bp and 1 of ≈1,000 bp, both specific for the 16S rRNA gene. The sets of primers used: set 1, forward: 5′-AGA GTT TGA TCM TGG CTC AG-3′, and reverse: 5′-CCG TCA ATT CMT TTR AGT TT-3′; set 2, forward: 5′-GCA AAC AGG ATT AGA TAC CC-3′, and reverse: 5′-GAC GTC RTC CNC DCC TTC CTC-3′. PCR products were separated by electrophoresis in ethidium bromide–stained 2% agarose gels, and were then sequenced on a 3130 Genetic Analyzer Capillary Electrophoresis DNA Sequencer (Applied Biosystems, https://www.thermofisher.com) and analyzed by using BLAST (https://blast.ncbi.nlm.nih.gov) giving 100% identity to *K. kingae*.

Antimicrobial treatment was switched to ceftriaxone. Echocardiography was performed and showed no evidence of vegetation on heart valves. Because of slow clinical improvement and the physical examination findings described, an endovascular focus was suspected. The patient underwent computed tomography angiography of the abdomen, pelvis, and lower limbs, which showed disseminated atherosclerotic plaques in the descending aorta. In addition, a plaque, surrounded by turbid fat, causing a major luminal stenosis was seen on the transition of the left external iliac artery and common femoral artery. Fluorodeoxyglucose positron emission tomography–computed tomography showed high uptake of fluorodeoxyglucose in the plaque in the transition of left external iliac artery and common femoral artery, a finding consistent with endovascular infection and an uptake in the left knee (Figure 2).

The patient was given intravenous ceftriaxone for 6 weeks and showed marked improvement in the C-reactive protein level and leukocyte count. However, 2 weeks later, the patient had a relapse of pain in left knee. Physical examination showed that her left leg was cold, with signs of worsening of arterial insufficiency and minimal swelling of the knee. A repeat fluorodeoxyglucose positron emission tomography–computed tomography showed increased uptake of fluorodeoxyglucose in the left knee, which was suspected for a flair-up of septic arthritis; uptake in the endovascular plaque; and worsening stenosis of the femoral artery. A repeat arthrocentesis trial failed.

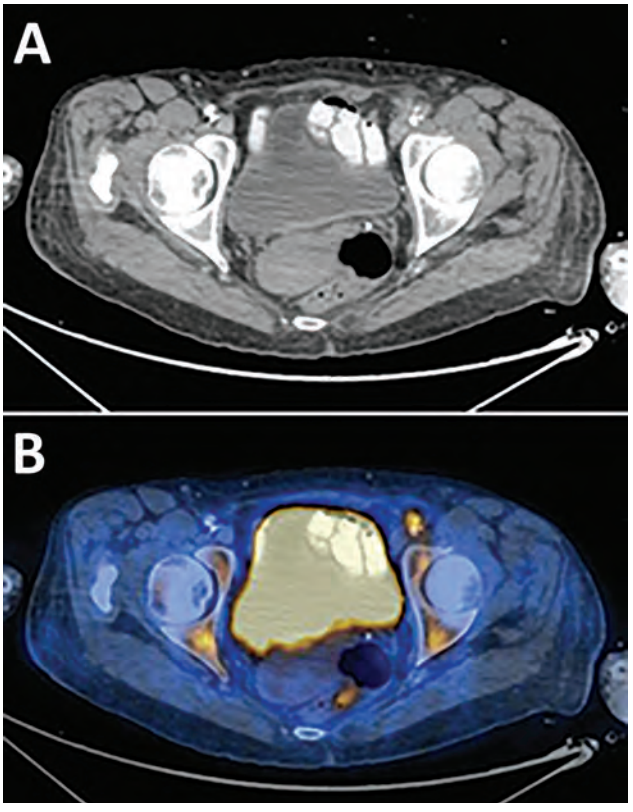

Figure 2. Imaging of an immunocompromised patient who had endovascular infection with *Kingella kingae* complicated by septic arthritis, Israel. A) Computed tomography scan shows a luminal stenosis in the transition zone of the left external iliac artery and common femoral artery along with surrounding turbid fat. B) Fluorodeoxyglucose positron emission tomography–computed tomography scan showing high fluorodeoxyglucose uptake in the plaque causing the stenosis.

Antimicrobial treatment with ceftriaxone was resumed for an additional 6 weeks, which led to improvement of clinical and inflammatory markers. Three months later, the patient showed no further clinical signs of active infection. We also monitored the patient for revascularization caused by worsening arterial insufficiency.

Conclusions

K. kingae usually causes septic arthritis in early childhood (*1*), but has been rarely reported in adults; only 10 such cases were identified in a literature review by using PubMed, Google, and Google Scholar and the words "*Kingella kingae*," "adult," and "arthritis." Previous reports included both male and female patients, of the entire adult age range, and in both immunosuppressed and immunocompetent patients (*3*–*8*). Other reported rare infections with *K. kingae* in adults include peritonitis (*9*), keratitis (*10*,*11*), stomatitis (*12*), urinary tract infection (*13*), and bacteremia (*14*).

The most common infection of *K. kingae* in adults is for persons with infective endocarditis, described in patients with native and prosthetic valves. In some of the cases, there is a clear oral source for the invasive infection. After transient bacteremia, the pathogen seeds heart valves that have damaged endothelium. In our patient, who was a heavy smoker, mucosal ulcers in the mouth caused by candidiasis could have been a port of entry, leading to transient bacteremia and resulting in seeding of the bacterium on the damaged endothelium in an atherosclerotic vascular lesion. The septic arthritis seemed to have been a complication of the infected vascular lesion in the femoral artery, caused either by seeding after bacteremia or after septic emboli to left leg, including the knee and skin of the sole of the left foot.

This case highlights the need for using molecular laboratory techniques to prompt early detection of causative agent in cases of culture-negative septic arthritis, especially in immunocompromised patients with a wide range of potential pathogens, some of which are difficult to identify in the standard laboratory techniques.

In the absence of endocarditis, slow clinical improvement in a patient with septic arthritis caused by *Kingella kingae* should raise suspicion of a deep-seated infections. These infections should include an endovascular source, especially for patients with risk factors for atherosclerosis, such as a history of smoking.

About the Author

Dr. Mustafa-Hellou is a physician, internal medicine specialist, and resident in the Infectious Disease Unit, Rambam Health Care Campus, Haifa, Israel. Her primary research interests are infectious diseases and diagnostic accuracy of laboratory tests.

References

1. Yagupsky P. *Kingella kingae*: carriage, transmission, and disease. Clin Microbiol Rev. 2015;28:54–79. https://doi.org/10.1128/CMR.00028-14
2. Shimeld LA. Essentials of diagnostic microbiology. Boston: Cenage; 1999.
3. Ducoulombier V, Dehecq E, Luraschi H, Prudhomme C, Bessard D, Houvenagel E. *Kingella kingae* spondylodiscitis in an adult [in French]. Med Mal Infect. 2011;41:110–2. https://doi.org/10.1016/j.medmal.2010.09.014
4. Elyès B, Mehdi G, Kamel BH, Hela Z, Imen BS. *Kingella kingae* septic arthritis with endocarditis in an adult. Joint Bone Spine. 2006;73:472–3. https://doi.org/10.1016/j.jbspin.2005.10.021
5. Estève V, Porcheret H, Clerc D, Dorfmann H, Le Pennec MP. Septic arthritis due to *Kingella kingae* in an adult. Joint Bone Spine. 2001;68:85–6. https://doi.org/10.1016/S1297-319X(00)00232-3
6. Ricketts J, Rehmatullah NN, Sutton P. *Kingella kingae* causing septic arthritis of the knee in an immunocompetent adult. Case Rep Orthop. 2015;2015:519190. https://doi.org/10.1155/2015/519190
7. Salminen I, von Essen R, Koota K, Nissinen A. A pitfall in purulent arthritis brought out in *Kingella kingae* infection of the knee. Ann Rheum Dis. 1984;43:656–7. https://doi.org/10.1136/ard.43.4.656
8. Wilmes D, Omoumi P, Squifflet J, Cornu O, Rodriguez-Villalobos H, Yombi JC. Osteomyelitis pubis caused by *Kingella kingae* in an adult patient: report of the first case. BMC Infect Dis. 2012;12:236. https://doi.org/10.1186/1471-2334-12-236
9. Bofinger JJ, Fekete T, Samuel R. Bacterial peritonitis caused by *Kingella kingae*. J Clin Microbiol. 2007;45:3118–20. https://doi.org/10.1128/JCM.00878-07
10. Muñoz-Egea MC, García-Pedrazuela M, González-Pallarés I, Martínez-Pérez M, Fernández-Roblas R, Esteban J. *Kingella kingae* keratitis. J Clin Microbiol. 2013;51:1627–8. https://doi.org/10.1128/JCM.03426-12
11. Yip H, Whiting M. *Kingella kingae* microbial keratitis in a human immunodeficiency virus patient with orthokeratology lens wear. Clin Exp Ophthalmol. 2017;45:420–1. https://doi.org/10.1111/ceo.12900
12. Van Damme PA, van Herpen CM, Meis JF. An adult case of oral infection with *Kingella kingae*. Int J Oral Maxillofac Surg. 2004;33:105–7. https://doi.org/10.1054/ijom.2002.0440
13. Ramana K, Mohanty S. An adult case of urinary tract infection with *Kingella kingae*: a case report. J Med Case Reports. 2009;3:7236. https://doi.org/10.1186/1752-1947-3-7236
14. Roiz MP, Peralta FG, Arjona R. *Kingella kingae* bacteremia in an immunocompetent adult host. J Clin Microbiol. 1997;35:1916. https://doi.org/10.1128/JCM.35.7.1916-1916.1997

Address for correspondence: Mona Mustafa-Hellou, Department of Internal Medicine E, Rambam Health Care Campus, Haifa 31999, Israel; email: monamhellou@gmail.com

Lymphocytic Choriomeningitis Virus Infections and Seroprevalence, Southern Iraq

Hussein Alburkat, Anne J. Jääskeläinen, Ali M. Barakat, Hassan J. Hasony, Tarja Sironen, Haider Al-hello, Teemu Smura, Olli Vapalahti

Acute febrile neurological infection cases in southern Iraq (N = 212) were screened for lymphocytic choriomeningitis virus (LCMV). Two LCMV IgM–positive serum samples and 2 cerebrospinal fluid samples with phylogenetically distinct LCMV strains were found. The overall LCMV seroprevalence was 8.8%. LCMV infections are common and associated with acute neurological disease in Iraq.

Lymphocytic choriomeningitis virus (LCMV) is a rodentborne pathogen that belongs to the genus *Mammarenavirus*, family *Arenaviridae*. The house mouse (*Mus musculus*) is considered the reservoir of LCMV (*1*). Humans can be infected with LCMV by inhaling particles contaminated with rodent excreta, during organ transplantation, or congenitally during pregnancy (*2*). The symptoms of LCMV infection range from subclinical to severe (*3*); severe infections may manifest as meningitis or encephalitis or as a congenital syndrome including microcephaly, for example (*4*).

Because of the cosmopolitan distribution of its reservoir host, LCMV most likely circulates globally. However, most epidemiologic studies on LCMV have been conducted in Europe, the United States, Japan, and China (*5*–*10*). The presence and seroprevalence of LCMV infections in the Middle East region have remained unknown (*11*,*12*). We report on LCMV seroprevalence, acute LCMV infections, and characterization of phylogenetically distinct local LCMV strains in southern Iraq.

The Study

We collected 261 serum samples (from 171 acute febrile patients and 90 healthy controls) in Nasiriyah region, Dhi Qar governorate, southern Iraq (Figure 1) during 2012–2016. In addition, we collected 41 cerebrospinal fluid (CSF) samples from another set of acute febrile patients. All samples were stored at –70°C.

We studied the occurrence of LCMV infection in the Nasiriyah region of southern Iraq by screening 171 serum and 41 CSF samples, from patients with fever and neurologic manifestations, for LCMV RNA and IgM and IgG. The inclusion criteria for the study were acute febrile illness and neurologic symptoms such as headache, muscle weakness, or fatigue (Table 1). The mean duration of illness was 4.29 days (range 3–7 days). We used the IgG positivity in serum samples from the symptomatic patients as well as healthy controls to estimate the LCMV seroprevalence in the region. Ethics permissions were obtained and stored in the Al Hussain General Teaching Hospital and Bint Al Huda Maternity and Children Teaching Hospital in the Nasiriyah region, southern Iraq.

We extracted viral RNA from acute infection samples (serum and CSF) (140 μL/sample) using a QIAamp Viral RNA Mini kit (QIAGEN, https://www.qiagen.com) according to the manufacturer's instructions. We performed a pan-arena reverse transcription PCR (RT-PCR) using SuperScript II One-Step RT-PCR system with Platinum Taq High Fidelity (Invitrogen, https://www.thermofisher.com), and primers described previously (*13*). RT-PCR products (≈300–400 bp) were sequenced using the Sanger method; sequencing was performed by the Sequencing laboratory of Institute for Molecular Medicine Finland FIMM Technology Centre, University of Helsinki. For antibody detection, indirect LCMV IgM and IgG immunofluorescence assays (IFAs) were conducted, as described previously (*6*). In general, IFAs are not very specific assays; therefore, one could assume cross-reaction between LCMV and other mammarenaviruses. The specificity and sensitivity of IFA were not examined in this study.

Author affiliations: University of Helsinki, Helsinki, Finland (H. Alburkat, A.J. Jääskeläinen, T. Sironen, T. Smura, O. Vapalahti); Helsinki University Hospital, Helsinki (A.J. Jääskeläinen, O. Vapalahti); University of Basrah, Basrah, Iraq (A.M. Barakat, H.J. Hasony); Finnish Institute for Health and Welfare, Helsinki (H. Al-hello)

DOI: https://doi.org/10.3201/eid2612.201792

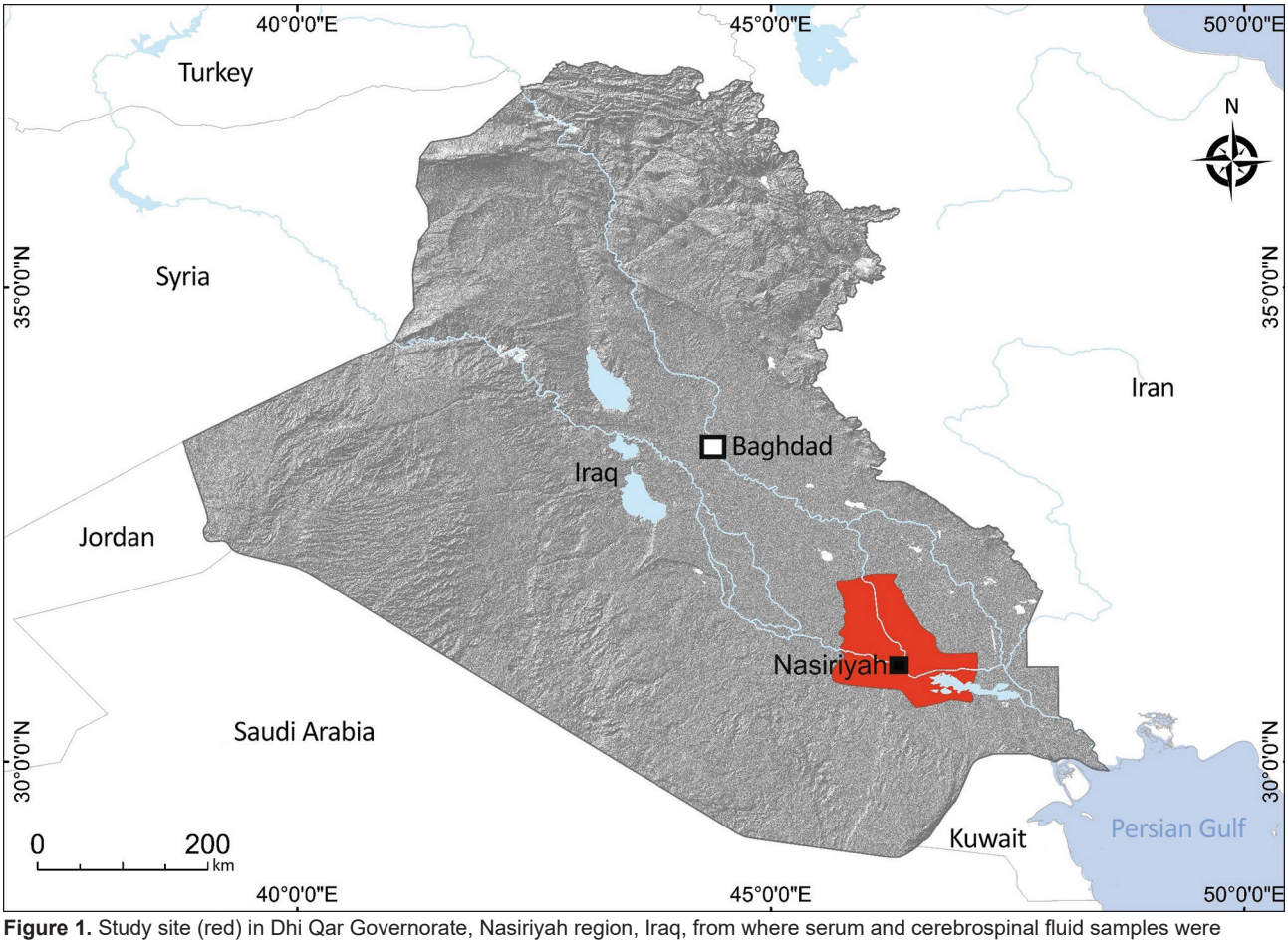

Figure 1. Study site (red) in Dhi Qar Governorate, Nasiriyah region, Iraq, from where serum and cerebrospinal fluid samples were collected from persons in rural and urban areas and screened for lymphocytic choriomeningitis virus.

The serum samples derived from patients with fever and neurologic symptoms were screened by IFA for both LCMV IgM and IgG. LCMV IgM was found in 2 serum samples (2/171) derived from patients with acute febrile illness; both serum samples were negative for LCMV IgG and LCMV RNA. These patients (a 65-year-old woman and a 70-year-old man) had fever and neurologic symptoms (Table 2).

Two CSF samples (from a 35-year-old woman and a 50-year-old man) derived from patients with fever and neurologic symptoms (Table 2) were positive for LCMV RNA by using panarenavirus RT-PCR and sequencing. Phylogenetic analysis showed that both of the sequences (GenBank accession nos. MT093202 for CSF_sample_11_Iraq_2012 and MT093203 for CSF_sample_64_Iraq_2012) grouped with other LCMV strains but formed a distinct subcluster (Figure 2). No corresponding serum samples were available for these patients, but CSF samples were further tested for LCMV IgM and IgG; all were negative.

Table 1. Signs and symptoms observed among 212 patients with acute febrile illness and neurologic symptoms screened for lymphocytic choriomeningitis virus, southern Iraq

Sign or symptom	Percentage
Fever	100
Headache	90
Joint pain	68
Vertigo	61
Severe malaise	48
Chills	46
Cough	46
Abdominal pain	34
Drowsiness	30
Anorexia	28
Stiff neck	28
Nausea	21
Retroorbital pain	19
Diarrhea	18
Vomiting	10
Confusion	8
Severe muscle weakness	6
Conjunctivitis	3
Lymphadenopathy	3
Rash	2
Ataxia	1
Shortness of breath	1

Table 2. Clinical observations in 4 patients with test results positive for lymphocytic choriomeningitis virus, southern Iraq*

	CSF RNA–positive patients		IgM–positive patients	
Observation	Male. no. 11	Female. no. 64	Male. no. 61	Female. no. 38
Diagnosis	Meningoencephalitis	Meningitis	None	No diagnosis
Duration of illness	7	4	3	3
Symptoms	Fever	Fever	Fever	Fever
	Chills	Chills	Headache	Chills
	Headache	Headache	Drowsiness	Headache
	Cough	Cough	Vertigo	General malaise
	Retroorbital pain	Retroorbital pain	Joint pain	Vertigo
	Severe muscle weakness	Severe malaise		Abdominal pain
	Drowsiness	Drowsiness		Fatigue
	Vertigo	Vertigo		
	Joint/ bone pain	Joint pain		
	Stiff neck			

*CSF, cerebrospinal fluid; LCMV, lymphocytic choriomeningitis virus.

Figure 2. Phylogenetic tree of lymphocytic choriomeningitis virus strains detected in southern Iraq (red triangles) and reference sequences. GenBank accession number, strain name, and country of origin are indicated. Bootstrap support values >70 are shown at the nodes. The phylogenetic tree was constructed using MEGA version 7 (https://www.megasoftware.net) and the maximum-likelihood algorithm on the basis of partial large segments of Kodoko virus and partial large segment sequences corresponding to sites 3210–3604 of strain Armstrong (accession no. NC_004291). Scale bar indicates substitutions per nucleic acid site. CSF, cerebrospinal fluid.

The overall LCMV IgG seroprevalence was 8.8% (23/261) in all serum samples. The seroprevalence of LCMV in our study was 12.2% (11/90) in the healthy control group and 7% (12/171) in the acute febrile patients. This difference was not statistically significant ($p = 0.2$ by χ^2 test). Because the patient samples were collected early after onset of illness (3–7 days), IgG had not yet developed; IgG serostatus thus reflects past immunity in this patient group. The healthy control population (mean age 42.9 years) was younger than acute febrile patients (mean age 46.3 years). Healthy men (7.9%) were more often LCMV seropositive than were women (5.6%), but in patients with acute febrile illness, the gender ratio was reversed (3.9% in women, 2.8% in men).The detected LCMV IgG–positive samples were derived from all age groups (21–80 years of age) included in this study. The differences concerning residency, age, and gender were not statistically significant. IgG titers measured among positive samples ranged from 20 to 80 in IFA.

Conclusions

Only limited information is available on LCMV infections beyond the United States, Europe, Japan, and China. In this work, we focused on both acute febrile infections (presence of IgM antibodies in serum or LCMV RNA in CSF) and seroprevalence of LCMV in southern Iraq. Considerable LCMV seroprevalence was detected in the Nasiriyah region of southern Iraq, and acute LCMV infection was confirmed by demonstration of LCMV RNA in 2 CSF samples and IgM antibodies in 2 serum samples. The phylogenetic analyses of these 2 findings revealed that the new sequences formed a unique subcluster, ancestral to previously known LCMV strains.

Overall, the seroprevalence rate (8.8%) of LCMV infection characterized in this study is in line with seroprevalences detected earlier in many countries in Europe, in which it varies from 5.0% in Finland (*14*) to 36% in a special subset in a rural area of the northern Croatian island of Vir (*15*). Collectively, the seroprevalence and detection of acute infection, including 2 phylogenetically distinct sequences, provide evidence that LCMV circulates in southern Iraq, and it is causing infections leading to acute neurologic manifestations in the population. More sequence data are needed to extend the knowledge on the molecular epidemiology and evolution of LCMV. In addition, further research to characterize LCMV in rodent reservoirs in southern Iraq is needed to plan vector control and public health recommendations.

Acknowledgments

We gratefully thank Ruut Uusitalo for her assistance in creating the map of Iraq.

This study was partially funded by a research grant to O.V. from the Sigrid Jusélius Foundation and from Helsinki University Hospital Funds.

About the Author

Mr. Alburkat is a PhD student at the Faculty of Medicine, Haartman Institute, University of Helsinki, Finland. His main research interests include emerging and reemerging rodent-borne viruses, virus evolution, and new pathogen discovery using next-generation sequencing techniques.

References

1. Zhou X, Ramachandran S, Mann M, Popkin DL. Role of lymphocytic choriomeningitis virus (LCMV) in understanding viral immunology: past, present and future. Viruses. 2012;4:2650–69. https://doi.org/10.3390/v4112650
2. Fischer SA, Graham MB, Kuehnert MJ, Kotton CN, Srinivasan A, Marty FM, et al.; LCMV in Transplant Recipients Investigation Team. Transmission of lymphocytic choriomeningitis virus by organ transplantation. N Engl J Med. 2006;354:2235–49. https://doi.org/10.1056/NEJMoa053240
3. Bonthius DJ, Mahoney J, Buchmeier MJ, Karacay B, Taggard D. Critical role for glial cells in the propagation and spread of lymphocytic choriomeningitis virus in the developing rat brain. J Virol. 2002;76:6618–35. https://doi.org/10.1128/JVI.76.13.6618-6635.2002
4. Barton LL, Hyndman NJ. Lymphocytic choriomeningitis virus: reemerging central nervous system pathogen. Pediatrics. 2000;105:e35. https://doi.org/10.1542/peds.105.3.e35
5. Blasdell KR, Duong V, Eloit M, Chretien F, Ly S, Hul V, et al. Evidence of human infection by a new mammarenavirus endemic to Southeastern Asia. eLife. 2016;5:e13135. https://doi.org/10.7554/eLife.13135
6. Kallio-Kokko H, Laakkonen J, Rizzoli A, Tagliapietra V, Cattadori I, Perkins SE, et al. Hantavirus and arenavirus antibody prevalence in rodents and humans in Trentino, Northern Italy. Epidemiol Infect. 2006;134:830–6. https://doi.org/10.1017/S0950268805005431
7. Knust B, Macneil A, Wong SJ, Backenson PB, Gibbons A, Rollin PE, et al. Exposure to lymphocytic choriomeningitis virus, New York, USA. Emerg Infect Dis. 2011;17:1324–5. https://doi.org/10.3201/eid1707.101349
8. Knust B, Ströher U, Edison L, Albariño CG, Lovejoy J, Armeanu E, et al. Lymphocytic choriomeningitis virus in employees and mice at multipremises feeder-rodent operation, United States, 2012. Emerg Infect Dis. 2014;20:240–7. https://doi.org/10.3201/eid2002.130860
9. Leibler JH, Zakhour CM, Gadhoke P, Gaeta JM. Zoonotic and vector-borne infections among urban homeless and marginalized people in the United States and Europe, 1990–2014. Vector Borne Zoonotic Dis. 2016;16:435–44. https://doi.org/10.1089/vbz.2015.1863
10. Takagi T, Ohsawa M, Morita C, Sato H, Ohsawa K. Genomic analysis and pathogenic characteristics of lymphocytic choriomeningitis virus strains isolated in Japan. Comp Med. 2012;62:185–92.

11. Albariño CG, Palacios G, Khristova ML, Erickson BR, Carroll SA, Comer JA, et al. High diversity and ancient common ancestry of lymphocytic choriomeningitis virus. Emerg Infect Dis. 2010;16:1093–100. https://doi.org/10.3201/eid1607.091902
12. Zhang L, Li S, Huang SJ, Wang ZD, Wei F, Feng XM, et al. Isolation and genomic characterization of lymphocytic choriomeningitis virus in ticks from northeastern China. Transbound Emerg Dis. 2018;65:1733–9. https://doi.org/10.1111/tbed.12946
13. Vieth S, Drosten C, Lenz O, Vincent M, Omilabu S, Hass M, et al. RT-PCR assay for detection of Lassa virus and related Old World arenaviruses targeting the L gene. Trans R Soc Trop Med Hyg. 2007;101:1253–64. https://doi.org/10.1016/j.trstmh.2005.03.018
14. Fevola C, Kuivanen S, Smura T, Vaheri A, Kallio-Kokko H, Hauffe HC, et al. Seroprevalence of lymphocytic choriomeningitis virus and Ljungan virus in Finnish patients with suspected neurological infections. J Med Virol. 2018;90:429–35. https://doi.org/10.1002/jmv.24966
15. Dobec M, Dzelalija B, Punda-Polic V, Zoric I. High prevalence of antibodies to lymphocytic choriomeningitis virus in a murine typhus endemic region in Croatia. J Med Virol. 2006;78:1643–7. https://doi.org/10.1002/jmv.20749

Address for correspondence: Hussein Alburkat, Rastilantie 2A 29, Helsinki 00960, Finland; email: hussein.alburkat@helsinki.fi

Range Expansion of Bombali Virus in *Mops condylurus* Bats, Kenya, 2019

Lauri Kareinen, Joseph Ogola, Ilkka Kivistö, Teemu Smura, Kirsi Aaltonen, Anne J. Jääskeläinen, Sospeter Kibiwot, Moses M. Masika, Philip Nyaga, Dufton Mwaengo, Omu Anzala, Olli Vapalahti, Paul W. Webala, Kristian M. Forbes, Tarja Sironen

Previously identified only in Sierra Leone, Guinea, and southeastern Kenya, Bombali virus–infected *Mops condylurus* bats were recently found ≈750 km away in western Kenya. This finding supports the role of *M. condylurus* bats as hosts and the potential for Bombali virus circulation across the bats' range in sub-Saharan Africa.

Bombali virus (BOMV) is the sixth and most recently identified virus of the genus *Ebolavirus* (*1*), first detected in Sierra Leone in oral and rectal swab samples from 2 species of insectivorous bats, *Mops condylurus* and *Chaerephon pumilus* (*2*). Since then, BOMV has been found in the tissues and excreta of *M. condylurus* bats in southeastern Kenya (*3*) and Guinea (*4*). To explore the role of *M. condylurus* bats as hosts for BOMV and the geographic distribution of the virus, we trapped bats in western Kenya, screened tissues for BOMV, and conducted next-generation sequencing on positive samples.

The Study

Bats were trapped in mist nets at 4 sites in Busia County: 2 house roosts, 1 orchard, and 1 cave. A total of 182 bats were captured, including 113 *M. condylurus* and 18 *C. pumilus* (Table 1). Similarly, at the original location in the Taita Hills, bats were trapped at a bridge site where an infected bat had previously been identified (*3*), at 4 additional building roosts, and over a water hole. From these sites, 396 bats were captured, including 177 *M. condylurus* and 219 *C. pumilus* (Table 1). Captured bats were euthanized with terminal isoflurane anesthesia followed by cervical dislocation. We collected mouth swab samples, fecal and blood samples, and major organs (kidney, spleen, liver, intestine, lung, and brain) and stored them in RNAlater (Invitrogen, https://www.thermofisher.com) as described previously (*3*).

Samples were stored at -20°C for up to 10 days in Kenya before being shipped to Helsinki, Finland, where they were stored at -70°C before processing in a Biosafety Level 3 laboratory. Tissue samples were treated with TRIzol (Invitrogen) for virus inactivation, and RNA was extracted according to the manufacturer's instructions. Because previous studies have identified the highest BOMV viral loads in bat lungs (*3*,*4*), we initially conducted reverse transcription PCR (RT-PCR) on pooled lung samples from 3 bats (same species, collection date, and location) by using the BOMV-specific RT-PCR protocol described earlier (*2*). Samples in positive pools were then screened individually, and other sample types (other organs, saliva, and excreta) from these bats were also tested.

We conducted next-generation sequencing on positive lung samples. Before sequencing, we applied

Table 1. Bats captured and screened for Bombali virus, Kenya, 2019

Species	No.	Sex ratio, M/F
Busia County		
Chaerephon pumilus	18	5/13
Coleura afra	19	11/8
Epomophorus labiatus	31	19/12
Mops condylurus	113	57/56
Neoromicia nana	1	1/0
The Taita Hills		
C. pumilus	177	91/86
M. condylurus	219	92/127
Mops spp.	2	2/0
Rhinolophus hildebrandtii	2	0/2

Author affiliations: University of Helsinki, Helsinki, Finland (L. Kareinen, I. Kivistö, T. Smura, K. Aaltonen, A.J. Jääskeläinen, O. Vapalahti, T. Sironen); University of Nairobi, Nairobi, Kenya (J. Ogola, M.M. Masika, P. Nyaga, D. Mwaengo, O. Anzala); Helsinki University Hospital, Helsinki (A.J. Jääskeläinen, O. Vapalahti); University of Eldoret, Eldoret, Kenya (S. Kibiwot) Maasai Mara University, Narok, Kenya (P.W. Webala); University of Arkansas, Fayetteville, Arkansas, USA (K.M. Forbes)

DOI: https://doi.org/10.3201/eid2612.202925

Figure 1. Known locations of bats infected with Bombali virus (BOMV) in Africa. The main map shows the 3 countries—Sierra Leone, Guinea, and Kenya (dark shading)—where BOMV-infected bats have been identified and the geographic range of *Mops condylurus* bats (light shading). The inset map shows the 2 sites in Kenya (red dots), ≈750 km apart, where BOMV-positive *M. condylurus* bats have been found.

a multiplex PCR protocol for amplification. The primers for the entire BOMV coding region were designed by using the PrimalScheme tool (*5*) with a target amplicon of 500 bp with 50-bp overlap. Complementary DNA was synthesized from RNA samples positive by RT-PCR by using SuperScript III enzyme (Invitrogen) and random hexamers; PCR was conducted by using a Q5 PCR kit (New England Biolabs, https://www.neb.com) (*5*). The PCR products were purified by using AMPure XP magnetic beads (Beckman Coulter, https://www.beckmancoulter.com), and sequencing libraries were prepared by using a Nextera XT kit (Illumina) according to the manufacturer's instructions. Sequencing was conducted with the Illumina MiSeq Reagent Kit v2, a sequencing kit with 150-bp paired-end reads. The raw sequence reads were trimmed by using Trimmomatic (Q-score >30, read length >50 bp) and assembled to the reference sequence (MK340750) by using the Burrows-Wheeler Aligner–Maximal Exact Match algorithm implemented in SAMTools version 1 ([*6*], H. Li et al. unpub. data, https://arxiv.org/abs/1303.3997?upload=1).

We identified 3 BOMV RNA–positive *M. condylurus* bats (Z153, Z178, and X030). All other bats were negative. Two of the BOMV-positive bats were captured in Busia (Z153 and Z178, both adult males) in 2 distinct trapping locations (both house roosts) ≈7 km apart (Figure 1). One BOMV-positive bat (X030, gravid female) was captured in the Taita Hills at the location previously reported to have a BOMV-infected bat (*3*). Among the bat samples, BOMV RNA was present in lung (3/3), spleen (2/3),

Table 2. Bombali virus RNA quantities in tissues, excreta, and saliva of infected bats, Kenya, 2019*

	Copies/ng of total RNA							
Bat no.	Lung	Mouth (swab sample)	Spleen	Liver	Feces	Kidney	Intestine	Brain
Z153	7,160	149	Neg	Neg	90	Neg	Neg	Neg
Z178	1,050	Neg	512	840	No sample	Neg	Neg	Neg
X030	217	Neg	694	Neg	Neg	Neg	Neg	Neg

*Neg, negative.

mouth (1/3), liver (1/3), and fecal (1/2) samples but absent from all kidney, intestine, and brain samples (Table 2). Of note, BOMV RNA was not consistently detected from the mouth swab or fecal samples of tissue-positive individuals. Viral loads were quantified as previously described (*3*); the highest viral loads were detected in the lungs (both male bats) and the spleen (female bat).

By sequencing, we obtained 2 full genomes (from X030 and Z153, GenBank accession nos. MW056492 and MW056493) and 1 partial genome (from Z178, GenBank accession no. MW056494). Phylogenetic analysis showed 99% nt identity between the complete sequences from Busia and Taita (200-nt difference) and 97% nt identity with the prototype strain from Sierra Leone (Figure 2). The virus sequence obtained from a bat at the Taita Hills in this study was almost identical to the sequence from a bat at the same site in 2018 (4-nt difference).

Conclusions

We identified 2 BOMV-positive *M. condylurus* bats from separate roost sites in western Kenya, expanding the known virus geographic range in East Africa. This new location in Busia County, on the Kenya–Uganda border, is ≈750 km from the previously reported site. We also identified a second BOMV-positive *M. condylurus* bat at the original site near the Taita Hills in southeastern Kenya, indicating sustained local persistence but limited prevalence.

Lack of evidence of infection in bats of other species, including *C. pumilus*, indicates a dominant host role for *M. condylurus* compared with other species. Although no evidence of human infection with BOMV has yet been reported (*3*), the close phylogenetic relationship of BOMV to pathogenic human ebolaviruses necessitates prudence. Because *M. condylurus* bats are one of the several synanthropic species of bat often found roosting in human-made structures (e.g., dwellings, schools, offices, and bridges in rural and urban areas [*8*,*9*]), the potential for human exposure to *M. condylurus* bats and the pathogens they carry is likely to be higher than exposure to bats of many other species. However, study of *M. condylurus* bats has been relatively limited, and other aspects of human exposure risk, such as bat movement range, are inferred from closely related species; *M. condylurus* bats are thought to travel only short distances in line with their feeding activities (*8*).

Our results expand the known distribution of BOMV and increase support for a role of *M. condylurus* bats as hosts. Although BOMV had been previously reported in 3 distinct locations, most evidence came from Sierra Leone and adjacent Guinea (*2*,*4*). Kenya is located on the opposite side of Africa, where only 1 BOMV-positive bat had been identified (*3*).

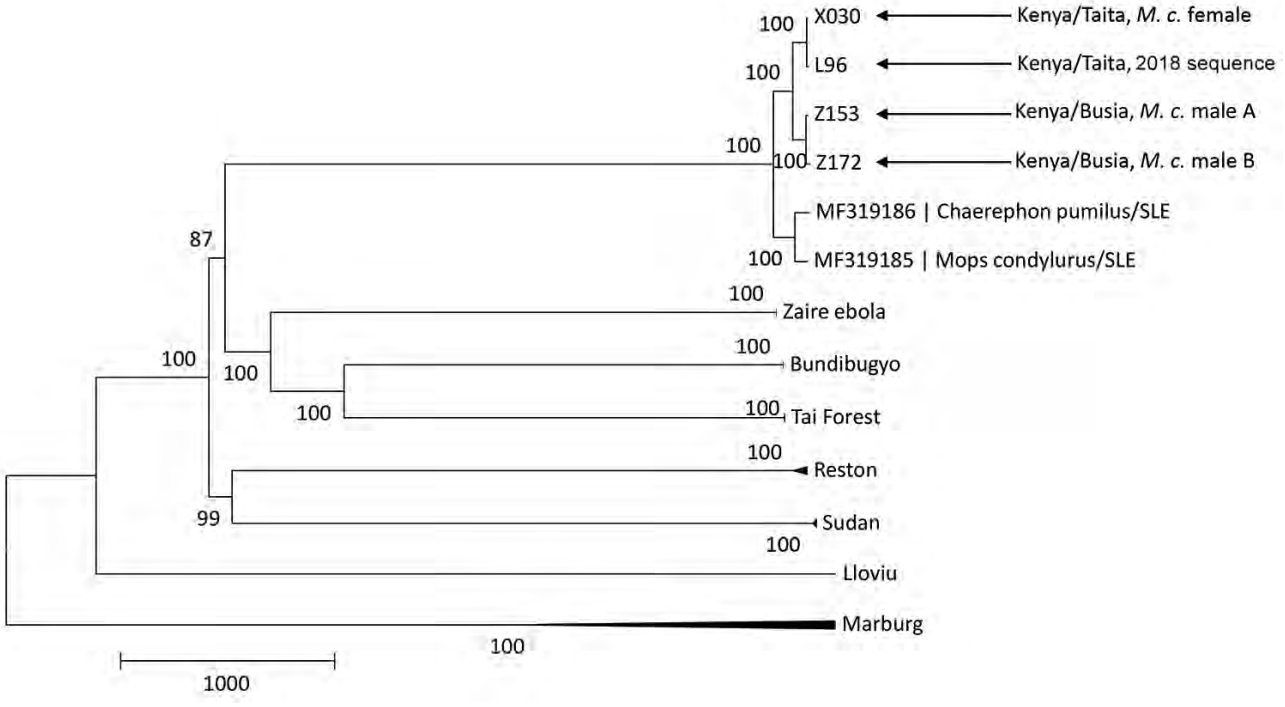

Figure 2. Phylogenetic tree showing 3 new sequences of Bombali virus found in Kenya in 2019 in relation to those of other filoviruses. The tree was built by using the maximum-likelihood approach implemented in MEGA7 (*7*). Bootstrap support percentage is shown at the nodes. Scale bar indicates genetic distance. *M.c.*, *Mops condylurus.*

These new findings from 2 disparate locations in Kenya demonstrate the established presence of BOMV in East Africa and the potential for BOMV circulation across the *M. condylurus* bat range in sub-Saharan Africa (*10*). The low virus prevalence observed in *M. condylurus* bats (1.7% in Busia, 0.6% in Taita), however, is below that for reservoir hosts in other bat pathogen systems (e.g., Marburg virus [*11*]). Therefore, questions remain as to how the virus is maintained within and transmitted among bat colonies and whether bats of other taxa are involved.

Acknowledgments

We thank Ali Mirazimi and Samir Abdurahman for their assistance with analyzing the mouth swab samples and Ruut Uusitalo for preparing the map image.

This research was supported by the Finnish Cultural Foundation, the Jenny and Antti Wihuri Foundation, the Academy of Finland (grant no. 318726), Helsinki University Hospital Funds, and the Jane and Aatos Erkko Foundation. Bat trapping and sample collections were conducted under permits from the National Commission for Science, Technology and Innovation (permit no. NACOSTI/P/18/76501/22243) and the Kenya Wildlife Service (permit no. KWS/BRM/500). Sample import to Finland was approved by the Finnish Food Safety Authority (EVIRA; 4250/0460/2016 and 2809/0460/2018).

About the Author

Dr. Kareinen is a veterinarian and a PhD student at the University of Helsinki. His research interests include the maintenance and circulation of zoonotic viruses in bat hosts.

References

1. Olival KJ, Hayman DT. Filoviruses in bats: current knowledge and future directions. Viruses. 2014;6:1759–88. https://doi.org/10.3390/v6041759
2. Goldstein T, Anthony SJ, Gbakima A, Bird BH, Bangura J, Tremeau-Bravard A, et al. The discovery of Bombali virus adds further support for bats as hosts of ebolaviruses. Nat Microbiol. 2018;3:1084–9. https://doi.org/10.1038/s41564-018-0227-2
3. Forbes KM, Webala PW, Jääskeläinen AJ, Abdurahman S, Ogola J, Masika MM, et al. Bombali virus in *Mops condylurus* bat, Kenya. Emerg Infect Dis. 2019;25:955–7. https://doi.org/10.3201/eid2505.181666
4. Karan LS, Makenov MT, Korneev MG, Sacko N, Boumbaly S, Yakovlev SA, et al. Bombali virus in *Mops condylurus* bats, Guinea. Emerg Infect Dis. 2019;25:1774–5. https://doi.org/10.3201/eid2509.190581
5. Quick J, Grubaugh ND, Pullan ST, Claro IM, Smith AD, Gangavarapu K, et al. Multiplex PCR method for MinION and Illumina sequencing of Zika and other virus genomes directly from clinical samples. Nat Protoc. 2017;12:1261–76. https://doi.org/10.1038/nprot.2017.066
6. Bolger AM, Lohse M, Usadel B. Trimmomatic: a flexible trimmer for Illumina sequence data. Bioinformatics. 2014;30:2114–20. https://doi.org/10.1093/bioinformatics/btu170
7. Kumar S, Stecher G, Tamura K. MEGA7: Molecular Evolutionary Genetics Analysis Version 7.0 for bigger datasets. Mol Biol Evol. 2016;33:1870–4. https://doi.org/10.1093/molbev/msw054
8. Noer CL, Dabelsteen T, Bohmann K, Monadjem A. Molossid bats in an African agro-ecosystem select sugarcane fields as foraging habitat. Afr Zool. 2012;47:1–11. https://doi.org/10.3377/004.047.0120
9. Bronrier GN, Maloney SK, Buffenstein R. Survival tactics within thermally-challenging roosts: heat tolerance and cold sensitivity in the Angolan free-tailed bat, *Mops condylurus.* S Afr Zool. 1999;34:1–10. https://doi.org/10.1080/02541858.1999.11448481
10. Happold M, Happold D. *Tadarida condylura* Angolan free-tailed bat. In: Happold M, Happold D, editors. Mammals of Africa. Vol. 4. London: Bloomsbury Publishing; 2013. p. 505–7.
11. Amman BR, Carroll SA, Reed ZD, Sealy TK, Balinandi S, Swanepoel R, et al. Seasonal pulses of Marburg virus circulation in juvenile *Rousettus aegyptiacus* bats coincide with periods of increased risk of human infection. PLoS Pathog. 2012;8:e1002877. https://doi.org/10.1371/journal.ppat.1002877

Address for correspondence: Tarja Sironen, University of Helsinki, Department of Medicine, Haartmaninkatu 3, FI-00290, Helsinki, Finland; email: tarja.sironen@helsinki.fi

Novel *Rickettsia* Species Infecting Dogs, United States

James M. Wilson, Edward B. Breitschwerdt, Nicholas B. Juhasz, Henry S. Marr, Joao Felipe de Brito Galvão, Carmela L. Pratt, Barbara A. Qurollo

In 2018 and 2019, spotted fever was suspected in 3 dogs in 3 US states. The dogs had fever and hematological abnormalities; blood samples were *Rickettsia* seroreactive. Identical *Rickettsia* DNA sequences were amplified from the samples. Multilocus phylogenetic analysis showed the dogs were infected with a novel *Rickettsia* species related to human *Rickettsia* pathogens.

In the United States, tickborne *Rickettsia parkeri*, *R. philipii* (*Rickettsia* 364D), and *R. rickettsii*, causative agents of Rocky Mountain spotted fever (RMSF), are well-documented human spotted fever group (SFG) rickettsioses (*1*). *R. rickettsii* is the only known cause of SFG rickettsioses in dogs (*2*). The extent to which other SFG *Rickettsia* are pathogenic in dogs is unclear; however, SFG *Rickettsia* seroprevalence is high among dogs in the United States and Mexico (*3*,*4*). The increased *R. rickettsii* seroprevalence in humans in the United States during the past decade has been attributed to SFG *Rickettsia* cross-reactivity (*1*,*5*).

We report 3 dogs with febrile illness located in different US states. Samples from the dogs were *R. rickettsii* seroreactive. Identical *Rickettsia* DNA gene sequences were obtained from each dog's blood specimen and used to investigate *Rickettsia* spp.

The Cases

On May 15, 2018, a 10-year-old male neutered mixed breed dog (case 1) from Tennessee was examined by a veterinarian for lethargy and hyporexia. The owner reported removing a tick (species unknown) within the previous 2 weeks. On physical examination, the dog had fever (39.8°C) and possible hepatomegaly. Radiographic imaging results were unremarkable. Thrombocytopenia was the only abnormality noted on complete blood count (CBC). Serum biochemistry panel (SBP) abnormalities included hyperglobulinemia, increased serum alkaline phosphatase activity, hypoglycemia, and hyponatremia (Table 1). Results of urine dipstick and sediment examination were unremarkable. The dog's samples were *R. rickettsii* seroreactive and PCR positive for *Rickettsia* (Table 2). Clinical abnormalities resolved after treatment with doxycycline, and the dog remained healthy during the 1-year follow-up period.

On May 8, 2019, a 9-year-old male neutered Boston terrier (case 2) from Illinois was examined by a veterinarian for lethargy, difficulty walking, and painful elbows. Clinical signs developed 3 days after returning from a tick-infested area in Arkansas. Abnormalities noted on physical examination included fever (40.1°C), dehydration, joint effusion, elbow pain, and shifting leg lameness. Thrombocytopenia and mild leukocytosis were the only CBC abnormalities (Table 1). SBP abnormalities included hypoalbuminemia, increased alanine amino transferase activity, alkaline phosphatase activity, hypercholesterolemia, and hypocalcemia (Table 1). Mild microalbuminuria was noted. Neutrophilic inflammation was documented by synovial fluid cytology in the right and left stifle joints, right tarsus, and left elbow joint. The left carpus contained moderate, chronic inflammation with very rare extracellular cocci; however, culture resulted in no bacterial growth. The dog experienced cardiorespiratory arrest during sedated arthrocentesis but recovered after CPR and sedative reversal. Thoracic radiographs were unremarkable. The dog's samples were *R. rickettsii* seroreactive and PCR–positive for *Rickettsia* and convalescent titers demonstrated 4-fold seroconversion (Table 2). Most clinical abnormalities resolved after administration of doxycycline to treat rickettsiosis, prednisone to treat potential immune-mediated component, omeprazole to prevent gastric ulcers, and metronidazole to treat

Author affiliations: North Carolina State University College of Veterinary Medicine, Raleigh, NC, USA (J.M. Wilson, E.B. Breitschwerdt, N.B. Juhasz, H.S. Marr, B.A. Qurollo); VCA Arboretum View Animal Hospital, Downers Grove, Illinois, USA (J.F. de Brito Galvão); Oklahoma Veterinary Specialists, Tulsa Oklahoma, USA (C.L. Pratt)

DOI: https://doi.org/10.3201/eid2612.200272

Table 1. Findings from physical examination, laboratory results, treatment regimens for 3 dogs infected with a novel *Rickettsia* species, United States*

Examination and treatment	Case 1	Case 2	Case 3
Physical examination	Febrile (39.8°C); lethargy; +/– hepatomegaly	Febrile (40.1°C); lethargy; dehydration; joint effusion (elbow, carpus, and tarsus); arthropathy; shifting leg lameness	Febrile (39.8°C); lethargy; abdominal pain
CBC	Platelets 141 × 10^3 cells/μL (RI 200–500 × 10^3 cells/μL)	Platelets 139 × 10^3 cells/μL (RI 170–400 × 10^3 cells/μL)	Platelets 60 × 10^3 cells/μL (RI 125–500 × 10^3 cells/μL); Hct 35.2% (RI 36%–55%); 2 d later platelets 25 × 10^3 cells/μL and Hct 26.8%
SBP	Globulins 4.5 g/dL (RI 2.1–4.4 g/dL); ALP 177 U/L (RI 11–140 U/L); glucose 73 mg/dL (RI 75–125 mg/dL); sodium 136.5 mmol/L (RI 143–153 mmol/L)	Albumin 2.2 g/dL (RI 2.7–4.4 g/dL); ALT 1,158 U/L (RI 12–118 U/L); ALP 1,702 U/L (RI 5–131 U/L); cholesterol 352 mg/dL (RI 92–324 mg/dL); calcium 8.4 mg/dL (RI 8.9–11.4 mg/dL)	Albumin 1.0 mg/dL (RI 2.5–4.3 mg/dL); calcium 8.4 mg/dL (RI 8.9–11.4 mg/dL); BUN 35 (35, RI 7–28 mg/dL)
Urinalysis	USG 1.007	Microalbuminuria 3.1 (RI <2.5 mg/dL)	USG 1.033; 3+ proteinuria; UPC 14.7 (RI 0.00–1.00)
Treatment regimen	Doxycycline (6 mg/kg every 12 h for 21 d)	Doxycycline (7 mg/kg every 12h for 28 d); prednisone (1 mg/kg every 12 h for 9 mo with gradual taper); omeprazole (1.4 mg/kg every 12h for 9 mo); ondansetron (0.5 mg/kg every 12h for 15 d); and metronidazole (17 mg/kg every 12 h for 15 d)	Doxycycline (7.5 mg/kg q12 h for 40 d); prednisone (1 mg/kg every 12 h for 14 d, then 0.5mg/kg every 12 h for 6 d, then every 24 h for 22 d until death), mycophenolate (12.5 mg/kg every 12 h for 22 d until death)

*ALP, alkaline phosphatase activity; ALT, alanine amino transferase activity; BUN, blood urea nitrogen; CBC, complete blood count; Hct, hematocrit; RI, reference interval; SBP, serum biochemistry panel; UA, urinalysis; UPC, urine protein/creatinine ratio; USG, urine specific gravity.

assumed dysbiosis. All SBP changes resolved within 5 months of treatment and the dog remained healthy during the 5-month follow-up.

On August 28, 2019, a 9-year-old male neutered terrier mixed-breed (case 3) from Oklahoma was examined by a veterinarian for lethargy, hyporexia, and polydipsia. Physical examination revealed fever (39.8°C) and palpable abdominal tenderness. CBC abnormalities included a normocytic normochromic anemia and thrombocytopenia. SBP abnormalities included hypoproteinemia, hypocalcemia, and mild azotemia. A protein-losing nephropathy (PLN) was documented by urine dipstick and protein/creatinine ratio. Blood samples were *R. rickettsii* seroreactive and *Rickettsia* PCR positive, and convalescent titers demonstrated 4-fold seroconversion (Table 2).

Table 2. CVBD diagnostic results for blood and serum samples from 3 dogs infected with a novel *Rickettsia* species*

			Rickettsia PCR§								
						gltA region			*ompA* region		
Sample dates	CVBD panel†	IFA‡	23S-5S ITS	*htrA* (17kDa)	*mmpA-purC* ITS	1	2	3	1	2	3
Case 1											
2018 May 5¶	–	1:512	+	+	+	+	+	+	+	+	–**
Case 2											
2019 May 8¶	–	1:256	+	+	+	+	NA††	+	+	+	NA††
2019 May 15	–	1:8,192	–	NA	NA	NA	NA	NA	NA	NA	NA
2019 May 28	–	1:1,024	–	NA	NA	NA	NA	NA	NA	NA	NA
2019 Jul 16	NA	1:2,048	NA	NA	NA	NA	NA	NA	NA	NA	NA
2019 Oct 2	–	1:2,048	–	NA	NA	NA	NA	NA	NA	NA	NA
2019 Nov 12	–	1:2,048	–	NA	NA	NA	NA	NA	NA	NA	NA
Case 3											
2019 Aug 28¶‡‡	–	1:1,024	+	+	+	+	+	+	+	+	+
2019 Sep 10	NA	1:8,192	–	NA	NA	NA	NA	NA	NA	NA	NA

*CVBD, canine vectorborne disease; IFA, immunofluorescence assay; NA, not applicable; +, positive; –, negative.
†Panel includes IFA serology for *Babesia canis vogeli*, *B. gibsoni*, *Bartonella henselae*, *B. koehlerae*, *B. vinsonii berkhoffii*, and *Ehrlichia canis*; point-of-care ELISA serology test SNAP 4DX Plus for *Dirofilaria immitis* antigen and antibodies against *Anaplasma phagocytophilum*, *A. platys*, *Borrelia burgdorferi*, *Ehrlichia canis*, and *E. ewingii*; and PCR for *Anaplasma*, *Babesia*, *Bartonella*, *Ehrlichia*, hemotropic *Mycoplasma, Neoehrlichia*, and *Neorickettsia.*
‡IFA results are reported as reciprocal titers. All samples were positive for *R. rickettsii.*
§PCR assay gene targets 23S-5S ITS, *htrA* (17 kDa), *mmpA-purC* ITS, *gltA*, and *ompA*.
¶Sample tested before doxycycline treatment administered.
**The PCR was negative despite repeated attempts. *ompA* region 3 PCR assay was designed to bridge *ompA* regions 1 and 2 to obtain an additional 281 bps. The total amplicon size of *ompA* region 3 is 533 bp (Appendix Table, https://wwwnc.cdc.gov/EID/article/26/12/20-0272-App1.pdf). DNA from case 1 was ≥1 year old when retrospective PCRs were performed. Poor DNA quality might have prevented amplification of the larger amplicon.
††PCR assays were not performed due to depleted blood sample for DNA extraction and testing.
‡‡GenBank accession nos. for sequences from case 3: 23S-5S ITS, MT050448; *htrA* (17 kDa), MT050446; *mmpA-purC* ITS, MT066187; *gltA*, MT050445; and *ompA*, MT050447.

The year before, in August 2018, the dog described in case 3 was examined by a veterinarian for lethargy after tick attachment. At that time, fever (39.7°C), anemia, thrombocytopenia, hyperbilirubinemia, and hypoproteinemia were documented. IFA serology tests performed by 1 diagnostic laboratory showed samples were *R. rickettsii* seroreactive (1:320) but seronegative for *Anplasma* spp., *Borrelia burdorferi*, and *Ehrlichia* spp. by SNAP 4Dx Plus (IDEXX Laboratories, https://www.idexx.com). Doxycycline and immunosuppressive doses of prednisone were administered concurrently for RMSF and potential immune-mediated disease. Clinical and hematologic abnormalities resolved, and treatment was transitioned from prednisone to cyclosporine due to adverse side effects. Cyclosporine was discontinued in January 2019 and serial monthly CBCs remained normal through March 2019. When rechecked on August 9, 2019, for joint pain, hematocrit and platelet count were normal, but hypoproteinemia, hypoalbuminemia, and hypocalcemia were detected. By August 30, 2019, the dog's anemia and thrombocytopenia worsened, despite treatment with doxycycline and prednisone. Marked abdominal effusion was documented by abdominal ultrasound, without evidence of an intra-abdominal mass. Prednisone and mycophenolate were administered for presumptive immune-mediated thrombocytopenia, and within 3 weeks, the platelet count normalized and titers increased by 4-fold. Despite medical therapy for PLN, nephrotic syndrome developed, and the dog was euthanized.

We obtained identical *Rickettsia* DNA gene sequences from each dog's blood specimen. We confirmed novel *Rickettsia* sp. by PCR targeting 3 genes (*gltA*, *htrA*, and *ompA*) and 2 intergenic spacer re-

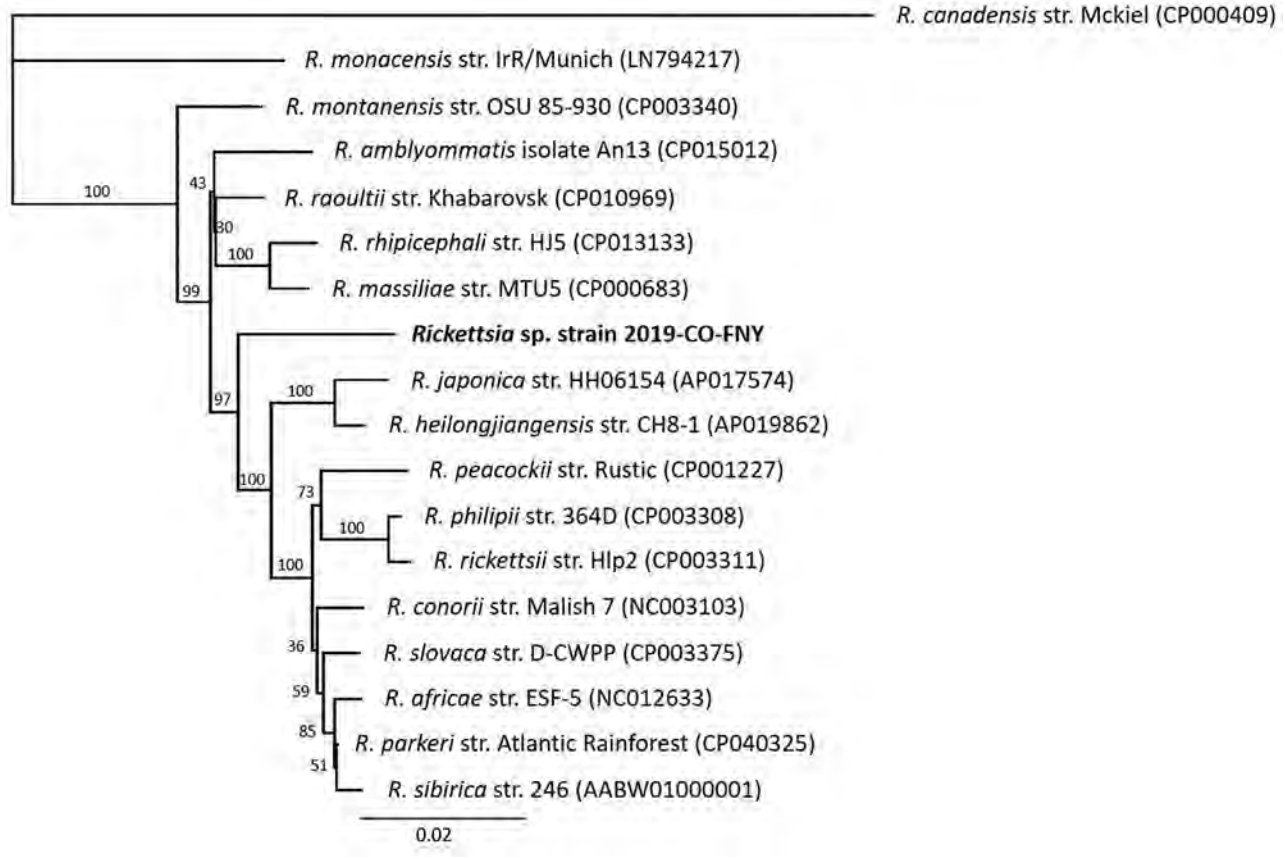

Figure. Multilocus phylogenetic tree of *Rickettsia* spp. obtained from a dog with Rocky Mountain spotted fever–type symptoms in 2019 (bold) compared with reference sequences. We noted 3 dogs with RSMF symptoms. *Rickettsia* DNA were identical among all 3 cases; however, complete sequences from all 5 regions were obtained only from case 3, which we used to represent the novel *Rickettsia* species strain 2019-CO-FNY. We used 2,576 nucleotides concatenated from regions within 3 genes (*gltA*, *htrA*, and *ompA*) and 2 intergenic spacer regions (23S-5S and *mmpA-purC*). We used the maximum-likelihood method and Tamura-Nei model (*6*,*7*) optimized for branch length, topology, and substitution rate to assemble the tree by using the PhyML 3.3.20180621 plugin in Geneious Prime 11.0.0+7 (https://www.geneious.com). Numbers at nodes indicate bootstrap percentages obtained from 1,000 resamplings. Numbers in parentheses are GenBank accession numbers. The tree is drawn to scale. Scale bar indicated the number of nucleotide substitutions per site.

gions (23S-5S and *mmpA-purC*) (Table 2). *Rickettsia* amplicons were 100% identical among the 3 dogs. We amplified a larger region of the *ompA* and *gltA* genes by using 3 different quantitative PCRs from case 3. We submitted sequences from this dog's serum samples to GenBank (accession nos. MT050445–8 and MT066187). We also used the *Rickettsia* sequences from case 3 to generate a phylogenetic tree (Table 2) based on concatenated novel *Rickettsia* sp. DNA sequences and reference *Rickettsia* spp. We generated the phylogenetic tree by using the maximum-likelihood method based on the Tamura-Nei model (Figure) (*6*,*7*). Multilocus phylogenetic analysis placed the novel *Rickettsia* sp. in a clade among SFG *Rickettsia* between the human pathogens *R. heilongjiangensis* and *R. massiliae*. We attempted cell culture isolation of the *Rickettsia* sp. from whole blood but were unsuccessful (Appendix, https://wwwnc.cdc.gov/EID/article/26/12/20-0272-App1.pdf).

Conclusions

We report similar illnesses among 3 dogs from different US states associated with tick exposures occurring in summer months. All 3 cases demonstrated fever, lethargy, and thrombocytopenia, abnormalities commonly associated with RMSF. Case 1 had a typical acute onset fever and rapidly responded to treatment with doxycycline; case 2 had a neutrophilic polyarthritis, which has been associated with RMSF in dogs (*8*). Case 3 was examined for acute onset febrile illness 1 year before the novel *Rickettsia* sp. infection was documented; *Rickettsia* IFA seroreactivity was documented on both occasions. This dog likely had an unidentified, concurrent disease process that contributed to PLN.

The cases were geographically distributed among 4 states; the dogs resided in Illinois, Oklahoma, and Tennessee, but the dog from Illinois had traveled to a tick-infested area of Arkansas. The tick species were not identified, but ticks common to these states include *Amblyomma americanum, Dermacentor variabilis,* and *Rhipicephalus sanguineus* sensu lato, all of which are known to transmit *Rickettsia* (*3*). *Haemophysalis longicornis*, an invasive tick species recently confirmed in the United States, including in Tennessee and Arkansas, should be considered a potential vector for *Rickettsia* spp. (*9*,*10*).

Based on serologic cross-reactivity, presence of *ompA*, and phylogenetic tree analysis, the new *Rickettsia* sp. is an SFG *Rickettsia*, phylogenetically related to human pathogenic *R. heilongjiangensis* and *R. massiliae*, with only 95% identity to each (*11*,*12*). Thus, we report a previously unknown and unique *Rickettsia* sp. with clinical significance for dogs and potentially humans. Because this novel *Rickettsia* cross-reacts with *R. rickettsia* on IFA, it could be underdiagnosed and more geographically widespread. Studies aimed at identifying the tick vector, potential animal reservoirs, and prevalence are ongoing. These 3 canine rickettsioses cases underscore the value of dogs as sentinels for emerging tickborne pathogens (*13*,*14*).

Acknowledgments

We thank Brad L. Fry for providing the clinical and diagnostic information for case 1 in this manuscript.

B.A.Q. is co-director of the North Carolina State Vector Borne Disease Diagnostic Lab (NC State VBDDL); IDEXX Laboratories (https://www.idexx.com) funds a portion of her salary. E.B.B. codirects the NC State VBDDL and the Intracellular Pathogens Research Laboratory at NC State, is chief scientific officer at Galaxy Diagnostics (https://www.galaxydx.com), and is a paid consultant for IDEXX Laboratories, Inc. No other authors have competing interests to declare.

About the Author

Mr. Wilson is a vectorborne disease research technician at the North Carolina State Vector Borne Disease Diagnostic Lab. His research interests include optimization of molecular testing and vectorborne infectious disease diagnoses.

References

1. Straily A, Stuck S, Singleton J, Brennan S, Marcum S, Condit M, et al. Antibody titers reactive with *Rickettsia rickettsii* in blood donors and implications for surveillance of spotted fever Rickettsiosis in the United States. J Infect Dis. 2020;221:1371–8. https://doi.org/10.1093/infdis/jiz316
2. Warner RD, Marsh WW. Rocky Mountain spotted fever. J Am Vet Med Assoc. 2002;221:1413–7. https://doi.org/10.2460/javma.2002.221.1413
3. Hardstone Yoshimizu M, Billeter SA. Suspected and confirmed vector-borne rickettsioses of North America associated with human diseases. Trop Med Infect Dis. 2018;3:2. https://doi.org/10.3390/tropicalmed3010002
4. Yancey CB, Hegarty BC, Qurollo BA, Levy MG, Birkenheuer AJ, Weber DJ, et al. Regional seroreactivity and vector-borne disease co-exposures in dogs in the United States from 2004–2010: utility of canine surveillance. Vector Borne Zoonotic Dis. 2014;14:724–32. https://doi.org/10.1089/vbz.2014.1592
5. Drexler NA, Dahlgren FS, Heitman KN, Massung RF, Paddock CD, Behravesh CB. National surveillance of spotted fever group rickettsioses in the United States, 2008–2012. Am J Trop Med Hyg. 2016;94:26–34. https://doi.org/10.4269/ajtmh.15-0472
6. Tamura K, Nei M. Estimation of the number of nucleotide substitutions in the control region of mitochondrial DNA in humans and chimpanzees. Mol Biol Evol. 1993;10:512–26. https://doi.org/10.1093/oxfordjournals.molbev.a040023
7. Guindon S, Dufayard JF, Lefort V, Anisimova M,

Hordijk W, Gascuel O. New algorithms and methods to estimate maximum-likelihood phylogenies: assessing the performance of PhyML 3.0. Syst Biol. 2010;59:307–21. https://doi.org/10.1093/sysbio/syq010
8. Gasser AM, Birkenheuer AJ, Breitschwerdt EB. Canine Rocky Mountain spotted fever: a retrospective study of 30 cases. J Am Anim Hosp Assoc. 2001;37:41–8. https://doi.org/10.5326/15473317-37-1-41
9. Raghavan RK, Barker SC, Cobos ME, Barker D, Teo EJM, Foley DH, et al. Potential spatial distribution of the newly introduced long-horned tick, *Haemaphysalis longicornis* in North America. Sci Rep. 2019;9:498. https://doi.org/10.1038/s41598-018-37205-2
10. Xu H, Zhang Q, Guan H, Zhong Y, Jiang F, Chen Z, et al. High incidence of a novel *Rickettsia* genotype in parasitic *Haemaphysalis longicornis* from China-North Korea Border. Sci Rep. 2019;9:5373. https://doi.org/10.1038/s41598-019-41879-7
11. Ando S, Kurosawa M, Sakata A, Fujita H, Sakai K, Sekine M, et al. Human *Rickettsia heilongjiangensis* infection, Japan. Emerg Infect Dis. 2010;16:1306–8. https://doi.org/10.3201/eid1608.100049
12. Vitale G, Mansuelo S, Rolain J-M, Raoult D. *Rickettsia massiliae* human isolation. Emerg Infect Dis. 2006;12:174–5. https://doi.org/10.3201/eid1201.050850
13. Estrada I, Balagot C, Fierro M, Kriner P, Iniguez-Stevens E, Kjemtrup A, et al. Spotted fever group *rickettsiae* canine serosurveillance near the US-Mexico border in California. Zoonoses Public Health. 2020;67:148–55. https://doi.org/10.1111/zph.12666
14. Smith FD, Ballantyne R, Morgan ER, Wall R. Estimating Lyme disease risk using pet dogs as sentinels. Comp Immunol Microbiol Infect Dis. 2012;35:163–7. https://doi.org/10.1016/j.cimid.2011.12.009

Address for correspondence: Barbara A. Qurollo, Department of Clinical Sciences College of Veterinary Medicine, North Carolina State University, Research Bldg, Office 464, 1060 William Moore Dr, Raleigh, NC 27606, USA; email: baquroll@ncsu.edu

Human Monocytic Ehrlichiosis, Mexico City, Mexico

Virginia E. Alcántara-Rodríguez,[1] Sokani Sánchez-Montes,[1] Hugo Contreras, Pablo Colunga-Salas,[1] Lauro Fierro-Flores, Sergio Avalos, Francisco Rodríguez-Rangel, Ingeborg Becker, David H. Walker

Little information is available about human infections by the members of the genus *Ehrlichia* in Mexico. Only 2 species, *Ehrlichia canis* and *E. chaffensis*, are known to cause disease in this country. We report a fatal case of human monocytic ehrlichiosis in Mexico City in a man who was homeless.

The genus *Ehrlichia* contains 6 species of obligately intracytoplasmic bacteria that have major roles in human and veterinary medicine. These bacteria can cause ehrlichiosis, an emerging zoonoses transmitted mainly by bites of several hard tick species of the genera *Amblyomma*, *Ixodes*, and *Rhipicephalus* (*1*). In the Americas, the most relevant species that involves public health is *Ehrlichia chaffeensis*, the etiologic agent of human monocytic ehrlichiosis, an acute disease characterized by fever, thrombocytopenia, leukopenia, alterations of coagulation, and hepatic and neurologic involvement; systemic complications can lead to death in 3% of case-patients (*1*,*2*).

Little is known about *Ehrlichia* infections in Mexico. A human case was reported in the Yucatan Peninsula during 1999 in a male patient who had fever, anorexia, lymphadenopathy, cutaneous bleeding, and sore throat. Peripheral blood morulae, PCR detection of *E. chaffeensis*, and anemia were also reported (*3*). Subsequently, a case of *E. canis* infection was detected in the coastal state of Oaxaca in a veterinary stylist who had close contact with dogs (*4*). A study published in 2016 reported a female resident of the state of Mexico who had fever, thrombocytopenia, and alteration of liver enzyme levels and died after a long hospitalization (*5*). We report a fatal case of human monocytic ehrlichiosis in Mexico City, Mexico.

The Study

On March 3, 2017, a 35-year-old man who was homeless (resident in Mexico City for 4 years) was admitted to the Emergency Department in the General Hospital of Xoco of the Ministry of Health of Mexico City because of trauma after a fall of 6 m from a bridge as a result of a suicide attempt. At admission, no lesions were detected in internal organs; a transtrochanteric fracture of the left femoral head was surgically repaired without complications. However, the patient had profuse bleeding during the surgical procedure, for which it was necessary to provide multiple blood transfusions. The blood units came from resident donors of Mexico City and the neighboring state of Mexico. In the postoperative period, the patient remained hospitalized for 65 days, during which behavioral alterations with several psychotic periods developed. He also had febrile episodes that evolved to a torpid state.

Routine laboratory analyses (blood count, blood chemistry, and serologic studies for infectious diseases) were performed. Because the patient was homeless and had persistent febrile episodes and dysfunction of the coagulation system, a possible infection by a rickettsial agent or *Bartonella* spp. was suspected because *Bartonella quintana* has been detected previously in human lice from persons who were homeless in Mexico City (*6*). For this reason 5 mL of whole blood was obtained, stored in EDTA, and processed for DNA extraction by using the QIAamp DNA Mini Kit (QIAGEN, https://www.qiagen.com) according to the manufacturer's instructions. Blood was then examined for *Bartonella*, *Ehrlichia*/*Anaplasma*, and *Rickettsia* spp. by amplifying fragments of the

Author affiliations: Secretaría de Salud de la Ciudad de México, Mexico City, Mexico (V.E. Alcántara-Rodríguez, H. Contreras, L. Fierro-Flores, S. Avalos, F. Rodríguez-Rangel); Universidad Veracruzana, Veracruz, Mexico (S. Sánchez-Montes); Universidad Nacional Autónoma de México, Mexico City (S. Sánchez-Montes, P. Colunga-Salas, I. Becker); University of Texas Medical Branch, Galveston, Texas, USA (D.H. Walker)

DOI: https://doi.org/eid2612.200520

[1]These authors contributed equally to this article.

gltA, *rrs*, and *sca5*, genes and using primers and PCR conditions specified (*7*–*9*). Positive controls (*E. canis* [GenBank accession no. MG917715], *B. vinsonii* [KT326174], and *Rickettsia amblyommatis* [KX363842) DNA]) were also included.

On April 27, 2017, antibodies against *Proteus* OX-19 at a titer of 1:320, leukocytosis, thrombocytosis, lymphopenia, anemia, hypoalbuminemia, and coagulation and liver enzyme alterations were reported (Table, https://wwwnc.cdc.gov/EID/article/26/12/20-0520-T1.htm). The patient was given a diagnosis of septic shock and urosepsis and died on day 63 of hospitalization.

During hospitalization, leukocytosis developed, which might have been associated with the multiple trauma. The patient initially had a platelet count within the reference range, but thrombocytosis developed, and the platelet count increased to 850,000/μL. However, with persistent leukocytosis, the platelet count dropped, and thrombocytopenia (108,000/μL) developed shortly before death.

Total serum protein and albumin concentrations at admission were within reference ranges, but during hospitalization they decreased, as would be expected for a diagnosis of ehrlichiosis. Alterations in liver enzyme levels and coagulation times also developed. Levels of alanine aminotransferase (ALT) and aspartate aminotransferase also increased after admission; ALT showed the largest increase. The level of γ-glutamyl transpeptidase increased by >10 times over its reference value (Table). The increase in the level of ALT could be related to hepatic alterations linked to ehrlichiosis.

Necropsy showed hepatosplenomegaly and pleural effusions. Molecular assays did not detect *Bartonella* or *Rickettsia* spp., but they did detect *Ehrlichia/Anaplasma* spp. when primers Ehr1/Ehr2 were used. We isolated a 400-bp fragment of the 16S rRNA gene, which showed 99% identity with that of the *E. chaffensis* strain Arkansas. In addition, a 500-bp fragment of the *dsb* gene (present only in the members of the genus *Ehrlichia*) was amplified (*10*) and showed 100% identity with the sequence of *E. chaffensis* strain Arkansas.

Phylogenetic analysis of the isolated sequences grouped them with sequences of 2 strains of *E. chaffensis* (strain Arkansas and West Paces) detected

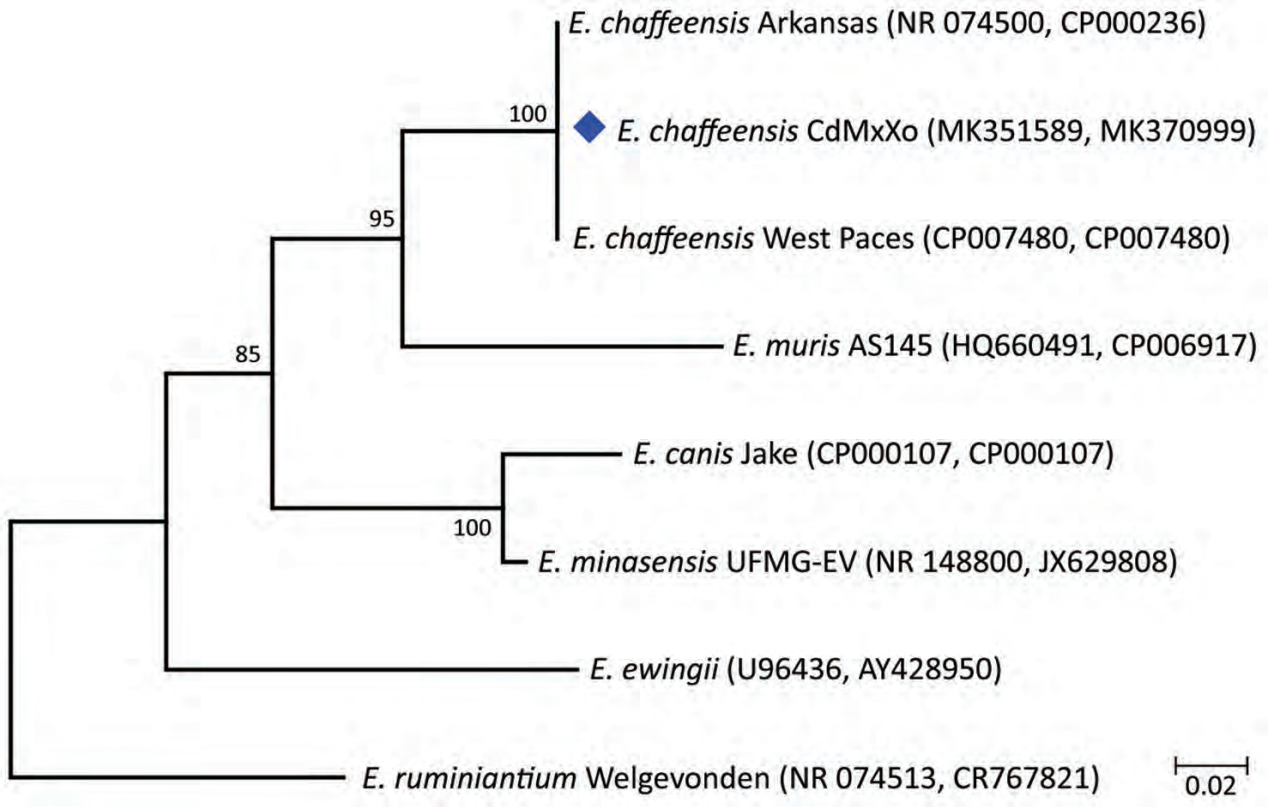

Figure. Maximum-likelihood phylogenetic tree for *Ehrlichia chaffensis* from a patient with human monocytic ehrlichiosis, Mexico City, Mexico (blue diamond), and reference sequences. The tree was generated by using concatenated fragments of 16S rRNA and *dsb* genes in an 850-bp alignment. GenBank accession numbers are indicated in parentheses. Numbers along branches are bootstrap values. Scale bar indicates nucleotide substitutions per site.

in the United States; these sequences had a bootstrap value of 99. The sequences we obtained were deposited in GenBank under accession numbers MK351589 and MK370999 (Figure).

Conclusions

Ehrlichioses represent systemic infections that can cause damage to different organs and systems, affecting the liver, meninges, brain, heart, and lungs. Because the pathophysiology of this disease is not well established, the findings obtained by necropsy are useful. During his hospitalization, the patient acquired some bacterial infections, which could explain the paradox that he initially had thrombocytosis and leukocytosis instead of thrombocytopenia and leukopenia, as would be expected for ehrlichiosis. Leukopenia and thrombocytopenia are present in >50% of patients given a diagnosis of *E. chaffeensis* infection (*5*).

The patient might have been infected by blood transfusion because the long period between hospital admission and detection of thrombocytopenia is compatible with the incubation period for infection with *E. chaffeensis*. The patient received multiple blood transfusions from donors in Mexico City and the state of Mexico; in this state, a fatal case of ehrlichiosis caused by blood transfusion has been reported (*5*). A study in Costa Rica reported a large number of *E. canis*–infected healthy blood donors (*11*), and a study in the United States reported a patient who was infected by blood transfusion containing *E. ewingii* (*12*). More recently, a potential case of transfusion-transmitted human monocytic ehrlichiosis was reported in a 59-year-old woman in the United States after she received a blood stem cell transplant (*13*).

Although this possibility is less likely, it cannot be ruled out that ehrlichiosis could be acquired by tick bite. *E. chaffeensis* was previously detected in 3 hard tick species (*Amblyomma americanum*, *A. mixtum*, and *Rhipicephalus sanguineus* sensu 1ato) (*14*) in Mexico. Only the lone star tick (*A. americanum*) has been implicated as a primary vector of this pathogen in the United States; however, its presence in Mexico has only been recorded restricted to the Nearctic region (*15*). Conversely, no studies demonstrate the role of the other 2 tick species as potential vectors of this pathogen or whether DNA of this pathogen came from an infected host from which these ticks fed.

For this reason, it is essential to perform systematic surveillance of this and other tick-borne pathogens in blood donors in Mexico. Studies should also be conducted with questing ticks to identify the risk to which the population is exposed and establish the actual distribution of the pathogen.

About the Author

Dr. Alcántara-Rodríguez is chief of the Unit of Epidemiologic Surveillance for hospitals of the Health Ministry, Mexico City, Mexico. Her primary research interest is rickettsioses.

References

1. Cabezas-Cruz A, Zweygarth E, Vancová M, Broniszewska M, Grubhoffer L, Passos LM, et al. *Ehrlichia minasensis* sp. nov., isolated from the tick *Rhipicephalus microplus*. Int J Syst Evol Microbiol. 2016;66:1426–30. https://doi.org/10.1099/ijsem.0.000895
2. Geier C, Davis J, Siegel M. Severe human monocytic ehrlichiosis presenting with altered mental status and seizures. BMJ Case Rep. 2016;2016:bcr2016215967. https://doi.org/10.1136/bcr-2016-215967
3. Gongóra-Biachi RA, Zavala-Velázquez J, Castro-Sansores CJ, González-Martínez P. First case of human ehrlichiosis in Mexico. Emerg Infect Dis. 1999;5:481. https://doi.org/10.3201/eid0503.990327
4. Beatriz Silva A, Pina Canseco S, Gabriel de la Torre MP, Mayoral Silva A, Mayoral MÁ, Pérez-Campos Mayoral L, et al. Asymptomatic human infection from contact with dogs: a case of human ehrlichiosis [in Spanish]. Gac Med Mex. 2014;150:171–4.
5. Sosa-Gutierrez CG, Solorzano-Santos F, Walker DH, Torres J, Serrano CA, Gordillo-Perez G. Fatal monocytic ehrlichiosis in woman, Mexico, 2013. Emerg Infect Dis. 2016;22:871–4. https://doi.org/10.3201/eid2205.151217
6. Alcántara V, Rolain JM, Eduardo AG, Raul MJ, Raoult D. Molecular detection of *Bartonella quintana* in human body lice from Mexico City. Clin Microbiol Infect. 2009;15(Suppl 2):93–4. https://doi.org/10.1111/j.1469-0691.2008.02176.x
7. Norman AF, Regnery R, Jameson P, Greene C, Krause DC. Differentiation of *Bartonella*-like isolates at the species level by PCR-restriction fragment length polymorphism in the citrate synthase gene. J Clin Microbiol. 1995;33:1797–803. https://doi.org/10.1128/JCM.33.7.1797-1803.1995
8. Roux V, Raoult D. Phylogenetic analysis of members of the genus *Rickettsia* using the gene encoding the outer-membrane protein rOmpB (*ompB*). Int J Syst Evol Microbiol. 2000;50:1449–55. https://doi.org/10.1099/00207713-50-4-1449
9. Murphy DS, Lee X, Larson SR, Johnson DK, Loo T, Paskewitz SM. Prevalence and distribution of human and tick infections with the *Ehrlichia muris*–like agent and *Anaplasma phagocytophilum* in Wisconsin, 2009–2015. Vector Borne Zoonotic Dis. 2017;17:229–36. https://doi.org/10.1089/vbz.2016.2055
10. Doyle CK, Labruna MB, Breitschwerdt EB, Tang YW, Corstvet RE, Hegarty BC, et al. Detection of medically important *Ehrlichia* by quantitative multicolor TaqMan real-time polymerase chain reaction of the *dsb* gene. J Mol Diagn. 2005;7:504–10. https://doi.org/10.1016/S1525-1578(10)60581-8
11. Bouza-Mora L, Dolz G, Solórzano-Morales A, Romero-Zuñiga JJ, Salazar-Sánchez L, Labruna MB, et al. Novel genotype of *Ehrlichia canis* detected in samples of human blood bank donors in Costa Rica. Ticks Tick Borne Dis. 2017;8:36–40. https://doi.org/10.1016/j.ttbdis.2016.09.012
12. Regan J, Matthias J, Green-Murphy A, Stanek D, Bertholf M, Pritt BS, et al. A confirmed *Ehrlichia ewingii*

infection likely acquired through platelet transfusion. Clin Infect Dis. 2013;56:e105–7. https://doi.org/10.1093/cid/cit177
13. Mah A, Viola GM, Ariza Heredia E, Rezvani K, Kebriaei P, Bhatti MM, et al. Graft loss attributed to possible transfusion-transmitted ehrlichiosis following cord blood stem cell transplant. Transpl Infect Dis. 2018;20:e12899. https://doi.org/10.1111/tid.12899
14. Sosa-Gutierrez CG, Vargas-Sandoval M, Torres J, Gordillo-Pérez G. Tick-borne rickettsial pathogens in questing ticks, removed from humans and animals in Mexico. J Vet Sci. 2016;17:353–60. https://doi.org/10.4142/jvs.2016.17.3.353
15. Guzmán-Cornejo C, Robbins RG, Guglielmone AA, Montiel-Parra G, Pérez TM. The *Amblyomma* (Acari: Ixodida: Ixodidae) of Mexico: identification keys, distribution and hosts. Zootaxa. 2011;2998:16–38 [cited 2020 Sep 8]. https://www.mapress.com/j/zt/article/view/zootaxa.2998.1.2

Address for correspondence: Virginia E. Alcántara Rodríguez, Unidad Departamental de Vigilancia Epidemiológica, Dirección General de Prestación de Servicios Médicos y Urgencias de la Secretaria de Salud de la Ciudad de México, SEDESA, Torre Insignia Avenida Insurgentes Norte No 423, Conjunto Urbano Nonoalco-Tlateloco, Alcaldía Cuauhtémoc, CP 06920 Ciudad de México, Mexico; email: vealcant55@yahoo.com

Hantavirus Cardiopulmonary Syndrome in Canada

Bryce M. Warner, Sebastian Dowhanik,[1] Jonathan Audet, Allen Grolla, Daryl Dick,[2] James E. Strong, Darwyn Kobasa, L. Robbin Lindsay, Gary Kobinger,[3] Heinz Feldmann,[4] Harvey Artsob,[2] Michael A. Drebot, David Safronetz

Hantavirus cardiopulmonary syndrome (HCPS) is a severe respiratory disease caused by Sin Nombre virus (SNV) in North America. As of January 1, 2020, SNV has caused 143 laboratory-confirmed cases of HCPS in Canada. We review critical aspects of SNV epidemiology and the ecology, biology, and genetics of HCPS in Canada.

Sin Nombre virus (SNV; family *Hantaviridae*, genus *Orthohantavirus*, species *Sin Nombre orthohantavirus*) is the primary etiologic agent of a severe respiratory illness known as hantavirus pulmonary syndrome (HPS) or hantavirus cardiopulmonary syndrome (HCPS), of which ≈1,000 cases have been confirmed across North America. SNV was identified after an outbreak in 1993, and association with the deer mouse (*Peromyscus maniculatus*) was established (*1*,*2*). In North America, the case-fatality rate (CFR) of HCPS is 30%–35% (*3*). Transmission of SNV to humans occurs predominantly through direct contact with infected deer mice or their excreta in peridomestic settings (*4*). We summarize critical aspects of SNV biology and the epidemiology of infections in Canada over the past 25 years, including a phylogenetic analysis of SNV from different geographic areas over time.

The Study

Public health authorities in Canada follow the case definition for HPS/HCPS of the Pan American Health Organization (*5*). Samples from suspected hantavirus-infected patients are sent for diagnostic testing to the National Microbiology Laboratory, Winnipeg, Manitoba (Appendix, https://wwwnc.cdc.gov/EID/article/26/12/20-2808-App1.pdf). Several criteria must be fulfilled for laboratory confirmation of an HCPS case: the presence of hantavirus-specific IgM; a ≥4-fold increase in hantavirus-specific IgG from sequential samples; and a positive reverse transcription PCR (RT-PCR) amplification of hantaviral RNA or positive immunohistochemical staining for hantaviral antigen in the tissues. Detection of IgM or a positive RT-PCR amplification occurs most often in early clinical disease, whereas IgG is typically detected throughout infection, even in the prodrome. Detection of hantavirus-specific antibodies remains the primary diagnostic criterion (*6*,*7*). It is difficult to propagate virus from clinical samples; therefore, isolation is not routinely attempted.

Active surveillance of HCPS began in Canada in 1994; it became a nationally notifiable disease in 2000 (*6*). Surveillance of small mammals across Canada was initiated in 1994 and has since documented SNV-infected deer mice in all provinces except Prince Edward Island and Nova Scotia, and in Yukon Territory but not in the Northwest Territories or Nunavut (*6*). The prevalence of SNV among deer mouse populations varies spatially and temporally, typically 10%–30% (*6*,*8*).

As of January 1, 2020, a total of 143 cases of HCPS had been laboratory confirmed in Canada, including 3 cases retrospectively identified since 1993 that were diagnosed in 1989, 1990, and 1992 (Figure 1; Figure 2, panel A). Annually, an average

Author affiliations: Public Health Agency of Canada, Winnipeg, Manitoba, Canada (B.M. Warner, S. Dowhanik, J. Audet, A. Grolla, D. Dick, J.E. Strong, D. Kobasa, L.R. Lindsay, G. Kobinger, H. Feldmann, H. Artsob, M.A. Drebot, D. Safronetz); University of Manitoba, Winnipeg (B.M. Warner, J.E. Strong, D. Kobasa, L.R. Lindsay, G. Kobinger, H. Feldmann, M.A. Drebot, D. Safronetz)

DOI: https://doi.org/10.3201/eid2612.20-2808

[1]Current affiliation: McMaster University, Hamilton, Ontario, Canada.

[2]Retired.

[3]Current affiliation: Université Laval, Quebec City, Quebec, Canada.

[4]Current affiliation: National Institutes of Health, Hamilton, Montana, USA.

of 4–5 cases (range 0–13 cases) are confirmed in Canada (Figure 2, panel A). Although cases of HCPS have been diagnosed in every month, they are most common in spring and summer (Figure 2, panel B), peaking in May–June and then gradually decreasing. Peaks in HCPS cases are likely driven by seasonal increases in deer mouse populations coupled with increased human contact with environments contaminated with SNV-infected rodent excreta. All cases except 1 have occurred in the 4 westernmost provinces of Manitoba, Saskatchewan, Alberta, and British Columbia; Alberta had the most cases (Figure 1; Figure 2, panel A). Most cases in these provinces have been in southern rural, often agricultural, settings. Most HCPS cases occur in geographic and spatial isolation, although clusters have been reported across communities and within households. The most northern case of HCPS in Canada was documented above the 59th parallel in British Columbia, <20 km from the border with Yukon Territory. Six cases have been diagnosed in patients from Quebec; 5 were directly attributed to military exercises or travel in western provinces (*9*,*10*). The sixth case-patient was a resident in the Nicolet-Yamaska municipality with no travel history except to a nearby recreational lakeside property. To date, this case remains the only HCPS case with autochthonous transmission east

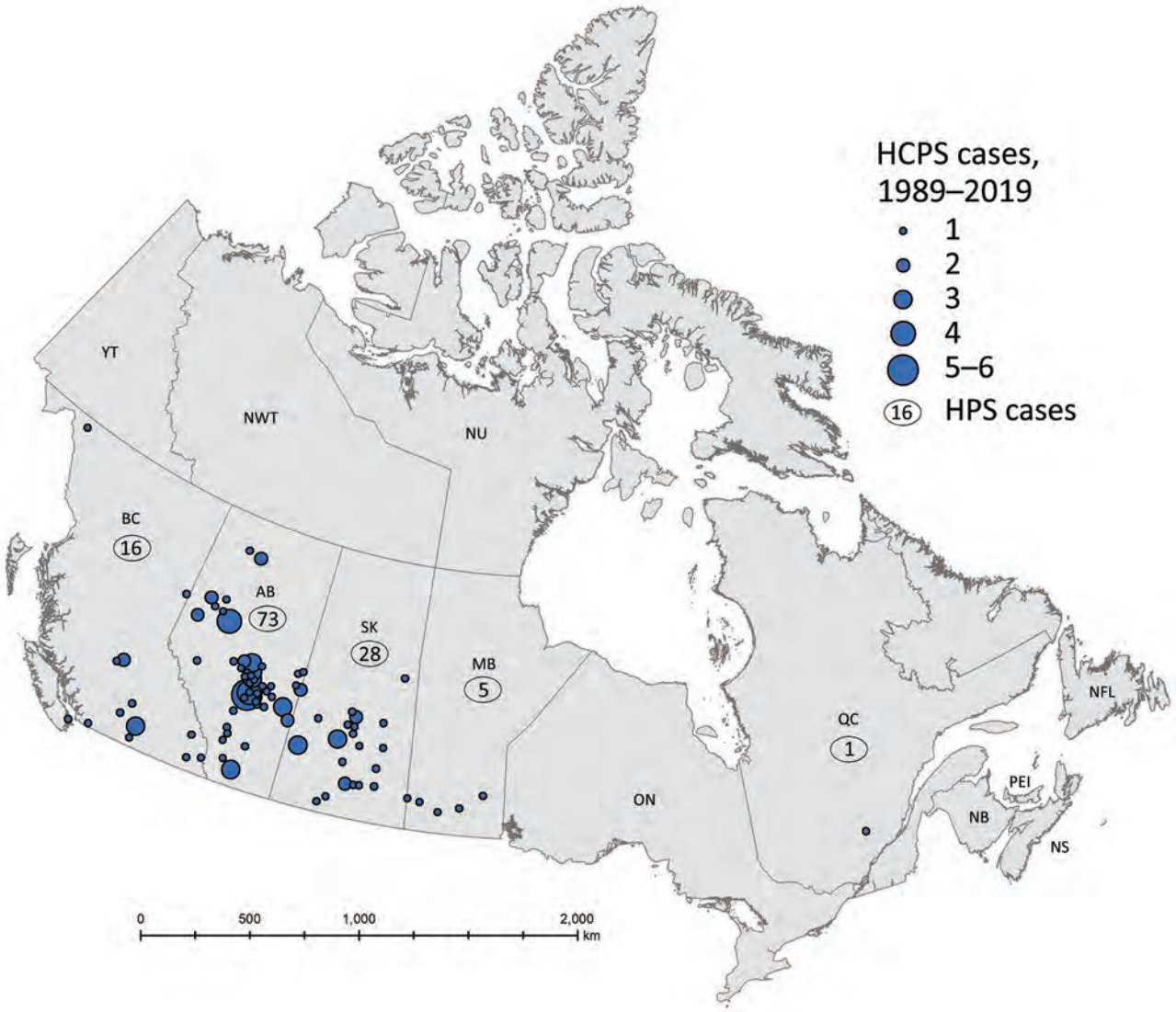

Figure 1. Geographic distribution of confirmed cases of hantavirus cardiopulmonary syndrome (HCPS) in Canada, 1989–2019. The map shows the locations of cases in Canada based on provinces where Sin Nombre virus infection was likely contracted; data were provided on diagnostic requisitions, physician reports, or follow-up investigations. Numbers in circles indicate number of cases for that province. The locations of 15 cases could not be mapped due to insufficient information.

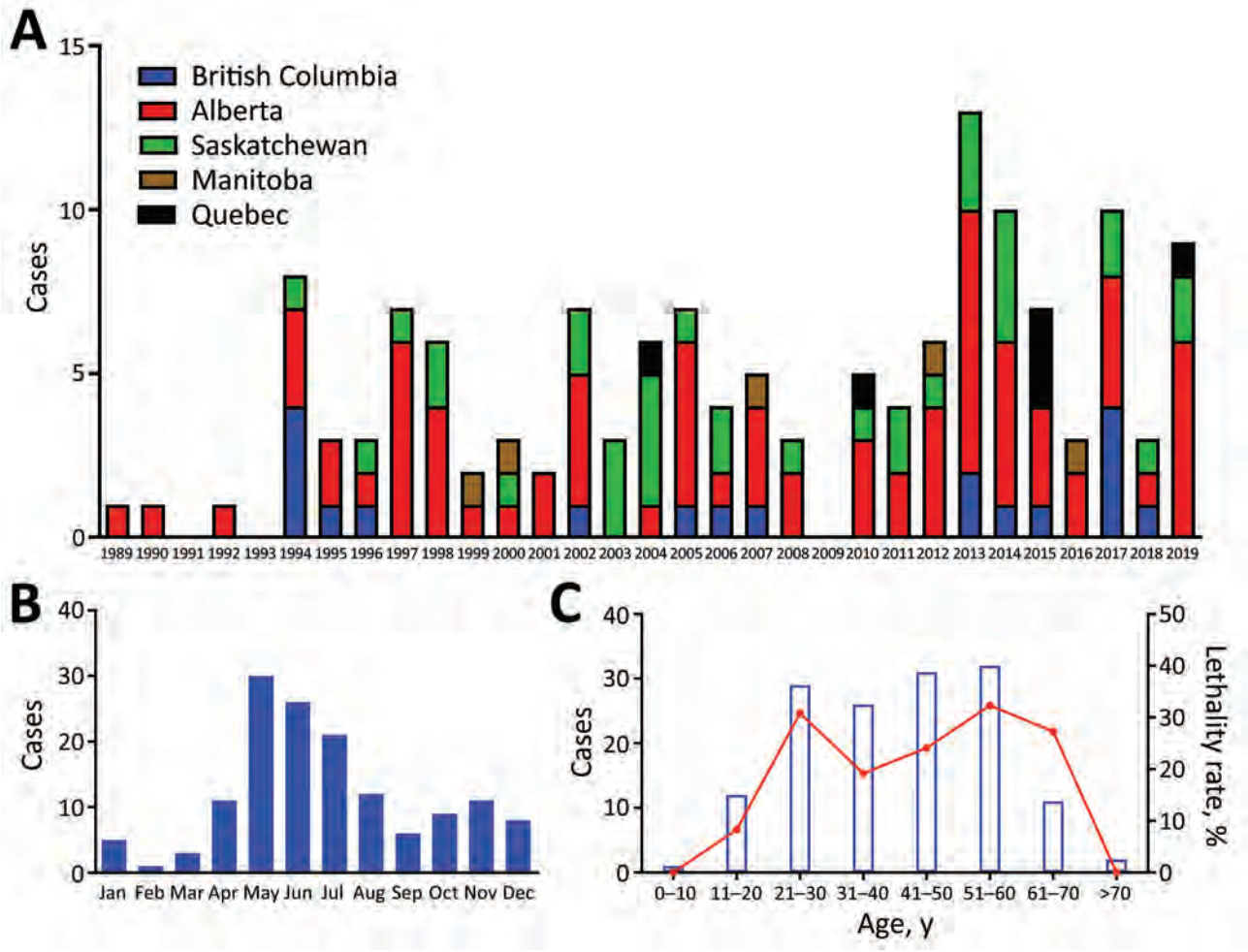

Figure 2. Cases of hantavirus cardiopulmonary syndrome (HPCS) by province, year, month, and patient age, Canada, 1989–2019. A) HCPS cases per year by province. B) Seasonal incidence of HCPS in Canada as shown by number of cases diagnosed in each month. A clear trend toward spring/summer contraction of disease can be seen. C) HCPS cases by age with associated case-fatality rate. Blue bars indicate the number of cases diagnosed in each age group; red line shows case-fatality rate associated with each age group.

of Manitoba. The western bias observed in HCPS case distribution in Canada mirrors that reported in the United States (*7*).

The mean age of HCPS patients in Canada is 40; cases have occurred in all age brackets from 10–70 years of age (median 42, range 7–76 years of age) (Figure 2, panel C). Overall, the CFR of HCPS in Canada is 25% (34/137 cases; 6 outcomes unknown). HCPS occurs more frequently in male patients (99/143 cases). CFR is higher in female than in male patients, although the difference is not statistically significant (15/43 [35%] vs. 19/94 [20%]; relative risk = 1.726 [0.9733–3.060]; p = 0.0651 by χ^2 test) (Table). Differences in infection outcome based on age and sex of patients is an area of research that could lead to insights into the pathogenesis of HCPS and, similar to immunological studies using patient samples, could provide a means of identifying important signatures associated with severe infection and poor outcome (*11*,*12*).

When available, sequence data for HCPS cases in Canada appear to share a relatively recent common ancestor. This ancestor appears to have diverged from viruses from deer mice in eastern Canada (Ontario eastward) before diversifying into the western Canada (Manitoba westward) genotypes that have most commonly caused clinical disease in humans and are also found in deer mice from western Canada (Appendix Figure 1, panels A–C). The eastern Canada genotypes cluster with a clinical isolate from a case in New York, USA, suggesting that, despite a lack of cases in eastern Canada, these viruses may also be pathogenic to humans.

For both the small (S) and medium (M) genomic segments, sequences from western Canada tend to

Table. Comparison of outcomes for confirmed cases of hantavirus cardiopulmonary syndrome in male and female patients, Canada

Sex	No. fatal cases	No. nonfatal cases	Relative risk (95% CI)	p value (χ^2 test)
M	19	75	1.726 (0.9733−3.060)	0.0651
F	15	28		
Total	34	103		

group relatively tightly together and with S segment sequences from Montana and New Mexico. This evidence suggests that latitude does not account for the variation in the S sequences the way longitude does, with a clear separation of eastern and western genotypes. However, M segment sequences from western Canada are more closely related to samples from California, USA, suggesting some M segment variation in the north–south gradient (*13*). The biologic relevance of these variances remains to be investigated.

The median estimate of the average mutation rate for the S segment is 1.03×10^{-3} substitutions/site/year (95% highest posterity density interval 0.51–1.72 $\times 10^{-3}$ substitutions/site/year) whereas the estimate for the M segment is 3.79×10^{-4} substitutions/site/year (95% highest posterity density interval 1.82–6.76 $\times 10^{-4}$ substitutions/site/year). However, we were unable to distinguish whether this difference is an artifact of the modeling or the underlying data, due to limited datasets for S (150–200 nt) and M (300–400 nt) segments, or analyzing variables versus conserved regions. Because of the limited data inherent with small nucleotide fragments, we could not assess if differences are potentially due to reassortment or recombination or if differing selective pressures cause different mutation rates.

On occasion non–SNV-related hantavirus infections have been diagnosed in Canada; however, studies on non-SNV hantaviruses within Canada are limited. Two imported HCPS cases from Argentina and Bolivia were detected in returning travelers by reverse transcription PCR analysis; amplicon sequencing determined the etiologic agent was Andes virus or a closely-related variant (*6*). In addition, a traveler returning from Siberia in 2002, who originally tested seronegative using an in-house ELISA, subsequently tested seropositive for Dobrava virus. A small proportion of coastal rats have shown seroreactivity for Seoul virus; however, human infections in Canada have been limited to a recent cluster associated with imported pet rats (*14*,*15*).

Conclusions

Although hantavirus infections in Canada remain rare, the high CFR and severe nature of the disease underscore the importance of surveillance-based awareness and risk prevention in at-risk populations and settings. Overall, close monitoring of SNV infections in Canada remains a key part of risk mitigation and will further our understanding of HCPS pathogenesis and SNV ecology and evolution.

Acknowledgments

We thank Yann Pelcat for preparing the map presented in this manuscript.

This work was funded by the Public Health Agency of Canada as a part of routine national diagnostic reference services. Field surveillance was conducted following the Canadian Council of Animal Care guidelines and in accordance with an animal use document approved by the Canadian Science Centre for Human and Animal Health's institutional animal care and use committee.

About the Author

Dr. Warner is a research biologist with the Public Health Agency of Canada in Winnipeg, Manitoba, Canada. His research interests include using animal models of infection of high-consequence pathogens for the testing of vaccines and therapeutics, currently focused primarily on understanding transmission dynamics of Sin Nombre virus in deer mice.

References

1. Hjelle B, Jenison S, Torrez-Martinez N, Yamada T, Nolte K, Zumwalt R, et al. A novel hantavirus associated with an outbreak of fatal respiratory disease in the southwestern United States: evolutionary relationships to known hantaviruses. J Virol. 1994;68:592–6. https://doi.org/10.1128/JVI.68.2.592-596.1994
2. Nichol ST, Spiropoulou CF, Morzunov S, Rollin PE, Ksiazek TG, Feldmann H, et al. Genetic identification of a hantavirus associated with an outbreak of acute respiratory illness. Science. 1993;262:914–7. https://doi.org/10.1126/science.8235615
3. Jonsson CB, Figueiredo LT, Vapalahti O. A global perspective on hantavirus ecology, epidemiology, and disease. Clin Microbiol Rev. 2010;23:412–41. https://doi.org/10.1128/CMR.00062-09
4. Warner BM, Stein DR, Griffin BD, Tierney K, Leung A, Sloan A, et al. Development and characterization of a Sin Nombre virus transmission model in *Peromyscus maniculatus*. Viruses. 2019;11:183. https://doi.org/10.3390/v11020183
5. Pan-American Health Organization. Hantaviruses in the Americas: guidelines for prevention, diagnosis, treatment, prevention and control. Technical paper 47. Washington: The Organization; 1999.
6. Drebot MA, Jones S, Grolla A, Safronetz D, Strong JE, Kobinger G, et al. Hantavirus pulmonary syndrome in Canada: An overview of clinical features, diagnostics, epidemiology, and prevention. Can Commun Dis Rep. 2015;41:124–31. https://doi.org/10.14745/ccdr.v41i06a02
7. Jenison S, Hjelle B, Simpson S, Hallin G, Feddersen R, Koster F. Hantavirus pulmonary syndrome: clinical,

diagnostic, and virologic aspects. Semin Respir Infect. 1995;10:259–69.
8. Drebot MA, Gavrilovskaya I, Mackow ER, Chen Z, Lindsay R, Sanchez AJ, et al. Genetic and serotypic characterization of Sin Nombre–like viruses in Canadian *Peromyscus maniculatus* mice. Virus Res. 2001;75:75–86. https://doi.org/10.1016/S0168-1702(01)00227-1
9. Weir E. Hantavirus: 'tis the season. Can Med Assoc J. 2005 Jul 19;173:147.
10. Parkes LO, Nguyen TT, Longtin J, Beaudoin M-C, Bestman-Smith J, Vinh DC, et al. A cluster of three cases of hantavirus pulmonary syndrome among Canadian military personnel. Can J Infect Dis Med Microbiol. 2016;2016:1. https://doi.org/10.1155/2016/2757969
11. Borges AA, Campos GM, Moreli ML, Moro Souza RL, Saggioro FP, Figueiredo GG, et al. Role of mixed Th1 and Th2 serum cytokines on pathogenesis and prognosis of hantavirus pulmonary syndrome. Microbes Infect. 2008;10:1150–7. https://doi.org/10.1016/j.micinf.2008.06.006
12. Morzunov SP, Khaiboullina SF, St. Jeor S, Rizvanov AA, Lombardi VC. Multiplex analysis of serum cytokines in humans with hantavirus pulmonary syndrome. Front Immunol. 2015;6:432. https://doi.org/10.3389/fimmu.2015.00432
13. Kjemtrup AM, Messenger S, Meza AM, Feiszli T, Yoshimizu MH, Padgett K, et al. New exposure location for hantavirus pulmonary syndrome case, California, USA, 2018. Emerg Infect Dis. 2019;25:1962–4. https://doi.org/10.3201/eid2510.190058
14. Himsworth CG, Bai Y, Kosoy MY, Wood H, DiBernardo A, Lindsay R et al. An investigation of Bartonella spp., Rickettsia typhi, and Seoul hantavirus in rats (Rattus spp.) from an inner-city neighborhood of Vancouver Canada: is pathogen presence a reflection of global and local rat population structure? Vector Borne Zoonotic Dis. 2015;15:21–6.
15. Kerins JL, Koske SE, Kazmierczak J, Austin C, Gowdy K, Dibernado A et al. Outbreak of Seoul virus among rats and rat owners—United States and Canada, 2017. MMWR Morb Mortal Wkly Rep. 2018. Feb 2;67:131–4.

Address for correspondence: David Safronetz, Zoonotic Diseases and Special Pathogens, National Microbiology Laboratory, Public Health Agency of Canada, 1015 Arlington St, Winnipeg, MB R3E 3R2, Canada; email: david.safronetz@canada.ca

Detection and Characterization of Bat Sarbecovirus Phylogenetically Related to SARS-CoV-2, Japan

Shin Murakami,[1] Tomoya Kitamura,[1] Jin Suzuki, Ryouta Sato, Toshiki Aoi, Marina Fujii, Hiromichi Matsugo, Haruhiko Kamiki, Hiroho Ishida, Akiko Takenaka-Uema, Masayuki Shimojima, Taisuke Horimoto

Epidemiology of bat *Betacoronavirus*, subgenus *Sarbecovirus* is largely unknown, especially outside China. We detected a sarbecovirus phylogenetically related to severe acute respiratory syndrome coronavirus 2 from *Rhinolophus cornutus* bats in Japan. The sarbecovirus' spike protein specifically recognizes angiotensin-converting enzyme 2 of *R. cornutus*, but not humans, as an entry receptor.

During the past 20 years, coronaviruses belonging to the genus *Betacoronavirus* have caused multiple human epidemic or pandemic diseases, including severe acute respiratory syndrome (SARS), Middle East respiratory syndrome (MERS), and coronavirus disease (COVID-19). Two viruses of the subgenus *Sarbecovirus* are severe acute respiratory syndrome coronavirus (SARS-CoV), which causes SARS, and SARS-CoV-2, which causes COVID-19. Although *Rhinolophus* spp. bats in Asia, Europe, and Africa are considered natural reservoirs of sarbecoviruses (*1*–*3*), the epidemiology and distribution of these viruses remain largely unknown, especially outside China. Previously, partial RNA-dependent RNA polymerase (RdRp) genes of betacoronaviruses were detected in little Japanese horseshoe bats (*Rhinolophus cornutus*) (*4*). However, limited sequence information left the genetic and virological properties unclear. We detected and determined the entire genome sequence of a bat sarbecovirus belonging to a phylogenetic clade that includes SARS-CoV-2 from *R. cornutus* bats in Japan. Further, we used a pseudotyped virus system to characterize an entry step of this virus into cells.

Author affiliations: The University of Tokyo, Tokyo, Japan (S. Murakami, T. Kitamura, M. Fujii, H. Matsugo, H. Kamiki, H. Ishida, A. Takenaka-Uema, T. Horimoto); Yamaguchi University, Yamaguchi, Japan (J. Suzuki); Iwate University, Iwate, Japan (R. Sato, T. Aoi); National Institute of Infectious Diseases, Tokyo, Japan (M. Shimojima)

DOI: https://doi.org/10.3201/eid2612.203386

The Study

R. cornutus is an endemic bat species in Japan and is found nationwide. These bats primarily inhabit caves and abandoned tunnels in the countryside during daytime and capture insects at night outside their roosts. *R. cornutus* bats often cohabit with other insectivorous bats, such as *R. ferrumequinum* or *Myotis macrodactylus*, and occasionally with wild animals, such as the masked palm civet (*Paguma larvata*), in their daytime roosts.

In 2013, we captured 4 *R. cornutus* bats in a cave in Iwate prefecture, Japan, and extracted RNA from fresh feces. Then, we used real-time reverse transcription PCR (rRT-PCR) to detect the partial RdRp gene of sarbecovirus from 2 samples by using a pair of primers designed to detect betacoronavirus. In 2020, we performed RNA sequencing and determined the full genome sequence of 1 sample, Rc-o319, which exhibited lower cycle threshold value by rRT-PCR.

We performed a BLAST (https://blast.ncbi.nlm.nih.gov/Blast.cgi) analysis of the full genome of Rc-o319, which showed Rc-o319 had the highest nucleotide homology to SARS-CoV-2 HKG/HKU-904a/2020 strain (GenBank accession no. MT365032) with a query cover of 96% and sequence identity of 81.47%. The maximum-likelihood analysis with sarbecoviruses demonstrated that the full genome and spike protein (S) gene of Rc-o319 were positioned within a specific clade that included SARS-CoV-2 (Figure 1, panels A, B). Amino acid sequences of open reading frame 1ab (ORF1ab) and S of Rc-o319 also were positioned within the SARS-CoV-2 clade (Figure 1 panels C and D). The phylogenetic trees maintained the same topology between ORF1ab and S, indicating that no recombination event occurred in Rc-0319, which was supported by similarity plot analysis (Appendix Figure 1, https://wwwnc.cdc.gov/EID/article/26/12/

[1]These authors contributed equally to this article.

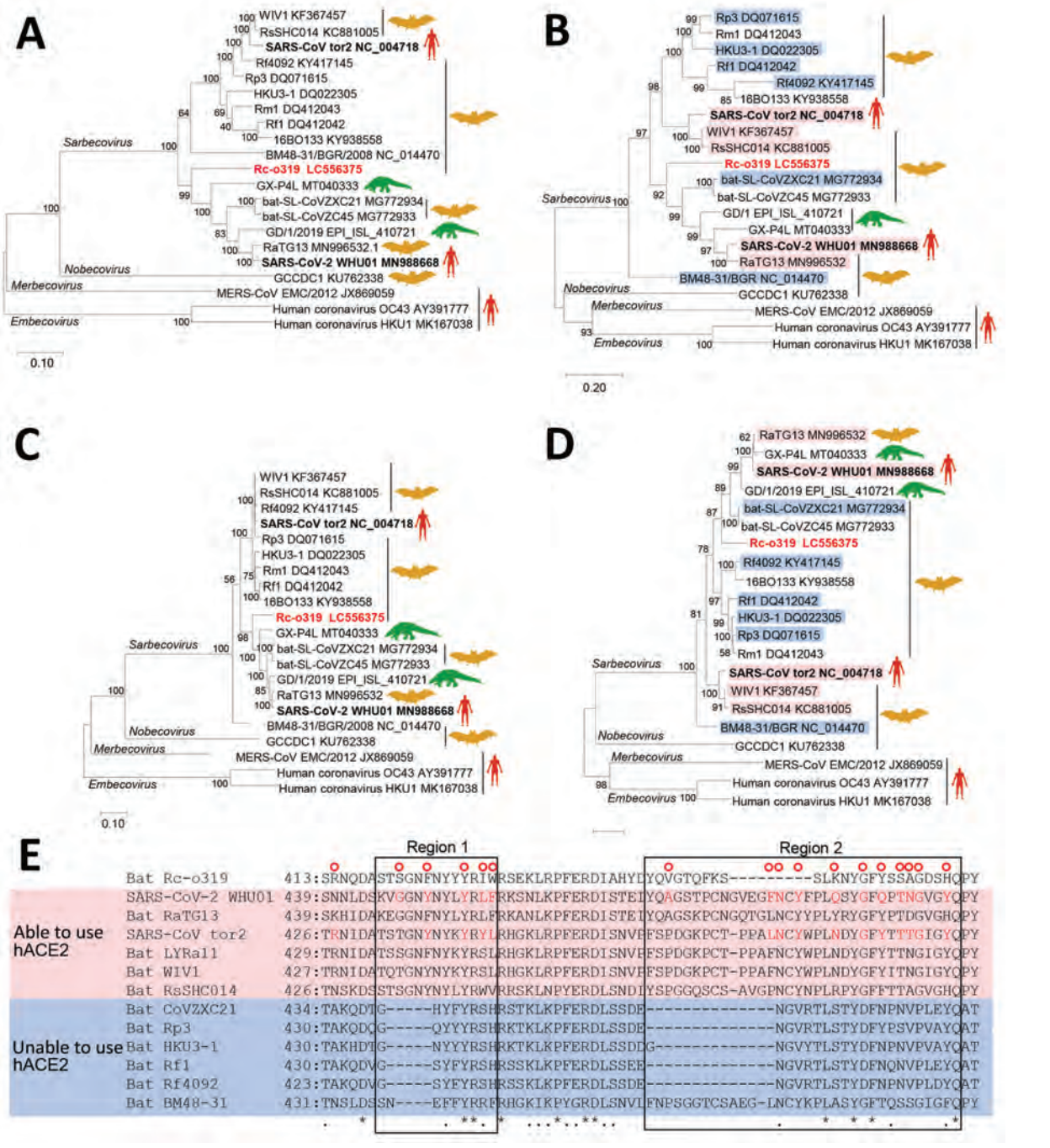

Figure 1. Phylogenetic analysis of sarbecovirus sequenced from little Japanese horseshoe bats (*Rhinolophus cornutus*) and genetically related to human SARS-CoV-2, Japan. A–D) Phylogenetic trees were generated by using maximum-likelihood analysis combined with 500 bootstrap replicates and show relationships between bat-, human-, and pangolin-derived sarbecoviruses. Phylogenetic trees are shown for nucleotide sequences of the full genome (A), the S protein gene and amino acid sequences (B), the ORF1ab (C), and the S protein (D). Red text indicates positions of Rc-o319, the sarbecovirus sequenced in this study. For panels B and D, magenta bands indicate viruses with S proteins that bind to human ACE2; blue bands indicate viruses with S proteins that do not bind to human ACE2. Bootstrap values are shown above and to the left of the major nodes. Scale bars indicate nucleotide or amino acid substitutions per site. E) Amino acid sequence alignment of the RBM of S proteins that are able or unable to bind to human ACE2. Amino acid residues of the RBM that contact human ACE2 of SARS-CoV-2 and SARS-CoV are indicated in the upper side by red circles. The 2 regions of S protein RBM known to interact with human ACE2 are indicated by boxes labeled region 1 and region 2. ACE2, angiotensin-converting enzyme 2; hACE2, human angiotensin-converting enzyme 2; ORF1ab, open reading frame 1ab; RBM, receptor-binding motif; S, spike protein; SARS-CoV, severe acute respiratory syndrome coronavirus; SARS-CoV-2, severe acute respiratory syndrome coronavirus 2.

20-3386-App1.pdf). The nucleotide and amino acid sequences of Rc-o319 were more homologous to those of viruses belonging to SARS-CoV-2 clade than the SARS-CoV clade (Table). These data suggest that Rc-o319 genetically is related to SARS-CoV-2.

To gain insight into the zoonotic potential of Rc-o319, we focused on angiotensin-converting enzyme 2 (ACE2) receptor binding motif (RBM) of the S protein (Figure 1, panel E). RBM has 2 regions (1 and 2); both are essential to human ACE2 (hACE2) recognition (*5*,*6*). Several S proteins of bat-origin sarbecoviruses that lack the ability to bind the hACE2 contain amino acid deletions in both regions (Figure 1, panel E) (*5*). However, the RBM of Rc-o319 S is unique because it has 9 aa deletions in region 2 only, which was not observed in other bat sarbecoviruses. Of note, most residues that contact hACE2, which were detected in the S protein of SARS-CoV-2 and SARS-CoV, were different or missing in the S protein of Rc-o319. Thus, current data do not enable inference for whether the Rc-o319 can use hACE2 as a cell entry receptor.

To evaluate the potential of ACE2 as a receptor for Rc-o319, we adopted a pseudotyped vesicular stomatitis virus (VSV) system, in which VSV glycoprotein envelope (G) gene is replaced by green fluorescent protein (GFP) gene. We generated VSV pseudotyped with S proteins of Rc-o319 (VSV-Rc-o319), SARS-CoV (VSV-SARS), SARS-CoV-2 (VSV-SARS-2), or VSV-G (VSV-VSV-G) in human embryonic kidney 293T (HEK293T) cells. We also constructed ACE2 expression plasmids from hACE2, *R. ferrumequinum* bats (Rf-ACE2), and *R. sinicus* bats (Rs-ACE2). *R. ferrumequinum* is another bat species inhabiting in Japan, and *R. sinicus* bats are a major host reservoir of bat sarbecoviruses. We also prepared a chimeric bat ACE2 from *R. cornutus* and *R. ferrumequinum* bats, Rc/Rf chimera, which has the N terminus of S protein interaction domain of Rc-ACE2 and the remaining region from Rf-ACE2 (Appendix Figure 2). The HEK293T cells expressing Rc-ACE2, Rf-ACE2, Rs-ACE2, Rc/Rf-ACE2, or hACE2 were produced by transfecting each ACE2-expression plasmid (Appendix Figure 3) and inoculating them with pseudotyped VSVs; their infectivity was titrated by counting GFP-positive cells at 20 hours postinfection (Figure 2). Our results showed that VSV-Rc-o319 infected Rc-ACE2– and Rc/Rf-ACE2–expressing cells, but not Rf-ACE2–, Rs-ACE2–, or hACE2–expressing cells or control cells transfected with empty vector plasmid. In contrast, VSV-SARS and VSV-SARS-2 more effectively infected hACE2-expressing cells than bat ACE2–expressing cells and control cells. VSV-VSV-G infected all tested cells to comparable levels, confirming ACE2-independent infectivity of VSV. These results suggest high specificity of ACE2 receptor between sarbecovirus and host cells and possibly a limited zoonotic potential of Rc-o319 in terms of cell receptor usage without adaptation to humans.

We next analyzed the membrane fusion step of Rc-o319 S. A previous study showed that human sarbecovirus S protein was proteolytically activated by cellular transmembrane serine protease 2 (TMPRSS2), in vitro and in vivo, inducing efficient virus-cell membrane fusion at the cell surface (*7*). We prepared a fusion assay, in which HEK293T cells were cotransfected with S-expression plasmid of Rc-o319, SARS-CoV, or SARS-CoV-2 and Rc-ACE2–, Rf-ACE2–, Rs-ACE2–, or hACE2-expression plasmid, together with fluorescent reporter Venus-expression plasmid with and without TMPRSS2-expression plasmid, and incubated for 24 h to assess syncytium formation. We observed that the S protein

Table. Identities of nucleotide and amino acid sequences of genome, genes, and proteins to representative sarbecoviruses used to investigate sarbecovirus Rc-o319 detected in bats, Japan

Virus	Entire genome	ORF1ab	S	ORF3a	E	M	ORF6	ORF7a	ORF7b	ORF8	N	ORF10
						Nucleotide %						
SARS-CoV-2	81.5	80.0	73.0	83.2	97.4	86.6	86.6	78.4	77.3	53.3	88.3	94.9
RaTG13	81.2	79.8	73.3	83.9	96.9	85.4	87.1	77.4	78.0	53.0	87.8	94.0
pangolin/P4L	80.4	79.8	72.5	83.5	97.8	85.5	85.5	74.5	–	53.2	86.8	91.5
CoVZXC21	80.4	80.2	72.5	79.9	96.1	86.0	83.3	75.1	–	50.8	85.9	53.9
SARS-CoV-1	81.0	78.8	73.6	76.6	93.1	87.0	77.1	73.4	74.8	–	86.1	63.3
Rf1	80.6	78.7	70.9	75.1	92.6	85.8	78.8	72.2	75.6	68.6	84.9	63.3
BM48–31	79.6	77.4	69.3	70.4	90.5	80.6	61.3	65.1	57.9	–	77.0	64.1
						Amino acid, %						
SARS-CoV-2	NA	88.2	76.7	87.0	98.7	91.0	83.6	73.8	69.8	27.5	89.5	87.2
RaTG13	NA	88.1	77.6	86.6	98.7	91.0	83.6	73.0	72.1	28.2	89.7	84.6
pangolin/P4L	NA	88.2	76.9	86.2	98.7	91.0	80.3	68.9	–	28.8	89.2	79.5
CoVZXC21	NA	87.9	75.5	83.3	98.7	91.4	77.1	68.9	–	20.5	88.1	28.2
SARS-CoV-1	NA	85.9	75.2	72.5	93.4	97.7	66.7	69.7	68.2	–	88.9	59.0
Rf1	NA	85.5	73.6	69.6	92.1	94.1	66.7	68.0	72.7	66.7	87.4	59.0
BM48–31	NA	83.7	71.9	64.5	93.4	88.1	48.5	52.5	58.1	–	85.9	61.5

*NA, not available; ORF, open reading frame; –, no ORFs found.

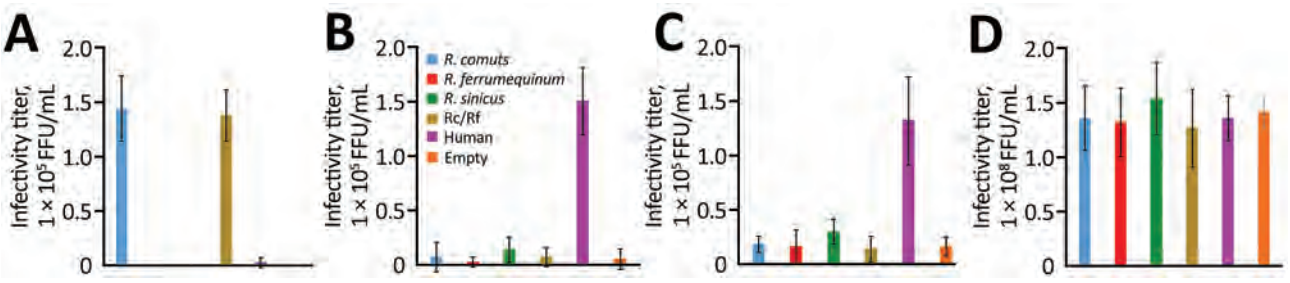

Figure 2. Infectivity titers of sarbecoviruses from bats and humans used to investigate bat sarbecovirus Rc-o319, which is genetically related to human SARS-CoV-2, Japan. Cells expressing each host-origin angiotensin-converting enzyme 2 were inoculated with VSV pseudotyped with spike proteins of Rc-o319 (A), SARS-CoV (B), SARS-CoV-2 (C), or glycoprotein of VSV (D). At 20 hours postinfection, GFP-positive cells were counted and the infectivity titers were calculated. Error bars indicate SDs from 3 independent experiments. CoV, coronavirus; GFP, green fluorescent protein; Rc/Rf, chimera of *Rhinolophus cornutus* and *R. ferrumequinum*; SARS, severe acute respiratory syndrome; VSV, vesicular stomatitis virus.

of SARS-CoV and SARS-CoV-2 required both hACE2 and TMPRSS2 for fusion activity (Appendix Figure 4), confirming the previous findings (*7*,*8*). In contrast, the S protein of Rc-o319 induced cell fusion only in Rc-ACE2–expressing cells, both in the presence and absence of TMPRSS2. These results suggest that unlike human sarbecoviruses, Rc-o319 uses Rc-ACE2 as a functional receptor, leading to membrane fusion independent of S-cleavage by TMPRSS2.

Conclusions

Among *R. cornutus* bats in Japan, we detected sarbecovirus Rc-o319, which is phylogenetically positioned in the same clade as SARS-CoV-2. Sarbecoviruses belonging to this clade previously were detected from other *Rhinolophus* spp. bats and pangolins (family Manidae) in China and could have played a role in the emergence of SARS-CoV-2 (*9*–*11*). We provide a hypothesis that a bat sarbecovirus with zoonotic potential might exist even outside China, because *Rhinolophus* spp. bats inhabit Asia, Europe, and Africa (*12*).

Receptor usage is one factor for cross-species transmission of viruses. Unlike a previous report that showed that some bat SARS-CoV–related viruses could use human and civet ACE2 and *R. sinicus* ACE2 as entry receptors (*5*,*13*,*14*), VSV-Rc-o319 was found to use only homologous Rc-ACE2, which arguably suggests that Rc-o319 and its related viruses might not jump the species barrier easily and cause infection. However, Rc-o319 and its related viruses could be transmitted accidentally from *R. cornutus* bats to cohabitant animals, such as civets, which are potential intermediate hosts for human infection (*15*). Therefore, further epidemiologic surveillance of bat betacoronaviruses, including evaluation of their zoonotic potential, is essential because betacoronaviruses that caused SARS, MERS, and COVID-19 outbreaks in humans during the past 20 years likely originated from bat betacoronaviruses.

S.M. is supported by a Kakenhi Grant-in-Aid for Challenging Research (Exploratory) from the Japan Society for the Promotion of Science (grant no. 17K19319).

About the Author

Dr. Murakami is an associate professor at the Graduate School of Agricultural and Life Sciences, University of Tokyo, Tokyo, Japan. His research interests include epidemiologic and molecular biological studies of animal viruses, including coronaviruses and influenza viruses.

References

1. Drexler JF, Gloza-Rausch F, Glende J, Corman VM, Muth D, Goettsche M, et al. Genomic characterization of severe acute respiratory syndrome-related coronavirus in European bats and classification of coronaviruses based on partial RNA-dependent RNA polymerase gene sequences. J Virol. 2010;84:11336–49. https://doi.org/10.1128/JVI.00650-10
2. Hu B, Zeng LP, Yang XL, Ge XY, Zhang W, Li B, et al. Discovery of a rich gene pool of bat SARS-related coronaviruses provides new insights into the origin of SARS coronavirus. PLoS Pathog. 2017;13:e1006698. https://doi.org/10.1371/journal.ppat.1006698
3. Tao Y, Tong S. Complete genome sequence of a severe acute respiratory syndrome-related coronavirus from Kenyan bats. Microbiol Resour Announc. 2019 8(28):e00548–19. https://doi.org/0.1128/MRA.00548-19
4. Suzuki J, Sato R, Kobayashi T, Aoi T, Harasawa R. Group B betacoronavirus in rhinolophid bats, Japan. J Vet Med Sci. 2014;76:1267–9. https://doi.org/10.1292/jvms.14-0012
5. Letko M, Marzi A, Munster V. Functional assessment of cell entry and receptor usage for SARS-CoV-2 and other lineage B betacoronaviruses. Nat Microbiol. 2020;5:562–9. https://doi.org/10.1038/s41564-020-0688-y
6. Lan J, Ge J, Yu J, Shan S, Zhou H, Fan S, et al. Structure of the SARS-CoV-2 spike receptor-binding domain bound to the

ACE2 receptor. Nature. 2020;581:215–20. https://doi.org/10.1038/s41586-020-2180-5
7. Glowacka I, Bertram S, Müller MA, Allen P, Soilleux E, Pfefferle S, et al. Evidence that TMPRSS2 activates the severe acute respiratory syndrome coronavirus spike protein for membrane fusion and reduces viral control by the humoral immune response. J Virol. 2011;85:4122–34. https://doi.org/10.1128/JVI.02232-10
8. Yamamoto M, Kiso M, Sakai-Tagawa Y, Iwatsuki-Horimoto K, Imai M, Takeda M, et al. The anticoagulant nafamostat potently inhibits SARS-CoV-2 S protein-mediated fusion in a cell fusion assay system and viral infection in vitro in a cell-type-dependent manner. Viruses. 2020;12:E629. https://doi.org/10.3390/v12060629
9. Zhou P, Yang XL, Wang XG, Hu B, Zhang L, Zhang W, et al. A pneumonia outbreak associated with a new coronavirus of probable bat origin. Nature. 2020;579:270–3. https://doi.org/10.1038/s41586-020-2012-7
10. Lau SKP, Luk HKH, Wong ACP, Li KSM, Zhu L, He Z, et al. Possible bat origin of severe acute respiratory syndrome coronavirus 2. Emerg Infect Dis. 2020;26:1542–7. https://doi.org/10.3201/eid2607.200092
11. Zhang T, Wu Q, Zhang Z. Probable pangolin origin of SARS-CoV-2 associated with the COVID-19 outbreak. Curr Biol. 2020;30:1346–51.e2. https://doi.org/10.1016/j.cub.2020.03.022
12. Stoffberg S, Jacobs DS, Mackie IJ, Matthee CA. Molecular phylogenetics and historical biogeography of Rhinolophus bats. Mol Phylogenet Evol. 2010;54:1–9. https://doi.org/10.1016/j.ympev.2009.09.021
13. Ge XY, Li JL, Yang XL, Chmura AA, Zhu G, Epstein JH, et al. Isolation and characterization of a bat SARS-like coronavirus that uses the ACE2 receptor. Nature. 2013;503:535–8. https://doi.org/10.1038/nature12711
14. Yang XL, Hu B, Wang B, Wang MN, Zhang Q, Zhang W, et al. Isolation and characterization of a novel bat coronavirus closely related to the direct progenitor of severe acute respiratory syndrome coronavirus. J Virol. 2015;90:3253–6. https://doi.org/10.1128/JVI.02582-15
15. Guan Y, Zheng BJ, He YQ, Liu XL, Zhuang ZX, Cheung CL, et al. Isolation and characterization of viruses related to the SARS coronavirus from animals in southern China. Science. 2003;302:276–8. https://doi.org/10.1126/science.1087139

Address for correspondence: Shin Murakami or Taisuke Horimoto, Department of Veterinary Microbiology, Graduate School of Agricultural and Life Sciences, University of T okyo, 1-1-1 Yayoi, Bunkyo-ku, Tokyo 113-8657, Japan; email: amurakam@mail.ecc.u-tokyo.ac.jp or ahorimo@mail.ecc.u-tokyo.ac.jp

Unique Outbreak of Rift Valley Fever in Sudan, 2019

Ayman Ahmed, Yousif Ali, Adel Elduma, Mawahib Hassan Eldigail, Rehab Abdallah Mhmoud, Nouh Saad Mohamed, Thomas G. Ksiazek, Isabelle Dietrich, Scott C. Weaver

We report a unique outbreak of Rift Valley fever in the Eldamar area, Sudan, May–July 2019, that resulted in 1,129 case-patients and 19 (1.7%) deaths. Patients exhibited clinical signs including fever (100%), headache (79%), and bleeding (4%). Most (98%) patients also reported death and abortions among their livestock.

Rift Valley fever (RVF) is an arboviral disease caused by RVF virus (RVFV; genus *Phlebovirus*, family *Phenuiviridae*) (*1*). RVFV periodically emerges to cause epizootics among livestock and epidemics in persons living nearby (*2*). It is mainly transmitted by the bite of infected mosquitoes or by direct contact with infected animals and their products (*3*). In addition, RVFV transmission is maintained vertically among both humans and vector mosquito populations (*4*,*5*).

The public health threat from arboviral diseases is growing rapidly in Sudan (*4*,*6*). Increasing human movement, often arising from armed conflict, is driving several arboviral diseases to emerge in Sudan, usually in the form of undifferentiated febrile illness. Recent epidemics include dengue fever (*6*,*7*), Crimean-Congo hemorrhagic fever, West Nile virus disease (*8*), yellow fever, and chikungunya fever (*4*). RVF outbreaks represent major public health and economic burdens on endemic countries, particularly those such as Sudan that rely on exporting animals and animal products (*3*,*4*,*9*). In a recent study, RVFV infection was also associated with spontaneous abortion among pregnant women in Sudan (*10*). We describe a unique, undeclared outbreak of RVF in River Nile state, in northern Sudan, leading to the potential spread of the virus to other states in Sudan or neighboring countries.

Author affiliations: University of Khartoum, Khartoum, Sudan (A. Ahmed); University of Texas Medical Branch, Galveston, Texas, USA (A. Ahmed, T.G. Ksiazek, S.C. Weaver); World Reference Center for Emerging Viruses and Arboviruses, Galveston (A. Ahmed, S.C. Weaver); Sudan Federal Ministry of Health, Khartoum (Y. Ali, A. Elduma, M.H. Eldigail); River Nile State Ministry of Health, Eldamar, Sudan (R.A. Mhmoud); Nile University, Khartoum (N.S. Mohamed); The Pirbright Institute, Pirbright, UK (I. Dietrich)

DOI: https://doi.org/10.3201/eid2612.201599

The Study

Rift Valley fever cases initially appeared on May 23, 2019, in Eldamar, the capital city of River Nile state (Figure 1). This region, characterized as a desert environment, is in general rural and peri-urban; most of the population relies on farming, animal breeding, and more recently, traditional gold mining. By July 18, a total of 1,129 cases had been identified on the basis of clinical signs and symptoms. The outbreak peaked in June 2019 with ≈96 cases reported daily (Figure 2).

Most RVF cases, 1,120 (99.2%), were from Eldamar, with only 7 cases reported in Barbar and 2 in Atbara (Table). The male:female ratio was 1.2:1. Adults 25–44 years of age were most affected (34.6%), but other age groups were similarly represented; however, only 6.1% of cases involved children <5 years old (Table). Many of the patients (34%) worked in farming and animal product production.

Among the 1,129 patients, 100% had fever, 79% (892/1,129) had headache, and only 4% (45/1,129) had clinically manifested bleeding. Almost all (98%; 1,104/1,129) patients (or their guardians, in the case of children) reported death or abortion among their domestic livestock. Of the 19 reported human deaths, 6 (32%) were children <15 years of age and 9 (47.4%) were farmers (Table 1).

We retrospectively analyzed data collected by active surveillance during this epidemic to confirm that RVFV was the exclusive causative agent of this outbreak, because it is normally associated with the rainy season in Sudan. Surveillance was established by the River Nile State Ministry of Health. In our analysis, we included variables such as patient age and sex; signs and symptoms, such as fever,

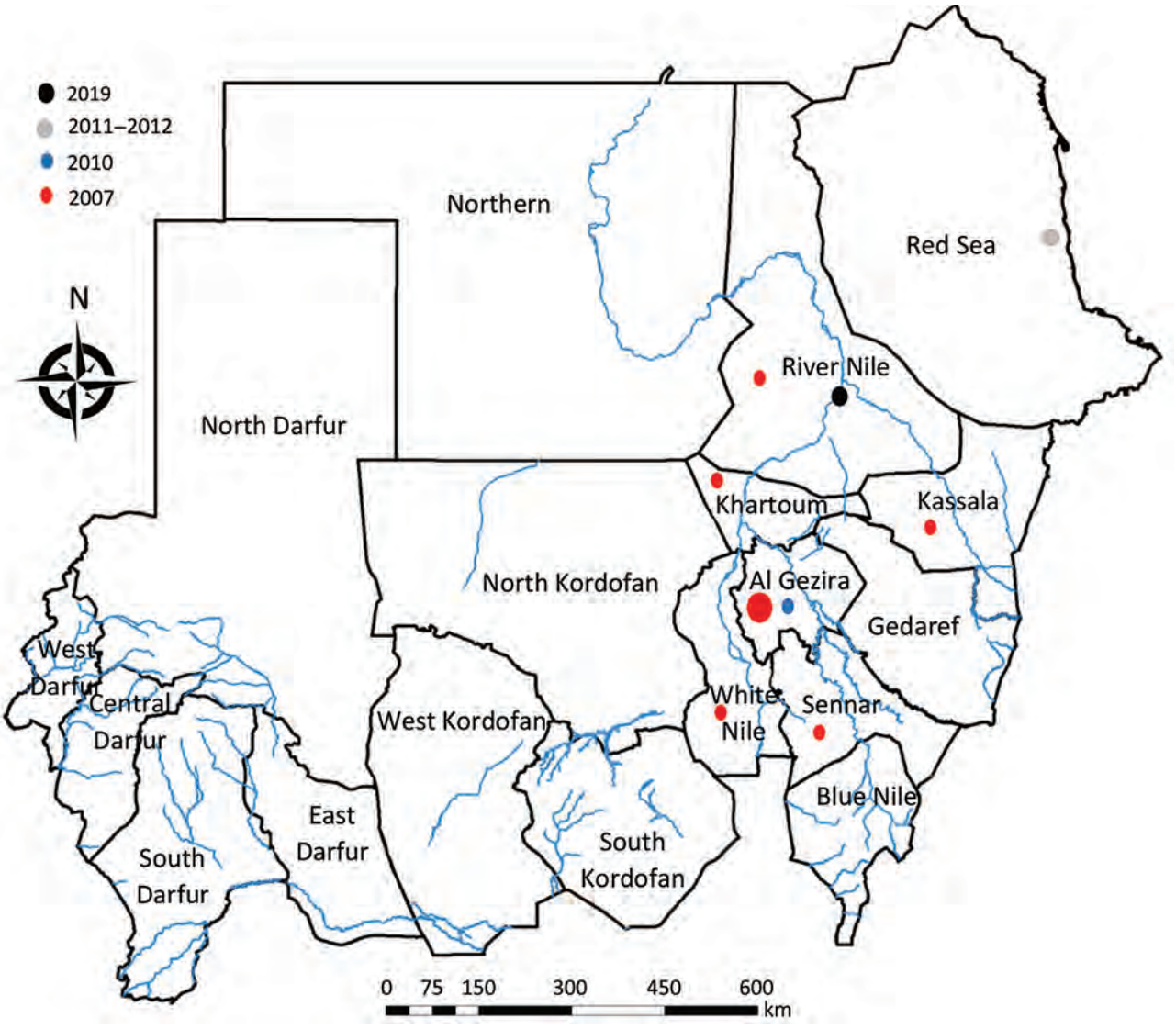

Figure 1. Distribution of Rift Valley fever outbreaks in Sudan, by year.

hemorrhagic manifestations, and headaches; where the patient lived; and if the patient had noted any death or abortion among livestock. We randomly collected 50 blood samples and tested them by reverse transcription PCR using the RealStar Rift Valley Fever Virus RT-PCR Kit 1.0 (Altona Diagnostics GmbH, https://altona-diagnostics.com) in the Sudanese National Public Health Laboratory, Khartoum, Sudan. PCR testing confirmed RVFV infection in 88% (44/50) of samples.

We report a unique outbreak of RVF that occurred before the typical transmission season, which in Sudan normally corresponds with rain and flooding during September–December. There were also an unusually large number of cases (1,129) and 19 related deaths. Although RVF epidemics and epizootics are common in Sudan because of the endemic transmission of RVFV (*4*), this outbreak was unique in the scale of human and animal infections over only 3 months. The timing of outbreak development was also unusual, which could be attributed to the nationwide political violence that forced many people to move with their animals from RVF-endemic to non–RVF-endemic areas and vice versa (*11*).

Three major RVF epidemics were documented in Sudan in 2007, 2010, and 2011–2012 (Figure 1) (*4*). During June 2011–November 2012, a total of 28 RVFV infections were detected among pregnant women in the governmental hospital of Port Sudan in Red Sea state (*10*). In 2010, the outbreak was more limited in size and geographic distribution; only 18 cases were reported, in El Gezira state (*12*). In 2007, a total of 747

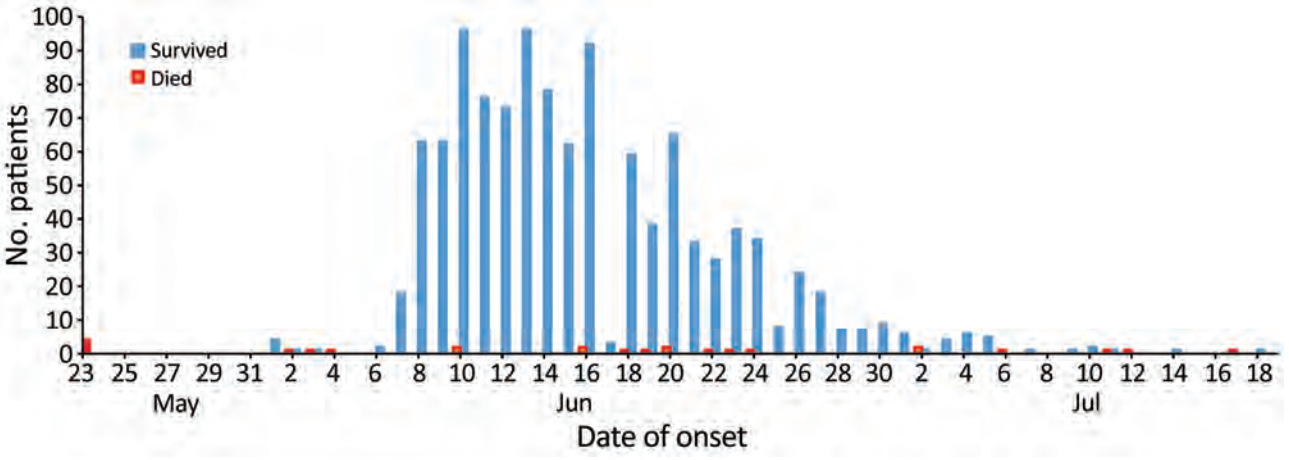

Figure 2. Cases of and deaths from Rift Valley fever, River Nile state, north Sudan, May 23–July 18, 2019.

human RVF cases, including 230 deaths, were reported from El Gezira, Sennar, White Nile, Kassala, Khartoum, and River Nile states; most cases (54%) and deaths (64%) were reported from El Gezira state (*9*).

In Sudan, there is no reliable estimate for RVF death and abortion rates among livestock animals due to limited health surveillance systems for both human and animal populations (*4*,*9*,*13*). However, a 2019 report shared with the World Organization for Animal Health showed that, in sheep, the death rate was 2.4% and the case-fatality rate 13.5%; in goats, the death rate was 2.1% and the case-fatality rate 18.8% (*14*).

As part of the recent unrest in Sudan, medical and health professionals have been intentionally targeted by military forces for their role in supporting national demonstrations. As a result, both health outcomes and records of cases might have been influenced by the escalating political violence throughout the country during the time of the 2019 RVF outbreak (*11*). These attacks impaired the health system, limiting its capacity to respond to and contain the outbreak in its early stages (*11*). This health system deficiency is underscored by the limited number of cases reported around June 16, 2019, when the outbreak was at its peak (Figure 1). In addition, Eldamar is a major market for domestic animals, particularly sheep and goats, which could have been an additional risk factor influencing the emergence of RVFV in the area and facilitating spread into other states, particularly Port Sudan in Red Sea state, the main seaport of the country for exporting animals (*15*). Unfortunately, Sudan typically experiences delays and deficiencies in data sharing during epidemics and health emergencies (*13*), which likely contributed to the slow reporting of this 2019 RVF outbreak and the general impairment of the health system during a time of national political change (*11*).

Table. Characteristics of case-patients during Rift Valley fever outbreak in Sudan, 2019

Characteristic	No. cases	% Of total
Sex		
F	505	45
M	624	55
Locality		
Eldamar	1,120	99.2
Barbar	7	0.6
Atbara	2	0.2
Age group, y		
<5	69	6.1
5–14	229	20.3
15–24	233	20.7
25–44	391	34.6
>44	207	183
Signs/symptoms		
Fever	1129	100
Headache	892	79
Bleeding	45	4
Reported disease/abortion among domestic animals		
Yes	1104	98
No	25	2

Conclusions

The risk of exporting RVFV across borders remains poorly characterized but real, stressing the need for a countrywide, One Health survey in Sudan to investigate the prevalence of RVFV among humans and domesticated animals and to identify the risk factors associated with its emergence. Further, we recommend vaccination of domestic animals at risk during the dry season when they cluster together before being moved to open pastures (*4*) and adherence by health authorities to the core of the World Health Organization's International Health Regulations, including sharing data in a timely manner to promote both local and international safety (*13*).

This major RFV outbreak underscores the urgent need in Sudan for improved surveillance systems and a robust health policy for the prevention, early detection, and control of arboviral epidemics. In the case of RVF, early reporting of information regarding animal health is particularly important, because it could be used to contain the disease before it spills over into people.

Acknowledgments

We acknowledge all the technical support from our colleagues at the state and federal Ministries of Health in acquiring and analyzing data.

S.C.W.'s research is supported by the World Reference Center for Emerging Viruses and Arboviruses, NIH Grant R24 AI120942.

About the Author

Mr. Ahmed is an arbovirology scientist. His research interests include epidemiology, the dynamics and evolution of arboviral zoonotic diseases, and their control through a One Health strategy. He works toward developing local health policy and global partnerships to prevent and control hemorrhagic fevers epidemics in Sudan.

References

1. Gaudreault NN, Indran SV, Balaraman V, Wilson WC, Richt JA. Molecular aspects of Rift Valley fever virus and the emergence of reassortants. Virus Genes. 2019;55:1–11. https://doi.org/10.1007/s11262-018-1611-y
2. Weaver SC, Reisen WK. Present and future arboviral threats. Antiviral Res. 2010;85:328–45. https://doi.org/10.1016/j.antiviral.2009.10.008
3. Grossi-Soyster EN, Lee J, King CH, LaBeaud AD. The influence of raw milk exposures on Rift Valley fever virus transmission. PLoS Negl Trop Dis. 2019;13:e0007258. https://doi.org/10.1371/journal.pntd.0007258
4. Ahmed A, Dietrich I, LaBeaud AD, Lindsay SW, Musa A, Weaver SC. Risks and challenges of arboviral diseases in Sudan: the urgent need for actions. Viruses. 2020;12:81. https://doi.org/10.3390/v12010081
5. Weaver SC, Barrett ADT. Transmission cycles, host range, evolution and emergence of arboviral disease. Nat Rev Microbiol. 2004;2:789–801. https://doi.org/10.1038/nrmicro1006
6. Elduma AH, LaBeaud AD, Plante JA, Plante KS, Ahmed A. High seroprevalence of dengue virus infection in Sudan: systematic review and meta-analysis. Trop Med Infect Dis. 2020;5:120. https://doi.org/10.3390/tropicalmed5030120
7. Ahmed A, Ali Y, Elmagboul B, Mohamed O, Elduma A, Bashab H, et al. Dengue fever in the Darfur area, western Sudan. Emerg Infect Dis. 2019;25:2126. https://doi.org/10.3201/eid2511.181766
8. Ahmed A, Elduma A, Magboul B, Higazi T, Ali Y. The first outbreak of dengue fever in greater Darfur, western Sudan. Trop Med Infect Dis. 2019;4:43. https://doi.org/10.3390/tropicalmed4010043
9. Hassan OA, Ahlm C, Sang R, Evander M. The 2007 Rift Valley fever outbreak in Sudan. PLoS Negl Trop Dis. 2011;5:e1229. https://doi.org/10.1371/journal.pntd.0001229
10. Baudin M, Jumaa AM, Jomma HJE, Karsany MS, Bucht G, Näslund J, et al. Association of Rift Valley fever virus infection with miscarriage in Sudanese women: a cross-sectional study. Lancet Glob Health. 2016;4:e864–71. https://doi.org/10.1016/S2214-109X(16)30176-0
11. Dahab M, Abdelmagid N, Osama T, Nurelhuda N, Abutalib Z, Spiegel P, et al. Political violence in Sudan: the need for a coordinated, locally led humanitarian health response. Lancet. 2019;394:549–51. https://doi.org/10.1016/S0140-6736(19)31618-6
12. Aradaib IE, Erickson BR, Elageb RM, Khristova ML, Carroll SA, Elkhidir IM, et al. Rift Valley fever, Sudan, 2007 and 2010. Emerg Infect Dis. 2013;19:246–53. https://doi.org/10.3201/eid1902.120834
13. Ahmed A. Urgent call for a global enforcement of the public sharing of health emergencies data: lesson learned from serious arboviral disease epidemics in Sudan. Int Health. 2020 Mar 6 [Epub ahead of print]. https://doi.org/10.1093/inthealth/ihz122
14. World Organisation for Animal Health. Rift Valley fever, Sudan. Follow-up report no. 1. 2019 [cited 2020 Feb 9]. https://www.oie.int/wahis_2/public/wahid.php/Reviewreport/Review?reportid=32246
15. Salih HAM, Elfadil AAM. Risk assessment and management for peste des petites ruminants (PPR) in Sudan [PhD thesis]. Khartoum (Sudan): Sudan University of Science and Technology; 2015 [cited 2020 Feb 9]. http://repository.sustech.edu//handle/123456789/11968

Address for correspondence: Ayman Ahmed, Institute of Endemic Diseases, University of Khartoum, PO Box 2318, Khartoum 11111, Sudan; email: ayman.ame.ahmed@gmail.com

Transmission of Multidrug-Resistant *Salmonella enterica* Subspecies *enterica* 4,[5],12:i:- Sequence Type 34 between Europe and the United States

Ehud Elnekave, Samuel L. Hong, Seunghyun Lim, Dave Boxrud, Albert Rovira, Alison E. Mather, Andres Perez, Julio Alvarez

Multidrug-resistant *Salmonella enterica* subspecies *enterica* 4,[5],12:i:- sequence type 34 represents a worldwide public health risk. To determine its origin in the United States, we reconstructed a time-scaled phylogeny with a discrete trait geospatial model. The clone in the United States was introduced from Europe on multiple occasions in the early 2000s.

Since the late 1990s, reports of an emerging multidrug-resistant *Salmonella enterica* subspecies *enterica* serotype 4,[5],12:i:- strain have been published in Europe (*1*). This strain is a monophasic variant of *Salmonella* Typhimurium, predominantly resistant to ampicillin, streptomycin, sulfonamides, and tetracycline (ASSuT). Its rapid increase in North America after 1998 has also been described (*2*). However, precise knowledge of the time of introduction and the initial influx of clinical cases caused by this serotype in the United States is not available because of inconsistent reporting before 2004 (*3*).

Previously, on the basis of high genetic similarity between *Salmonella* 4,[5],12:i:- sequence type (ST) 34 isolates from the United States and Europe and *Salmonella* Typhimurium strains from Europe, we suggested a European origin for the *Salmonella* 4,[5],12:i:- ST34 clade (*4*). With this study, we aimed to reconstruct a time-scaled phylogeny of the emerging ST34 clade by using a Bayesian modeling approach to determine its origin in United States.

Author affiliations: Hebrew University of Jerusalem, Jerusalem, Israel (E. Elnekave); University of Minnesota, St. Paul, Minnesota, USA (E. Elnekave, S. Lim, A. Rovira, A. Perez, J. Alvarez); University of Leuven, Leuven, Belgium (S.L. Hong); Minnesota Department of Health, St. Paul (D. Boxrud); Quadram Institute Bioscience, Norwich, UK (A.E. Mather); University of East Anglia, Norwich (A.E. Mather); Universidad Complutense, Madrid, Spain (J. Alvarez)

DOI: https://doi.org/10.3201/eid2612.200336

The Study

We used publicly available whole-genome sequences of 1,431 *Salmonella* 4,[5],12:i:- ST34 isolates from the United States and Europe from 2008–2017, including sequences from 690 isolates from Europe (mainly from the United Kingdom and Denmark) and 741 isolates from multiple US states (Appendix 1, https://wwwnc.cdc.gov/EID/article/26/12/20-0336-App1.xlsx). We used BEAST version 1.8.4 (*5*) to estimate divergence times, mutation rates, and location trait transitions. We applied the modeling approach to 10 subsets of 112 sequences selected from the study population. These sequences represented 33% (474/1,431) of the study population and included 242 sequences from Europe (76% from humans, 8% from food products, 8% from livestock, and 8% from other sources) and 232 from the United States (62% from humans, 13% from food products, 21% from livestock, and 3% from other sources). Time-scaled phylogenies of each subset were reconstructed by using a general time-reversible nucleotide substitution model, an uncorrelated lognormal relaxed molecular clock, and an exponential growth coalescent model with asymmetric trait transitions (Figure 1; Appendix 2 Figures 1–10, https://wwwnc.cdc.gov/EID/article/26/12/20-0336-App2.pdf). All time-scaled phylogenies presented similar topology to a maximum-likelihood phylogeny constructed by using all 1,431 study isolates (based on visual inspection; Appendix 2 Figure 11). Overall, averaged estimates from all subsets were in agreement as follows (Figure 2): the evolutionary rate was 3.64×10^{-7} substitutions/site/year (95% highest posterior density [HPD] $2.65–4.64 \times 10^{-7}$), which corresponds to an accumulation of ≈1–2 single-nucleotide

polymorphisms/genome/year; the time to most recent common ancestor was 1994 (95% HPD 1988–2000); the number of collection location state transitions (Markov jumps) from Europe to the United States was 7.7 (95% HPD 5.9–9.3) and from the United States to Europe was 0.8 (95% HPD 0–2.2); and the waiting times (in years; Markov rewards) were 519.9 (95% HPD 393.1–667.8) in Europe and 318.6 (95% HPD 234.0–417.6) in the United

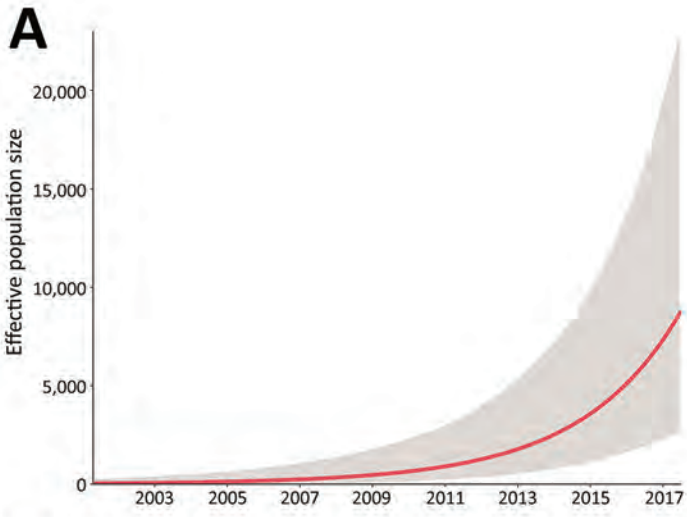

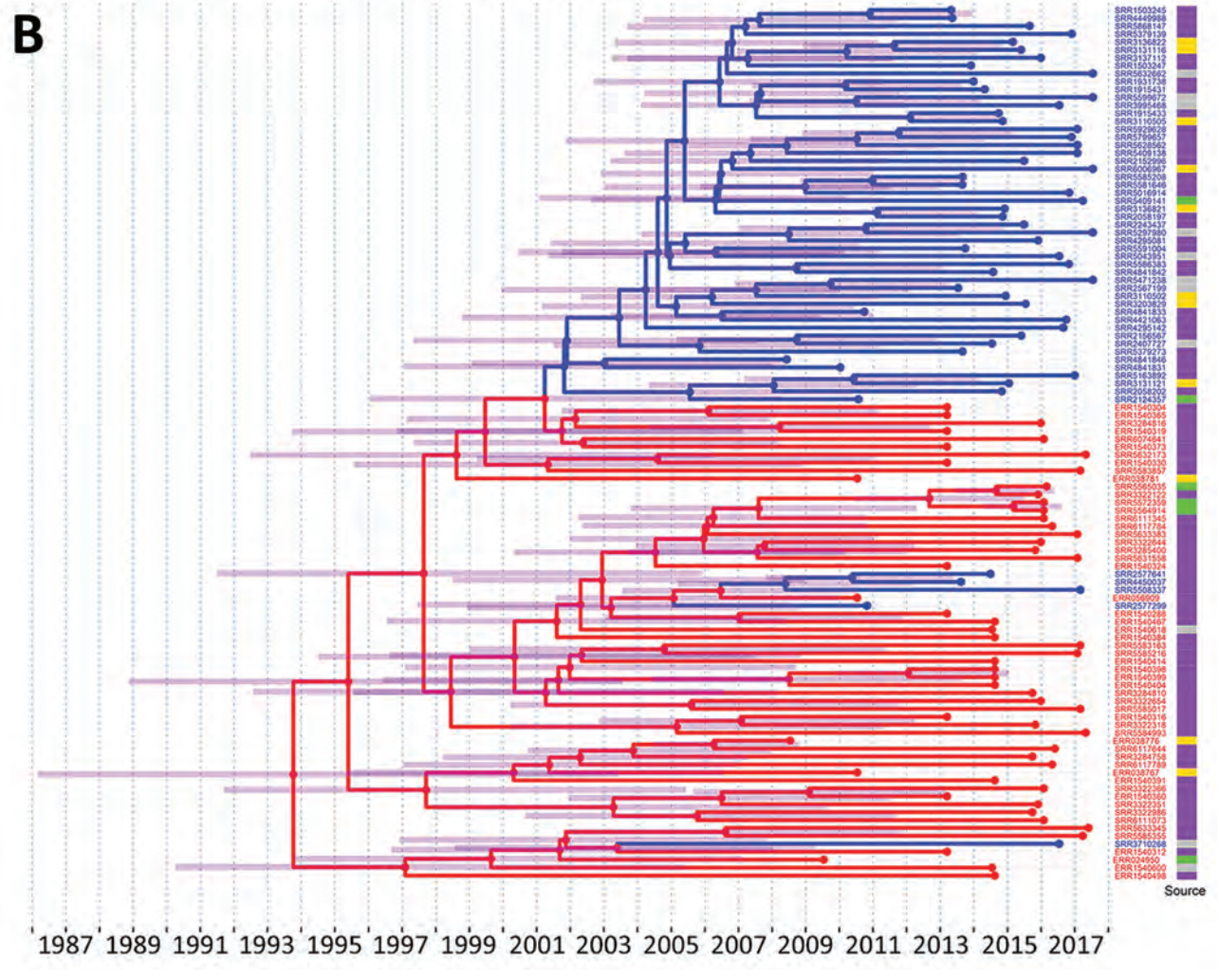

Figure 1. Demographic reconstruction and phylogenetic analysis of *Salmonella enterica* subspecies *enterica* 4,[5],12:i:- sequence type 34 isolates. A) Demographic reconstruction (subset 2) shows the population exponential growth of over time. The red line indicates the median effective population size with 95% highest posterior density credible interval (gray). B) Time-scaled phylogenetic analysis of isolates in subset 2 (n = 110 sequences after duplicates removal). Isolates were collected from multiple sources in the United States (blue) and Europe (red) during 2008–2017. An asymmetric discrete trait analysis model was used to reconstruct the locations on the nodes. The nodes, branches, and tree tips were annotated according to the collection location. The 95% highest posterior density credible intervals of node heights are indicted with transparent purple bars. The posterior probability for all inferred ancestral locations was >70%. The isolate source (food product, gray; human, purple; livestock, yellow; and other, green) is depicted in the heatmap appended to the tree tips.

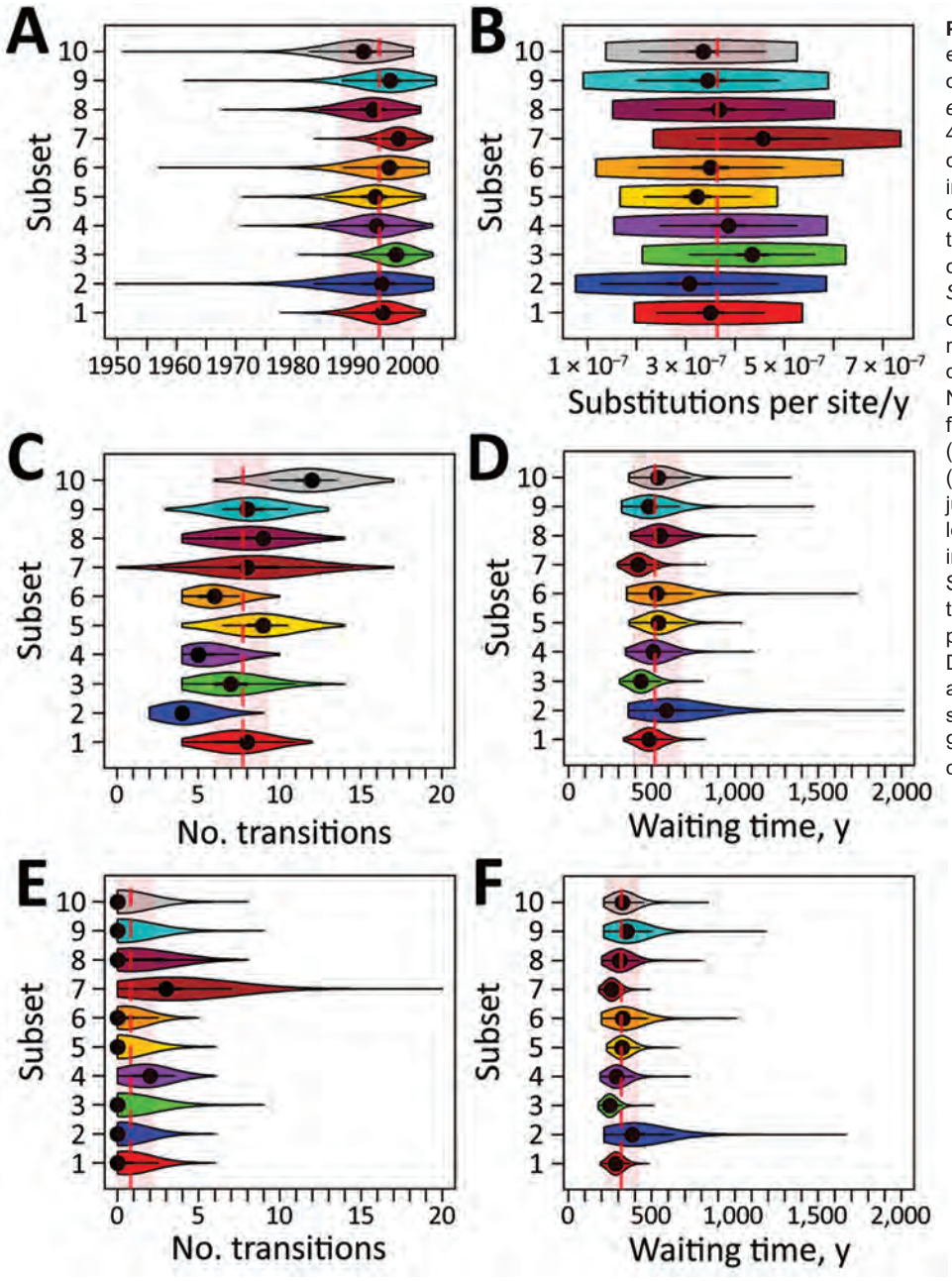

Figure 2. Summary of posterior estimates of all 10 subsets of sequences of *Salmonella enterica* subspecies *enterica* 4,[5],12:i:- sequence type (ST) 34 collected from multiple sources in the United States and Europe during 2008–2017. A) Inferred time (year) of the most recent common ancestor of the emerging *Salmonella* 4,[5],12:i:- ST34 clade. B) Estimated mutation rate (uncorrelated log-normally distributed mean parameter). C–F) Number of unobserved transitions from Europe to the United States (C) and United States to Europe (E) along each branch (Markov jumps) and total phylogenetic tree length spent (Markov rewards) in Europe (D) and the United States (F). Violin plots illustrate the posterior distribution and probability density of each subset. Dashed red vertical lines indicate average posterior value; red shaded areas indicate average 95% highest posterior density credible interval of all subsets.

States. The exponential growth rate of the population was estimated at 0.316/year (averaged across all subset means; Figure 1). In addition, the estimated (averaged) main introduction into the United States was 2004 (95% HPD 2000–2006; Appendix 2 Table 1). The occurrence of several additional smaller introductions was suggested by 48 sequences (6 from Europe and 42 from the United States). The 6 sequences from Europe were recovered from human sources; among sequences from the United States, 28 were from humans, 5 from food products, 6 from livestock, and 3 from other sources. Information on recent international travel was obtained for 22/28 of US isolates from humans, 2 of whom had traveled (1 to the Philippines and the other to France [S. Meyer et al., Minnesota Department of Health, pers. comm., 2019 Sep 23]).

Among the 1,431 *Salmonella* 4,[5],12:i:- ST34 sequences, 978 (68.34%) had genetic determinants contributing to the ASSuT profile, 108 (7.55%) conferred resistance to quinolones, and 82 (5.73%) conferred resistance to extended-spectrum cephalosporins. The probability of harboring most predominant acquired antimicrobial resistance genes (AARGs) conferring the resistance phenotypes described above was significantly higher for

Table. Association between collection location and presence of resistance genetic determinants in sequences of *Salmonella enterica* subspecies *enterica* serotype 4,[5],12:i:- sequence type 34 isolates collected in Europe and the United States, 2008–2017*

Conferring resistance to	Presence of genetic resistance determinants	No. positives/total (%)		Odds ratio (95% CI), United States vs. Europe	p value†
		Europe	United States		
ASSuT	ASSuT‡	406/690 (58.84)	572/741 (77.19)	2.37 (1.87–3.00)	**<0.001**
Extended-spectrum cephalosporins	bla_{CTX-M} genes§	4/690 (0.58)	14/741 (1.89)	3.30 (1.03–13.84)	0.032
	bla_{CMY-2}	2/690 (0.29)	37/741 (4.99)	18.06 (4.63–155.09)	**<0.001**
	bla_{SHV-12}	0/690¶	27/741 (3.64)	53.15 (3.24–873.11)	**<0.001**
Quinolones	*qnrB19*	9/690 (1.3)	51/741 (6.88)	5.59 (2.70–13.01)	**<0.001**
	qnrB2	0/690¶	20/741 (2.7)	39.24 (2.36–650.05)	**<0.001**
	qnrS1	6/690 (0.87)	13/741 (1.75)	2.03 (0.72–6.57)	0.22
	aac(6')-Ib-cr	1/690 (0.14)	19/741 (2.56)	18.11 (2.86–751.91)	**<0.001**

*ASSuT indicates ampicillin, streptomycin, sulfonamides, and tetracycline.
†A statistically significant *p value* (boldface) is <0.05/8 = 0.00625 (adjusted for multiple comparisons using Bonferroni's correction).
‡Simultaneous presence of bla_{TEM-1}, *strA*, *strB*, *sul2*, and *tet(B)* genes (Appendix 2, https://wwwnc.cdc.gov/EID/article/26/12/20-0336-App2.pdf).
§Including $bla_{CTX-M-1}$ (n = 1), $bla_{CTX-M-14}$ (n = 2), $bla_{CTX-M-55}$ (n = 14), and $bla_{CTX-M-65}$ (n = 1).
¶Haldane-Anscombe correction (adding 0.5 to all 4 cells) was used to account for cells with a value of 0.

sequences of US isolates (odds ratio 2.37–26.05; Table). Yet associations between the collection location and the presence of bla_{CTX-M} or *qnrS1* genes were not significant (Table). In addition, AARGs conferring resistance to colistin (*mcr*-1/*mcr*-3/*mcr*-5; Appendix 1) were detected in isolates from Europe only (n = 5).

Conclusions

Salmonella 4,[5],12:i:- ST34 was introduced into the United States from Europe on multiple occasions since the beginning of the 21st century. The main introduction occurred in 2004; additional independent introductions resulted in small clades for which the predominant sources were human travelers and imported food products. Human travelers (*6*) and imported food products (*7*) have been described as potential vehicles for introduction of salmonellae.

The date of introduction of the main clade into the United States is later than the first peer-reviewed report of a *Salmonella* 4,[5],12:i:- infection in the country in 1998 (*2*). However, given the antimicrobial susceptibility profile of isolates from that report (mostly not ASSuT) (*2*), they most likely belonged to the nonemerging ST19 clade, which was described elsewhere (*4*). In addition, the incidence of *Salmonella* 4,[5],12:i:- in humans increased only modestly (9.5%) during 2006–2011 but increased dramatically (78.3%) during 2011–2016 (*8*). A similar increase in detection after 2011 was described for clinical cases in swine from the midwestern United States (*9*). The difference between the date of main introduction into the United States found in this study and the later sharp increase in its prevalence in animals and humans may in part result from changes in reporting practices and increasing awareness (*8*). However, the increase since 2011 can be the result of rapid propagation of the ST34 population, possibly associated with swine (*4*). Moreover, White et al. (*10*) recently reported that according to the National Antibiotic Resistance Monitoring System, the percentage of ASSuT-resistant *Salmonella* 4,[5],12:i:- from humans increased from 17% in 2009 to 59.1% in 2015 (out of all *Salmonella* 4,[5],12:i:- clinical isolates from humans). This increase probably resulted to a large extent from ST34 strains, in which this phenotype is predominant. The estimated exponential yearly growth rate determined in our model (0.316/year), which corresponds to a population doubling time of 2.2 years, is in agreement with this dramatic increase of the ST34 population.

The presence of AARGs conferring resistance to quinolones and extended-spectrum cephalosporins has mainly been observed since 2014 and may be biased by the lack of sequences before 2013 (Appendix 2 Figure 12). Yet AARGs conferring resistance to quinolones were not found in *Salmonella* 4,[5],12:i:- ST34 strains from Europe collected before 2010 (*1*), and therefore our findings may reflect an increasing prevalence of these resistance determinants. Given time and overall unidirectionality of *Salmonella* 4,[5],12:i:- ST34 transmission from Europe to the United States, it is likely that the acquisition of AARGs to quinolones occurred independently in the United States and in Europe. Yet introduction of resistant strains from the United States to Europe is also possible. Contributors to the acquisition of resistance in the United States might be the approval for enrofloxacin use in swine in the United States since 2008 (*11*) and the potential dissemination of plasmids harboring AARGs to quinolones between *Salmonella* serotypes (*12*). Independent acquisition of resistance to quinolones by *Salmonella* in Asia has also been suggested (*13*). The presence of *mcr* resistance genes conferring resistance to colistin in sequences from Europe (n = 5) is alarming, given their recent worldwide spread (*14*). However, further investigation of the travel history associated with these cases may be required because the acquisition of *mcr* genes

may be travel associated (*15*). The spread of *Salmonella* 4,[5],12:i:- ST34 from Europe to the United States and the presence of plasmid-mediated resistance genes to key antimicrobial classes such as quinolones, extended-spectrum cephalosporins, and colistin in this clade further highlights its potential risk to public health and emphasizes the need for robust surveillance and mitigation programs for such transboundary pathogens.

Acknowledgments

We thank staff members from the Minnesota Department of Health Foodborne, Waterborne, Vectorborne, and Zoonotic Diseases Section for providing the travel history records and for their advice on this work.

This work was supported by the Global Food Venture-MnDRIVE Initiative, the National Institute of Food and Agriculture (Animal Health Formula Fund project MIN-62-091) of the US Department of Agriculture, the Rapid Agricultural Response Fund, and the Swine Disease Eradication Center at the University of Minnesota. In addition, the United States-Israel Binational Agricultural Research and Development Fund awarded a Vaadia-BARD postdoctoral fellowship (no. FI-565-17) to E.E. A.E.M. is a Food Standards Agency research Fellow and is supported by the Biotechnology and Biological Sciences Research Council Institute Strategic Programme Microbes in the Food Chain BB/R012504/1 and its constituent project BBS/E/F/000PR10348 (Theme 1, Epidemiology and Evolution of Pathogens in the Food Chain). The Ramón y Cajal postdoctoral contract from the Spanish Ministry of Economy, Industry and Competitiveness (MINECO) (RYC-2016-20422) was awarded to J.A.

About the Author

Dr. Elnekave is a veterinarian and epidemiologist who has been working as a postdoctoral fellow in the Veterinary Population Medicine Department, University of Minnesota, and is a faculty member in the Koret School of Veterinary Medicine at the Robert H. Smith Faculty of Agricultural, Food and Environmental Sciences at the Hebrew University of Jerusalem, Israel. His primary research interest is the epidemiology of bacterial foodborne pathogens. He uses genetic tools and Bayesian models to study pathogen emergence, evolution, and antimicrobial resistance.

References

1. Petrovska L, Mather AE, AbuOun M, Branchu P, Harris SR, Connor T, et al. Microevolution of monophasic *Salmonella* Typhimurium during epidemic, United Kingdom, 2005–2010. Emerg Infect Dis. 2016;22:617–24. https://doi.org/10.3201/eid2204.150531
2. Agasan A, Kornblum J, Williams G, Pratt CC, Fleckenstein P, Wong M, et al. Profile of *Salmonella enterica* subsp. enterica (subspecies I) serotype 4,5,12:i:- strains causing food-borne infections in New York City. J Clin Microbiol. 2002;40:1924–9. https://doi.org/10.1128/JCM.40.6.1924-1929.2002
3. Centers for Disease Control and Prevention. National *Salmonella* surveillance overview. Atlanta: US Department of Health and Human Services; 2011.
4. Elnekave E, Hong S, Mather AE, Boxrud D, Taylor AJ, Lappi V, et al. *Salmonella enterica* serotype 4,[5],12:i:- in swine in the United States midwest: an emerging multidrug-resistant clade. Clin Infect Dis. 2018;66:877–85. https://doi.org/10.1093/cid/cix909
5. Drummond AJ, Rambaut A. BEAST: Bayesian Evolutionary Analysis by Sampling Trees. BMC Evol Biol. 2007;7:214. https://doi.org/10.1186/1471-2148-7-214
6. Williamson DA, Lane CR, Easton M, Valcanis M, Strachan J, Veitch MG, et al. Increasing antimicrobial resistance in nontyphoidal *Salmonella* isolates in Australia from 1979 to 2015. Antimicrob Agents Chemother. 2018;62:e02012-17. https://doi.org/10.1128/AAC.02012-17
7. Gould LH, Kline J, Monahan C, Vierk K. Outbreaks of disease associated with food imported into the United States, 1996–2014. Emerg Infect Dis. 2017;23:525–8. https://doi.org/10.3201/eid2303.161462
8. Centers for Disease Control and Prevention. National *Salmonella* surveillance annual report, 2016: Atlanta: US Department of Health and Human Services; 2018.
9. Hong S, Rovira A, Davies P, Ahlstrom C, Muellner P, Rendahl A, et al. Serotypes and antimicrobial resistance in *Salmonella enterica* recovered from clinical samples from cattle and swine in Minnesota, 2006 to 2015. PLoS One. 2016;11:e0168016. https://doi.org/10.1371/journal.pone.0168016
10. White PL, Green AL, Holt KG, Hale KR. Multidrug-resistant *Salmonella enterica* subspecies I serovar 4,[5],12:i:- isolates recovered from Food Safety and Inspection Service-regulated products and food animal ceca, 2007-2016. Foodborne Pathog Dis. 2019;16:679–86. https://doi.org/10.1089/fpd.2018.2573
11. Food and Drug Administration. NADA 141–068 in the approved animal drug products (Green Book) [cited 2020 Aug 31]. https://animaldrugsatfda.fda.gov/adafda/views/#/home/previewsearch/141-068
12. Elnekave E, Hong SL, Lim S, Hayer SS, Boxrud D, Taylor AJ, et al. Circulation of plasmids harboring resistance genes to quinolones and/or extended-spectrum cephalosporins in multiple *Salmonella enterica* serotypes from swine in the United States. Antimicrob Agents Chemother. 2019;63:e02602-18. https://doi.org/10.1128/AAC.02602-18
13. Mather AE, Phuong TLT, Gao Y, Clare S, Mukhopadhyay S, Goulding DA, et al. New variant of multidrug-resistant *Salmonella enterica* serovar Typhimurium associated with invasive disease in immunocompromised patients in Vietnam. MBio. 2018;9:e01056-18. https://doi.org/10.1128/mBio.01056-18
14. McEwen SA, Collignon PJ. Antimicrobial resistance: a One Health perspective. Microbiol Spectr. 2018;6.
15. Arnott A, Wang Q, Bachmann N, Sadsad R, Biswas C, Sotomayor C, et al. Multidrug-resistant *Salmonella enterica* 4,[5],12:i:- sequence type 34, New South Wales, Australia, 2016–2017. Emerg Infect Dis. 2018;24:751–3. https://doi.org/10.3201/eid2404.171619

Address for correspondence: Ehud Elnekave, Koret School of Veterinary Medicine, Robert H. Smith Faculty of Agricultural, Food and Environmental Sciences, The Hebrew University, PO Box 12, Rehovot 76100, Israel; email: ehud.elnekave@mail.huji.ac.il or udie79@gmail.com

Hypervirulent *Klebsiella pneumoniae* as Unexpected Cause of Fatal Outbreak in Captive Marmosets, Brazil

Juliana Mariotti Guerra, Natália Coelho Couto de A. Fernandes, Alessandra Loureiro Morales dos Santos, Joana de Souza Pereira Barrel, Bruno Simões Sergio Petri, Liliane Milanelo, Monique Ribeiro Tiba-Casas, Alcina Maria Liserre, Cláudia Regina Gonçalves, Cláudio Tavares Sacchi, José Luiz Catão-Dias, Carlos Henrique Camargo.

After the sudden death of captive marmosets in São Paulo, Brazil, we conducted a histologic and microbiologic study. We found hyperacute septicemia caused by hypermucoviscous sequence type 86 K2 *Klebsiella pneumoniae.* We implemented prophylactic antimicrobial therapy, selected dedicated staff for marmoset interactions, and sanitized the animals' fruit to successfully control this outbreak.

Klebsiella pneumoniae is an opportunistic bacteria that is a normal part of the nasopharyngeal and gastrointestinal tract microbiome of humans and animals (*1*). The hypermucoviscous variant of *K. pneumoniae* (hvKp), initially described in Southeast Asia, has emerged as a pathogen affecting young and healthy persons worldwide (*2*). The development of prominent polysaccharide capsules associated with capsular serotypes K1 or K2 have been reported as the major virulence determinants for human hvKp in liver abscesses, perhaps because it seems to protect the bacteria from phagocytosis and prevents destruction by bactericidal serum factors (*2*).

K. pneumoniae strains have also been associated with a variety of diseases in animals, especially in Old World (Africa, Asia, and Europe) and New World (Oceana, North America, and South America) nonhuman primates (*3*–*5*). Sudden death or various clinical signs, including anorexia, prostration, fever, cough, dyspnea, mucopurulent discharge, meningitis, pneumonia, peritonitis, and sepsis are strongly associated with sporadic infections of *K. pneumoniae* in common marmosets research colonies (*5*,*6*).

Despite the well-recognized zoonotic importance of hvKp and the public health risk of emerging multidrug-resistant strains (*7*–*9*), information is incomplete about the genotypic and phenotypic characterization of the etiologic agent essential to adequately diagnose and treat this pathogen in captive and wild nonhuman primates. The aim of this study was to report an epizootic among common marmosets in a wildlife rehabilitation center in Brazil and to describe the serotype, sequence typing, virulence properties, and resistance profile of the *K. pneumoniae* strains involved.

The Study

On February 10–11, 2019, a total of 11 captive marmosets (8 *Callithrix penicillata*, 2 C. *jacchus*, and 1 hybrid) died suddenly without clinical signs of disease. All of the animals were maintained in Parque Ecológico do Tietê, located in São Paulo municipality, São Paulo, Brazil, which is a center for receiving, rehabilitating, and referring wildlife. All animals had been in captivity 123–399 days. No new animals had been introduced into the cages in the previous 25 days. Each necropsy was performed <24 h after death in accordance with the Brazil Ministry of Health's guide for surveillance of epizootics in nonhuman primates (*10*). Tissue samples were preserved in phosphate-buffered formalin 10% and processed for routine histopathology and for 12 hours in refrigeration for microbiologic and molecular analyses. This study was approved by the Ethics Committee for the Use of

Author affiliations: Instituto Adolfo Lutz, São Paulo, Brazil (J.M. Guerra, N.C.C.A. Fernandes, A.L.M. dos Santos, J.S.P. Barrel, M.R. Tiba-Casas, A.M. Liserre, C.R. Gonçalves, C.T. Sacchi, C.H. Camargo); Universidade de São Paulo, São Paulo (Fernandes N.C.C.A., A.L.M. dos Santos, J.L. Catão-Dias); Parque Ecológico do Tietê, São Paulo (B.S.S. Petri, L. Milanelo)

DOI: https://doi.org/10.3201/eid2612.191562

Table 1. Histologic findings for tissue samples from captive marmosets analyzed by microscopic evaluation in investigation of a fatal epizootic caused by highly virulent *Klebsiella pneumoniae* sequence type 86 strain P04 in Brazil, 2019

Organ	No. samples	Histologic findings	Positive/total
Liver	10	Sinusoidal leukocytosis, predominantly with neutrophilia	9/10
		Hemorrhagic foci	7/10
		Hepatitis necrotizing, suppurative, acute, multifocal	2/10
		Intravascular fibrin deposition	1/10
Spleen	9	Splenitis necrotizing, suppurative, acute, multifocal	8/9
		Hemorrhage	8/9
		Many bacilli on the red pulp	8/9
Lung	10	Subacute interstitial pneumonia	8/10
		Occasional free bacilli	7/10
		Hemorrhage	1/10
Cerebrum	10	Bacilli on leptomeninges	1/10
Adrenal	2	Adrenalitis necrotizing, suppurative, acute, multifocal	2/2
Heart	7	Myocarditis necrotizing, acute, multifocal	1/7
Intestine	7	Enteritis neutrophilic, acute, diffuse	2/7
Kidney	8	Granular tubular casts	4/8
		Tubular acute necrosis	1/8

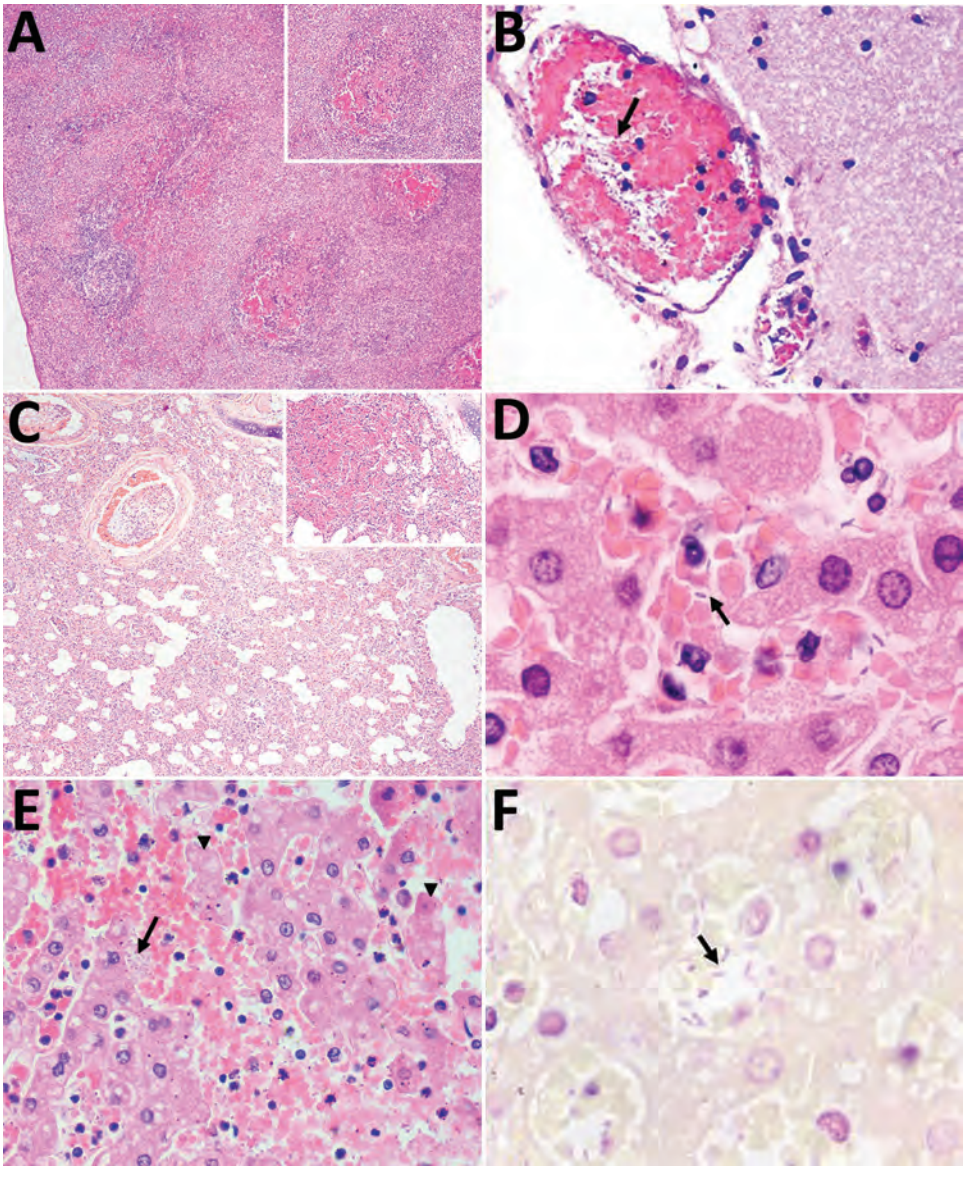

Figure 1. Microscopic findings of histological and histochemical examination of tissue samples from captive marmosets in investigation of a fatal epizootic caused by highly virulent *Klebsiella pneumoniae* sequence type 86 strain P04 in Brazil, 2019. A) Spleen shows necrosis in germinal centers, suppurative splenitis, and hemorrhage (inset: necrosis in germinal center). Hematoxylin and eosin stain (H&E); original magnification ×4. B) Brain (meninges) shows bacterial rods inside vascular lumen (arrow). H&E stain; original magnification ×40. C) Lung shows sinterstitial pneumonia (H&E stain; original magnification ×4) and alveolar hemorrhage (inset; H&E stain; original magnification ×10). D–F) Liver samples. D) Numerous intravascular bacilli (arrow). H&E stain; original magnification ×100. E) Hepatocellular necrosis (arrowheads) associated with numerous bacterial rods (arrow) and neutrophils in the sinusoids. H&E stain; original magnification ×40. F) Sinusoids filled with gram-negative bacterial structures (arrow) and neutrophils. Gram stain; original magnification ×1,000.

Animals (CEUA) of Adolfo Lutz Institute, Brazil (protocol no. 11/2016), SISBIO registration no. 50551 for the manipulation of wildlife material, and SISGEN registration nos. A1A2A72 and A7EB4B6.

Histologic findings from all of the animals were compatible with hyperacute septicemia. Multiple sections of liver, spleen, and adrenal tissue were similarly affected by suppurative and necrotizing multifocal lesions associated with intrahistiocytic gram-negative bacteria, 1–2-μm long. We also observed numerous intravascular gram-negative bacilli in samples from the liver (10 of 10 samples; the sample from 1 marmoset was excluded because the animal showed severe postmortem autolysis), cerebrum (8/10), lungs (3/10), heart (1/7), intestines (1/7), thymus (1/2), and skeletal muscle (1/1). Other relevant microscopic findings from different tissues are summarized in Table 1 and Figure 1. We found no microscopic alterations in the analyzed fragment samples from the stomach, tongue, testis, thymus, skin, uterus, or lymph nodes.

Pure cultures of *K. pneumoniae,* positive for the string test (*11*), were recovered from the brain and liver in 8 different animals. The representative isolate P04 displayed susceptibility to all the antimicrobial agents we evaluated using the broth microdilution methodology with Sensititre plate (Thermo Fisher Scientific, https://www.thermofisher.com), according to the manufacturer's instructions (Table 2). We screened for *K. pneumoniae* in environmental samples of water from a lake near the primate cages by filtration and in drag swabs from their cages by direct growth on MacConkey agar plates. Although we recovered *K. pneumoniae* isolates from both samples, all of them were negative in the string test. We subjected all isolates identified as *K. pneumoniae* to DNA macrorestriction by using 30 U of XbaI enzyme followed by pulsed-field gel electrophoresis (PFGE) (https://www.cdc.gov/pulsenet/pathogens/pfge.html). PFGE results showed the same restriction profile among the isolates recovered from the dead animals; however, environmental isolates clustered apart from the invasive isolates (Figure 2).

We subjected the P04 strain to whole genome sequencing using the Thermo Fisher Ion Torrent S5 platform, resulting in 1,049,163 reads; the de novo assembled genome comprised 5,358,608 bps grouped in 62 contigs, with an average coverage depth of 53. The whole-genome shotgun project reported here was deposited in DDBJ/EMBL/GenBank under accession number SPSP00000000.

We employed online platforms from PubMLST (https://pubmlst.org) to definitively identify species as *K. pneumoniae*, sequence type (ST) 86, capsular type K2, and multiple virulence genes: *mrkABCDFHIJ* cluster (mannose-resistant *Klebsiella*-like type III fimbriae cluster, associated with adhesiveness and fimbrial filament formation to adhere to eukaryotic cells) (*12*) in the same contig of the *kvgAS* genes; *iroBCD* genes (salmochelin) in the same contig with the *rmpA* gene (regulator of mucoid phenotype A); and *rmpA2* gene within the contig along the *iucABD* with the *iutA* genes (aerobactin) (http://bigsdb.pasteur.fr). We detected only the constitutive antimicrobial-resistant genes bla_{SHV-1}, *oqx*AB, and *fos*A by the in silico analysis (Comprehensive Antibiotic Resistance Database, https://card.mcmaster.ca). Phylogenetic analysis of high quality single-nucleotide polymorphisms (SNPs) built on the CSI Phylogeny 1.4 (Center for Genomic Epidemiology, https://cge.cbs.dtu.dk/services/CSIPhylogeny) showed that the ST86 isolates were closely related and the P04 strain clustered closely with IPEUC340, an isolate recovered in 1975 in France (Appendix, https://wwwnc.cdc.gov/EID/article/26/12/19-1562-App1.pdf). The isolate RJF293, ST374, clustered apart from the ST86 isolates (Appendix Figure).

To contain the spread of hvKp to other animals, metaphylatic therapy with trimethoprim/sulfamethoxazole was implemented by adding the antimicrobial to the water supply of animals during the first 5 days after the fatal cases were identified. In addition, access to the cages was restricted to a dedi-

Table 2. Antimicrobial susceptibility profile of highly virulent *Klebsiella pneumoniae* sequence type 86 strain P04 from a fatal epizootic among captive marmosets in Brazil, 2019*

Antimicrobial	MIC, mg/L†	Category
Amikacin	<4.0	Susceptible
Ampicillin/sulbactam	8/4	Susceptible
Aztreonam	<2	Susceptible
Cefepime	<2	Susceptible
Cefotaxime	<2	Susceptible
Ceftazidime	<1.0	Susceptible
Ciprofloxacin	<0.06	Susceptible
Colistin	<0.25	Susceptible
Doripenem	<0.5	Susceptible
Doxycycline	2.0	Susceptible
Gentamicin	<1.0	Susceptible
Imipenem	<1.0	Susceptible
Levofloxacin	<1.0	Susceptible
Meropenem	<1.0	Susceptible
Minocycline	4.0	Susceptible
Piperacillin/tazobactam	<8/4	Susceptible
Polymyxin B	<0.25	Susceptible
Sulfamethoxazole/trimethoprim	<0.5/9.5	Susceptible
Ticarcillin/clavulanic Acid	<16/2	Susceptible
Tigecycline‡	0.5	Susceptible
Tobramycin	<1.0	Susceptible

*Susceptibility determined by Sensititre (ThermoFisher, https://www.thermofisher.com).
†MIC values were categorized as susceptible, intermediate, or resistance following Clinical and Laboratory Standards Institute (https://clsi.org) M100-S30 breakpoints (http://em100.edaptivedocs.net/dashboard.aspx).
‡Tigecycline breakpoint followed Food and Drug Administration recommendations.

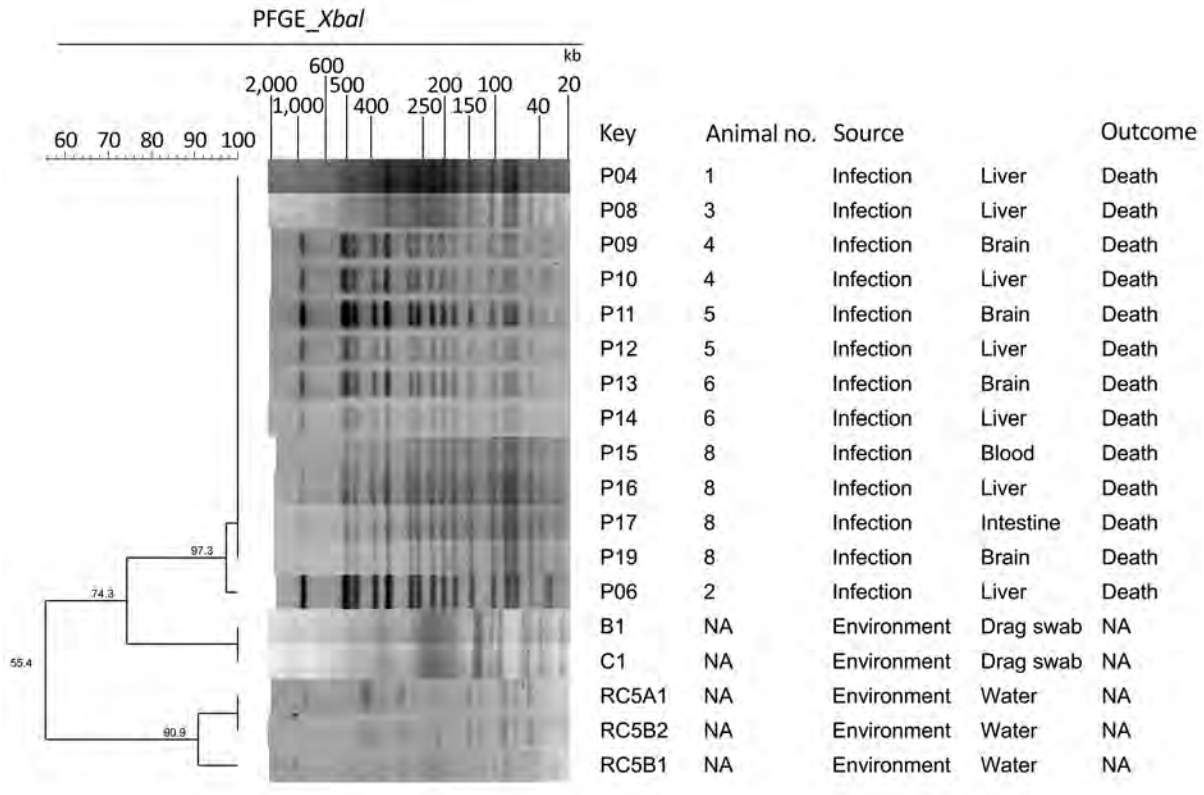

Figure 2. Dendrogram and pulsed-field gel electrophoresis (PFGE) typing of XbaI-restricted *Klebsiella pneumoniae* strains from captive marmosets in investigation of a fatal epizootic caused by highly virulent *K. pneumoniae* sequence type 86 in Brazil, 2019. PFGE profiles were defined based on 100% Dice similarity cutoff value of the UPGMA clustering method (1.5% optimization; 1.5% tolerance). The Universal Size Standard Strain H9812 (*Salmonella* Braenderup) was used as reference in all gels. NA, not applicable.

cated employee, who wore clothing exclusively for accessing the cages for the duration of the outbreak. We also implemented additional steps for sanitizing fruit eaten by the marmosets with 2% sodium hypochlorite for 15 minutes and dedicated space and staff for preparing the marmosets' meals after the epizootic event.

Conclusions

We report the detection of hypermucoviscous *K. pneumoniae* ST86 K2 as cause of a sudden fatal outbreak in captive marmosets. Implementing prompt containment measures led to successful control of this outbreak. The burden of hypermucoviscous *K. pneumoniae* ST86 K2 in unexpected reservoirs, including those in contact with people, deserves further investigation. The emergence of these strains is a concern for human and veterinary health because of the potential for these bacteria to acquire multidrug-resistant genes, their capacity to persist in the environment and to infect a wide range of hosts, and the unavailability of vaccines against these strains for humans and animals (*13*). The expansion of this emerging pathogen among different reservoirs should be carefully surveilled, because the relationship between hypervirulent and multidrug-resistant strains is narrowing.

Acknowledgments

We thank the team of curators of the Institut Pasteur MLST and whole genome MLST databases for curating the data and making them publicly available and all contributors from the Center of Pathology at Adolfo Lutz Institute in São Paulo for routine sample processing.

About the Author

Dr. Guerra is a veterinary pathologist and scientific researcher at the Center of Pathology at Adolfo Lutz Institute in São Paulo, Brazil. Her research focuses on the comparative pathology of emerging and reemerging infectious diseases in the context of an integrated One Health approach.

References

1. Bueno MG, Iovine RO, Torres LN, Catão-Dias JL, Pissinatti A, Kierulff MC, et al. Pneumonia and bacteremia in a golden-headed lion tamarin (*Leontopithecus chrysomelas*) caused by *Klebsiella pneumoniae* subsp. pneumoniae during a translocation program of free-ranging animals in Brazil. J Vet Diagn Invest. 2015;27:387–91. https://doi.org/10.1177/1040638715584792
2. Russo TA, Marr CM. Hypervirulent *Klebsiella pneumoniae*. Clin Microbiol Rev. 2019;32:e00001-19. https://doi.org/10.1128/CMR.00001-19
3. Fox JG, Rohovsky MW. Meningitis caused by *Klebsiella* spp in two rhesus monkeys. J Am Vet Med Assoc. 1975;167:634–6.
4. Gonzalo A, Montoya E. *Klebsiella pneumoniae* infection in a New World nonhuman primate center. Laboratory Primate Newsletter 1991;30:13–20 [cited 2019 Oct 20]. https://www.brown.edu/Research/Primate/lpn30-2.html#kleb
5. Pisharath HR, Cooper TK, Brice AK, Cianciolo RE, Pistorio AL, Wachtman LM, et al. Septicemia and peritonitis in a colony of common marmosets (*Callithrix jacchus*) secondary to *Klebsiella pneumoniae* infection. Contemp Top Lab Anim Sci. 2005;44:35–7.
6. Kindlovits A, Kindlovits L. Clinic and therapeutics in neotropical primates [in Portuguese]. 2nd ed. Rio de Janeiro: L.F. Livros; 2009.
7. Wu F, Ying Y, Yin M, Jiang Y, Wu C, Qian C, et al. Molecular characterization of a multidrug-resistant *Klebsiella pneumoniae* strain R46 isolated from a rabbit. Int JGenomics. 2019;2019:5459190. https://doi.org/10.1155/2019/5459190
8. Osman KM, Hassan HM, Orabi A, Abdelhafez AST. Phenotypic, antimicrobial susceptibility profile and virulence factors of *Klebsiella pneumoniae* isolated from buffalo and cow mastitic milk. Pathog Glob Health. 2014;108:191–9. https://doi.org/10.1179/2047773214Y.0000000141
9. Boszczowski I, Salomão MC, Moura ML, Freire MP, Guimarães T, Cury AP, et al. Multidrug-resistant *Klebsiella pneumoniae*: genetic diversity, mechanisms of resistance to polymyxins and clinical outcomes in a tertiary teaching hospital in Brazil. Rev Inst Med Trop São Paulo. 2019;61:e29. https://doi.org/10.1590/s1678-9946201961029
10. Brasil Ministério da Saúde. Guide for surveillance of epizootics in nonhuman primates and entomology applied to yellow fever surveillance [in Portuguese]. 2nd ed. Brasília: Brazil Ministry of Health; 2014.
11. Siu LK, Yeh K-M, Lin J-C, Fung C-P, Chang F-Y. *Klebsiella pneumoniae* liver abscess: a new invasive syndrome. Lancet Infect Dis. 2012;12:881–7. https://doi.org/10.1016/S1473-3099(12)70205-0
12. Gerlach GF, Clegg S, Allen BL. Identification and characterization of the genes encoding the type 3 and type 1 fimbrial adhesins of *Klebsiella pneumoniae*. J Bacteriol. 1989;171:1262–70. https://doi.org/10.1128/JB.171.3.1262-1270.1989
13. Cox BL, Schiffer H, Dagget G Jr, Beierschmitt A, Sithole F, Lee E, et al. Resistance of *Klebsiella pneumoniae* to the innate immune system of African green monkeys. Vet Microbiol. 2015;176:134–42. https://doi.org/10.1016/j.vetmic.2015.01.001

Address for correspondence: Carlos Henrique Camargo, Instituto Adolfo Lutz, Centro de Bacteriologia, Núcleo de Doenças Entéricas e Infecções por Patógenos Especiais, Avenida Dr. Arnaldo, 351–9° Andar, Pacaembú, São Paulo, Brazil; email: carlos.camargo@ial.sp.gov.br

Identification of a Novel α-herpesvirus Associated with Ulcerative Stomatitis in Donkeys

Vito Martella, Gianvito Lanave, Michele Camero, Vittorio Larocca, Eleonora Lorusso, Cristiana Catella, Paolo Capozza, Maria Tempesta, Canio Buonavoglia

An outbreak of ulcerative stomatitis with was observed in a donkey (*Equus asinus*) dairy herd. Similar lesions were also observed on the dams' udders and, sporadically, in genital areas. The lesions typically resolved in 1–3 weeks. An α-herpesvirus, *Varicellovirus*, genetically related to equid herpesvirus type 3, was identified.

Vesicular stomatitis is a consequential disease of equids. Vesicular stomatitis virus (family *Rhabdoviridae*, genus *Vesiculovirus*) is a major infectious agent with zoonotic potential that is common in the Americas. A few other infectious viral agents (equine arteritis virus, bunyavirus, caliciviruses, equine adenoviruses, and herpesviruses) have been associated with this condition in horses, but on several occasions the etiology of vesicular and ulcerative stomatitis remains undiagnosed (*1*). Noninfectious etiology may include plant- and drug-related toxicoses and photosensitization (*1*).

In October 2011, an outbreak of ulcerative stomatitis started in a donkey (*Equus asinus*) dairy herd, comprising 106 animals, located in the prefecture of Bari, Apulia region, Italy. The outbreak appeared related to the introduction of a pregnant female 8 weeks before the onset of the disease. The mare was clinically healthy and in good physical condition at arrival and gave birth to a foal after 7 weeks. Clinical signs developed in neither the dam nor the foal.

Initially, the outbreak affected 34 animals (17 lactating mares with their foals). This group was separated with wood fences from the other animals, but not strictly. Fever and small nodular lesions, evolving into painful ulcers, were observed on the oral mucosa, tongue, and skin around the lips of young animals (2 weeks–4 months old) (Figure 1). Similar lesions were also observed sporadically on the dams' udders and genital areas. The lesions typically resolved in 1–3 weeks. The herd owner reported weight loss in foals and interruption of lactation in dams. Two weeks after onset in the original group, the disease was observed in a separate group of animals, comprising 63 adult or yearling females and 5 yearling males. In this group, however, oral lesions were observed only in 5 yearlings and 1 mare. A third group of 4 adult males was kept apart from the other animals and was not affected by the disease.

Oral swab and serum samples collected from 8 animals with acute disease were sent to the laboratories at the University of Bari (Valenzano, Italy) for virologic investigation. Using an electron microscope, we observed herpesvirus-like particles in the oral swabs and detected herpesvirus DNA using consensus herpesvirus primers for the DNA polymerase and inverse terminase (*2*,*3*). We used BLASTn (https://blast.ncbi.nlm.nih.gov) to search the GenBank genetic sequence database and found the virus to be highly related to equid herpesvirus (EHV) 3 in the DNA polymerase (93.35% nt identity) and terminase (90.71% nt identity) regions.

We isolated the virus onto equine dermal cells from oral swab specimens. The virus was titrated and used for screening serum samples collected from the donkeys in virus neutralization assays. We detected specific neutralizing antibodies in the serum samples collected from approximately three quarters (80/106) of the animals 2 months after the beginning of the outbreak but not in the serum samples of 8 animals with acute infection, suggesting seroconversion.

To sequence the DNA of the isolate, we performed next generation sequencing using the Illumina MiSeq platform (https://www.illumina.com) and used Nextera XT (Illumina) for library preparation. We obtained the full genome sequence (147,607 bp) of asinine herpesvirus (AsHV) strain AsHV/Bari/2011/740 and annotated it using the software ORF Finder (https://www.bioinformatics.org).

Author affiliation: University of Bari, Valenzano, Italy

DOI: https://doi.org/10.3201/eid2612.200201

Figure 1. Foals with herpesviral infection, part of an outbreak of ulcerative stomatitis in a donkey dairy herd, Bari, Italy. Ulcerative lesions were observed on the lips (A), oral mucosa (B), and tongue (C).

On full genome sequence analysis, strain AsHV/Bari/2011/740 appeared genetically related (87.02% nt identity) to EHV-3 strain AR/2007/C3A (accession no. KM051845) (subfamily *a-Herpesviridae*, genus *Varicellovirus*). Three different full-length gene targets (glycoproteins B, C, and D) of strain AsHV/Bari/2011/740 were aligned with cognate sequences representative of the genus *Varicellovirus* listed by the International Committee on Taxonomy of Viruses (https://talk.ictvonline.org) by using Geneious software version 9.1.8 (Biomatters Ltd., https://www.geneious.com) and the MAFFT algorithm (*4*). We performed phylogenetic analyses with MEGAX software (https://www.megasoftware.net) (*5*) using the

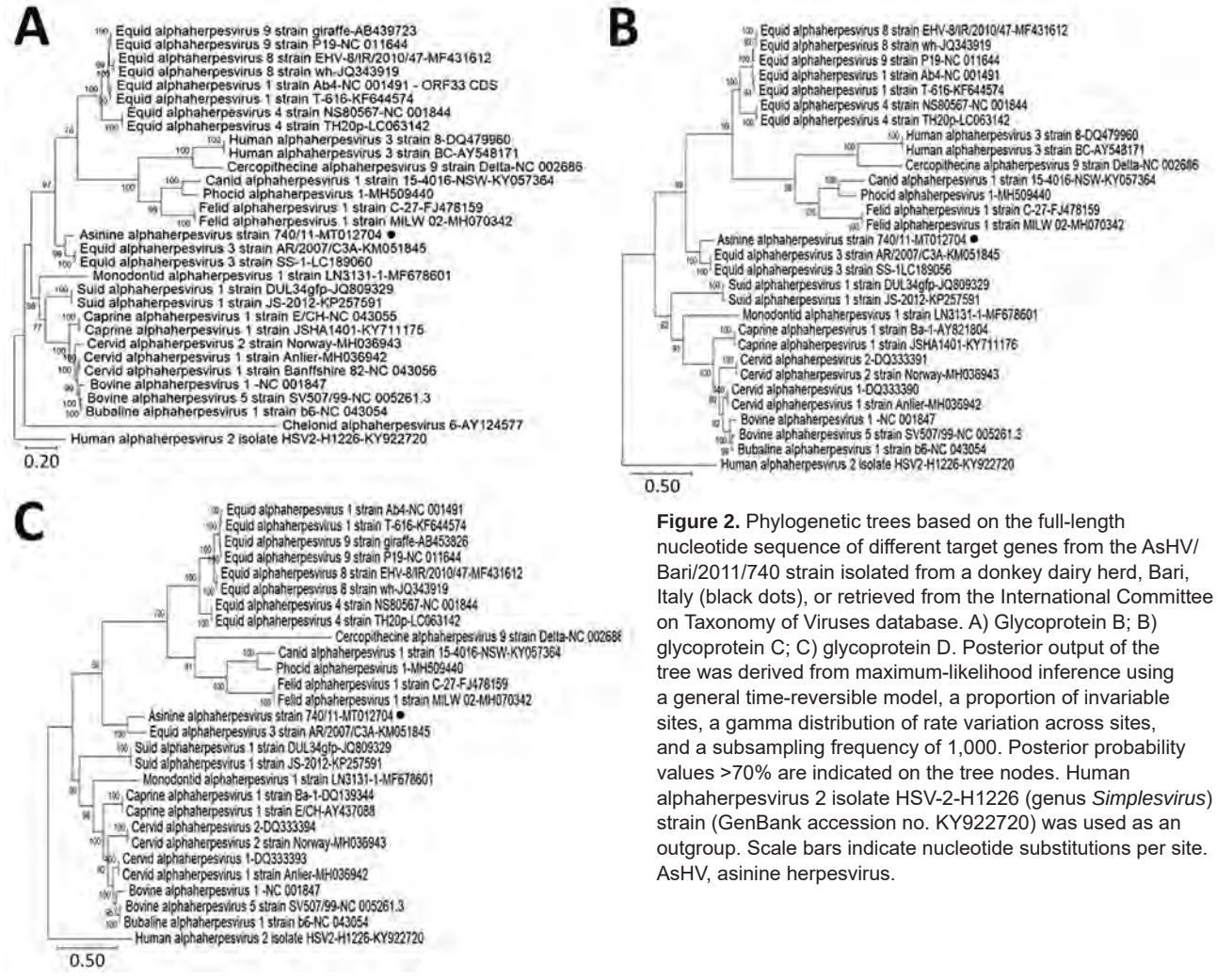

Figure 2. Phylogenetic trees based on the full-length nucleotide sequence of different target genes from the AsHV/Bari/2011/740 strain isolated from a donkey dairy herd, Bari, Italy (black dots), or retrieved from the International Committee on Taxonomy of Viruses database. A) Glycoprotein B; B) glycoprotein C; C) glycoprotein D. Posterior output of the tree was derived from maximum-likelihood inference using a general time-reversible model, a proportion of invariable sites, a gamma distribution of rate variation across sites, and a subsampling frequency of 1,000. Posterior probability values >70% are indicated on the tree nodes. Human alphaherpesvirus 2 isolate HSV-2-H1226 (genus *Simplesvirus*) strain (GenBank accession no. KY922720) was used as an outgroup. Scale bars indicate nucleotide substitutions per site. AsHV, asinine herpesvirus.

Table. List of equid herpesviruses recognized in the ICTV database or other sources*

Species	Subfamily	Related to	Other designations	Source
EHV-1	Alpha	NA	Equine abortion	ICTV
EHV-2	Gamma	NA	NA	ICTV
EHV-3	Alpha	NA	Coital exantema	ICTV
EHV-4	Alpha	NA	Equine rhinopneumonitis	ICTV
EHV-5	Gamma	NA	NA	ICTV
EHV-6	Alpha	EHV-3	AsHV-1	(*6*); this study
EHV-7	Gamma	EHV-2/EHV-5	AsHV-2	ICTV
EHV-8	Alpha	EHV-1	AsHV-3	ICTV
AsHV-4	Gamma	EHV-2/EHV-5	NA	(*11*)
AsHV-5	Gamma	EHV-2/EHV-5	NA	(*11*)
AsHV-6	Gamma	EHV-2/EHV-5	NA	(*2*)
EHV-9	Alpha	EHV-1	Zebra, gazelle, giraffe herpesviruses	ICTV

*AsHV, asinine herpesvirus; EHV, equine herpesvirus; ICTV, International Committee on Taxonomy of Viruses; NA, not applicable.

maximum-likelihood method with the general time-reversible model, a proportion of invariant sites, and a discrete gamma distribution (5 categories) to model evolutionary rate differences among sites, and bootstrap analyses with 1,000 pseudoreplicate datasets. In the consensus phylogenetic trees (Figure 2), strain AsHV/Bari/2011/740 was closely related to EHV-3 sequences and distantly related to other members of the genus *Varicellovirus*. We deposited the full-genome sequence of strain AsHV/Bari/2011/740 in the GenBank database (accession no. MT012704).

To date, several herpesviruses have been discovered in donkeys (Table). AsHV type 1, also called EHV-6, is an α-herpesvirus associated with ulcerative lesions (*6*). AsHV-2 (EHV-*7*) is a γ-herpesvirus identified in leukocytes of healthy animals (*7*). AsHV-3 (EHV-8) was isolated from the nose of immunodepressed animals (*8*) and was classified as an α-herpesvirus on the basis of the glycoprotein G sequence and poor antigenic cross-reactivity with EHV-1 and EHV-4 (*8*–*10*). AsHV-4, -5, and -6 are γ-herpesviruses identified from donkeys with interstitial pneumonitis (*2*,*11*).

We report the detection and isolation of a novel AsHV from an outbreak of vesicular and ulcerative stomatitis and mammillitis in a donkey dairy herd. By comparing it with other herpesvirus sequences from the databases, we identified 3 targets (glycoproteins B, C, and D) for which the sequences were available across all the varicelloviruses listed in the ICTV database and that were used for phylogenetic analysis. In these analyses, the AsHV strain appeared similar to EHV-3. By reviewing the literature, we found another donkey herpesvirus, AsHV-1, genetically related to EHV-3 on the basis of restriction enzyme and hybridization analyses (*6*). AsHV-1 was originally isolated from the vesicular and erosive lesions of the muzzle of a foal and the external genitalia and udder of its dam (*12*). Unfortunately, the prototype AsHV-1 is no longer available and it is not possible to determine its genome sequence for precise comparison (G.F. Browning, pers. comm.). It is possible that AsHV/Bari/2011 is actually an AsHV-1 strain, although this possibility cannot be confirmed.

Overall, based on the chronology of the health events observed in the herd, the tendency of herpesviruses to reactivate from latent infection under stress conditions, and the seroconversion observed in the monitored animals, we hypothesized that the newly introduced mare was the vehicle for herpesvirus infection in the herd, although this possibility could not be conclusively confirmed. Also, we screened only 8 animals during the acute phase of the disease, and we do not have an exact picture of the immunological status of the animals before the onset of the disease.

In conclusion, we identified a novel AsHV, genetically related to EHV-3, from an outbreak of infectious ulcerative stomatitis in donkey foals. These findings extend the spectrum of pathologies potentially attributable to herpesviruses in donkeys. Considering the nature and shape of the lesions, the virus should be included in the differential diagnosis of vesicular and ulcerative stomatitis among equids. Also, it needs to be determined whether the novel AsHV can be transmitted to horses.

Acknowledgments

We are grateful to Aristide Maggiolino for collecting the animal samples and to Carlo Armenise and Arturo Gentile for their support in laboratory work.

The authors dedicate this work to the memory of Professor Leland Eugene "Skip" Carmichael (June 15 1930–July 27 2020), College of Veterinary Medicine, Cornell University, Ithaca, NY, USA, for his contribution to the growth of veterinary virology, his decades-long friendship and scientific collaboration, and his profound sense of humanity.

About The Author

Dr. Martella is a full professor in the Department of Veterinary Medicine, University of Bari, Italy. His research

is focused on diagnosis, epidemiology, and characterization of human and animal viruses, with particular interest for zoonotic viruses.

References

1. McCluskey BJ, Mumford EL. Vesicular stomatitis and other vesicular, erosive, and ulcerative diseases of horses. Vet Clin North Am Equine Pract. 2000;16:457–69, viii–ix. https://doi.org/10.1016/s0749-0739(17)30089-5
2. Kleiboeker SB, Chapman RK. Detection of equine herpesvirus 3 in equine skin lesions by polymerase chain reaction. J Vet Diagn Invest. 2004;16:74–9. https://doi.org/10.1177/104063870401600113
3. VanDevanter DR, Warrener P, Bennett L, Schultz ER, Coulter S, Garber RL, et al. Detection and analysis of diverse herpesviral species by consensus primer PCR. J Clin Microbiol. 1996;34:1666–71. https://doi.org/10.1128/JCM.34.7.1666-1671.1996
4. Katoh K, Misawa K, Kuma K, Miyata T. MAFFT: a novel method for rapid multiple sequence alignment based on fast Fourier transform. Nucleic Acids Res. 2002;30:3059–66. 10.1093/nar/gkf436 https://doi.org/10.1093/nar/gkf436
5. Kumar S, Stecher G, Li M, Knyaz C, Tamura K. MEGA X: molecular evolutionary genetics analysis across computing platforms. Mol Biol Evol. 2018;35:1547–9. https://doi.org/10.1093/molbev/msy096
6. Browning GF, Ficorilli N, Studdert MJ. Asinine herpesvirus genomes: comparison with those of the equine herpesviruses. Arch Virol. 1988;101:183–90. https://doi.org/10.1007/BF01310999
7. Bell SA, Pusterla N, Balasuriya UB, Mapes SM, Nyberg NL, MacLachlan NJ. Isolation of a gammaherpesvirus similar to asinine herpesvirus-2 (AHV-2) from a mule and a survey of mules and donkeys for AHV-2 infection by real-time PCR. Vet Microbiol. 2008;130:176–83. https://doi.org/10.1016/j.vetmic.2007.12.013
8. Crabb BS, Allen GP, Studdert MJ. Characterization of the major glycoproteins of equine herpesviruses 4 and 1 and asinine herpesvirus 3 using monoclonal antibodies. J Gen Virol. 1991;72:2075–82. https://doi.org/10.1099/0022-1317-72-9-2075
9. Ficorilli N, Studdert MJ, Crabb BS. The nucleotide sequence of asinine herpesvirus 3 glycoprotein G indicates that the donkey virus is closely related to equine herpesvirus 1. Arch Virol. 1995;140:1653–62. https://doi.org/10.1007/BF01322539
10. Paweska JT, Gerdes T, Van Heerden J. Serological relationship between a donkey alphaherpesvirus (isolate M7/91) and equid herpesvirus type 1 and 4. J S Afr Vet Assoc. 1994;65:64–6.
11. Kleiboeker SB, Schommer SK, Johnson PJ, Ehlers B, Turnquist SE, Boucher M, et al. Association of two newly recognized herpesviruses with interstitial pneumonia in donkeys (*Equus asinus*). J Vet Diagn Invest. 2002;14:273–80. PubMed https://doi.org/10.1177/104063870201400401
12. Burrows R. Discussion. In: Bryans JT, Gerber H, editors. Equine infectious diseases III. Proceedings of the Third International Conference on Equine Infectious Diseases; 1972 Jul 17–21; Paris. Basel: S Karger; 1973

Address for correspondence: Vito Martella, Department of Veterinary Medicine, University of Bari, S.p. per Casamassima km 3, 70010, Valenzano, Bari, Italy; email: vito.martella@uniba.it

Human Rickettsiosis Caused by *Rickettsia parkeri* Strain Atlantic Rainforest, Urabá, Colombia

Margarita Arboleda, Leidy Y. Acevedo-Gutiérrez, Alejandra Ávila, Dairo Ospina, Francisco J. Díaz, David H. Walker, Juan D. Rodas

We describe the clinical, serologic, and molecular findings of a new human rickettsiosis in Colombia. Antibodies against *Rickettsia* spp. were detected. PCR showed amplification of genes for *R. parkeri* strain Atlantic Rainforest. This new rickettsiosis of minor virulence could explain some of the undifferentiated acute febrile diseases in Colombia.

Among the numerous causes of acute undifferentiated nonmalarial febrile illness, rickettsiae are amenable to treatment that can prevent death or, in the case of non–life-threatening diseases, shorten and ameliorate the course of illness (*1*). Awareness and knowledge of these infectious diseases are crucial and necessary. In Colombia, Rocky Mountain spotted fever was recognized in the 1930s and then rediscovered in the 21st century (*2*). Clusters of cases were documented in the departments of Cundinamarca, Córdoba, and Antioquia (*2*–*4*). Five fatal cases of Rocky Mountain spotted fever occurred in the village of Las Changas in the district of Necoclí in 2006, and 4 fatal cases occurred in a village in the district of Turbo in 2008 (*4*). Prevalence of antibodies to spotted fever group (SFG) rickettsiae of 25.6% among healthy residents of several areas in Colombia suggests contact of persons with less-virulent SFG rickettsiae, such as *Rickettsia parkeri*, which has previously been reported in Colombia in ticks of the species *Amblyomma ovale*, and *R. amblyommatis,* previously reported in *A. cajennense* ticks (*5*–*7*).

Author affiliations: Instituto Colombiano de Medicina Tropical–CES, Medellín, Colombia (M. Arboleda); Universidad de Antioquia, Medellín (L.Y. Acevedo-Gutiérrez, F.J. Díaz, J.D. Rodas); Clínica Aurora y Universidad Pontificia Bolivariana, Medellín (A. Ávila); Clínica Chinita, Apartadó, Colombia (D. Ospina); University of Texas Medical Branch, Galveston, Texas, USA (D. Walker)

DOI: https://doi.org/10.3201/eid2612.200388

The Case

A previously healthy 47-year-old male farmer who lived in a rural area near the village of Puerto López in the district of Turbo, Department of Antioquia, Colombia, came to a clinic in Apartadó with a 5-day history of fever. He also reported chills, asthenia, nausea, loss of appetite, dark urine, and dysuria that began 1 day after discovery of a tick on the left flank of his abdomen. On physical examination he appeared to be in generally good condition; no rash was identified, and he was afebrile with normal vital signs.

A 13 × 16 mm crust with an erythematous halo and scaling collaret was seen above the left iliac crest at the site of the tick bite, accompanied by ipsilateral visible tender inguinal lymphadenopathy 3.5 cm in length (Figure). Results of the patient's complete blood counts were within reference ranges, and blood smear detected no plasmodia.

Because of the eschar, draining lymphadenopathy, and history of tick bite, a rickettsial infection was suspected, and the patient was referred to the Colombian Institute of Tropical Medicine in Apartadó, Antioquia. There, a punch biopsy of the inoculation eschar and scraping of the eschar base and blood samples were obtained, and treatment with doxycycline (200 mg/d for 7 d) was initiated. The patient subsequently reported defervescence after 48 hours, with disappearance of symptoms and decreased lymphadenopathy.

The patient's serum samples were examined by indirect immunofluorescence assay for antibodies reactive with 6 rickettsiae: *R. rickettsii* strain Uramita, *R. parkeri* strain At24, *R. amblyommatis* strain Ac37, *R. rhipicephali* strain HJ5, *R. bellii* strain Mogi, and *Candidatus* Rickettsia colombianensi (slides donated by Marcelo Labruna, Faculdade de Medicina Veterinária e Zootecnia, Universidade de São Paulo, São Paulo, Brazil). DNA was extracted from the eschar crust,

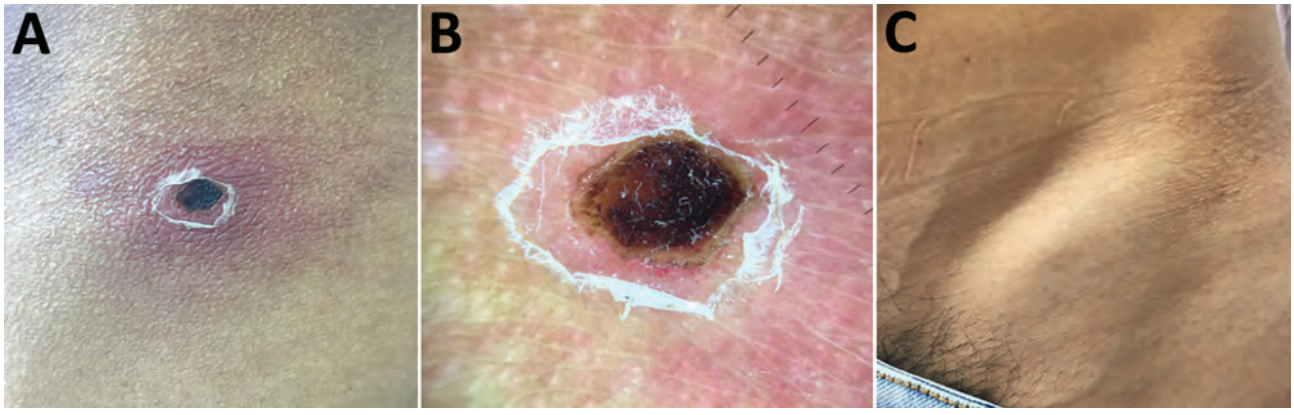

Figure. Eschar of inoculation and lymphadenopathy in patient with febrile syndrome caused by a strain of *Rickettsia parkeri*, Colombia. A) A 1 .3 × 1.6 cm eschar with an erythematous halo is present at the site of a tick bite above the left iliac crest. B) A closer view reveals a brown-black crust and a collarette of desquamation. C) Distended skin overlying enlarged draining lymph nodes, 3.5 cm in length, is visible in the left inguinal region.

eschar biopsy, and scrapings with the DNeasy Blood and Tissue kit (QIAGEN, https://www.qiagen.com), according to the manufacturer's instructions. The samples were processed by PCR for *gltA*, *sca0*, *sca4*, and *sca5* genes of *Rickettsia* using previously described primers and methods (*8*). The amplification products were sent for sequencing to Macrogen, and the sequences were analyzed with BLASTn (https://blast.ncbi.nlm.nih.gov), MEGA 7.0 (https://www.megasoftware.net), and MrBayes 3.2.6 (https://www.geneious.com). The human protocol was approved by the Bioethical Committee at the University of Antioquia (act 001/2016).

Indirect fluorescent antibody testing demonstrated seroconversion to all 6 *Rickettsia* antigens. Acute serum samples showed reactivity with none of the antigens at a titer of 64, whereas seroconversion to each of the antigens was observed by reactivity with *R. parkeri* (titer 1,024); *R. rickettsii* (titer 512); *R. bellii* (titer 256); and *R. amblyommatis*, *Candidatus* R. colombianensi, and *R. rhipicephali* (titer 128), without a quadruple difference between the different antigens.

Amplicons were obtained for all genes tested and all samples analyzed. All the sequences demonstrated 100% identity with *R. parkeri* strain Atlantic Rainforest and were submitted to GenBank (accession nos. MK860199–202).

Previous patients with rickettsial infections in the Department of Antioquia were gravely ill with rapid deterioration and respiratory and renal compromise, hepatic injury, and case-fatality rates of 28%–35% (*4*). In contrast, *R. parkeri* infections are mild or moderate acute febrile illnesses with fever, chills, headache, arthromyalgia, inoculation eschar, maculopapular or vesicular rash, and painful lymphadenopathy at lymphatic drainage sites of the entry lesion. Some patients do not manifest lymphadenopathy or, as in this patient, a rash (*9*).

In 2004, a new SFG human infection attributed to *R. parkeri* sensu stricto was described in the United States (*10*); later, Spolidorio et al. described a patient in Brazil with a clinically identical moderate febrile condition, with myalgia, arthralgia, and eschar, caused by a strain of *R. parkeri* designated Atlantic Rainforest (*11*). Human infections with similar signs and symptoms caused by *R. parkeri* sensu stricto and *R. parkeri* strain Atlantic Rainforest have been documented in the United States, Brazil, Uruguay, Argentina, and now in Colombia; meanwhile, these bacteria have also been demonstrated in ticks (in the absence of recognized human infections) in Bolivia, Peru, Nicaragua, Belize, and Mexico. *Amblyomma maculatum*, *A. triste*, and *A. tigrinum* ticks have been found infected with *R. parkeri* sensu stricto in nature; *R. parkeri* strain Atlantic Rainforest has been reported in *A. ovale, A. aureolatum*, and *Dermacentor parumapertus* ticks (*12*,*13*). *R. parkeri* strain Atlantic Rainforest was previously identified in *A. ovale* ticks in Colombia, where dogs are suspected of bringing the ticks into homes (*6*).

Conclusions

There may be a substantial unrecognized occurrence of *R. parkeri* infections in South and Central America. Increased awareness and knowledge by primary care physicians and establishment of effective national surveillance programs and guidelines, including empiric treatment with doxycycline, would lead to improved patient outcomes. Enhanced research to identify the range of vectors, vertebrate hosts, and risk factors to predict human exposure to this and other agents that may be causing similar diseases would contribute to the elucidation of the causes of acute febrile illnesses in Latin America.

Acknowledgments

We are grateful to Colciencias through the National Doctorate program (647/2014) and to Andrés Londoño for the confirmation of the *ompA* gene. We express our gratitude to the Fogarty International Center for the help and advice obtained through the Research Training Program on the Impact of Zoonotic and Vector-borne Viruses, Rickettsiae, and Leptospira in Acute Undifferentiated Febrile Illnesses (D43 TW010331).

The Universidad de Antioquia provided financial support through the CODI project 2014-321 and the Sustainability Program 2018–2019.

About the Author

Dr. Arboleda is the coordinator of the Colombian Institute of Tropical Medicine Branch in Apartado, Colombia. She works as a clinician, taking care of patients with endemic febrile diseases such as dengue, malaria, leptospirosis, and other acute undifferentiated febrile illnesses.

References

1. Lin L, Decker CF. Rocky Mountain spotted fever. Dis Mon. 2012;58:361–9. https://doi.org/10.1016/j.disamonth.2012.03.008
2. Patino L, Afanador A, Paul JH. A spotted fever in Tobia, Colombia: preliminary report. Am J Trop Med Hyg. 1937; s1-17:639–53. https://doi.org/10.4269/ajtmh.1937.s1-17.639
3. Hidalgo M, Lizarazo D, Ovalle M, Castañeda E, Heredia D, Zambrano P, et al. Brote de rickettsiosis en Los Córdobas, departamento de Córdoba, Febrero–Marzo 2007. Inf Quinc Epidemiol Nac. 2007;12:118–20.
4. Pacheco O, Giraldo M, Martinez M, Hidalgo M, Galeano A, Echeverri E, et al. Estudio de brote febril hemorrágico en el corregimiento de Alto de Mulatos—Distrito Especial Portuario de Turbo, Antioquia, enero de 2008. Inf Quinc Epidemiol Nac. 2008;13:145–60.
5. Quintero V JC, Paternina T LE, Uribe Y A, Muskus C, Hidalgo M, Gil J, et al. Eco-epidemiological analysis of rickettsial seropositivity in rural areas of Colombia: a multilevel approach. PLoS Negl Trop Dis. 2017;11:e0005892. https://doi.org/10.1371/journal.pntd.0005892
6. Faccini-Martínez ÁA, Ramírez-Hernández A, Forero-Becerra E, Cortés-Vecino JA, Escandón P, Rodas JD, et al. Molecular evidence of different *Rickettsia* species in Villeta, Colombia. Vector Borne Zoonotic Dis. 2016;16:85–7. https://doi.org/10.1089/vbz.2015.1841
7. Londoño AF, Díaz FJ, Valbuena G, Gazi M, Labruna MB, Hidalgo M, et al. Infection of *Amblyomma ovale* by *Rickettsia* sp. strain Atlantic rainforest, Colombia. Ticks Tick Borne Dis. 2014;5:672–5. https://doi.org/10.1016/j.ttbdis.2014.04.018
8. Oteo JA, Nava S, Sousa R de, Mattar S, Venzal JM, Abarca K, et al. Guías Latinoamericanas de la RIICER para el diagnóstico de las rickettsiosis transmitidas por garrapatas. Rev Chil Infectología. 2014;31:54–65.
9. Kelman P, Thompson CW, Hynes W, Bergman C, Lenahan C, Brenner JS, et al. *Rickettsia parkeri* infections diagnosed by eschar biopsy, Virginia, USA. Infection. 2018;46:559–63. https://doi.org/10.1007/s15010-018-1120-x
10. Paddock CD, Sumner JW, Comer JA, Zaki SR, Goldsmith CS, Goddard J, et al. *Rickettsia parkeri*: a newly recognized cause of spotted fever rickettsiosis in the United States. Clin Infect Dis. 2004;38:805–11. https://doi.org/10.1086/381894
11. Spolidorio MG, Labruna MB, Mantovani E, Brandão PE, Richtzenhain LJ, Yoshinari NH. Novel spotted fever group rickettsiosis, Brazil. Emerg Infect Dis. 2010;16:521–3. https://doi.org/10.3201/eid1603.091338
12. Parola P, Paddock CD, Socolovschi C, Labruna MB, Mediannikov O, Kernif T, et al. Update on tick-borne rickettsioses around the world: a geographic approach. Clin Microbiol Rev. 2013;26:657–702. https://doi.org/10.1128/CMR.00032-13
13. Nieri-Bastos FA, Marcili A, De Sousa R, Paddock CD, Labruna MB. Phylogenetic evidence for the existence of multiple strains of *Rickettsia parkeri* in the New World. Appl Environ Microbiol. 2018;84:e02872-17. https://doi.org/10.1128/AEM.02872-17

Address for correspondence: David Walker, University of Texas Medical Branch, 301 University Blvd, Keiller Bldg, Galveston, TX 77555-0609, USA; email: dwalker@utmb.edu

Shedding of Marburg Virus in Naturally Infected Egyptian Rousette Bats, South Africa, 2017

Janusz T. Pawęska, Nadia Storm, Wanda Markotter, Nicholas Di Paola, Michael R. Wiley, Gustavo Palacios, Petrus Jansen van Vuren

We detected Marburg virus RNA in rectal swab samples from Egyptian rousette bats in South Africa in 2017. This finding signifies that fecal contamination of natural bat habitats is a potential source of infection for humans. Identified genetic sequences are closely related to Ravn virus, implying wider distribution of Marburg virus in Africa.

The genus *Marburgvirus*, family *Filoviridae*, comprises 1 species, *Marburg marburgvirus*, which comprises 2 marburgviruses, Marburg virus (MARV) and Ravn virus (RAVV) (*1*). Marburgviruses cause sporadic but often fatal MARV disease in humans and nonhuman primates (*2*). The Egyptian rousette bat (*Rousettus aegyptiacus*) has been implicated as the primary reservoir for marburgviruses (*3*–*9*), but the mechanisms by which they are maintained in these bats remain elusive. Evidence of marburgvirus circulation was reported from countries where MARV disease outbreaks have not been recorded (*10*–*12*). Determining the risks for spread and developing evidence-based public health strategies to prevent zoonotic transmission requires up-to-date knowledge about marburgvirus geographic range; genetic diversity; and transmission mechanisms, including natural ports of entry and shedding patterns. To clarify which marburgviruses are circulating and how they are maintained in Egyptian rousette bat populations in South Africa, we tested oral and rectal swab samples and blood samples collected during a previously identified peak season of marburgvirus transmission in a local Egyptian rousette bat population (*13*).

Author affiliations: National Institute for Communicable Diseases of the National Health Laboratory Service, Johannesburg, South Africa (J.T. Pawęska, N. Storm, P. Jansen van Vuren); Boston University, Boston, Massachusetts, USA (N. Storm); University of Pretoria, Pretoria, South Africa (J.T. Pawęska, W. Markotter); University of Nebraska Medical Center, Omaha, Nebraska, USA (N. Di Paola, M.R. Wiley, G. Palacios); US Army Medical Research Institute of Infectious Diseases, Frederick, Maryland, USA (N. Di Paola, M.R. Wiley, G. Palacios); Australian Centre for Disease Preparedness, Commonwealth Scientific and Industrial Research Organisation–Health and Biosecurity, Geelong, Victoria, Australia (P. Jansen van Vuren)

DOI: https://doi.org/10.3201/eid2612.202108

The Study

We conducted this work in accordance with approved protocols by animal ethics committees of the National Health Laboratory Service (Johannesburg, South Africa; AEC 137/12) and the University of Pretoria (Pretoria, South Africa; EC054–14). During February–November 2017, a total of 1,674 Egyptian rousette bats (February, 107 bats; April, 600; May, 563; September, 214; November, 190) were captured, aged, and sampled at Matlapitsi Cave, Limpopo Province, South Africa, as described previously (*13*). We collected and processed oral and rectal swab samples from each bat and blood from a subset of 423 bats, as described previously (*7*). Swab samples were collected and pooled by aliquoting 4 × 25 μL of the media of each sample into a microcentrifuge tube, yielding a total of 416 pools containing 100 μL of pooled rectal swab samples and 4 pools containing 50 or 75 μL of pooled oral swab samples. We conducted serologic, virologic, and molecular tests as described previously (*7*). In addition, we conducted real-time quantitative reverse transcription PCR (qRT-PCR) for individual swab samples when the pool tested positive. We prepared sequencing libraries using the TruSeq RNA Access Kit (Illumina, https://www.illumina.com) with MARV-specific bait enrichment, followed by sequencing on an Illumina NextSeq, genomic alignment and phylogenetic analysis (*13*). We calculated the significance of differences in several positive swab samples and seropositivity using the Fisher exact test in Stata version 13 (StataCorp, https://www.stata.com).

Seven rectal swab pools (5 from April 2017 and 2 from September 2017) were qRT-PCR positive; the remaining rectal swab samples collected during

February–November 2017 were all negative. The number of individual positive rectal swab samples ranged from 1 to 3 per positive pool, totaling 11 positive samples. Only 1 oral swab sample pool, from April 2017, yielded a positive qRT-PCR result, containing a single positive oral swab sample (Table 1). Of 600 rectal swab samples collected during 3 nights in April, 9 (1.5%) were positive; of 215 rectal swab samples collected during 2 nights in September, 2 (0.9%) were positive. We found no significant difference between the number of positive rectal swab samples collected in April and the number collected September. The number of positive rectal swab samples differed significantly from the number of positive oral swab samples collected in April ($p = 0.02$). Attempts to culture marburgvirus from qRT-PCR–positive swab samples were unsuccessful. Identical results from specimens with cycle threshold (C_t) >30 were obtained in other studies (*6*,*13*).

Table 1. qRT-PCR results of oral and rectal swab samples from juvenile Egyptian rousette bats (*Rousettus aegyptiacus*) at Matlapitsi Cave, Limpopo Province, South Africa, February–November 2017*

			Swab sample type and qRT-PCR result, C_t†	
Bat ID	Capture date	Sex	Oral	Rectal
Apr-77	Apr 4	F	Negative	30.61
Apr-117	Apr 4	F	Negative	30.57
Apr-118	Apr 4	F	Negative	30.95
Apr-124	Apr 4	F	Negative	30.66
Apr-133	Apr 4	F	Negative	30.46
Apr-232	Apr 5	F	33.01	Negative
Apr-369	Apr 6	F	Negative	31.9
Apr-380	Apr 6	M	Negative	32.67
Apr-399	Apr 6	F	Negative	31.7
Apr-470	Apr 6	M	Negative	31.8
8025	Sep 26	F	Negative	31.7
0895	Sep 20	F	Negative	33.05

*C_t, cycle threshold; ID, identification; qRT-PCR, quantitative real-time reverse transcription PCR.
†Negative, C_t >40.

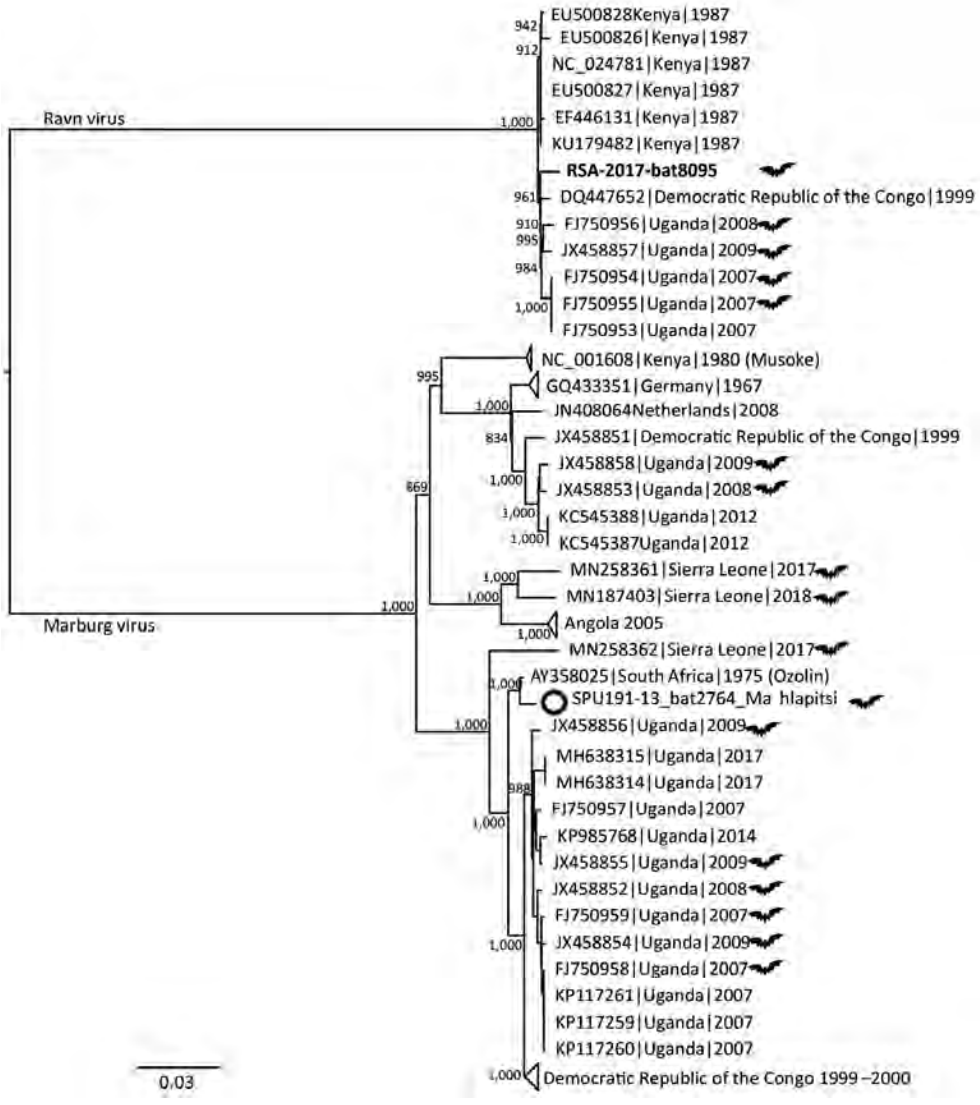

Figure 1. Midpoint-rooted, maximum-likelihood phylogeny of complete and near-complete MARV and RAVV genomes. Phylogenetic tree shows evolutionary relationships of marburgvirus detected in a rectal swab sample from a subadult Egyptian rousette female bat (*Rousettus aegyptiacus*) in Matlapisi Cave, Limpopo Province, South Africa, 2017 (black filled circle; GenBank accession no. MT321489), and reference viruses, including the SPU191-13 bat 2764 Mahlapitsi strain (white circle; GenBank accession no. MG725616), detected in the same cave in July 2013. Complete and near-complete genome sequences from GenBank (accession numbers indicated) were aligned with the partial MARV sequence obtained from RSA-8095bat using MUSCLE version 3.8.31 (https://www.drive5.com/muscle), and RAxML version 8.2.10 (https://cme.h-its.org/exelixis/web/software/raxml/index.html) was used to infer the best-scoring maximum-likelihood tree after 1,000 bootstrap replicates. Node values indicate the bootstrap support values. Genomes isolated from bats are shown using a bat symbol. Scale bar indicates nucleotide substitutions per site. MARV, Marburg virus; RAVV, Ravn virus.

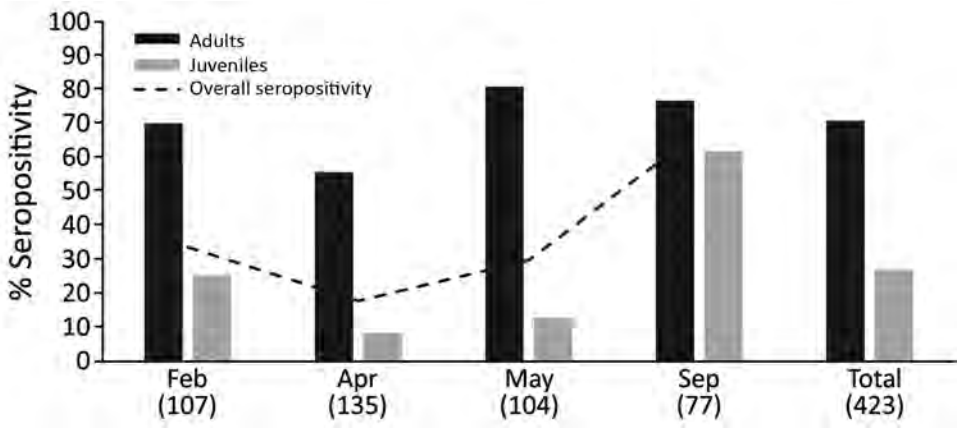

Figure 2. Marburgvirus seropositivity in adult and juvenile Egyptian rousette bats (*Rousettus aegyptiacus*), Matlapitsi Cave, Limpopo Province, South Africa, February–September 2017. Numbers in parentheses indicate the numbers of bats tested per month. Juvenile bats represent the new generation of bats born mostly during November 2016–January 2017.

We obtained sufficient marburgvirus-specific sequence data only from 1 of the 12 individual positive swab samples for phylogenetic analysis: a rectal swab sample, collected from a juvenile female (bat 8095) in September 2017, from which we recovered 79.2% (15.1/19.1 kb) of the genome. We merged sequencing reads from replicate sequencing runs and mapped 2,472 reads to the MARV reference genome. Maximum coverage per base obtained was 291 reads; some regions had no coverage. The average coverage per base across the genome was 18.5 reads (when we included 0 coverage regions), and the average coverage when we excluded 0 coverage regions was 40 reads. We obtained near-complete coding sequences for the viral protein (VP) 35 (972/990 nt; 98.2%) and VP40 (898/912 nt; 98.5%) genes; coverage ranged from 49.7% (VP24) to 89.3% (glycoprotein) in other open reading frames of the genome.

The marburgviruses sequence (strain RSA-2017-bat8095) detected from the rectal swab sample of bat 8095 shared a common ancestor with all other RAVV complete or near-complete genome sequences, including 3 human isolates from Kenya (*14*), Uganda (*15*), and the Democratic Republic of Congo (*3*) and several bat isolates from Uganda (*4*) (Figure 1). The RSA-2017-bat8095 nt sequence shared ≈77% identity with the MARV SPU191–13bat2764 Mahlapitsi strain (GenBank accession no. MG725616) that was collected and characterized from Matlapitsi Cave 4 years earlier.

Of 423 bats tested, 143 (33.8%) were positive for antibodies against marburgviruses (73 adults and 70 juveniles). Lowest overall seroprevalence occurred in April 2017 (17.78%) and ranged from 8.3% in juveniles (9/108) to 55.6% in adults (15/27) (Figure 2). Overall seropositivity did not differ significantly between male and female bats, but the overall seropositivity differed significantly between juvenile (forearm <89 mm; <1-year-old) and adult bats ($p = 0.03$). We detected seroconversion in 6 (33.3%) of 18 recaptured bats (Table 2).

Conclusions

The period of the lowest seropositivity in juveniles (April–May) resulting in the highest number of potentially susceptible bats at Matlapitsi Cave was the same as previously identified (*13*). This finding coincides with demonstrable seroconversions and virus shedding and represents a period of increased exposure. The significantly higher number of marburgvirus-positive rectal than oral swab samples we detected contrasts with results from experimentally infected Egyptian rousette bats and field studies in Uganda (*4*,*8*,*9*). Experimental data on marburgvirus shedding were obtained from subcutaneously inoculated and colonized Egyptian rousette bats (*7*–*9*). Whether this mode of infection represents a natural portal of entry for marburgviruses in Egyptian rousette bats and to what extent viral shedding patterns in colonized bats can be extrapolated to natural settings are unknown.

Table 2. Marburgvirus seroconversion in 6 of 18 Egyptian rousette bats (*Rousettus aegyptiacus*) recaptured at Matlapitsi Cave, Limpopo Province, South Africa, February 2017–September 2017*

	First capture		Recapture	
Bat ID	iELISA, %†	Capture date	iELISA, %†	Capture date
SMB676	2.2	2016 Apr	23.3	2017 Feb
SMB797	12.4	2016 Jun	23.7	2017 Apr
SMA780	0.7	2014 Jul	61.7	2017 Sep
SM906	15.2	2013 Sep	202.4	2017 Sep
SMB160	2.5	2015 Mar	51.3	2017 Sep
SMB978	11.1	2016 Nov	142.2	2017 Sep

*Recaptured bats were identified by a previously applied unique tattoo number. iELISA, indirect ELISA.
†Percent positivity of the internal positive control serum in I-ELISA calculated as (average optical density of the test serum replicates/average optical density of the positive control serum replicates) × 100; cutoff percent positivity of iELISA = 16.78% (7).

Our findings highlight the risk for marburgvirus fecal environmental contamination and for Egyptian rousette bat roosting sites as a possible source of virus spillover. Roosting behavior enabling direct physical contact suggests that fecal–oral transmission of marburgviruses in bats can occur. Biting among animals or biting by hematophagous ectoparasites might result in inoculation of wounds with contaminated feces or exposure to contaminated fomites.

Our findings, combined with earlier detection of an Ozolin-like MARV in Egyptian rousette bats roosting at Matlapitsi Cave (*13*), suggest local co-circulation of multiple marburgviruses genetic variants. Detection of RAVV in South Africa, closely related to East African isolates, indicates that long-distance movement of Egyptian rousette bats contributes to widespread geographic dispersion of marburgviruses. Moreover, it implies that more virulent strains, such as the MARV Angolan strain (*2*), might be co-circulating. Entering caves and mining have been associated with MARV spillover (*3*–*6*,*14*,*15*) and detection of viral RNA in rectal swab samples, highlight the potential route of transmission. Confirmation of the period for the highest virus exposure risk further highlights the value of biosurveillance and demonstrates that marburgviruses continue endemic circulation in South Africa. This circulation represents a potential threat that needs to be communicated to at-risk communities as a part of evidence-based public health education and prevention of pathogen spillover.

Acknowledgments

We thank the students of the Centre for Viral Zoonoses, University of Pretoria, and the staff of the Center for Emerging Zoonotic and Parasitic Diseases, National Institute for Communicable Diseases of the National Health Laboratory Service, for technical assistance during field work. We also thank the Ga Mafefe community in the Limpopo Province for supporting our research at Matlapitsi Cave.

This work was supported by the South African National Research Foundation (grant no. UID 98339); the Poliomyelitis Research Foundation (grant no.12/14); the Division of Global Disease Detection, Center for Global Health, US Centers for Disease Control and Prevention, under Cooperative Agreement no. 5, NU2GGH001874-02-00; the US Defense Threat Reduction Agency (CB10246); and the US Defense Biological Product Assurance Office through task order award (FA4600-12-D-9000).

About the Author

Dr. Paweska is head of the Center for Emerging Zoonotic and Parasitic Diseases at the National Institute for Communicable Diseases, Johannesburg, South Africa. His research interests include diagnostic testing, epidemiology, and ecology of Biosafety Level 4 zoonotic viral agents.

References

1. Amarasinghe GK, Aréchiga Ceballos NG, Banyard AC, Basler CF, Bavari S, Bennett AJ, et al. Taxonomy of the order Mononegavirales: update 2018. Arch Virol. 2018;163:2283–94. https://doi.org/10.1007/s00705-018-3814-x
2. Amman BR, Swanepoel R, Nichol ST, Towner JS. Ecology of filoviruses. Curr Top Microbiol Immunol. 2017;411:23–61. https://doi.org/10.1007/82_2017_10
3. Bausch DG, Nichol ST, Muyembe-Tamfum JJ, Borchert M, Rollin PE, Sleurs H, et al.; International Scientific and Technical Committee for Marburg Hemorrhagic Fever Control in the Democratic Republic of the Congo. Marburg hemorrhagic fever associated with multiple genetic lineages of virus. N Engl J Med. 2006;355:909–19. https://doi.org/10.1056/NEJMoa051465
4. Towner JS, Amman BR, Sealy TK, Carroll SAR, Comer JA, Kemp A, et al. Isolation of genetically diverse Marburg viruses from Egyptian fruit bats. PLoS Pathog. 2009; 5:e1000536. https://doi.org/10.1371/journal.ppat.1000536
5. Towner JS, Khristova ML, Sealy TK, Vincent MJ, Erickson BR, Bawiec DA, et al. Marburgvirus genomics and association with a large hemorrhagic fever outbreak in Angola. J Virol. 2006;80:6497–516. https://doi.org/10.1128/JVI.00069-06
6. Amman BR, Carroll SA, Reed ZD, Sealy TK, Balinandi S, Swanepoel R, et al. Seasonal pulses of Marburg virus circulation in juvenile *Rousettus aegyptiacus* bats coincide with periods of increased risk of human infection. PLoS Pathog. 2012;8:e1002877. https://doi.org/10.1371/journal.ppat.1002877
7. Paweska JT, Jansen van Vuren P, Fenton KA, Graves K, Grobbelaar AA, Moolla N, et al. Lack of Marburg virus transmission from experimentally infected to susceptible in-contact Egyptian fruit bats. J Infect Dis. 2015;212(Suppl 2):S109–18. https://doi.org/10.1093/infdis/jiv132
8. Amman BR, Jones MEB, Sealy TK, Uebelhoer LS, Schuh AJ, Bird BH, et al. Oral shedding of Marburg virus in experimentally infected Egyptian fruit bats (*Rousettus aegyptiacus*). J Wildl Dis. 2015;51:113–24. https://doi.org/10.7589/2014-08-198
9. Schuh AJ, Amman BR, Jones ME, Sealy TK, Uebelhoer LS, Spengler JR, et al. Modelling filovirus maintenance in nature by experimental transmission of Marburg virus between Egyptian rousette bats. Nat Commun. 2017;8:14446. https://doi.org/10.1038/ncomms14446
10. Towner JS, Pourrut X, Albariño CG, Nkogue CN, Bird BH, Grard G, et al. Marburg virus infection detected in a common African bat. PLoS One. 2007;2:e764. https://doi.org/10.1371/journal.pone.0000764
11. Kajihara M, Hang'ombe BM, Changula K, Harima H, Isono M, Okuya K, et al. Marburgvirus in Egyptian fruit bats, Zambia. Emerg Infect Dis. 2019;25:1577–80. https://doi.org/10.3201/eid2508.190268
12. Amman BR, Bird BH, Bakarr IA, Bangura J, Schuh AJ, Johnny J, et al. Isolation of Angola-like Marburg virus from

Egyptian rousette bats from West Africa. Nat Commun. 2020;11:510. https://doi.org/10.1038/s41467-020-14327-8

13. Pawęska JT, Jansen van Vuren P, Kemp A, Storm N, Grobbelaar AA, Wiley MR, et al. Marburg virus infection in Egyptian rousette bats, South Africa, 2013–2014. Emerg Infect Dis. 2018;24:1134–7. https://doi.org/10.3201/eid2406.172165
14. Johnson ED, Johnson BK, Silverstein D, Tukei P, Geisbert TW, Sanchez AN, et al. Characterization of a new Marburg virus isolated from a 1987 fatal case in Kenya. Arch Virol Suppl. 1996;11:101–14. https://doi.org/10.1007/978-3-7091-7482-1_10
15. Adjemian J, Farnon EC, Tschioko F, Wamala JF, Byaruhanga E, Bwire GS, et al. Outbreak of Marburg hemorrhagic fever among miners in Kamwenge and Ibanda Districts, Uganda, 2007. J Infect Dis. 2011;204(Suppl 3):S796–9. https://doi.org/10.1093/infdis/jir312

Address for correspondence: Janusz T. Pawęska, Center for Emerging Zoonotic and Parasitic Diseases, National Institute for Communicable Diseases of the National Health Laboratory Service, 1 Modderfontein Rd, Sandringham 2131, Johannesburg, South Africa: email: januszp@nicd.ac.za

Lyssaviruses in Insectivorous Bats, South Africa, 2003–2018

Jessica Coertse, Colyn S. Grobler, Claude T. Sabeta, Ernest C.J. Seamark, Teresa Kearney, Janusz T. Paweska, Wanda Markotter

We detected 3 lyssaviruses in insectivorous bats sampled in South Africa during 2003–2018. We used phylogenetic analysis to identify Duvenhage lyssavirus and a potentially new lyssavirus, provisionally named Matlo bat lyssavirus, that is related to West Caucasian bat virus. These new detections highlight that much about lyssaviruses remains unknown.

Lyssaviruses cause fatal encephalitic disease in mammals; 6 viral species have been implicated in human deaths (*1*). Bats are the primary hosts for members of the *Lyssavirus* genus, which belongs to the family *Rhabdoviridae*. Researchers have described 17 lyssavirus species, and a putative species is awaiting formal classification (*1*). The genus can be divided into ≥3 phylogroups on the basis of genetic, immunogenic, and pathogenic properties (*2*). Rabies vaccines and postexposure prophylaxis protect against infection by members of phylogroup I but provide limited protection against phylogroups II or III (*3*).

In Africa, 6 lyssaviruses are in circulation: rabies virus, which is associated with terrestrial carnivores; Duvenhage virus (DUVV), which is associated with insectivorous bats, specifically the Egyptian slit-faced bat (*Nycteris thebaica*); Lagos bat virus, which is associated with various species of frugivorous bats; Mokola virus, for which the reservoir host is unknown; Shimoni bat virus, which is associated with the striped leaf-nosed bat (*Macronycteris vittatus*); and Ikoma lyssavirus, for which the reservoir host is unknown (*1*). Only rabies virus, DUVV, and Mokola virus have been associated with human deaths on the continent. Lyssavirus surveillance in Africa is inadequate. As a result, genetic diversity, geographic distribution, and host species associations of lyssaviruses are poorly understood (*1*). However, this information is crucial for making treatment decisions, especially in resource-limited settings (*1*).

We report the results of 16 years of surveillance of insectivorous bats in South Africa. We used genetic characterization to identify DUVV and a potential novel lyssavirus from phylogroup III.

The Study

During 2003–2018, we tested 605 insectivorous bats (Appendix Tables 1, 2, https://wwwnc.cdc.gov/EID/article/26/12/20-3592-App1.pdf) of 41 species across South Africa (Figure 1; Appendix Tables 1, 2). Most bats were collected as part of a broader biosurveillance program in collaboration with bat taxonomists for species identification and classification. Among the bats collected, 562 appeared healthy and 28 were dead. Another 12 exhibited signs of disease or abnormal behavior, and 3 had been involved in human contact; we submitted these samples for rabies testing.

We anesthetized the sampled bats with isoflurane inhalant (Safeline Pharmaceuticals, https://safeline.co.za), exsanguinated them by cardiac puncture, and then performed full necropsies. We identified bats on the basis of morphologic (*4*) and genetic characteristics (*5*). The sampling protocol was approved by the University of Pretoria Animal Ethics Committee (approval no. EC054-14). Permission to conduct research was obtained from the Department of Agriculture, Land Reform and Rural Development (formerly Department of Agriculture, Forestry, and Fisheries) of the Republic of South Africa under Section 20 of the Animal Diseases Act 1984 with additional provincial permits granted (Appendix Table 3).

We extracted total RNA from the bats' brain material and subjected it to real-time reverse transcription PCR selective for 126 bp of the nucleoprotein gene

Author affiliations: University of Pretoria, Pretoria, South Africa (J. Coertse, C.S. Grobler, T. Kearney, J.T. Paweska, W. Markotter); National Institute of Communicable Diseases of the National Health Laboratory Service, Sandringham, South Africa (J. Coertse, J.T. Paweska); Onderstepoort Veterinary Institute, Pretoria (C.T. Sabeta); AfricanBats NPC, Pretoria (E.C.J. Seamark, T. Kearney); Ditsong National Museum of Natural History, Pretoria (T. Kearney)

DOI: https://doi.org/10.3201/eid2612.203592

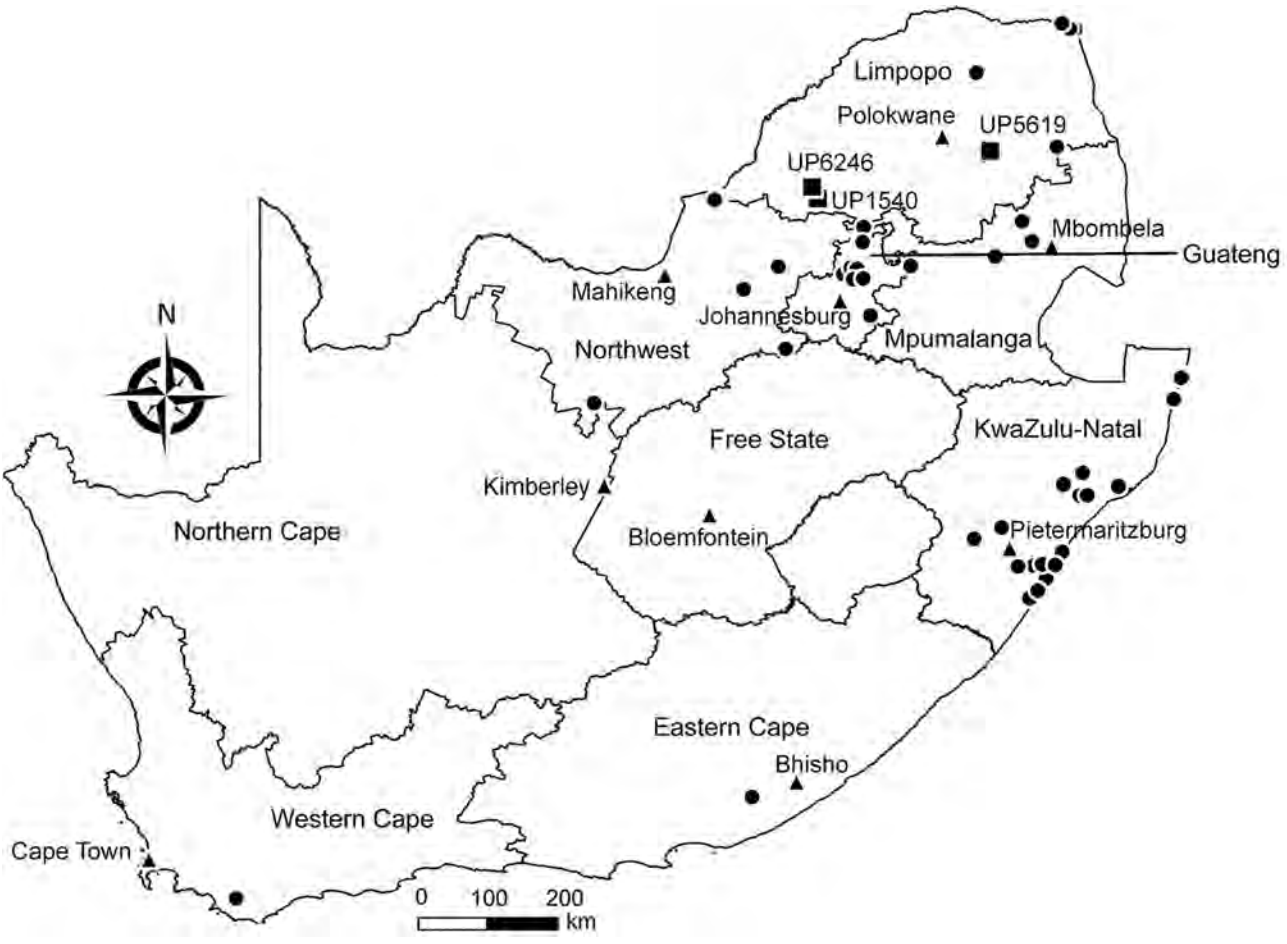

Figure 1. Locations of bat collection sites, South Africa, 2003–2018. Circles indicate collection sites, squares indicate sites with lyssavirus-positive bats, and triangles indicate capitals.

(*6*). Samples from 3 bats tested positive for lyssavirus RNA; we sequenced the amplicons (*7*). One of these samples came from an Egyptian slit-faced bat (sample no. UP1540) collected in 2012 from the Rooiberg area, Limpopo. This bat, which was collected by members of a bat interest group in August 2012, tested positive for DUVV (Figure 1). We also obtained sequences of a potentially novel lyssavirus in samples from 2 apparently healthy Natal long-fingered bats (*Miniopterus natalensis*, sample nos. UP5619 and UP6246); these sequences were distantly related to West Caucasian bat virus (WCBV). We collected these samples from Matlapitsi cave, Limpopo, in 2015 and Madimatle cave, Limpopo, in 2016 (Figure 1).

To infer the phylogeny, we used the complete nucleoprotein gene sequences of the 3 lyssaviruses according to a method described previously (*8*). We used Bayesian inference to compare our samples with representative sequences from GenBank (Appendix Table 4). We analyzed the dataset with BEAST (*9*); we used the general time-reversible substitution model as determined by jmodeltest2 (*10*), invariant sites, and gamma distribution. We assumed an underlying coalescent process with constant population size and Markov chain Monte Carlo chains of 50 million generations.

The results indicated that the sequences from Natal long-fingered bats were most closely related to, but distinct from, WCBV (Figure 2); they might belong to a novel species of *Lyssavirus*, provisionally called Matlo bat lyssavirus (MBLV). These 2 novel sequences had a shared nucleotide identity of 99.2%. Compared with other lyssaviruses, they shared the highest nucleotide identity with WCBV (80.9%–81%) and the lowest with Ikoma lyssavirus (70.5%). The DUVV sequence was 91.6%–99.3%, similar to previously described DUVV sequences (Table).

Conclusions

From 2003–2018, we detected 3 lyssavirus infections in insectivorous bats from South Africa, indicating

active but low-level circulation of lyssaviruses in this population. The Egyptian slit-faced bat is the only species of bat that has been conclusively linked with DUVV (*11*). Our finding is 1 of only 6 known DUVV cases, 3 of which caused fatal infection in humans (*1*). This finding suggests that these infections are underreported. The Egyptian slit-faced bat is widely distributed in Africa. It co-roosts with bats of various other species and switches roosts frequently, implicating a wider potential to infect other species (*12*).

We detected a novel lyssavirus, MBLV, that belongs to phylogroup III and is most closely related to a sequence of WCBV that was isolated from a common long-fingered bat (*Miniopterus schreibersii*) from the Russian Caucasus in 2002 (*13*). The nucleotide identity for MBLV falls within the species demarcation criteria determined by the International Committee for the Taxonomy of Viruses of 80%–82% for the complete nucleoprotein gene (*2*). If MBLV is not pronounced a new lyssavirus species, this virus would be a distinct lineage of WCBV. In 2006–2007, detection of virus neutralizing antibodies (seroprevalence 17%–26%) against WCBV in *Miniopterus* bats in Kenya spurred speculation that WCBV, or a closely related virus, was circulating in Africa (*14*). The bat family Miniopteridae, which includes ≥23 species in Africa, does not host known lyssaviruses in phylogroup I or II (*12*). The long-fingered bats are widely distributed throughout Africa (*12*).

Models have demonstrated that WCBV can cause fatal encephalitis in animals; commercial human and veterinary vaccines do not offer significant protection (*3*). Considering genetic diversity and phylogenetic grouping, we speculate that current vaccines will probably provide little to no protection against

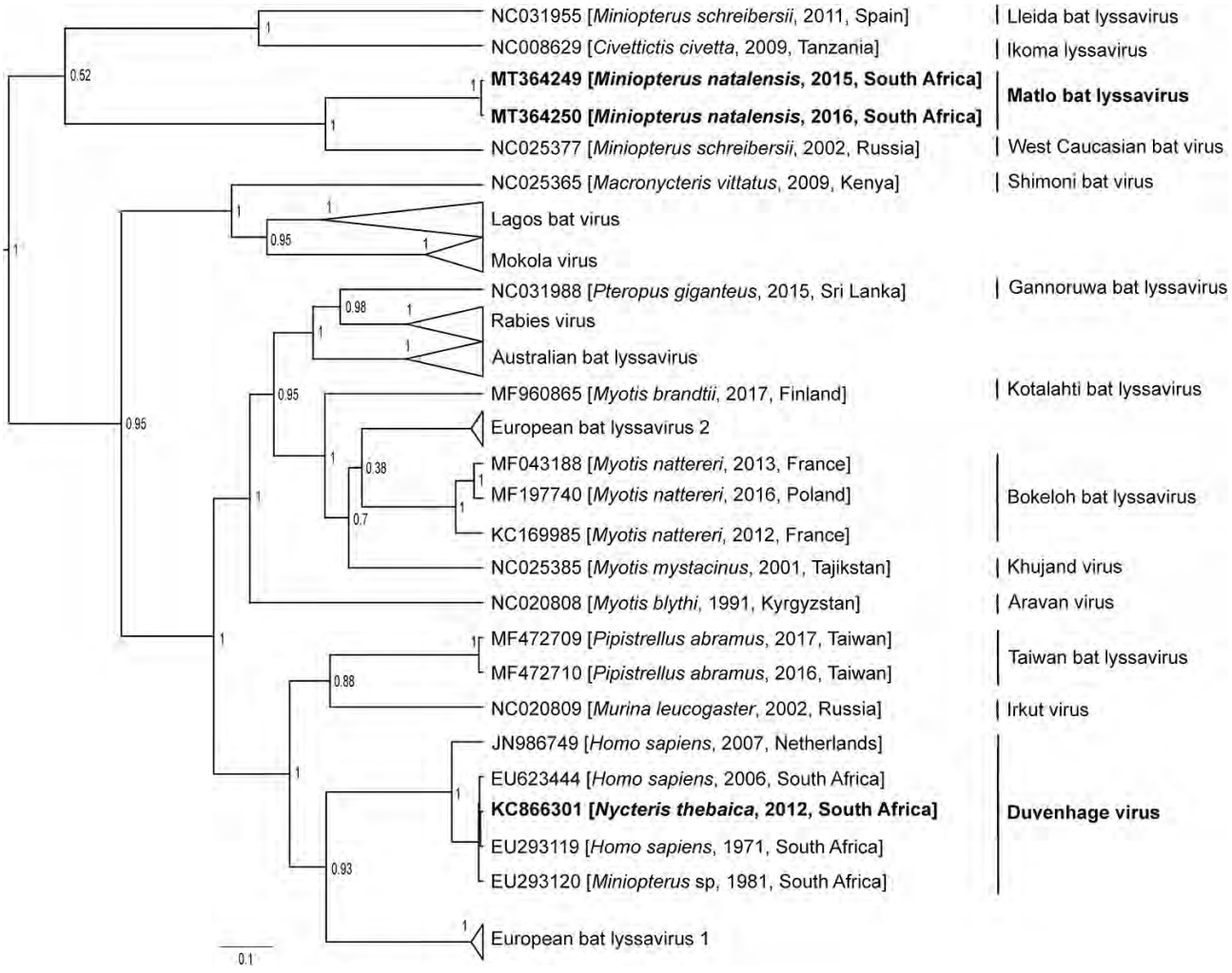

Figure 2. Phylogenetic reconstruction by Bayesian inference of nucleoprotein gene sequences of lyssavirus sequences from bats collected in South Africa, 2003–2018 (bold), and other representative lyssaviruses. Node numbers indicate posterior probabilities. GenBank accession number, host species, year of detection, and country of origin are indicated for each sequence. Scale bar indicates number of substitutions per site.

Table. Genetic similarities of 3 lyssaviruses found in insectivorous bats in South Africa, 2003–2018, and representative lyssavirus species from GenBank*

	% Similarity					
	UP5619 (MT364249)		UP6246 (MT364250)		UP1540 (KC866301)	
Virus	Nucleotide	Amino acid	Nucleotide	Amino acid	Nucleotide	Amino acid
Aravan virus	72.7	83.3	72.6	84.0	NA	NA
Australian bat lyssavirus	72.7–74.4	82–83.3	72.8–74.7	82.4–83.7	NA	NA
Bokeloh bat lyssavirus	72.9–73.3	81.5	73–73.4	81.8	NA	NA
European bat lyssavirus 1	71.1–72.4	82.2–82.4	71.2–72.5	82.7–82.9	NA	NA
European bat lyssavirus 2	71–72.4	80.0–80.7	71–72.4	80.2–80.9	NA	NA
Gannoruwa bat lyssavirus	70.6	83.1	70.6	83.5	NA	NA
Ikoma lyssavirus	70.5	79.5	70.5	79.5	NA	NA
Irkut virus	72	83.3	72.4	83.8	NA	NA
Khujand virus	72.5	81.3	72.5	81.8	NA	NA
Kotalahti bat lyssavirus	71.9	81.8	71.9	82.4	NA	NA
Lagos bat virus	71.1–74.2	82.6–84	71.3–74.5	83.1–84.4	NA	NA
Lleida bat lyssavirus	71.3	81.5	71.4	81.5	NA	NA
Mokola virus	72.2–73.8	82.4–83.7	72.3–73.7	82.8–84.2	NA	NA
Rabies virus	71.1–72.4	80.6–82	71–72.2	80.8–82.4	NA	NA
Shimoni bat virus	73.1	83.5	73.6	84.2	NA	NA
Taiwan bat lyssavirus	73.6–73.9	83.3	73.7–73.9	83.8	NA	NA
West Caucasian bat virus	80.9	95.5	81	96.2	NA	NA
DUVVs						
EU293119	72.9	84	72.9	84.4	99.3	99.5
EU293120	72.9	84	72.9	84.4	98.5	99.5
JN986749	73	84	73	84.4	91.6	99.3
EU623444	72.8	84	72.8	84.4	98.6	99.3

*GenBank accession numbers are shown for sequences from this study and reference DUVV sequences. DUVV, Duvenhage virus; NA, not applicable.

infection with MBLV (as with WCBV). Because of the lack of diagnostic capability in Africa (*6*), the potential threat of this virus is unknown. Continued surveillance and development of improved pharmaceuticals are necessary for the prevention of these infections. We observed a low prevalence (0.5%), similar to other lyssaviruses (*1*). Additional longitudinal surveillance, including serologic testing, among bats of this species and other potential hosts must be implemented to determine if Natal long-fingered bats are the reservoir host of MBLV. This study did not obtain equally representative samples of all bat species from all sampling sites; MBLV might exist in other bat species in South Africa.

In summary, the mechanisms of lyssavirus maintenance in bats is still unknown and could be influenced by various environmental and ecologic factors (*1*). Additional surveillance and comparative seroprevalence studies are needed to establish the host range and distribution of MBLV and other lyssaviruses. Although the public health impact of MBLV is currently unknown, DUVV can cause fatal infection and should be taken seriously. Surveillance is needed to understand the epidemiology and diversity of bat lyssaviruses and inform prevention efforts.

Acknowledgments

We thank the students and staff of the Centre for Viral Zoonoses, University of Pretoria, for technical assistance during fieldwork. We also thank the bat rehabilitator community, the bat interest groups for submission of bats for testing, and the Ga Mafefe community in the Limpopo Province for supporting our research at Matlapitsi cave. All participants in this project were vaccinated against rabies according to the World Health Organization preexposure prophylaxis guidelines. We also thank Motjoli Resources, Aquila Steel, and Aquila Resources for their support and permission to conduct surveillance at Meletse.

This research is supported in part by the South African Research Chair Initiative (held by Wanda Markotter) of the Department of Science and Innovation and administered by the National Research Foundation of South Africa (UID: 98339). The National Research Foundation funded the equipment based at the DNA Sanger sequencing facility in the Faculty of Natural and Agricultural Sciences, University of Pretoria (UID: 78566). This research was also supported in part by Cooperative Agreement no. 5 NU2GGH001874-02-00, funded by the US Centers for Disease Control and Prevention. These contents are solely the responsibility of the authors. C.S.G. was additionally supported by the Poliomyelitis Research Foundation (grant no. 18/54).

About the Author

Dr. Coertse is a postdoctoral fellow in the Centre for Viral Zoonoses at the University of Pretoria. Her research interests are focused on zoonoses, particularly those related to lyssaviruses and bats.

References

1. Markotter W, Coertse J. Bat lyssaviruses. Rev Sci Tech. 2018;37:385–400. https://doi.org/10.20506/rst.37.2.2809
2. Walker PJ, Blasdell KR, Calisher CH, Dietzgen RG, Kondo H, Kurath G, et al.; ICTV Report Consortium. ICTV virus taxonomy profile: *Rhabdoviridae*. J Gen Virol. 2018;99:447–8. https://doi.org/10.1099/jgv.0.001020
3. Hanlon CA, Kuzmin IV, Blanton JD, Weldon WC, Manangan JS, Rupprecht CE. Efficacy of rabies biologics against new lyssaviruses from Eurasia. Virus Res. 2005; 111:44–54. https://doi.org/10.1016/j.virusres.2005.03.009
4. Meester J. Classification of southern African mammals. Pretoria (South Africa): Transvaal Museum Monograph; 1986. p. 1–359.
5. Folmer O, Black M, Hoeh W, Lutz R, Vrijenhoek R. DNA primers for amplification of mitochondrial cytochrome c oxidase subunit I from diverse metazoan invertebrates. Mol Mar Biol Biotechnol. 1994;3:294–9.
6. Coertse J, Weyer J, Nel LH, Markotter W. Reverse transcription recombinase polymerase amplification assay for rapid detection of canine associated rabies virus in Africa. PLoS One. 2019;14:e0219292. https://doi.org/10.1371/journal.pone.0219292
7. Coertse J, Weyer J, Nel LH, Markotter W. Improved PCR methods for detection of African rabies and rabies-related lyssaviruses. J Clin Microbiol. 2010;48:3949–55. https://doi.org/10.1128/JCM.01256-10
8. Markotter W, Kuzmin I, Rupprecht CE, Randles J, Sabeta CT, Wandeler AI, et al. Isolation of Lagos bat virus from water mongoose. Emerg Infect Dis. 2006;12:1913–8. https://doi.org/10.3201/eid1212.060514
9. Drummond AJ, Suchard MA, Xie D, Rambaut A. Bayesian phylogenetics with BEAUti and the BEAST 1.7. Mol Biol Evol. 2012;29:1969–73. https://doi.org/10.1093/molbev/mss075
10. Darriba D, Taboada GL, Doallo R, Posada D. jModelTest 2: more models, new heuristics and parallel computing. Nat Methods. 2012;9:772–772. https://doi.org/10.1038/nmeth.2109
11. Foggin C. Rabies and rabies-related viruses in Zimbabwe: Historical, virological and ecological aspects. Harare (Zimbabwe): University of Zimbabwe; 1988. p. 186–221.
12. AfricanBats NPC. African Chiroptera report 2019. 2019 [cited 2020 Apr 13]. https://africanbats.org/publication/african-chiroptera-report-2019
13. Botvinkin AD, Poleschuk EM, Kuzmin IV, Borisova TI, Gazaryan SV, Yager P, et al. Novel lyssaviruses isolated from bats in Russia. Emerg Infect Dis. 2003;9:1623–5. https://doi.org/10.3201/eid0912.030374
14. Kuzmin IV, Niezgoda M, Franka R, Agwanda B, Markotter W, Beagley JC, et al. Possible emergence of West Caucasian bat virus in Africa. Emerg Infect Dis. 2008;14:1887–9. https://doi.org/10.3201/eid1412.080750

Address for correspondence: Wanda Markotter, Centre for Viral Zoonoses, Department of Medical Virology, Faculty of Health Sciences, Private Bag X323, Room 2-66, Pathology Bldg, Prinshof Campus, University of Pretoria, Gezina, Pretoria 0031, South Africa; email: wanda.markotter@up.ac.za

Circulation of 2 Barmah Forest Virus Lineages in Military Training Areas, Australia

Wenjun Liu, Joanne R. Kizu, David R. Matley, Richard Grant, Fiona J. McCallum, Christopher G. Moller, Tracy L. Carthew, Jun Hang, Ania J. Gubala, John G. Aaskov

During 2017–2018, Barmah Forest virus was recovered from mosquitoes trapped in military training areas in Australia and from a soldier infected at 1 of these areas. Phylogenies of the nucleotide sequences of the envelope glycoprotein gene E2 and the 3′ untranslated region suggest that 2 lineages are circulating in eastern Australia.

With ≈15,000 laboratory-confirmed cases over the last decade, Barmah Forest virus (BFV) is the second most common cause of human arboviral disease in Australia, after Ross River virus (RRV) (*1*). BFV is a positive-sense, single-strand, enveloped RNA virus of genus *Alphavirus*, family *Togaviridae*. Other viruses in this genus include chikungunya virus, RRV, Sindbis virus, and Eastern and Western equine encephalitis viruses. BFV was first isolated in 1974 from *Culex annulirostris* mosquitoes trapped near Barmah Forest, northern Victoria, Australia (*2*); the first case of a clinical BFV infection in humans was reported in 1986 (*3*). Since then, BFV has been reported throughout mainland Australia and Papua New Guinea (*4*,*5*). Clinical signs and symptoms of BFV infection, including polyarthritis, arthralgia, and myalgia, are similar to but milder than those of RRV infection (*6*–*7*). Through phylogenetic analyses of the nucleotide sequences of complete E2 envelope protein genes and of the 3′ untranslated region (3′ UTR), we identified 3 BFV lineages. However, we found only 1 example of 2 of the lineages (*5*,*8*).

Author affiliations: Australian Defence Force Malaria and Infectious Disease Institute, Enoggera, Queensland, Australia (W. Liu, J.R. Kizu, R. Grant, F.J. McCallum, C.G. Moller, T.L. Carthew); Enoggera Health Centre, Brisbane, Queensland, Australia (D.R. Matley); Walter Reed Army Institute of Research, Silver Spring, Maryland, USA (J. Hang); Australian Defence Science and Technology Group, Fishermans Bend, Victoria, Australia (A.J. Gubala); Institute of Health and Biomedical Innovation, Brisbane (J.G. Aaskov)

DOI: https://doi.org/10.3201/eid2612.191747

RRV caused epidemic polyarthritis outbreaks in military personnel in Australia during and after short military exercises in the Shoalwater Bay Training Area in northeastern Australia in 2016 and 2017 (*9*). The soldier in this study was among personnel who sought treatment during the 2017 outbreak with a suspected RRV infection. Signs and symptoms included rash on the face and body, nausea, headache, fatigue, lethargy, and joint and muscle pain. This retrospective study was approved by the Australian Department of Defence and Department of Veterans' Affairs Human Research Ethics Committee (DDVA HREC), Joint Health Command Low-Risk Ethical Review Panel (no. 16-021). We obtained formal written consent from the soldier.

During a retrospective investigation of the outbreak, using PanBio ELISA kits (Abbott, https://www.abbott.com), we detected BFV IgG and IgM, but not RRV IgG and IgM, in convalescent serum samples collected 23, 28, and 38 days after onset of symptoms in the patient. After inoculating 100 μL of the serum into cultures of C6/36 mosquito cells and 2 subsequent passages in this cell line, we did not detect infectious virus in the acute-phase serum sample collected on the day of symptom onset. However, we detected BFV RNA, but not RRV RNA, using a quantitative reverse-transcription PCR assay of RNA extracted from 140 μL of the acute-phase sample using a QiaAMP Viral RNA Mini Kit (QIAGEN, https://www.qiagen.com). BFV E2 RNA was present at 4.2×10^6 copies/mL, with a forward primer 8985F (5′-AGTGTGGCAGTACAACTCCCAAT-3′) corresponding to genome position 8985–9006 and a reverse primer (5′-AAGGCACATGGATCTTTCCTTTC-3′) corresponding to genome position 9036–9058.

For sequencing, we amplified the E2 and 3′ UTR genes by reverse transcription PCR using primers E2 forward 8205F 5′-GCTGTCTGACCACTACTACCA-3′ and E2 reverse 9833R 5′-GACTTAATCACTACTAAAGATAGCG-3′, and 3′ UTR forward 10923F 5′-TCCATCCATCTCTACTACCG-3′ and reverse poly-T

Table 1. Details of BFV strains used for phylogenetic study of virus lineages circulating in military training areas, Australia*

No.	Isolate	Location	Isolation year	Hosts	GenBank accession no.
1	BFVBH2193	Barmah Forest, Victoria	1974	*Culex annulirostris*	NC_001786
2	BFVC583	Beatrice Hill, Northern Territory	1978	*Culicoides marksi*†	MK169381
3	BFV16313	Charleville, Queensland	1974	*Cx. annulirostris*	MK169382
4	BFVC530SAB8	Beatrice Hill, Northern Territory	1975	*Cx. annulirostris.*	MK169383
5	BFV19493	Charleville, Queensland	1976	*Aedes normanensis*	MK169384
6	BFV19418BF	Charleville, Queensland	1976	*Cx. annulirostris*	MK169385
7	BFV16287	Charleville, Queensland	1974	*Ae. normanensis*	MK169386
8	BFVMIDI4	Brisbane, Queensland	2015	*Homo sapiens*	MH618665
9	BFV-TullyA	ADF Tully Beach training area, Queensland	2017	*Verrallina spp*	MK169387
10	BFVWBTA	ADF Wide Bay training area, Queensland	2018	*Ae. vigilax*	MH618666
11	BFVSWBTA40	Shoal Water Bay training area, Queensland	2017	*Homo sapiens*	MK169388
12	BFV18295	Australia	1993	*Cx. annulirostris*	JX855115
13	BFV145357	Australia	2008	*Cx. annulirostris*	JX855116
14	BFV106287	Australia	1995	*Ae. vigilax*	JX855117
15	BFV80504	Australia	2006	*Ae. vigilax*	JX855118
16	BFV76707	Australia	2006	*Ae. procax*	JX855119
17	BFV78362	Australia	NR	NR	JX855120

*ADF, Australian Defence Force; BFV, Barmah Forest virus; NR, Not recorded.
†Biting midge species.

5′-TTTTTTTTTTTTTTTTTTTTG-3′ designed from the nucleotide sequence of the prototype BFV strain (BH2193) and synthesized by Sigma (https://www.sigmaaldrich.com). The PCR amplifications were performed using *pfu* DNA polymerase (Promega, https://www.promega.com), which has 3′–5′ exonuclease proofreading activity. The PCR amplicons were separated by agarose gel electrophoresis and recovered using a rapid gel extraction system (QIAGEN). Sequencing was performed at the Australian Genome Research Facility as described elsewhere (*10*). Sequences were assembled and edited using Geneious version 11.2 (https://www.geneious.com). The human isolate was named SWBTA40/2017. Two strains of BFV (TullyA/2017 and WBTA/2018) isolated from mosquitoes collected in the Tully and Wide Bay military training

Table 2. Nucleotide and deduced amino acid differences in E2 of the Barmah Forest virus from the Shoalwater Bay Training Area compared with the prototype strain and strains isolated by the Australian Defence Force, Australia*

	Strain (GenBank accession no.)			
Characteristic	BH2193 (NC_001786)	SWBTA40 (MK169388)	WBTA (MH618665)	TullyA (MK169387)
Geographic origin	Northern Victoria	Central Queensland	Central Queensland	Central Queensland
Year of isolation	1974	2017	2018	2017
Nucleotide no.†	Changes in nt seq (aa)	Changes in nt seq (aa)	Changes in nt seq (aa)	Changes in nt seq (aa)
8313	C	NC	U	U
8394	C	NC	U	U
8412	C	NC	U	U
8466	U	NC	C	C
8472	U	NC	C	C
8556	A	NC	U	U
8619	U	NC	C	C
8628	A	NC	G	G
8631	A	NC	G	G
8673	C	NC	U	U
8692	A (Asn)	G (Asp)	NC	NC
8745	U	NC	C	C
8835	U	C	NC	NC
8865	G	NC	A	A
9108	A	G	NC	NC
9197	G (Ser)	NC	A (Asn)	A (Asn)
9229	A (Ser)	NC	G (Gly)	NC
9246	U	NC	C	C
9295	C	NC	U	U
9315	A	NC	U	U
9342	U	NC	A	A
9354	A	NC	U	U
9427	U (Ser)	C (Pro)	NC	NC
9433	U (Phe)	NC	C (Leu)	C (Leu)
9510	C	NC	U	U

*A, adenine; aa, amino acids; C, cytosine; G, guanine; NC, no changes; nt seq, nucleotide sequence; U, uracil.
†Nucleotide numbers correspond to those of the prototype BH2193 strain.

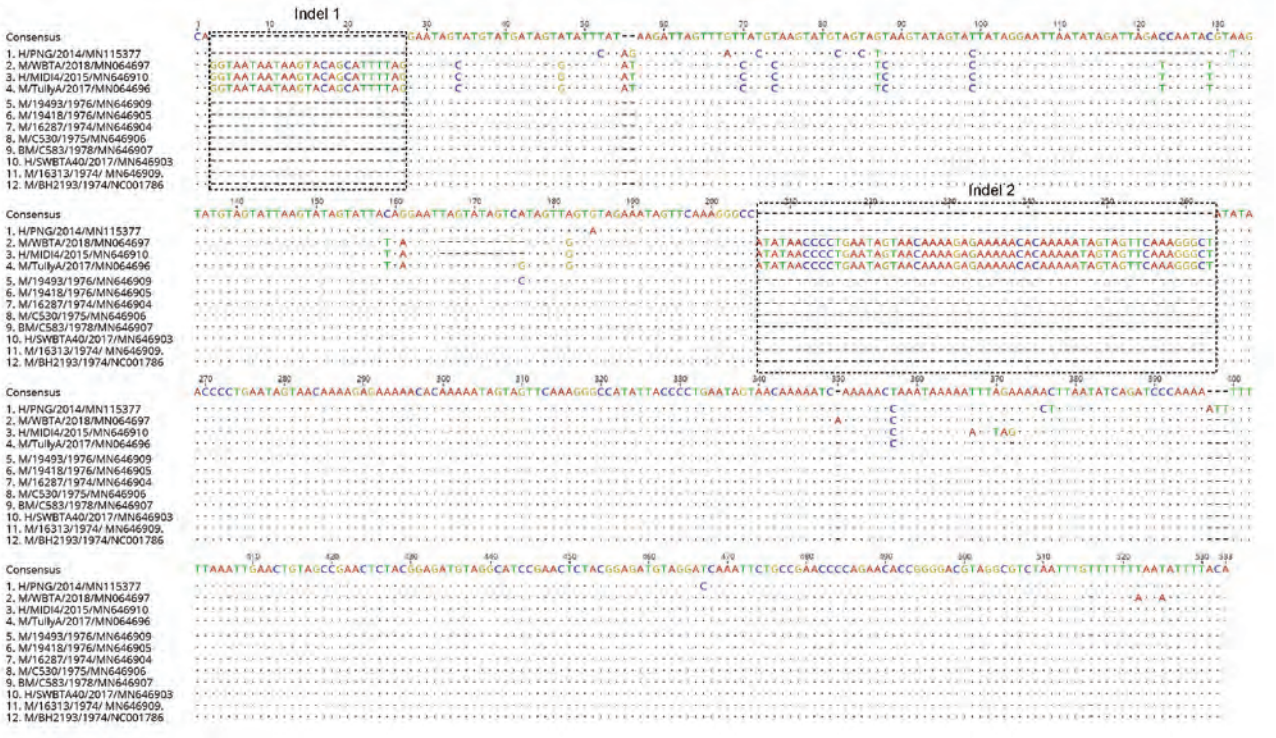

Figure 1. Nucleotide alignment of 3′ untranslated region sequences of Barmah Forest virus strains from Australia with that of the prototype BH2193 strain using muscle alignment method in Geneious version 11.2 (https://www.geneious.com). The dots indicate the consensus sequence of Barmah Forest virus strains, whereas letters in individual sequences indicate nucleotide substitutions. Dashes indicate insertions/deletions. The naming convention of the strains is name of host/strain/year of isolation/GenBank accession number. H, humans; M, mosquitoes; BM, biting midges.

areas in Queensland, eastern Australia, in 2017 and 2018 (Table 1), as well as 7 BFV strains collected previously in Australia during 1974–2015, were also sequenced in the same manner. All sequences were submitted to GenBank (accession no. MK169381-6 and MH618666). Seven BFV E2 gene sequences within GenBank, including that of a recent isolate from Papua New Guinea (*5*), were included in phylogenetic analyses.

The SWBTA40/2017 E2 comprised 1263 nt corresponding to nucleotides 8290–9552 of the genomic RNA of the BFV prototype strain BH2193. The sequence similarity among all 17 E2 sequences we examined was remarkably high, with an overall divergence of ≤4.1%. The nucleotide sequence of SWBTA40/2017 was most closely related to that of the BFV prototype strain BH2193, but differed from it at 4 sites, 8692 (A→G), 8835 (U→C), 9108 (A→G), and 9427 (U→C), resulting in nucleotide divergence of 0.32% (Table 2). The A→G substitution at 8692 resulted in an amino acid substitution of Asn→Asp and the U→C substitution at 9427 resulted in a Ser→Pro amino acid change. SWBTA40/2017 E2 gene diverged from TullyA/2017 in 24 (1.9%) nt positions and from WBTA/2018 in 25 (1.98%) nt positions (Table 2). The A→G substitution at 9197 resulted in a Ser→Asn change and a U→C substitution at 9433 resulted in a Phe-to-Leu change in both the TullyA and WBTA BFV strains.

The SWBTA40/2017 3′ UTR comprised 443 nt corresponding to nucleotides 11047–11488 of the prototype strain BH2193 but with a single-nucleotide insertion at position 11128 (Figure 1); it differed from that of the TullyA/2017 strain by 110 nt and the WBTA/2018 strain by 114 nt (Figure 1), with multiple insertions/deletions (indels) occurring in the recent TullyA/2017 and WBTA/2018 strains. The noticeable differences were the finding of 2 large indels at nucleotide positions 3–27 and 205–263 of the 3′ UTR (Figure 1). The potential influence of these indels on BFV replication and transmission warrants further study because the 3′ UTR region plays critical roles in alphaviral gene expression, replication, protein translation, and host tropism (14).

We derived phylogenies using Geneious version 11.2 with neighbor joining, maximum-likelihood, and Bayesian analysis for 17 complete E2 and twelve 3′ UTR sequences. E2 sequences segregated into 3 lineages with strong bootstrap support (Figure 2, panel A), instead of the 1 (*8*) or 2 (*5*) lineages reported

previously. The lineages are numbered chronologically; the strain from the central province of Papua New Guinea from 2014, which appears to be the oldest, was denoted as lineage I (5). The isolates described in this study (SWBTA40/2017, TullyA/2017, and WBTA/2018) were placed into 2 distinct lineages,

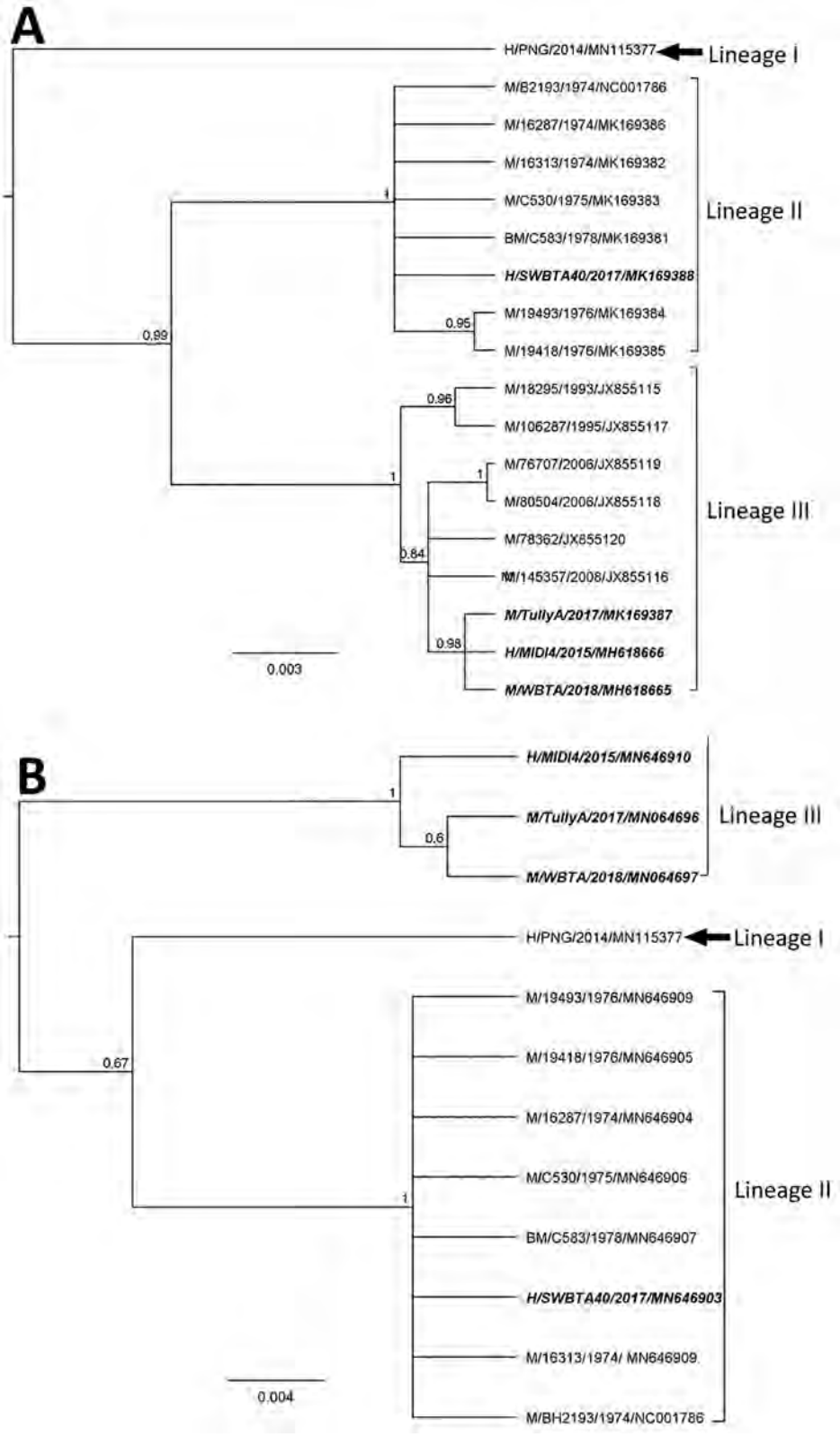

Figure 2. Phylogenies based on 17 complete BFV E2 sequences (1,263 bp) (A) and twelve 3′ untranslated region sequences (B) classify Barmah Forest virus isolates into 3 distinct lineages. We used Bayesian phylogenetic analysis method in Geneious version 11.2 (https://www.geneious.com) to analyze the aligned E2 and 3′ untranslated region sequences, applying the Hasegawa-Kishino-Yano plus gamma substitution model with a gamma molecular clock model of uniform branch lengths, a chain length of 1 million, and a 10% burn-in length. The naming convention of the strains is name of host/strain/year of isolation/GenBank accession number. Scale bar indicates the length of the branches of each tree. H, humans; M, mosquitoes; BM, biting midges.

lineages II and III. The conclusion about 3 lineages was supported by the analysis of the 3′ UTR regions (Figure 2, panel B).

All amino acid substitutions were located in the C domain of the E2 protein in areas that are involved in interaction with other proteins (E1, capsid, and 6k), as well as in the process of budding of alphavirus envelope proteins from host cell membranes (*11*,*12*). BM/C583/1978 in lineage II was isolated from *Culicoides* midges rather than mosquitoes and may reflect BFV in a blood meal rather than this insect being a vector for BFV. Nonetheless, given the position of BFV in the phylogeny of alphaviruses, exploration of vectors other than mosquitos for this virus might be warranted.

Given the relatively recent detection of BFV in western Australia (*13*,*14*) and the basal position in phylogenetic trees of the only isolate of BFV from Papua New Guinea, the cocirculation of 2 lineages of BFV in eastern Australia points to a poor understanding of population dynamics and evolution in this virus. The ongoing replacement of strains of RRV and the appearance of strains with epidemic potential (*15*) suggests that BFV may warrant more detailed virological surveillance.

Acknowledgment

The authors would like to thank the soldier for participating in the study and Dennis Shanks for proofreading the manuscript.

Joint Health Command of Australian Defence Force funded this investigation. The funder had no role in the study design, data collection and analysis, decision to publish, or preparation of the manuscript.

About the Author

Dr. Liu is head of the Arbovirology Department at the Australian Defence Force Malaria and Infectious Disease Institute. His primary research interests are epidemiology, and the evolution and transmission of emerging arboviral diseases.

References

1. Australian Government Department of Health National Notifiable Diseases Surveillance System. Number of notifications of Ross River virus and Barmah Forest virus infection, Australia, in the period of 1991 to 2018 and year-to-date notifications for 2019 [cited on 2019 Oct 15]. http://www9.health.gov.au/cda/source/rpt_3.cfm
2. Dalgarno L, Short NJ, Hardy CM, Bell JR, Strauss JH, Marshall ID. Characterization of Barmah Forest virus: an alphavirus with some unusual properties. Virology. 1984;133:416–26. https://doi.org/10.1016/0042-6822(84)90407-0
3. Vale TG, Carter IW, McPhie KA, James GS, Cloonan MJ. Human arbovirus infections along the south coast of New South Wales. Aust J Exp Biol Med Sci. 1986;64:307–9. https://doi.org/10.1038/icb.1986.32
4. Australian Government Department of Health National Notifiable Diseases Surveillance System. Number of notifications of Barmah Forest virus infection, Australia, in the period of 1991 to 2018 and year-to-date notifications for 2019 [cited 2019 Oct 15]. http:// http://www9.health.gov.au/cda/source/rpt_3_sel.cfm
5. Caly L, Horwood PF, Vijaykrishna D, Lynch S, Greenhill AR, Pomat W, et al. Divergent Barmah Forest virus from Papua New Guinea. Emerg Infect Dis. 2019;25:2266–9. https://doi.org/10.3201/eid2512.191070
6. Jacups SP, Whelan PI, Currie BJ. Ross River virus and Barmah Forest virus infections: a review of history, ecology, and predictive models, with implications for tropical northern Australia. Vector Borne Zoonotic Dis. 2008;8:283–98. https://doi.org/10.1089/vbz.2007.0152
7. Jeffery JAL, Kay BH, Ryan PA. Role of *Verrallina funerea* (Diptera: Culicidae) in transmission of Barmah Forest virus and Ross River virus in coastal areas of eastern Australia. J Med Entomol. 2006;43:1239–47. https://doi.org/10.1093/jmedent/43.6.1239
8. Poidinger M, Roy S, Hall RA, Turley PJ, Scherret JH, Lindsay MD, et al. Genetic stability among temporally and geographically diverse isolates of Barmah Forest virus. Am J Trop Med Hyg. 1997;57:230–4. https://doi.org/10.4269/ajtmh.1997.57.230
9. Liu W, Kizu JR, Le Grand LR, Moller CG, Carthew TL, Mitchell IR, et al. Localized outbreaks of epidemic polyarthritis among military personnel caused by different sublineages of Ross River virus, northeastern Australia, 2016–2017. Emerg Infect Dis. 2019;25:1793–801. https://doi.org/10.3201/eid2510.181610
10. Liu WJ, Rourke MF, Holmes EC, Aaskov JG. Persistence of multiple genetic lineages within intrahost populations of Ross River virus. J Virol. 2011;85:5674–8. https://doi.org/10.1128/JVI.02622-10
11. Jose J, Snyder JE, Kuhn RJ. A structural and functional perspective of alphavirus replication and assembly. Future Microbiol. 2009;4:837–56. https://doi.org/10.2217/fmb.09.59
12. Li L, Jose J, Xiang Y, Kuhn RJ, Rossmann MG. Structural changes of envelope proteins during alphavirus fusion. Nature. 2010;468:705–8. https://doi.org/10.1038/nature09546
13. Ehlkes L, Eastwood K, Webb C, Durrheim D. Surveillance should be strengthened to improve epidemiological understandings of mosquito-borne Barmah Forest virus infection. Western Pac Surveill Response J. 2012;3:63–8. https://doi.org/10.5365/wpsar.2012.3.1.004
14. Gyawali N, Taylor-Robinson AW, Bradbury RS, Potter A, Aaskov JG. Infection of western gray kangaroos (*Macropus fuliginosus*) with Australian arboviruses associated with human infection. Vector Borne Zoonotic Dis. 2020;20:33–9. https://doi.org/10.1089/vbz.2019.2467
15. Aaskov J, Jones A, Choi W, Lowry K, Stewart E. Lineage replacement accompanying duplication and rapid fixation of an RNA element in the nsP3 gene in a species of alphavirus. Virology. 2011;410:353–9. https://doi.org/10.1016/j.virol.2010.11.025

Address for correspondence: Wen Jun Liu, Australian Defence Force Malaria and Infectious Disease Institute, Weary Dunlop Drive, Gallipoli Barracks, Enoggera, Brisbane, QLD 4051, Australia; email: wenjun.liu@defence.gov.au

Effects of Cocooning on Coronavirus Disease Rates after Relaxing Social Distancing

Xutong Wang, Zhanwei Du, George Huang, Remy F. Pasco, Spencer J. Fox, Alison P. Galvani, Michael Pignone, S. Claiborne Johnston, Lauren Ancel Meyers

Author affiliations: The University of Texas at Austin, Austin, Texas, USA (X. Wang, Z. Du, G. Huang, R.F. Pasco, S.J. Fox, L. Ancel Meyers); Yale School of Public Health, New Haven, Connecticut, USA (A.P. Galvani); The University of Texas at Austin Dell Medical School, Austin (M. Pignone, S. Claiborne Johnston); Santa Fe Institute, Santa Fe, New Mexico, USA (L. Ancel Meyers)

DOI: https://doi.org/10.3201/eid2612.201930

As coronavirus disease spreads throughout the United States, policymakers are contemplating reinstatement and relaxation of shelter-in-place orders. By using a model capturing high-risk populations and transmission rates estimated from hospitalization data, we found that postponing relaxation will only delay future disease waves. Cocooning vulnerable populations can prevent overwhelming medical surges.

In March 2020, cities and states throughout the United States issued social distancing orders to mitigate the coronavirus disease (COVID-19) pandemic (*1*). In response to growing political and economic pressures, the White House and the Centers for Disease Control and Prevention issued guidelines for relaxing such measures on April 16, 2020 (*2*). However, the gating criteria in these guidelines do not include provisions, such as cocooning, to protect vulnerable populations. Residents of long-term care facilities (LTCFs) are particularly vulnerable because of congregate living, shortages in qualified workers, and the need for physical contact between caregivers and residents. In LTCFs, cocooning includes measures to increase staff; cohort residents; test for severe acute respiratory syndrome 2 (SARS-CoV-2), the causative agent of COVID-19; and assess availability of personal protective equipment and other infection control resources (*3*). Among other groups, cocooning involves incentivizing persons with high-risk underlying conditions to remain at home, helping persons experiencing homelessness to social distance, and broadly encouraging hand hygiene and facemask wearing for persons at high risk for severe illness or death and their caregivers (*4*).

By June 16, 2020, nursing home residents constituted 42.8% (50,919/119,055) of US COVID-19 deaths (*5*). In Austin, Texas, patients in LTCFs represented approximately half the COVID-19 deaths and ≥20% (81/398) of COVID-19 hospitalizations among persons with known residence (*6*).

To quantify the need for proactively protecting these vulnerable populations, we projected the effects of relaxation of shelter-in-place orders, with and without additional cocooning measures. We built a granular mathematical model of COVID-19 spread in US cities that incorporates age-specific and risk-stratified heterogeneity in the transmission and severity of COVID-19 (Appendix, https://wwwnc.cdc.gov/EID/article/26/12/20-1930-App.pdf) (*7*). The model uses 70 stochastic differential equations to track the disease status in 10 subpopulations: low-risk and high-risk persons in each of 5 age groups, 0–4 years, 5–17 years, 18–49 years, 50–64 years, and >64 years of age. We focused on the Austin-Round Rock Metropolitan Statistical Area in Texas, the fastest-growing large city area in the United States, because we provide decision support for city leaders and have access to patient-level COVID-19 hospitalization and death data.

Persons initially are susceptible SARS-CoV-2 and infection rates are dependent on age-specific contact rates and prevalence of infection. Upon infection, persons incubate SARS-CoV-2 asymptomatically before progressing to a symptomatic or asymptomatic infectious state. Depending on age and risk group, symptomatic COVID-19 case-patients might be hospitalized and die. To model cocooning of high-risk populations, we reduced the transmission rate to and from persons >64 years of age and in younger high-risk subgroups.

Social distancing began in Austin with school closures on March 14, 2020 and ramped up on March 24, 2020 with a Stay Home–Work Safe order (order 20200324-007; https://www.austintexas.gov). We assumed published values for most model parameters (Table; Appendix) and calibrated the transmission rate before and after the stay-home order based on hospitalization counts (Figure). During March 24–April 23, data suggest that SARS-CoV-2 transmission dropped by 70% (95% CI 45%–100%). If social distancing measures were completely relaxed on May 1, 2020, we estimated that COVID-19 hospitalizations would surpass Austin's surge capacity of 3,440 beds in 27 (95% CI 16–43) days, on May 28 (Figure). Assuming instead that individual behavior and public health efforts continued to reduce transmission by 75% relative to the stay-home order, hospital surge capacity would

Table. Key parameters of a transmission model for coronavirus disease, Austin, Texas, USA*

Parameter	Value				
Incubation period, d (range)	2.9 (1.9–3.9)				
Infectious period, d (range)	6.3 (5.3–7.3)				
Asymptomatic proportion, %	43				
Average hospitalization, d					
Recovered	10.96				
Died	8.2				
Transmission reduction during Stay Home–Work Safe Order, % (95% CI)†	70 (45%–100%)				
Cocooning efficacy, % reduction in transmission relative to Stay–Home Work Safe Order‡					
Cocooning			100		
Enhanced cocooning			125		
Age group, y	0–4	5–17	18–49	50–64	≥65
Symptomatic case hospitalization rate, %§					
Low-risk group	0.0279	0.0215	1.3215	2.8563	3.3873
High-risk group	0.2791	0.2146	13.2154	28.5634	33.8733
Infected fatality rate, %‡					
Low-risk group	0.0009	0.0022	0.0339	0.2520	0.6440
High-risk group	0.0092	0.0218	0.3388	2.5197	6.4402

*Detailed parameter distributions and references are given in Appendix Tables 3, 4 (https://wwwnc.cdc.gov/EID/article/26/12/20-1930-App.pdf).
†Estimated by fitting the model to coronavirus disease hospitalization counts March 13–April 23.
‡The Appendix provides sensitivity analyses with respect to 2 key assumptions of the model: age-specific contact patterns, which might have changed during the recent unprecedented social distancing; and equally effective cocooning of persons at high risk across all age groups. Cocooning and enhanced cocooning are for persons ≥65 years of age and persons <65 years of age with high-risk underlying conditions.
§The hospitalization rate and fatality rate for the high-risk group is assumed to be 10 times higher than the corresponding low-risk group in the same age range. The overall hospitalization rate and fatality rate is based on the age-specific values listed in corresponding literature.

be reached after 84 (95% CI 41–137) days, on July 24. When we superimposed cocooning to reduce transmission risk by 125% relative to the stay-home period for 547,474 persons at high risk among the total population of 2,168,316 (Appendix), Austin could avoid hospital surge and reduce cumulative COVID-19 hospitalizations by 62% and deaths by 70% (Appendix Table 1). Postponing relaxation

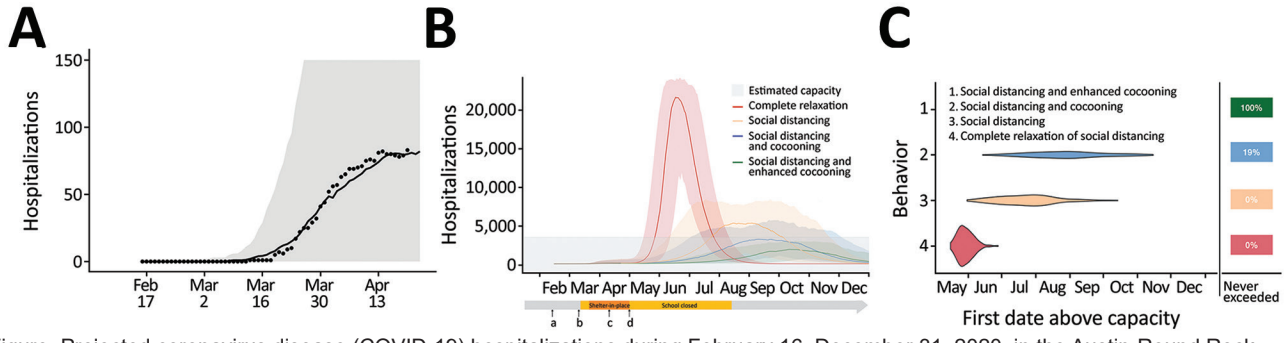

Figure. Projected coronavirus disease (COVID-19) hospitalizations during February 16–December 31, 2020, in the Austin-Round Rock Metropolitan Statistical Area, Texas, USA, assuming strict social distancing measures are relaxed on May 1, 2020. A) To calibrate transmission rates before and after Austin's March 24 Stay Home–Work Safe Order (order 20200324-007; https://www.austintexas.gov), we used least squares to fit our age- and risk-structured susceptible-exposed-infection-recover (SEIR) compartmental model of COVID-19 transmission. Black dots represent daily hospitalization data for the metropolitan area from February 16–April 20, 2020. The curve is the median projection across 200 simulations. Shading represents 95% prediction interval, based on the estimated transmission reduction of 70% beginning March 24. B) Model fitting indicating the ongoing COVID-19 epidemic in Austin. Schools were closed, on March 15 and the shelter-in-place order was issued on March 24. a) Date of possible local COVID-19 introduction, February 16; b) date of the first detected case reported, March 13; c) date shelter-in-place order was amended to include cloth face coverings in public, April 13; d) date Texas governor mandated for statewide reopening, May 1. After May 1, we project 4 scenarios in which transmission in low-risk and high-risk groups change relative the reductions achieved during the March 24–May 1 stay-home period: 1) a complete relaxation of measures with transmission rates rebounding to baseline (red); partially relaxed social distancing measures that are 75% as effective as the stay-home order in low-risk groups, with either 2) identical relaxation in high-risk populations (yellow), 3) cocooning that continues to reduce transmission in high-risk groups at the level achieved during the stay-home order (blue), or 4) enhanced cocooning that reduces transmission in high-risk groups further, by 125% relative to the stay home order (green). Lines indicate the median and shading indicates 95% CI across 200 stochastic simulations. Gray shading at bottom indicates 80% of the estimated total daily hospital capacity in the Austin–Round Rock MSA for COVID-19 patients of the 4,299 total beds (3,440). The projections assume that schools open on August 18th. C) The projected first date in 2020 that COVID-19 hospital bed requirements will exceed local capacity for each scenario, as indicated by corresponding colors. The right column indicates the chance that hospitalizations will not exceed capacity in 2020. For example, under enhanced cocooning, we would not expect hospitalizations to exceed capacity.

of shelter-in-place measures would not prevent a second pandemic wave but could buy more time to protect vulnerable populations (Appendix Figure 1).

Cities likely will experience additional waves of COVID-19 when social distancing orders are relaxed. Our model indicates that Austin must aggressively reduce SARS-CoV-2 spread to avoid overwhelming hospital capacity by the end of 2020. Without cocooning, measures that reduce transmission with ≥90% the efficacy of the stay-home order are needed; with cocooning, social distancing measures for persons at lower risk can be more relaxed (Appendix Figure 1). Cocooning of older adults and persons with known high-risk conditions (*8*) can protect thousands in Austin and millions worldwide. The high-risk population in Austin, like many cities, is diverse; 66% are ≥65 years of age, »5,000 are residents in LTCs, and almost 3,000 are persons experiencing homelessness (*9*). Cocooning should be resourced proactively and tailored to meet the distinct needs of high-risk subgroups, including work-at-home and paid leave programs that enable high-risk workers to self-isolate (*10*). Concerted efforts also are needed to shelter residents of LTCs (*3*) and persons experiencing homelessness, where risks are compounded by group living conditions that amplify COVID-19 transmission. Thus, cocooning should be added to the national gating criteria prior to relaxation of social distancing.

This article was published as a preprint at https://www.medrxiv.org/content/10.1101/2020.05.03.20089920v1.

Acknowledgments

We thank Matthew Biggerstaff, Michael Johannson, the FluCode network at CDC, Austin Mayor Steven Adler, and the White House Coronavirus Task Force for providing critical discussions and parameter guidance.

This research was supported by National Institutes of Health grant R01 AI151176 and Tito's Handmade Vodka.

About the Author

Ms. Wang is a PhD candidate at the University of Texas at Austin under the supervision of Dr. Ancel Meyers. Her research interest is in mathematical and statistical modeling of infectious disease dynamics.

References

1. Mervosh S, Lu D, Swales V. See which states and cities have told residents to stay at home. NY Times. 2020 Apr 20 [cited 2020 Jun 1]. https://www.nytimes.com/interactive/2020/us/coronavirus-stay-at-home-order.html
2. White House, Centers for Disease Control and Prevention. Guidelines: opening up America again. Washington: The White House and The Centers; 2020 [cited 2020 Jun 1]. https://www.whitehouse.gov/wp-content/uploads/2020/04/Guidelines-for-Opening-Up-America-Again.pdf
3. Centers for Disease Control and Prevention. Coronavirus disease 2019 (COVID-19): performing facility-wide SARS-CoV-2 testing in nursing homes [cited 2020 Jun 1]. https://www.cdc.gov/coronavirus/2019-ncov/hcp/nursing-homes-facility-wide-testing.html
4. Centers for Disease Control and Prevention. Coronavirus disease 2019 (COVID-19): CDC COVID data tracker. 2020 Jun 17 [cited 2020 Jun 22]. https://www.cdc.gov/coronavirus/2019-ncov/cases-updates/cases-in-us.html
5. Kamp J, Mathews AW. Coronavirus deaths in U.S. nursing, long-term care facilities top 50,000. WSJ Online. 2020 Jun 16 [cited 2020 Jun 16]. https://www.wsj.com/articles/coronavirus-deaths-in-u-s-nursing-long-term-care-facilities-top-50-000-11592306919
6. Plohetski T. Coronavirus chronicles: heartache inside Austin, Texas, nursing home. USA Today. 2020 May 8 [cited 2020 Jun 20]. https://www.usatoday.com/story/news/investigations/2020/05/08/covid-chronicles-heartache-one-u-s-citys-deadliest-nursing-home/3095807001
7. Wang X, Pasco RF, Du Z, Petty M, Fox SJ, Galvani AP, et al. Impact of social distancing measures on coronavirus disease healthcare demand, central Texas, USA. Emerg Infect Dis. 2020 [Epub ahead of print]. https://doi.org/10.3201/eid2610.201702
8. US Centers for Disease Control and Prevention. Coronavirus disease 2019 (COVID-19): people with certain medical conditions [cited 2020 Jun 1]. https://www.cdc.gov/coronavirus/2019-ncov/need-extra-precautions/people-with-medical-conditions.html
9. ECHO. 2020 Point-in-time count results 2020 May 18 [cited 2020 Jun 20] https://www.austinecho.org/leading-system-change/data-and-reports/#pit-count-results
10. US Department of Labor. Temporary rule: paid leave under the families first coronavirus response act [cited 2020 Jun 18]. https://www.dol.gov/agencies/whd/ffcra

Address for correspondence: Lauren Ancel Meyers, Department of Integrative Biology; 1 University Station C0990; Austin, TX 78712, USA; email: laurenmeyers@austin.utexas.edu

SARS-CoV-2 Natural Transmission from Human to Cat, Belgium, March 2020

Mutien Garigliany, Anne-Sophie Van Laere, Cécile Clercx, Didier Giet, Nicolas Escriou, Christèle Huon, Sylvie van der Werf, Marc Eloit, Daniel Desmecht

Author affiliations: University of Liège, Liège, Belgium (M. Garigliany, A.-S. Van Laere, C. Clercx, D. Giet, D. Desmecht); Institut Pasteur, Paris, France (N. Escriou, C. Huon, S. van der Werf, M. Eloit); Alfort National Veterinary School, Maisons Alfort, France (M. Eloit)

In March 2020, a severe respiratory syndrome developed in a cat, 1 week after its owner received positive test results for severe acute respiratory syndrome coronavirus 2. Viral RNA was detected in the cat's nasopharyngeal swab samples and vomitus or feces; immunoglobulin against the virus was found in convalescent-phase serum. Human-to-cat transmission is suspected.

DOI: https://doi.org/10.3201/eid2612.202223

We report the investigation of illness and infection with severe acute respiratory syndrome coronavirus 2 (SARS-CoV-2) in a household cat in Belgium (*1*). The cat was a female domestic shorthair, ≈15 years of age, that had been adopted 2 years earlier. The owner considered the cat to have been healthy since adoption, although it had never been assessed by a veterinarian. In February 2020, the owner took part in a 7-day tour to a mountain resort in Lombardy, Italy. The day after returning home, March 2, the owner felt suddenly too short of breath to conduct normal activities. As a precautionary measure, the family doctor decided to take a deep oropharyngeal swab sample and asked the patient to remain at home until the test result was reported. Over the next 10 days, the patient experienced a series of general, respiratory, and then digestive symptoms consistent with the clinical signs associated with coronavirus disease (COVID-19) (Figure). On March 6, the swab sample was declared positive for the SARS-CoV-2 genome, and home quarantine was extended until the end of March.

During that time, the patient's household cat was asymptomatic (Video 1, https://wwwnc.cdc.gov/EID/article/26/12/20-2223-V1.htm). However, 1 week later, the cat suddenly demonstrated clinical signs; the cat was found prostrated and vomiting in her litter, then showed pronounced lethargy, poor appetite to anorexia, vomiting, and diarrhea (Figure). Several days later, the clinical signs worsened. The cat demonstrated sneezing (Video 2, https://wwwnc.cdc.gov/EID/article/26/12/20-2223-V2.htm; Video 3, https://wwwnc.cdc.gov/EID/article/26/12/20-2223-V3.htm); a harsh, productive cough several times a day; episodes of paroxysmal reverse sneezing (Video 4 https://wwwnc.cdc.gov/EID/article/26/12/20-2223-V4.htm; Video 5, https://wwwnc.cdc.gov/EID/article/26/12/20-2223-V5.htm); labored breathing with increased respiratory effort and frequency; and emaciation (Video 6, https://wwwnc.cdc.gov/EID/article/26/12/20-2223-V6.htm). The clinical impression at this time was that of a restrictive breathing pattern suggestive of substantial involvement of parenchyma, pleura, or both. The cat's condition then gradually improved; she became less lethargic, vomiting stopped, feces resumed normal consistency, episodes of cough became less frequent, and appetite quickly improved. The cat recovered completely within <2 weeks.

A series of laboratory analyses were then conducted (Appendix, https://wwwnc.cdc.gov/EID/article/26/12/20-2223-App1.pdf). The cat's owner collected 26 swab samples according to instructions received by telephone; 16 samples contained varying amounts of the SARS-CoV-2 genome (Table). Overall, positive samples were detected March 11–24. The cat was examined by veterinarians at the time of blood sampling on day 22 after onset of first symptoms. Clinical examination of the cat was unremarkable at that time, and auscultation of the thorax revealed no abnormalities. Results of a complete blood count and a serum biochemistry panel were within reference ranges. Presence of serum IgG was first sought by Western blotting of mock-exposed and SARS-CoV-2–exposed Vero E6 cells lysates. In convalescent-phase serum, 5 protein bands that were simultaneously absent from mock-exposed Vero E6 cell lysates were identified (Appendix Figure). Furthermore, the convalescent-phase serum was positive by double-epitope sandwich ELISA and for 2 of the 3 antigens tested by double-epitope luciferase assay (Table; Appendix Table). Whereas serum samples from 30 control cats and 10 control humans were negative by virus neutralization assay, the convalescent-phase serum samples from the cat and her owner were positive; endpoints were 1:512 for the cat and 1:128 for the human.

The cat at first showed general signs, then gastrointestinal signs, and finally respiratory signs, similar to those observed in humans. Subsequently examined samples from the cat revealed viral RNA persisting for about 10 days. With the exception of a vomitus fluid sample collected on March 13, the amounts of viral RNA were relatively low. For this reason, and

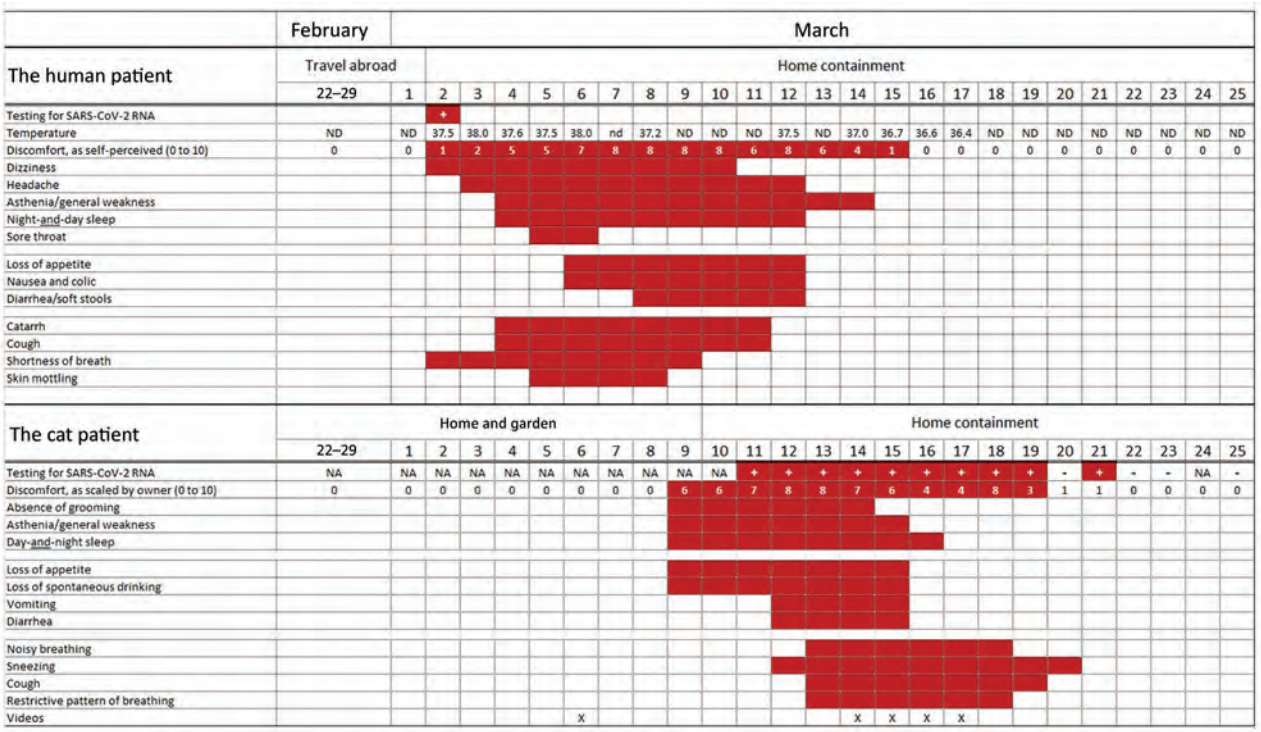

Figure. Timeline of disease course for human and cat with SARS-CoV-2 infection, by days from illness onset according to the cat owner, Belgium, February 22–March 25, 2020. NA, not available; ND, not determined; SARS-CoV-2, severe acute respiratory syndrome coronavirus 2.

despite the simultaneous presence of a compatible clinical syndrome and a suggestive chronology of events, we cannot automatically rule out passive contamination of the cat's samples by its owner.

To confirm the hypothesis of a productive infection of the cat, we conducted a series of serologic analyses by using 4 different testing approaches and targeting distinct viral protein targets. All procedures

Table. Severe acute respiratory syndrome coronavirus 2 genome loads measured by qRT-PCR in a series of consecutive swab samples from cat, Belgium, March 2020*

	Oropharyngeal swab samples		Vomitus		Feces	
Date	β-actin gene	N gene	β–actin gene	N gene	β-actin gene	N gene
11	NS	NS	26.95	23.5 ± 0.1	35.5	33.3 ± 0.2
12	33.4	38.2 ± 0.5	NS	NS	32.9	34.8 ± 0.0
13	37.8	37.9 ± 0	ND	34.9 ± 0.1	34.4	37,6 ± 0,1
14	25.1	39.3 ± 0.1	NS	NS	30.7	35.1 ±0.1
15	35.9	35.7 ± 0.1	NS	NS	27.8	33.2 ± 0.1
16	38.2	Negative	NS	NS	26.0	35.1 ± 0
17	27.1	38.2 ± 0	NS	NS	28.7	Negative
18	26.7	Negative	NS	NS	36.1	37.9 ± 0
19	NS	NS	NS	NS	27.9	39.0 ± 0
20	NS	NS	NS	NS	30.1	Negative
21	NS	NS	29.9	33.8 ± 0.1	32.8	Negative
22	37.9	Negative	NS	NS	31.7	Negative
23	NS	NS	NS	NS	33.8	Negative
25	NS	NS	34.9	Negative	35.0	Negative

*Numbers reported are defined as the number of cycles required for the real-time PCR assay fluorescent signal curve to intersect with a threshold line that exceeds background level (mean ± SD). It is a relative measure of the concentration of the genomic target in the qRT-PCR reaction (the severe acute respiratory syndrome coronavirus 2 N gene or cat β-actin gene); values >40 are considered negative. All samples with qRT-PCR values <40 were analyzed further by a standard gel RT-PCR targeting the coding sequence of the virus spike protein gene followed by Sanger sequencing of the correctly sized amplicon retrieved (≈370 bp). Only samples positive for all 3 tests were defined as positive, which was the case for all samples with a value <40 for the N gene aggregated in this table. NS, no sample available; negative, RT-qPCR and/or gel PCR and/or sequencing test failed; qRT-PCR, quantitative reverse transcription PCR.

converged toward the same result: the convalescent-phase serum from the cat contained immunoglobulins against SARS-CoV-2, which were absent from the serum from control cats. These antibodies target several distinct viral proteins, and they caused a total neutralizing effect up to a much higher dilution than those from the owner's serum. This household cat was therefore productively infected with the SARS-CoV-2 virus excreted by its owner, and the infection caused a nonfatal but nevertheless severe disease, mainly of the respiratory system (Videos 2–6).

Public health officials are still learning about SARS-CoV-2, but no current evidence indicates that pets play a role in spreading the virus. Therefore, taking measures against companion animals that may compromise their welfare is not justified.

Acknowledgments

We thank Emmanuel Vidal and Sébastien Quesney for serologic testing. In addition, in alphabetical order, we thank K.-Y. Chen, C. Demeret, M. Franssen, and S. Temmam for their interventions in various capacities in the establishment of molecular and serologic diagnostics.

About the Author

Prof. Garigliany is a senior researcher and professor of General and Molecular Pathology at Liège University, Belgium. His primary research interests include host–pathogen interactions between animals and RNA viruses.

Reference

1. ProMED-mail. COVID-19 update (58): Belgium, animal, cat, clinical case, RFI. 2020 May 20 [cited 2020 Jul 31]. http://www.promedmail.org, archive no. 20200327.7151215

Address for correspondence: Daniel Desmecht, University of Liège, Faculty of Veterinary Medicine, Department of Pathology, Sart Tilman B43, 4000 Liège, Belgium; email: daniel.desmecht@uliege.be

SARS-CoV-2 in Quarantined Domestic Cats from COVID-19 Households or Close Contacts, Hong Kong, China

Vanessa R. Barrs,[1] Malik Peiris,[1] Karina W.S. Tam, Pierra Y.T. Law, Christopher J. Brackman, Esther M.W. To, Veronica Y.T. Yu, Daniel K.W. Chu, Ranawaka A.P.M. Perera, Thomas H.C. Sit

Author affiliations: City University of Hong Kong, Hong Kong, China (V.R. Barrs); The University of Hong Kong, Hong Kong (M. Peiris, D.K.W. Chu, R.A.P.M. Perera); Government of the Hong Kong Special Administrative Region, Hong Kong (K.W.S. Tam, P.Y.T. Law, C.J. Brackman, E.M.W. To, V.Y.T. Yu, T.H.C. Sit)

DOI: https://doi.org/10.3201/eid2612.202786

We tested 50 cats from coronavirus disease households or close contacts in Hong Kong, China, for severe acute respiratory syndrome coronavirus 2 RNA in respiratory and fecal samples. We found 6 cases of apparent human-to-feline transmission involving healthy cats. Virus genomes sequenced from 1 cat and its owner were identical.

Naturally occurring human-to-animal transmission of severe acute respiratory syndrome (SARS) coronavirus was reported during 2003 when viral RNA was detected in oropharyngeal and rectal swab specimens from healthy domestic cats in a housing estate at the center of a large SARS cluster in Hong Kong, China; infections were confirmed serologically (*1*). Susceptibility of cats to infection with this virus and transmission between cats were demonstrated experimentally (*2*). Pulmonary pathologic changes, similar to those for humans with SARS, developed in infected cats, but the cats remained asymptomatic (*2*,*3*).

These findings informed the current precautionary strategy of the Agriculture, Fisheries and Conservation Department of Hong Kong to quarantine mammalian pets from households with confirmed human coronavirus disease (COVID-19) or their close contacts (defined as a person who had face-to-face contact for >15 min with a person who had confirmed SARS Coronavirus-2 [SARS-CoV-2] infection) in a holding facility, when alternative care was unavailable. Pets are swabbed for SARS-CoV-2 testing and confined until reverse transcription PCR (RT-PCR) results are negative on 2 consecutive oc-

[1]These authors contributed equally to this article.

casions. Findings for 2 infected dogs have been reported (*4*). We report testing results for cats.

Swab (nasal, oral, rectal) specimens and feces collected from nonsedated cats after admission were tested for SARS-CoV-2 RNA at the Agriculture, Fisheries and Conservation Department Veterinary Laboratory by using a commercial RT-PCR targeting the partial envelope and RNA-dependent RNA polymerase genes (Molbiol Lightmix; TIB MOLBIOL, https://www.tib-molbiol.com). This PCR does not

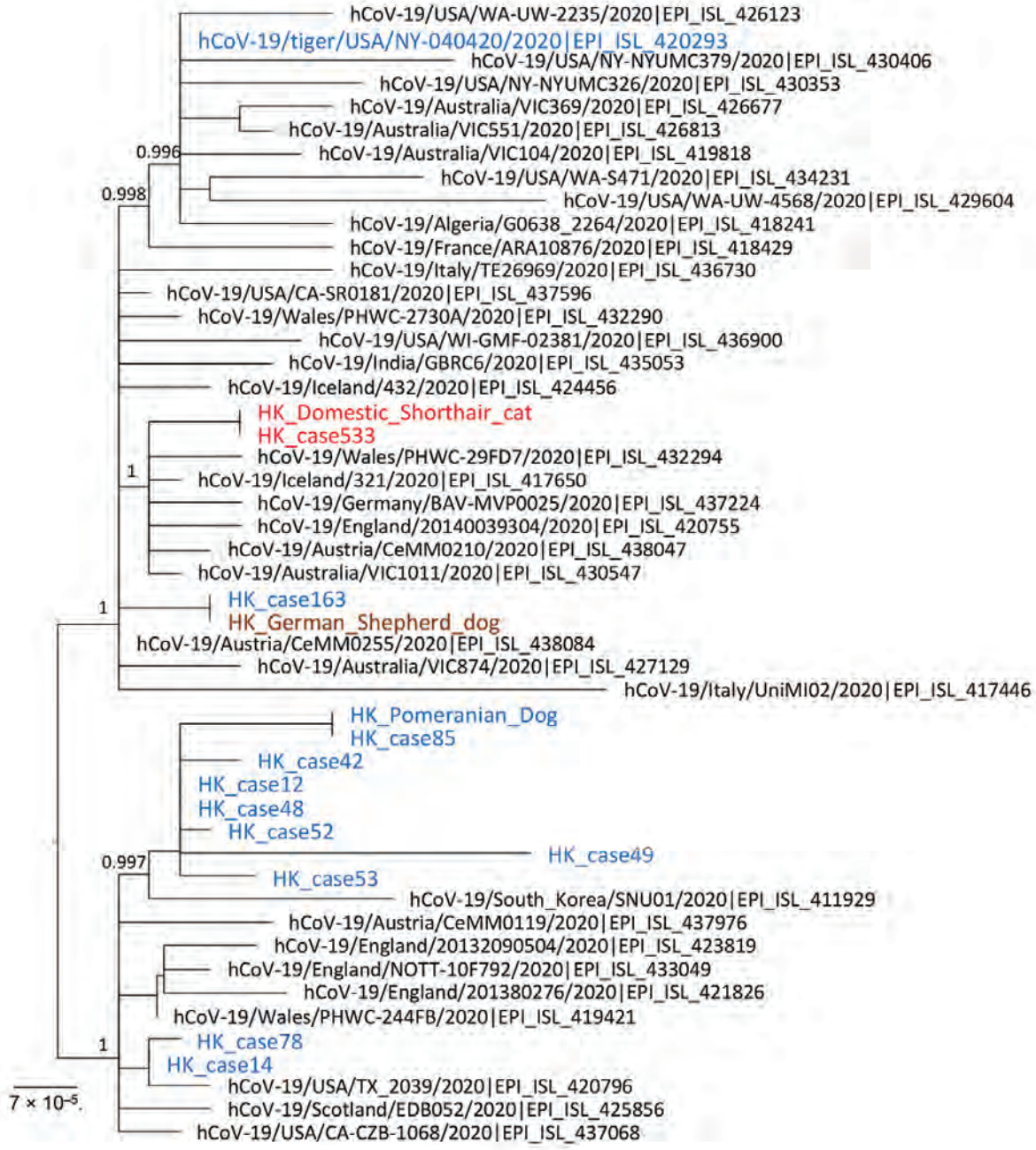

Figure. Phylogenetic analysis of SARS-CoV-2 full genome from an infected cat and the human index case-patient, Hong Kong, China. A virus sequenced directly from a tiger in a zoo in United States was included in this analysis. Virus genome alignment was prepared and manually trimmed at genome 5′ and 3′ ends for low-alignment quality. A resulting alignment of 29,655 nt was analyzed by using PhyML (http://www.atgc-montpellier.fr) and the generalized time reversible nucleotide substitution model. Branch support identified by using the fast approximate likelihood ratio test are shown at major nodes. The Hong Kong feline virus from cat 1 and that of its owner are shown in red. Canine and human viruses from Hong Kong, including from the dogs' owners (HK_case 163 and HK_case 85) are shown in blue. Numbers along branches are bootstrap values. Scale bar indicates nucleotide substitutions per site. SARS-CoV-2, severe acute respiratory syndrome coronavirus 2.

show cross-reactivity with these genes from enteric coronavirus (*5*).

For samples with positive or equivocal results, confirmatory quantitative RT-PCRs targeting nonstructural protein 4, nonstructural protein 16, nucleoprotein, and membrane genes were performed at the World Health Organization COVID-19 Reference Laboratory at the University of Hong Kong (*4*). Animals with positive results were evaluated by repeated sampling to monitor viral shedding by RT-PCR. Serologic analysis was used selectively.

We sampled 50 cats during February 11–August 11, 2020. Time from onset of COVID-19 symptoms in owners to first sampling of their cats was available for 21 owners of 35 cats and ranged from 3 to 15 (median 8, interquartile range 4) days. SARS-CoV-2 RNA was detected in samples from 6 (12%) of 50 cats (Table, https://wwwnc.cdc.gov/EID/article/26/12/20-2786-T1.htm).

The first positive case (cat 1) was from a household that had 3 persons with confirmed cases of COVID-19; their symptoms (fever, cough, or shortness of breath) started on March 20, 29, and 30, 2020. Their 7-year old, female, domestic shorthair cat was examined by a veterinarian at admission on day 1 (March 30), and reported to be clinically healthy. Nasal, oral, and rectal swab specimens collected on day 1 were positive for SARS-CoV-2 RNA; viral nucleoprotein gene copy numbers were $\log_{10}$ 6.3/mL, $\log_{10}$ 5.6/mL, and 3.2 $\log_{10}$/mL, respectively.

Attempts to culture virus from day 1 samples on Vero E6 (ATCC CRL-1586) cells as described (*4*) were unsuccessful. Viral RNA was detected in oral swab specimens for 8 days and nasal swab specimens for 11 days, but rectal swab specimens were negative after day 1 (Table).

We performed serologic analysis to detect neutralizing antibodies by using a 90% plaque reduction neutralization test for SARS-CoV-2 (*4*). The result was positive for the only serum sample collected (on day 19) and had titer ≥1:320 (*4*).

Viral genomes from cat 1 and 1 owner were sequenced by using a MiSeq Sequencing Platform (Illumina, https://www.illumina.com) after reverse transcription of viral RNA and multiple, overlapping, ≈2-kb PCRs that targeted the viral genome (*4*). Both genome sequences (29,830 nt sequenced; 99.8% of the genome) were identical (Figure) and deposited in GenBank (accession no. MT628701).

Four of the other 5 positive cats were from confirmed COVID-19–infected households, and 1 indoor-only cat belonged to a close contact who was not confirmed to be infected. Time from onset of COVID-19 symptoms in owners to animal sampling was known for 3 cats (5, 11, and 8 days); 1 had equivocal envelope gene PCR results but was positive by a novel surrogate virus neutralization test (*6*). Signs of disease did not develop in any infected cats, consistent with experimental feline infections, which are also usually subclinical (*7*; A. Bosco-Lauth et al., unpub. data).

COVID-19–like signs have been reported in domestic cats naturally infected with SARS-CoV-2 in other countries (*8*). In addition, 4 tigers and 3 lions with respiratory signs in a zoo in New York, New York, USA, were confirmed to be shedding SARS-CoV-2 in feces (S.L. Bartlett et al., unpub. data). Susceptibility to SARS-CoV-2 might differ between felid species.

SARS-CoV-2 RNA persisted longest in nasal secretions in 1 case for 11 days at low levels. Viral RNA was detected in nasal washes from kittens experimentally inoculated with SARS-CoV-2 for 8–9 days, after which sampling was stopped (*7*). Cats acquiring infection from being cohoused with experimentally infected cats shed virus in respiratory secretions longer (7 days) than directly inoculated cats (5 days) (*8*).

Although feline-to-human transmission is theoretically possible, we did not find any evidence of this transmission. The timeline of infection in cat 1 and the finding of an identical SARS-CoV-2 genome sequence in a human from the same household is consistent with human-to-animal transmission. In support of these findings, the cat had no outdoor access.

More widespread serologic surveillance of cats in contact with COVID-19 patients is warranted to determine the prevalence of human-to-cat transmission. Some infected cats might have stopped shedding virus before being quarantined because viral shedding periods as short as 3 days have been reported in experimentally infected cats (*7*).

Acknowledgment

We thank Dominic N.C. Tsang for providing the human specimen.

M.P. was supported by the US National Institutes of Health (contract no. HHSN272201400006C).

About the Author

Dr. Barrs is a chair professor of companion animal health and disease at the City University of Hong Kong, Hong Kong, China. Her primary research interests are One Health infectious diseases; viral diseases of cats, dogs, and wildlife; and shared environmental pathogens of public health concern, especially cryptic species of *Aspergillus*.

References

1. World Health Organization. Consensus document on the epidemiology of severe acute respiratory syndrome (SARS). Department of Communicable Disease Surveillance and Response; 2003. WHO/CDS/CSR/GAR/2003.11:1–47 [cited 2020 Sep 10]. https://www.who.int/csr/sars/en/WHOconsensus.pdf
2. Martina BE, Haagmans BL, Kuiken T, Fouchier RA, Rimmelzwaan GF, Van Amerongen G, et al. Virology: SARS virus infection of cats and ferrets. Nature. 2003;425:915. https://doi.org/10.1038/425915a
3. van den Brand JM, Haagmans BL, Leijten L, van Riel D, Martina BE, Osterhaus AD, et al. Pathology of experimental SARS coronavirus infection in cats and ferrets. Vet Pathol. 2008;45:551–62. https://doi.org/10.1354/vp.45-4-551
4. Sit TH, Brackman CJ, Ip SM, Tam KW, Law PY, To EM, et al. Infection of dogs with SARS-CoV-2. Nature. 2020. May 14 [Epub ahead of print]. https://doi.org/10.1038/s41586-020-2334-5
5. Corman VM, Landt O, Kaiser M, Molenkamp R, Meijer A, Chu DK, et al. Detection of 2019 novel coronavirus (2019-nCoV) by real-time RT-PCR. Euro Surveill. 2020;25:2000045. https://doi.org/10.2807/1560-7917.ES.2020.25.3.2000045
6. Tan CW, Chia WN, Qin X, Liu P, Chen MI, Tiu C, et al. A SARS-CoV-2 surrogate virus neutralization test based on antibody-mediated blockage of ACE2-spike protein-protein interaction. Nat Biotechnol. 2020;38:1073–8. https://doi.org/10.1038/s41587-020-0631-z
7. Shi J, Wen Z, Zhong G, Yang H, Wang C, Huang B, et al. Susceptibility of ferrets, cats, dogs, and other domesticated animals to SARS-coronavirus 2. Science. 2020;368:1016–20. https://doi.org/10.1126/science.abb7015
8. World Organisation for Animal Health. Questions and answers on COVID-19, Jun 4, 2020 [cited 2020 Jun 8]. https://www.oie.int/scientific-expertise/specific-information-and-recommendations/questions-and-answers-on-2019novel-coronavirus/

Address for correspondence: Vanessa R. Barrs, Department of Veterinary Clinical Sciences, Jockey Club College of Veterinary Medicine, City University of Hong Kong, Kowloon Tong, Hong Kong, China; email: vanessa.barrs@cityu.edu.hk

Lack of Susceptibility to SARS-CoV-2 and MERS-CoV in Poultry

David L. Suarez, Mary J. Pantin-Jackwood, David E. Swayne, Scott A. Lee, Suzanne M. DeBlois, Erica Spackman

Author affiliation: US Department of Agriculture, Athens, Georgia, USA

DOI: https://doi.org/10.3201/eid2612.202989

We challenged chickens, turkeys, ducks, quail, and geese with severe acute respiratory syndrome coronavirus 2 or Middle East respiratory syndrome coronavirus. We observed no disease and detected no virus replication and no serum antibodies. We concluded that poultry are unlikely to serve a role in maintenance of either virus.

Coronaviruses of animals periodically transmit to humans (*1*), as recently occurred with severe acute respiratory syndrome coronavirus 2 (SARS-CoV-2). SARS-CoV-2 was recognized in December 2019 in cases of atypical pneumonia in hospitalized patients in Wuhan, China. The virus is a novel betacoronavirus, related to the now-eradicated severe acute respiratory syndrome coronavirus (SARS-CoV) from 2003, with which SARS-CoV-2 has 82% identity across the genome (*2*). SARS-CoV-2 is highly transmissible among humans and particularly virulent for elderly persons and those with certain underlying health conditions. Multiple studies have examined the susceptibility of domestic animals to SARS-CoV-2 to establish the risk for zoonotic transmission; 2 studies have shown chickens and Pekin ducks were not susceptible to infection (*3*,*4*).

Middle East respiratory syndrome coronavirus (MERS-CoV), another coronavirus of high concern associated with zoonotic infection, was first detected in patients with severe acute lower respiratory tract disease in Saudi Arabia in 2012. MERS-CoV causes lower respiratory disease, similar to the SARS-CoVs (*5*). Unlike SARS-CoV-2, MERS-CoV transmits poorly to humans and does not exhibit sustained human-to-human transmission; however, it has a high case fatality rate of ≈30%. Although the MERS-CoV case count is low, human cases continue to be reported, therefore there is a possibility for the virus to adapt to humans.

Based on sequence similarity, the closest relatives of SARS-CoV-2 and MERS-CoV are believed to be bat betacoronaviruses (*6*); the sequence difference

between human and bat isolates suggests the existence of an intermediary host. For MERS-CoV, dromedary camels appear to be the primary natural reservoir of infection to humans, but other domestic animals seem to be susceptible to infection (*7*,*8*). Hemida et al. looked for MERS-CoV antibodies in chickens; all samples were negative (*9*).

Because poultry are so widespread and have close and extended contact with humans and other mammals in many production systems, including live animal markets, we conducted susceptibility studies with SARS-CoV-2 and MERS-CoV in 5 common poultry species. Embryonating chicken eggs (ECE) have been used for virus isolation culture, including use in vaccine production, for diverse avian and mammalian viruses; therefore, we tested ECE for their ability to support the replication of both viruses.

We examined 5 poultry species: chickens (*Gallus gallus domesticus*), turkeys (*Meleagris gallopavo*), Pekin ducks (*Anas platyrhinchos domesticus*), Japanese quail (*Coturnix japonica*), and white Chinese geese (*Anser cygnoides*). The US National Poultry Research Center Institutional Animal Care and Use Committee reviewed and approved all procedures involving animals; the Institutional Biosafety Committee approved the use of the viruses.

To evaluate their susceptibility to these viruses, 10 birds of each species were challenged with a virus isolate obtained from the Biodefense and Emerging Infections Research Resources Repository (BEI Resources; National Institute of Allergy and Infectious Diseases, National Institutes of Health). We used either the USA-WA1/2020 isolate of SARS-CoV-2 (BEI NR-58221) or the Florida/USA-2_SaudiArabia_2014 isolate of MERS-CoV (BEI NR-50415) (Appendix, https://wwwnc.cdc.gov/EID/article/26/12/20-2989-App1.pdf).

We collected oropharyngeal and cloacal swabs from all birds at 2, 4, and 7 days postchallenge (dpc) and tested them for virus by real-time reverse transcription PCR. At 14 dpc we collected serum specimens from the birds and tested for antibody to the challenge virus by microneutralization. No clinical signs were observed at any time in any species, and virus was not detected in any swab material (Table). Antibodies were not detected in serum from any birds at 14 dpc. These results suggest that neither virus replicated in any of the avian species evaluated or that they replicated at a level that was too low to be detected.

We tested ECE for their ability to support SARS-CoV-2 or MERS-CoV replication after inoculation with any of the 3 most common routes: yolk sac, chorioallantoic sac, or chorioallantoic membrane (Appendix). We collected yolk, allantoic fluid (albumin), and embryo tissues from inoculated eggs; we tested for viral replication by attempting virus isolation in Vero cells from the egg material after each of 2 ECE passages. We did not recover either virus in Vero cells from the inoculated ECEs, nor did we observe lesions in any of the embryos inoculated with SARS-CoV-2 or MERS-CoV. The ECE results with SARS-CoV-2 are consistent with the results reported by Barr et al. (*10*).

Identifying potential reservoir hosts of the novel coronaviruses is critical to controlling exposure and subsequent infection, as well as to preserving a safe and consistent food supply. None of the avian species nor the ECE appeared to support replication of either virus. Our findings demonstrate that poultry are unlikely to serve a role in the maintenance or transmission of either SARS-CoV-2 or MERS-CoV, and furthermore that ECE are not a viable laboratory host system.

Table. Poultry testing positive for SARS-CoV-2 or MERS-CoV, United States*

	SARS-COV-2							MERS-CoV						
	No. positive at 2 dpc		No. positive at 4 dpc		No. positive at 7 dpc			No. positive at 2 dpc		No. positive at 4 dpc		No. positive at 7 dpc		
Species	OP	CL	OP	CL	OP	CL	Antibody	OP	CL	OP	CL	OP	CL	Antibody
Chickens (*Gallus gallus domesticus*)	0	0	0	0	0	0	0	0	0	0	0	0	0	0
Turkeys (*Meleagris gallopavo*)	0	0	0	0	0	0	0	0	0	0	0	0	0	0
Japanese quail (*Coturnix japonica*)	0	0	0	0	0	0	0	0	0	0	0	0	0	0
Pekin ducks (*Anas platyrhinchos*)	0	0	0	0	0	0	0	0	0	0	0	0	0	0
Chinese domestic geese (*Anser cygnoides*)	0	0	0	0	0	0	0	0	0	0	0	0	0	0

*Real-time reverse transcription PCR was used to test the oropharyngeal and cloacal swabs collected from 10 individuals of each poultry species inoculated with SARS-CoV-2 or MERS-CoV. We tested serum samples for antibody 14 dpc by virus neutralization assay. Three birds of each species served and noninoculated controls. CL, cloacal swab; dpc, days postchallenge; MERS-CoV, Middle East respiratory syndrome coronavirus; OP, oropharyngeal swab; SARS-CoV-2, severe acute respiratory syndrome coronavirus 2.

Acknowledgments

We thank Jesse Gallagher, Melinda Vonkungthong, Anne Hurley-Bacon, Jasmina Luczo, James Doster, and Charles Foley for technical assistance with this work.

Severe acute respiratory syndrome coronavirus 2, isolate USA-WA1/2020, NR-52281 was deposited by the Centers for Disease Control and Prevention and obtained through BEI Resources, NIAID, NIH. Middle East respiratory syndrome coronavirus, Florida/USA-2_Saudi Arabia_2014, NR-50415 was obtained through BEI Resources, NIAID, NIH. Vero African green monkey kidney cells (ATCC CCL-81), FR-243, were obtained through the International Reagent Resource, Influenza Division, WHO Collaborating Center for Surveillance, Epidemiology and Control of Influenza, Centers for Disease Control and Prevention, Atlanta, GA, USA.

This work was supported by USDA-Agricultural Research Service (project no. 6040-32000-066-00-D).

About the Author

Dr. Suarez is the research leader for the Exotic and Emerging Avian Viral Disease Research Unit of the Agricultural Research Service, USDA. His primary research interests are in the understanding and control of avian influenza and Newcastle disease viruses in poultry and other emerging viral diseases that threaten the poultry industry.

References

1. Corman VM, Muth D, Niemeyer D, Drosten C. Hosts and sources of endemic human coronaviruses. Adv Virus Res. 2018;100:163–88. https://doi.org/10.1016/bs.aivir.2018.01.001
2. Chan JF, Kok KH, Zhu Z, Chu H, To KK, Yuan S, et al. Genomic characterization of the 2019 novel human-pathogenic coronavirus isolated from a patient with atypical pneumonia after visiting Wuhan. Emerg Microbes Infect. 2020;9:221–36. https://doi.org/10.1080/22221751.2020.1719902
3. Schlottau K, Rissmann M, Graaf A, Schön J, Sehl J, Wylezich C, et al. SARS-CoV-2 in fruit bats, ferrets, pigs, and chickens: an experimental transmission study. Lancet Microbe. 2020;1;e218–e225. https://doi.org/10.1016/S2666-5247(20)30089-6
4. Shi J, Wen Z, Zhong G, Yang H, Wang C, Huang B, et al. Susceptibility of ferrets, cats, dogs, and other domesticated animals to SARS-coronavirus 2. Science. 2020;368:1016–20. https://doi.org/10.1126/science.abb7015
5. The Lancet. MERS-CoV: a global challenge. Lancet. 2013;381:1960. https://doi.org/10.1016/S0140-6736(13)61184-8
6. Hui DS, Azhar EI, Memish ZA, Zumla A. Human coronavirus infections—severe acute respiratory syndrome (SARS), Middle East respiratory syndrome (MERS), and SARS-CoV-2. Reference Module in Biomedical Sciences. 2020 [cited 2020 Sep 23]. https://doi.org/10.1016/B978-0-12-801238-3.11634-4
7. Ferguson NM, Van Kerkhove MD. Identification of MERS-CoV in dromedary camels. Lancet Infect Dis. 2014;14:93–4. https://doi.org/10.1016/S1473-3099(13)70691-1
8. Kandeil A, Gomaa M, Shehata M, El-Taweel A, Kayed AE, Abiadh A, et al. Middle East respiratory syndrome coronavirus infection in non-camelid domestic mammals. Emerg Microbes Infect. 2019;8:103–8. https://doi.org/10.1080/22221751.2018.1560235
9. Hemida MG, Perera RA, Wang P, Alhammadi MA, Siu LY, Li M, et al. Middle East respiratory syndrome (MERS) coronavirus seroprevalence in domestic livestock in Saudi Arabia, 2010 to 2013. Euro Surveill. 2013;18:20659. https://doi.org/10.2807/1560-7917.ES2013.18.50.20659
10. Barr IG, Rynehart C, Whitney P, Druce J. SARS-CoV-2 does not replicate in embryonated hen's eggs or in MDCK cell lines. Euro Surveill. 2020;25. https://doi.org/10.2807/1560-7917.ES.2020.25.25.2001122

Address for correspondence: Erica Spackman, US National Poultry Research Center, USDA Agricultural Research Service, 934 Station Rd, Athens, GA 30605, USA; email: erica.spackman@usda.gov

Serologic Responses in Healthy Adult with SARS-CoV-2 Reinfection, Hong Kong, August 2020

Paul K.S. Chan, Grace Lui, Asmaa Hachim, Ronald L.W. Ko, Siaw S. Boon, Timothy Li, Niloufar Kavian, Fion Luk, Zigui Chen, Emily M. Yau, Kin H. Chan, Chi-hang Tsang, Samuel M.S. Cheng, Daniel K.W. Chu, Ranawaka A.P.M. Perera, Wendy C.S. Ho, Apple C.M. Yeung, Chit Chow, Leo L.M. Poon, Sophie A. Valkenburg, David S.C. Hui, Malik Peiris

Author affiliations: The Chinese University of Hong Kong, Hong Kong, China (P.K.S. Chan, G. Lui, S.S. Boon, T. Li, F. Luk, Z. Chen, W.C.S. Ho, A.C.M. Yeung, C. Chow, D.S.C. Hui); The University of Hong Kong, Hong Kong (A. Hachim, R.L.W. Ko, N. Kavian, E.M. Yau, K.H. Chan, C. Tsang, S.M.S. Cheng, D.K.W. Chu, R.A.P.M. Perera, L.L.M. Poon, S.A. Valkenburg, M. Peiris)

DOI: https://doi.org/10.3201/eid2612.203833

In March 2020, mild signs and symptoms of coronavirus disease developed in a healthy 33-year-old man in Hong Kong. His first infection did not produce virus neutralizing antibodies. In August, he had asymptomatic reinfection, suggesting that persons without a robust neutralizing antibody response might be at risk for reinfection.

Severe acute respiratory syndrome coronavirus 2 (SARS-CoV-2) is the causative agent of coronavirus disease, which has caused a pandemic in humans. Whether SARS-CoV-2 infection induces serologic immunity and the duration of that immunity is unknown. In humans, reinfection with seasonal coronaviruses occurs naturally and in experimental conditions (*1*,*2*).

Within 30 days after infection, most persons with SARS-CoV-2 begin producing antibodies against the spike and N proteins of the virus (*3*,*4*). An outbreak of SARS-CoV-2 on a fishing vessel showed that persons with prior neutralizing antibodies against SARS-CoV-2 were not reinfected (*5*). We analyzed the serologic and cytokine responses of a patient who had 2 episodes of SARS-CoV-2 infection (*6*). These findings have implications for population immunity generated from natural infection or vaccines.

On March 23, 2020, fever, headache, cough, and sore throat developed in a 33-year-old Caucasian man with no underlying conditions in Hong Kong. Six days later, the patient was admitted to the hospital with mildly elevated levels of alanine aminotransferase (73 U/L, reference range <50 U/L) and lactate dehydrogenase (236 U/L, reference range 106–218 U/L). Chest radiographs did not show any infiltrates. He tested negative for hepatitis B surface antigen and antibodies against HIV and hepatitis C virus. He had IgG against measles virus and varicella zoster virus. Symptoms resolved completely within 3 days. A sample of the patient's deep throat saliva tested positive for SARS-CoV-2 RNA by reverse transcription PCR (RT-PCR). During days 6–20 after symptom onset, the patient tested positive 7 more times; RT-PCR cycle thresholds ranged from 31 through 36 (Figure). He was isolated in the hospital until twice testing negative for SARS-CoV-2 by RT-PCR, on days 21 and 22. At a follow-up visit on day 43 (i.e., May 5, 2020), he was asymptomatic and had resumed his usual work. We took serum samples on days 10 and 43 (Figure).

On August 15, 2020, the patient returned to Hong Kong after a 1-week trip in Spain. As a part of border surveillance, he submitted a deep throat saliva sample for RT-PCR; this sample tested positive for SARS-CoV-2 RNA. He remained asymptomatic throughout his second infection. The clinical course of this second episode has been reported elsewhere (Figure) (*6*). We confirmed the previous report (*6*) that viruses from the first and second infection of this patient were phylogenetically distinct (Appendix Figure 1, https://wwwnc.cdc.gov/EID/article/26/12/20-3833-App1.pdf), demonstrating reinfection. We collected baseline serum on day 3 after detection of reinfection (day 148 after symptom onset of his first infection) to infer his probable preinfection serologic results.

The 50% plaque reduction neutralization test (*3*) and surrogate virus neutralization test (*7*) on the serum samples collected on days 10, 43, and 148 did not detect antibodies against SARS-CoV-2. ELISA showed decreasing titers of serum IgG against the spike receptor-binding domain (RBD) of SARS-CoV-2; on day 148, the patient tested negative for these antibodies (*3*). All 3 serum samples tested negative for IgM against spike RBD (Appendix Figure 2). On day 10, the patient tested negative for N-specific serum IgG by chemiluminescent microparticle immunoassay assay (Abbott, https://www.corelaboratory.abbott) and indirect microtiter plate enzyme immunoassay; he tested weakly positive on day 43 in a validated luciferase immunoprecipitation assay (*4*) (Figure). As reported previously (*6*), a strong antibody response to N protein developed by day 5 of reinfection. This

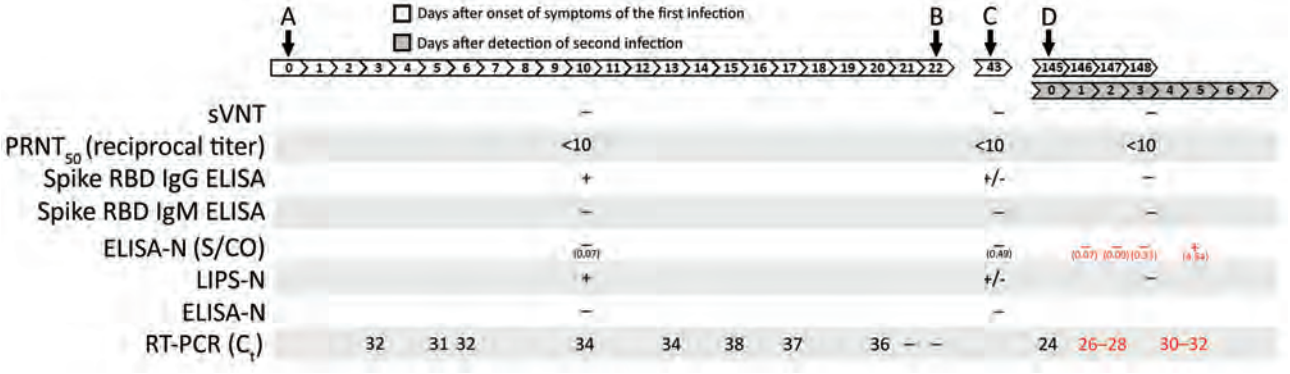

Figure. Timeline of primary infection and reinfection with severe acute respiratory syndrome coronavirus 2, Hong Kong, August, 2020. A) Onset. B) Discharge. C) Clinical follow-up. D) Mandatory testing. Black font indicates data from this investigation; red font indicates data from To et al. (*6*). C_t, cycle threshold; ELISA-N, enzyme linked immunosorbent assay for N protein; LIPS, luciferase immune precipitation assay; $PRNT_{50}$, 50% plaque reduction neutralization test titer; RBD, receptor binding domain; RT-PCR, reverse transcription PCR; S/CO, ratio of optical density readings of sample divided by cutoff (ratio of ≥1.4 considered positive); sVNT, surrogate virus neutralization test; +, positive; –, negative; +/–, borderline.

response suggests that antibody against SARS-CoV-2 developed on reinfection.

Levels of adaptive cytokine interleukin-2 were elevated on days 10 and 43 (Appendix Figure 3, panels A, B). Reinfection coincided with a stronger interleukin-21 memory type response on day 148 than on days 10 and 43.

Previous studies show that most patients with mild, severe, or asymptomatic SARS-CoV-2 infection produce neutralizing antibodies and antibodies against spike RBD and N proteins (*3*,*4*). This case was unusual because the patient had low or undetectable levels of neutralizing and binding antibodies against multiple viral proteins during his primary infection and acute stage of asymptomatic reinfection. He was not immunodeficient because he had IgG against measles and varicella zoster viruses and no history of recurrent infections. The virus from the first infection had a truncation in the 58AA open reading frame 8 gene, which mediates immune evasion through downregulation of major histocompatibility complex and interferon responses (Y. Zhang et al., unpub. data, https://www.biorxiv.org/content/10.1101/2020.05.24.111823v1) (*8*). However, it is unclear if this mutation contributed to the patient's lack of antibody production.

Reasons for this patient's unusual response need to be further investigated. He recovered from his primary infection within 3 weeks, and his secondary infection was asymptomatic. These findings indicate that, in the absence of primary neutralizing antibodies, T cells and mucosal immunity might have played a critical role in resolving the infection. Given the unusual antibody response in this patient to his first infection, researchers must be cautious about generalizing more widely from this patient's experience.

Acknowledgments

We thank Rity Wong, Vickie Li, Miu Ling Chin, Barry Wong, and Kitty Fung for their assistance in this study.

The study was supported by the Health and Medical Research Fund–Commissioned Research on the Novel Coronavirus Disease (COVID-19) (reference nos. COVID190107, COVID190126, COVID190205, and COVID190115) from the Food and Health Bureau, Hong Kong Special Administrative Region Government; and the US National Institutes of Health (contract no. HHSN272201400006C).

About the Author

Prof. Chan is a clinical virologist at the Chinese University of Hong Kong, Hong Kong. His research interests include diagnostics, epidemiology, and pathogenesis.

References

1. Kiyuka PK, Agoti CN, Munywoki PK, Njeru R, Bett A, Otieno JR, et al. Human coronavirus NL63 molecular epidemiology and evolutionary patterns in rural coastal Kenya. J Infect Dis. 2018;217:1728–39. https://doi.org/10.1093/infdis/jiy098
2. Callow KA. Effect of specific humoral immunity and some non-specific factors on resistance of volunteers to respiratory coronavirus infection. J Hyg (Lond). 1985;95:173–89. https://doi.org/10.1017/S0022172400062410
3. Perera RA, Mok CK, Tsang OT, Lv H, Ko RL, Wu NC, et al. Serological assays for severe acute respiratory syndrome coronavirus 2 (SARS-CoV-2), March 2020. Euro Surveill. 2020;25:2000421. https://doi.org/10.2807/1560-7917.ES.2020.25.16.2000421
4. Hachim A, Kavian N, Cohen CA, Chin AWH, Chu DKW, Mok CKP, et al. ORF8 and ORF3b antibodies are accurate serological markers of early and late SARS-CoV-2 infection. [Erratum in: Nat Immunol. 2020 Aug 27; Epub ahead of print].
Nat Immunol. 2020 Aug 17 [Epub ahead of print].
5. Addetia A, Crawford KHD, Dingens A, Zhu H, Roychoudhury P, Huang ML, et al. Neutralizing antibodies correlate with protection from SARS-CoV-2 in humans during a fishery vessel outbreak with high attack rate. J Clin Microbiol. 2020;Aug 21:JCM.02107-20. https://doi.org/10.1128/JCM.02107-20
6. To KK, Hung IF, Ip JD, Chu AW, Chan WM, Tam AR, et al. COVID-19 re-infection by a phylogenetically distinct SARS-coronavirus-2 strain confirmed by whole genome sequencing. Clin Infect Dis. 2020 Aug 25 [Epub ahead of print]. https://doi.org/10.1093/cid/ciaa1275
7. Tan CW, Chia WN, Qin X, Liu P, Chen MI, Tiu C, et al. A SARS-CoV-2 surrogate virus neutralization test based on antibody-mediated blockage of ACE2-spike protein-protein interaction. Nat Biotechnol. 2020;38:1073–8. https://doi.org/10.1038/s41587-020-0631-z
8. Li JY, Liao CH, Wang Q, Tan YJ, Luo R, Qiu Y, et al. The ORF6, ORF8 and nucleocapsid proteins of SARS-CoV-2 inhibit type I interferon signaling pathway. Virus Res. 2020;286:198074. https://doi.org/10.1016/j.virusres.2020.198074

Address for correspondence: Malik Peiris, School of Public Health, Li Ka Shing Faculty of Medicine, The University of Hong Kong, No. 7 Sassoon Rd., Pokfulam, Hong Kong, China; email: malik@hku.hk; Grace Lui, Department of Medicine and Therapeutics, Faculty of Medicine, The Chinese University of Hong Kong, Prince of Wales Hospital, 30-32 Ngan Shing St., Shatin, New Territories, Hong Kong, China; email: gracelui@cuhk.edu.hk

Brucella canis in Commercial Dog Breeding Kennels, Ontario, Canada

J. Scott Weese, Kathleen Hrinivich, Maureen E.C. Anderson

University of Guelph, Guelph, Ontario, Canada (J.S. Weese); Animal Hospital of Cambridge, Cambridge, Ontario (K. Hrinivich); Ministry of Agriculture, Food and Rural Affairs, Guelph (M.E.C. Anderson)

DOI: https://doi.org/10.3201/eid2612.201144

We evaluated the prevalence of *Brucella canis* seropositivity in a convenience sample of dogs from commercial breeding kennels in Ontario, Canada. Overall, 127/1,080 (11.8%) dogs from 23/63 (37%) kennels were seropositive. The prevalence of positive dogs within kennels with ≥1 positive dog ranged from 3.9% to 100% (median 33%).

Brucella canis is a dog-adapted *Brucella* species that most commonly causes reproductive disease and diskospondylitis in dogs and can be carried long-term and subclinically. Zoonotic infections are uncommonly reported (*1*–*4*), but may be underdiagnosed (*3*,*5*).

In Canada, *Brucella canis* has been found predominantly in imported dogs. However, it was identified in 2 adult female dogs from a commercial breeding kennel in Ontario, Canada, in March 2019. We conducted an investigation of prevalence and distribution of *B. canis* in the broader commercial dog breeding population.

We collected serum samples from a convenience sample of dogs at commercial breeding kennels in southern Ontario, Canada. We used rapid slide agglutination test (RSAT) and followed up with positive results using 2-mercaptoethanol RSAT (2ME-RSAT). We performed PCR on whole (EDTA treated) blood from a subset of *B. canis*–seropositive dogs.

We identified positive RSAT and 2ME-RSAT tests in 127/1,080 (11.8%) clinically normal dogs from 23/63 (37%) kennels during March 15–December 18, 2019 (1–61 dogs/kennel, median 7). We considered reactive an additional 82 (7.6%) dogs that were positive by RSAT but negative by 2ME-RSAT; 63 (77%) of those were from kennels from which positive dogs were identified. The prevalence of positive dogs within kennels that had ≥1 positive dog ranged from 3.9% to 100% (median 33%). Whole blood samples from 20 dogs tested by PCR were all negative. We retested 130 dogs 4–6 weeks after the initial test (Table).

The seropositive rate contrasts with a 1980 study that reported 0.3% seroprevalence in dogs from southwestern Ontario (*6*). Studies in other regions have reported seroprevalence rates of 0%–4.6%; higher rates (e.g., 20%–83%) were reported in some breeding kennels (*1*,*7*–*9*). A structured approach to enrollment was not possible because enrollment was based on kennel operators' willingness to participate. Various population enrollment biases might be present in the prevalence estimate. These results should be taken as an indication of widespread presence of *B. canis* bacteria in this population, with high rates in some kennels and the potential for introduction of infected puppies into households.

Because *B. canis* infection is a notifiable disease in Ontario, we obtained data from 2013–2018 from the Ontario Ministry of Agriculture Food and Rural Affairs. Provincially, there were no positive test results for *B. canis* in dogs in 2013, 2015 and 2017, and 1–3 cases in each of 2014, 2016, and 2018. Because prior surveillance was limited, it is unclear whether this is a new problem or one that was previously overlooked. However, these 0–3 diagnoses/year and anecdotal data about recent reproductive disease in some affected kennels make it unlikely that *B. canis* infection was present but undiagnosed. The origin of the infection could not be properly investigated, but it was suspected to have originated from breeding dogs imported from eastern Europe in 2018.

Without a standard approach for clinical or surveillance testing for *B. canis* bacteria, we used the sensitive RSAT followed by the more specific 2ME-RSAT, which is considered a confirmatory test (*10*). Cases with RSAT-positive but 2ME-RSAT–negative results were common; most were subsequently negative. A possible cause was transient cross-reaction with *Bordetella bronchiseptica* vaccination or another pathogen; we could not investigate specifically because information about *B. bronchiseptica* vaccination or infection in these dogs was not available. The potential for false-positive results should be considered, particularly because infected dogs are often euthanized in accordance with regulatory requirements.

Table. Initial and follow-up serologic testing for *Brucella canis* in 130 dogs, Canada

Initial result	No.	Follow-up result*	No. (%)
Negative	84	Positive	0 (0)
		Reactive	0 (0)
		Negative	84 (100)
Positive	9	Positive	6 (67)
		Reactive	1 (11)
		Negative	2 (22)
Reactive	37	Positive	1 (0.3)
		Reactive	2 (0.5)
		Negative	34 (92)

*Follow-up testing was performed 4–6 weeks after the initial test.

Limited PCR testing was performed because of negative results in the first 20 samples; negative results were presumed due to the intermittent nature of *B. canis* bacteremia in clinically normal animals. Although PCR or culture can provide a definitive diagnosis, sensitivity can be low for screening; it is higher when testing reproductive or fetal fluids or tissues from abortions or stillbirths for *B. canis*.

Limited clinical data were available. Some affected kennels reported substantial reproductive challenges presumably associated with brucellosis (e.g., small litter sizes, abortions, stillbirths, low conception rates) whereas no problems were reported in others. Whether this reflects lack of recognition of problems, subclinical infection, or early infection that had not yet resulted in overt reproductive disease is unclear.

Underdiagnosis of *B. canis* as a cause of nonspecific disease (e.g., undulating fever, fatigue, headache, malaise, chills, weight loss, hepatomegaly, splenomegaly, lymphadenopathy) and human brucellosis is a concern; physicians are more likely to perform serologic tests that target smooth *Brucella* species (*B. abortus, B. suis*, and *B. melitensis*). Physicians should consider the potential presence of *B. canis* in patients with disease suggestive of brucellosis, especially those with animal contact, and realize the limitations of serologic testing.

Brucella canis should be considered endemic to commercial dog kennels in Ontario, with potential human health risks. *B. canis* screening of breeding dogs is recommended (*10*), and testing of puppies from parents of unknown *Brucella* status is reasonable.

Acknowledgments

We thank Tim Pasma for providing *B. canis* reports from previous years in Ontario.

This study was supported by the Ontario Animal Health Network.

About the Author

Dr. Weese is a veterinary internist at the University of Guelph, Guelph, Ontario, Canada. His primary research interests are infectious diseases and infection control, and he has a particular interest in emerging diseases, zoonotic diseases, and antimicrobial stewardship.

References

1. Johnson CA, Carter TD, Dunn JR, Baer SR, Schalow MM, Bellay YM, et al. Investigation and characterization of *Brucella canis* infections in pet-quality dogs and associated human exposures during a 2007–2016 outbreak in Michigan. J Am Vet Med Assoc. 2018;253:15.
2. Lucero NE, Corazza R, Almuzara MN, Reynes E, Escobar GI, Boeri E, et al. Human *Brucella canis* outbreak linked to infection in dogs. Epidemiol Infect. 2010;138:280–5. https://doi.org/10.1017/S0950268809990525
3. Lucero NE, Escobar GI, Ayala SM, Jacob N. Diagnosis of human brucellosis caused by *Brucella canis*. J Med Microbiol. 2005;54:457–61. https://doi.org/10.1099/jmm.0.45927-0
4. Dentinger CM, Jacob K, Lee LV, Mendez HA, Chotikanatis K, McDonough PL, et al. Human *Brucella canis* infection and subsequent laboratory exposures associated with a puppy, New York City, 2012. Zoonoses Public Health. 2015;62:407–14. https://doi.org/10.1111/zph.12163
5. Hensel ME, Negron M, Arenas-Gamboa AM. Brucellosis in dogs and public health risk. Emerg Infect Dis. 2018;24:1401–6. https://doi.org/10.3201/eid2408.171171
6. Bosu WTK, Prescott JF. A serological survey of dogs for *Brucella canis* in southwestern Ontario. Can Vet J. 1980; 21:198–200.
7. Brower A, Okwumabua O, Massengill C, Muenks Q, Vanderloo P, Duster M, et al. Investigation of the spread of *Brucella canis* via the U.S. interstate dog trade. Int J Infect Dis. 2007;11:454–8. https://doi.org/10.1016/j.ijid.2006.12.009
8. Dahlbom M, Johnsson M, Myllys V, Taponen J, Andersson M. Seroprevalence of canine herpesvirus-1 and *Brucella canis* in Finnish breeding kennels with and without reproductive problems. Reprod Domest Anim. 2009;44:128–31. https://doi.org/10.1111/j.1439-0531.2007.01008.x
9. Higgins R, Hoquet F, Bourque R, Gosselin Y. A serological survey for *Brucella canis* in dogs in the Province of Quebec. Can Vet J. 1979;20:315–7.
10. Bramlage DJ, Fortney W, Kesler RM, Mabray CJ, Mason JW, Reinhold H, et al. Best practices for *Brucella canis* prevention and control in dog breeding facilities. US Department of Agriculture. 2015 [cited 2020 Oct 21]. https://www.aphis.usda.gov/animal_welfare/downloads/brucella_canis_prevention.pdf

Address for correspondence: J. Scott Weese, Centre for Public Health and Zoonoses, Ontario Veterinary College, University of Guelph, Guelph, ON, N1G2W1 Canada; email: jsweese@ovc.uoguelph.ca

Novel Serotype of Epizootic Hemorrhagic Disease Virus, China

Heng Yang,[1] Zhuoran Li,[1] Jinping Wang, Zhanhong Li, Zhenxing Yang, Defang Liao, Jianbo Zhu, Huachun Li

Author affiliation: Yunnan Animal Science and Veterinary Institute, Kunming, China

DOI: https://doi.org/10.3201/eid2612.191301

In 2018, a strain of epizootic hemorrhagic disease virus (EHDV), named YNDH/V079/2018, was isolated from a sentinel calf in Mangshi County, Yunnan Province, China. Nucleotide sequencing and neutralization tests indicated that the virus belongs to a novel serotype of EHDV that had not been reported previously.

Epizootic hemorrhagic disease virus (EHDV; family *Reoviridae*, genus *Orbivirus*) is transmitted between ruminants by *Culicoides* spp. biting midges. It is widespread in tropical and subtropical regions and primarily infects white-tailed deer and cattle (*1*); EHDV infection often causes death in white-tailed deer. Seven serotypes of EHDV (EHDV-1, -2, -4, -5, -6, -7, and -8) have been officially assigned; EHDV-3 (NIG1967/01 strain) has been combined into EHDV-1 (*1*,*2*). Recently, 2 novel EHDV strains isolated from South Africa (*3*) and Japan (*4*) were suggested as new serotype candidates. Although only Ibaraki virus (a strain of EHDV-2 from Japan) was previously known to cause a bluetongue-like illness in cattle (*1*), EHDV-1, EHDV-2, EHDV-6, and EHDV-7 have recently been associated with illness and death in cattle in Asia, the Mediterranean Basin, South Africa, North America, and Réunion Island (*1*,*5*–*7*), suggesting that the distribution and the pathogenicity associated with EHDV infection are increasing. EHDVs belonging to serotypes 1, 5, 6, and 7, as well as a nontyped serotype, have been isolated from sentinel cattle in southern China (H. Li et al., unpub. data).

In 2018, we placed 10 Yunnan yellow cattle 6–12 months of age and free of EHDV antibodies under field conditions at Sanjiaoyan village, Mangshi County, Dehong Prefecture, Yunnan Province, China (Appendix Figure 1, https://wwwnc.cdc.gov/EID/article/26/12/19-1301-App1.pdf) as sentinel animals. We took blood samples at weekly intervals during May–October: whole blood for serology, EDTA samples for viral nucleic acid detection, and heparin blood samples for virus isolation.

During June–September, we confirmed EHDV infections in 3 of the sentinel cattle by EHDV competitive ELISA (cELISA; ID-Vet, https://www.id-vet.com) and real-time quantitative reverse transcription PCR (qRT-PCR) (*3*). We isolated viruses from blood samples by inoculating C6/36 cells and blindly passaging for 5 times on BHK-21 cells (*1*). We isolated EHDV-1 and EHDV-5 strains from 2 of the cattle and an additional strain of EHDV, YNDH/V079/2018, from the third animal. Serotype identification of YNDH/V079/2018 displayed uniform negative results through serotype-specific RT-PCR (*8*) and virus neutralization tests using serum samples against EHDV-1, EHDV-2, EHDV-5, EHDV-6, EHDV-7, EHDV-8, and nontyped serotype reference strains. Furthermore, serum from the YNDH/V079/2018-infected calf showed no neutralization to tested serotypes of EHDV reference strains.

Double-stranded RNA extracted from YNDH/V079/2018 generated a genome segment migration pattern typical of bluetongue virus or EHDV (Appendix Figure 2) by agarose gel electrophoresis. Transmission electron microscopy revealed virus particles ≈80 nm in diameter, with a ring-shaped capsomere characteristic of *Orbivirus* (Appendix Figure 3). Full-length cDNA copies of segments 2 and 3 (Seg-2 and Seg-3) of YNDH/V079/2018 were synthesized and sequenced as described by Maan et al. (*9*). BLAST analyses (https://www.ncbi.nlm.nih.gov/BLAST) of Seg-2 and Seg-3 sequences (GenBank accession nos. MN418446 and MN418447) revealed the highest matching identities with equivalent genome segments of other EHDVs.

Subcore shell viral protein (VP) 3 of EHDV, encoded by Seg-3, is highly conserved, showing >95.5% amino acid sequence identity within EHDVs (*10*). Seg-3/VP3 of YNDH/V079/2018 showed overall nucleotide/amino acid identity levels of 78.5%/94.6% to 80.0%/96.5% with other EHDVs, confirming its identity as an EHDV isolate. However, Seg-3 of YNDH/V079/2018 did not cluster with previously identified Eastern or Western EHDV topotypes (*10*); maximum sequence identities were 80.0% nt and 78.9% aa, which placed YNDH/V079/2018 as a distinct topotype in the phylogenetic tree (Figure, panel A).

The outer capsid protein VP2 of EHDV, encoded by Seg-2, is highly variable and is definitive for serotype determination (*2*). Seg-2/VP2 of YNDH/V079/2018 sharing sequence identities of 44.3%–50.9% nt and 31.0%–40.6% aa to previously recognized EHDV serotypes, which supports it as a distinct EHDV Seg-2 group (*2*), herein named group E (Figure, panel B). This finding coincides with the results of neutralization tests and indicates that YNDH/V079/2018 represents a novel serotype of EHDV.

[1]These authors contributed equally to this article..

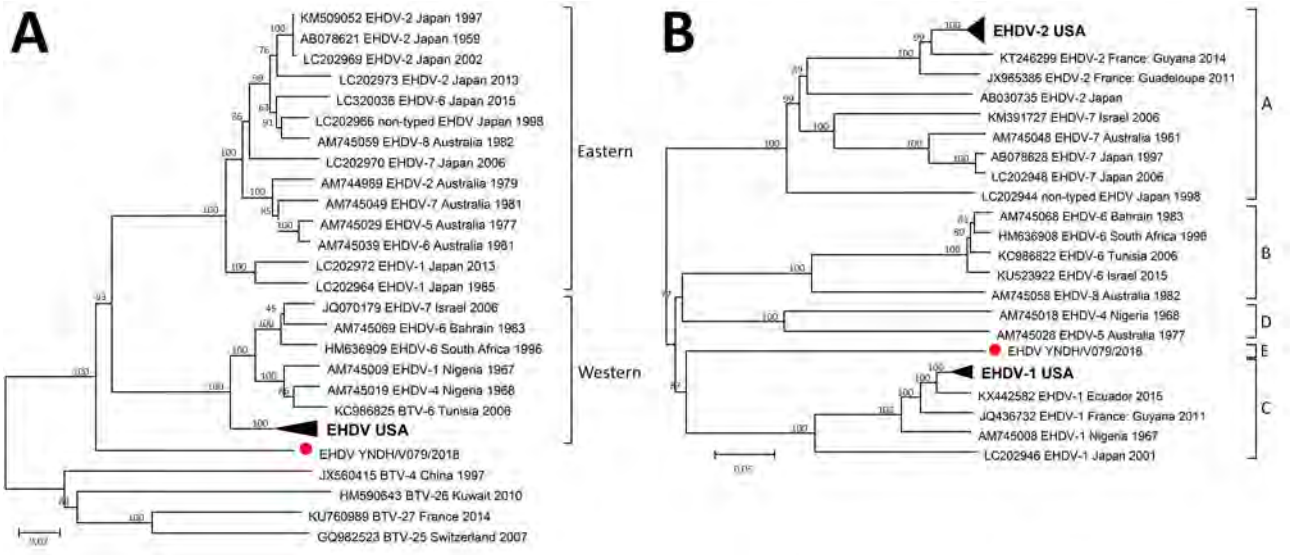

Figure. Phylogenetic analyses of EHDV based on segment 3 (A) and segment 2 (B) of YNDH/V079/2018 from Mangshi County, Yunnan Province, China (red dot), compared with other global EHDV isolates. The following convention was used to identify sequences: GenBank accession no., EHDV-serotype, country, isolation year. Eastern and Western topotypes of segment 3 and A–D groups of segment 2 were assigned as described by Anthony et al. (*2*,*10*); a distinct segment 2 group of the strain YNDH/V079/2018 isolated in China (*2*) is marked as group E. The nontyped strain from Japan isolated in 1998 is included in accession nos. LC202966 and LC202944 (*4*). We did not include the nontyped strain from South Africa, due to the lack of sequence information in GenBank. BTV strains were used as the outgroups. Number at each branch indicates a bootstrap value. Scale bars indicate nucleotide substitutions per site. BTV, bluetongue virus; EHDV, epizootic hemorrhagic disease virus.

We developed conventional RT-PCR and qRT-PCR targeting Seg-2 of YNDH/V079/2018 (Appendix Table 1) and used them in combination with cELISA and serum neutralization tests to trace progress of the infection in the sentinel animal (Appendix Table 2). We defined the earliest week in which the virus was detectable in the blood using qRT-PCR as infection week 1. We isolated YNDH/V079/2018 in week 2 from the sentinel calf, which experienced fever to 40.2°C, anorexia, and respiratory distress. Viral nucleic acid in the blood peaked in weeks 1–2; levels decreased gradually until none was detected at week 14. cELISA and neutralization antibodies first appeared at week 2, peaked in weeks 7–8, and remained elevated until week 17, when blood sampling ceased.

To determine the prevalence of YNDH/V079/2018, we tested 87 EDTA cattle blood samples from 3 farms in Mangshi County during April–October 2018 but detected no nucleic acid consistent with YNDH/V079/2018. Additional genome sequencing, type-specific diagnostic tests, and epidemiologic and pathogenic investigations of this novel EHDV are planned. Our study will help clarify the diversity of EHDV serotypes and the distribution and pathogenicity of this novel EHDV and its potential risk to ruminants.

Acknowledgments

We thank colleagues from the Center for Animal Disease Control and Prevention of Dehong Prefecture who collected blood samples from sentinel animals.

This study, "Arbovirus Disease Research in Cattle and Sheep," was supported by Special Fund for Agro-scientific Research in the Public Interest (project no. 201303035) and National Key R&D Program of China (project no. 2017YFC1200500).

About the Author

Dr. Yang is a research fellow in Yunnan Animal Science and Veterinary Institute, Kunming, China. His current research interests include characterization of bluetongue virus and other related arboviruses of ruminants.

References

1. World Organisation for Animal Health. Epizootic hemorrhagic disease (infection with epizootic hamorrhagic disease virus). In: Manual of diagnostic tests and vaccines for terrestrial animals 2019. Paris; The Organisation: 2018. p. 422–32.
2. Anthony SJ, Maan S, Maan N, Kgosana L, Bachanek-Bankowska K, Batten C, et al. Genetic and phylogenetic analysis of the outer-coat proteins VP2 and VP5 of epizootic haemorrhagic disease virus (EHDV): comparison of genetic and serological data to characterise the EHDV serogroup. Virus Res. 2009;145:200–10. https://doi.org/10.1016/j.virusres.2009.07.012

3. Maan NS, Maan S, Potgieter AC, Wright IM, Belaganahalli M, Mertens PPC. Development of real-time RT-PCR assays for detection and typing of epizootic haemorrhagic disease virus. Transbound Emerg Dis. 2017;64:1120–32. https://doi.org/10.1111/tbed.12477
4. Shirafuji H, Kato T, Yamakawa M, Tanaka T, Minemori Y, Yanase T. Characterization of genome segments 2, 3 and 6 of epizootic hemorrhagic disease virus strains isolated in Japan in 1985-2013: identification of their serotypes and geographical genetic types. Infect Genet Evol. 2017;53:38–46. https://doi.org/10.1016/j.meegid.2017.05.010
5. Golender N, Bumbarov VY. Detection of epizootic hemorrhagic disease virus serotype 1, Israel. Emerg Infect Dis. 2019;25:825–7. https://doi.org/10.3201/eid2504.180149
6. Temizel EM, Yesilbag K, Batten C, Senturk S, Maan NS, Mertens PPC, et al. Epizootic hemorrhagic disease in cattle, western Turkey. Emerg Infect Dis. 2009;15:317–9. https://doi.org/10.3201/eid1502.080572
7. Kamomae Y, Kamomae M, Ohta Y, Nabe M, Kagawa Y, Ogura Y, et al. Epizootic hemorrhagic disease virus serotype 6 infection in cattle, Japan, 2015. Emerg Infect Dis. 2018;24:902–5. https://doi.org/10.3201/eid2405.171859
8. Maan NS, Maan S, Nomikou K, Johnson DJ, El Harrak M, Madani H, et al. RT-PCR assays for seven serotypes of epizootic haemorrhagic disease virus & their use to type strains from the Mediterranean region and North America. PLoS One. 2010;5:e12782. https://doi.org/10.1371/journal.pone.0012782
9. Maan S, Rao S, Maan NS, Anthony SJ, Attoui H, Samuel AR, et al. Rapid cDNA synthesis and sequencing techniques for the genetic study of bluetongue and other dsRNA viruses. J Virol Methods. 2007;143:132–9. https://doi.org/10.1016/j.jviromet.2007.02.016
10. Anthony SJ, Maan N, Maan S, Sutton G, Attoui H, Mertens PP. Genetic and phylogenetic analysis of the core proteins VP1, VP3, VP4, VP6, and VP7 of epizootic haemorrhagic disease virus (EHDV). Virus Res. 2009;145:187–99. https://doi.org/10.1016/j.virusres.2009.07.011

Address for correspondence: Huachun Li or Heng Yang, Yunnan Animal Science and Veterinary Institute, Jindian St, Kunming 650224, China; email: Li_huachun@hotmail.com or yangheng2008.cool@163.com

Pathogenic New World Relapsing Fever *Borrelia* in a *Myotis* Bat, Eastern China, 2015

Hui-Ju Han, Jian-Wei Liu, Hong-Ling Wen, Ze-Min Li, Si-Cong Lei, Xiang-Rong Qin, Chuan-Min Zhou, Hao Yu, Xiao Xiao, Xue-Jie Yu

Author affiliations: Wuhan University, Wuhan, China (H.-J. Han, J.-W. Liu, Z.-M. Li, S.-C. Lei, X.-R. Qin, C.-M. Zhou, H. Yu, X.-J. Yu); Shandong University, Jinan, China (H.-L. Wen); Hubei University of Chinese Medicine, Wuhan (X. Xiao)

DOI: https://doi.org/10.3201/eid2612.191450

We identified *Candidatus* Borrelia fainii, a human pathogenic bacterium causing New World relapsing fever in a *Myotis* bat in eastern China. This finding expands knowledge about the geographic distribution of *Borrelia* spp. and the potential for infection with New World relapsing fever in China.

Borrelia is a genus comprising 3 groups of spirochetes: the Lyme disease group, the relapsing fever group, and a nonconformist third group. Typically, Lyme disease borreliae are transmitted by hard ticks and have a worldwide distribution, but most relapsing fever *Borrelia* are transmitted by soft ticks, except for louse-borne *B. recurrentis*. Relapsing fever borreliae are further classified into 2 subgroups, New World relapsing fever (NWRF) *Borrelia* and Old World relapsing fever, on the basis of epidemic regions and the genetic lineage of the causative agent. *B. lonestari* and *B. miyamotoi* are transmitted by hard ticks, but are more closely related to relapsing fever borreliae than to Lyme disease borreliae and are distributed both in the New World (North and South America and Oceania) and the Old World (Europe, Asia, and Africa). The nonconformist third group includes an orphan *Borrelia* species named *B. turicata* (*1*). We identified *Candidatus* Borrelia fainii in a *Myotis* bat from eastern China.

During March–October 2015, with the help of local farmers, we caught a total of 145 bats from various niches in Mengyin County, Shandong Province, China, using mist nets or butterfly nets and took tissue samples (liver, spleen, lung, or kidney). The captured bats included 4 *Rhinolophus ferrumequinum* and 14 *Rh. pusillus* from a karst cave, 26 *Eptesicus serotinus* from 2 farm houses, 34 *Myotis fimbriatus* and 10 *M. ricketti* from a city sewer, and 57 *M. pequinius* from a cave. We extracted DNA from the bat tissue, then screened for *Borrelia* by amplifying the *rrs*, *flaB*, and *glpQ* genes using methods

described previously (2–4); after gel extraction, we cloned the PCR products into pMD19 T-vectors (TaKaRa, https://www.takarabio.com) for sequencing.

We found 1 *M. ricketti* bat positive for *Borrelia* (GenBank accession nos. MG832412 for *rrs*, MG832413 for *flaB*, and MG921625 for *glpQ*). BLAST searches showed that *rrs* exhibited 99.7% (1,491/1,495 bp) identity with *Candidatus* Borrelia fainii (accession no. LC382043), *flaB* exhibited 97.9% (756/772 bp) identity with *B. turicatae* (accession no. CP015629), and *glpQ* exhibited 97.6% (859/880 bp) identity with *B. parkeri* (accession no. AY934633).

We performed multilocus sequence typing (MLST) by amplifying 8 housekeeping genes (*clpA*, *clpX*, *nifS*, *pepX*, *pyrG*, *recG*, *rplB*, and *uvrA*) with degenerate primers from the *Borrelia* MLST database (https://pubmlst.org/borrelia). Sequence query showed that all 8 housekeeping genes were novel alleles, which were assigned the following novel allele numbers: *clpA* (298), *clpX* (261), *nifS* (235), *pepX* (264), *pyrG* (277), *recG* (292), *rplB* (254) and *uvrA* (268); the *Borrelia* species of this study was designated sequence type (ST) 927.

Sequences of the 8 housekeeping genes were concatenated in the order *clpA*, *clpX*, *nifS*, *pepX*, *pyrG*, *recG*, *rplB*, and *uvrA* and imported into MEGA7 (MEGA, https://www.megasoftware.net) for phylogenetic analysis. We constructed a phylogenetic tree using the maximum-likelihood method with the Kimura 2-parameter model. The ST927 *Borrelia* species was phylogenetically closely related to multiple NWRF

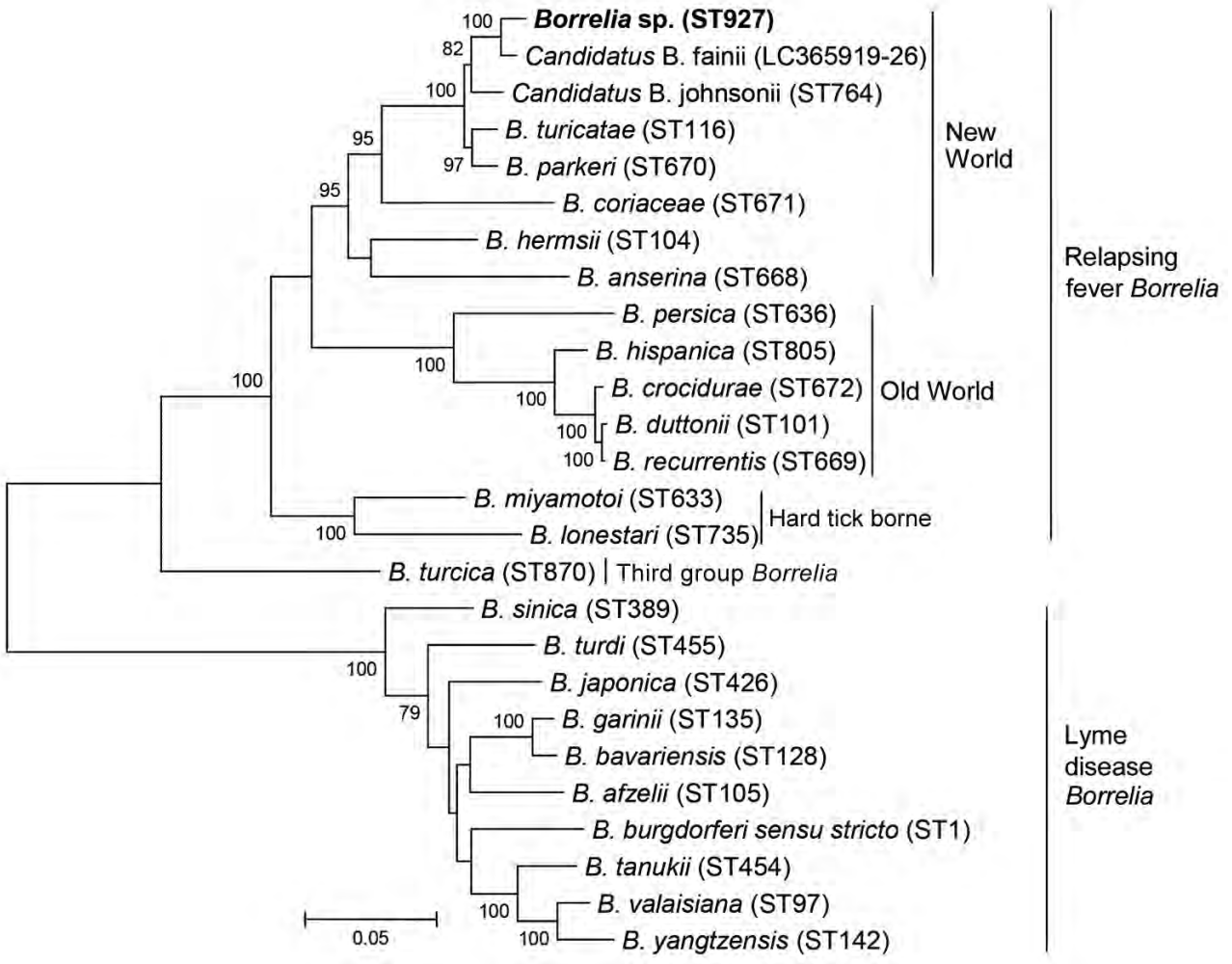

Figure. Phylogenetic analysis of *Borrelia* species based on 8 concatenated housekeeping genes (*clpA-clpX-nifS-pepX-pyrG-recG-rplB-uvrA*). Bold indicates *Borrelia* species identified in study of pathogenic New World relapsing fever *Borrelia* in a *Myotis* bat, eastern China, 2015. The tree was constructed by using the maximum-likelihood method in MEGA7 (https://www.megasoftware.net). Bootstrap values were calculated with 1,000 replicates. There were a total of 4,776 positions in the final dataset. Reference sequences of *Borrelia* species were downloaded from the *Borrelia* MLST database; the corresponding sequence type (ST) number of each *Borrelia* species is shown in parentheses. For *Candidatus* Borrelia fainii, the GenBank accession number is shown instead of an ST number because the 8 housekeeping gene sequences of *Candidatus* Borrelia fainii were only submitted to GenBank and no ST number was assigned. Scale bar indicates 5% divergence.

Borrelia species, including *B. turicatae*, *B. parkerii*, and *Candidatus* Borrelia johnsonii, which are endemic in the United States, as well as *Candidatus* Borrelia fainii, which was recently identified in Zambia (Figure 1).

We calculated pairwise genetic distances using the Kimura 2-parameter model and identified relapsing fever *Borrelia* spp. using the threshold of 98.3% similarity and genetic distance 0.017 (*5*). Genetic distance analysis of the 8 concatenated housekeeping genes (4,776 bp) revealed a value of 0.015 compared with *Candidatus* Borrelia fainii, strain Qtaro. Thus, the *Borrelia* sp. in our study was identified as *Candidatus* Borrelia fainii.

There have been several reports of NWRF *Borrelia* spp. in the Old World, although exclusively in Africa. A new human pathogenic *Borrelia* spp. was identified in *Ornithodoros* ticks from Tanzania that grouped together with NWRF borreliae rather than the relapsing fever–inducing spirochetes previously known to be endemic in East Africa (*6*). Another study described the discovery of a NWRF *Borrelia*, *Candidatus* Borrelia kalaharica, in a traveler returning from the Kalahari Desert (*7*). Finally, a 2019 study reported on a NWRF *Borrelia*–like spirochete, *Candidatus* Borrelia fainii, recently isolated from a febrile patient as well as from bats and bat ticks in Zambia (*8*).

Whether bats are reservoirs for *Borrelia* remains inconclusive. A new Old World relapsing fever *Borrelia* species, CPB1, was found responsible for the death of a *Pipistrelle* bat in the United Kingdom (*9*) and was also detected in bat soft ticks in France (*10*). A recent study found that bats and bat soft ticks collected from a cave in Zambia showed a high infection rate for *Candidatus* Borrelia fainii, and the authors proposed that bats contribute to the environmental cycle of *Candidatus* Borrelia fainii as hosts and bat soft ticks as vectors (*8*). For this study, we found only 1 bat infected with *Candidatus* Borrelia fainii, and it remains unclear whether bats serve as reservoirs of this *Borrelia* species. However, with the discovery of *Candidatus* Borrelia fainii in China, both health officials and physicians should pay attention to its potential emergence.

Acknowledgments

We are grateful to Dr. Gabriele Margos, the curator of the *Borrelia* MLST database (https://pubmlst.org/borrelia), for providing us the degenerate primers for relapsing fever *Borrelia* MLST.

The collection of bats for microbiological studies was approved by the Ethics Committee of Prevention Medicine of Shandong University (No. 20150501).

This work was supported by the National Natural Science Funds of China (grant numbers: 81971939) and the China Postdoctoral Science Foundation Funded Project (grant numbers: 2019M662720).

About the Author

Dr. Han is a postdoctoral researcher in School of Health Sciences, Wuhan University. Her research interests include emerging infectious diseases and vector-borne diseases, especially bat-borne diseases.

References

1. Cutler SJ, Ruzic-Sabljic E, Potkonjak A. Emerging borreliae—expanding beyond Lyme borreliosis. Mol Cell Probes. 2017;31:22–7. https://doi.org/10.1016/j.mcp.2016.08.003
2. Evans NJ, Brown JM, Demirkan I, Singh P, Getty B, Timofte D, et al. Association of unique, isolated treponemes with bovine digital dermatitis lesions. J Clin Microbiol. 2009;47:689–96. https://doi.org/10.1128/JCM.01914-08
3. Assous MV, Wilamowski A, Bercovier H, Marva E. Molecular characterization of tickborne relapsing fever *Borrelia*, Israel. Emerg Infect Dis. 2006;12:1740–3. https://doi.org/10.3201/eid1211.060715
4. Toledo A, Anda P, Escudero R, Larsson C, Bergstrom S, Benach JL. Phylogenetic analysis of a virulent *Borrelia* species isolated from patients with relapsing fever. J Clin Microbiol. 2010;48:2484–9. https://doi.org/10.1128/JCM.00541-10
5. Kingry LC, Anacker M, Pritt B, Bjork J, Respicio-Kingry L, Liu G, et al. Surveillance for and discovery of *Borrelia* species in US patients suspected of tickborne illness. Clin Infect Dis. 2018;66:1864–71. https://doi.org/10.1093/cid/cix1107
6. Kisinza WN, McCall PJ, Mitani H, Talbert A, Fukunaga M. A newly identified tick-borne *Borrelia* species and relapsing fever in Tanzania. Lancet. 2003;362:1283–4. https://doi.org/10.1016/S0140-6736(03)14609-0
7. Fingerle V, Pritsch M, Wächtler M, Margos G, Ruske S, Jung J, et al. "*Candidatus* Borrelia kalaharica" detected from a febrile traveller returning to Germany from vacation in southern Africa. PLoS Negl Trop Dis. 2016;10:e0004559. https://doi.org/10.1371/journal.pntd.0004559
8. Qiu Y, Nakao R, Hang'ombe BM, Sato K, Kajihara M, Kanchela S, et al. Human borreliosis caused by a New World relapsing fever *Borrelia*-like organism in the Old World. Clin Infect Dis. 2019;69:107–12. https://doi.org/10.1093/cid/ciy850
9. Evans NJ, Bown K, Timofte D, Simpson VR, Birtles RJ. Fatal borreliosis in bat caused by relapsing fever spirochete, United Kingdom. Emerg Infect Dis. 2009;15:1331–3. https://doi.org/10.3201/eid1508.090475
10. Socolovschi C, Kernif T, Raoult D, Parola P. *Borrelia*, *Rickettsia*, and *Ehrlichia* species in bat ticks, France, 2010. Emerg Infect Dis. 2012;18:1966–75. https://doi.org/10.3201/eid1812.111237

Address for correspondence: Xiao Xiao, Institute of Epidemiology Research, Hubei University of Traditional Chinese Medicine, Huangjiahuxi Road No.16, Wuhan 430065, Hubei, China, email: xiaoalltheway@gmail.com; Xue-Jie Yu, State Key Laboratory of Virology, School of Health Sciences, Wuhan University, Donghu Road No. 115, Wuhan 430071, Hubei, China, email: yuxuejie@whu.edu.cn

High *Coxiella burnetii* Seroconversion Rate in Veterinary Students, the Netherlands, 2006–2010

Marit M.A. de Lange, Wim van der Hoek, Peter M. Schneeberger, Arno Swart, Dick J.J. Heederik, Barbara Schimmer, Inge M. Wouters

Author affiliations: National Institute for Public Health and the Environment, Bilthoven, the Netherlands (M.M.A. de Lange, W. van der Hoek, A. Swart, B. Schimmer); Jeroen Bosch Hospital, 's-Hertogenbosch, the Netherlands (P.M. Schneeberger); Utrecht University, Utrecht, the Netherlands (D.J.J. Heederik, I.M. Wouters)

DOI: https://doi.org/10.3201/eid2612.200063

We examined *Coxiella burnetii* seroconversion rates by measuring *C. burnetii* IgG among 2 cohorts of veterinary students. During follow-up of 118 seronegative veterinary students, 23 students seroconverted. Although the clinical importance of the presence of antibodies is unknown, veterinary students should be informed about the potential risks for Q fever.

Q fever is caused by the bacteria *Coxiella burnetii* and can manifest as acute or chronic illness. Veterinarians who care for livestock are prone to *C. burnetii* infection (*1*,*2*). A high seroprevalence among veterinary students has been reported (*3*–*5*). However, the incidence of Q fever and associated risk factors during veterinary training are still unknown. We conducted a longitudinal study at the Faculty of Veterinary Medicine of Utrecht University (FVMUU), Utrecht, the Netherlands, in which we followed incoming, seronegative veterinary students and investigated potential associated factors for seroconversion.

Veterinary students who started in 2006 or 2008 at FVMUU were invited to participate. After obtaining written informed consent, we collected blood samples, and participants completed a baseline questionnaire. From participants who began at FVMUU in 2006 (cohort 2006), ≤2 additional blood samples and follow-up questionnaires were obtained in 2008 and 2010. Students who started in 2008 (cohort 2008) provided 1 follow-up blood sample and 1 follow-up questionnaire in 2010.

Serum samples were tested for IgG against phase I and II of *C. burnetii*, using an indirect immunofluorescence assay as previously described (*3*). Those samples with IgG phase I or II IgG ≥1:32 were classified as *C. burnetii* seropositive. Seroconversion was defined as the change observed in a participant who was IgG seronegative at baseline and seropositive in a follow-up sample.

We determined differences in demographics and past animal exposure between seropositive and seronegative participants at baseline. Risk factors for seroconversion were estimated by using univariable logistic regression analyses through generalized estimating equations models (Appendix, https://wwwnc.cdc.gov/EID/article/26/12/20-0063-App1.pdf).

At the beginning of their veterinary training, 447 students were invited to participate in the study. Of those, 131 participated, of whom 13 (10%) were *C. burnetii* IgG seropositive at baseline. Students who were seropositive at baseline were more likely to have lived on a farm and to have had contact with cattle and poultry (Appendix Table 1).

Of the 118 participants seronegative at baseline, 78 started their training in 2006 and 40 in 2008 (Figure). Of those students, 23 seroconverted during the follow-up period of 362 person-years, translating to an incidence of 0.06/person-year. Of the 17 seroconversions in cohort 2006, 11 occurred between baseline and the

	2006	2008	2010
No. in 2006 cohort	78	77	73
Questionnaire no., %	77/78 (99)	77/77 (100)	71/73 (97)
Blood no., %	78/78 (100)	72/77 (94)	63/73 (86)
Seropositive no., %	0/78 (0)	11/77 (15)	17/63 (27)
No. in 2008 cohort		40	40
Questionnaire no., %		39/40 (98)	38/40 (95)
Blood no., %		40/40 (100)	40/40 (100)
Seropositive no., %		0/40/(0)	6/40 (15)

Figure. Follow-up timeline illustrating number and percentages of seronegative participants at baseline, per follow-up moment, in study of *Coxiella burnetii* seroconversion rate in veterinary students, the Netherlands, 2006–2010. The 17 seropositive students in 2010 include the 11 students who already seroconverted during 2006–2008 and were censored from risk factor analysis in 2010.

Table. Characteristics from follow-up questionnaire in association with *Coxiella burnetii* seroconversion among 118 veterinary students seronegative at baseline, the Netherlands*

Characteristic	Odds ratio (95% CI)	p value
Age group, y		
≤20	Referent	
21	0.9 (0.2–3.5)	0.85
≥22	1.3 (0.4–4.2)	0.69
Sex		
M	Referent	
F	0.7 (0.2–2.3)	0.53
Regular exposure to cigarette smoke		
Yes	1.1 (0.4–2.8)	0.81
No	Referent	
Living on a farm with cattle		
Yes	ND	
No	ND	
Living on a farm with sheep or goats		
Yes	6.2 (1.4–28.1)	0.02
No	Referent	
Living on a farm with pigs		
Yes	ND	
No	ND	
Living on a farm with chickens		
Yes	3.0 (0.3–35.0)	0.39
No	Referent	
Regular contact with cattle outside veterinary training		
Yes	0.3 (0.1–2.7)	0.31
No	Referent	
Regular contact with goats outside veterinary training		
Yes	0.6 (0.1–3.8)	0.56
No	Referent	
Regular contact with horses outside veterinary training		
Yes	0.7 (0.3–1.7)	0.40
No	Referent	
Regular contact with pigs outside veterinary training		
Yes	ND	
No	ND	
Regular contact with chickens outside veterinary training		
Yes	0.5 (0.1–3.8)	0.50
No	Referent	
Regular contact with sheep outside veterinary training		
Yes	4.4 (1.2–16.7)	0.03
No	Referent	
History of performing animal nursing on farm where they lived		
Yes	3.6 (0.9–14.3)	0.07
No	Referent	
History of working with straw or hay on farm where they lived		
Yes	6.4 (1.6–26.1)	<0.01
No	Referent	
History of working with fertilizers on farm where they lived		
Yes	3.2 (0.5–19.6)	0.21
No	Referent	
History of performing plant nursing on farm where they lived		
Yes	3.1 (0.3–33.5)	0.35
No	Referent	
No. years after study start†		
2	Referent	
4	1.0 (0.3–2.9)	0.96
Cohort‡		
2006	Referent	
2008	0.7 (0.3–2.0)	0.56
Chosen specialization during veterinary training		
Individually kept animals	Referent	
Veterinary public health or farm animals	1.6 (0.5–5.0)	0.38

*ND, not determined because of low numbers.
†Only adjusted for cohort.
‡Only adjusted for number of years after the study.

first follow-up, and 4 occurred between the first and second follow-up (Appendix Table 2). None of the seroconverted participants reported a diagnosis of acute Q fever from a general practitioner or medical specialist, suggesting all cases were mild or asymptomatic. In addition, no participants had serologic indication of a chronic infection. Of the 20 investigated characteristics, "living on a sheep or goat farm," "having contact with sheep outside [veterinary] training," and "working with hay, straw, silage grass, or animal feed" outside FVMUU increased the odds of seroconversion (Table).

We were not able to identify education-related potential risk factors, such as courses taken, for 2 reasons. First, the curriculum changed during our study, so participants from the 2006 and 2008 cohorts took different courses, causing low power in the analysis. Second, within each cohort, little variation occurred in courses taken. Another limitation of this study is our assumption of a constant risk for *C. burnetii* exposure during the study period. Students seem to have been at higher risk for infection in the first 2 study years, although we cannot draw definite conclusions from this small group of students.

Identified risk factors for seroconversion were not education-related. Proximity to (aborting) small ruminants, such as goats and sheep, was a risk factor in an outbreak in the Netherlands (*6*). Veterinary students have a high prevalence of animal contacts outside their education (*7*). In addition, contact with hay, straw, silage grass, or animal feed, is a known risk factor for human Q fever (*8*). A major outbreak of acute Q fever occurred in the Netherlands during 2007–2010 (*9*), and some students might have contracted the infection then, although increased seroprevalence of Q fever in veterinary students before that outbreak has been reported (*3*).

In conclusion, we found a considerable *C. burnetii* seroconversion rate among veterinary students. Although the clinical importance of the presence of antibodies is unknown, students should be advised at the beginning of their education about potential risks and instructed to seek care if they experience symptoms of acute or chronic Q fever infection.

Acknowledgments

We would like to express our gratitude to all participants of the study. Many thanks to coworkers at the Institute for Risk Assessment Sciences involved in recruitment of the participants and serum sample collection (Lot Bannink, Manon Bogaerts, Isabella van Schothorst, Esmeralda Krop, Siegfried de Wind, Jack Spithoven, Marieke Oldenwening, Lidwien Smit, Haitske Gravenland, and Bernadette Aalders). We would like to thank the laboratory technicians in the Serology Unit of the Department of Medical Microbiology and Infection Control at Jeroen Bosch Hospital for their work in analyzing serum samples. We would also like to thank Roel Coutinho of the Julius Center University Medical Center Utrecht for reviewing the manuscript.

About the Author

Dr. de Lange is an epidemiologist at the National Institute for Public Health and the Environment. She conducted her PhD research on Q fever. Her other research interests include respiratory infections, such as influenza and respiratory syncytial virus.

References

1. Van den Brom R, Schimmer B, Schneeberger PM, Swart WA, van der Hoek W, Vellema P. Seroepidemiological survey for *Coxiella burnetii* antibodies and associated risk factors in Dutch livestock veterinarians. PLoS One. 2013;8:e54021. https://doi.org/10.1371/journal.pone.0054021
2. Dal Pozzo F, Martinelle L, Léonard P, Renaville B, Renaville R, Thys C, et al. Q fever serological survey and associated risk factors in veterinarians, Southern Belgium, 2013. Transbound Emerg Dis. 2017;64:959–66. https://doi.org/10.1111/tbed.12465
3. de Rooij MM, Schimmer B, Versteeg B, Schneeberger P, Berends BR, Heederik D, et al. Risk factors of *Coxiella burnetii* (Q fever) seropositivity in veterinary medicine students. PLoS One. 2012;7:e32108. https://doi.org/10.1371/journal.pone.0032108
4. Meadows SL, Jones-Bitton A, McEwen SA, Jansen J, Patel SN, Filejski C, et al. Prevalence and risk factors for *Coxiella burnetii* seropositivity in small ruminant veterinarians and veterinary students in Ontario, Canada. Can Vet J. 2017;58:397–9.
5. Valencia MC, Rodriguez CO, Puñet OG, de Blas Giral I. Q fever seroprevalence and associated risk factors among students from the Veterinary School of Zaragoza, Spain. Eur J Epidemiol. 2000;16:469–76. https://doi.org/10.1023/A:1007605414042
6. Roest HI, Tilburg JJ, van der Hoek W, Vellema P, van Zijderveld FG, Klaassen CH, et al. The Q fever epidemic in the Netherlands: history, onset, response and reflection. Epidemiol Infect. 2011;139:1–12. https://doi.org/10.1017/S0950268810002268
7. Samadi S, Spithoven J, Jamshidifard AR, Berends BR, Lipman L, Heederik DJ, et al. Allergy among veterinary medicine students in the Netherlands. Occup Environ Med. 2012;69:48–55. https://doi.org/10.1136/oem.2010.064089
8. Rustscheff S, Norlander L, Macellaro A, Sjöstedt A, Vene S, Carlsson M. A case of Q fever acquired in Sweden and isolation of the probable etiological agent, *Coxiella burnetii* from an indigenous source. Scand J Infect Dis. 2000;32:605–7. https://doi.org/10.1080/003655400459496
9. van der Hoek W, Morroy G, Renders NH, Wever PC, Hermans MH, Leenders AC, et al. Epidemic Q fever in humans in the Netherlands. Adv Exp Med Biol. 2012;984:329–64. https://doi.org/10.1007/978-94-007-4315-1_17

Address for Correspondence: Marit M.A. de Lange, National Institute for Public Health and the Environment, Centre for Infectious Disease Control Netherlands, Antonie van Leeuwenhoeklaan 9, 3721 MA, Bilthoven, the Netherlands; email: marit.de.lange@rivm.nl

Phylogenetic Analysis of MERS-CoV in a Camel Abattoir, Saudi Arabia, 2016–2018

Maged Gomaa Hemida,[1] Daniel K.W. Chu,[1] Yen Y. Chor, Samuel M.S. Cheng, Leo L.M. Poon, Abdelmohsen Alnaeem, Malik Peiris

Author affiliations: Kafrelsheikh University, Kafrelsheikh, Egypt (M. Hemida); King Faisal University, Al-Hasa, Saudi Arabia (M. Hemida, A. Alnaeem); The University of Hong Kong (D.K.W. Chu, Y.Y. Chor, S.M.S. Cheng, L.L.M. Poon, M. Peiris)

DOI: https://doi.org/10.3201/eid2612.191094

We detected Middle East respiratory syndrome coronavirus (MERS-CoV) RNA in 305/1,131 (27%) camels tested at an abattoir in Al Hasa, Eastern Province, Saudi Arabia, during January 2016–March 2018. We characterized 48 full-length MERS-CoV genomes and noted the viruses clustered in MERS-CoV lineage 5 clade B.

Middle East respiratory syndrome (MERS) coronavirus (MERS-CoV) is a zoonotic disease of concern for global public health (*1*,*2*). Dromedary camels are the source of zoonotic infection (*3*). During 2016–2018, a total of 80 full-length MERS-CoV genome sequences were available from human infections in the Arabian Peninsula where all zoonotic disease has occurred, but only 30 sequences from dromedary camels were available, highlighting the need for contemporary dromedary MERS-CoV sequence data.

During November 2015–June 2018, nasal and rectal swab specimens were collected, typically on a monthly basis, from dromedary camels slaughtered at an abattoir and camel market complex in Al Hasa, Eastern Province, Saudi Arabia (Appendix, https://wwwnc.cdc.gov/EID/article/26/12/19-1094-App1.pdf). Most camels for slaughter were bred locally, but some camels were imported from Somalia or Sudan for slaughter. Imported camels came through the port of Jeddah, usually via a large central camel market in Riyadh.

Nasal and rectal swab specimens were collected from 1,131 camels; 4–143 camels were sampled each month. Overall, 288 (25.5%) nasal and 85 (7.5%) rectal swabs were MERS-CoV–positive as confirmed by reverse transcription PCR (RT-PCR; Appendix); cycle threshold values ranged from 15.3 to 39.1 (median 33.6). Most (68/85; 80%) positive rectal swab specimens were collected from animals that also had a positive nasal swab. Overall, 305 (27%) camels sampled were MERS-CoV–positive from either nasal or rectal swabs. Despite regular exposure to infected camels, none of the abattoir workers had diagnosed clinical MERS disease.

MERS-CoV–positive samples were detected during most months in which samples were tested. Age, sex, date of sampling, and breed data were available for 847 camels. Among animals for which age and sex data were available, RT-PCR positive rates for MERS-CoV were not statistically significantly different by age or sex. Among local camels, MERS-CoV–positive rates by breed were 81/227 (35.7%) Magaheem, 19/87 (21.8%) Sofor, and 27/158 (17.1%) Wodaoh. Among imported camels, 21/146 (14.4%) from Somalia and 64/221 (29%) from Sudan were MERS-CoV–positive.

We obtained 48 full genomes of MERS-CoV from the camel samples; dates of sampling were available for 35 (GenBank accession nos. MN654970–5017). We did not detect evidence of deletions in accessory or other genes. Our newly generated virus genomes phylogenetically clustered within the recombinant lineage 5 clade, a novel recombinant clade that has become progressively dominant in Saudi Arabia since 2014 (*4*,*5*) (Appendix Figure). The 48 sequences in this study appear to cluster into 2 groups, which we named group A and group B for ease of description rather than a formal taxonomic designation (Figure). Other sublineages within lineage 5 appear to have gone extinct with no human or animal viruses detected since 2016. Virus group A had viruses sampled from 2014–2017, whereas group B had viruses sampled in 2014–2018. Both virus groups cocirculated in the region during the study period (Figure).

Genetically identical viruses were collected mostly during the same sampling period, suggesting cross-infection in the market. However, identical viruses sometimes were from samples collected 1 month apart, such as SA2557 and SA2626, or 3 months apart, such as SA2199, SA2159, and SA2247, suggesting reintroduction of viruses from the same herd or area into the abattoir at different times. Although we sampled imported camels from Somalia and Sudan, the viruses we detected were clade B lineage 5 viruses rather than the clade C viruses that are known to be enzootic in Africa (*6*). In several instances, viruses from camels from Sudan (for example, SA4104/2017 in December 2017 or SA2687/2017 in May 2017) were almost identical to viruses concurrently detected in camels from Saudi Arabia, indicating likely cross-infection in the camel market. Virus cross-infection and amplification in the camel market could explain the high overall MERS-CoV–positive rate in the abattoir.

[1]These authors contributed equally to this article.

A virus from a patient from Saudi Arabia who had diagnosed MERS in the United Kingdom in August 2018 (MERS-CoV_England-KSA_1/2018-08-22) was found to be closely genetically related (99.81% similarity) to a camel virus sampled during this study in 2018 (Figure). As previously reported, viruses from camels and humans interleave within the phylogenetic tree (*7*), suggesting that viruses in

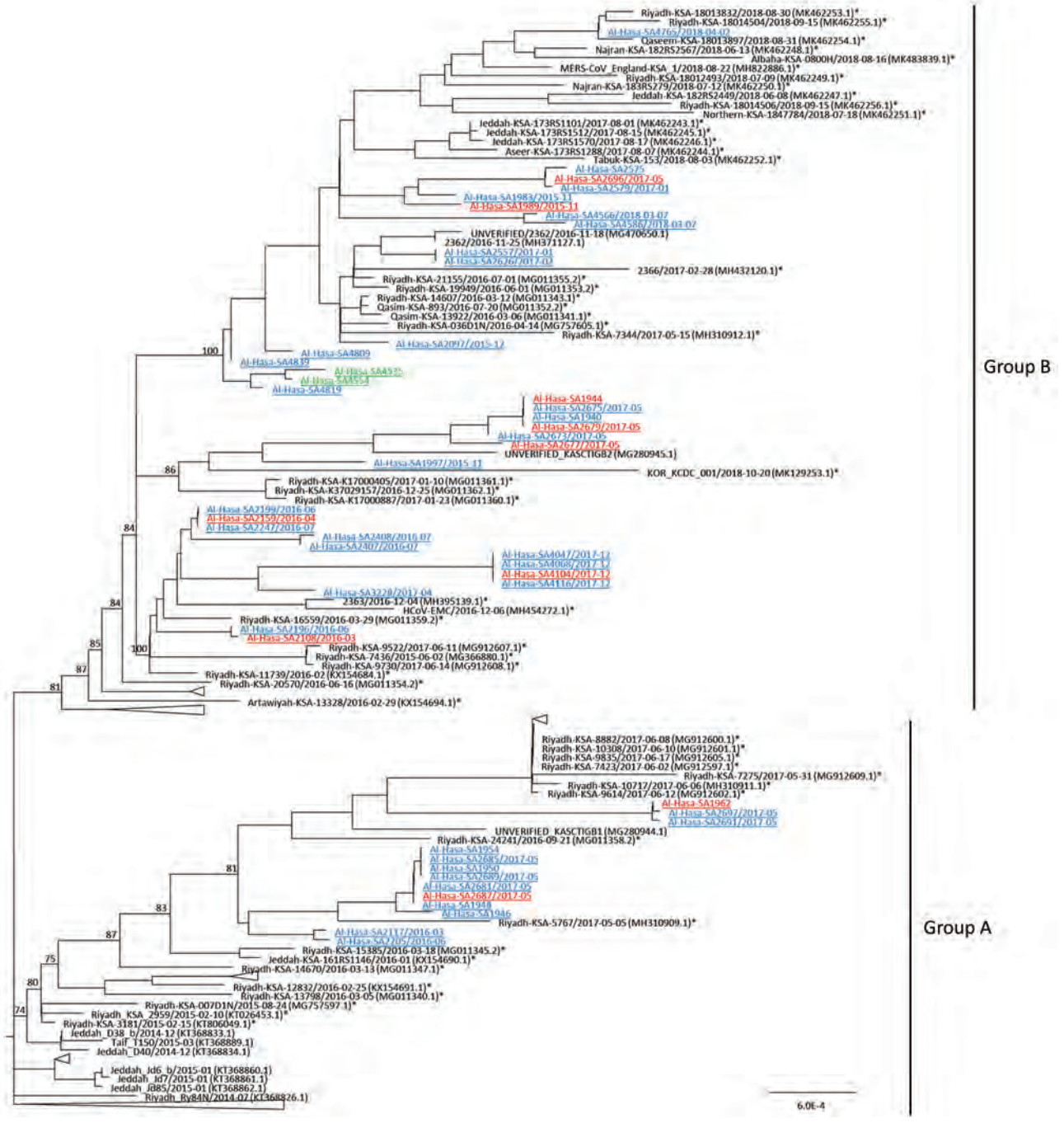

Figure. Phylogeny of Middle East respiratory syndrome coronavirus (MERS-CoV) sequenced from nasal and rectal samples collected from camels in an abattoir, Saudi Arabia. Phylogeny was constructed by using IQTREE (http://www.iqtree.org) with the automatic nucleotide transition model selection. Branch supports, shown at major nodes, were generated by ultrafast bootstrap approximation (Appendix, https://wwwnc.cdc.gov/EID/article/26/12/19-1094-App1.pdf). Genomes generated from this study are underlined; asterisks (*) indicate viruses from humans. Blue indicates viruses from camels from Saudi Arabia; red indicates viruses in camels imported from Sudan; green indicates viruses in camels imported from Somalia. The overall topology of the phylogeny of MERS-CoV also is available (Appendix Figure). Scale bar indicates 10^4 mutations per site.

camels continue to be the source of human infections through separate zoonotic transmission events without sublineage separation between viruses in camels and humans.

In conclusion, our study suggests multiple lineage 5 clade B viruses continue to be dominant among camels in eastern Saudi Arabia. Camels imported from Sudan and Somalia also had evidence of MERS-CoV B lineage 5 clade viruses prevalent in the Arabian Peninsula, rather than clade C viruses known to be enzootic in camels in Africa. These data suggest imported camels likely acquired MERS-CoV after arriving in Saudi Arabia and that lineage 5 viruses have the greater evolutionary fitness and appear to outcompete other viral lineages, which is concordant with other recently reported data (*8*). The high rates of MERS-CoV we detected and viral phylogeny suggest likely cross-transmission of MERS-CoV within the camel market and abattoir complex, even among imported animals.

King Abdul-Aziz City for Science and Technology provided funding through the MERS-CoV research grant program (grant no. 20-0004), which is a part of the KACST Targeted Research Program.

About the Author

Dr. Hemida is an assistant professor of molecular virology in the Department of Microbiology, College of Veterinary Medicine, King Faisal University, Saudi Arabia. His primary research interests are virus–host interactions and the molecular biology of coronaviruses.

References

1. Mehand MS, Al-Shorbaji F, Millett P, Murgue B. The WHO R&D Blueprint: 2018 review of emerging infectious diseases requiring urgent research and development efforts. Antiviral Res. 2018;159:63–7. https://doi.org/10.1016/j.antiviral.2018.09.009
2. World Health Organization. WHO MERS global summary and assessment of risk, July 2019 [cited 2020 Jan 21]. https://apps.who.int/iris/bitstream/handle/10665/326126/WHO-MERS-RA-19.1-eng.pdf
3. Haagmans BL, Al Dhahiry SH, Reusken CB, Raj VS, Galiano M, Myers R, et al. Middle East respiratory syndrome coronavirus in dromedary camels: an outbreak investigation. Lancet Infect Dis. 2014;14:140–5. https://doi.org/10.1016/S1473-3099(13)70690-X
4. Sabir JS, Lam TTL, Ahmed MM, Li L, Shen Y, Abo-Aba SE, et al. Co-circulation of three camel coronavirus species and recombination of MERS-CoVs in Saudi Arabia. Science. 2016;351:81–4. https://doi.org/10.1126/science.aac8608
5. Assiri AM, Midgley CM, Abedi GR, Bin Saeed A, Almasri MM, Lu X, et al. Epidemiology of a novel recombinant Middle East respiratory syndrome coronavirus in humans in Saudi Arabia. J Infect Dis. 2016;214:712–21. https://doi.org/10.1093/infdis/jiw236
6. Chu DKW, Hui KPY, Perera RAPM, Miguel E, Niemeyer D, Zhao J, et al. MERS coronaviruses from camels in Africa exhibit region-dependent genetic diversity. Proc Natl Acad Sci U S A. 2018;115:3144–9. https://doi.org/10.1073/pnas.1718769115
7. Dudas G, Carvalho LM, Rambaut A, Bedford T. MERS-CoV spillover at the camel-human interface. eLife. 2018;7:e31257. https://doi.org/10.7554/eLife.31257
8. El-Kafrawy SA, Corman VM, Tolah AM, Al Masaudi SB, Hassan AM, Müller MA, et al. Enzootic patterns of Middle East respiratory syndrome coronavirus in imported African and local Arabian dromedary camels: a prospective genomic study. Lancet Planet Health. 2019;3:e521–8. https://doi.org/10.1016/S2542-5196(19)30243-8

Address for correspondence: Malik Peiris, School of Public Health, The University of Hong Kong, No 7 Sassoon Rd, Pokfulam, Hong Kong; email: malik@hku.hk

One-Year Retrospective Review of Psychiatric Consultations in Lassa Fever, Southern Nigeria

Esther O. Okogbenin,[1] Michael O. Obagaye,[2] Benjamin E. Aweh,[3] Williams O. Eriyo,[3] Sylvanus A. Okogbenin,[3] Peter O. Okokhere[2]

Author affiliations: Ambrose Alli University, Ekpoma, Edo State, Nigeria and Institute of Lassa Fever Research and Control, Irrua Specialist Teaching Hospital, Edo State, Nigeria (E.O. Okogbenin, S.A. Okogbenin, P.O. Okokhere); Institute of Lassa Fever Research and Control, Irrua Specialist Teaching Hospital, Edo State (M.O. Obagaye, B.E. Aweh, W.O. Eriyo)

DOI: https://doi.org/10.3201/eid2612.200084

We conducted a retrospective review of psychiatric consultations for hospitalized patients with Lassa fever in southern Nigeria. Ten (8.8%) of 113 patients had psychiatric consultations. Delirium was the most common psychiatric manifestation complicating Lassa fever. Findings suggest that psychiatric intervention could improve overall outcomes of Lassa fever.

[1]This author was the principal investigator.

[2]These authors were co-principal investigators.

[3]These authors contributed equally to this article.

Viral hemorrhagic fever viruses may cause a wide spectrum of neurologic manifestations, including psychiatric syndromes (*1*–*3*). To the best of our knowledge, only 1 study, performed in 1991 in Sierra Leone, attempted to show that psychiatric syndromes are possible in acute Lassa fever (LF) (*3*). This case series, reported by Solbrig and McCormick, showed psychiatric syndromes including delirium, depression, and abnormal behavior in 3 of 9 patients with central nervous system (CNS) manifestations (*3*).

This review was conducted at the Institute of Lassa Fever Research and Control, Irrua Specialist Teaching Hospital Irrua, Edo state, Nigeria, a national LF referral center. We retrospectively reviewed the files of patients with Lassa virus reverse transcription PCR–positive blood samples, who were admitted at the center during 2012, and included in the study patients who had psychiatric consultations. A questionnaire designed by the researchers was used to collect information from patient files. We examined each file for psychopathology and coded the eventual diagnosis using the International Classification of Diseases, Tenth Revision (ICD-10) (*4*).

Ten (8.8%) of 113 hospitalized patients with LF had psychiatric consultations. All 10 patients met ICD-10 criteria for delirium (hyperactive motor type) and 2 had co-occurring depression. None of the 10 patients had a history of psychiatric illness. All 10 patients received supportive psychotherapy and haloperidol in low doses (2.5-5 mg daily). Citalopram (20 mg) was used for depression. All 113 patients were given ribavirin and received symptomatic management and treatment of medical complications and other preexisting conditions by the infectious disease physicians. All patients recovered from delirium and depression within 3 weeks and survived the infection despite an overall mortality rate of 45.1% (54/113) in the hospitalized patients (Table).

The finding of delirium in 100% of our patients with psychiatric manifestations is comparable with findings of a study that evaluated psychiatric illness in a typhoid fever cohort in Nigeria, where delirium was reported in 73% of 26/136 patients with psychiatric symptoms (*5*). Although mild and self-limiting confusion occurs in many febrile illnesses, delirium has been reported to be associated with prolonged hospital stay (14–40 days) in patients with infectious diseases; this was statistically significant ($p<0.001$) when compared with patients without delirium (hospital stay ≤14 days) in Nigeria (*6*). The strict ICD-10 criteria require symptoms of delirium to be present in each of the following 5 areas: disturbance of consciousness and attention, cognition, psychomotor, emotional, and sleep-wake cycle disturbances (*4*). Using these criteria, we found delirium in our patients, who were all hyperactive, and ruled out mild confusion. Of note is that fever had subsided in 4 of our patients by the time of onset of psychiatric symptoms. No patient with anxiety was seen, and only 2 patients had co-occurring depression.

The absence of past psychiatric illness in the patients we studied suggests that LF was likely the direct or indirect cause of delirium/depression in these patients. Psychiatric manifestations and viral infections are linked through a complex interaction; in our patients, this interaction could have been a direct cytopathic effect of LF virus on their CNS. Generally, viruses enter the CNS through several pathways, which

Table. Sociodemographic and clinical characteristics observed in a retrospective review of psychiatric consultations in patients with Lassa fever conducted at the Irrua Specialist Teaching Hospital, Irrua, Edo State, Nigeria, January–December 2012*

ID	Age, y/ sex	Duration of fever, d	Temperature at onset of psychiatric symptoms, °C	Medical complications	Preexisting conditions	Family history of mental illness	ICD-10 diagnosis
1	25/M	14	38.0	Acute renal failure	No	No	Delirium
2	30/F	14	37.2	Acute renal failure	No	No	Delirium
3	31/M	6	38.0	Anemia, hypokalemia	No	No	Delirium
4	33/F	6	36.8	Low platelet levels	No	No	Delirium
5	38/M	14	38.6	Altered liver enzyme levels, hypernatremia	Diabetes	No	Delirium
6	45/F	14	38.0	Uremia	No	No	Delirium
7	55/F	14	36.5	Anemia	Hypertension	Yes	Delirium
8	60/M	6	38.0	Acute renal failure, septicemia	Hypertension	No	Delirium, depression
9	38/M	14	38.5	Anemia	Diabetes	No	Delirium, depression
10	20/F	10	37.6	Acute renal failure, seizures, anemia	No	No	Delirium

*All patients had fever and tested positive for Lassa fever by reverse transcription PCR. All patients survived. ICD-10, International Statistical Classification of Diseases and Related Health Problems, 10th revision; ID, identification.

may include a hematogenous route, directly breaching the blood–brain barrier, or through infected leukocytes, which then infect vascular endothelial cells (*2*,*7*). A case of infection with Lassa virus in cerebrospinal fluid has been reported in a patient with blood samples negative for Lassa virus (*8*). In fact, psychiatric symptoms without neurologic symptoms may be the initial presentation of viral encephalitis (*9*).

All our patients, like some other patients with severe LF, had various medical complications, such as acute renal failure, septicemia, and electrolyte disturbances. These are well documented etiologic factors for delirium (*10*) and could have contributed to delirium in our patients.

All 10 patients recovered from delirium and depression within 3 weeks of intervention and survived the infection despite an overall mortality rate of 45.1% for patients admitted to the hospital with LF. This is irrespective of the presence of poor prognostic factors in these patients and the fact that the same LF case management protocol was applied to all patients admitted to the center. Unfortunately, there were no data on viral load and oxygen saturation for comparison between our patients and other patients with LF who did not receive psychiatric intervention. Although we cannot adequately explain this excellent prognosis, we note that identifying and managing psychiatric complications could contribute to improved LF outcome.

The limitation of this study was that it was retrospective and looked at only those who had psychiatric consultations, which made the sample size small and did not permit causal inferences. A prospective study might have identified more cases and given more room for a comparative study design. Based on our findings, we recommend prospective studies to determine the pattern of psychiatric manifestations in LF and integrating mental healthcare into the management of LF.

About the Author

Dr. Esther O. Okogbenin is an associate professor of psychiatry at Ambrose Alli University Ekpoma Edo State, Nigeria, and a consultant psychiatrist at the Irrua Specialist Teaching Hospital in Edo State. She is the head of the Department of Mental Health at Ambrose Alli University, with primary research in consultation–liaison psychiatry.

References

1. Okokhere PO, Bankole IA, Akpede GO. Central nervous system manifestations of Lassa fever in Nigeria and the effect on mortality. J Neurol Sci. 2013;333(suppl1):e604. https://doi.org/10.1016/j.jns.2013.07.2107
2. Ruzek D, Holbrook M, Yakimenko V, Karan L, Tkachev S. Omsk hemorrhagic fever virus. In: Manual of security sensitive microbes and toxins, Liu D, editor. Boca Raton (FL): CRC Press; 2014. p. 193–200.
3. Solbrig MV, McCormick JB. Lassa fever: central nervous system manifestations. J Trop Geogr Neurol. 1991;1:23–30.
4. World Health Organization. ICD-10: the ICD-10 classification of mental and behavioral disorders: clinical descriptions and diagnostic guidelines. Geneva: The Organization; 1992.
5. Aghanwa HS, Morakinyo O. Correlates of psychiatric morbidity in typhoid fever in a Nigerian general hospital setting. Gen Hosp Psychiatry. 2001;23:158–62. https://doi.org/10.1016/S0163-8343(01)00130-X
6. Taru MY, Bamidele LI, Faith AO, Annah GB, Mayowa OK, Yushau AA. Delirium and length of hospital stay among medical inpatients in Jos University Teaching Hospital, North-Central Nigeria. Open J Psychiatr. 2018;8:297–314. https://doi.org/10.4236/ojpsych.2018.83024
7. Koyuncu OO, Hogue IB, Enquist LW. Virus infections in the nervous system. Cell Host Microbe. 2013;13:379–93. https://doi.org/10.1016/j.chom.2013.03.010
8. Okokhere PO, Erameh CO, Alikah F, Akhideno PE, Iruolagbe CO, Osazuwa OO, et al. Acute Lassa virus encephalitis with Lassa virus in the cerebrospinal fluid but absent in the blood: a case report with a positive outcome. Case Rep Neurol. 2018;10:150–8. https://doi.org/10.1159/000490374
9. Wilson LG. Psychiatric aspects of acute viral encephalitis. In: Viruses, immunity, and mental disorders. Kurstak E, Lipowski ZJ, Morozov PV, editors. Boston: Springer; 1987. https://doi. org/10.1007/978-1-4613-1799-9_40
10. MacLullich AM, Ferguson KJ, Miller T, de Rooij SE, Cunningham C. Unravelling the pathophysiology of delirium: a focus on the role of aberrant stress responses. J Psychosom Res. 2008;65:229–38. https://doi.org/10.1016/j.jpsychores.2008.05.019

Address for correspondence: Esther Osemudiamen Okogbenin, Irrua Specialist Teaching Hospital, KM 87, Benin Auchi Rd, PMB 08, Irrua, Edo State, Nigeria; email: eokogbenin@gmail.com

Low Pathogenicity Avian Influenza (H5N2) Viruses, Dominican Republic

David H. Chung, Dejelia R. Gomez, Julia M. Vargas, Belkis L. Amador, Mia K. Torchetti, Mary L. Killian, David E. Swayne, Dong-Hun Lee

Author affiliations: University of Connecticut, Storrs, Connecticut, USA (D.H. Chung, D.-H. Lee); Ministry of Agriculture, Roseau, Dominican Republic (D.R. Gomez, J.M. Vargas, B.L. Amador); US Department of Agriculture, Athens, Georgia, USA (D.E. Swayne); US Department of Agriculture, Ames, Iowa, USA (M.K. Torchetti, M.L. Killian)

DOI: https://doi.org/10.3201/eid2612.200268

Low pathogenicity avian influenza (H5N2) virus was detected in poultry in the Dominican Republic in 2007 and re-emerged in 2017. Whole-genome sequencing and phylogenetic analysis show introduction of an H5N2 virus lineage from Mexico into poultry in the Dominican Republic, then divergence into 3 distinct genetic subgroups during 2007–2019.

Low pathogenicity avian influenza virus (LPAIV) subtype H5N2 has caused outbreaks in poultry in Mexico since 1993 and mutated into highly pathogenic avian influenza virus (HPAIV) H5N2 during 1994–1995 (*1*). In 1994, a vaccination program against H5N2 in poultry was established in Mexico; HPAIV H5N2 was eradicated there in 1995 (*2*). However, LPAIV H5N2 persisted and related viruses spread to neighboring countries (*1*,*3*,*4*). In addition, the H5N2 virus lineage from Mexico was introduced to Taiwan in 2003, likely because of inadequately inactivated vaccines. The virus then reassorted with the local avian influenza (H6N1) virus strain that has been enzootic in chickens in Taiwan since 1997 to produce reassortant H5N2 virus possessing hemagglutinin (HA) and neuraminidase (NA) genes of H5N2 virus from Mexico and internal genes of the Taiwan H6N1 virus. The reassortant H5N2 virus mutated into an HPAIV and caused outbreaks in poultry in Taiwan during 2012 (*5*).

In 2007, outbreaks of LPAIV H5N2 occurred among chickens in Santo Domingo and Higüey-La Otra Banda, Dominican Republic, and were reported to the World Organisation for Animal Health (OIE) (*6*). The OIE Reference Laboratory detected LPAIV H5N2 lineages from Mexico in samples from the Dominican Republic outbreaks on December 21, 2007. During December 2007–February 2008, a total of 11 avian influenza A viruses were detected in the Dominican Republic from backyard birds, fighting birds, and a live bird market (*7*) (Appendix Table 1, https://wwwnc.cdc.gov/EID/article/26/12/20-0268-App1.pdf). During 2007–2016, serologic surveillance of poultry detected 364/45,440 (0.80%) samples exhibiting positive antibody responses, suggesting low level circulation of LPAIVs in the Dominican Republic, but the HA and NA subtypes were not identified (data not shown). During September–November 2017, the H5N2 LPAIV re-emerged and affected 5 commercial chicken farms in Espaillat, San Juan, and La Vega (Appendix Table 2). Subsequently, the viruses were detected in 23 commercial and backyard poultry flocks during September 2018–February 2019 (*8*). During the 2017–2019 H5N2 LPAIV outbreak period, seropositivity reached 52% (8,740/16,543).

Since 2007, limited information on H5N2 LPAIVs and few genetic sequences have been reported. We provide sequenced genomes of 19 H5N2 LPAIVs identified in the Dominican Republic during 2007–2019: 1 virus from 2007, 6 from 2017, 1 from 2018, and 11 from 2019.

The 2007 H5N2 LPAIV, Ck/Dominican_Republic/2007(H5N2), had an HA cleavage site sequence with 2 basic amino acids (PQRETR/G). However, the 2017–2019 viruses possessed 3 monobasic amino acids (PQRGKR/G, PQREKR/G, and LQREKR/G) (Appendix Table 3). Seven representative isolates were of low pathogenicity in chickens on intravenous inoculation (intravenous pathogenicity index = 0.0). The acquisition of an additional basic amino acid in the HA cleavage site raises a concern regarding the increased risk for mutation to an HPAIV.

All genes formed a well-supported monophyletic clade (bootstrap support of 98–100 in maximum likelihood phylogeny and posterior probability of 0.99–1.00 in Bayesian phylogeny), suggesting their close relationship from a single viral introduction into the poultry population descended from A/Ck/Hidalgo/28159–232/94 (H5N2)–like virus and maintenance in poultry in the Dominican Republic (Figure 1; Appendix Figures 1–8). The inferred time to most recent common ancestor (tMRCA) for each gene of H5N2 viruses identified in the Dominican Republic ranged from February 2005 to August 2006, suggesting that ancestors of these viruses emerged from an H5N2 virus lineage introduced from Mexico during this period (Appendix Table 4). Phylogenetic analyses show divergence of all 8 gene segments into 3 genetic sublineages

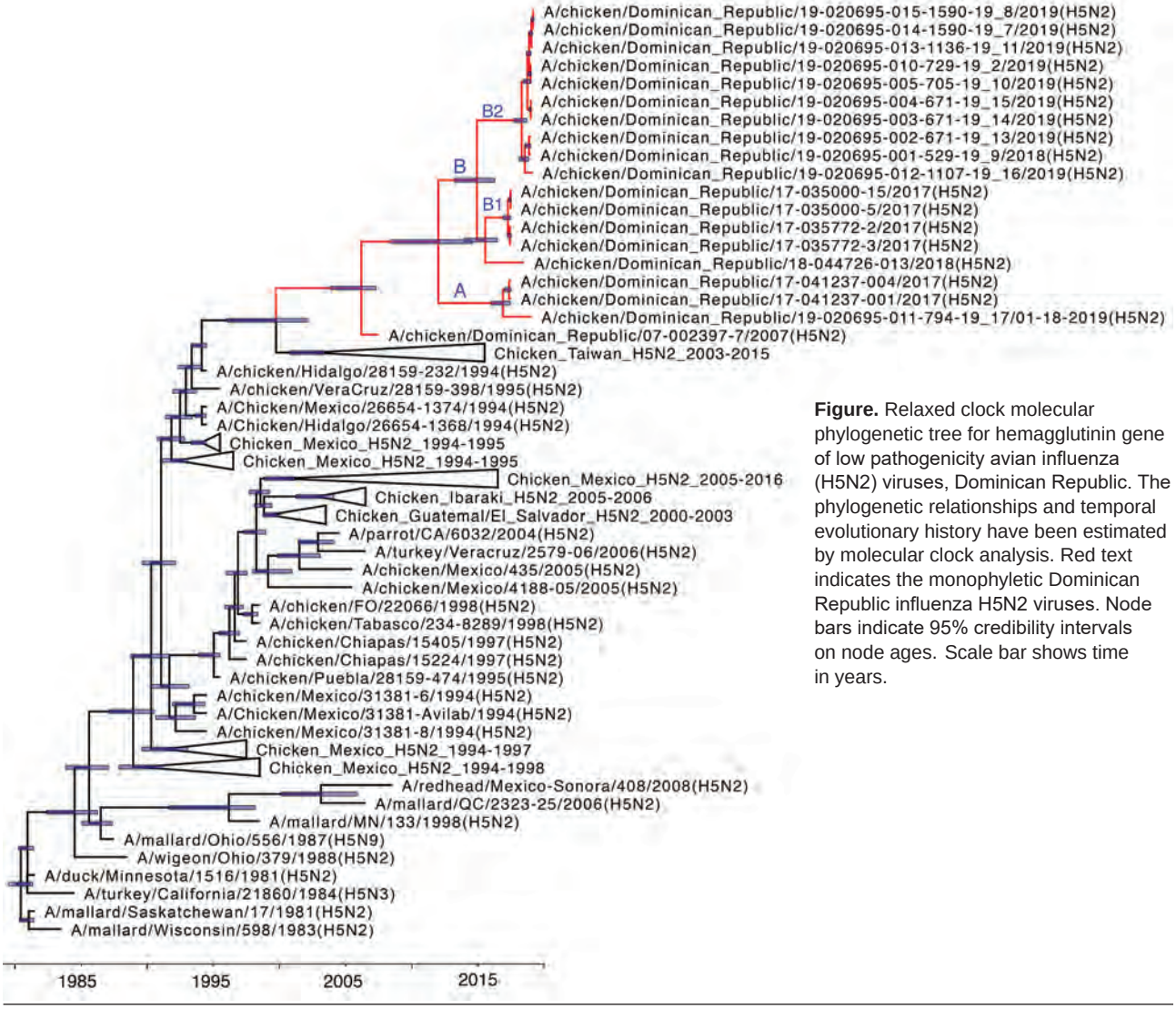

Figure. Relaxed clock molecular phylogenetic tree for hemagglutinin gene of low pathogenicity avian influenza (H5N2) viruses, Dominican Republic. The phylogenetic relationships and temporal evolutionary history have been estimated by molecular clock analysis. Red text indicates the monophyletic Dominican Republic influenza H5N2 viruses. Node bars indicate 95% credibility intervals on node ages. Scale bar shows time in years.

designated as sublineage A, which contains viruses collected in 2017 and 2019; B1, which contains viruses collected during 2017; and B2, which contains viruses collected during 2018–2019. The 8 gene segments of Ck/Dominican_Republic/044726_013/2018(H5N2) fell into sublineage B (Appendix Table 3).

The prediction of N-linked glycosylation sites in the HA protein revealed that the H5N2 LPAIVs have 9 potential glycosylation sites at position 27, 39, 142, 181, 252, 277, 302, 496, and 555 (H5 numbering system), with a range of 6–8 sites for individual isolates (Appendix Table 5, Figure 9). The potential glycosylation at positions 142, 181, and 252 were found within antigenic sites (*9*). The initially identified Ck/Dominican_Republic/2007(H5N2) was predicted to contain N-linked glycosylation at the antigenic sites at positions 181 and 252. Sublineage A and B1 did not have the predicted glycosylation at position 252 but gained additional glycosylation at position 142. However, sublineage B2 was predicted to possess glycosylation at all antigenic sites at positions 142, 181, and 252, except for the Ck/Dominican_Republic/020695-012-1107-19-16/2019 (H5N2) strain, which has N-glycosylation only at positions 142 and 252.

Enhanced active surveillance is required to monitor the evolution and spread of H5N2 viruses in the Dominican Republic; such efforts could further the epidemiologic understanding and the design of improved prevention strategies. Additional studies could elucidate whether the genetic changes in glycosylation and antigenic sites contribute to the alterations in antigenicity of the H5N2 LPAIV from the Dominican Republic against current H5 virus vaccine strains.

Acknowledgment

We thank Julia Desiato for technical assistance.

D.-H.L. and D.H.C. are partially supported by the US Department of Agriculture, Agricultural Research Service project no. 6040-32000-066-51S.

About the Author

Mr. Chung is a PhD student at the University of Connecticut, Storrs, Connecticut, USA. His primary research interests include the molecular epidemiology of avian influenza and other zoonotic viruses.

References

1. Villarreal-Chávez C, Rivera-Cruz E. An update on avian influenza in Mexico. Avian Dis. 2003;47(Suppl):1002–5. https://doi.org/10.1637/0005-2086-47.s3.1002
2. Escorcia M, Vázquez L, Méndez ST, Rodríguez-Ropón A, Lucio E, Nava GM. Avian influenza: genetic evolution under vaccination pressure. Virol J. 2008;5:15. https://doi.org/10.1186/1743-422X-5-15
3. Abdelwhab SM, Veits J, Mettenleiter TC. Genetic changes that accompanied shifts of low pathogenic avian influenza viruses toward higher pathogenicity in poultry. Virulence. 2013;4:441–52. https://doi.org/10.4161/viru.25710
4. Bublot M, Pritchard N, Swayne DE, Selleck P, Karaca K, Suarez DL, et al. Development and use of fowlpox vectored vaccines for avian influenza. Ann N Y Acad Sci. 2006;1081:193–201. https://doi.org/10.1196/annals.1373.023
5. Lee CC, Zhu H, Huang PY, Peng L, Chang YC, Yip CH, et al. Emergence and evolution of avian H5N2 influenza viruses in chickens in Taiwan. J Virol. 2014;88:5677–86. https://doi.org/10.1128/JVI.00139-14
6. World Organization for Animal Health. Report on low pathogenic avian influenza virus in Dominican Republic, H5N2 2007. 2007 Dec 21 [cited 2019 Dec 10]. https://www.oie.int/wahis_2/public/wahid.php/Reviewreport/Review?page_refer=MapEventSummary&reportid=6616
7. World Organization for Animal Health. Report on low pathogenic avian influenza virus in Dominican Republic, H5N2 2009. 2009 Aug 21 [cited 2019 Dec 10]. https://www.oie.int/wahis_2/public/wahid.php/Reviewreport/Review?reportid=6882
8. World Organization for Animal Health. Report on low pathogenic avian influenza virus in Dominican Republic, H5N2 2019. 2019 Oct 16 [cited 2019 Dec 10]. https://www.oie.int/wahis_2/public/wahid.php/Reviewreport/Review?reportid=31880
9. Kaverin NV, Rudneva IA, Govorkova EA, Timofeeva TA, Shilov AA, Kochergin-Nikitsky KS, et al. Epitope mapping of the hemagglutinin molecule of a highly pathogenic H5N1 influenza virus by using monoclonal antibodies. J Virol. 2007;81:12911–7. https://doi.org/10.1128/JVI.01522-07

Address for correspondence: Dong-Hun Lee, Department of Pathobiology & Veterinary Science, University of Connecticut, 61 N Eagleville Rd, Unit-3089, Storrs, CT 06269, USA; email: dong-hun.lee@uconn.edu

Autochthonous Ratborne Seoul Virus Infection in Woman with Acute Kidney Injury

Jörg Hofmann,[1] Elisa Heuser,[1] Sabrina Weiss,[2] Beate Tenner, Konrad Schoppmeyer, Jutta Esser, Christiane Klier, Stephan Drewes, Rainer G. Ulrich, Detlev H. Kruger

Author affiliations: Charité–Universitätsmedizin Berlin, Berlin, Germany (J. Hofmann, S. Weiss, B. Tenner, D.H. Kruger); Friedrich-Loeffler-Institut, Greifswald-Insel Riems, Germany (E. Heuser, S. Drewes, R.G. Ulrich); Euregio-Klinik, Medizinische Klinik II, Nordhorn, Germany (K. Schoppmeyer); Laborarztpraxis Osnabrück, Georgsmarienhütte, Germany (J. Esser); German Center for Infection Research, Partner Site Hamburg-Lübeck-Borstel-Insel Riems, Germany (E. Heuser, R.G. Ulrich); Public Health Agency of Lower Saxony, Hannover, Germany (C. Klier)

DOI: https://doi.org/10.3201/eid2612.200708

Outside Asia, Seoul virus (SEOV) is an underestimated pathogen. In Germany, autochthonous SEOV-associated hantavirus disease has not been unequivocally diagnosed. We found clinical and molecular evidence for SEOV infection in a young woman; her pet rat was the source of infection.

Hantavirus infections cause febrile and often life-threatening zoonoses known as hemorrhagic fever with renal syndrome and hantavirus cardiopulmonary syndrome. Human pathogenic hantavirus species usually are carried by specific rodent reservoirs, which shed infectious virus in their excreta (*1*).

Seoul virus (SEOV), a species within the genus *Orthohantavirus*, is hosted by Norway or brown rats (*Rattus norvegicus*) and other *Rattus* species as main reservoir. SEOV-associated hantavirus disease is characterized by fever, acute kidney injury, often hepatitis and gastroenteritis, associated with transient thrombocytopenia and proteinuria (*2*,*3*). Most clinical cases are known to originate from China and South Korea; however, SEOV infection can occur worldwide because of the global distribution of Norway rats in the wild. Moreover, human infection has been described from contact with breeder rats (laboratory rats and laboratory rat–derived tissue cultures), pet rats, and feeder rats (*3*–*6*).

SEOV-caused hantavirus disease, especially in areas outside Asia to which it is not endemic, is

[1]These authors contributed equally to this article.

[2]Current affiliation: Robert Koch Institute, Berlin, Germany.

Table. Biochemical parameters of the patient with Seoul virus during hospitalization, Germany, 2018*

Parameter (reference range)	Day 1	Day 2	Day 3	Day 4	Day 6	Day 7	Day 8	Day 9	Day 11	Day 12
Platelets (150–400/μL)	183	93	73	89	167	185	334	379	515	537
Leukocytes (4–10/μL)	3.4	4.7	4.4	5.5	10.4	10.8	10.1	9.1	9.4	8.6
CRP (0–0.5 mg/dL)	4.7	12.4	11.5	7.8	6.2	4.8	4.1	3.6	1.4	0.9
Serum creatinine (0.5–0.9 mg/dL)	0.92	1.42	1.93	1.81	2.27	2.72	2.93	2.33	1.18	1.16
Serum urea (16.6–48.5 mg/dL)	ND	41.5	ND	55.2	63.3	67.5	67.8	53.0	17.9	17.0
GFR (>89 mL/min)	91	54	37	40	31	25	22	30	67	69
Protein in urine (0 mg/dL)	ND	ND	75	ND	ND	75	75	ND	ND	–
γGT (6–42 U/L)	67	202	206	172	187	177	159	141	110	156
ALT (10–35 U/L)	28	164	233	140	117	96	67	55	39	54

*ALT, alanine aminotransferase; CRP, C-reactive protein; γGT, gamma-glutamyltransferase; GFR, glomerular filtration rate; –, negative; ND, not determined.

often misdiagnosed, perhaps because of its sometimes mild/atypical clinical presentation and healthcare providers' low clinical awareness (*2*,*3*). A lack of appropriate routine diagnostic tools also complicate the correct diagnosis. SEOV nucleocapsid protein shares a high antigenic similarity to related orthohantaviruses, such as Hantaan virus (HTNV) and Dobrava-Belgrade virus (DOBV), and is not always included in commercial assays (*1*,*7*).

Therefore, the use of molecular methods is the best way to unequivocally prove SEOV infections in Europe. Molecular evidence for SEOV infection has been found in patients from France and the Netherlands (*6*,*8*). Molecularly proven SEOV hantavirus disease in a German patient was reported in 2018, but the infection probably was acquired in Indonesia (*7*). Except for this travel-associated infection, neither SEOV-specific antibodies nor SEOV RNA had been detected in humans in Germany.

In October 2019, an 18-year-old woman was admitted to the intensive care unit of a hospital in Nordhorn in northwestern Germany with high fever and in critical condition. During the clinical course of her illness, acute kidney injury, gastroenteritis, and hepatopathy developed. Thrombocytes were lowest at day 3 and normal from day 6 on. Leukocytosis was evident during days 6–8, C-reactive protein as an inflammation parameter was above normal, peaked on day 2, and then decreased continuously until day 12. Serum creatinine and urea were elevated, and glomerular filtration rate was reduced with most critical values of all 3 parameters on day 8. We also detected proteinuria. The >3-fold increase in serum creatinine concentration from day 1 to day 8 is consistent with an acute kidney injury severity level 3 in the 3-stage KDIGO (Kidney Disease: Improving Global Outcomes) classification (*9*). These parameters of kidney function reached normal or nearly normal levels on day 12. Liver enzymes were elevated during the entire period and peaked on day 3 (Table). After receiving antimicrobial treatment and treatment for her symptoms, the patient was discharged from the hospital on day 13 in largely normal condition.

Serologic diagnostic approaches were based on *recom*Line HantaPlus IgG and IgM immunoblot assays (Mikrogen GmbH, https://www.mikrogen.de). The *recom*Line IgM blot showed strong reactivity to DOBV, HTNV, and SEOV nucleocapsid antigens, and in the IgG blot, we found a single weak reactivity to HTNV. A follow-up sample drawn 2 months after discharge revealed comparable band intensities in the IgM blot. The IgG blot showed a strong HTNV band but no DOBV or SEOV reactivities. However, neither DOBV nor HTNV are prevalent in the patient's residential area, and she reported not traveling.

We conducted molecular virus typing. A serum sample collected on day 5 of hospitalization was tested by the pan-hanta reverse transcription PCR (RT-PCR) addressing a 412-nt region of the viral large (L) segment (*10*). The identified nucleotide sequence demonstrated SEOV infection.

The patient reported that she kept Norway rats as pets in her flat. RT-PCR investigation of lung tissue of 1 of these rats yielded an L segment sequence identical to the patient-derived sequence (Figure). A subsequent small (S) segment RT-PCR enabled amplification of a 673-nt sequence from both the patient and the pet rat. Sequence alignment showed only a single silent nucleotide exchange. The analyzed S segment sequences exhibited the highest similarity to breeder-rat derived SEOV strains from the Netherlands and United Kingdom (Figure). The identities of the patient- and pet rat-derived sequences support the zoonotic transmission of the virus to the woman.

This case illustrates the importance of clinical awareness for SEOV infection after contact with rats. Along with this human case, we report a molecularly proven SEOV infection in a pet rat in Germany. More information regarding the SEOV prevalence in domestic and wild rat populations in Germany is needed to assess the risk for infection in the general public, pet rat owners, and breeder-rat handlers.

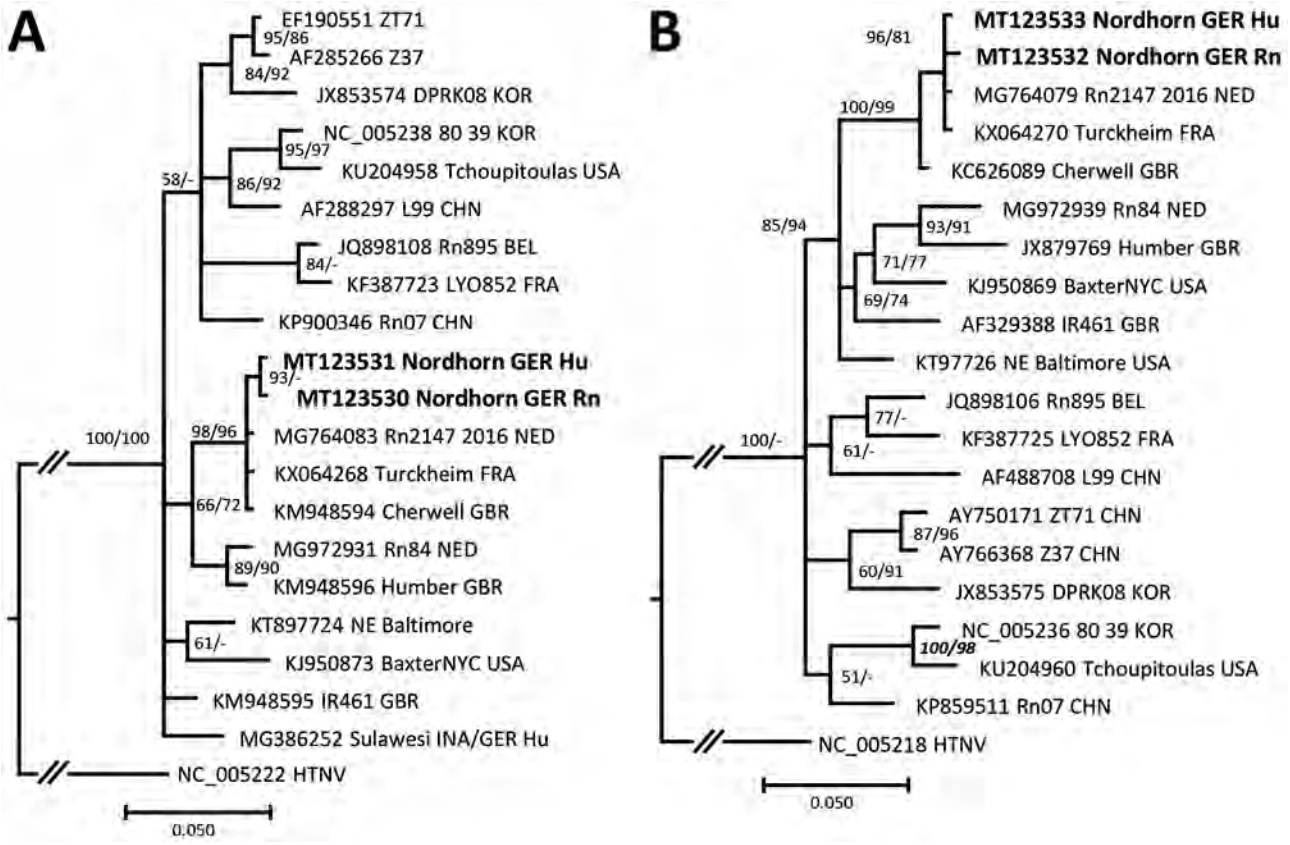

Figure. Molecular phylogenetic analysis of the amplified large (L) and small (S) segment regions of human and rat origin from Nordhorn/Germany (strains Nordhorn GER Hu and Nordhorn GER Rn, designated in bold). The consensus tree is based on a 412-nt region of the L segment (A) and a 673-nt region of the S segment (B). Alignments were constructed with Bioedit software package version7.2.5) (https://bioedit.software.informer.com) using the Clustal W Multiple Alignment algorithm. The best fitting substitution model was determined with jModeltest version 2.1.10 (https://github.com/ddarriba/jmodeltest2). Trees were reconstructed with MrBayes version 3.2.6 (http://www.mrbayes.net) and FasttreeMP version 2.1.10 (http://microbesonline.org/fasttree) executed on the CIPRES portal (https://www.phylo.org) according to maximum-likelihood and Markov chain Monte Carlo algorithms. The consensus tree is based on Bayesian analyses with 2 × 106 generations, a burn-in phase of 25%, and the Hasegawa-Kishono-Yano substitution model with gamma distribution. Bootstrap values were transferred to the Bayesian tree behind posterior probabilities only if they were >50% and if branches of both trees were consistent. Hantaan virus was used as outgroup. The L and S segment sequences were deposited in GenBank under accession nos. MT123530–33. At the end of the strain names the country of origin is given: BEL, Belgium; CHN, China; FRA, France; GBR, Great Britain; GER, Germany; INA, Indonesia; KOR, South Korea; NED, the Netherlands; USA, United States. Scale bars indicate nucleotide substitutions per site.

Acknowledgments

We thank J. Dreesman and M. Oskamp for their support in patient contact. We gratefully acknowledge the expert technical assistance of C. Stephan, S. Schwarz, and D. Kaufmann.

Work was supported by the German Federal Ministry of Public Health via Robert Koch-Institute (grant no 1369-382/435, 1362-924/980), by Deutsches Zentrum, für Infektionsforschung (area "Emerging Infections"), and the Bundesministerium für Bildung und Forschung through the Research Network Zoonotic Infections (project 01KI1721A, C, D).

About the Author

Dr. Hofmann is the chair of the National Consultation Laboratory for Hantaviruses, Institute of Virology, Charité–Universitätsmedizin Berlin, Germany. His primary research interest is human infections with viral pathogens.

References

1. Kruger DH, Figueiredo LT, Song JW, Klempa B. Hantaviruses—globally emerging pathogens. J Clin Virol. 2015;64:128–36. https://doi.org/10.1016/j.jcv.2014.08.033
2. Lee HW. Hemorrhagic fever with renal syndrome in Korea. Rev Infect Dis. 1989;11(Suppl 4):S864–76. https://doi.org/10.1093/clinids/11.Supplement_4.S864
3. Clement J, LeDuc JW, Lloyd G, Reynes JM, McElhinney L, Van Ranst M, et al. Wild rats, laboratory rats, pet rats: global Seoul hantavirus disease revisited. Viruses. 2019;11:E652. https://doi.org/10.3390/v11070652
4. Childs JE, Klein SL, Glass GE. A case study of two rodent-borne viruses: not always the same old suspects. Front Ecol Evol. 2019;7:35. https://doi.org/10.3389/fevo.2019.00035

5. McElhinney L, Fooks AR, Featherstone C, Smith R, Morgan D. Hantavirus (Seoul virus) in pet rats: a zoonotic viral threat. Vet Rec. 2016;178:171–2. https://doi.org/10.1136/vr.i817
6. Reynes JM, Carli D, Bour JB, Boudjeltia S, Dewilde A, Gerbier G, et al. Seoul virus infection in humans, France, 2014–2016. Emerg Infect Dis. 2017;23:973–7. https://doi.org/10.3201/eid2306.160927
7. Hofmann J, Weiss S, Kuhns M, Zinke A, Heinsberger H, Kruger DH. Importation of human Seoul virus infection to Germany from Indonesia. Emerg Infect Dis. 2018;24:1099–102. https://doi.org/10.3201/eid2406.172044
8. Swanink C, Reimerink J, Gisolf J, de Vries A, Claassen M, Martens L, et al. Autochthonous human case of Seoul virus infection, the Netherlands. Emerg Infect Dis. 2018;24:2158–63. https://doi.org/10.3201/eid2412.180229
9. Weiss R, Meersch M, Pavenstädt HJ, Zarbock A. Acute kidney injury. Dtsch Arztebl Int. 2019;116:833–42.
10. Klempa B, Fichet-Calvet E, Lecompte E, Auste B, Aniskin V, Meisel H, et al. Hantavirus in African wood mouse, Guinea. Emerg Infect Dis. 2006;12:838–40. https://doi.org/10.3201/eid1205.051487

Address for correspondence: Jörg Hofmann, Institute of Virology, Helmut-Ruska-Haus, Charité – Universitätsmedizin Berlin, Charitéplatz 1, 10117 Berlin; Germany. e-mail: joerg.hofmann@charite.de

Pediatric Lyme Disease Biobank, United States, 2015–2020

Lise E. Nigrovic, Desire N. Neville, Fran Balamuth, Michael N. Levas, Jonathan E. Bennett, Anupam B. Kharbanda, Amy D. Thompson, John A. Branda, Aris C. Garro, the Pedi Lyme Net Working Group

Author affiliations: Boston Children's Hospital, Boston, Massachussetts, USA (L.E. Nigrovic); Children's Hospital of Pittsburgh, Pittsburgh, Pennsylvania, USA (D.N. Neville); Milwaukee Children's Hospital, Milwaukee, Wisonsin, USA (F. Balamuth); Children's Hospital of Philadelphia, Philadelphia, Pennsylvania, USA (M.N. Levas); Nemours/Alfred I. duPont Children's Hospital, Wilmington, Delaware, USA (J.E. Bennett, A.D. Thompson); Children's Minnesota, Minneapolis, Minnesota, USA (A.B. Kharbanda); Massachusetts General Hospital, Boston (J.A. Branda); Rhode Island Hospital, Providence, Rhode Island, USA (A.C. Garro)

DOI: https://doi.org/10.3201/eid2612.200920

In 2015, we founded Pedi Lyme Net, a pediatric Lyme disease research network comprising 8 emergency departments in the United States. Of 2,497 children evaluated at 1 of these sites for Lyme disease, 515 (20.6%) were infected. This network is a unique resource for evaluating new approaches for diagnosing Lyme disease in children.

Children are disproportionally affected by Lyme disease, which is diagnosed in ≈300,000 persons in the United States each year (*1*). Clinicians diagnose Lyme disease using a 2-tier examination of enzyme immunoassay (EIA) and immunoblot results. Current Lyme disease diagnostic tests have well-described limitations that include false negatives early in disease (*3*) and inability to distinguish between resolved, active, and recurrent infections (*4*). Clinicians must also wait several days for Lyme disease serologic results, a delay that might contribute to late or unnecessary treatment with antimicrobial drugs. The increased incidence of Lyme disease, limitations of current tests, and lack of studies in children demonstrate the need for a systematic approach to Lyme disease diagnosis in children.

Developing improved diagnostic techniques relies on biobanks of samples collected from patients with Lyme disease and clinical mimics (i.e., patients with similar signs and symptoms caused by non-Lyme illnesses). The US Centers for Disease Control and Prevention (Atlanta, GA, USA) curated the first Lyme disease biobank with samples from 86 adults with Lyme disease, 144 clinical mimics, and 203 healthy controls from 11 collection sites (*5*). The Study of Lyme Disease Immunology and Clinical Events (http://www.slicestudies.org) at the Johns Hopkins Lyme Disease Research Center (Baltimore, MD, USA) enrolled 40 adults with an erythema migrans (EM) lesion and followed up with patients for 1 year. The Lyme Disease Biobank, supported by the Bay Area Lyme Foundation, has enrolled 550 adults with Lyme disease evaluated at 7 primary-care collection sites (*6*). To date, none of these biobanks have included children or used emergency departments for enrollment.

In 2015, we founded Pedi Lyme Net, a pediatric Lyme disease research network comprising 8 emergency departments in a diverse range of areas to which Lyme disease is endemic. We conducted a prospective cohort study of children evaluated for Lyme at 1 of of these emergency departments (Appendix Figure 1, https://wwwnc.cdc.gov/EID/article/26/12/20-0920-App1.pdf). The Pediatric Lyme Disease Biobank, housed at Boston Children's Hospital (Boston, MA, USA), stores and distributes the biosamples collected from enrolled children (*7*).

Table. Characteristics of enrolled children with Lyme disease and clinical mimics, United States, 2015–2020*

Characteristics	Lyme disease	Clinical mimics	p value
Total	515	1,982	
Demographics			
Median age, y (IQR)	8 (6–11)	9 (5–14)	0.02
Sex			
M	345 (67.0)	1,048 (52.9)	<0.01
F	170 (33.0)	934 (47.1)	
Race			
White	438 (85.0)	1,482 (74.8)	<0.01
Black	42 (8.2)	255 (12.9)	
Asian	8 (1.6)	53 (2.7)	
Pacific Islander	0	3 (0.1)	
Native American	0	2 (0.1)	
Other	22 (4.3)	156 (7.9)	
Missing data	5 (1.0)	31 (1.6)	
Ethnicity			
Hispanic	33 (6.4)	234 (11.8)	<0.01
Non-Hispanic	480 (93.2)	1,734 (87.5)	
Missing data	2 (0.4)	14 (0.7)	
History			
Presentation during peak Lyme season†	343/515 (66.6)	1,187/1,982 (59.9)	<0.01
Previous Lyme disease	47/514 (9.1)	79/1,945 (4.1)	<0.01
Tick bite within past year	73/468 (15.6)	150/1,808 (8.3)	<0.01
Fever	176/507 (34.7)	732/1,959 (37.4	0.35
Headache	152/510 (29.8)	760/1,926 (39.5)	<0.01
Examination			
Erythema migrans lesion	54 (10.5)	NA	NA
Facial palsy	59 (11.5)	158 (8.0)	<0.01
Lumbar puncture performed	47 (9.1)	155 (7.8)	0.33
Meningitis	21/47 (44.7)	57/155 (36.8)	
Arthritis (joint swelling)	286 (55.5)	556 (28.1)	<0.01

*Values are no. (%) except as indicated. NA, not applicable.
†June–October.

We describe enrolled children 1–21 years of age who underwent emergency department evaluation for Lyme disease during June 1, 2015–January 31, 2020 (Table). We obtained informed consent from parents/guardians for study participation and child assent for those ≥8 years of age. Informed consent documents were available in English and Spanish. We defined disease stage on the basis of signs and symptoms: early (i.e., single EM lesion), early disseminated (i.e., multiple EM lesions, cranial neuritis, meningitis, or carditis) or late (i.e., arthritis or arthralgia). In addition, as asymptomatic controls, we enrolled children undergoing intravenous cannulation for procedural sedation for fracture reduction or laceration repair without acute infectious symptoms. We implemented standard operating procedures at each of the participating sites (Appendix Table). All deidentified data were collected electronically with Research Electronic Data Capture housed at Harvard University (https://catalyst.harvard.edu/services/redcap).

We defined Lyme disease on the basis of an EM lesion diagnosed by the treating clinician or positive serologic results with compatible symptoms. We took serum samples from all enrolled patients, including asymptomatic controls, and conducted a C6 EIA on each sample. If the EIA results were positive or equivocal, we also conducted a Western immunoblot interpreted using standard criteria (*8*). We considered a positive IgM immunoblot paired with a negative IgG immunoblot to be positive only if symptoms lasted ≤30 days (*10*). We classified symptomatic children who tested negative for Lyme disease as clinical mimics. We compared characteristics of children with Lyme disease and mimics using the χ^2 test for categorical variables and the Mann-Whitney test for continuous variables with SPSS Statistics 23.0 (IBM Corp., https://www.ibm.com).

We enrolled and obtained samples from 2,497 symptomatic and 377 asymptomatic control patients (Appendix Figure 2). Overall, 515 (20.6% of symptomatic patients) had Lyme disease; of these children, 46 (8.9%) had an EM lesion alone, 461 (89.5%) had a positive 2-tier serology alone, and 8 (1.6%) had both. Of the asymptomatic control patients, 4 (1.1%) had positive 2-tier serology.

Our Pediatric Lyme Disease Biobank is unique because it includes biosamples from pediatric patients, clinical mimics, and diverse geographic regions. The samples are linked to demographic, clinical, laboratory, and treatment data about each patient. With >2,800 children enrolled, this biobank is a unique resource for researching Lyme disease diagnosis in children.

Our biobank has a few limitations. First, we enrolled a convenience sample of children depending on the availability of study staff. However, in this study, the proportion of children with Lyme disease did not differ between enrolled and unenrolled but eligible patients. Second, some children with early or early-disseminated Lyme disease might have had false negative serologic results. However, we conducted follow-up to identify children who had initially negative 2-tier Lyme serologic results but tested positive within 30 days of enrollment. Finally, because our network includes only 8 enrollment sites, we were unable to include all regions to which Lyme disease is endemic.

Acknowledgments

We would like to thank patients and families who agreed to participate in the study.

This study received funding from Boston Children's Hospital and Global Lyme Alliance.

Interested collaborators should contact Pedi Lyme Net to discuss potential collaborations.

About the Author

Dr. Nigrovic is an associate professor of Pediatrics and Emergency Medicine at Harvard Medical School. Her research interests include the diagnosis of Lyme disease in children.

References

1. Hinckley AF, Connally NP, Meek JI, Johnson BJ, Kemperman MM, Feldman KA, et al. Lyme disease testing by large commercial laboratories in the United States. Clin Infect Dis. 2014;59:676–81. https://doi.org/10.1093/cid/ciu397
2. Wormser G-PP, Dattwyler R-JJ, Shapiro E-DD, Halperin JJ, Steere AC, Klempner MS, et al. The clinical assessment, treatment, and prevention of Lyme disease, human granulocytic anaplasmosis, and babesiosis: clinical practice guidelines by the Infectious Diseases Society of America. Clin Infect Dis. 2006;43:1089–134. https://doi.org/10.1086/508667
3. Branda JA, Body BA, Boyle J, Branson BM, Dattwyler RJ, Fikrig E, et al. Advances in serodiagnostic testing for Lyme disease are at hand. Clin Infect Dis. 2018;66:1133–9. https://doi.org/10.1093/cid/cix943
4. Garro A, Bennett J, Balamuth F, Levas MN, Neville D, Branda JC, et al.; Pedi Lyme Net. Positive 2-tiered Lyme disease serology is uncommon in asymptomatic children living in endemic areas of the United States. Pediatr Infect Dis J. 2019;38:e105–7. https://doi.org/10.1097/INF.0000000000002157
5. Molins CR, Sexton C, Young JW, Ashton LV, Pappert R, Beard CB, et al. Collection and characterization of samples for establishment of a serum repository for Lyme disease diagnostic test development and evaluation. J Clin Microbiol. 2014;52:3755–3762. https://doi.org/10.1128/JCM.01409-14
6. Horn EJ, Dempsey G, Schotthoefer AM, Prisco UL, McArdle M, Gervasi SS, et al. The Lyme Disease Biobank: characterization of 550 patient and control samples from the East Coast and Upper Midwest of the United States. J Clin Microbiol. 2020;58:1–12.
7. Boston Children's Hospital. Pedi Lyme Net. 2020 [cited 2020 Aug 3]. http://www.childrenshospital.org/research/centers-departmental-programs/Pedi-Lyme-Net
8. Centers for Disease Control and Prevention. Recommendations for test performance and interpretation from the Second National Conference on Serologic Diagnosis of Lyme Disease. MMWR Morb Mortal Wkly Rep. 1995;44:590–1.
9. Nowakowski J, Schwartz I, Liveris D, Wang G, Aguero-Rosenfeld ME, Girao G, et al.; Lyme Disease Study Group. Laboratory diagnostic techniques for patients with early Lyme disease associated with erythema migrans: a comparison of different techniques. Clin Infect Dis. 2001;33:2023–7. https://doi.org/10.1086/324490
10. Lantos PM, Lipsett SC, Nigrovic LE. False positive Lyme disease IgM immunoblots in children. J Pediatr. 2016;174:267–269.e1. https://doi.org/10.1016/j.jpeds.2016.04.004

Address for correspondence: Lise Nigrovic, Division of Emergency Medicine, Boston Children's Hospital, 300 Longwood Avenue, Boston, MA 02115, USA; email: lise.nigrovic@childrens.harvard.edu

Transmission Electron Microscopy Confirmation of *Orientia tsutsugamushi* in Human Bile

Yujeong Lee,[1] Seung Il Kim,[1] Yoon-sun Yi, Hayoung Lee, Joo-Hee Hwang, Edmond Changkyun Park, Sangmi Jun,[2] Chang-Seop Lee[2]

Author affiliations: Korea Basic Science Institute, Cheongju, South Korea (Y. Lee, S.I. Kim, Y.-s. Yi, H. Lee, E.C. Park, S. Jun); Korea Research Institute of Chemical Technology, Daejeon, South Korea (Y. Lee, S.I. Kim, E.C. Park, S. Jun); University of Science and Technology, Daejeon (S.I. Kim, H. Lee, E.C. Park); Jeonbuk National University, Jeonju, South Korea (J.-H. Hwang, C.-S. Lee); Jeonbuk National University Hospital, Jeonju (J.-H. Hwang, C.-S. Lee)

[1]These authors contributed equally to this article.

[2]These authors were co-principal investigators.

Scrub typhus, the third most frequently reported infectious disease in South Korea, causes serious public health problems. In 2019, we collected a bile specimen from a patient with scrub typhus through percutaneous transhepatic gallbladder drainage and performed transmission electron microscopy to confirm the ultrastructure of *Orientia tsutsugamushi*.

Orientia tsutsugamushi is a gram-negative obligately intracellular coccobacillus and a causative pathogen of scrub typhus, which is transmitted to humans by bites from trombiculid (chigger) mites (*1*). Scrub typhus is a prevalent acute febrile disease that mainly occurs in the Asia-Pacific region, infecting ≈1 million persons worldwide each year. In South Korea, infections have increased rapidly since 2014 because of climate change, increased outdoor activities, and numbers of elderly farmers (*2*). The most typical clinical manifestation of scrub typhus is an eschar at the site of the bite (Figure, panel A); symptoms include fever, headache, muscle pain, nausea, and vomiting (*3*). Without proper diagnosis and antimicrobial drug treatment, severe illness with multiple organ system involvement can occur; the death rate is ≈10% (*4*). Immunohistochemical staining for *O. tsutsugamushi* antigens have revealed extensive endothelial cell infection in the heart, lung, kidney, pancreas, skin, and brain (*5*). Bacteria also have been detected in cardiac muscle cells and in macrophages in the liver and spleen (*5*,*6*).

In humans, the liver secretes ≈1 L of bile daily into the intestinal tract. However, little information is available about the presence of gram-negative bacteria in bile (*7*). Pathogenic microorganisms must endure potential impediments, such as variations in pH, low oxygen levels, nutrient limitation, and elevated osmolarity, to survive in this harsh environment (*7*). We collected bile from a patient with scrub typhus in South Korea (Figure, panel B) and visualized the ultrastructure of *O. tsutsugamushi* in the clinical sample using transmission electron microscopy.

In 2019, a 68-year-old woman reported fever, drowsy mental state, abdominal pain, and reduced oral intake. These symptoms had begun 7 days earlier. Her vital signs were blood pressure 100/60 mm Hg and body temperature 38.9°C. Laboratory analysis revealed a leukocyte count 10,350/mL (reference range 4,800–10,800/mL), platelet count 45,000/mL (reference 130,000–450,000/mL), serum creatinine 0.4 mg/dL (reference 0.7–1.7 mg/dL), aspartate aminotransferase 31 IU/L (reference 12–33 IU/L), alanine aminotransferase 41 IU/L (reference 5–35 IU/L), total bilirubin 1.72 mg/dL (reference 0.2–1.2 mg/dL), and C-reactive protein 196.86 mg/L (reference <5 mg/L). Abdominal computed tomography scan detected acute cholecystitis, and percutaneous transhepatic gallbladder drainage was performed. The presence of acute cholecystitis in scrub typhus cases is rare (5 [1.1%] instances of 442 cases) (*8*). *O. tsutsugamushi* can

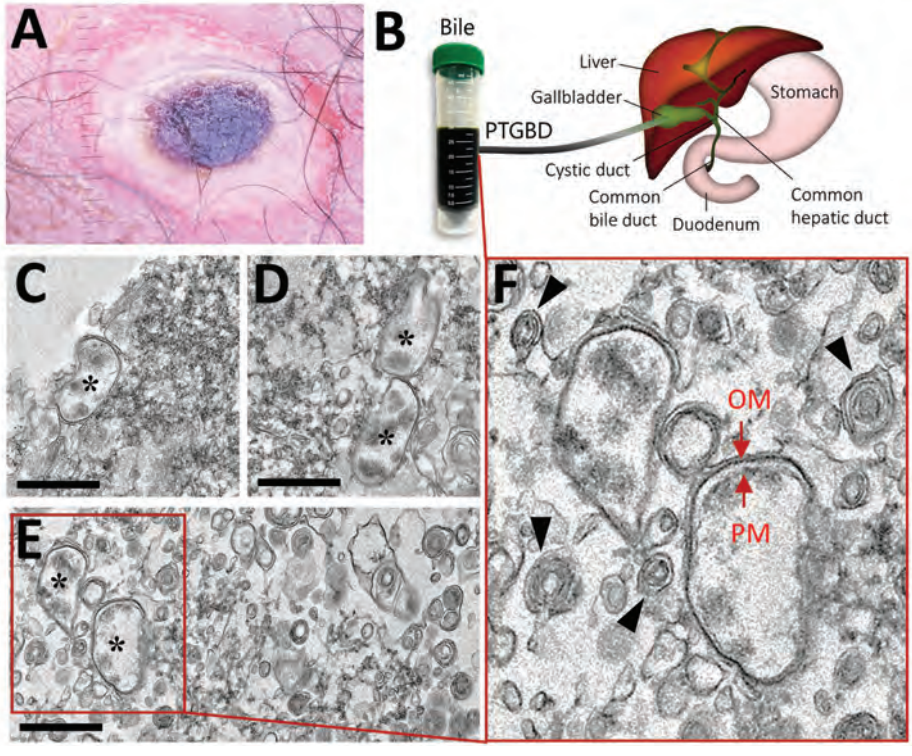

Figure. Findings from a 68-year-old woman with scrub typhus, South Korea, 2019. A) Eschar in the right inguinal area. B) Human bile collected through percutaneous transhepatic gallbladder drainage in the gallbladder of a patient affected with scrub typhus. C–F) Transmission electron microscopy images of *Orientia tsutsugamushi* in the bile. Bacteria (black asterisks); outer membrane (OM) and plasma membrane (PM) (red arrows); multilamellar body (black arrowheads); Scale bars indicate 1 μm.

also cause liver injury in some patients, but the patient reported here did not have any such signs (*9*). We confirmed scrub typhus using indirect immunofluorescence assay (IgG 5,120) and nested PCR selective for the 56-kDa gene of *O. tsutsugamushi* (Appendix, https://wwwnc.cdc.gov/EID/article/26/12/20-2188-App1.pdf). The *O. tsutsugamushi* identified belonged to the Boryong strain (the most common strain in South Korea). We also detected an eschar in the right inguinal area (Figure, panel A). The patient completely recovered after doxycycline treatment.

A drainage tube was placed in the patient's gallbladder, and the bile was directly discharged and collected through the tube (Figure, panel B). We tested the bile specimen for pathogens using nested quantitative reverse transcription PCR and DNA sequencing to detect a specific *O. tsutsugamushi* gene encoding a 56-kDa protein (Appendix) (*10*). After chemical fixation, the sample was embedded in 100% Epon 812 resin and ultrathin (≈80-nm thick) sections were stained with 2% uranyl acetate and 1% lead citrate (Appendix) (*10*). This sample preparation method might not preserve the ultrastructure of live bacteria, but structural features of the bacteria can be clearly observed. The ultrastructural details were acquired using transmission electron microscopy at 120 kV. Despite the presence of a wide variety of components, we detected *O. tsutsugamushi* in the bile (asterisks in Figure, panels C–E). The bacteria showed a coccobacillus shape and were 0.5–0.7-μm in diameter and 1.2–2.5-μm long, all typical features of *O. tsutsugamushi* (*5*,*10*). The bacterial cytoplasm was surrounded by an outer membrane, an internal plasma membrane, and a peptidoglycan layer (Figure, panel F). Moreover, the periplasmic space appeared as an electron-lucent gap between the 2 membranes. We also observed a thicker outer leaflet of the cell wall membrane, which is a typical and diagnostic sign of *Orientia* (*5*). We also detected multilamellar bodies, which are cholesterol-carrying particles, in the bile sample (black arrowheads in Figure, panel F).

Previously, human scrub typhus disease was studied using a mouse model mimicking the disease and examining clinical samples postmortem (*5*,*6*). However, the host cell of *O. tsutsugamushi* in humans has not been completely defined. In this study, we confirmed detection of *O. tsutsugamushi* in human bile, an environment in which bacterial survival is challenging. This observation (i.e., the presence of *O. tsutsugamushi* in human bile) might be useful for diagnosing scrub typhus in patients who do not show clear eschars or skin rash, broadening the potential routes for diagnosing the disease.

This work was supported by the Basic Science Research Programs (NRF-2015R1D1A1A01060251 and 2018R1D-1A3B07049557) of the National Research Foundation of Korea, which is funded by the Ministry of Education; the Korea Basic Science Institute grant (C030221), and National Research Council of Science & Technology grant by the Korea government (CRC-16-01-KRICT).

About the Authors

Ms. Y. Lee is a researcher at the Korea Basic Science Institute. Her primary interests are electron microscopy of infectious viral and bacterial diseases. Dr. Kim is a senior researcher at the Korea Basic Science Institute. His research interests are in the proteomics of infectious diseases.

References

1. Liu YX, Cao WC, Gao Y, Zhang JL, Yang ZQ, Zhao ZT, et al. *Orientia tsutsugamushi* in eschars from scrub typhus patients. Emerg Infect Dis. 2006;12:1109–12. https://doi.org/10.3201/eid1207.050827
2. Kim DM. Clinical features and diagnosis of scrub typhus. Infect Chemother. 2009;41:315–22. https://doi.org/10.3947/ic.2009.41.6.315
3. Lee CS, Hwang JH. Images in clinical medicine. Scrub syphus. N Engl J Med. 2015;373:2455. https://doi.org/10.1056/NEJMicm1503639
4. VieBrock L, Evans SM, Beyer AR, Larson CL, Beare PA, Ge H, et al. *Orientia tsutsugamushi* ankyrin repeat-containing protein family members are type 1 secretion system substrates that traffic to the host cell endoplasmic reticulum. Front Cell Infect Microbiol. 2015;4:186. https://doi.org/10.3389/fcimb.2014.00186
5. Moron CG, Popov VL, Feng HM, Wear D, Walker DH. Identification of the target cells of *Orientia tsutsugamushi* in human cases of scrub typhus. Mod Pathol. 2001;14:752–9. https://doi.org/10.1038/modpathol.3880385
6. Shelite TR, Saito TB, Mendell NL, Gong B, Xu G, Soong L, et al. Hematogenously disseminated *Orientia tsutsugamushi*–infected murine model of scrub typhus [corrected]. Erratum in: PLoS Negl Trop Dis. 2014;8:e3175. PLoS Negl Trop Dis. 2014;8:e2966. https://doi.org/10.1371/journal.pntd.0002966
7. Begley M, Gahan CG, Hill C. The interaction between bacteria and bile. FEMS Microbiol Rev. 2005;29:625–51. https://doi.org/10.1016/j.femsre.2004.09.003
8. Lee H, Ji M, Hwang JH, Lee JY, Lee JH, Chung KM, et al. Acute cholecystitis in patients with scrub typhus. J Korean Med Sci. 2015;30:1698–700. https://doi.org/10.3346/jkms.2015.30.11.1698
9. Chung JH, Lim SC, Yun NR, Shin SH, Kim CM, Kim DM. Scrub typhus hepatitis c onfirmed by immunohistochemical staining. World J Gastroenterol. 2012;18:5138–41. https://doi.org/10.3748/wjg.v18.i36.5138
10. Ro HJ, Lee H, Park EC, Lee CS, Il Kim S, Jun S. Ultrastructural visualization of *Orientia tsutsugamushi* in biopsied eschars and monocytes from scrub typhus patients in South Korea. Sci Rep. 2018;8:17373. https://doi.org/10.1038/s41598-018-35775-9

Address for correspondence: Sangmi Jun, Center for Research Equipment, Korea Basic Science Institute, 162 Yeongudanji-ro, Ochang-eup, Cheongwon-gu, Cheongju-si, Chungcheongbuk-do, 28119, South Korea; email: smjun@kbsi.re.kr

Etymologia: Buruli Ulcer

Tony M. Korman, Paul D.R. Johnson, John Hayman

Author affiliations: Monash University, Melbourne, Victoria, Australia (T.M. Korman); Austin Health, Melbourne (P.D.R. Johnson); University of Melbourne, Melbourne (P.D.R. Johnson, J. Hayman)

DOI: https://doi.org/10.3201/eid2612.200744

To the Editor: The recent etymologia by Henry in the March 2020 issue of Emerging Infectious Diseases recounts the fascinating origin of the name Buruli ulcer (*1*). Further to the history, in 1948, pathologist Peter MacCallum first described the clinical features for 6 patients from Victoria, Australia, each with an ulcer with undermined edges on an arm or a leg, and the characteristic histopathologic findings, including extensive necrosis and abundant acid-fast bacilli without granuloma formation (*2*). Five of the patients were identified by general practitioners D.G. Alsop, L.E. Clay, and J.R. Searls from the city of Bairnsdale (thus, another eponym "Bairnsdale ulcer") (*3*). Glen Buckle and Jean Tolhurst at the Alfred Hospital in Melbourne established experimental animal infections, and eventually isolated the causative organism (*2*), which they later named *Mycobacterium ulcerans* (*4*). The growth of *M. ulcerans* required prolonged incubation at a temperature of 30°C–33°C (*2*), which was only realized after the inadvertent use of a faulty incubator.

In 1964, Clancey described a "new" mycobacterium causing chronic skin ulcers in Uganda that "resembled" *M. ulcerans* which he named "*Mycobacterium buruli*" (*5*). However, the causative organism of Buruli ulcer was subsequently recognized as *Mycobacterium ulcerans,* which had been originally described in Australia.

About the Author

Dr. Korman is an adjunct clinical professor at Monash University; Director, Monash Infectious Diseases; and Director of Microbiology, Monash Health, Clayton, Australia. He has a wide range of clinical, laboratory, and research interests.

References

1. Henry R. Etymologia: Buruli ulcer. Emerg Infect Dis. 2020;26:504. https://doi.org/10.3201/eid2603.ET2603
2. MacCallum P, Tolhurst JC, Buckle G, Sissons H. A new mycobacterial infection in man. J Pathol Bacteriol. 1948;60:93–122. https://doi.org/10.1002/path.1700600111
3. Johnson PD. Buruli ulcer in Australia. In: Pluschke G, Roltgen K, editors. Buruli ulcer. *Mycobacterium ulcerans* disease. New York: Springer; 2019. p. 61–76. https://doi.org/10.1007/978-3-030-11114-4
4. Fenner F. The significance of the incubation period in infectious diseases. Med J Aust. 1950;2:813–8. https://doi.org/10.5694/j.1326-5377.1950.tb106945.x
5. Clancey JK. Mycobacterial skin ulcers in Uganda: description of a new mycobacterium (*Mycobacterium buruli*). J Pathol Bacteriol. 1964;88:175–87. https://doi.org/10.1002/path.1700880123

Address for correspondence: Tony M. Korman, Monash Infectious Diseases, Monash Health Centre, 246 Clayton Rd, Clayton, VIC 3168, Australia; email: tony.korman@monash.edu

Arthritis Caused by MRSA CC398 in Patient without Animal Contact, Japan

Anders R. Larsen, Jesper Larsen

Author affiliation: Statens Serum Institut, Copenhagen, Denmark

DOI: https://doi.org/10.3201/eid2612.202780

To the Editor: In their recent article, Nakaminami et al. describe a case of human infection caused by Panton-Valentine leucocidin (PVL)–positive livestock-associated methicillin-resistant *Staphylococcus aureus* clonal complex 398 (MRSA CC398) in Japan (*1*). *S. aureus* CC398 includes 2 major MRSA variants with distinct genetic and epidemiologic properties, a highly transmissible and virulent human variant comprising both PVL-positive and PVL-negative strains and a more benign PVL-negative livestock-associated variant (*2*). We have previously shown that, in Denmark, nearly all case-patients colonized or infected with PVL-positive MRSA CC398 strains of the human variant have links to countries in mainland Asia, where the strain is endemic in the community (*3*). Our analysis revealed the existence of 2 phylogenetically distinct lineages (L1 and L2) with unique sequence types (STs), ST398 linked to China and ST1232 linked to Vietnam, Thailand, and Cambodia. Besides being PVL-positive and belonging to ST1232, the isolate described by Nakaminami et al. (*1*) also shared other genetic and phenotypic characteristics with the L2 strains: it carried *spa* type t034 and SCC*mec* type V and was resistant to aminoglycosides (gentamicin), lincosamides (clindamycin),

macrolides (clarithromycin), and tetracyclines (tetracycline). We therefore suspect that the isolate belongs to the human variant of MRSA CC398.

In recent years, Denmark has witnessed increased importation of PVL-positive MRSA CC398 from mainland Asia because of international travel, in 1 case leading to a large hospital outbreak among mothers and infants in a maternity ward (*3*), and it seems possible that Japan and other countries might face a similar risk in the near future. Strain identification, source attribution, and knowledge about the transmission dynamics are essential for maintaining an effective MRSA infection control and prevention program. We therefore advocate using genotypic methods (e.g., as described by Stegger et al. [*4*]) that can accurately distinguish the human variant of MRSA CC398 from the livestock-associated variant.

References

1. Nakaminami H, Hirai Y, Nishimura H, Takadama S, Noguchi N. Arthritis caused by MRSA CC398 in a patient without animal contact, Japan. Emerg Infect Dis. 2020;26:795–7. https://doi.org/10.3201/eid2604.190376
2. Price LB, Stegger M, Hasman H, Aziz M, Larsen J, Andersen PS, et al. *Staphylococcus aureus* CC398: host adaptation and emergence of methicillin resistance in livestock. MBio. 2012;3:e00305–11. https://doi.org/10.1128/mBio.00305-11
3. Møller JK, Larsen AR, Østergaard C, Møller CH, Kristensen MA, Larsen J. International travel as a source of an unusual meticillin-resistant *Staphylococcus aureus* clonal complex 398 outbreak in a Danish hospital, 2016. Euro Surveill. 2019;24:1800680. https://doi.org/10.2807/1560-7917.ES.2019.24.42.1800680
4. Stegger M, Liu CM, Larsen J, Soldanova K, Aziz M, Contente-Cuomo T, et al. Rapid differentiation between livestock-associated and livestock-independent *Staphylococcus aureus* CC398 clades. PLoS One. 2013;8:e79645. https://doi.org/10.1371/journal.pone.0079645

Address for correspondence: Jesper Larsen, Department of Bacteria, Parasites, and Fungi, Statens Serum Institut, Artillerivej 5, DK-2300 Copenhagen S, Denmark; e-mail: jrl@ssi.dk

Hidemasa Nakaminami

Author affiliation: Tokyo University of Pharmacy and Life Sciences, Tokyo, Japan

DOI: https://doi.org/10.3201/eid2612.203738

In Response: In our article (*1*), we hypothesized that the transmission route of the Panton-Valentine leukocidin (PVL)–positive sequence type (ST) 1232 (CC398) MRSA strain is not only from humans but also from imported edible meat for humans. However, in their letter, Larsen and Larsen (2) indicated that *S. aureus* CC398 includes 2 major MRSA variants with distinct genetic and epidemiologic properties; 1 being a highly transmissible and virulent human variant comprising both PVL-positive and PVL-negative strains, and the other being a more benign PVL-negative livestock-associated variant (3). The presence of PVL genes and immune evasion cluster (IEC) genes in CC398 strain provides supportive evidence for the association of human colonization or infections. Furthermore, they showed that most case-patients in Denmark who were colonized or infected with PVL-positive MRSA CC398 strains of the human variant have links to countries in mainland Asia (4).

Actually, we confirmed *scn*, *chp*, and *sak* of the IEC genes in the PVL-positive ST1232 strain. Hence, as Larsen and Larsen suggested, the ST1232 strain might be a human variant of CC398. We recently reported a second case of the ST1232 strain with characteristics similar to the previous patient in Japan (*5*). The data strongly suggest that the incidence of human variant of CC398 has been increasing in Japan. Therefore, I agree with their opinion that accurate discrimination of the human variant of MRSA CC398 from the livestock-associated variant is essential for maintaining effective MRSA infection control. I presume that detection of PVL and IEC genes might be a useful simplified marker for classification of the human variant of CC398.

References

1. Nakaminami H, Hirai Y, Nishimura H, Takadama S, Noguchi N. Arthritis caused by MRSA CC398 in a patient without animal contact, Japan. Emerg Infect Dis. 2020;26:795–7. https://doi.org/10.3201/eid2604.190376
2. Larsen AR, Larsen J. Arthritis caused by MRSA CC398 in a patient without animal contact, Japan. Emerg Infect Dis. 2020 Dec [cited 2020 Aug 10]. https://doi.org/10.3201/eid2612.202780
3. Price LB, Stegger M, Hasman H, Aziz M, Larsen J, Andersen PS, et al. *Staphylococcus aureus* CC398: host adaptation and emergence of methicillin resistance in livestock. MBio. 2012;3:e00305-11. https://doi.org/10.1128/mBio.00305-11
4. Møller JK, Larsen AR, Østergaard C, Møller CH, Kristensen MA, Larsen J. International travel as source of a hospital outbreak with an unusual meticillin-resistant *Staphylococcus aureus* clonal complex 398, Denmark, 2016. Euro Surveill. 2019;24. https://doi.org/10.2807/1560-7917.ES.2019.24.42.1800680
5. Nakaminami H, Kawasaki H, Takadama S, Kaneko H, Suzuki Y, Maruyama H, et al. Threat of dissemination, Panton-Valentine leukocidin-positive livestock-associated methicillin-resistant *Staphylococcus aureus* (LA-MRSA) CC398 clone in Tokyo, Japan. Jpn J Infect Dis. 2020. https://doi.org/10.7883/yoken.JJID.2020.345

Address for correspondence: Hidemasa Nakaminami, Department of Microbiology, School of Pharmacy, Tokyo University of Pharmacy and Life Sciences, 1432-1 Horinouchi, Hachioji, Tokyo 192-0392, Japan; email: nakami@toyaku.ac.jp

Large SARS-CoV-2 Outbreak Caused by Asymptomatic Traveler, China

Andrei R. Akhmetzhanov

Author affiliation: College of Public Health, National Taiwan University, Taipei, Taiwan

DOI: https://doi.org/10.3201/eid2612.203437

To the Editor: Liu et al. (*1*) reported on a large outbreak of >70 cases of severe acute respiratory syndrome coronavirus 2 (SARS-CoV-2) infection. The origin of the outbreak was traced back to an asymptomatically infected traveler. However, delays in detecting SARS-CoV-2 infections in families B and C1 represent missed opportunities for earlier isolation and interruption of disease transmission.

After reading Lui et al. (*1*), we questioned whether April 7 was the first day of illness onset for the initial confirmed case, B2.3. Because viral load and infectiousness peak around the time of symptom onset and exposure of family C1 to case B2.3 was 9 days before that date, presymptomatic transmission would be highly unlikely (*2*). Although B2.2, who was an asymptomatic carrier, also could have played a role in exposing the family of C1, a close examination of publicly available records (*3*) altered this hypothesis.

Exposed on March 26, case B2.3 transmitted the virus to family C1 3 days later, on March 29, which appears to be 1 day before his first symptoms. Case B2.3 went to an outpatient clinic with a subjective fever on March 30 but was not tested for SARS-CoV-2. He was not isolated until he went to a clinic again on April 7 with worsening symptoms. Earlier isolation and testing of B2.3 could have prompted earlier contact tracing and triggered earlier diagnosis of C1 during his hospital stay, potentially preventing the chain of >60 SARS-CoV-2 transmissions in 2 hospitals.

The uncooperative behavior of cases B2.2 and B2.3 complicated efforts for early contact tracing (*3*), demonstrating cooperation with medical officers, coupled with proactive case-finding and earlier case isolation, clearly are crucial in curbing disease spread (*4*,*5*). If timely actions had been implemented, the outbreak could have been prevented or greatly reduced in size.

References

1. Liu J, Huang J, Xiang D. Large SARS-CoV-2 outbreak caused by asymptomatic traveler, China. Emerg Infect Dis. 2020;26:2260–3. https://doi.org/10.3201/eid2609.201798
2. He X, Lau EHY, Wu P, Deng X, Wang J, Hao X, et al. Temporal dynamics in viral shedding and transmissibility of COVID-19. Nat Med. 2020;26:672–5. https://doi.org/10.1038/s41591-020-0869-5
3. Health Commission of Heilongjiang Province China. Patient trajectory: release of new confirmed cases, asymptomatic infection trajectory of 10 April [in Chinese] [cited 2020 Jul 25]. http://yiqing.ljjk.org.cn/index/pcontrol/newsinfo/id/1823.html
4. Wang CJ, Ng CY, Brook RH. Response to COVID-19 in Taiwan: big data analytics, new technology, and proactive testing. JAMA. 2020;323:1341–2. https://doi.org/10.1001/jama.2020.3151
5. Dinh L, Dinh P, Nguyen PDM, Nguyen DNH, Hoang T. Vietnam's response to COVID-19: prompt and proactive actions. J Trav Med. 2020;27(3):taaa047. PubMed https://doi.org/10.1093/jtm/taaa047

Address for correspondence: Andrei R. Akhmetzhanov, Global Health Program & Institute of Epidemiology and Preventive Medicine, College of Public Health, National Taiwan University, No. 17, Xuzhou Rd, Zhongzheng District, Taipei City 100025, Taiwan; email: akhmetzhanov@ntu.edu.tw

Interpreting Transmissibility of COVID-19 in Children

Eun Young Cho, Eun Hwa Choi, Jong-Hyun Kim

Author affiliations: Chungnam National University Hospital, Daejeon, South Korea (E.Y. Cho); Seoul National University College of Medicine, Seoul (E.H. Choi); College of Medicine, The Catholic University of Korea, Seoul (J-H. Kim)

DOI: https://doi.org/10.3201/eid2612.203452

To the Editor: We read with great interest the article by Park et al. (*1*) on contact tracing of 5,706 patients with coronavirus disease (COVID-19) during the early phase of the pandemic in South Korea. In the study, the overall detection rate of COVID-19 among household contacts was 11.8%; the highest detection rate (18.6%) was in household contacts of those 10–19 years of age and the lowest detection rate (5.3%) in household contacts of those 0–9 years of age. The media have reported the research as evidence that transmissibility in adolescents and adults is similar (*2*). Such an interpretation may influence decision-making on the reopening of schools.

Although this study nicely demonstrated the effectiveness of contact tracing strategy during a period of school closure, understanding transmissibility and the implications for the reopening of schools requires reinterpretation of the data. As of April 29, 2020, a total of 37.8% of the 10–19 age group were 19 years of age (223/590) and, therefore, were not school children (*3*). A recently published study in South Korea (*4*) reported 107 primary source children (aged 0–18) had 248 household contacts and only 1 became infected, giving a secondary attack rate of 0.5%. Data from source and contact tracing in the Netherlands (*5*) also confirmed low transmissibility in children <18 years of age (0/43, 0%) compared with persons ≥18 years (55/566, 8.3%).

Accumulating data, including this study, suggest low transmissibility in infected children <10 years of age. However, transmissibility in the adolescent age group is unclear at this time. The 10–19 years age group includes diverse students who have completely different contact patterns from elementary school through college; thus, transmission dynamics of COVID-19 may be different. Further detailed studies on understanding transmissibility of the virus by each school level can provide helpful insights for safe reopening of schools.

About the Author

Dr. Cho is a clinical associate professor at Department of Pediatrics, Chungnam National University Hospital. Her primary research focuses on pediatric infectious diseases.

References

1. Park YJ, Choe YJ, Park O, Park SY, Kim YM, Kim J, et al.; COVID-19 National Emergency Response Center, Epidemiology and Case Management Team. Contact tracing during coronavirus disease outbreak, South Korea, 2020. Emerg Infect Dis. 2020;26:1666–70. https://doi.org/10.3201/eid2610.201315
2. Mandavilli A. Older children spread the coronavirus just as much as adults, large study finds. The New York Times. 2020 Jul 18 [cited 2020 Aug 13]. https://www.nytimes.com/2020/07/18/health/coronavirus-children-schools.html
3. Korea Centers for Disease Control and Prevention. Updates on COVID-19 in Republic of Korea, 29 April 2020 [cited 2020 Nov 13]. https://www.kdca.go.kr/board/board.es?mid=a30402000000&bid=0030&act=view&list_no=367037
4. Kim J, Choe YJ, Lee J, Park YJ, Park O, Han MS, et al. Role of children in household transmission of COVID-19. Arch Dis Child. 2020 Aug 7 [Epub ahead of print]. https://doi.org/10.1136/archdischild-2020-319910
5. National Institute for Public Health and the Environment. Children and COVID-19. 2020 Jul 20 [cited 2020 Aug 13]. https://www.rivm.nl/en/novel-coronavirus-covid-19/children-and-covid-19

Address for correspondence: Jong-Hyun Kim, Department of Pediatrics, St. Vincent's Hospital, College of Medicine, The Catholic University of Korea, 93 Jungbu-daero, Paldal-gu, Suwon 16247, South Korea; email: jh00mn@catholic.ac.kr; Eun Hwa Choi, Department of Pediatrics, Seoul National University Children's Hospital, Seoul National University College of Medicine, 101 Daehak-ro, Jongno-gu, Seoul 03080, South Korea; email: eunchoi@snu.ac.kr

In Consideration of Our Mutual Relationship with Cats

Byron Breedlove and Jana Igunma

Felis catus, the only domesticated species of cat in the family *Felidae*, flourishes on every continent except Antarctica. Able to thrive in almost any climate and habitat, it is among the world's most invasive species. Current estimates of the global cat popula-tion, including pet, stray, and feral cats, range from 200 million to 600 million. Where there are humans, more than likely there are also cats.

Humans living in agricultural villages in northern Africa and the Near East are believed to have domesticated the African wildcat (*Felis lybica)* between 8,000 to 12,000 years ago. Archaeologist Magdalena Krajcarz and colleagues noted, "The cat's way to domestication is a complex and still unresolved topic with many questions concerning the chronology of its dispersal with agricultural societies and the nature of its evolving relationship with humans." Likely stored grains and trash piles in villages attracted rodent pests, which in turn lured local wildcats and initiated a nascent mutualistic relationship that has since flourished.

From those villages, cats found their way around the world. Authors Lee Harper and Joyce L. White wrote that ancient sailors "were quick to see the advantage of having cats aboard ship during long voyages to protect their food supplies from damage by rodents." Trade and commerce helped spread cats from the Middle East to various ports of call in Europe, the Far East and Orient, and the Americas. Throughout this common history, cats have been both reviled and revered by humans.

During the Middle Ages in Europe, some religious institutions considered cats evil, leading to thousands being killed. Later, however, the Black Death spread by fleas on rats contributed to cats' redemption. Harper and White noted, "The cat's skill as a hunter of vermin was desperately needed. Its reputation was salvaged. Owning a cat was back in style."

Ancient Egyptians ascribed to cats many characteristics shared with deities they worshipped. Freyja, Norse goddess of love, beauty, and fertility, rode on a cat-drawn chariot. Temples in medieval Japan often kept a pair of cats to protect precious manuscripts from being ruined by mice. In the Kingdom of Siam, which is modern-day Thailand, Buddhist monks welcomed cats into their temples, where they were protected as *Maeo Wat* (Temple Cats).

This month's cover art, "two lucky cats to support leadership," is the second folio from *A Thai Treatise on Cats*, created in the 19th century in central Thailand and acquired by the British Library in 2011. Such manuscripts about cats were made for breeders in Thailand at least from the 18th century on, although it is believed that cat breeding goes back to the beginnings of the ancient Thai Kingdom of Ayutthaya in the 14th century.

This work comprises 12 folios that open from top to bottom to reveal illustrations of 23 different types of Thai cats with brief captions. Author and researcher Martin R. Clutterbuck notes that this Thai treatise (and similar ones) ascribes 18 of these cats to be "lucky" and to bring their owners good luck, rank, prosperity, or health. The remaining cats were deemed unlucky. As is often the case with manuscripts from this period in Thailand, the author or illustrator is not identified nor is this example dated.

The cat depicted at the top is called *Wilat* (Beauty) and described as "having green eyes and dark fur, except the legs, stomach, back and tail which are white." The other cat is named *Kao Taem* (Nine Points) and has shiny emerald eyes and a white coat with nine darker spots of fur. Both males and females make a strong, melodious "*maeo*" sound, and keeping this cat "is understood to result in leadership." (The names for the different cats in the booklet are commonly used by cat breeders and owners in Thailand.) All cats in this manuscript are depicted on a small pedestal, which is a symbol of respect—deities, monks, royals, and sacred white elephants are often also depicted on pedestals.

Siamese cats, called *Maeo Boran* in Thai, have a wide variety of coat colors resulting from tyrosinase (TYR) mutations, and their eyes range from blue and green to yellow and gold. Naturally attached and loyal to humans, Maeo Boran are easy to keep in the home and to train to walk on a leash; they often have a beautiful, chatty voice and behave as if they were engaging in lively conversations.

The positive side of cat ownership, as celebrated in those cat treatises, is acknowledged on the CDC website, "Research has shown that cats can provide emotional support, improve moods, and contribute to the overall morale of their owners. Cats are also credited

Author affiliations: Centers for Disease Control and Prevention, Atlanta, Georgia, USA (B. Breedlove); British Library, London, UK (J. Igunma)

DOI: https://doi.org/10.3201/eid2612.AC2612

Artist Unknown. *Tamrā maeo—Cat treatise*, 1800–1870. Paper folding book, 12 folios, 2 images per side, ink, and water color on mulberry paper, Thai script. 14.2 in × 4.7 in/27.31 cm × 28.57 cm. British Library (Or 16797), London, UK. Public domain.

with promoting socialization among older individuals and physically or mentally disabled people." Cats, as noted earlier, have also historically helped control the spread of rodent-borne diseases among humans.

Nonetheless, living in close quarters with cats carries some health risks. Cats can transfer various zoonotic diseases, including *Campylobacter* infection, cat–scratch disease, cryptosporidiosis, hookworm infection, plague, rabies, and salmonellosis. Cats are the only animal in which the *Toxoplasma gondii* parasite completes its life cycle, and humans in close contact with cat litter, for example, are at risk of developing toxoplasmosis, which pregnant women can potentially transmit to a fetus. Much less common is transfer of disease from humans to animals, such as the suspected case of human-to-cat transmission of severe acute respiratory syndrome coronavirus 2 reported in this issue. (Both owner and cat recovered.)

Detecting, responding to, and preparing for emerging zoonotic infections—which, like cats, have made their way around the world with our help—are major challenges for public health leaders. Even if cats are not actual talismans or have the power to improve leadership, spending a few minutes considering these lucky cats may provide public health officials a brief respite or serendipitous insight.

Bibliography

1. Barbash Y. Cats, Bastet and the worship of feline gods [cited 2020 Oct 6]. https://www.arce.org/resource/cats-bastet-and-worship-feline-gods
2. British Library. Cat treatise, 1800–1870. Paper folding book [cited 2020 Oct 1]. https://www.bl.uk/manuscripts/Viewer.aspx?ref=OR_16797_f001r
3. Centers for Disease Control and Prevention. Healthy pets, healthy people. Cats [cited 2020 Oct 6]. https://www.cdc.gov/healthypets/pets/cats.html
4. Clutterbuck MR. The legend of Siamese cats. Bangkok: White Lotus; 1998 pp 19–29.
5. Driscoll CA, Macdonald DW, O'Brien SJ. From wild animals to domestic pets, an evolutionary view of domestication. Proc Natl Acad Sci U S A. 2009;106(Suppl 1):9971–8. https://doi.org/10.1073/pnas.0901586106
6. Driscoll CA, Menotti-Raymond M, Roca AL, Hupe K, Johnson WE, Geffen E, et al. The Near Eastern origin of cat domestication. Science. 2007;317:519–23. https://doi.org/10.1126/science.1139518
7. Garigliany M, Van Laere A-S, Clercx C, Giet D, Escriou N, Huon C, et al. SARS-CoV-2 natural transmission from human to cat, Belgium, March 2020. Emerg Infect Dis. 2020;26:3069–71. https://doi.org/10.3201/eid2612.202223
8. Harper L, White JL. The complete illustrated encyclopedia of cats. New York: Metro Books; 2008. p. 11–29.
9. Igunma J. Animals in Thai manuscript art [cited 2020 Oct 2]. https://www.bl.uk/animal-tales/articles/animals-in-thai-manuscript-art#authorBlock1
10. Igunma J. A treatise on Siamese cats [cited 2020 Oct 2]. https://southeastasianlibrarygroup.wordpress.com/2013/06/07/a-treatise-on-siamese-cats
11. Krajcarz M, Krajcarz MT, Baca M, Baumann C, Van Neer W, Popović D, et al. Ancestors of domestic cats in Neolithic central Europe: isotopic evidence of a synanthropic diet. Proc Natl Acad Sci U S A. 2020;117:17710–9. https://doi.org/10.1073/pnas.1918884117
12. Medina FM, Bonnaud E, Vidal E, Tershy BR, Zavaleta E, Donlan C, et al. A global review of the impacts of invasive cats on island endangered vertebrates. Glob Change Biol. 2011;17:3503–10. https://doi.org/10.1111/j.1365-2486.2011.02464.x

Address for correspondence: Byron Breedlove, EID Journal, Centers for Disease Control and Prevention, 1600 Clifton Rd NE, Mailstop H16-2, Atlanta, GA 30329-4027, USA; email: wbb1@cdc.gov

EMERGING INFECTIOUS DISEASES®

Emerging Infectious Diseases **thanks the following reviewers for their support through thoughtful, thorough, and timely reviews in 2020. Please contact us if your name is missing from this list.**

Preben Aavitsland
Abu Abdul-Quader
Joseph Abrams
Omar Abu Saleh
Nisha Acharya
Anna Acosta
Eisuke Adachi
Amesh Adalja
Laura Adams
Tolulope Adebanjo
Toidi Adekambi
Bishwa Adhikari
Jennifer Adjemian
Amos Adler
Cornelia Adlhoch
Danielle Adney
Nsiire Agana
Rakesh Aggarwal
Charles Agoti
Clas Ahlm
Faruque Ahmed
Kamruddin Ahmed
Kaylynn Aiona
Hossein Akbarialiabad
Andrei Akhmetzhanov
Lara Akinbami
Ana Alastruey-Izquierdo
M. John Albert
James Alexander
Afsar Ali
Ibne Ali
Sheikh Ali
Franz Allerberger
Celia Alpuche Aranda
Abeer Alshukairi
Arshad Altaf
Miriam Alter
Benjamin Althouse
Gerardo Alvarez
C. J. Alverson
Carmen Amaro
Roberto Amato
Avnika Amin
Brian Amman
Shuchi Anand
Cheryl Andam
Albert Anderson
Cole Anderson
Kathryn (Katie) Anderson
Kristi Anderson
Larry Anderson
Maureen Anderson
John Anderton
Nick Andrews
Emmanouil Angelakis
Andrea Angheben
Vernon Ansdell
Gregory Anstead
Assaf Anyamba
Yaseen Arabi
Diego Aragón-Caqueo
Matthew Arduino
Paul Arguin
Aziza Arifkhanova
Philip Armstrong
Melissa Arons
Naomi Aronson
Valentina Arsic Arsenijevic
Garret Asay
Victor Asensi
Danny Asogun
Katie Atkins
Houssam Attoui
Maite Aubry
Jonathan Auguste
Sara Auld
Tatjana Avsic
Abdu Azad
Eid Azar
Taj Azarian
Esther Babady
Hamid Badali
Edgar Badell
Martina Badell
Travis Baggett
Daniel Bailey
Kristina Bajema
Waheed Bajwa
Agoritsa Baka
Anthony Baker
Sapna Bamrah
Padmapriya Banada
Antonio Bandeira
Gad Baneth
Bettina Bankamp
A.-Lan Banks
Shisan Bao
Keith Baptiste
Galileu Barbosa Costa
Brianne Barker
Bridget Barker
Alex-Mikael Barkoff
John Barnes
Sophie Baron
Alan Barrett
Vanessa Barrs
Albert Barskey
Lisa Barton
Casey Barton Behravesh
Sridhar Basavaraju
Leonardo Basco
Anirban Basu
Michael Batz
Iacopo Baussano
Matthew Baylis
Lauren Bayliss
Bernard Beall
Ben Beard
Julia Beatty
Julien Beauté
J. David Beckham
Tammy Beckham
Robert Bednarczyk
Emily Beeler
Martin Beer
Nancy Beerens
Robin Behn
Jelena Bekvalac
John Belisle
David Bell
Fernando Bellissimo-Rodrigues
Jessica Belser
Karima Benameur
Adriana Benavides Lara
Eran Bendavid
Jeff Bender
Kaitlin Benedict
Camilla Benfield
Albert Bensaid
John Benson
Dennis Bente
Alberto Berardi
Michael Bergman
James Berkley
Kathryn Bernard
Theresa Bernardo
Kateri Bertran
Marianne Besnard
Pascal Bessong
Giulia Besutti
Elisa Bevilacqua
Nahid Bhadelia
Amrita Bharat
Narayan Bhattarai
Kyle Bibby
Dorothee Bienzle
Brad Biggerstaff
Dean Biggins
Bridgette Jeanne Billioux
Fabrice Biot
Paritosh Biswas
Aaron Bivins
Anders Björkman
Jason Blackard
Jason Blackburn
Stuart Blacksell
Carol Blair
Isobel Blake
David Blaney
Lucas Blanton
Alexandre Bleibtreu
Bradley Blitvich
Karen Bloch
Sandra Blome
Patrick Boerlin
Jérôme Boissier
Sameh Boktor
Trent Bollinger
Stephane Bonacorsi
James Bono
Jesse Bonwitt

John Boone
Martin Bootsma
Matthias Borchert
Nicole Borel
Andrew Borman
Ray Borrow
Albert Bosch
Steven Bosinger
Arnold Bosman
Graham Bothamley
Lorenzo Botto
Valerie Bouchez
Herve Bourhy
Anna Bowen
Richard Bowen
Carol Bower
William Bower
Victoria Bowes
O. Boyarchuk
Doug Brackney
Richard Bradbury
Robert Bradsher
Mary Brandt
Aaron Brault
Mike Bray
Byron Breedlove
Edward Breitschwerdt
Paul Brett
Annika Brinkmann
Melanie Brinkmann
Seth Britch
Francesco Broccolo
Tim Brooks
Lisa Brosseau
Julia Brotherton
Clive Brown
Corrie Brown
Joe Brown
Nicole Brown
Raffaele Bruno
James Brust
Gertrude Buehring
Canio Buonavoglia
Rachel Burke
Nathan Burkett-Cadena
Howard Burkom
Rachel Burns
Felicity Burt
Julian Burton
Luca Busani
Michael Busch
Marine Butin
Rachel Byrne
Viktória Čabanová
Andrea Calcagno
Charles Calisher
Vitaliano Cama
Magda Campins Martí
Fabricio Campos
Josefina Campos
Paul Cantey
Van-Mai Cao-Lormeau
Julien Cappelle
Mabel Carabali
Stephen Carden
Nora Cardona-Castro
Luis Cardoso
Christina Carlson
Chris Carr
Spencer Carran
Laura Carroll
Gail Carson
Jordi Casal
Irene Casas
Kelsie Cassell
Pamela Cassiday
Kenneth Castro
Godfred Cato
Marco Cavaleri
Joseph Cavanaugh
Catherine Cètre-Sossah
Thomas Chambers
Benedict Shing Bun Chan
Chung-Hong Chan
Derwin King Chung Chan
Kok Hoe Chan
Martin Chi-Wai Chan
Paul Chan
Luan-Yin Chang
Rémi Charrel
Christopher Chase
Sudha Chaturvedi
Vishnu Chaturvedi
Lakshmi Chauhan
Saurabh Chawla
Hualan Chen
Liang Chen
Lin Chen
Tzay-Jinn Chen
Zhiming Chen
Zhongdan Chen
Zhuo "Adam" Chen
Ziqiang Chen
Hao-Yuan Cheng
Vincent Cheng
Yi-Ning Cheng
Harrell Chesson
Veronique Chevalier
Tom Chiller
Alex Chin
Young June Choe
Eun Hwa Choi
Mary Choi
George Cholankeril
B.B. Chomel
Ka Chun Chong
Terence Chorba
Eric Chow
Nancy Chow
Anuradha Chowdhary
Gerardo Chowell
Jens Jørgen Christensen
Rebecca Christofferson
Daniel Chu
Victoria Chu
Helen Chun
Hyunjung Chung
Cansu Cimen
Elisa Cinotti
Daniela Cirillo
Cornelius Clancy
Hannah Clapham
Kristie Clarke
Gary Clifford
Barnett Cline
Katie Clow
Frank Cobelens
Nicole Cohen
Samuel Cohn
Robert Colebunders
Philippe Colson
Iñaki Comas
Emilyn Conceicao
Bruce Conn
Andrea Conroy
Gail Sondermeyer Cooksey
Laura Cooley
Victor Corman
Solenne Costard
Matthew Cotten
James Cotton
Deborah Couldwell
Julien Coussement
Logan Cowan
Benjamin Cowling
Pascal Crépey
Julio Croda
Samuel Crowe
Andrea Cruz
Bart Currie
Andrew Curtis
Felicity Cutts
Juliana Da Silva
Cristina Da Silva Carias
F. Scott Dahlgren
Charles Daley
Delesa Damena
Heath Damron
David Dance
Alexandra Dangel
Rachel Daniels
Kostas Danis
M. Carolina Danovaro-Holliday
Alexandre Dasilva
Virginia Dato
Michael David
Carlo Davila Payan
Charles Davis
Stephanie Davis
Bernard Davoust
Marcos de Almeida
Raoul de Groot
Pablo De Salazar
Thushan de Silva
Rita De Sousa
Daniela de Souza Rajao
Rik de Swart
Emmie de Wit
Nicola Decaro
Martin Dedicoat
Sylviane Defres
Carlos del Rio
Alexis Delabouglise
Giles DeLage
Mark Delorey
Eric Delwart
Grant Dewell
Walter Demczuk
Olivier Denis
Peter Deplazes
Stan Deresinski
Abhishek Deshpande
Guillaume Desoubeaux
Antonino Di Caro
Kadiatou Diallo
Georges Diatta
Francisco Diaz
James Diaz

Daniel Diekema
Emilio Dirlikov
Linda Dixon
Kevin Dobbin
Gerhard Dobler
Pete Dodd
Roger Dodd
Stephen Doggett
Yohei Doi
Dragoslav Domanović
Hopkins Donald
Lu Dong
Yuanyuan Dong
Christine Doyle
John Drake
Michel Drancourt
Michael Drebot
Jan Drexler
Rikard Dryselius
Zhanwei Du
Mignon du Plessis
Grégory Dubourg
Birgitta Duim
Roger Dumke
John Stephen Dumler
Veasna Duong
Claire Duployez
Alan Dupuis
Mariana Perez Duque
Lance Durden
Clare Dykewicz
Gregory Ebel
Mark Eberhard
Hideki Ebihara
Isabella Eckerle
Chris Edens
Kathryn Edwards
Morven Edwards
Paul Effler
Joseph Egger
Maren Eggers
Lars Eisen
Rebecca Eisen
Khalid El Karkouri
Adi Elias
Sascha Ellington
Robert Ellis
Esteban Engel
David Engelthaler
J. A. Englund
Julia Enkelmann
Delia Enria
Lauren Epstein
Dean Erdman
Laura Erdman
Lauren Erickson-Mamane
Luis Escobar
Pedro Esteves
Charles Evans
Jim Evermann
Samira Fafi-Kremer
Anna Fagre
Joseph Falkinham
Dennis Falzon
Cuifang Fan
Seamus Fanning
Nuno Faria
Claudio Farina
Amy Feehan
Kristen Feemster
Arnaud Fekkar
Heinz Feldmann
Leora Feldstein
Shuo Feng
Florence Fenollar
Jessica Ferguson
Maria Fernandez
Stefan Fernandez
James Fielding
Lyn Finelli
Alyssa Finlay
Leah Fischer
Peter Fischer
Thea Fischer
Matthew Fisher
David Fisman
Stefan Flasche
Katherine Fleming-Dutra
Antje Flieger
Jannik Fonager
Anthony Fooks
Pierre Formenty
Erik Foster
Monique Foster
Rob Foster
T.J. Foster
Pierre-Edouard Fournier
Robert Fowler
Joshua Francis
Kristina Franck
Jose Franco
Neil Franklin
Eelco Franz
Mark Fraser
John Frean
David Freedman
Scott Fridkin
Matthew Frieman
Rebecca Trout Fryxell
King-wa Fu
Pan Fu
Hans-Peter Fuehrer
Paul Fuerst
Paula Fujiwara
Isaac Chun-Hai Fung
Jennifer Furin
Nathan Woo Furukawa
Yuki Furuse
Alice Fusaro
Giovanni Gadda
Holly Gaff
Ken Gage
Romeo Galang
Maria Teresa Galán-Puchades
Renee Galloway
Cooper Galvin
Shantini Gamage
Manoj Gambhir
Emily Garner
Philippe Gautret
Yang Ge
Thomas Geisbert
William Geisler
Jon Gentsch
Sue Gerber
Peter Gerner-Smidt
Lorenzo Giacani
Connie Gibas
Katherine Gibney
Crystal Gigante
Leah Gilbert
Martin Gilbert
Thomas Gillespie
Robert Gilman
Howard Ginsberg
Maria Giufrè
Rebecca Gladstone
Mindy Glass
John Glasser
Janet Glowicz
Judith Glynn
Jacques Godfroid
Matthew Goetz
Jeremy Gold
Tony Goldberg
Paul Goldwater
Natalia Golender
Diego Gomez-Nieto
Gabriel Gonzalez
Fernando Gonzalez-Candelas
Alexander Gorbalenya
Catherine Gordon
Rachel Gorwitz
Neela Goswami
Magnus Gottfredsson
Marcelo Gottschalk
Ionela Gouandjika-Vasilache
Ernest Gould
Frédérique Gouriet
Jerome Gouttenoire
Fernando Gouvea-Reis
Joelle Gouy de Bellocq
Nelesh Govender
Tarini Goyal
Christopher Graber
Marc Grandadam
Stephen Gray
Pascal Grébaut
Bradford Greening
Luisa Gregori
Alexander Greninger
Karen Grépin
Daniel Griffin
Daniel Grint
Wolfgang Grisold
Martin Groschup
Nathan Grubaugh
Beate Grüner
Youyang Gu
Alfredo Guarino
Jeannette Guarner
Ania Gubala
Larisa Gubareva
Jonathan Gubbay
Alice Guh
Claire Guinat
Jonathan Guito
Paul Gulig
Karolina Gullsby
Cliff Gunthel
Emily Gurley
Alan Guthrie
Amanda Guthrie
Julie Gutman
Bart Haagmans
Maryam Haddad
Andrew Haddow
Liesl Hagan

Ferry Hagen
Jan Hajek
Pete Halfmann
Carina Hall
Patricia Hall
Francois Halleen
Benjamin Hallowell
Eric Halsey
Scott Halstead
Davidson Hamer
Gabriel Hamer
Sarah Hamer
Yiping Han
William Hanage
Julie Hand
Andreas Handel
Aidan Hanrath
Andrew Hansen
Fatmah Hansi
Jennifer Harcourt
Timm Harder
Gitte Hartmeyer
Yoshihisa Hashiguchi
Barbara Hasse
Ayesha Hassim
Norimichi Hattori
Arie Havelaar
Harry Haverkos
Joshua Havumaki
Hal Hawkins
Laura Hawks
Michael Hayashi
Frederick Hayden
David Hayman
Andrew Hayward
Daihai He
Fang He
Lihong He
Qiushui He
Yingchao He
Selwyn Headley
Craig Hedberg
Sonia Hegde
Fabian Heinrich
Marie Helleberg
Maged Hemida
Petr Heneberg
Emily Henkle
Thomas Hennessy
Bonnie Henry
Erine Henry
Ronnie Henry
Carolyn Herzig
David Heymann
Sarah Hill
Susan Hills
Charlotte Hobbs
Natasha Hochberg
Richard Hodinka
Markus Hoffmann
Regina Hofmann-Lehmann
Catherine A. Hogan
Mike Holbrook
David Holcomb
Matthew Holden
David Holland
F. Hollinger
Deirdre Hollingsworth
Edward Holmes
Margaret Honein
Chae Moon Hong
Yogesh Hooda
Roberta Horth
Katja Hoschler
Paul Hoskisson
Surui Hou
Rein Houben
Daniela Hozbor
Hui-Min Hsieh
Lewis Hsu
Haitao Hu
William Hu
Zhibin Hu
Yhu-Chering Huang
Falk Huettmann
Lucas Huggins
Holly Hughes
Ivan Hung
Yuen Wai Hung
Hiroshi Ichimura
Kazuhiko Ikeuchi
Allison Imrie
Kenichiro Inoue
Hon Ip
Stuart Isaacs
Badrul Islam
Nahed Ismail
Michael Ison
Claire Italiano
Naoya Itoh
Miren Iturriza-Gómara
Danielle Iuliano
Jesica Jacobs
Kathryn Jacobsen
Jóhanna Jakobsdóttir
Hee-Chang Jang
Sophie Jarraud
Aude Jary
Lauren Jatt
Claire Jenkins
Amy Jennison
Jørgen Skov Jensen
Seonghye Jeon
Walter Jeske
Libin Jiang
Min Jin
Reimar Johne
Christina Johns
Barbara Johnson
Nick Johnson
Paul Johnson
Stuart Johnson
Jefferson Jones
Jeffery Jones
Martin Jones
Morris Jones
Nicholas Jones
Susan Jones
T. Stephen Jones
Terry Jones
Colleen Jonsson
Brian Jordan
Joerg Jores
Naima Joseph
M. Joyce
John Jude Prakash
Emily Kahn
Adriana Kajon
Aley Kalapila
Alexander Kallen
Mary Kamb
Hajime Kamiya
Sanjat Kanjilal
Edward H. Kaplan
Edward L. Kaplan
Jon Kaplan
Shanthi Kappagoda
Alexandros Karamanlidis
Abraar Karan
Ruwandi Kariyawasam
John Karon
Imad Kassis
Morgan Katz
Carol A. Kauffman
Daniel Kaul
Ruian Ke
Bridget Kelly
Asis Khan
Grishma Kharod
Zohre Khodamoradi
Surender Khurana
Sarah Kidd
Marie Killerby
Alfred Kim
Bongyoung Kim
Bryan Kim
Choong-Hyo Kim
Dong-Min Kim
Hee-Jin Kim
Ann Marie Kimball
Anne Kimmerlein
Laura King
Michael King
Sally Wolff King
Luke Kingry
Joseph Kipkoech
Amy Kirby
Hannah Kirking
Noriko Kitamura
Jeffrey Klausner
Boris Klempa
Jonas Klingstrom
Amy Klion
Timothee Klopfenstein
Kathryn Knoop
Barbara Knust
Albert Ko
Kristin Kobaly
Miwako Kobayashi
Gary Kobinger
Guus Koch
Marleen Kock
Anson Koehler
Aaron Kofman
Jeroen Kortekaas
Christian Kositz
Peter Kotanko
Camille Kotton
Barbara Kowalcyk
Phyllis Kozarsky
Alicia Kraay
Colleen Kraft
Sarah Kramer
Florian Krammer
Annika Kratzel
Peter Krause
Mirjam Kretzschmar
S. Krishna
Marnar Kristiansen
Pavla Krizova

Jürgen Krücken
Detlev Kruger
Thomas Ksiazek
Adam Kucharski
Sharon Kuhlmann-Berenzon
Thijs Kuiken
Ekaterina Kurbatova
Kin On Kwok
Ricardo La Hoz
Bernard La Scola
Marcelo Labruna
Marcus Vinicius Lacerda
Philippe Lagacé-Wiens
Jean-Christophe Lagier
Katrien Lagrou
Katherine Laiton-Donato
Theresa Lamagni
Amy Lambert
Calvin Lambert
Gael Lamielle
Patrick Lammie
Adam Langer
Louise Lansbury
Timothy Lant
Paul Lantos
Tatiana Lanzieri
Romaric Larcher
Maureen Laroche
Amparo Larrauri
Marilynn Larson
Cornelia Lass-Floerl
Eric Lau
Joseph Lau
Max Siu Yin Lau
Rachel Lau
Susanna K. P. Lau
Becki Lawson
James Lawson
Mai Le
Tan Le Van
Sixto Leal
Jerome Lechien
Karin Leder
Phillip Lederer
John Lednicky
James LeDuc
Christopher Lee
Dong-Hun Lee
Jaehyeon Lee
Jin Yong Lee
Keun Hwa Lee
Lisa Lee
Sang Won Lee
Vernon J. Lee
Youn-Jeong Lee
Molly Leecaster
Fabian Leendertz
Sonja Leonhard
Christopher Lepczyk
Eyal Leshem
Justin Lessler
Gabriel Leung
George Ka Wai Leung
Jessica Leung
Kathy Leung
Kenneth Siu-Sing Leung
Tiffany Leung
Anthony Levasseur
Paul Levett
Michael Levy
Dingchen Li
Jingyun Li
Peng Li
Sheng Li
Yuguo Li
Hai Liang
Wanqing Liao
Michael Libman
Amelia Licari
Zachary Liederman
Poh Lian Lim
Travis Lim
Mauricio Lima
Brandi Limbago
Direk Limmathurotsakul
Chiou-Feng Lin
Hsien-Ho Lin
Jessica Lin
Sally Lin
Yen Ting Lin
Monika Lindemann
Daniel Linder
Rebecca Lindsey
Natalie Linton
Bodo Linz
Timothy Littlewood
Anastasia Litvintseva
Hsi Liu
Jing Liu
Wei Liu
Yaping Liu
Michael Lo
Stephanie Lo
Shawn Lockhart
Catherine Logue
Benjamin Lopman
Jacob Lorenzo-Morales
Ahmed Loukil
Jianyun Lu
Lu Lu
Xiaoyan Lu
Yinghong Lu
Inke Lubis
Stephen Luby
Sebastian Lucas
Naomi W. Lucchi
Jay Lucidarme
Martin Ludlow
Benjamin Luft
Grace Lui
Jinxin Lui
Alexander Lukashev
Tao Luo
Yaniv Lustig
Laurence Luu
Samantha Lycett
Joseph Lykins
Xiaoming Lyu
Mai-Juan Ma
Eve MacDonald
Emily MacLean
Oscar MacLean
Zachary Madewell
Hugo Madrid
Ken Maeda
Anna-Pelagia Magiorakos
James Maguire
Christine Mahle
Carla Maia
George Kam Wah Mak
Anna Majury
Hardeep Malhotra
Alexander Malogolovkin
Svenn-Erik Mamelund
Kenneth Mandl
Floréale Mangin
Lisa Manhart
S. Manoharan
Barbara Mann
Hui Mao
Nina Marano
Kalisvar Marimuthu
Wanda Markotter
Lauri Markowitz
Adriana Marques
Linsey Marr
Theodore Marras
Tom Marrie
Douglas Marthaler
Irene Martin
Javier Martin
Roosecelis Martines
Talkmore Maruta
Haruhiko Maruyama
Rasmus Marvig
Grace Marx
Santiago Mas-Coma
Amy Mathers
Blaine Mathison
Wasin Matsee
Yasufumi Matsumura
Keita Matsuno
Max Maurin
Carla Mavian
Lauren Maxwell
Tilicia Mayo-Gamble
Sarah A. Mbaeyi
Kimberly McCarthy
Charles McClure
J. Trenton McClure
Jennifer McClure
Andrea McCollum
John McCormick
Anita K. McElroy
Lesley McGee
Kenneth McIntosh
Brian McKay
Sara McLafferty
Temet McMichael
Meredith McMorrow
Laura McMullan
Lucy McNamara
Samir Mechai
Oleg Mediannikov
Freddy Medina
Jennifer Meece
Paul Meechan
Adam Meijer
Jacques Meis
Cléa Melenotte
Pierrette Melin
Martin Meltzer
Nicolas Menzies
Rachel Mercaldo
Matthias Merker
Stefano Merler
Kevin Messacar
Lauren Meyers
Georgies Mgode
Claire Midgley

Amy Mikhail
Gabrielle Miller
Ian Miller
Lorin Miller
Michael Miller
Michele Miller
Alexander Millman
Donald Milton
Anna Minta
Eric Mintz
A. Mirand
Adriana Miu
Kenji Mizumoto
Arash Mohazzab
Chris Mok
Igor Mokrousov
Marc Monot
April Monroe
Susan Montgomery
Andrew Moon
Patrick Moonan
Brittany Moore
Ramana Moorthy
Kathleen Morales
Aurelie Morand
Jacob Moran-Gilad
Kristine Mørch
Leah Moriarty
Chihiro Morishima
Gabriella Morley
Joan Morris
Stephen Morse
Kathleen Moser
Eric Mossel
Joshua Mott
Francois Mouawad
Heather Moulton-Meissner
Damien Mouly
Alexandra Moura
Marcel Mueller
Barbara Mühlemann
Sanjay Mukhopadhyay
Mick Mulders
John Mulhall
Kamalich Muniz-Rodriguez
Flor Munoz
José F. Muñoz
Vincent Munster
Pablo Murcia
Frederick Murphy
Kristy Murray
Megan Murray
Benoit Muylkens
Cameron Myhrvold
Khin Myint
Khin Saw Myint
Pierre Nabeth
Scott Nabity
Helen Nabwera
Robyn Nadolny
Hidemasa Nakaminami
Satosi Nakano
Allyn Nakashima
Srinivas Nanduri
Naganori Nao
Mitsuo Narita
Farooq Nasar
Roger Nasci
Avindra Nath
Momar Ndao
Mark Nelder
Christina Nelson
Cody Nelson
Kristin Nelson
Martha Nelson
Noele Nelson
Nicole Nemeth
Andreas Neumayr
Paul Newton
Olivier Neyrolles
Sophia Ng
Terry Fei Fan Ng
Billy Ngasala
Minh Ly Nguyen
Nathalie Nicolay
Megan Niederwerder
Eva Møller Nielsen
Silke Niemann
Stefan Niemann
Vladyslav Nikolayevskyy
Muhammad Imran Nisar
Allan Nix
Douglas Nixon
Diego Nobrega
João Nobrega de Almeida Júnior
Melissa Nolan
Jacqueline Nolting
Keri Norman
Erling Norrby
Philip Norris
Shannon Novosad
Norbert Nowotny
Andrew Noymer
Thomas Nutman
Conor O'Halloran
David O'Connor
Sylvia Ofori
Myoung-don Oh
Makoto Ohnishi
Tomohiro Oishi
Nisreen Okba
Liset Olarte
Peter Olbrich
Catherine Oldenburg
Francisco Olea Popelka
Jane Oliver
Sara Oliver
Sonja Olsen
Donald Olson
Ken Olson
Linus Olson
Hanna Oltean
Maurice Ope
Kathy Orloski
Anthony Orvedahl
Miguel O'Ryan
Stephen Ostroff
José A. Oteo
Domenico Otranto
Ken Otsuji
Simon Otto
Jorge Oyhenart
Christopher Paddock
Clinton Paden
Stephen Page
Madhukar Pai
Mark Pallansch
Mitchell Palmer
Melody Palmore
Sherri Pals
Stanley Pang
Yu Pang
Gitika Panicker
Indu Panicker
Mary Pantin-Jackwood
Costas Papagiannitsis
Igor Paploski
John Papp
Linde Parcels
Sang-Won Park
Sang Woo Park
Sun Hee Park
Wan Beom Park
Daniel Parker
William Parks
Philippe Parola
Jonathan Parr
Gabriel Parra
Colin Parrish
Clyde Partin
Katelyn Pastick
Diana Pastrana
Samir Patel
David Paterson
Janusz Paweska
Daniel Payne
Gabriela Paz-Bailey
Carl Pearson
Gisele Peirano
Malik Peiris
L. Peixe
Steve Pelton
Zhiyong Peng
Mary-Louise Penrith
Pasi Penttinen
João Perdigão
Sabine Pereyre
Nicole Perez
Juan Pericas
Lara Perinet
Alex Perkins
Stanley Perlman
Stephanie Perniciaro
Thomas Peterman
Christine Petersen
Jeannine Petersen
Lyle Petersen
Maria Skaalum Petersen
Karin Peterson
William Petri
Marco Pezzi
Michael A. Pfaller
Nisha Philip
Nick Phin
Melissa Phuong
Andrea Piana
Allan Pillay
Alexis Pillsbury
Rachael Piltch-Loeb
Maria Ines F. Pimentel
Stuart Pimm
Talia Pindyck
Benjamin Pinsky
Sara Pires
Johann Pitout
Watcharapong Piyaphanee
Louis Plessis

Kari Plewniak
Nottasorn Plipat
Mateusz Plucinski
Gerd Pluschke
Alexander Podboy
Laurent Poirel
Philip Polgreen
Guillaume Poliquin
Maria Politis
Zvonimir Poljak
Michael Pollanen
Lap Tak Poon
Leo Poon
Shalini Pooransingh
Vsevolod Popov
Sven Poppert
David Powell
Krista Powell
Ann Powers
Wisit Prasithsirikul
John Prescott
D. Rebecca Prevots
Bobbi Pritt
Lisa Prosser
Amy Pruden
Christine Prue
Michael Purdy
Jie Qiao
Liu Quan
Juarez Quaresma
Krista Queen
Flávio Queiroz-Telles
Elisabeth Rabold
Vincent Racaniello
Christian P. Raccurt
Lewis Radonovich
A. Raja
Thendavarayan Ramamurthy
Andrew Ramey
David Ramilo
M. Ramirez
Ian Ramsey
Stéphane Ranque
Didier Raoult
Giammarco Raponi
Mohammed Rasheed
Magnus Rasmussen
Sonja Rasmussen
Adrian Rauchfleisch
James Ravin
Simon Rayner
Krystle L. Reagan
Carrie Reed
Jennita Reefhuis
Johan Reimerink
Arthur Reingold
Richard Reithinger
Tamara Remington
Lili Ren
Adam Retchless
Chantal Reusken
Matthieu Revest
Jean-Marc Reynes
Mary Reynolds
Giovanni Rezza
Guilherme Ribeiro
Bruce Ribner
Ketra Rice
Stephen Rich
Gabriele Richardson
Jan Hendrik Richardus
Holly Richmond-Woods
Emily Ricotta
Renee Ridzon
Hans Rieder
William Ristenpart
Michele Riva
Vanessa Rivera-Amill
Suelee Robbe-Austerman
Florence Robert-Gangneux
Evan Roberts
Stephen Roberts
Emmanuel Robesyn
Stacie Robinson
Haresh Rochani
Benjamin Roche
Barry Rockx
Guenael Rodier
Aline Rodrigues
Alfonso Rodriguez Lainz
Jesús Rodríguez-Baño
Pierre Rollin
Ethan Romero-Severson
Jane Rooney
Pierre Roques
Dominic Rose
Jennifer Rosen
John Rossow
Paul Rota
Camilla Rothe
Janell Routh
Anne Rowley
Alison Roxby
Chad Roy
Sharon Roy
Jose Rubio
Horacio Ruiseñor-Escudero
Brandy Russell
Thomas Russo
Sadie Ryan
Jamal Saad
Claude Saegerman
Marco Aurelio Safadi
David Safronetz
Masayuki Saijo
Ryota Sakamoto
Yoshihiro Sakoda
Katherine Salciccioli
Marco Salemi
Jeanne Salje
Stefania Salmaso
Johanna Salzer
Aaron Samuels
Steven Sanche
Santiago Sanchez-Pacheco
Avnish Sandhu
Frank Sandmann
Cheryl Sangster
Gilberto Santiago
Sarah Sapp
Anita Saxena
Elaine Scallan Walter
Gaia Scavia
Charles Schable
Patrick Scheid
Alan Schenkel
Jarad Schiffer
Oliver Schildgen
Jonas Schmidt-Chanasit
Randal Schoepp
Michael Schotsaert
Simon Schröder
Amy Schuh
Constance Schultsz
Stacey Schultz-Cherry
Claudia Schulz
Ilan Schwartz
Ira Schwartz
Jessica Schwind
Doug Scott
Barbara Seaworth
William Secor
Isaac See
James Sejvar
Tara Sell
Rangaraj Selvarangan
Parham Sendi
Daniel Sexton
Jessica Sexton
Melisa Shah
Prakesh Shah
Sharaf Shah
Jeffrey Shaman
Shokoofeh Shamsi
Andi Shane
Manjunath Shankar
G. Dennis Shanks
Adrienne Shapiro
Eugene Shapiro
Carrie Shapiro-Mendoza
Tyler Sharp
Frederic Shaw
Xinghua Shen
Harsha Sheorey
Samendra Sherchan
Huiying Shi
Zhengli Shi
Jennifer Shield
M. R. Shivaprakash
Suisan Shriner
James Shultz
Carol Sibley
Peter Simmonds
Les Sims
Andreas Sing
Brajendra (Braj) Singh
Om Singh
Pranay Sinha
Theresa Sipe
Tarja Sironen
Helen Skaltsa
Kim Skrobarcek
Rachel Slayton
David Šmajs
David Smith
Duncan Smith
Jessica Smith
Kirk Smith
Robert Smith
Tara Smith
Sigrun Smola
Eveline Snelders
James Snyder
Abigail Snyder-Keller
Jeremy Sobel
Olusegun Soge
Antoni Soriano-Arandes

Frank Sorvillo
Brian Southwell
Erica Spackman
Jessica Spengler
Gianfranco Spiteri
Armand Sprecher
Siddhartha Srivastava
Elyse Stachler
Henry Staines
Claire Standley
J. Staples
Lindsay Starkey
Mieke Steensels
Allen Steere
Arjan Stegeman
Eike Steinmann
John Stelling
John Stenos
Dennis Stevens
Heather Stevenson
O. Stine
Gregory Storch
John Stothard
Michael Stoto
Susan Stramer
Marc Strassburg
Thomas Strecker
Tanja Strive
Franc Strle
D. Michael Strong
Samuel Stubbs
Ashely Styczynski
Miranda Suchomel
David Sue
Yi Nam Suen
Eric Suhler
Gang Sun
Pei-Lun Sun
Rebecca Sunenshine
Mehul Suthar
Colin Sutherland
Satowa Suzuki
Susan Swindells
Ayato Takada
Shannon Takala-Harison
Taichiro Takemura
Paul Tambyah
Azaibi Tamin
G.S. Tan
Kathrine Tan
Junko Tanaka
An Tang
Julian Tang
Robert Tanz
Yelena Tarasenko
Jaime Tarigo
Phillip Tarr
Kathy Tatti
Robert Tauxe
Joanne Taylor
Asmaa Tazi
Anders Tegnell
Halil Tekiner
Sam Telford
Zelalem Temesgen
Daniel Tena
Chong G. Teo
Karen Terio
Joel Terriquez
Eyasu Teshale
Harsh Thaker
Kiran Thakur
Elitza Theel
Roger Thomas
Andrew Thompson
Natalie Thornburg
Mingmei Tian
Peter Timoney
Boghuma Titanji
Tejpratap Tiwari
Kelvin To
James Tobias
Farrell Tobolowsky
Mitsuru Toda
Eugenia Tognotti
Joao Toledo
Yan Topilsky
Mia Torchetti
Noël Tordo
Paul Torgerson
Jeff Tornheim
Pritish Tosh
Machell Town
Jonathan Towner
Rita Traxler
Eija Trees
Mary Jo Trepka
William Trick
Raymond Tsang
Tim Tsang
Sarah Tschudin-Sutter
Theocharis Tsoleridis
Apichal Tuanyok
Damien Tully
Ho-Jui Tung
Mike Turell
Kenneth Tyler
Gregory Tyrrell
Yih-Ling Tzeng
Venkatachalam Udhayakumar
Peter Ueda
Robert Ulrich
Gérald Umhang
Thomas Unnasch
Timothy Uyeki
Nicolas Vabret
Ronald Valdiserri
Snigdha Vallabhaneni
Alex van Belkum
Chris Van Beneden
Andrew van den Hurk
Gerard Van der Auwera
Lia van der Hoek
Mark van der Linden
Wim van der Poel
Tjip van der Werf]
Neeltje van Doremalen
Michel van Herp
Maria Van Kerkhove
Debby van Riel
Ivo van Walle
Philippe Vanhems
Amelie Vantaux
Pedro Vasconcelos
Niccolo Vendramin
Meera Venkatesan
Harry Vennema
Timothée Vergne
Sten Vermund
Andrew Vernon
Thomas Verstraeten
Marcos Vieira
Simone Villa
Julie Villanueva
Amy Vincent
Jan Vinjé
Charles Vitek
Erika Vlieghe
Chantal Vogels
Maarten Voordouw
Setu Vora
Emily Vraga
Srinivas Vunnam
Timothy Wade
Jesse Waggoner
Sherrilyn Wainwright
Diane Waku-Kouomou
David Walker
Megan Wallace
Ryan Wallace
Gabriel Wallau
Andrew Waller
Julia Walochnik
Birgit Walther
Henry (Xiufeng) Wan
Divine Wanduku
Dayan Wang
Jia-Sheng Wang
Kejia Wang
Leyi Wang
Lin Wang
Lin-Fa Wang
Lunan Wang
Xianbo Wang
Xin Wang
Honorine Ward
Julie Ward
David Warhurst
Michael Washington
Marine Wasniewski
Tokiko Watanabe
Ray Waters
John Watson
Matthew Watts
Scott Weaver
Robert Webster
Scott Weese
George Wehby
Wycliffe Wei
Michael Weigand
Francois-Xavier Weill
Zachary Weiner
Robert Weinstein
Jim Wellehan
Rory Welsh
Bruce Weniger
Guido Werner
Joseph L. Wheat
A. Clinton White
Alexandre White
Jennifer White
Richard White
Cyndy Whitney
Nathan Wiederhold
Annelies Wilder-Smith
Hendrik Wilking
John Williams
Nick Wilson
William Wilson
Marc Windisch
Carla Winston

Kevin Winthrop
Timo Wolf
Katja Wolthers
Carlos Wong
Sunny Wong
Corine Sau Man Wong
Joseph Wood
Kate Woodworth
Gary Wormser
Michael Worobey
Henry Wu
Anne Wyllie
Dandan Xiang
Jingyi Xiao
Qian Xiao
Jiancheng Xu
Yingchun Xu
Yuqing Xue
Joseph Yabes
Hayley Yaglom
Pablo Yagupsky
Dafna Yahav
Bingyi Yang
Chunfu Yang
Yang Yang
Jiro Yasuda
Hui-Ling Yen
Jae-Joon Yim
Jingjing Yin
Dongwan Yoo
Takashi Yoshiyama
Barnaby Young
Hongjie Yu
Ignatius Yu
Lili Yu
Wen-Liang Yu
Xue-jie Yu
Kwok-Yung Yuen
Dawood Yusef
Sherif Zaki
Rashid Zaman
Laura Zambrano
Fabio Zampieri
Souheil Zayet
Jing Zeng
Xinyan Zhang
Xu Zhang
Yuan Zhen Zhang
Yue Zhang
Bao-Liang Zhong
Bin Zhou
Haijian Zhou
Tingting Zhuang
John Ziebuhr
Emily Zielinski-Gutierrez
Stephan Zientara
Wen-Quan Zou

EMERGING INFECTIOUS DISEASES®

Upcoming Issue

- Aspergillosis Complicating Severe Coronavirus Disease
- Nosocomial COVID-19 Outbreak Containment, Hanoi, Vietnam, March–April 2020
- Impact of Human Papillomavirus Vaccination, Rwanda and Bhutan
- Comparative Omics Analysis of Historic and Recent Isolates of Bordetella pertussis and Effects of Genome Rearrangements on Evolution
- Estimate of Burden and Direct Healthcare Cost of Infectious Waterborne Disease in the United States
- Using Repeated Serosurveys to Estimate the Force of Dengue Virus Infection in Ouagadougou, Burkina Faso
- Performance of Nucleic Acid Amplification Tests for Detection of Severe Acute Respiratory Syndrome Coronavirus 2 in Prospectively Pooled Specimens
- Intrafamilial Exposure to SARS-CoV-2 Associated with Cellular Immune Response without Seroconversion
- Differential Yellow Fever Susceptibility in New World Nonhuman Primates, Comparison with Humans, and Implications for Surveillance
- Using Structured Expert Judgment for Attribution of Foodborne and Waterborne Illnesses to Comprehensive Transmission Pathways, United States
- Prevalence of SARS-CoV-2, Verona, Italy, April–May 2020
- Cellular Immunity in COVID-19 Convalescents with PCR-Confirmed Infection but with Undetectable SARS-CoV-2–Specific IgG
- Human Diversity of Killer Cell Immunoglobulin-Like Receptors and Human Leukocyte Antigen Class I Alleles, and Ebola Virus Disease Outcomes
- IgG Seroconversion and Pathophysiology in Severe Acute Respiratory Syndrome Coronavirus 2 Infection
- Hospitalization for Invasive Pneumococcal Diseases in Young Children Before Use of 13-Valent Pneumococcal Conjugate Vaccine, Suzhou, China
- Hannibal's Ophthalmia—A New Answer to An Ancient Question
- Primary Amebic Meningoencephalitis Associated with Recreational Aquatic Exposures, USA, 1978–2018
- In Vivo Observation of Cutaneous Larva Migrans by Fluorescence-Advanced Videodermatoscopy
- Listeriosis Caused by Persistence of *Listeria monocytogenes* Serotype 4b Sequence Type 6 in Cheese Production Environment
- Fatal Case of Chronic Jamestown Canyon Virus Encephalitis Diagnosed by Metagenomic Sequencing in a Patient on Rituximab
- Severe Human Bocavirus-Associated Pneumonia in Adults at a Referral Hospital, Seoul, South Korea

Complete list of articles in the January issue at http://www.cdc.gov/eid/upcoming.htm

Earning CME Credit

To obtain credit, you should first read the journal article. After reading the article, you should be able to answer the following, related, multiple-choice questions. To complete the questions (with a minimum 75% passing score) and earn continuing medical education (CME) credit, please go to http://www.medscape.org/journal/eid. Credit cannot be obtained for tests completed on paper, although you may use the worksheet below to keep a record of your answers.

You must be a registered user on http://www.medscape.org. If you are not registered on http://www.medscape.org, please click on the "Register" link on the right hand side of the website.

Only one answer is correct for each question. Once you successfully answer all post-test questions, you will be able to view and/or print your certificate. For questions regarding this activity, contact the accredited provider, CME@medscape.net. For technical assistance, contact CME@medscape.net. American Medical Association's Physician's Recognition Award (AMA PRA) credits are accepted in the US as evidence of participation in CME activities. For further information on this award, please go to https://www.ama-assn.org. The AMA has determined that physicians not licensed in the US who participate in this CME activity are eligible for AMA PRA Category 1 Credits™. Through agreements that the AMA has made with agencies in some countries, AMA PRA credit may be acceptable as evidence of participation in CME activities. If you are not licensed in the US, please complete the questions online, print the AMA PRA CME credit certificate, and present it to your national medical association for review.

Article Title

Clinical and Multimodal Imaging Findings and Risk Factors for Ocular Involvement in a Presumed Waterborne Toxoplasmosis Outbreak, Brazil

CME Questions

1. Your patient is a 32-year-old man with blurred vision and floaters who may have been exposed to Toxoplasma gondii. According to the report of an outbreak in 2015 in Gouveia, Brazil, by Brandão-de-Resende and colleagues, which of the following statements about clinical and multimodal imaging findings at presentation and prevalence of and risk factors for ocular involvement in toxoplasmosis is correct?

A. Two distinct patterns of retinochoroiditis were seen on multimodal imaging: necrotizing focal and punctate retinochoroiditis
B. Age ≥40 years doubled the risk for ocular involvement
C. Female sex was a strong risk factor for retinochoroiditis
D. At baseline, one-tenth of patients had retinochoroiditis

2. According to the report by Brandão-de-Resende and colleagues, which of the following statements about recurrences and complications of toxoplasmosis reported during an outbreak in 2015 in Gouveia, Brazil, is correct?

A. Among patients with baseline ocular involvement, 21% had recurrent retinochoroiditis during follow-up after starting classic therapy
B. All cases of recurrent retinochoroiditis occurred within 1 year
C. Similar proportions of patients with binocular vs monocular involvement had recurrent lesions
D. Complications included epiretinal membranes (25%); and 1 each had rhegmatogenous retinal detachment with pars plana vitrectomy, transient intraocular pressure elevation, and posterior vitreous detachment

3. According to the report of an outbreak in 2015 in Gouveia, Brazil, by Brandão-de-Resende and colleagues, which of the following statements about clinical implications of findings, course, and risk factors for ocular involvement in toxoplasmosis is correct?

A. Only patients with initial ocular involvement need long-term ophthalmologic follow-up
B. Careful retinal examination with multimodal imaging is needed to detect punctate retinal infiltrates, distinct from the classical pattern of necrotizing retinochoroiditis
C. Among patients with confirmed acute infection, only patients with ocular symptoms need thorough eye examination
D. Baseline parasite load is unlikely to affect risk for recurrence of retinochoroiditis

Earning CME Credit

To obtain credit, you should first read the journal article. After reading the article, you should be able to answer the following, related, multiple-choice questions. To complete the questions (with a minimum 75% passing score) and earn continuing medical education (CME) credit, please go to http://www.medscape.org/journal/eid. Credit cannot be obtained for tests completed on paper, although you may use the worksheet below to keep a record of your answers.

You must be a registered user on http://www.medscape.org. If you are not registered on http://www.medscape.org, please click on the "Register" link on the right hand side of the website.

Only one answer is correct for each question. Once you successfully answer all post-test questions, you will be able to view and/or print your certificate. For questions regarding this activity, contact the accredited provider, CME@medscape.net. For technical assistance, contact CME@medscape.net. American Medical Association's Physician's Recognition Award (AMA PRA) credits are accepted in the US as evidence of participation in CME activities. For further information on this award, please go to https://www.ama-assn.org. The AMA has determined that physicians not licensed in the US who participate in this CME activity are eligible for AMA PRA Category 1 Credits™. Through agreements that the AMA has made with agencies in some countries, AMA PRA credit may be acceptable as evidence of participation in CME activities. If you are not licensed in the US, please complete the questions online, print the AMA PRA CME credit certificate, and present it to your national medical association for review.

Article Title

Tuberculosis among Children and Adolescents at HIV Treatment Centers in Sub-Saharan Africa

CME Questions

1. You are advising a pediatric HIV/tuberculosis (TB) center in sub-Saharan Africa about strategies to improve patient outcomes. According to the analysis of data from 7 integrated pediatric HIV/TB centers in 6 countries in sub-Saharan Africa by Mandalakas and colleagues, which of the following statements about TB Incidence and period prevalence among children and adolescents living with HIV (C/ALHIV) is correct?

A. During 57,525 patient-years (PY) of follow-up, there were 1,160 cases of TB in C/ALHIV (2017/100,000 PY)
B. TB incidence rate was similar across sites and substantially lower than the population level incidence estimated by the World Health Organization (WHO) in the respective countries
C. Rates of bacteriologically confirmed TB were higher in adolescents age 10 to 19 years than in young children
D. Prevalence of TB disease remained stable during the analytic period

2. According to the analysis of data from 7 integrated pediatric HIV/TB centers in 6 countries in sub-Saharan Africa by Mandalakas and colleagues, which of the following statements about TB outcomes and risk factors among C/ALHIV is correct?

A. Every 10% increase in ART uptake was associated with a 1.2% decrease in TB prevalence
B. Good TB outcomes were linked to increased time in care, early ART initiation, and immune preservation whereas severe immunosuppression was linked to death
C. Younger age at the time of starting ART was linked to lower risk for death
D. Risk factors for unfavorable outcome included extrapulmonary disease and previous TB treatment

3. According to the analysis of data from 7 integrated pediatric HIV/TB centers in 6 countries in sub-Saharan Africa by Mandalakas and colleagues, which of the following statements about clinical implications of the association between ART and TB prevalence and risk factors for adverse TB outcomes among C/ALHIV is correct?

A. Early TB case detection and treatment initiation is unlikely to improve TB outcome among C/ALHIV, as ART and ATT cannot be given simultaneously because of adverse events (AEs)
B. A population with excellent ART coverage should not have an elevated risk for TB
C. The study showed that in children, HIV infection significantly reduces the likelihood of bacteriologic TB disease confirmation
D. The findings show that increasing ART uptake > 90% is linked to decreased TB incidence in high-burden settings and support integrated HIV/TB services for C/ALHIV

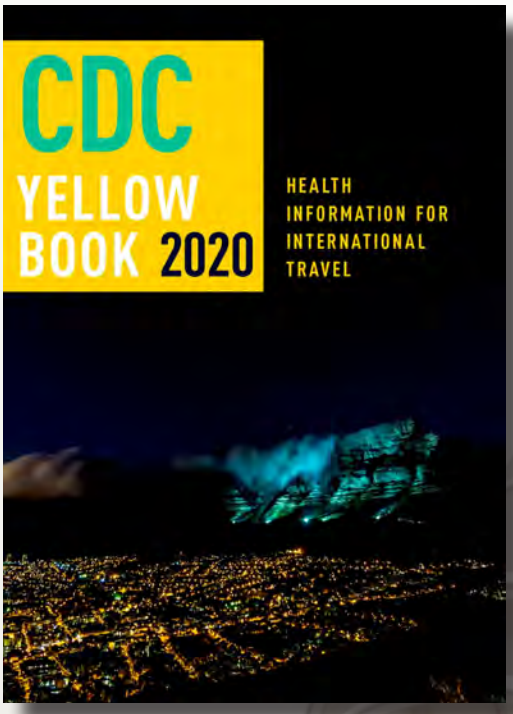

Available Now
Yellow Book 2020

The fully revised and updated CDC Yellow Book 2020: Health Information for International Travel codifies the US government's most current health guidelines and information for clinicians advising international travelers, including pretravel vaccine recommendations, destination-specific health advice, and easy-to-reference maps, tables, and charts.

ISBN: 978-0-19-006597-3 | $115.00 | May 2019 | Hardback | 720 pages

ISBN: 978-0-19-092893-3 | $55.00 | May 2019 | Paperback | 687 pages

Yellow Book 2020 includes important travel medicine updates

- **The latest information on emerging infectious disease threats, such as Zika, Ebola, and henipaviruses**
- **Considerations for treating infectious diseases in the face of increasing antimicrobial resistance**
- **Legal issues facing clinicians who provide travel health care**
- **Special considerations for unique types of travel, such as wilderness expeditions, work-related travel, and study abroad**

OXFORD
UNIVERSITY PRESS

Order your copy at:
www.oup.com/academic

DEPARTMENT OF
HEALTH & HUMAN SERVICES
Public Health Service
Centers for Disease Control and Prevention (CDC)
Mailstop D61, Atlanta, GA 30329-4027

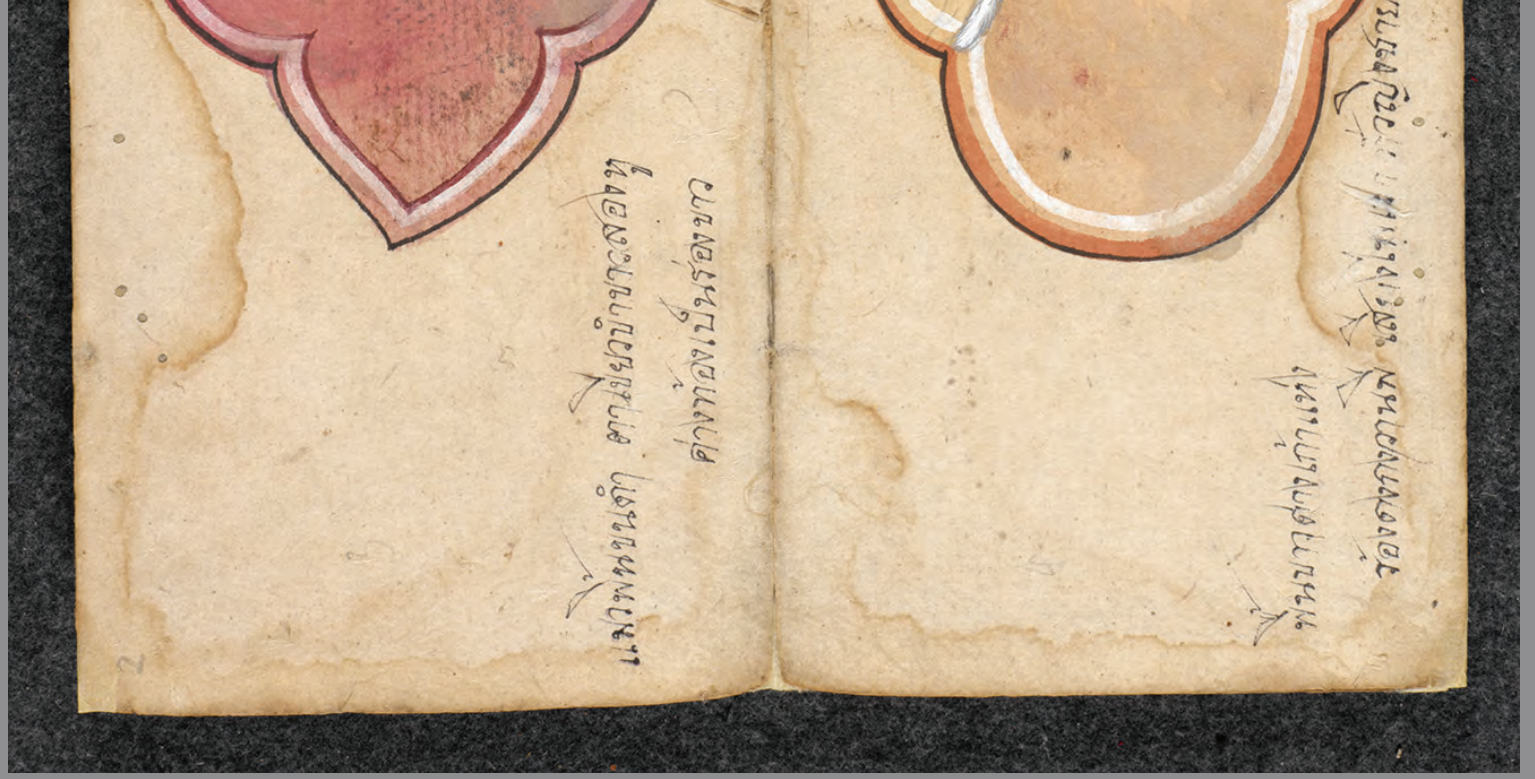

ISSN 1080-6040